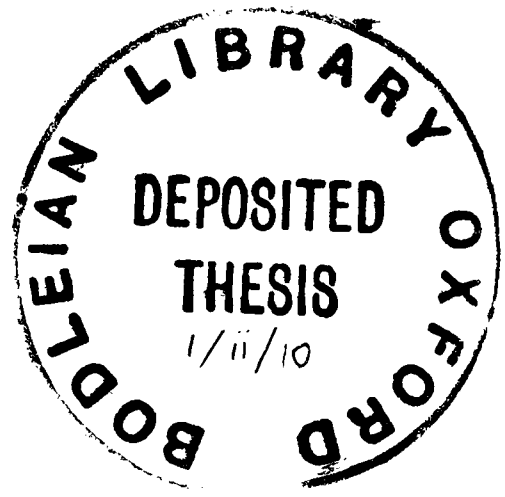
THE CHARACTERISATION OF CALCRETE BASED ON ITS ENVIRONMENTAL SETTINGS WITHIN SELECTED REGIONS OF THE KALAHARI, SOUTHERN AFRICA



Alexander Iain Shaw
Christ Church
Oxford

Submitted for the degree of D.Phil.

[2009]

TABLE OF CONTENTS

I. TABLE OF FIGURES viii

II. LIST OF TABLES xviii

III. LIST OF APPENDICES xx

IV. ABREVIATIONS USED xxi

V. AKNOWLEDGEMENTS xxii

VI. ABSTRACT xxv

1. INTRODUCTION 1

1.1 How does understanding Cenozoic terrestrial carbonate processes within the Kalahari of southern Africa add to global palaeoclimatic understanding? 8

2. TERRESTRIAL CARBONATE 12

2.1 Introduction 12

2.2 Carbonate Duricrusts 14

2.2.1 Types of Calcic Horizons and their Nomenclature 17

2.2.2 Occurrence According to Climatic Zones 19

2.2.3 Genesis 21

2.2.3.1 Pedogenetic Modes of Formation 25

2.2.3.1.1 Downward Movement 26

2.2.3.1.2 Upward movement of $CaCO_3$ 28

2.2.3.1.3 Lateral transport of $CaCO_3$ 29
2.2.3.1.4 Liberation or formation of $CaCO_3$ from parent material. 30
2.3 Organic Agency 31
2.4 Palustrine Carbonates 33
2.4.1 Development 33
2.4.2 Mechanism of Water Supply 36
2.4.3 Diagenesis 37
2.5 Non-Pedogenic Carbonates 39
2.6 Pedogenic Calcrete 42
2.7 Calcite or Dolomite? 44
2.8 Kalahari Carbonate 48
2.8.1 Dolocrete-Silcrete-Calcrete Intergrade Duricrusts 52
2.8.1.1 Duricrusts Containing Secondary Silica within a Carbonaceous Matrix 53
2.8.1.2 Duricrusts Containing Secondary Carbonate within a Siliceous Matrix 55
2.8.1.3 Duricrusts with Contemporaneous Silica and Carbonate Precipitation 56
2.9 Conclusion 56

3. ISOTOPIC ANALYSIS OF TERRESTRIAL CARBONATES 58
3.1 Introduction 58
3.2 Terrestrial Carbonate and Isotope Geochemistry 59
3.3 Problems associated with Pedogenic Carbonates 73
3.4 Conclusion 76

4. METHODOLOGY AND TECHNIQUES 80

4.1 Sampling 80
4.2 Mapping and Remote Sensing 81
4.3 Physical and Chemical Sedimentology 82
4.3.1 Description 82
4.3.2 Grain Size Analysis Techniques 83

4.3.3	Petrographic Investigation	85
4.3.4	XRD	89
4.3.5	Environmental Magnetic Susceptibility	91
4.3.6	LOI Organic Carbon	93
4.3.7	LOI Inorganic Carbon	94
4.3.8	Electrical Conductivity	95
4.3.9	pH	96
4.3.10	Cations	96
4.3.11	Anions	100
4.3.12	Isotopes	101
4.3.13	C/N and $\delta^{13}C$ Organic Analysis	103
4.4	Hydrogeochemistry of the Okavango Alluvial Fan	104
4.4.1	Preparation of Containers for Aqueous Samples	104
4.4.2	Water Sampling Protocol	105
4.4.3	Alkalinity	106
4.4.4	TDS	107
4.4.5	Anion and Cation Analysis of Ground and Surface Waters	108
4.5	Conclusion	109

5. THE GEOMORPHOLOGY, PETROGRAPHY, MINERALOGY AND ISOTOPE GEOCHEMISTRY OF THE MOKALANEN FORMATION, KALAHARI GROUP AT SELECTED SITES IN THE SW KALAHARI 110

5.1	Introduction	110
5.2	Geomorphology	110
5.2.1	The Auob River Valley	110
5.2.2	The Olifants River Valley	114
5.2.3	The Nossob River Valley	115
5.2.4	The Molopo River Valley	116
5.2.5	The Kuruman River Valley	119
5.3	Lithofacies of the Mokalanen Formation	120

5.3.1 Channel Carbonates 121
5.3.2 Hardpan Calcrete 122
5.3.3 Intergrade Nodular Carbonate 124
5.3.4 Massive Intergrade Carbonate 126
5.3.5 Carbonate Cemented Conglomerate Member 130
5.4 Isotope Geochemistry 132
5.5 Interpretation and Discussion 134
5.6 Conclusion 141

6. GROUNDWATER AND PEDOGENIC MODIFICATION OF CARBONATES FROM SELECTED SITES WITHIN THE PANNETJIESVELD OF THE KALK WEISSRAND, EASTERN NAMIBIA 143

6.1 Introduction 143
6.2 Lithostratigraphy and Depositional Environments 143
6.3 Geomorphology and Hydrology 146
6.4 Petrofabric and Mineralogical analysis of the Upper Makalanen Formation 150
6.5 Discussion 152
6.6 Conclusion 156

7. THE RELATIONSHIP BETWEEN GEOMORPHOLOGY AND CHEMICAL SEDIMENTS AT KEY LOCATIONS IN THE KGALAGADI DISTRICT, SW BOTSWANA 158

7.1 Introduction 158
7.2 Physical Environment 159
7.3 Geomorphology 163
7.4 Chemical Sediments 166
7.4.1 Petrographic Characteristics 167
7.4.1.1 Pedogenic Deposits 167
7.4.1.2 Groundwater Modified Pedogenic Deposits 169
7.4.1.3 Pedogenically Modified Groundwater Deposits 171

7.4.1.4 Pan Terrace Deposits 173
7.4.1.5 Pan Deposits 176
7.4.2 Mineralogy 179
7.5 Discussion and Conclusion 181

8. THE GEOMORPHOLOGY AND NEAR SURFACE CHEMICAL AND CLASTIC DEPOSITS ASSOCIATED WITH THE ETOSHA PAN, NORTHERN NAMIBIA 187

8.1 Introduction 187
8.2 Geological Setting 187
8.3 Geomorphology of the Etosha Pan 190
8.4 Lithological Units and Facies Assemblages 198
8.4.1 Unconsolidated Deposits 198
8.4.2 Consolidated Deposits 208
8.4.2.1 The Etosha Limestone 208
8.4.2.2 Andoni Formation Chemical Sediments 217
8.5 Conclusion 220

9. CHEMICAL SEDIMENTS OF THE PALAEO AND ACTIVE OKAVANGO ALLUVIAL FAN, BOTSWANA: EVIDENCE FOR VARIATIONS IN THE PROCESSES OF FORMATION 225

9.1 Introduction 225
9.2 Clastic and Chemical Sedimentation 229
9.3 Alluvial Carbonates 230
9.3.1 Relict Interdune Calcretes 231
9.3.2 Calcretes of the Thamalakane Valley 237
9.3.3 Sandveld and Thaoge Valley Calcretes 239
9.3.4 Islands in the Permanent Swamps of the Delta 242
9.3.5 The Seasonal Floodplains 249
9.4 Hydro-Geochemistry 252
9.5 Conclusion 254

10. THE GEOMORPHOLOGY AND CHEMICAL SEDIMENTS OF THE LINYANTI SYSTEM, EASTERN CAPRIVI, NAMIBIA **256**

10.1 Introduction 256
10.2 Geomorphology 257
10.3 Near Surface Deposits of the Linyanti 260
10.3.1 Physical Characteristics of the Deposits 260
10.3.2 Petrography 264
10.4 Mineralogy and Geochemistry of the Alluvial Deposits 266
10.4.1 XRD Mineralogy 266
10.4.2 Carbon and Oxygen Isotope Analysis of the Carbonate Fraction 270
10.5 Discussion and Conclusion 274

11. THE USE OF MINERALOGY, PETROGRAPHY, MAJOR ELEMENT GEOCHEMISTRY AND LIGHT STABLE ISOTOPES TO UNDERSTAND FORMATIVE PROCESSES AND DEPOSITIONAL ENVIRONMENTS OF CHEMICAL SEDIMENTS IN THE NGAMI SUB-BASIN, WESTERN CENTRAL BOTSWANA **277**

11.1 Introduction 277
11.2 Geomorphology and Depositional Context 277
11.3 Sedimentary Units 280
11.3.1 Palaeo-Lake Bed Deposits (923-928 m) 281
11.3.2 928-932 m Strandline Deposits 285
11.3.3 940-945 m Strandline Deposits 296
11.4 Discussion and Conclusion 301

12. DISCUSSION AND CONCLUSION **306**

12.1 Depositional Environments, Palaeoenvironmental

	Conditions and the Relative Age of Kalahari Carbonates	306
12.1.1	Pans	310
12.1.2	Alluvial	313
12.1.3	Lacustrine/Palustrine	317
12.1.4	Pedogenic	319
12.2	Isotope Geochemistry – its role in elucidating carbonate precipitation and epigenesis within the Kalahari	319
12.3	Kalahari Chemical Sediments: Are Micro-Fabrics Linked to Paragenetic and Epigenetic Environments?	323
12.3.1	Biogenic Processes	324
12.4	A Holistic Lithostratigraphy within the Kalahari	327
12.5	Conclusion	334

13. REFERENCES **336**

14. APPENDICES 1 - 17

I. TABLE OF FIGURES

Fig 1.1 – Location of areas investigated within the Mega Kalahari. ... 5

Fig 4.1 – Comparison of XRD techniques from various clay minerals from Ouhadia and Yong (2003). ... 90

Fig 5.1 – Map of the SW Kalahari showing drainages and sample sites. ... 111

Fig 5.2 – LANDSAT image of the Skaap River degenerating into the pans of the pannetjieveld and the adjacent pot-hole and incised carbonate surface among the NNW/SSE orientated linear dunes of the SW Kalahari. The Usib River to the west intersects the drainage emanating from the pannetjiesveld to form the Auob River. ... 113

Fig 5.3 – LANDSAT image of the Auob/Olifants confluence at Tweerivier. ... 114

Fig 5.4 – LANDSAT image of the confluence between the Olifants and Seeis Rivers and the adjacent flowing Skaap River. ... 115

Fig 5.5 – LANDSAT image of the confluence between the Auob and Nossob Rivers at Twee Rivieren. ... 116

Fig 5.6 – Neogene uplift within southern Africa after Partridge and Maud (2000). ... 117

Fig 5.7 – LANDSAT image of the middle and lower course of the Molopo drainage. ... 118

Fig 5.8 – (a) Photograph of Kalahari dunes capping the upper surface of the incised Olifants River. (b) Photograph of the profile exposed in the northern bank of the incised Auob River at site NC27. ... 120

Fig 5.9 – Photograph of the incised lower Auob River Valley. ... 121

Fig 5.10 – PPL thin-section photomicrographs: (a) Extremely dense micrite (upper right) and micrite coated detrital quartz grains and peloids cemented by sparmicrite (lower left) (b) cavity within the dense micrite fabric filled with detrital quartz grains cemented by a late stage micrite (c) lithoclast of the sandy dolo/limestone with small remnant detrital grains floating

within the later micrite fabric with detrital quartz grains. ... 122

Fig 5.11 – PPL thin-section photomicrographs: (a) micro-laminated micrite with dispersed floating corroded detrital quartz grains (b) fenestrae within the dense micrite fabric (c) micrite coated grains, pisoliths and ooids floating in a sparmicrite fabric (d) sparite filled vugs and micrite peloids floating within a sparmicrite cement (e) sparite fabric with patches of sparmicrite (f) increased detrital quartz content with sparry haloes towards the base of the hardpan unit. ... 123

Fig 5.12 – A nodular intergrade carbonate profile capped by hardpan exposed at site NC28. ... 124

Fig 5.13 – PPL thin-section photomicrographs: (a) transition from a dense micrite fabric with abundant floating detrital quartz grains to a less dense sparmicrite fabric (b) pelletal micrite and micrite coated detrital quartz grains floating in a sparmicrite fabric (c) authigenic microcrystalline quartz precipitated as fracture and vug fills within the micrite and sparmicrite fabric. ... 125

Fig 5.14 – The moderately consolidated upper massive unit of the Mokalanen Formation exposed along the upper terrace of the Kuruman Valley at site NC23. ... 125

Fig 5.15 – PPL thin-section photomicrographs: (a) Coarse, crystalline dolomite, authigenic silica, and sparry calcite fabric (b) authigenic silica lined vug within the sparmicrite fabric (c) dolomicrite and sparmicrite coated floating corroded detrital quartz grains ... 126

Fig 5.16 – Photograph of the unconformity between the upper and lower sandy massive carbonate units of the Mokalanen Formations at site NC25. ... 127

Fig 5.17 – PPL thin-section photomicrographs: (a) micrite and sparmicrite fabric with numerous floating corroded detrital quartz grains and a central cavity lined with sparmicrite and micrite (b) pelletal micrite, peloids and coated detrital quartz grains floating in a sparmicrite fabric (c) bioclast (possibly a fragment of ostracod?) floating in the micrite fabric with corroded detrital

quartz grains. ... 128
Fig 5.18 – Photograph of biotubes weathered out of the carbonate at site NC25. ... 128
Fig 5.19 – Ferric iron and manganese oxides and hydroxides nodules exposed within the upper massive intergrade carbonate. ... 129
Fig 5.20 – Photograph of well rounded quartzite clasts within the carbonate cemented conglomerate member at site N13. ... 131
Fig 5.21 – PPL thin-section photomicrographs: (a) detrital quartz grains with variably developed micrite grain coatings, pelletal micrite and peloids floating in a sparmicrite fabric (b) well developed sparry calcite coatings around detrital quartz grains in zones characterized by a sparmicrite fabric (c) fabric dominated by non-planar anhedral dolomite with minor authigenic silica and micrite and a single floating detrital quartz grain (lower left corner). ... 132
Fig 6.1 – LANDSAT image of the pot-holed landscape of the Kalk Weissrand, the adjacent linear dunes of the SW Kalahari and the major drainages. ... 144
Fig 6.2 – Location map of the Kalk Weissrand and sample sites. ... 145
Fig 6.3 – LANDSAT image of the NW/SE aligned pans with those nearest the western margin of the Kalahari Plateau characterized by incised centripetal drainage and the pothole depressions of the central pannetjiesveld. ... 147
Fig 6.4 – LANDSAT image of the Koes-Haksteen pan corridor. ... 149
Fig 6.5 – PPL thin-section photomicrographs: (a) Dense micrite fabric with floating highly corroded detrital quartz grains (b) complex micrite, sparmicrite and authigenic silica fabric developed 5-10 cm below the surface (c) fabric containing micrite peloids, glaebules, silica filled fracture, sparmicrite lacy fabric and numerous corroded detrital quartz grains some with micrite coatings (d) detrital quartz with a sparite (inner) and micrite (outer) grain coating (e) micrite peloids, silica glaebules and intraclasts (F-fabric glaebular fabric (Summerfield, 1983b)) have diffused edges and become less distinguishable (ghosts) as the fabric becomes devoid of structures and increasingly crystalline in texture

(M-fabric massive (Summerfield, 1983b)) (f) lower vuggy authigenic micro-crystalline silica fabric devoid of floating detrital grains. ... 151

Fig 7.1 – Location map of the Kgalagadi sample sites. ... 159

Fig 7.2 – Kalahari Group Isopach map of the study area, based on BGS and WCS (1994, 1996) drill data. ... 160

Fig 7.3 – LANDSAT image of the well developed lunettes on the southern side of Kakwe Pan and the linear and curvilinear features (boxes) in the vicinity of Hukuntsi, Lokgwabe, Tshane, Kakwe and Katlwe Pans. ... 164

Fig 7.4 – PPL thin-section photomicrographs: (a) Detrital quartz forming a grain supported fabric cemented by simple inter-granular micrite precipitation structures. (b) simple grainstone fabric containing numerous coated detrital quartz grains, pelletal micrite and glaebules (c) dispersed corroded detrital quartz grains floating in a mixed equant sparite (top left), sparmicrite (center) and micrite (lower right) fabric. ... 168

Fig 7.5 – PPL thin-section photomicrographs: (a) Dense micrite fabric with sparse floating detrital quartz grains in the upper section of the ridge believed to be indicative of pedogenic micritisation (b) network of silica micro-veins and stringers within the mixed micrite and sparite fabric (c) sparite dominated fabric with a micrite filled fracture and pervasive micritisation along the margin. ... 169

Fig 7.6 – PPL thin-section photomicrographs: (a) micrite with anastomosing laminae, cryptocrystalline vug fills and floating detrital quartz grains (b) dense pedogenic wackestone containing floating detrital quartz grains, pelletal micrite and peloids with authigenic silica filled fenestrae (c) sparmicrite filled circum-granular cracks within the dense micrite fabric (d) sparite fill undergoing micritisation within the dense micrite fabric (e) authigenic silica filled vug within the dense micrite fabric (f) the sparmicrite fabric undergoing micritisation along the fracture network and around detrital grains producing a chicken-wire type appearance. ... 172

Fig 7.7 – LANDSAT image of the concentric pits (box) investigated west

of Pepane Pan. ... 174

Fig 7.8 – PPL thin-section photomicrographs: (a) micro-laminated micrite with occasional floating corroded detrital quartz grains (b) dense micrite and dolomicrite fabric containing floating corroded detrital quartz grains and a bioclast (center - possibly a fragment of gastropod or ostracod test) (c) an array of intraclasts, peloids/glaebules, coated detrital quartz grains, alveolar septal fabric and micro-vugs present within the micrite fabric (d) geopetal authigenic silica fill within the micrite and sparmicrite fabric (e) authigenic silica filled vug (top left) with a network of lined veinlets intruding the adjacent micrite fabric – suggestive of corrosion and replacement by silica (f) lower packstone characterized by concentric micrite grain coatings and occasional peloids floating within a sparmicrite fabric. ... 175

Fig 7.9 – PPL thin-section photomicrographs: (a) extremely dense wackestone fabric consisting of dark brown micrite intraclasts and peloids floating in a vuggy biege dolomicrite, micrite and sparmicrite fabric (b) moderately corroded detrital quartz grains and a bioclast (possibly a fragment of ostracod test) floating in the dense micrite fabric with authigenic silica filled vugs (c) a lined and filled solution void with radial veins and lined fractures indicating the pervasive nature of the silica replacement of the original micrite fabric. ... 178

Fig 8.1 – MODIS image of the Etosha Basin. ... 188

Fig 8.2 – An aerial photograph of the terrace along the southern rim of Etosha Pan. ... 191

Fig 8.3 – LANDSAT image of Poachers Point, the Odila River delta and the bar and peninsula features of the NE sector of Etosha Pan. ... 192

Fig 8.4 – LANDSAT image of dust blowing off NW Namibia. ... 194

Fig 8.5 – Map of Etosha indicating the location of sample sites. ... 196

Fig 8.6 – An aerial photograph of the complex channel morphology associated with the anabranching and meandering Ekuma River. ... 198

Fig 8.7 – Photograph of the western terrace of the Ekuma River at the old horse camp north of Etosha Pan. ... 199
Fig 8.8 – Gravel, sand and mud fraction versus depth below surface from the Odila River channel. ... 200
Fig 8.9 – Gravel, sand and mud fraction versus depth below surface from the Oshigambo River channel. ... 201
Fig 8.10 – Aerial photographs of the Ekuma River's birds-foot delta debouching into the Etosha Pan (a) from the south and (b) from the north. ... 202
Fig 8.11 – Profiles (a) EKA1 and (b) EKA2 taken along a transect across the lower Ekuma River illustrating the gravel, sand and mud fraction versus depth below surface. ... 205
Fig 8.12 – PPL thin-section photomicrographs: (a) extremely dense fine grained micrite and dolomicrite fabric with silica filled fractures (b) & (c) detrital quartz grains, intraclasts, ooids, pseudo-ooids and peloids floating within late stage carbonate and silica fabrics (d) shell fragment (possibly from an ostracod) within the micrite fabric (e) & (f) authigenic silica filled fractures, voids and fenestrae within the dense micrite and dolomicrite fabric (g) intraclast formed as a result of a circum-granular crack structure within the dense micrite and dolomicrite fabric (h) pervasive silica (i) pseudobreccia of carbonate intraclasts with silica fracture fills ... 210
Fig 8.13 – PPL thin-section photomicrographs: (a) authigenic silica void fill and silicification of the fabric with residual micrite preserved (b) crenellated authigenic fracture fill and pervasive margin with micro-veins. ... 214
Fig 8.14 – Vegetation map of Etosha National Park (Le Roux, 1980). ... 216
Fig 8.15 – PPL thin-section photomicrographs: (a) authigenic microcrystalline quartz filled fractures with pervasive silica along the margins which have partially silicified the adjacent micrite fabric (b) a micrite intraclast with corroded edges floating within a microcrystalline silica replacement fabric. ... 217
Fig 9.1 – Location map of the Okavango alluvial fan in Northwest Botswana. Shaded area indicates extent of the seasonal

swamps (modified from McCarthy *et al.*, 1991a). ... 226
Fig 9.2 – LANDSAT image of the Okavango alluvial fan showing the main faults systems of the region (Ellery and Ellery, 1997). ... 228
Fig 9.3 – Photographs of linear dune dissected by the Okavango River. (a) Profile shows carbonate nodules formed within the aeolian sediment in the lower section. (b) Close up of calcrete nodules of various sizes and morphologies formed within the lower part of the profile. ... 232
Fig 9.4 – PPL thin-section photomicrographs of calcrete collected from various locations on the Okavango alluvial fan: (a) Pelletal micrite and pseudo-oolitic textured nodular calcrete at site E; (b) Complex spar fill structure with laminated micrite and authigenic quartz lining of voids within a clotted micrite fabric. Massive Fe and Mn mottled calcrete collected at site G; (c) Corroded detrital quartz grains within a micrite matrix. Void structure with spar lining and dolomite fill. Sample collected from massive poorly consolidated calcrete/dolocrete at site U; (d) Clotted micrite and sparite matrix with pseudo-oolitic and oolitic texture containing corroded detrital quartz grains. Massive nodular pedogenic calcrete collected at site O; (e) Section through a calcrete nodule collected from the capillary fringe on Xhamoga Island showing a banded micrite fabric, Fe and Mn staining, highly corroded detrital quartz grains and authigenic silica void fills; (f) Dense micritic alpha fabric containing corroded detrital quartz grains and a skeletal shell fragment. Sample collected at site V on the seasonal floodplain. ... 233
Fig 9.5 – Photograph of massive groundwater calcrete profile (A) with Mn and Fe nodules and staining (B), Thamalakane Valley. ... 237
Fig 9.6 – Photograph of an extensive calcrete sequence exposed next to the Thaoge River. ... 241
Fig 9.7 – A plot of electrical conductivity in μS versus distance from the channel edge/island perimeter for each of the three islands sampled in the permanent swamps. Letters show the location of

samples within the transect from perimeter to island core for each island. ... 244
Fig 9.8 – Idealised cross-section through Xhamoga Island showing the location of sample pits. Modified from Ellery and Ellery (1997). ... 247
Fig 9.9 – Simplified summary schematic of the processes, mechanisms and resultant mineralogies within the Okavango. ... 251
Fig10.1 – Location map of sample sites within the Linyanti Swamps. ... 256
Fig10.2 – MODIS image of the Chobe-Linyanti-Okavango-Ngami-Makgadikgadi system. ... 257
Fig 10.3 – Dominant fault lineaments within the Okavango Region, from Mendelsohn and el Obeid (2004). ... 258
Fig 10.4 – LANDSAT image of the Savuti Channel, Magwikhwe Sand Ridge, Mababe Depression and the Mogogelo Channel. ... 259
Fig 10.5 – Photograph of a palaeo-channel profile exposed at site L6. An upper unconsolidated white fluvial sand horizon (containing numerous bee-eater burrows) overlies a moderately consolidated feruginised sand. ... 261
Fig 10.6 – Photograph of the down-profile increase in carbonate at site L4. ... 262
Fig 10.7 – PPL thin-section photomicrographs of: (a) peloidal micrite and corroded detrital quartz grains within a lacy sparite fabric; (b) crypto-crystalline quartz with poorly corroded floating detrital quartz grains; (c) concentric laminations of micrite forming an ooid around an aggregate of detrital quartz grains; (d) calcified root cortex cells (possibly microcodium); (e) calcified root hair; (f) detrital quartz grains with very well developed sparite grain coating floating within a crystalline sparite fabric which has been partially micritised (lower left corner). ... 265
Fig 11.1 – LANDSAT image of the Ngami Basin. ... 278
Fig 11.2 – Map of Ngami Basin with sample sites and geomorphic features. ... 279
Fig 11.3 – An aerial photograph of the meandering NW/SE orientated incised Nhabe River and the adjacent Kunyere River feeding

into Lake Ngami. ... 280
Fig 11.4 – An aerial photograph of the confluence of the Nhabe and Thamalakane Rivers at Dikatlhong. ... 281
Fig 11.5 – Photograph of the powdery sil-calcrete section exposed within a trench at site B31. ... 281
Fig 11.6 – PPL thin-section photomicrographs: (a) highly corroded floating detrital quartz grains floating within a mixture micrite and sparmictrite fabric; (b) corroded floating detrital quartz grain and bioclast (possibly a fragment of a diatom) floating within a mixture micrite and sparmictrite fabric; (c) peliods, pelletal micrite and circum-granular crack structures within a lacy micrite and sparmictrite fabric; (d) manganese enriched micritic nodule floating within the mixed micrite and sparmicrite fabric; (e) manganese enriched micritic fabric containing a bioclast (possibly a fragment of a diatom) adjacent the mixed micrite and sparmictrite fabric containing highly corroded detrital quartz grains. Note the distinct interface between the two fabric types; (f) lacy micrite and sparmicrite fabric with authigenic silica filled secondary porosity. ... 284
Fig 11.7 – PPL thin-section photomicrographs of the 928-932 m strandline deposits: (a) grain supported silcrete packstone composed of well sorted sub-angular to sub-round medium sand cemented by a micro-crystalline quartz fabric with small floating crypto-crystalline nodules; (b) grain supported packstone with sub-round to well-rounded detrital quartz grains of various sizes cemented by micrite; (c) a rhizoliths feature consisting of calcified root cells adjacent to micro-laminated micrite containing floating detrital quartz grains; (d) dense pelletal micrite within a sparmicrite fabric with occasional floating detrital quartz grains and manganese stained micro-nodules (top left corner); (e) micro- and crypto-crystalline silica filled fenestrae within the mixed pelletal micrite and sparmicrite fabric; (f) micrite grain envelopes around detrital quartz grains illustrate the extent of micritisation within the sparite fabric; (g) lacy fabric illustrating the dissolution and reprecipitation/

replacement of the sparry calcite by micrite; (h) micrite lined and sparry calcite filled rhizolith structures (believed to be calcified root hairs); (i) sparry calcite fabric with minor crypto- and micro-crystalline quartz. ... 293

Fig 11.8 – PPL thin-section photomicrographs of the 940-945m strandline deposits: (a) crystalline alpha fabric consisting of abundant blocky spar calcite and sparmicrite with corroded floating detrital quartz grains; (b) two contrasting fabrics with a distinct boundary – (left) crystalline alpha sparry calcite fabric and (right) sparmicrite and micrite fabric, both with floating corroded detrital quartz grains; (c) mixed sparry calcite and sparmicrite fabric with highly corroded floating detrital quartz grains. Some of the floating detrital grains have very well developed sparry calcite grain coatings (haloes) while other grains have poorly developed quartz overgrowths; (d) grain supported silcrete packstone with micrite rim cements around the corroded detrital quartz grains and authigenic silica filled intergranular spaces with occasional overgrowths; (e) micro-laminated micrite containing floating detrital quartz grains; (f) complex cal-silcrete fabric consisting of an original micro-crystalline authigenic silica fabric which has been partially micritised by pervasive micrite. ... 299

Fig 12.1 – Graph of $\delta^{18}O$ values for all sediment samples analysed (sample numbers correspond with Appendix 11). ... 320

Fig 12.2 – Graph of inorganic $\delta^{13}C$ values for all sediment samples analysed (sample numbers corresponds with Table 4). Pure C_4 vegetation = 1.8‰ and pure C_3 vegetation = -11.8‰. ... 322

II. LIST OF TABLES

Table 4.1 – Classification based on the proportional fabric mineralogy in grain and fabric supported chemical sediments. ... 86

Table 5.1 – Kalahari Group sediments in South Africa. ... 119

Table 5.2 – Summary of XRD analysis. ... 130

Table 7.1 – Probability of locating calcrete adjacent to pans in the Botswana, from Lawrence and Toole (1984). ... 177

Table 7.2 – Summary of XRD analysis. ... 179

Table 8.1 – Sedimentology of unconsolidated samples. ... 197

Table 8.2 – Summary of XRD analysis. ... 204

Table 8.3 – Summary of loss on ignition (LOI) analysis conducted on unconsolidated sediment. ... 206

Table 8.4 – Summary of carbon and oxygen isotope values. ... 216

Table 8.5 – Summary of loss on ignition (LOI) conducted on consolidated carbonates. ... 219

Table 9.1 – A summary of XRD results for samples A-V. (++++) >75%, (+++) 50-74%, (++) 25-49% and (+) 0.1-24%. ... 235

Table 9.2 – A summary of Xhamoga Island's sedimentology. ... 243

Table 9.3 – A summary of Xhamoga Island's mineralogy. For XRD data (++++) >75%, (+++) 50-74%, (++) 25-49% and (+) 0.1-24%. ... 245

Table 9.4 – A summary of Gaenga and Mosupatsela Islands' sedimentology. ... 246

Table 9.5 – A summary of Gaenga and Mosupatsela Islands' mineralogy. For XRD data (++++) >75%, (+++) 50-74%, (++) 25-49% and (+) 0.1-24%. ... 248

Table 10.1 – Summary of XRD analysis. ... 266

Table 10.2 – Summary of loss on ignition (LOI) analysis conducted on unconsolidated and consolidated sediments. ... 268

Table 10.3 – Summary of carbon and oxygen isotope values. ... 271

Table 11.1 – Summary of XRD analysis. ... 282

Table 11.2 – Summary of loss on ignition (LOI) analysis. ... 283

Table 11.3 – Summary of magnetic susceptibility of consolidated and unconsolidated deposits. ... 286
Table 11.4 – Summary of carbon and oxygen isotope values. ... 287
Table 11.5 – Summary of major cations and principal metals detected within a water leach of consolidated and unconsolidated deposits. ... 288
Table 11.6 – Summary of oxygen isotope values from rain samples collected. ... 298

III. LIST OF APPENDICES

Appendix 1 – Atlas of micro-structures within terrestrial carbonate.

Appendix 2 – International stratigraphic chart 2000.

Appendix 3 – Inventory of rock and sediment samples analysed

Appendix 4 – Summary of XRD results

Appendix 5 – A selection of 30 X-ray diffraction traces

Appendix 6 – Summary of magnetic susceptibility

Appendix 7 – Summary table of loss on ignition (LOI) results

Appendix 8 – Summary table of the sediments EC

Appendix 9 – Summary table of the water soluble cation content of the sediments

Appendix 10 – Summary table of the water soluble anion content of the sediments

Appendix 11 – Summary table of isotope analysis

Appendix 12 – Summary table of nitrogen and organic carbon content of the island sediments

Appendix 13 – Mohembo hydrograph 2000-2004

Appendix 14 – Surface and ground water samples collected from the Okavango Delta March 2001-July 2002

Appendix 15 – Summary table of TDS (mg/l) in the surface Okavango water

Appendix 16 – Summary table of groundwater TDS (mg/l) levels in the Okavango region

Appendix 17 – Summary table of groundwater cations in the Okavango region

IV. ABBREVIATIONS USED

AAS – atomic absorption spectroscopy

a.s.l. – above sea level

B.P. – before present (ie. 1950)

b.s.l. – below surface level

BSR – bacterial sulphate reduction

CEC – cation exchange capacity

EC – electrical conductivity

EPS – exopolysaccharides

ICP-MS – inductively coupled plasma mass-spectrometer

ka – thousand years

LGM – last glacial maximum

LOI – loss on ignition

Ma – million years

MAP – mean annual precipitation

MAT – mean annual temperature

m.b.s. – meters below surface

NIGL – NERC Isotope Geoscience Laboratory

OSL – optically stimulated luminescence

PDB – Pee Dee formation Belemnite

PET – potential evaporation

SMOW – Standard Mean Ocean Water

SOM – soil organic matter

SRB – sulphate reducing bacteria

TDS – total dissolved substances

TDIC – total dissolved inorganic carbonate

VCF – vertical at centroid-of-flow

XRD – X-ray diffraction

V. ACKNOWLEDGEMENTS

The list of people to whom I am eternally grateful for their assistance with my research is extensive. However, by no means does it do justice to the kindness and generosity of the numerous people who unceremoniously provided advice and assistance.

Foremost I would like to thank Tamara, my parents - Ian and Christina, and Andrew Goudie for their patience, support and guidance. I am indebted to my brother Christopher and Brett Smith for their unfaltering assistance during the extensive fieldwork conducted; without their assistance much of this work would never have been possible. I would like to thank my sisters Joscelyne and Arabel for their support and assistance during the thesis roller-coaster. Prof. Michael Meadows is thanked for his logistical assistance, advice and friendship. I am eternally grateful to Dr. Baruch Spiro for his endless enthusiasm for scientific advancement. Dr. Marty McFarlane is thanked for her kindness, hospitality, insight and assistance during fieldwork in the Okavango. Prof. Paul Wright is sincerely thanked for help interpreting calcrete petrography and numerous discussions on mechanisms of formation.

I would like to thank The Office of the President, Republic of Botswana for permission to undertake research in Botswana. The Department of Water Affairs, Division of Hydrology and in particular Tshito Babusi, Lethebe Zambo, Jane Prince-Nengu and the members of the Maun and Gumare Offices are thanked for their extraordinary hospitality, insight into the hydrology of the Okavango and

assistance in collecting samples, obtaining monitoring data and logistical support. Clinton Gielink, Koos and Labinda of Game Trails Maun are thanked for providing logistical support during March 2001. Dr. Susan Ringrose and Dr. Martin Krah are thanked for their insight and logistical assistance during 2001. I am extremely grateful to Dr. Frank Eckardt for his hospitality and advice while in Gaborone. Wellfields Consulting Services, Botswana are thanked for the access granted to the borehole logs and reports from the Tshane area.

Colin Craig and Holger Kolberg at the Ministry of Environment and Tourism, Namibia are acknowledged for their assistance in obtaining research permits. Wouter van Zijl of Burmeister and Partners, Namibia is thanked for his helpful advice, access to documentation on the Cuvelai and Cunene systems, hospitality and an unforgettable flight from Windhoek to Ondangwa. Alex Verlinden and Stuart Kean of the Northern Namibia Environmental Project, Inga Brasche and the Police Commissioner, Oshakati District are thanked for their hospitality and assistance during fieldwork in Owamboland during 1998-99. I would like to thank the staff of the Etosha National Park and the Ecological Institute, in particular Nigel Berryman, Wynand Du Plessis and Martin Hipondoka, for their support, access and advice on the Etosha Pan region. Justine Eixas, and numerous other staff members at the Ministry of Mines and Energy, Namibia, are thanked for their enthusiasm and assistance in locating geological maps, borehole logs and reports. I am most grateful to the numerous other people of the northern Namibia and southern Angola who provided accommodation, advice and assistance during fieldwork.

Toni Balt, South African Council for Geoscience, is sincerely thanked for her assistance with the majority of the XRD analyses. Willem Kirsten at the Institute for Soil, Water and Climate, South Africa is thanked for supplementary XRD analyses.

Prof. Melanie Leng, Carol Arrowsmith and Hilary Sloane at NIGL are thanked for their assistance in analysing the isotope content of the samples. Dr. John Arden, Department of Earth Sciences, University of Oxford is thanked for his enthusiasm and assistance with ICP-MS analysis. Chris Jackson is thanked for his assistance with laboratory analyses. The staff of the Map Room, Bodleian Library, Linda Atkinson and Sue Bird are thanked for their assistance in obtaining and accessing maps, aerial photography and documentation relating to the research area.

I am extremely grateful for the financial support I received for this research from the NRF Overseas Doctoral Scholarship, South Africa; The Carl and Emily Fuchs Scholarship, South Africa; The RBHS Old Boys Scholarship, South Africa; Christ Church and the Trapnell Fund.

Finally I would like to thank the staff of the School of Geography and Christ Church for giving me the opportunity to conduct my research and their support during my time in Oxford. My D.Phil has been a life changing experience during which I have learnt a great deal about my chosen discipline, southern Africa and myself. I am eternally grateful to Mike Meadows for that last minute invitation to the Okavango Delta in June/July 1997 which sparked a love affair with the Kalahari!

VI. ABSTRACT

THE CHARACTERISATION OF CALCRETE BASED ON ITS ENVIRONMENTAL SETTING WITHIN SELECTED REGIONS OF THE KALAHARI, SOUTHERN AFRICA.

Alexander Iain Shaw
Christ Church / School of Geography
Submitted for the degree of D.Phil.
Trinity 2008

Chemical sediments in a variety of geomorphic environments (pedogenic, fluvial, palustrine, lacustrine and pan) were investigated from seven regions (SW Kalahari, Kgalagadi, Kalkweissrand, Etosha, Linyanti, Okavango and Ngami) in the Kalahari of southern Africa. These primary and multi-phase sediments were characterised by a range of pure and intergrade silcrete, calcrete and dolocrete fabrics which contained an array of structures indicative of the crystalline and biogenic processes responsible for their precipitation, epigenesis and paragenesis.

Petrography, mineralogy and isotope geochemistry provided significant insight regarding the environmental and geochemical conditions at the time of precipitation. Petrography indicated that the majority of chemical sediments were undergoing epigenetic modification as a consequence of the desiccation induced transition from phreatic to vadose diagenetic and geochemical conditions. The role of rapidly infiltrating meteoric water, associated with unstable wetting fronts, is believed to be instrumental in vadose diagenesis and the precipitation of crystalline/alpha fabric carbonate. Salinisation within the capillary fringe and deeper vadose zone is believed to be responsible for the sequence dolomitisation of crystalline calcite within mature sequences. Highly saline pan conditions instigate the precipitation of authigenic dolomite, calcite and K-feldspar within the

surface sediments and authigenic silica at depth. Phreatic water beneath the islands, floodplains and fluvial systems of the Okavango, which undergoes evapotranspirational and transmission salinisation and ultimately terminal desiccation, are similarly precipitating silcrete. Pedogenic processes principally associated with C_4 vegetation are responsible for the grainification of carbonate mud within desiccating lacustrine, palustrine and pan sediments. Within the thin sandy Kalahari soils, pedogenesis is limited, but biogenic/beta fabric precipitation linked to mycorrihizae and tree/shrub savanna vegetation is instrumental in the formation of hardpans and the modification of upper calcrete horizons. The dominance of a distinct assemblage (smectite/kaolinite or sepiolite/palygorskite) of authigenic clay minerals present within all the environments provides evidence of semi-arid precipitation within Mg and Ca enriched saline/rapidly evaporating water or brackish/reduced permeability environments.

1. INTRODUCTION

The extensive Cenozoic sag basin deposits of the Kalahari Group which characterise large areas of the southern African landscape are dominated by a mixture of fluvio-aeolian siliciclastic sediments and silica-carbonate dominated duricrusts. Extensive research has been conducted on all aspects of geomorphology and sedimentology within the Mega Kalahari Basin, but investigation of the linkages between geomorphology, geochemical processes, depositional and epigenetic environments and paragenesis of duricrusts has been fairly limited. It is this thesis' main objective to describe and interpret the complex epigenetic, syngenetic and diagenetic processes recorded by pedogenic and phreatic intergrade terrestrial carbonates (including the Mokalanen formation and the Kalahari Limestone) within the near surface Cenozoic sediments of the vast and poorly understood Kalahari Group. This information will be used to obtain a better understanding of the mega-basin architecture, depositional environments and mechanisms, conditions and processes which induced epigenesis and paragenesis within the sediments and ultimately facilitate a better understanding of the Kalahari lithologies and their stratigraphic relationships. In addition light stable isotope geochemistry, mineralogical and other geochemical data obtained from the analysis of these deposits will add substantial proxy palaeo climatic and environmental information to the ever expanding database of information on southern African environments during the last 100 million years. This increasingly detailed information provides a background of past climatic fluctuations against which present climatic variability can be tested and potentially provide a better understanding of possible future conditions along with

an understanding of the mechanisms and processes responsible for the formation of these sediments, the geomorphic features they are associated with and the context of their preservation within the landscape.

Advances in understanding carbonate epigenesis, diagenesis and paragenesis, elucidating the role of biotic and abiotic processes of precipitation, predicting lithologic responses to environmentally and climatically forced variables and using the simple and complex geochemical relationships that occur within the geosphere, has provided valuable insight when reconstructing palaeoenvironments. Thus the diagenetic record can often be used to reconstruct surface paleoenvironments not otherwise recorded by sediment deposition.

Appreciation of the role of terrestrial geochemical sediments in surface and near-surface diagenesis has grown over the past few decades. This is especially the case with duricrusts which have assisted in the interpretation of lithostratigraphy, facies and their palaeoenvironmental settings. Cenozoic duricrusts are widespread (Goudie, 1973) and form an integral part of many terrestrial sedimentary sequences and can be a powerful tool in the recognition of depositional environments. To date much of the work performed in the field of terrestrial chemical sedimentology has focused on either lacustrine/palustrine carbonates or calcretes (pedogenic, valley and phreatic). More recent investigation (see Wright and Tucker, 1991; Alonso-Zarza, 2003; Wright 2005) has indicated that there may be a transition from one form to the other under the right conditions, revealing the interplay between sedimentary, pedogenic, epigenetic and diagenetic processes. Even though the study of terrestrial carbonates has increased in recent years, still

much less is known about them than marine carbonates. Presently, earth scientists have placed emphasis on obtaining a better understanding of terrestrial basin development and sequence/litho stratigraphy due to their economic value as reservoirs for oil, gas and water along with alluvial and aeolian deposits (diamonds, gold, base metals and heavy minerals) and secondary stratiform type mineralization (base, rare earth and heavy minerals). The role of terrestrial carbonates in deciphering basin evolution is based on their stratigraphic role as indicators of depositional hiatuses and landscape stability during which time the chemical deposits accumulate often through weathering and supergene enrichment. In this study their presence and characteristics can thus be used as indicators of basin stability, aggradation, subsidence and accommodation rates, and tectonic activity within the Mega Kalahari throughout the Cenozoic.

Calcretes and calcium/magnesium carbonate cemented deposits are important features of many dryland environments, covering as much as 13% of the Earth's land surface (Goudie, 1983). They range from powdery through to massive highly indurated types (Netterberg, 1980), and are produced by a combination of pedogenic and non-pedogenic processes that cause the dissolution, mobilisation and precipitation of carbonates in the near-surface environment. Carbonates typically exhibit alpha and/or beta fabrics which provide evidence of physicochemical or biological processes of precipitation (Wright and Tucker, 1991; Wright, 2005). This study has shown that although alpha fabrics tend to occur in silicate-rich hosts and are typically associated with arid climates and reduced biological activity, solution and reprecipitation along with epigenesis of fabrics tends to promote the preservation of crystalline fabrics within the Kalahari.

The initial objective of this study was to compile a detailed atlas of micro and macro structures associated with terrestrial carbonates in order to facilitate accurate description and cross-referencing of proposed mechanisms, processes and depositional environments (Appendix 1). The majority of these structures have been recorded in very different climatic and biogeographical zones but frequently similar geomorphic conditions to those of the Kalahari. However, despite this range of climatic conditions and associated vegetation, the structures appear to be universal and attest to commonalities in the mechanisms and processes of precipitation if the geochemical conditions are suitable.

The majority of terrestrial carbonates within southern Africa are pedogenic, frequently exposed as surface hardpan which is indicative of a mature stable landscape which has been stripped of its original A and upper B horizons leaving the carbonate residue of the lower B horizon to form a chemically and physically weathered armoured surface which constrains further denudation. However, studies to date in southern Africa have focussed on non-pedogenic carbonates, principally due to their accessibility (Nash and McLaren, 2003). The aim of this study was to investigate carbonates from the entire spectrum of geomorphic environments within four regions (Fig 1.1) in order to understand how both pedogenic and non-pedogenic carbonate formation, epigenesis and diagenesis occurs.

As highlighted by Summerfield (1983a,b,c), petrographic, mineralogical and geochemical characterisation of chemical sediments is crucial to their

identification and interpretation. As such this study aims to complement and supplement the work of Blumel (1982), Eitel (1993, 2000), Eitel and Blumel (1997), Goudie (1973, 1983), Nash (1996, 1997), Nash *et al.* (1994, 1998), Nash and Shaw (1998), Nash and McLaren (2003, 2005), Netterberg (1969a,b,c, 1980), Shaw and De Vries (1988), Shaw and Nash (1998), Summerfield (1978, 1981, 1982, 1983a,b,c), Watts (1977a,b, 1978, 1980) and others in southern Africa by detailed description of chemical sedimentary sequences and depositional environments (pedogenic, palustrine, lacustrine, pan, aeolian, valley, channel, phreatic and bedrock) in order to characterise the modes of formation associated with specific processes and environments. Thus the majority of the investigation is centred on the interaction between geomorphology, macro and micro petrography, mineralogy and geochemistry.

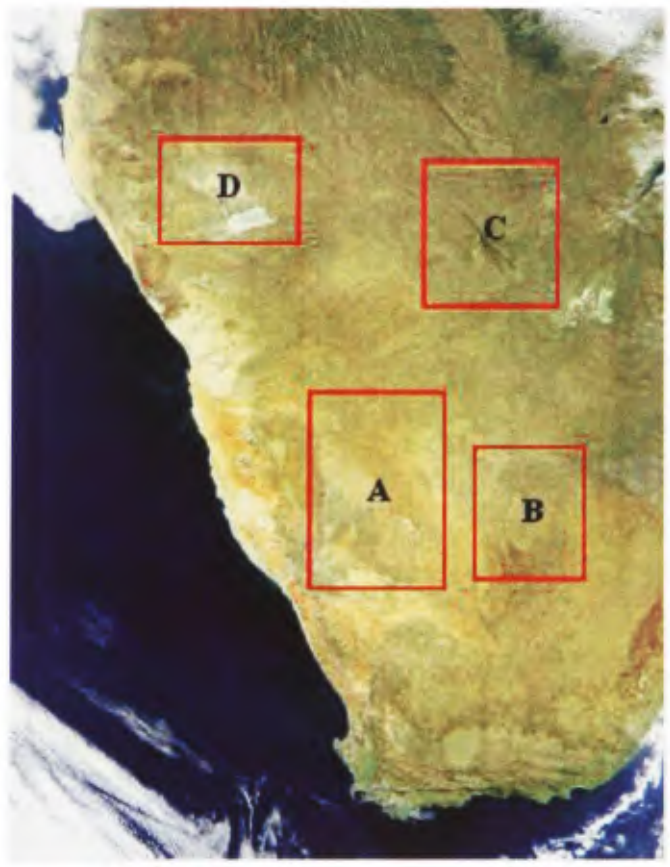


Figure 1.1: Areas of the Kalahari investigated. A = SW Kalahari and Kalkweissrand, B = Kgalagadi, C = Linyanti, Okavango and Ngami D = Etosha.

Three main factors control the formation of chemical sediments: the position of the water table, the host material, and the period of sub-aerial exposure. In pedogenic environments, precipitation takes places mostly in the vadose zone, and within host rock or sediment. In phreatic, valley and channel environments precipitation occurs within the capillary fringe or around the level of the groundwater table. In pan, palustrine and lacustrine environments precipitation occurs within the water body and may then undergo sub-aerial exposure. The period of sub-aerial exposure needed to form palustrine sediments may by relatively short (even a season), whereas pedogenic sediments need more time (several years to millions of years). Phreatic precipitates by nature form below the surface and stable surfaces favour the development of thick sequences (Arakel and McConchie, 1982; Arakel, 1986a,b; Arakel *et al.*, 1989). Changes to the location of the phreatic zone cause epigenesis in all three types of terrestrial carbonates. This has been identified as a major process within the Kalahari chemical sediments, due to the maturity of the sequences and the long-term desiccation of southern Africa during the Cenozoic. The resultant mixing of characteristic features makes interpretation complicated.

The formation of carbonates is controlled by geochemical and palaeoenvironmental factors and light stable isotope geochemistry is a powerful tool to help elucidate this information from the entire range of pure to impure carbonates. It is widely accepted (e.g. Netterberg, 1969a; Watts, 1980; Nash and Shaw, 1998; Nash and McLaren, 2003) that the semi-arid and sub-humid climate of the Kalahari is favourable for the formation of authigenic carbonate. The $\delta^{18}O$ content of the inorganic carbonate provides significant insight into the origin and

evolution of the solutions (degree of evaporitic fraction and temperature) responsible for primary precipitation and subsequent modification. Considerable proxy data on the palaeovegetation (*c.f.* Ehleringer *et al.*, 2000) associated with the precipitation of the chemical sediments was also obtained from the inorganic $\delta^{13}C$ values of the carbonate. Identification of the vegetation communities contributing soil organic matter (SOM) and CO_2 at the time of carbonate precipitation indicated that periods of pedogenic carbonate accumulation are associated with mixed C_3/C_4 savanna vegetation that generally shows higher levels of C_3 vegetation than most of the contemporary communities associated with carbonate deposits. This suggests increased precipitation associated with higher levels of atmospheric CO_2 and cooler climatic conditions, although there is abundant evidence to suggest contemporary vadose carbonate precipitation at a number of sites. In addition, by using the $\delta^{13}C$ and $\delta^{18}O$ signatures together the extent of detrital contamination associated with epigenesis can be evaluated.

In order to obtain a better understanding of the processes and mechanisms responsible for carbonate precipitation a detailed study was conducted on an environment within the modern Kalahari where intergrade carbonate was believed to be forming. The Okavango Delta has extensive phreatic and pedogenic terrestrial carbonate deposits. Modern calcrete was believed to be forming beneath the islands of the permanent swamps (McCarthy and Ellery, 1995), however, investigation revealed that active carbonate precipitation and epigenesis is only occurring within the pedogenic horizons and vadose zone of the islands and the seasonal and abandoned floodplains (Shaw and Goudie, 2004). Saline shallow groundwater, principally the result of evapotranspirational pumping by vegetation

(McCarthy *et al.*, 1993a), although often supersaturated with respect to calcium carbonate is precipitating authigenic silcrete below the islands of the permanent swamps, within the phreatic zone and along the channels of the Thamalakane and Boteti (Shaw and Nash, 1998) in the terminal reaches of the Delta. The Okavango study provided significant insight to the processes operational within pan and fluvial environments (discussed in the other chapters) where palustrine carbonate has often undergone epigenetic silicification as a result of evaporitic geochemical processes.

1.1 How does understanding Cenozoic terrestrial carbonate processes within the Kalahari of southern Africa add to global palaeoclimatic understanding?

The Cenozoic is a globally significant period due to the fact that the uniform and stable warm humid climate which existed for the previous ~140 Ma, since the late Triassic, suddenly became more dynamic during the late Cretaceous and experienced a number of significant cooling events which caused significant global disruption (Zachos *et al.*, 2001a). The first was a ~10°C temperature drop at the end of the Cretaceous and then after temperatures recovered during the Paleogene there was another major temperature decrease of ~12°C during the late Eocene/early Oligocene and Antarctica which had drifted over the south pole experienced its first major glaciation since the Ordovician. During this same period sea-level fluctuations, the initiation of the circum-polar current, the formation of cold oxygen rich oceanic bottom water, the initiation of the thermo-haline circulation pattern, changing albedo and fluctuating atmospheric CO_2 levels (Pearson and Palmer, 2000) all had a major affect on global climates. The

combined effect was a drier and generally cooler global climate. These changes also have to be considered within the geological context of long term plate dynamics. The collisions involving the Arabian, European, Indian and Australian plates and the closure of the Isthmus of Panama had a significant affect on ocean circulation and topography. The initiation of rifting between the African and Arabian plates around 35 Ma and the later East African rifting which commenced around 15 Ma had a considerable influence on African climatology and geology. The change to warm dry conditions during the Miocene and cool dry conditions with warm phases during the Pliocene (Zachos *et al.*, 1997, 2001a,b; Ravelo *et al.*, 2004; Westerhold *et al.*, 2005) resulted in changes to depositional environments and the evolution and dominance of C_4 grasslands and savannas during the Neogene (Cerling *et al.*, 1989, 1998; Cerling, 1997; Ehleringer *et al.*, 1997; Beerling and Royer, 2002). The transition from the late Pliocene to early Pleistocene signalled increased climatic complexity in the form of rapid climatic fluctuations linked to glacial/interglacial cycles and the onset of marked seasonality.

A crucial debate in science is centred around the issue of climate change, its magnitude, frequency and the anthropogenic influence. Environmental summits such as Rio, Kyoto and Johannesburg often failed to reach consensus on issues such as quotas and management of resources due to the simple fact that climates of the past and their natural variability are so poorly understood and hence future projections are often seen as educated guess work at best. Process studies have highlighted the link between global change and continental weathering. A better understanding of the mechanisms and processes active in the formation and

weathering of terrestrial calcium carbonate in arid and semi-arid landscapes, which account for a significant proportion of the Earth's surface, is fundamental to understanding the global carbon budget.

The palaeoclimatic community has historically needed reliably dated, continuous, high-resolution time series data that can be related to climate proxies. However, such palaeoclimatic data are still relatively rare in the Southern Hemisphere and even more so in southern Africa (Tyson, 1999). This study does not add this type of palaeoenvironmental information to the Cenozoic database. It does however add detailed information on the geomorphology, depositional environments, mechanisms and processes responsible for chemical sediment formation and subsequent alteration along with palaeovegetation indicators throughout the Cenozoic to the sparse and low resolution information on terrestrial systems that currently exists.

The palaeoenvironmental information obtained from this study spans the entire Cenozoic and therefore can play a role in the formulation and testing of regional climate, sedimentation and process models. Tyson (1999) states that the sophisticated analysis of sediments and precipitates, in particular light stable isotope analysis, provides a powerful means to trace the movement of elements through surface systems (Graustein and Armstrong, 1983; Starinsky *et al.*, 1987; Miller *et al.*, 1993; Clow *et al.*, 1997) and hence can provide relatively accurate information on palaeoclimates (Retallack, 2001; Pierrehumbert, 2004). This geochemical research has played a significant role in improving the progress of regional palaeoclimatic understanding when coupled with the recent advances in

the sophistication and capabilities of coupled land, ocean and atmosphere general circulation models (GCM's).

The detailed investigation of four key areas within the Kalahari undertaken during this study has contributed a wealth of knowledge to the description and understanding of key mechanisms controlling the precipitation of authigenic terrestrial chemical sediments, their epigenesis and paragenesis as environmental and climatic conditions fluctuated throughout the Cenozoic.

2. TERRESTRIAL CARBONATE

2.1 Introduction

Carbonates in terrestrial settings form within a range of environments from permanent water bodies to sub-aerial and under various diagenetic conditions. The active processes are not easy to characterise and often make identifying the facies or describing sections extremely difficult.

The correct identification of carbonates and their features is vital if the conditions in which they formed are to be understood and the valuable environmental information contained within them is to be correctly interpreted. Their study can provide data that can help interpret the sedimentary record as well as determine the main controls that took part in their formation and thus provide proxy evidence for palaeoenvironmental reconstruction (Wright and Tucker, 1991; Wright, 2005). These processes are compound and may be the result of biogenic influences, climate, composition of rainwater, movements and characteristics of groundwater, sedimentary regime, length of sub-aerial exposure, tectonism, source area, and many other factors (Alonso-Zarza, 2003). A synthesis of the pedogenic, diagenetic, and sedimentary processes that interact in the formation of terrestrial carbonate (intergrade pedogenic, groundwater and palustrine carbonates are the focus of this thesis) and their interpretation is considered the best way to present a general overview.

Adams and MacKenzie (1998) refer to carbonate sediments as having six main components:

- The grains, which comprise discrete, organised aggregates of calcium carbonate or amorphous silica. These are the allochemical components or allochems and are comprised mainly of coated grains, peloids, intraclasts and bioclasts.
- Carbonate mud sediments which occur as the matrix between grains. These clay and silt sized carbonate particles are deposited with the grains or infiltrate into the sediment. This matrix material has many possible origins, but the fine material (< 5 μm) known as micrite (microcrystalline calcite) within a pedogenic or groundwater environment is most commonly associated with direct precipitation from supersaturated waters.
- Terrigenous components, consisting of detrital quartz, clay or other non-carbonate minerals.
- Large calcium carbonate crystals known as sparry calcite (also refered to as sparite or spar). These are generally associated with pore-filling cements and are thus related to secondary diagenesis within the sediments.
- Replacive crystals of microcrystalline quartz, dolomite, gypsum (all evaporite minerals have this replacive capacity) and other minerals (e.g. secondary iron and magnesium accumulations).
- Pore-space, referring to any space in the sediment, filled by gasses or fluids.

Any classification system has to consider the proportional contribution of each of these components.

2.2 Carbonate Duricrusts

There are numerous definitions of the various types of surface and near-surface chemically precipitated crusts and pans, collectively termed duricrusts and duripans when indurated. The most commonly occurring duricrusts are calcrete (where the clastic host material is cemented by a $CaCO_3$ dominated precipitate), silcrete (silica dominated), ferricrete (iron oxide dominated) and gypcrete (gypsum dominated) (Goudie, 1973). Of these types, calcrete is the most widespread, covering ~ 13% of the Earth's land surface (Yaalon, 1981, 1988). When studying these deposits it may be difficult to identify a dominant cement type, and hence a specific duricrust type, particularly where a crust contains almost equal proportions of different cementing agents. This may arise due to a number of factors including co-deposition of minerals, constructional and degradational processes occurring within a pedogenic environment, and post-formational near-surface epigenetic or diagenetic alteration of a pre-existing crust, all of which can lead to the generation of extremely complex intergrade duricrust forms (Nash and Shaw, 1998).

To date no true petrographic or chemical definition exists for the most common form, calcrete. Material is recognised as calcrete simply if it appears to be a surface or near-surface crust where the host material is cemented by or enriched in calcium carbonate. A useful working definition of calcrete is: 'calcrete is a near surface, terrestrial, accumulation of predominantly calcium carbonate, which occurs in a variety of forms from powdery to nodular to highly indurated. It results from the cementation of displacive and replacive introduction of calcium carbonate into soil profiles, bedrock and sediments, in areas where vadose and

shallow phreatic groundwaters become saturated with respect to calcium carbonate' (Wright and Tucker 1991, pg. 1).

Nash and Shaw (1998) noted that variations in the chemical components within calcretes can be attributed to three main factors. Firstly, the relative proportion of carbonate and silica will vary between individual samples dependent upon the percentage of detrital quartz grains and other host materials within the calcrete. Hence, it is useful to classify calcrete as fabric or grain supported using the nomenclature of either Folk (1959, 1962) or Dunham (1962) as this provides insight regarding genesis. Secondly, variability can occur within and between individual profiles dependent upon the types of calcrete present (Netterberg, 1980) and the degree of induration (Machette, 1985). Powdery calcretes generally contain the lowest proportion of $CaCO_3$ whilst hardpan varieties have a much higher $CaCO_3$ content. Thirdly, the percentage of dolomite [$CaMg(CO_3)_2$] present within a calcrete will influence its bulk chemistry, with Netterberg (1980) suggesting that only duricrusts containing < 5% dolomite by mass of total carbonates be termed calcrete. In addition a general distinction is made between high- (unstable) and low-Mg calcites within the carbonate mineralogy with the cut-off taken as 4.0 mol% $MgCO_3$ (Chave, 1952 in Watts, 1980) and not 8.0% as proposed by Winland (1968, 1969).

The formation of calcretes occurs throughout a sedimentary profile. In a sub-aerial environment they may form surface crusts or case hardened precipitates. Within a soil profile (pedogenic calcretes) they may precipitate as a result of pedogenic processes of calcification or calcium relocation. In addition they also occur below

the zone of soil formation but within the vadose zone, at the capillary fringe or below the water table to form groundwater/phreatic calcrete. Pedogenic calcretes are finely crystalline and in their more mature forms, consist of a continuous secondary matrix of microspar carbonate. This fabric differs from the coarsely crystalline grain supported fabric common in groundwater calcrete.

Pedogenic calcretes or calcic and petrocalcic horizons (if continuous and indurated), in the terminology of soil scientists, are the most widespread form of terrestrial carbonate. They are a prominent feature in climatic zones where a seasonal moisture deficit occurs, allowing calcium carbonate to accumulate (Goudie, 1973, 1983). Calcretes are important in landscape development, providing a significant geomorphic 'threshold' for erosion and generally indicate prolonged periods of landscape stability. Intergrade calcretes are particularly resistant to erosion due to the fact that the higher calcium carbonate content of pure calcretes makes them more vulnerable to dissolution. The resistance of calcrete to erosion results in calcrete maintaining its integrity long after climatic changes have occurred.

In addition the displacive nature of calcrete precipitation often results in the formation of subtle surface topography as an adjustment to horizontal compression due to volume increase or as a result of numerous phases of calcrete formation taking advantage of porosity, fractures and solution channels within pre-existing sediments and thus magnifying deformation (Watts, 1977a; Mann and Horwitz, 1979).

2.2.1 Types of Calcic Horizons and their Nomenclature

While most sedimentologists working on calcrete sequences interpret calcretes using the terminology and concepts of soil science many carbonate sedimentologists treat calcretes as diagenetic features. This has resulted in parallel approachs to some degree. However, recently the divisions have become blurred with far more 'cross-pollenation' of ideas.

The term 'calcic horizon' is defined in Soil Survey Staff (1975) as an accumulation of calcium carbonate or of calcium- and magnesium-carbonate that may be located in a variety of horizons. Its equivalents in the carbonate sedimentology literature are: 'calcrete', 'croûte calcaire' and 'caliche' (Goudie, 1972a,b). Soil Survey Staff (1975) do not set minimum requirements for thickness and carbonate content; rather these are set according to the nature of the other mineral constituents and according to the character of the underlying material. For hard calcic horizons the following from Soil Survey Staff (1975) applies: 'the petrocalcic horizon is a continuous, cemented or indurated calcic horizon that is cemented by calcium carbonate or in some places by calcium- and some magnesium-carbonate. The petrocalcic horizon is continuously cemented throughout the pedon to the degree that dry fragments do not slake in water.' Special depth and carbonate content requirements are set for laminar petrocalcic horizons resting directly on bedrock. For horizons with carbonate accumulation that do not fulfil the requirements of either calcic or petrocalcic horizons, the suffix 'ca' is used to denote calcium enrichment.

In the horizon nomenclature for soil description, horizons with calcium carbonate accumulation are denoted by the suffix 'ca', even when these horizons have morphologies dominated entirely by this material. In order to express this, Gile *et al.* (1965) proposed the term 'K horizon'. They set absolute limits for K1, K2 and K3 horizons to indicate the degree of development as measured by the percentage of the so-called K-fabric (K from the German 'kalk'). As such, accumulations of carbonates are indicated by 'k', cementation by 'm' and a petrocalcic horizon by 'km'.

Elbersen (1982) discusses how the literature on calcic horizons and ca-horizons makes numerous attempts to subdivide the phenomena. The criteria used for subdivision are:

1. Measurable characteristics of the horizon proper, i.e. (macro)morphology, carbonate content and hardness: Brown (1956), Durand (1959) cited in Elbersen (1982), Gile (1961), Wilbert (1962), Ruellan (1970), Soil Survey Staff (1975), Netterberg (1980).
2. Micromorphology: Blokhuis *et al.* (1968), Brewer (1972), James (1972), Siesser (1973), Bal (1975).
3. Like 1, together with occurrence in the landscape: Dumas (1969) cited in Elbersen (1982), Lattman (1973).
4. Like 1, together with age and/or degree of development: Gile *et al.* (1965), Gile *et al.* (1966), Netterberg (1969b).
5. Like 1, together with presumed genesis: Dumas (1969) cited in Elbersen (1982).

Of all these subdivisions those of type 1 are preferred over 3, 4 and 5 due to the fact that there is no consensus about the genesis of the different types. As such age and degree of development are arbitrary values. Position in the landscape becomes insignificant if no reliable genetic conclusions can be drawn from it. Micromorphology is a useful tool for characterisation, if superimposed upon the types distinguished according to 1.

The micromorphology literature on calcic horizons can be separated into two disciplines: micropedology and carbonate petrography. Pedologists study these formations in order to decipher their genesis (Brewer, 1976) and to characterise certain properties important for agricultural use. Petrographers study both exposed and buried calcic horizons. Their main aim is to define criteria by which calcic horizons are indicative of sub-aerial diagenesis and can be distinguished from other formations with which they can be confused. Such horizons can act as stratigraphic markers.

2.2.2 Occurrence According to Climatic Zones

The occurrence and distribution of carbonates in soils depends heavily on climate, principally effective leaching (Donner and Lynn, 1989). According to Reeves (1970), well developed calcic horizons do not form in arid or in humid climates. In arid climates rainfall is insufficient to allow for substantial accumulations of $CaCO_3$, while in humid climates leaching is too strong. Cerling (1984) believes that authigenic soil carbonate is common in soils where mean annual rainfall is < 750 mm while it is rarely found in soils receiving > 1000 mm precipitation per year. Jenny and Leonard (1939) were the first to propose that the zone of

carbonate precipitation is a function of the MAT and in general represents a first approximation of the vertical extent of leaching. Arkley (1963), however, showed that this relationship only applies in areas which don't experience pronounced seasonality of rainfall or orographic effects. In general it is assumed that calcic horizons occur where leaching is sufficient to wash $CaCO_3$ into, but not out of, the soil.

Apart from precipitation, factors influencing the drainage conditions of the soil play a key role (Gile *et al.* 1981). The $CaCO_3$ content of the material on which the calcic horizon is developed is another influencing factor. Strongly calcareous materials may contain calcic horizons even in humid climates (James, 1972). Mediterranean climates, where most of the precipitation is concentrated in the cool season, seem particularly likely to develop calcic horizons even where the rainfall is rather low (Klappa, 1978a). In addition, windblown dust has been identified as a major source of calcium carbonate and will influence the development of calcic horizons (Goudie, 1973).

The aforementioned factors make it difficult to establish a very specific climatic zone in which calcic horizons occur (Marion *et al.* 1985; Mayer *et al.* 1988). If the mitigating factors are considered it can be stated that the zone in which they are encountered varies from arid to sub-humid but the zone in which they still seem to be actively formed is semi-arid (Dumas, 1969; Franz and Franz, 1969 both cited in Elbersen, 1982). Ruellan (1968) states that calcic horizons have a tendency to become thinner and closer to the surface as one moves from areas with a precipitation range of 500-700 mm/yr towards drier zones and if the rainfall drops

to 200 mm/yr they tend to disappear altogether. Thick soft calcic horizons are more common in the moister climatic range, while the occurrence of petrocalcic horizons increases progressively towards the drier areas.

In addition however, despite the dominance of climatic conditions and parent material in determining pedogenic carbonate accumulation, Schlesinger (1985) noted that there is also a special relationship between types of vegetation and the process of calcification.

2.2.3 Genesis

The abundance of pedogenic and non-pedogenic calcretes in the geological record, and their use in the geomorphic analysis of alluvial sequences (e.g. McCarthy and Metcalfe, 1990; McCarthy *et al.*, 1993a; McCarthy and Ellery, 1995; Pimentel *et al.*, 1996; Shaw and Nash, 1998; Khadkikar *et al.*, 1998, 2000; Candy *et al.*, 2003; Shaw and Goudie, 2004), valley development (e.g. Shaw and De Vries, 1988; Ringrose *et al.*, 2002; Nash and McLaren, 2003) or as indicators of subaerial exposure, has resulted in a large database of case studies and of criteria for their recognition.

Interest in pedogenic calcretes has resulted in a number of well documented 'models' of formation (Gile *et al.*, 1966; Goudie, 1973; Arakel, 1982; Klappa, 1983; Machette, 1985; West *et al.*, 1988; Rabenhorst *et al.*, 1991; Wang *et al.*, 1994). These have a common component in that the development of a calcrete profile is the result of the progressive increase of secondary calcium carbonate (or

dolomite) within the host material (soil, sediment or rock), via a combination of cementation, replacement and displacement.

Replacement is the most difficult to account for geochemically because it requires simultaneous removal of large amounts of silicates and import of large amounts of calcium carbonate. Wang *et al.* (1994) believe that the replacement process is directly related to the fluctuation of dry-wet seasons and the appropriate soil/pore water composition. Their reaction-transport model accounts for replacement within calcretes and their mineralogy under these conditions. During the dry season, evaporation of soil water causes localised alkalinity and the precipitation of calcium carbonate and sepiolite. At the same time if the porewater contains sufficient Mg^{2+} ions, authigenic sepiolite precipitation by the chemical-divide mechanism will deplete the silica enriched porewater. This results in the continued dissolution of parent silicates rather than continued enrichment and subsequent supersaturation of soluble silica which is then precipitated within the carbonate as authigenic secondary silica. In the following wet season the sepiolite is at least partially dissolved and silica and cations in solution are leached away by rainwater, making room for calcium carbonate precipitation in the next dry season. As this climate cycle repeats, calcium carbonate slowly accumulates and silicates are removed. The authigenic sepiolite (or Mg-smectite (Shaw and Goudie, 2004)) serves as a temporary storage for silicates between seasons. If the soil/pore water contains too little aqueous Mg then the model predicts the growth of calcium carbonate without removing silicates, thus producing a predominance of void fillings and displacive textures instead of replacement, although both tend to happen as the natural system is more complex than the model predicts. In this

manner Wang *et al.* (1994) were able to simulate the precipitation of near surface pedogenic calcrete and conclude that low P_{CO_2}, intensive evaporation and long dry seasons within a semi-arid climate combine to produce thick pedogenic calcrete profiles.

Thus carbonates constitute an effective geochemical tool that, via replacement, removes parent silicate rocks and shapes semi-arid landscapes. As a consequence, the host becomes substituted by a calcic-rich horizon eventually resulting, if time permits, in a continuous, indurated and typically impermeable horizon (the hard pan or petrocalcic layer). This acts as a barrier to further movement of calcium carbonate, resulting in the formation of laminar units on the impermeable horizon. As a result of processes still unresolved, the laminar and hard pan horizons eventually fracture and brecciate. This developmental sequence is the basis of the models offered by Gile *et al.*, (1966), Goudie (1973), Arakel (1982), Machette (1985), West *et al.*, (1988) and Rabenhorst *et al.*, (1991).

Although these processes (cementation, replacement and displacement) operate on siliciclastic and calcareous host materials, the nature of the host is a critical factor influencing fabric development. The contrasting behaviour of silicate grains, as opposed to carbonate grains, to calcite cement growth is particularly important. Chadwick and Nettleton (1990) have suggested that while calcite forms cohesive bonds with other carbonate crystals, reflecting the chemical affinity of the ionic bonding in calcite, it forms adhesive bonds with non-carbonate grains causing displacement during calcretisation.

Another key factor appears to be the degree of biological activity and biological 'fixing' of calcium carbonate in the soil. Some calcretes exhibit microfabrics predominantly of biogenic origin, particularly by fungi, while others consist of simple crystalline structures (the beta and alpha calcrete microfabrics, respectively of Wright, 1990d).

Calcium is the seventh most abundant element of the earth's crust and hydrosphere (Delwiche, 1975). As such $CaCO_3$ is a constituent of many rocks. In many other cases in which it is not a constituent, calcium carbonate is formed in the weathering zone upon liberation of Ca-ions from minerals such as anorthite, titanite and augite. It is also found as a result of the reduction of sulphates by bacterial action. $CaCO_3$ is highly mobile and is easily recycled thus it can also be sourced from atmospheric dust, rainfall, seaspray, surface runoff, bioclasts and vegetation litter (Goudie, 1983). As such the relation between calcic horizons and the materials upon which or within which they are encountered, is not always properly described by the term 'parent material'.

In order to discuss the interrelationships between various carbonate types, the practice of dividing profiles into simple and composite forms (Allen, 1974) should be employed (*c.f.* Watts, 1980). Although the divisions are generally intended to be descriptive, aspects of calcrete development/maturity should also be considered. Simple profiles represent a single episode of calcrete formation, show a variety of stages of maturity and are unaffected by later periods of calcrete formation. They are therefore discrete units and are separated from overlying and underlying profiles by uncalcretised material. Composite profiles represent

recurring episodes of calcrete formation. They may be identified by a stacking, with overlap, of individual calcrete profiles. Where sediment accretion or erosion takes place, a simple profile may experience renewed calcrete formation producing an 'upward-composite' or 'downward-composite' profile.

To date there is little concensus about the main process involved in calcrete formation. The main problem lies in the origin of the often quite large quantities of $CaCO_3$. In most cases they are too large to be accounted for by simple leaching from the present surface sediment.

A factor which adds to the confusion is that most authors fail to mention whether they consider the calcic horizons which they study as static features formed in the position they presently occupy, or exposed by subsequent erosion of the material from which the $CaCO_3$ originated, or as dynamic features capable of transforming themselves from one form into another and migrating downwards in a denuding landscape, adapting themselves in the process to the relief forms as they are shaped.

2.2.3.1 Pedogenetic Modes of Formation

Pedogenetic modes of origin can be subdivided according to source and mode of transport of the $CaCO_3$. The question of whether the calcic horizons are considered to be dynamic or static cannot be avoided. Under certain conditions there is no need to envisage a mode of transport of $CaCO_3$ towards the calcic horizon since this is dynamic and can be assumed to be moving towards the $CaCO_3$ and not vice versa. However, mode of transport and source are not

independent factors since the assumption of a source implies the assumption of a mode of transport in accordance with the position of that source in relation to the position of the calcic horizon (Elbersen, 1982).

The following sources are frequently assumed: sediment overlying the calcic horizon which are recipients of $CaCO_3$ contained in aeolian material deposited on the surface; horizons and/or strata underlying the calcic horizon; or materials at the surface located upslope from the point where the calcic horizon is located (Elbersen, 1982).

The commonly assumed mechanism of transport from source to calcic horizon is water. The $CaCO_3$ is transported in dissolved form as bicarbonate which can move downward, upward or in a lateral sense through the sediment. Alternative mechanisms of transport for $CaCO_3$ are illuviation of carbonate particles (Gile, 1977) and diffusion (Reeves, 1976).

2.2.3.1.1 *Downward Movement*

If the amount of $CaCO_3$ that accumulates in sediment is considered to be relatively minor, then it can be assumed that the majority of $CaCO_3$ must have been leached from horizons presently overlying the accumulation zone. Goudie (1983) refers to this downward movement of dissolved $CaCO_3$ and the development of calcrete well above the water-table and on non-calcareous substrates as the 'per descensum' model.

In order to account for the discrepancy between the amount of $CaCO_3$ and the thickness of the overlying horizon, many authors assume aeolian additions to the surface soil. Capo and Chadwich (1999) concluded that > 95% of the Ca in pedogenic carbonates in New Mexico was from atmospheric sources.

Due to this significant atmospheric deposition of $CaCO_3$ a number of researchers favour aeolian aggradations to the surface soil and downward leaching of $CaCO_3$ towards the calcic horizon. Gile *et al.* (1966) proposed that downward leaching of $CaCO_3$ in unsaturated flow resulted in the formation of an impermeable zone at the depth of frequent wetting. This downward movement results in the gradual increase of precipitated $CaCO_3$ under the right conditions and slowly 'plugs' the horizon. This causes the formation of a zone where percolating water is retarded and accumulates. Capillary rise and evaporation of this water results in the formation of a solution supersaturated with respect to $CaCO_3$ and leads to the formation of a hard laminated crust. This will grow in an upwards displacive manner and gradually lifts the overlying soil.

Lattman (1973) found that the strongest $CaCO_3$ cementation of non-carbonate detritus occurred downwind of playas, high in carbonates. Lattman and Lauffenburger (1974) suggest that areas downwind of major outcrops of gypsiferous rocks are also characterised by thick calcrete as a result of gypsum being reduced in the soil by bacteria. This bacterial sulphate reduction (BSR) leads ultimately to the transformation of gypsum to $CaCO_3$, incorporating CO_2 from the soil and liberating H_2S (Machel, 2001).

A mass-balance calculation by Gardner (1972) in an almost carbonate-free alluvial sand in Nevada suggested that 36.5 m of primary material was equivalent in $CaCO_3$ content to the $CaCO_3$ contained in the calcrete. In order to derive the same amount of $CaCO_3$ from calcium liberated on weathering, over 90 m of material would have been needed. As a result he discarded the hypothesis that the overlying sand was the only source of $CaCO_3$ since the weathering residue was not present and no explanation for its uniform removal could be found. Rather, he proposed that the $CaCO_3$ was supplemented by airborne dust and bicarbonate enriched rainwater. Blumel (1979) also assumed aeolian additions to the surface soil as one of the principal sources of $CaCO_3$ forming calcretes studied in Namibia and Spain. These calcic horizons overlie materials out of which hardly any $CaCO_3$ can be liberated by weathering.

2.2.3.1.2 *Upward movement of $CaCO_3$*

A common mechanism of $CaCO_3$ transport is evaporation and capillary rise or the 'per ascensum' model (Goudie, 1983). Other options are a fluctuating groundwater table and the pumping action of vegetation (evapotranspiration). It is important to dispel the misconception that $CaCO_3$ precipitation due to surface evaporation and soil moisture stress is equivalent to carbonate cementation associated with capillary rise and the capillary fringe which sources bicarbonate directly from the groundwater (Wright and Tucker, 1991). The capillary fringe is strongly controlled by the texture of the host sediment which affects the amount of capillary rise, which may be a few metres in clays and far less in sand and coarse material (Wright and Tucker, 1991). Pedogenic calcretes generally form near the surface and the groundwater table is invariably many metres below the surface

(Gile and Grossman, 1979; Wright and Tucker, 1991). Thus capillary rise is of most relevance to groundwater calcretes (Nash and McLaren, 2003) unless the water-table is close to the surface. Some authors indicate that capillary rise of $CaCO_3$ would imply transport of soluble salts which would cause salinisation and alkalinisation of sections of the profile. Intergrade deposits and a dynamic precipitation/solution equilibrium (Nash and Shaw, 1998; Shaw and Goudie, 2004) provides evidence for this mode of formation.

2.2.3.1.3 *Lateral transport of $CaCO_3$*

The transport of $CaCO_3$ mainly in the form of a solution may occur as overland flow or subsurface flow and occasionally in the form of a suspension over the soil surface. These percolation (diffuse or conduit flow), sheetwash or channelised systems obtain the majority of their carbonate from solution of carbonate rich catchment material or aeolian dust (Goudie, 1973). Ruellan (1968), Dumas (1969 cited in Elbersen, 1982) and Blumel (1979) determined that where calcic horizons are found on materials that do not contain $CaCO_3$ and do not liberate calcium upon weathering, the $CaCO_3$ must have been transported laterally from sources upslope. This relationship was found to be valid over distances of several kilometres in the more arid areas but only over tens of meters in sub-humid areas.

Carlisle (1983) classifies a number of genetic calcrete types (e.g. laminar crusts, case hardening, valley and channel calcrete) all of which can form by either surficial or subterranean lateral transport of $CaCO_3$. Changes in any one of many physicochemical conditions as a result of the common ion effect, CO_2 degassing or evaporitic concentration can initiate the precipitation of carbonate from

solution at the surface, within the vadose zone of the host sediment, within the capillary fringe or below the water table. In these areas $CaCO_3$ is often contributed via ground or river water rich in bicarbonate. Khadkikar *et al.* (1998) suggest that the presence of relict and active non-pedogenic calcretes which are abundant within alluvial sediments (Carlisle, 1983) may act as a local source of $CaCO_3$ for pedogenic carbonates and may contribute to recycling of carbonate in solution and thus saturation of river water. Thus within these environments calcrete formation is generally accelerated due to the abundance of $CaCO_3$, which results in faster accretion rates (Khadkikar *et al.*, 1998) which may lead to misjudgement regarding the maturity of the pedogenic calcretes derived on the basis of the morphogenetic sequences of Gile *et al.* (1966).

2.2.3.1.4 *Liberation or formation of $CaCO_3$ from parent material*

This mode of formation envisages no transport towards the calcic horizon as it is assumed that the horizon moves downwards with the weathering front of the parent material. This mode of formation is supposed to be accompanied by removal of the weathering products from the surface synchronous with the downward movement of the calcic horizons and weathering front (Elbersen, 1982). As such it is mostly referred to in the literature as a degradational mode of formation and is commonly associated with bedrock calcrete.

Gigout (1960 cited in Elbersen, 1982) and Lattman (1973) investigated the differential development of $CaCO_3$ cementation associated with lithologies. The highest levels of cementation were found on carbonate and basic igneous rock detritus, less on silicious sedimentary detritus, and least on acid igneous rock

material. The process may first lead to an enrichment in $CaCO_3$ and secondly to induration of this $CaCO_3$. In certain cases the weathered rock surface becomes case hardened. Blank and Tynes (1965) and James (1972) reported the formation of soft powdery $CaCO_3$ as a result of *in situ* sub-aerial weathering of limestone in Texas, USA and Barbados respectively. Blank and Tynes (1965) suggest that the soft powdery $CaCO_3$ is not brought in from overlying soil or rocks by migrating water, but is due to *in situ* dissolution and reprecipitation, which transforms coarse calcite into microcrystalline calcium carbonate. James (1972) cites the presence of the same fossils within the limestone and the soft $CaCO_3$ layer as evidence of this *in situ* weathering and calcretisation.

2.3 Organic Agency

The role of biological organisms and the resultant biogenic 'fixing' of $CaCO_3$ in sediment can be a significance process (Goudie, 1996a). Many carbonates exhibit macroscopic organo-sedimentary structures (Klappa, 1980a; Jones and Ng, 1988; Wright and Tucker, 1991; Jaillard *et al.*, 1991) and microfabrics (Wright, 1990c) indicative of biogenic processes which may be dominant or complimentary to physicochemical processes. Wright (1990c) initiated the use of a two end-member microfabric classification system to describe features attributable to either crystalline (alpha) or biogenic (beta) processes. Although many carbonates contain both 'alpha' and 'beta' fabrics there appears to be a degree of climatic and host sediment control on the dominant fabric type (Wright, 1990c; Wright and Tucker, 1991). Beta fabrics typically occur within carbonate-rich hosts and reflect high biological activity associated with well vegetated semi-arid to sub-humid

environments, while alpha fabrics tend to occur in silicate-rich hosts and are associated with arid climates and reduced biological activity.

Rhizoliths, stromatolites, rhizogenic and laminar calcretes (Kahle, 1977; Klappa, 1979a; Krumbein and Giele, 1979; Cohen, 1982; Mount and Cohen, 1984; Wright *et al.*, 1988, 1995; Wright, 1989; Mack and James, 1992; Rossinsky *et al.*, 1992; Fedoroff *et al.*, 1994) are typically associated with pedogenic carbonate and have a range of root zone and biogenic structures indicative of extra- and intra-cellular calcification and replacement. Glaebules, peloids (in most cases believed to be representative of faecal pellets in carbonates (Wright, 1983; Jones and Squair, 1989)) and pisoids are also components of pedogenic carbonate sequences and can have a range of structures (needle-fibre calcite, fungal tubules, spherulites, microcodium, etc.) which allude to the role of micro-organisms, principally soil fungi, cyanobacteria and root mycorrhizae mediation, in carbonate precipitation (James, 1972; Harrison, 1977; Knox, 1977; Klappa, 1979b, 1980a; Calvet, 1982; Calvet and Julia, 1983; Wright, 1984, 1986; Solomon and Walkden, 1985; Beier, 1987; Phillips and Self, 1987; Phillips *et al.*, 1987; Wright and Wilson, 1987; Goldstein, 1988; Wright and Tucker, 1991; Callot *et al.*, 1995; Wright, 2005).

Plants naturally absorb atmospheric carbon dioxide (CO_2) during photosynthesis and then pump surplus carbon through their roots into the soil around them. In most soils, much of this carbon can escape back to the atmosphere or enters groundwater. But in soils containing calcium-bearing silicates the carbon dioxide reacts with calcium to form calcium carbonate grain coatings or grains. Macrophytes and microbes drive this precipitation and modification process by

changing bulk and pore-water chemistry through metabolic activity or by concentrating ions and nucleating crystals on cell walls or producing exopolysaccharides (EPS) around detrital or authigenic minerals. Globally nutrient-acquiring processes associated with the mutualistic relationship between plant roots and mycorrhizae are the principle agents of biogenic carbonate precipitation even in arid regions (Verrecchia *et al.*, 1990).

2.4 Palustrine Carbonates

Freytet and Plaziat (1982) defined palustrine carbonates as palaeosols formed on lacustrine carbonate substrates. Freytet and Verrecchia (2002) state that the original characteristics of the primary lacustrine deposit (organisms, sedimentary features) must co-exist with characteristics indicative of later pedogenic transformation (organisms, root traces, desiccation, pedogenic remobilizations). Palustrine carbonates are generally associated with shallow, low gradient lakes which have low energy margins (Platt and Wright, 1992; Alonso-Zarza, 2003) and ephemeral ponds, playas or pans (Nickel, 1985; Sanz *et al.*, 1995). Under these conditions, the carbonate mud with its associated charophytes, molluscs, and ostracods, is subaerially exposed when there is a slight waning of the lake, pond or pan level. Pedogenic processes then modify the lacustrine mud giving rise to a variety of palustrine facies and microfabrics (*c.f.* Freytet and Verrecchia, 2002).

2.4.1 Development

Palustrine carbonates are highly sensitive to climate. Very arid or very humid climates do not favour carbonate deposition in lakes, ponds or pans (Cecil, 1990), whereas semi-arid to sub-humid climates with marked seasonality are more

appropriate (Platt and Wright, 1992; Sanz *et al.*, 1995; Gierlowski-Kordesch, 1998). In sub-humid climates, palustrine deposits include more organic matter (Alonso-Zarza and Calvo, 2000) which may develop into coal (Cabrera and Saez, 1987). On the contrary, semi-arid climates are characterised by wide pseudo-microkarst development on top of the sequences, and organic matter is rarely preserved. More arid climates favour the presence of abundant evaporite minerals and nodules within the palustrine carbonates, or palustrine carbonates dominated by dolomite (Sanz *et al.*, 1999).

Climate also affects the carbonate precipitation rate since most of the carbonate precipitated within the lakes is biogenic. This is commonly associated with algal and microbial photosynthesis (Platt and Wright, 1992). Temperature also plays a role in carbonate production with some carbonate being inorganically precipitated as a result of seasonal and diurnal temperature fluctuations (Kelts and Hsu, 1978).

Climate not only controls the palustrine environment itself but also the activity of the adjacent, usually siliciclastic, depositional environments (rivers, alluvial fans, etc.), and therefore the arrangement of palustrine sequences. However, even in tectonically passive regions it is difficult to evaluate the relative role of climate and tectonism separately.

In lacustrine basins, tectonism seems to be the main agent responsible for generating accommodation space for deposition (De Wet *et al.*, 1998), whereas sediment plus water supply, which is mostly climatically controlled, is the critical factor in defining the main features of both recent and ancient lake fills (Carroll

and Bohacs, 1999). The interplay between these two factors has been used to establish a complete framework of lacustrine basins using a sequence-stratigraphy approach. This framework establishes three types of lake basins: overfilled basins characterised by the association of fluvial–lacustrine facies, balance-fill basins dominated by the association of fluctuating–profundal facies, and underfill basins characterised by evaporite facies association (Bohacs *et al.*, 2000). Palustrine carbonates may be present in any of the three types, but are most prominent in overfilled basins and in the highstand depositional systems of balanced-fill and underfill basins.

Palustrine deposition requires shallow water bodies within relatively flat depressions. It is the adjacent alluvial systems within the alluvial basin that control the stability and permanence of the water body. In terms of accommodation space and/or sequence stratigraphy, two scenarios are possible (Alonso-Zarza, 2003):

(1) Low activity alluvial/fluvial systems which allow long periods of water body permanence, and favour the development of vertically stacked palustrine sequences. This situation usually occurs at the final stages of the infilling of endoreic basins where very often the carbonates extend right to the basin margins (Alonso-Zarza *et al.*, 1992a). This reflects either a progressive decrease of tectonic activity along the basin margins or the change of the topography from a steeper to less steep gradient due to basin infilling or the reduced activity of alluvial systems, during periods of low subsidence rate and thus may represent stages of reduced accommodation space.

(2) When alluvial–fluvial systems occasionally reach the shallow water body or pond systems, interbedded clastic alluvial deposits develop. This is common in stages of high accommodation space that favour high levels of storage of floodplain sediments, resulting in isolated channels, weakly developed soils (Wright and Marriott, 1993) and seasonal ponds. These features are characteristic of transgressive depositional systems (Alonso-Zarza *et al.*, 1998; Khadkikar *et al.*, 1998) which are common throughout the sub-humid northern Kalahari.

On a smaller scale (decimetres to a few metres), the development of palustrine sequences responds to the relationship between the subsidence rate and the vertical aggradation of the basin (Alonso-Zarza, 2003). In alluvial basins, pulses of subsidence due to the tilting of the basin floor are often associated with dramatic reorientation of the fluvial systems. In contrast, the equilibrium between tectonic subsidence and sedimentation favours a slow, but continuous aggradation of the floodplain and a gradual rise of the water table.

2.4.2 Mechanism of Water Supply

The origin of the water accumulated within the lake/pond/pan plays an important role in determining the hydrochemistry and therefore the mineralogy of the sediments and latter transformations during early diagenesis (Gierlowski-Kordesch, 1998). A purely meteoric supply gives rise to relatively fresh water and chemical precipitates are usually calcite. However, chemical precipitation may be inhibited, as surface water will also carry significant quantities of clastic material that may constitute the majority of any deposit. If the system is mainly fed by

groundwaters directly or via springs, a more complex hydrogeochemistry can be expected and the mineralogy of the palustrine deposits will reflect this composition. Factors such as the distance that the groundwater has flowed, the composition of the catchment areas, and the ratio of rock–water interaction and evaporation rates, all control groundwater composition and therefore the mineralogy of the primary precipitates and their possible transformation during early diagenesis (Arakel and McConchie, 1982; Alonso-Zarza, 2003).

Low-Mg calcite is a common precipitate if groundwater flows only relatively short distances or if the catchment area is dominated by low-Mg calcite and little evaporation occurs (Alonso-Zarza, 2003). Dolomite and gypsum may form from more evolved groundwaters due to evaporation during flow towards the lake/pond/pan or within the lake/pond/pan itself (Wright and Sandler, 1994; Calvo *et al.*, 1995). However, the evolution of groundwaters and the formation of other precipitates such as dolomite, gypsum or Mg clays (Arakel, 1986a,b; Wright and Tucker, 1991; Shaw and Goudie, 2004) depends not only on hydrology but also on climate and/or the lithologies within the catchment which can contribute anions and cations to the solution.

2.4.3 Diagenesis

Diagenetic processes are commonly difficult to separate from sedimentation processes in many depositional environments, but in palustrine environments it is almost impossible (Alonso-Zarza, 2003). It has been suggested by Alonso-Zarza (2003) that it is appropriate to consider diagenesis in palustrine carbonates as those processes controlled by the chemistry and position of the groundwater.

Therefore, diagenetic processes in palustrine environments are those that result from the interaction of pedogenically modified carbonates with groundwaters (Alonso-Zarza, 2003). The most common processes are:

(1) Cementation is normally associated with meteoric processes. Vadose cements are commonly acicular and both pendant and meniscus structures are common, whereas phreatic cements are typically coarse calcite spar (Freytet and Plaziat, 1982).

(2) Mineralogical stabilisation and recrystallisation. Palustrine sediments are commonly highly indurated despite not undergoing significant compaction associated with burial. The induration of these deposits is interpreted to be the result of epigenesis and mineralogical stabilization (Wright *et al.*, 1997; Anadon *et al.*, 2000) of the initial lacustrine muds. Pseudo-sparitic and microsparitic textures are common, forming irregular patches with sharp to gradual boundaries with the micrite host (Valero Garces and Gisbert, 1992).

(3) Karstification may be an early or late stage process occurring when the meteoric waters that infiltrate the lacustrine carbonates are undersaturated with respect to calcite. The effects of karst-related processes on terrestrial carbonates are similar to those developed in marine environments (Canaveras *et al.*, 1996) but the geochemical and textural changes may be different. Karstification causes dissolution and collapse features, extensive recrystallisation, dissolution of intrasedimentary evaporites and dedolomitisation (Arenas *et al.*, 1999; Bustillo and Bustillo, 2000).

(4) Dolomitization is commonly an early diagenetic process, which results in the formation of dolomicrites in which the primary fabric is well preserved. In these shallow pond environments, dolomitization is the result of intense evaporation by the pumping of water through the mudflats or lake margins during periods of exposure, allowing an increase in the Mg/Ca ratio. This favours intrasedimentary growth of evaporites, primary dolomites, dolomitization and silicification (Wells, 1983; Arenas *et al.*, 1999; Bustillio *et al.*, 2002).

2.5 Non-Pedogenic Carbonates

Non-pedogenic carbonates are characterised by crystalline (alpha) fabrics which cement and replace/displace large volumes of sediment and are an important component of present-day arid alluvial basins (Wright and Tucker, 1991). However, as discussed by Nash and McLaren (2003), there is a great deal of confusion regarding the characterisation of non-pedogenic calcretes based on their macro- and micro- morphological properties, their landscape context and geomorphological setting (Goudie, 1983). The term groundwater calcrete has until recently been used interchangeably with non-pedogenic calcrete to imply any calcrete precipitated at or below the groundwater table (Mann and Horwitz, 1979; Jacobson *et al.*, 1988; Wright and Tucker, 1991). However, Nash and McLaren (2003) argue that while there is a genetic link between many forms of non-pedogenic calcrete (phreatic, valley and channel calcrete (Carlisle, 1983)) a distinction between phreatic and groundwater calcrete is necessary in order to identify the mode of origin, which is indicative of subtle hydrological variation, and to enable its palaeoenvironmental significance to be correctly assessed.

Phreatic calcretes are those in which cementation has occurred predominantly at or below the groundwater table (Arakel, 1986a,b; Wright and Tucker, 1991; Nash and McLaren, 2003). Groundwater calcretes form as a result of carbonate precipitation in the zone of capillary rise directly above the water table (Nash and McLaren, 2003). Significantly these calcretes should be considered separate to valley and channel calcretes which although they develop at or below the groundwater table are associated with specific geomorphological settings (Nash and McLaren, 2003). Channel calcretes are carbonate deposits which cement alluvium within confined impermeable bedrock channels or exhumed palaeochannels, and may occupy the entire channel cross-section (Nash and McLaren, 2003).Valley calcretes are calcium carbonate cemented alluvium within broad, shallow, drainage courses, but they do not necessarily occupy the entire valley width (Nash and McLaren, 2003).

Groundwater and phreatic carbonates are commonly associated with weathered regolith and unconsolidated sediment (Mann and Deutscher, 1978; Mann and Horwitz, 1979; Arakel and McConchie, 1982; Carlisle, 1983; Arakel, 1986a,b; Lee and Gilkes, 2005). These geochemical sediments are often intergrade (Arakel *et al.*, 1989; Lee and Gilkes, 2005) and lensoid with local thickening occurring as a result of displacive growth which forms mounds or domes which may break the surface (Wright and Tucker, 1991).

The carbonate is precipitated mainly in the capillary fringe, directly above laterally moving subsurface water, but it can also be precipitated below the water

table. It is triggered by any one of or a combination of several factors, the most important being: carbon dioxide degassing, evaporation/evapotranspiration and the common ion effect (Wright and Tucker, 1991). Precipitation preferentially occurs at 'highs' where basement irregularities force groundwater nearer the surface, facilitating degassing and evaporation/evapotranspiration (Wright and Tucker, 1991). Also where calcium or magnesium bicarbonate enriched waters mix with calcium or magnesium sulphate or chlorite-rich groundwaters from localised evaporitic systems, precipitation due to the common ion effect occurs (Wright and Tucker, 1991). Preferential formation of groundwater and phreatic carbonate also occurs where surface drainages converge, flow gradients decrease, saline waters mix, or where permeabilities are low (Wright and Tucker, 1991).

Groundwater and phreatic carbonates typically have a micritic and densely crystalline fabric which often contains shinkage cracks and dissolution features (Wright and Tucker, 1991). The carbonate fabric often contains authigenic silica, authigenic clays (usually smectite, sepiolite or palygorskite) and gypsum (Wright and Tucker, 1991). Arakel (1986a) observed that groundwater and phreatic calcrete in Australia underwent distinctive mineralogical changes down-dip as the groundwaters evolve. The growth of the carbonates is both displacive and replacive and, as a result the deposits are usually characterised by a nodular, massive or brecciated macromorphology (Wright and Tucker, 1991). In addition phreatophytic plants have been identified as being responsible for the formation of laminar and rhizocretionary calcrete at the capillary fringe zone in dunes (Semeniuk and Meagher, 1981). These carbonates will preferentially occur in the coarser, more permeable lithologies but precipitation of carbonate within the

profile over extended periods results in a decrease in porosity and permeability as the pore-throats and inter-granular spaces become plugged (Wright and Tucker, 1991). As this happens the groundwater flow is affected and eventually forced to adjust its flow path to reach an equilibrium position relative to the hydrostatic pressure and gradient. If this occurs in fluvial environments the lateral shift of groundwater creates wide, ribbon-like channel or valley calcretes. These cemented channel zones are responsible for inverted relief if erosion of the surrounding, less cemented, deposits occurs (Reeves, 1983; McCarthy *et al.*, 1988; Smith and Mason, 1991; Smith *et al.*, 1997; Gumbricht *et al.*, 2001; Nash and McLaren, 2003). Desiccation features and rhizobrecciation are generally not commonly associated with non-pedogenic calcretes but relief inversion and large-scale doming (Mann and Horwitz, 1979) result in local zones of fracturing and weathering which aid in regeneration of porosity and hence renewed precipitation (Wright and Tucker, 1991).

2.6 Pedogenic Carbonate

Pedogenic calcretes typically form distinctive sub-profiles within the host profile (Wright and Tucker, 1991). They are typically strongly asymmetric with regards to the vertical concentration of carbonate and exhibit maximum carbonate content in the upper part of the profile (Wright and Tucker, 1991).

Numerous authors have provided idealized pedogenic calcrete profiles (see reviews by Klappa, 1983, and Esteban and Klappa, 1983) which are widely identified in palaeocalcretes. Profiles develop in stages, the most basic process being the progressive accumulation of carbonate within the host soil. This

involves several processes besides precipitation and cementation, most importantly the replacement and displacement of the host material (Wright and Tucker, 1991). Many calcretes exhibit clear evidence of partial or complete replacement of detrital silicate grains and ultimately the replacement of carbonate grains to produce a diagenetic wackstone fabric (Read, 1974; Arakel, 1982; Wang *et al.*, 1994). Displacive growth is similarly a very important process in carbonate sedimentation and accounts for the volume of carbonate in mature profiles which typically significantly exceeds the original pore space of the host material (Wright and Tucker, 1991). Machette (1985) calculated that the floating detrital grains commonly observed in calcrete matrices require a 400-700% expansion of the original grain framework. This results in the formation of pseudo-anticlines (Watts, 1977a) although the hydration of clays within the calcrete fabric may also contribute to this deformation. Displacive growth appears to be the dominant process in the formation of alpha-fabrics and features such as grain fracturing and 'floating grains' are directly attributable to this process.

Brecciation is a striking feature of many calcretes, reflecting pedoturbation caused by the displacive growth of carbonate, wetting and drying cycles, thermal expansion, swelling clays and root activity (Klappa, 1980b; Semeniuk, 1986).

The importance of clay translocation and the formation of argillic horizons in calcrete-bearing soils, particularly aridisols, is still debated (Nettleton and Peterson, 1983; Allen, 1985; Wright and Tucker, 1991). It is generally accepted that the alkaline conditions associated with the high Ca^{2+} content causes clays to flocculate, thereby reducing their mobility (Wright and Tucker, 1991). Within the

calcrete fabric illuviated clay coatings, which form on peloids or detrital grains, are often destroyed due to wetting and drying cycles or by the displacive growth of carbonate (Wright and Tucker, 1991). As a result the majority of clay coats within carbonate rich soils are believed to have formed through stress and are not illuvial in origin (Ranson and Bidwell, 1990).

Silica is a key component of many calcretes. The type and location of secondary silica relative to carbonate within the profile, depends on a number of environmental, geochemical and biological factors (Folk and Pittman, 1971; Reeves, 1976; Chadwick *et al.*, 1987; Shaw *et al.*, 1990; Wright and Tucker, 1991).

2.7 Calcite or Dolomite?

Primary precipitation of dolomite typically occurs as very fine grained crystals within environments experiencing capillary evaporation and evaporative pumping. However, the majority of dolomite is precipitated gradually from pore-fluids during early and late diagenesis as a coarse replacement of pre-existing $CaCO_3$ or as a void filling cement. Two major considerations in the formation of dolomite in the Kalahari are the source of the Mg^{2+} ions (high-Mg calcite and smectite clays) and the process whereby the dolomitising fluid (modified meteoric water) is pumped through the carbonate sediments (Tucker and Wright, 1990). Climate is extremely important as groundwater circulation will be most active under a humid climate with strong seasonal rainfall (Tucker and Wright, 1990).

Although most research on dolomite involves marine influence, four of the dolomitisation models (Land, 1985) can be used to interpret the purely terrestrial dolomites of the Kalahari: evaporative (Coorong-type), seepage-reflux, mixing-zone and burial.

Fine grained evaporative dolomite is precipitated within the sediments of the highly evaporitic pans of the Kalahari. These systems are recharged with meteoric water during short duration high intensity rain storms and temporary wetting fronts penetrate the sediments to recharge the groundwater at depth. During the remainder of the year the systems desiccate to highly alkaline and saline brines which are dominated by intense evaporative pumping, a process which induces an upward flow of shallow groundwater to the capillary zone until the water-table falls below a level where capillary evaporation can occur (Hsü and Siengenthaler, 1969). This process is believed to be most active immediately after recharge events when the capillary zone expands and the water-table is temporarily elevated. Changes in porewater chemistry across a pan results from evaporation-mineral precipitation and mixing of the pan brine with the groundwater which results in the majority of the dolomite being precipitated between 15 cm and 75 cm of the surface.

The seepage-reflux dolomitisation model involves the generation of hypersaline dolomitising fluids through the evaporation of water and porewaters which then descends into the underlying sediment as a result of its increased density (Tucker and Wright, 1990). This model relies on Mg^{2+}-rich fluids being produced by evaporation, and sulphate (gypsum and anhydrite) and chloride (halite)

precipitation, which descend into the underlying sediments and displace the less dense porewaters (Tucker and Wright, 1990). Another seepage-reflux model is that of localised solution cannibalisation (Goodell and Garman, 1969). This model is based on the dissolution of metastable high-Mg calcite during meteoric weathering. The conversion of high-Mg to low-Mg calcite or the total dissolution of the calcite results in an enrichment of the pore-fluids in Mg^{2+} which subsequently percolate downwards, due to their increased density, to dolomitise the underlying sediments.

The mixing-zone model is based on the hypothesis that dolomite will precipitate from solutions despite a dilution of their high Mg/Ca ratio, usually by meteoric water or as a result of mixing of aquifers, if some of the kinetic obstacles (e.g. high ionic strength) are removed (Hanshaw *et al.*, 1971; Folk and Land, 1975; Tucker and Wright, 1990). The key features of this model are that saline groundwater supplies the Mg^{2+} and active groundwater movement pumps the dolomitising solutions through the sediment. Dolomites formed by this model tend to be located within more porous sediments which act as conduits for groundwater and typically have negative $\delta^{18}O$ values which reflect the meteoric dilution (Tucker and Wright, 1990).

Dolomite precipitation as a result of burial is a result of compactional dewatering of mud and clay rich sediments which expel Mg^{2+}-rich porewater into the adjacent (common where mud and clay rich horizons are interbedded with porous calcarenites and sandstones) and overlying sediments (Magara, 1978; Tucker and Wright, 1990). The transformation of clay minerals during burial, particularly the

conversion of smectite to illite, is responsible for the release of significant quantities of Mg^{2+}, Fe^{2+}, Ca^{2+}, Si^{4+} and Na^{+} (Boles and Franks, 1979; McHargue and Price, 1982). Ca^{2+} and Si^{4+} are released during early burial diagenesis and precipitate as calcite and quartz cements, while Fe^{2+} and Mg^{2+} are only released later (Tucker and Wright, 1990). In addition the diagenesis of organic matter, which is normally associated with such clay rich deposits, contributes CO_3^{2-} (Tucker and Wright, 1990). However, mass balance calculations (e.g. Given and Wilkinson, 1987) indicate that the Mg^{2+} released during the dewatering and conversion of clays is generally insufficient to account for large scale dolomitisation. This accounts for the occurrence of dolomite in thin lenses close to clay horizons and within stylolites and pressure dissolution seams in limestones (Tucker and Wright, 1990).

Dolomite is believed to form from the carbonate anion (CO_3^{2-}) rather than the bicarbonate anion (HCO_3^{-}) since the former has the ability to dislodge water dipoles from Mg^{2+} ions on the growing crystal surface (Lippmann, 1973) thus preventing hydration. This suggests that dolomitisation is favoured from solutions with high alkalinity, high pH and high PCO_2 where the CO_3^{2-} ion dominates over the HCO_3^{-} (Tucker and Wright, 1990).

Replacement dolomite ranges from fabric destructive to retentive and from fabric selective to pervasive (Tucker and Wright, 1990). The controls on dolomite replacement are precursor mineralogy and grain/crystal size. High-Mg calcite is preferentially dolomitised relative to low-Mg calcite (Blake *et al.*, 1982). High-Mg calcite grains are typically dolomitised with good fabric retention while low-

Mg calcite grains experience only minor replacement. Replacement dolomite crystals will often pseudomorph the crystal form, sedimentary structures and gross textures of the most susceptible components; finely crystalline low-Mg calcite and high-Mg calcite (Murray and Lucia, 1967) when the saturation state of the dolomitising fluid is low. When the saturation state of the dolomitising fluid is high and pervasive dolomitisation of all the components has occurred over an extended period rather than a single event, very little of the original sedimentary fabric is preserved (Tucker and Wright, 1990). Dolomite crystals with cloudy centres indicate the presence of inclusions, mineral relics of the $CaCO_3$ precursor and empty or fluid-filled microcavities (Tucker and Wright, 1990). These mineral relics and residues suggest that during the early stages of dolomitisation, the fluids were unable to dissolve the $CaCO_3$ completely.

2.8 Kalahari Carbonate

The Mega Kalahari is characterised by a series of endoreic drainages which extend from the Northern Cape Province of South Africa, through Botswana, eastern Angola, Zambia and into the Congo Basin (Thomas, 1984; Thomas and Shaw, 1991; Haddon, 1999, 2000; Shaw and Goudie, 2002). The majority of the Kalahari is semi-arid with extremely high rates of evaporation. Within the central part of the basin there is an aridity gradient with the southeast being the wettest area and the southwest and northwest being more arid (Stokes *et al.*, 1997a).

Nash and McLaren (2003) highlight the fact that pedogenic carbonates predominate within the Kalahari but are generally the least well exposed due to the limited dissection of the landscape. The most commonly encountered

carbonates are therefore non-pedogenic and are usually found within dry valleys and pan/lake systems (Nash and McLaren, 2003).

Duricrust maturity is related to a number of interdependent factors: time, climate, host materials, carbonate source, geomorphological position, organic influences, sedimentation (or erosion) rate and various localised conditions (Watts, 1980; Wright and Tucker, 1991). The interplay of these parameters over an area as large as the Mega Kalahari Basin results in a highly diverse suite of pure and intergrade carbonate types (Nash and Shaw, 1998). Therefore, broad conclusions regarding mechanisms of carbonate formation and modification within the Kalahari must be treated with caution.

There are two broad groups of Kalahari duricrusts: the 'older' duricrusts (King, 1963; Netterberg, 1969a; Cooke, 1975; Watts, 1980; Mallick *et al.*, 1981; Shaw and De Vries, 1988; Nash *et al.*, 1994; Ringrose *et al.*, 2002) and the 'younger' Quaternary duricrusts (Goudie 1973; Watts 1977b; Nash and McLaren, 2003; Shaw and Goudie, 2004). Based on Late Cenozoic palaeoclimatic change, Netterberg (1969a) suggests four major episodes of calcrete formation within southern Africa: (1) Pliocene times and this includes the Mid-Pliocene 'Kalahari Limestone'; (2) Acheulian or Middle Pleistocene times; (3) Upper Pleistocene times; and (4) Late Pleistocene-Recent (which is equivalent to and includes the two younger phases of calcrete described by Cooke (1975)). As discussed by Nash and McLaren (2003) a number of studies have attempted to obtain absolute dates for Kalahari carbonate material and construct chronosequences, with TL dating of detrital quartz currently providing the most useful dates (Ringrose *et al.*, 2002).

However, the accuracy of these dates is highly debatable as the material dated was detrital bleached quartz grains and not authigenic carbonate. Hence these siliciclastic grains almost certainly predate the formation of the carbonate matrix and thus should be viewed as a maximum age. The use of radiocarbon is highly problematic (Rust *et al.*, 1984) due to included detrital 'old' carbon and the processes of formation which includes significant solution and reprecipitation of carbonate. Thus this technique when used on matrix material can only provide a youngest possible age but significant insight into resolution and precipitation. However, Shaw *et al.* (1992) have successfully used radiocarbon on biogenic material (gastropods and reed casts) included within valley calcretes of the central Kalahari. Despite problems dating 'dirty carbonates' there is a great deal of potential for uranium series dating in light of recent work on calcrete sequences in Spain by Candy (2002) and Candy *et al.* (2003).

The terrestrial carbonates of the Kalahari are probably amongst the thickest in the world (Goudie, 1973) with calcrete sequences often being between 50-100 m thick. Simple profiles are generally <2.5 m thick but may be thicker where sediment accretion has been constant and sufficiently slow (Hugo, 1969; Watts, 1980; BGS and WCS, 1994, 1996). A number of authors have suggested a relationship between duricrust thickness and geomorphological position, with calcrete generally thinning with increased slope or over positive areas (McFarlane, 1975) and thickening adjacent to river channels and pans which reflects the role of groundwater in their precipitation (Goudie, 1973; Watts, 1980).

Non-pedogenic carbonates form a significant component of the Kalahari Group within alluvial systems (e.g. Nossob/Molopo, Etosha-Cuvalei, Linyanti-Chobe-Okavango-Makgadikgadi systems) and are precipitated as inter-channel and extra-channel deposits. Their precipitation is the result of laterally migrating river/ground water which is saturated with respect to carbonate. Active Kalahari alluvial systems are rarely stable and are thus prone to avulsion. Channel and valley calcretes may consequently be abandoned and then later form banks of subsequent channels (McCarthy *et al.*, 1991b, 1992; Khadkikar *et al.* 1998). In a similar fashion groundwater calcretes may be abandoned due to falling groundwater levels, redirection of groundwater or changes in hydrogeochemistry linked to changes in the water's provenance. The latter may result in corrosion and re-solution or the groundwater calcrete but other changes are likely to be linked to localised landscape inversion which may result in subaerial exposure and initiation of pedogenesis (Pimentel *et al.*, 1996; Nash, 1997; Khadkikar *et al.* 1998; Shaw and Goudie, 2004). Pedogenesis of sediments containing groundwater calcretes often leads to the development of a vertisol calcrete association through the formation of authigenic clays (Khadkikar *et al.* 1998; Shaw and Goudie, 2004). Once formed, pedogenic calcretes may become permanent features of the sedimentary sequence or be remobilized as a result of changing geomorphic conditions (Khadkikar *et al.* 1998; Shaw and Goudie, 2004).

Although some carbonates are developed in and on bedrock, the majority form within host Kalahari sand of mixed fluvial and aeolian origin (Moore and Dingle, 1998). The thickness of sand overlying the carbonates is rarely >30 m and is usually <3 m (Grove, 1969) and the dominant mineralogy is quartz with

subsidiary feldspar, lithic fragments, biotite, occasional weathered silcrete fragments, authigenic carbonate, evaporites and clay minerals (Watts, 1980; Moore and Dingle, 1998). The red colour of the sands is due to haematitic and limonitic coats (ferrans-terminology of Brewer, 1976) around the detrital grains. This iron is attributed to *in situ* weathering of ferro-magnesian minerals and clays (e.g. smectite) with the released iron migrating to grain boundaries as outlined by Walker (1967), Walker and Honea (1969) and others (review by Van Houten, 1973). Detrital grains within the majority of carbonates lack iron coatings, which suggest that primary precipitation or dissolution reprecipitation of the carbonate has occurred from pore-fluids under reducing conditions (negative Eh) where the iron and manganese has been in solution and thus incorporated to form a ferroan-calcite or dolomite (even ankerite). Detrital grains in carbonates precipitated in near-surface pedogenic environments which have not undergone significant burial and diagenesis tend to retain their coatings since most near-surface fluids are oxidising.

2.8.1 Dolocrete-Silcrete-Calcrete Intergrade Duricrusts

Nash and Shaw (1998) highlight the fact that the majority of reviews on carbonate duricrusts recognise secondary silica as being the most important, if not only, silica-carbonate association commonly occurring within duricrusts. However, thin-section and geochemical analyses of Kalahari duricrusts by Watts (1980), Summerfield (1982, 1983a) Nash and Shaw (1998) Ringrose *et al.* (2002) and Shaw and Goudie (2004) suggest that there are numerous geochemical equilibrium and epigenetic carbonate combinations and three main silcrete-calcrete/dolocrete intergrade duricrust types (Nash and Shaw, 1998). These have

been grouped by Nash and Shaw (1998) into duricrusts where secondary silica occurs within a primary calcareous matrix, varieties where secondary carbonate occurs within a dominantly siliceous matrix, and crusts where the precipitation of carbonate and silica appears to have been contemporaneous.

2.8.1.1 Duricrusts Containing Secondary Silica within a Carbonaceous Matrix

Pure carbonates are relatively uncommon within the Kalahari and it is rather the widespread partial silicification of carbonates that appears to be norm as silica is released when calcite corrodes and replaces detrital silicate minerals within the host sediment (Walker, 1960; Watts, 1980; Nash and Shaw, 1998). The inverse solubility of calcite and silica is well-documented; strongly alkaline conditions (> pH 9) favour the precipitation of calcite and the solution of silica, whilst the reverse occurs under more neutral and acidic conditions (Wright and Tucker, 1991; Nash and Shaw, 1998). Therefore silica rich porewaters are characteristic of zones of active carbonate precipitation due to the related silica solution (Wang *et al.*, 1994; Nash and Shaw, 1998).

The ongoing active precipitation of carbonate and associated corrosion of detrital host silica is expected to result in the sediment's porewater becoming increasingly saturated with silica. With increased carbonate precipitation there is a complementary reduction in porosity and increase in fabric density, both of which limit the ability of the silica enriched porewater to drain or be flushed away (percolation changes from diffuse to conduit flow as the sediment changes from unconsolidated to consolidated), thus increasing the likelihood of silicification within vugs and fractures. As discussed by Nash and Shaw (1998) there is some

disagreement over where silicification most commonly occurs within the carbonate profile. Reeves (1970), Watts (1980) and Shaw and Goudie (2004) identify silica precipitation in the lower parts of pedogenic calcretes. Nash *et al.* (1994a), Ringrose *et al.* (2002, 2005), and Nash and McLaren (2003) record a tendency for the upper parts of calcrete profiles exposed within the flanks of valleys in Botswana and Namibia to be more strongly silicified. Arakel *et al.* (1989) notes silicification throughout calcrete profiles developed within Australian palaeodrainages. Due to the fact that the local conditions are so instrumental in determining if and where authigenic silica accumulates in conjunction with carbonate precipitation the best suggestion is that of Summerfield (1982) who believes that the occurrences of silicified zones within Kalahari calcretes are largely unpredictable.

Nash and Shaw (1998) identify three main occurrences of authigenic silica within the Kalahari calcretes. The most common form of silicification is where chalcedonic and opaline silica and megaquartz occur as late stage void fills. This form of silicification is due to replacement of the carbonate by silica as a result of dissolution along void boundaries, as well as more pervasive replacement of the matrix in the absence of voids. There is a tendency for replacement to be greatest along the margins of major voids or fractures as they act as conduits for the greatest flow of silica bearing solutions through the material (Ribet and Thiry, 1990). Vugs and veins filled by silica are common in Kalahari calcretes and generally exhibit a clear sequence of authigenic silica precipitation (Nash and Shaw, 1998). They are commonly lined by a thin (<5 μm) opaline silica layer, followed by a zone of chalcedonic silica (40-90 μm) which may include both

length-fast and length-slow species (Folk and Pittman, 1971), with a euhedral quartz (megaquartz) fill which may partially or completely fill the remaining void space (Watts, 1980; Nash and Shaw, 1998). The other occurrence of secondary silica in Kalahari carbonates identified by Nash and Shaw (1998) is where silica has replaced the carbonate matrix material in the absence of voids. In this case pervasive silicification invariably occurs in combination with the other forms of silica enrichment (Nash and Shaw, 1998).

2.8.1.2 Duricrusts Containing Secondary Carbonate within a Siliceous Matrix

Intergrade Kalahari silcretes with carbonate inclusions have been described by Summerfield (1983a,b,c), Nash *et al.* (1994b), McCarthy and Ellery (1995), Nash and Shaw (1998) and Shaw and Nash (1998). As in the case of silicified calcretes, Nash and Shaw (1998) have described three main types of carbonate occurrence within Kalahari silcretes; carbonate as a late stage void or vein fill, carbonate replacement of the silcrete matrix in the vicinity of voids or veins, and pervasive replacement of the silcrete matrix away from voids or veins.

The most common occurrence of carbonate within Kalahari silcretes is in the form of void fills or veins associated with *in situ* fracturing and brecciation of the pre-existing duricrust. Replacement of the silicrete fabric by carbonate tends to occur along the margins of major voids as opposed to minor cracks (Nash and Shaw, 1998). Nash and Shaw (1998) believe this is due to the carbonate originating outside the silcrete body and migrating into the void. Therefore the degree of replacement appears to be governed by the ability of carbonate rich porewaters to interact with the void walls and the ability of any dissolved silica to be removed,

both of which are controlled by the rate of movement of porewater through the silcrete (Nash and Shaw, 1998). The rate of porewater movement is therefore likely to control the extent of replacement and explains why there is an absence of alteration away from voids or veins in well-cemented Kalahari silcretes (Nash and Shaw, 1998).

2.8.1.3 Duricrusts with Contemporaneous Silica and Carbonate Precipitation

Duricrusts in which both silica and carbonate appear to have been precipitated either contemporaneously or in close succession are very rare and are limited to cyanobacterial activity which precipitates laminar crusts in hyper-saline pan brines (Shaw *et al.*, 1990; Harrison and Shaw, 1995). These intergrade duricrusts form in the upper 10-15 cm of pan sediments and comprise detrital quartz grains within wavy laminae of interspaced microcrystalline calcite and cryptocrystalline silica (Shaw *et al.*, 1990; Harrison and Shaw, 1995). Nash and Shaw (1998) believe these crusts are the result of lithification processes operating at and above the water table as a result of capillary rise. The wavy laminae of alternating siliceous and calcareous matrix appear to have been precipitated as a result of evaporation and changes in pH and salinity levels in the pan surface sediments with possible cyanobacterial assistance (Nash and Shaw, 1998).

2.9 Conclusion

Carbonate distribution is not merely a reflection of geomorphological and geochemical factors. Climate, host material, sediment accretion rate, carbonate source (and its availability), vegetation and time all play important roles in

carbonate formation and may consequently greatly influence the form, type and thickness of the deposit produced.

3. ISOTOPIC ANALYSIS OF TERRESTRIAL CARBONATES

3.1 Introduction

Inorganic carbon as the main constituent of carbonate accumulations provides the ideal material for stable isotope stratigraphy and as a tool for understanding environments and mechanisms of formation, diagenesis and recrystallisation processes. Stable isotope stratigraphy is particularly useful for lithostratigraphic correlations where there is a scarcity of biostratigraphic information, such as within the arid and semi-arid environments associated with the Kalahari Group sediments. Stable isotopes of carbon and oxygen in terrestrial pedogenic carbonate are generally used to estimate palaeoclimatic and environmental parameters, such as temperature, effective moisture, and atmospheric carbon dioxide concentration, recorded at the time of carbonate formation based on the assumption that the isotopic composition of ancient pedogenic carbonates was controlled by the same factors as modern ones (Talma and Netterberg, 1983; Cerling, 1991; Hays and Grossman, 1991; Cerling *et al.*, 1992; Cerling and Quade, 1993; Smith *et al.*, 1993; Pendall *et al.*, 1994; Eckardt *et al.*, 1999, 2001). The nature of the stable isotopes in pedogenic carbonates means that they provide useful indicators as to the influence of meteoric water and climatic conditions on soil-forming processes, the origins of the pedogenic carbonate (Rabenhorst *et al.*, 1984; Quade and Cerling, 1990; Marion *et al.*, 1991) and can also be used as ground-surface markers and indicators of landscape stability (Callen *et al.*, 1983; Cerling, 1984, Lui *et al.*, 1994, Lui *et al.*, 1996). In addition they are also good

indicators of palaeoecological conditions (e.g. Cerling *et al.*, 1989; Kelly *et al.*, 1991, Jiamao *et al.*, 1997).

3.2 Terrestrial Carbonate and Isotope Geochemistry

Soil carbonate forms at a rate of approximately 1 x 10^{-6} to 1 x 10^{-5} moles cm^{-2} y^{-1} (Arkley, 1963; Goudie, 1973; Gile *et al.*, 1981), the main control on the $\delta^{18}O$ and $\delta^{13}C$ composition is the $\delta^{18}O$ of the soil water and the $\delta^{13}C$ composition of soil carbon dioxide. Soil water ultimately derives from local meteoric water, whose isotopic composition is a well-known function of the meteoclimatic parameters of the region (Cerling, 1984). Thus a strong correlation of decreasing $\delta^{18}O$ with decreasing mean annual temperature has been observed for modern soils (Cerling, 1984; Quade et al., 1989). However, soil moisture may be lost through plant transpiration or by direct evaporation. The former process does not involve large isotopic fractionation, while the latter leads to an enrichment of the heavy isotope in the residual soil water. Thus, soil water should approach the isotopic composition of local meteoric water in well-vegetated soils and 'humid' climates, whereas 'arid' climates are characterised by soil water noticeably enriched in $\delta^{18}O$ compared with meteoric water (Quade et al., 1989; Liu et al., 1996).

Lui et al. (1996) demonstrated that the $\delta^{18}O$ precipitated from the soil solution as soil carbonate is in isotopic equilibrium with the $\delta^{18}O$ of seasonally-mixed soil water in the deeper parts of the soil. Two of the factors strongly influencing the isotopic composition of the pedogenic carbonate are probably of general significance for

interpretation of palaeoenvironmental information from measurements on soils: (1) the isotopic composition reflects isotopic equilibrium at maximum summer temperatures, and (2) the soil solution that precipitates the carbonate has been enriched by evaporation.

Ideally, in a soil of homogeneous porosity, organic matter distribution, and isotopic composition, carbonate $\delta^{13}C$ values should change gradually with depth, reflecting the diffusion gradient of $\delta^{13}C$-depleted, plant-derived soil carbon dioxide out of the profile and the mixing of $\delta^{13}C$-enriched, atmospheric carbon dioxide down into the profile (Cerling, 1984; Pendall, 1994). This model assumes that the carbonate system (soil $CO_{2(g)}$, carbonate, and soil solution) is in isotopic equilibrium (i.e., sufficient time exists for complete isotopic exchange of carbon and oxygen between all components), which implies that $\delta^{14}C$ is also in isotopic equilibrium within the system (Pendall *et al.*, 1994). There is no model however which adequately describes the isotopic composition of soil carbon dioxide. Soils have higher carbon dioxide partial pressures than the atmosphere, this is a result of soil respiration, the carbon dioxide produced by root respiration and by microbial oxidation of organic material in the soil (Cerling, 1984). However few studies of carbonate in modern soils have been performed to assess this model, but generally the isotopic pattern with depth is found to follow the predicted model (Quade *et al.*, 1989b; Amundson *et al.*, 1989; Pendall and Amundson, 1990).

The observed differences in the $\delta^{13}C$ contents of soil carbonates is not due to carbonate formation in a closed system, but rather can result from changes in the soil respiration rate and changes in the proportion of plant biomass that uses the C_3, C_4 or CAM photosynthetic pathway seasonally or over a long time interval (Cerling, 1984). C_4 plants are well adapted to conditions of high water stress, particularly when that stress is related to high temperatures. The observed difference between the isotopic composition of soil carbon dioxide and the associated organic matter in soil is expected because of the difference in diffusion coefficients for $^{13}CO_2$ and $^{12}CO_2$.

Thus the main control on the $\delta^{13}C$ of modern soil carbonates at depths below about 50 cm (where the influence of atmospheric CO_2 is small) has been found to be the relative proportions of C_3 compared to C_4 plants. Since the Early Neogene, C_3 plants are characteristic of vegetation in temperate regions, whereas many C_4 plants are found in areas of tropical or subtropical climate. It is assumed that past changes in vegetation would also have resulted in temporal shifts in the $\delta^{13}C$ of soil carbonate. This simplified scenario is made more complex by the many factors that concur in determining the structure of the climate and the typology of the vegetation. Furthermore, physicochemical effects, like the temperature dependence of isotopic fractionation, may act in an opposite direction with respect to climatic parameters, when the whole process is considered (Cerling and Quade, 1993). Nevertheless, it is generally thought that local climate and vegetation types govern the stable isotope composition of pedogenic carbonates.

Good correlation is expected between $\delta^{13}C$ and $\delta^{18}O$ for pedogenic carbonates (Cerling and Hay, 1986). This is expected in soil environments from continental climates since the $\delta^{18}O$ value of soil carbonates is related to the isotopic composition of meteoric waters, and the $\delta^{13}C$ value of soil carbonates is related to the proportion of plants using the C_4 photosynthetic pathway, both of which tend to increase with increasing mean annual temperature (Cerling, 1984). C_4 plants use the Hatch-Slack cycle of photosynthesis and have $\delta^{13}C$ values of about -13‰ while C_3 plants, which use the Calvin cycle of photosynthesis, have $\delta^{13}C$ values of -27‰ (Deines, 1980; Cerling, 1984). Because the diffusion coefficients for $^{12}CO_2$ and for $^{13}CO_2$ differ by a factor of 1.0044 the isotopic composition of soil CO_2 is expected to be at least 4.4‰ enriched in ^{13}C relative to soil organic matter (Cerling, 1984). This model predicts $\delta^{13}C$ values for soil CO_2 produced by pure C_4 flora to be about -8.5‰ and for pure C_3 flora to be about -22.2‰. Since the fractionation factor for carbon between CO_2 and calcium carbonate is 1.01036 at 25°C (Friedman and O'Neil, 1977), predicted end-member carbonate isotopic values are about +1.8‰ and -11.8‰ for pure C_4 and pure C_3 components, respectively. Wang and Zheng (1989) inferred a relationship to estimate the C_3/C_4 ratio of the biomass from the $\delta^{13}C$ in a soil on the basis of the model first developed by Cerling (1984). Their equation is: $C_3 = (2.1-\delta^{13}C_{CaCO3})/14.0$, where C_3 represents the fraction of C_3 biomass.

There are several other potential sources of CO_2 present during the formation of carbonates. Amtospheric CO_2 (-6‰, the value for the preindustrial atmosphere), oxidation of plant material (-27‰ to -13‰, in proportion to the abundance of C_4

flora), respiratory soil CO_2 [-22.2‰ to -8.5‰, in proportion to the abundance of C_4 flora (Cerling, 1984)], and CO_2 produced in the fermentation of organic material ($\delta^{13}C$ = ca. +20‰).

However, in order to use stable isotopes to study carbonate formation and the inherent relationship to climate, it is necessary to eliminate the problem of external carbonate sources. Thus, the term soil carbonate is used to represent only the carbonate in the soil or palaeosol that is authigenic. Therefore all standard isotopic interpretations based on palaeosols, requires that sampled carbonate form pedogenically, does not undergo subsequent reprecipitation, and be formed during a relatively homogeneous climate (Pendall *et al.*, 1994). It is thus necessity to understand regional environmental conditions and diagenetic histories prior to the use of pedogenic carbonates in palaeoreconstructions. However, epigenetic dissolution and reprecipitation processes occur readily in arid and semi-arid soil environments thereby seriously affecting the palaeorecord and the potential for accurate interpretation (Salomons and Mook, 1976; Gile and Grossman, 1979; Amundson *et al.*, 1989; Deutz et al., 1995, 2001). Budd et al. (2002) have described how diagenetic alteration of pedogenic carbonate nodules in the presence of dissolved inorganic groundwater carbon linked to a fluctuating regional groundwater table resulted in significant differences between the $\delta^{13}C$ values of coexisting soil organic matter (SOM) and the carbonate nodules. These results (Budd et al., 2002) highlight potential problems for (1) the use of some pedogenic carbonate isotopic records as proxies for environmental change; and (2) the way 'altered' $\delta^{18}O$ values and

'unaltered' $\delta^{13}C$ values have been used as a screening tool for the presence or absence of diagenesis (Shafiqual Alam, et al., 1997). In this regard if isotopic variations within any one horizon are less than those observed between horizons, it may not necessarily be evidence for a lack of diagenesis but rather evidence for varied degrees of diagenetic overprinting (Budd et al., 2002).

When using isotopes as proxies for making palaeoclimatic interpretations, if other factors are considered to remain constant, increased rainfall means increased removal of carbonates from upper layers and deposition in deeper layers or complete removal from the soil. Movement of carbonate within the soil can be vertical and/or lateral depending on the slope, texture, and stratigraphy of the material (as discussed in Chapter 2; Donner and Lynn, 1989). In environments with greater effective leaching, no carbonates remain in the soil.

The transport of $CaCO_3$ within soils by water is complex and has been well documented by many authors, particularly Jenny (1941). Arkley (1963) concluded that evapotranspiration is an important parameter controlling depth of carbonate movement in soil. Of additional importance is the fact that soil carbonate formation is generally considered to result not only from carbonate supersaturation due to evapotranspiration, but also due to the effect of evaporation, and the lowering of the partial pressure of carbon dioxide, $P(CO_2)$, on carbonate supersaturation (Cerling, 1984). But of these additional two factors, evaporation is probably of little

significance because evapotranspiration is the dominant mechanism for soil water loss in areas covered by vegetation (Jenny, 1980; Black, 1968).

Soil waters do not become nearly as enriched in ^{18}O as do closed-basin lake waters. Modern East African lakes are enriched by 5 to 10‰ in ^{18}O compared to their inflowing waters, whereas soil waters may be enriched by less than 4‰ as a result of evaporation (Cerling and Hay, 1986) since transpiration is nonfractionating with respect to soil water.

The average temperature of the soil at the earth's surface is approximately the same as the mean annual temperature. However, the instantaneous soil temperature depends on the season of the year, the albedo of the surface, and the diurnal temperature fluctuations (Cerling and Hay, 1986). The diurnal fluctuation is dampened with depth, and is unimportant below about 50 cm (Baver *et al.*, 1972; Kirkham and Powers, 1972). One can estimate the annual temperature due to changes in mean monthly temperature from (Carslaw and Jaeger, 1959):

$$T = T_0 +/- (A_0/2)_e\text{-}kZ$$

where:

T = temperature

T_0 = mean annual temperature

A_0 = mean monthly temperature range

Z = depth (m)

$k = (\omega/2\alpha)^{1/2}$ = thermal conductivity

$\omega = 2\pi/t$

t = period (yr)

α = thermal diffusivity

Using $\alpha = 32\ m^2yr^{-1}$, a typical value for unconsolidated earth materials (Kappelmeyer and Haenel, 1974; Baver *et al.*, 1972), it is possible to estimate the annual temperature range at a given depth. This method was used by Cerling and Hay (1986), whereby the mean soil temperature could be calculated according to Craig's equation (1953; 1961; 1965), as recalculated by Bowen (1991), assuming an oxygen isotope composition of palaeoprecipitation similar to present day rainfall.

The temperature of formation of soil carbonate and the oxygen isotope composition of water are combined by an equilibrium relationship. Therefore a quantitative calculation of one of these parameters requires a previous assessment of one of them. A relationship has been proposed between the oxygen isotope composition of pedogenic carbonates and local meteoric water using Cerling's (1984) data from modern world-wide soils: $\delta^{18}O_{H2O} = 1.361 + 0.955\delta^{18}O_{CaCO3}$ (Jiamao et al., 1997). The major advantage of this empirical relationship is that it incorporates the evaporative effect in soil however, according to Cerling (1984) and Jiamao et al. (1997), knowledge of the statistical relationship between the mean annual local surface temperature and the oxygen isotope composition of precipitation are required. This relationship can be deduced from IAEA (International Atomic Energy Agency)

data, as elaborated by Rozanski et al. (1993). Clearly, all these numerical evaluations of the climate of the past must be considered cautiously. This is because: (a) they originate from empirical relationships, which have been deduced on a broad scale and not tested for each local area; and (b) the present relationships may not hold for all periods in the past.

The stable isotope composition of soil carbonate is best described as a dynamic system in which isotopic re-equilibrium occurs as a result of recurrent dissolution and reprecipitation. The degree of carbonate isotope re-equilibration is determined by the depth of water penetration into the soil profile, as well as soil age (Pendall *et al.*, 1994). Dissolution and reprecipitation of pedogenic carbonate in soils has been shown to be an equilibrium process following the reaction:

$$CaCO_3 + H_2O + CO_2 = Ca^{2+} + 2HCO_3^-$$

where CO_2 is derived from plant and microbial respiration mixed with some proportion of atmospheric carbon dioxide in an open system (Cerling, 1984; Amundson *et al.*, 1989; Quade *et al.*, 1989b). An additional issue of debate is the fact that some suggest that the bicarbonate produced by this reaction is influenced by isotopic composition of parent material or pre-existing detrital carbonate (e.g., Solomons and Mook, 1976; Schlesinger *et al.*, 1989); however others have shown that limestone does not contribute substantially to the carbon isotope signature of pedogenic carbonate (Quade *et al.*, 1989b). Soil carbon dioxide, even at low

respiration rates in desert soils, apparently is the primary contributor to $\delta^{13}C$ in pedogenic carbonate. The atmospheric component is only likely to be important when soil respiration rates are very low or at very shallow depths (less than 10 cm), or a combination of both (Cerling, 1984). Pedogenic carbonate thus generally acquires carbon from soil gas and calcium from weathering of dust or detrital minerals. It is however not always possible to determine petrographically whether carbonate in soil is pedogenic, detrital, or a mixture; if it is pedogenic, it is not possible to determine whether it has undergone re-equilibrium since the time of deposition without radiocarbon analysis. Work with stable isotopes has shown that up to 100% of the carbonates in soil may have dissolved and reprecipitated (Salomon and Mook, 1976).

Newly-formed calcite in soils can probably be considered to be in isotopic equilibrium with the gas phase since rates of change in $P(CO_2)$ in soils are much slower than those used in laboratories to determine equilibrium isotopic fractionation (Turner, 1982). Magaritz *et al.* (1981) and Salomons *et al.* (1978) considered carbonate formation in soils to take place in a closed system so that the carbon isotopic composition of the soil solution changes according to a simple Rayleigh process. This is unlikely because of the continuous carbon dioxide flux due to soil respiration (Cerling, 1984). Thus, soil solutions are considered to be in equilibrium with a carbon dioxide reservoir whose isotopic composition is unchanged by carbonate formation.

Stable isotope ratios of $^{13}C/^{12}C$ are hence used to account for carbonate dissolution, transport, and precipitation processes and rates (Amundson and Lund, 1987). Any phase transition involves a change in isotopic ratio. In general, the heavier isotope (^{13}C) is concentrated in the solid phase, and the lighter isotope (^{12}C) is concentrated in the liquid or gaseous phase. Since this is a kinetically controlled distribution, it depends on the temperature of the environment.

In Holocene soils that have experienced relatively uniform climate conditions and dust deposition rates, carbonate "ages" can be compared to ages predicted from two simple models. These models are meant to be end-members of a continuum of possibilities. As one end-member, we assume that carbonate accumulating due to dust is immediately 'reset' to modern ^{14}C content upon leaching down into the profile (probably starting as 'dead' carbonate before rewetting), accumulates at a constant rate, and after deposition undergoes only radioactive decay (no further re-equilibrium)(Pendall *et al.*, 1994). In this 'dust model,' one can use 10-yr time steps as Pendall *et al.* (1994) did, incrementally adding modern carbonate to the existing pool (starting with none in the soil), not allowing the existing carbonate to re-equilibrate. 'Modern' carbonate has the ^{14}C content of 1950 carbon dioxide (the spike of atmospheric ^{14}C produced by nuclear bomb testing can be detected in soil organic matter, but not yet in carbonate)(Pendall *et al.*, 1994). The mass of carbonate added does not effect the age, as long as the input rate is constant. The dust model assumes pedogenic re-equilibration of all incoming carbonate as soon as it is added, but not after.

The other end-member model ('detrital model') considers a nonaccumulating, nonpedogenic system: detrital carbonate can be completely reset to modern at the time of deposition and decay radioactively to the present, or as with Pendall *et al.* (1994) it can start out with an 'age' of 10 000 yr at the time of deposition (based on the deepest C horizon in their late Marble Creek soil) and decay radioactively until the present. Importantly though neither model takes into consideration decreasing $^{14}CO_2$ concentrations with increased depth in the soil, due to the presence of an increasing proportion of old organic matter, as suggested by another alternative model developed by Wang *et al.* (1994).

Only carbonate that has the dust-model age or younger can be considered primarily pedogenic, since it requires equilibration with soil carbon dioxide (Pendall *et al.*, 1994). Measured ages that are younger than modelled ages reflect more dissolution and reprecipitation than would be due to accumulation alone. Ages older than the dust-model ages reflect the presence of some proportion of detrital (or non-equilibrated) carbonate.

At shallow depths, input of new carbonate apparently cannot "keep-up" with re-equilibration due to wetting events. Consistency with the dust model suggests that even at reasonably shallow depths, as pedogenic carbonate precipitates, it re-equilibrates with contemporaneous soil carbon dioxide, but importantly it will not dissolve and reprecipitate once it has formed (Pendall *et al.*, 1994). Therefore,

carbonate from these depths reflect the average pedogenic conditions over the lifetime of the soil. Below 90 cm, the carbonate has experienced fewer wetting events and thus retains inherited isotopic values (Pendall *et al.*, 1994).

Pedons generally have progressively older carbonate ^{14}C ages with depth, which is a pattern predicted by the production-diffusion model of Amundson *et al.* (1994) and Wang *et al.* (1994). This model emphasizes that the soil CO_2, the master variable controlling ^{14}C content in pedogenic carbonate, is derived from two sources: root respiration and microbial decomposition (Wang *et al.*, 1994). Although the ^{14}C content of CO_2 from root respiration is ca. 0 radiocarbon years, the CO_2 from microbial decomposition can have radiocarbon ages that are several thousand years B.P., making carbonate samples appear older than they really are. Application of the ^{14}C model of Amundson *et al.* (1994) and Wang *et al.* (1994, 1996) to ^{14}C ages is complicated for two reasons. First, their model applies to non-aggrading, relict soils and assumes carbonate accumulation since soil formation began. Many soils, however, are buried and out of the zone of modern carbonate deposition, and thus the pedogenic carbonate is not cumulative over the life span of the soil. Second, the amount and type of soil organic matter and respiration rates may have changed significantly over the life span of the soils. Currently, soil organic carbon content is much less than 0.5% in most soils, especially the sandy soils of the Kalahari and the coarse, desert scrub soils investigated by Gile and Grossman (1979) that can have A horizons with values as low as 0.2%. During pluvial periods of the Late Pleistocene,

however, vegetation density, soil organic matter and respiration rates may have been significantly higher.

As evidence of dissolution-reprecipitation, Pendall *et al.* (1994) reported enrichment of $\delta^{13}C$ and $\delta^{18}O$ values towards the soil surface. With commencement of sedimentation carbonate deposition was presumably pulled upward and travelled in a subsoil zone of about 15 to 45 cm beneath the aggrading land surface. Similarly, the zone of organic matter deposition would have lifted with aggradation.

In addition to dissolution-reprecipitation of carbonates as described by Pendall *et al.* (1994), other factors can complicate the use of pedogenic carbonates as palaeovegetation indicators. First, if plants are sparse and plant-respired CO_2 is low, atmospheric CO_2 (having a $\delta^{13}C$ average of about –6‰ to –8‰) can diffuse into the upper portion of the soil and enrich the carbonates (Cerling, 1984; Quade *et al.*, 1989a; Wang *et al.*, 1996). Second, if fossil organic matter remains in the soil, CO_2 from microbial decomposition could affect carbonate signatures (Wang *et al.*, 1994). Third, desert succulents, such as cacti, can be mixed with both the C_4 grassland communities and C_3 shrubland communities. Succulents use the CAM photosynthetic pathway, producing isotopic values intermediate between C_4 and C_3 plants (Ehleringer and Cooper, 1988; Ehleringer *et al.*, 1986, 1997). However, this is not a major factor in the Kalahari. Forth, if limestone detritus is not removed before acid treatment to extract CO_2, it may alter the isotopic signal (Rabenhorst *et al.*, 1984; Cerling and Quade, 1993).

Interpreting $\delta^{18}O$ values in soil carbonate can be complicated because ^{18}O content is controlled by both the isotopic signature of rain and any fractionation in the soil (Cerling, 1984; Cerling and Quade, 1993; Pendall *et al.*, 1994; Amundson *et al.*, 1994; Liu *et al.*, 1995; 1996; Luz and Barkan, 2005). The isotopic signature of rain, is influenced by several factors: (1) latitudinal location (isotopically lighter rain occurs polewards); (2) seasonality (winter rain is isotopically lighter and percolates deeper into the soil); (3) mountain ranges and distance from the coast (lighter rain at higher altitudes and greater distances from coast); (4) the amount of rain (rain becomes lighter as the amount of rain increases, this includes both monthly rainfall and individual rainfall events); (5) storm trajectories (source-area, including vapour from land, yields different $\delta^{18}O$ values); and (6) mean annual air temperature (as temperature increases, $\delta^{18}O$ values increase) (Rozanski *et al.*, 1993). Fractionation of ^{18}O in soil also occurs because of (1) evapotranspiration, (2) elevated soil temperatures, (3) reequilibration caused by dissolution and reprecipitation of carbonate and (4) biogeochemical processes (Cerling and Quade, 1993; Pendall *et al.*, 1994; Amundson *et al.*, 1994; Luz and Barkan, 2005).

Despite these variables, Cerling and Quade (1993) reported a correlation ($r^2 = 0.84$) between $\delta^{18}O$ values in soil carbonate and meteoric water. In desert soils of southern Arizona, Liu *et al.* (1995) found that $\delta^{18}O$ varied seasonally in the upper 40 cm, with the highest $\delta^{18}O$ values occurring in the hot, dry seasons. Below 40 cm and deeper,

the isotopic values became more closely related to the composition of the local average annual precipitation.

Although isotopic signatures of rainwater correlate with mean annual air temperatures (Dansgaard, 1964; Rozanski *et al.*, 1993), and theoretical relationships have been developed that link carbonate $\delta^{18}O$ values to palaeotemperatures, changes in rainfall seasonality, storm trajectories, and differential enrichment in soil profiles may mask palaeotemperature information. An additional factor to consider is that the following assumptions are generally made (Naiman *et al.*, 2000):

1. all surface waters are in equilibrium with atmospheric CO_2, and soil waters are in equilibrium with soil CO_2;
2. the $\delta^{18}O$ values of surface waters, especially in floodplains and playas, may be higher than meteoric water values due to evaporation;
3. the $\delta^{18}O$ value of soil water is the same as the $\delta^{18}O$ value of meteoric water (i.e., soil waters are not significantly enriched in ^{18}O by evaporation); and
4. carbonate precipitates in oxygen isotopic equilibrium with water, and carbon isotopic equilibrium with the dissolved CO_2 of that water.

3.3 Problems associated with Pedogenic Carbonates

One of the main problems in studying the origins of carbonate minerals in soil is deciding which minerals are formed through pedogenic processes (secondary) and which are the remains of the original parent material (primary). The most abundant

carbonate minerals in sedimentary rocks are calcite and dolomite, followed by siderite and ankerites (Fe-bearing dolomites)(Lippmann, 1973). Only calcite and Mg-calcite commonly form in soils as a precipitation product.

Reworked carbonate derived by erosion from an older soil or original parent material, produces ^{14}C ages which are too old. Recrystallization will produce dates that are too young. The combined results of these effects are impossible to estimate quantitatively (Callen *et al.*, 1983). Widespread reworking with transportation is not thought to be a major factor in readjusting the carbon content of pedogenic carbonates. A more likely factor is the fluctuating groundwater table that occurred during the Quaternary, together with continual percolation of rainwater down through the sediment (Callen *et al.*, 1983). Sites situated on the margins of channels or lakes, or alluvial fans where fluctuating groundwater is likely to have a maximum effect and result in the precipitation of a combination of pedogenic and non-pedogenic carbonates (Pimentel *et al.*, 1996; Shaw and Goudie, 2004) which will have compromised carbonate values (Quade and Cerling, 1990). These factors just reinforce the inherent dynamic nature of carbonate in the soil environment.

Callen *et al.* (1983) found that radiocarbon ages of pedogenic carbonate were younger than the surface age and inconsistent with depth in the profile and even within individual horizons. The result is that the stratigraphical impossibility of the age/depth plot means that radiocarbon ages can not be taken as being absolute, but rather they must be taken as minimum ages. Williams and Polach (1971) found that

carbonate precipitated in semi-arid to arid climates (<500 mm precipitation) were likely to be "too old," while in sub-humid climates (~500 mm precipitation), carbonate appeared to have undergone reprecipitation and was "too young." The result of this is that radiocarbon dates from pedogenic carbonates are often several thousand years too young or too old, which is contrary to the opinion that suggests dates on such material were reasonably reliable within arid and semi-arid zones (Botha, 1992). But even though the dates from soil carbonates in these arid and semi-arid zones are not reliable estimates for the age of pedogenesis, they can be useful as environmental indicators if their limitations are recognised (Pendall *et al.*, 1994; Koch *et al.*, 1995; Connin *et al.*, 1997; Geyh and Eitel, 1998; Deutz *et al.*, 2001).

Palaeosol carbonates may be useful in some cases in determining palaeoclimates since, if they are unaltered by diagenesis, they record information concerning both the isotopic composition of meteoric water and the proportion of C_3, C_4 or CAM biomass present in the ecosystem. Two problems are of immediate concern: epigenetic overprinting and diagenesis (Cerling, 1984). Overprinting refers to the imposition of later climatic information on previous information. This could have taken place if the soil carbonate in a single horizon formed during several different climatic episodes. It is likely that some of the variation observed in soil carbonates, especially in calcretes, is due to this problem. In evaluating this as a potential problem, one can consider the relationship between the zone of soil carbonate formation and the sedimentation rate. Soil carbonate horizons are approximately one metre thick; periods of climate change are on the order of 10 000 years or more (Cerling, 1984). Studies of terrestrial

sequences show that intervals of climatic change may be rapid (< 50 000 years) but long intervals of relatively constant climatic conditions (400 000 years) have persisted during the Cenozoic (Cerling, 1984). Sedimentation rates must take this into account: very low sedimentation rates (less than 1cm/1000 years) may have an isotopic record that spans several different climatic regimes; this is probably the case for many carbonates (Cerling, 1984). Higher sedimentation rates (greater than 10 cm/1000 years) may result in the preservation of soil carbonate that retains higher resolution climatic information (Cerling, 1984).

Diagenetic and epigenetic effects are not easily evaluated and understood. A primary issue is the fact that carbonate precipitation and partial redissolution in soils is most sensitive in the A and B horizons of soils. This is due to the fact that changes in the partial pressure of carbon dioxide and water loss due to evapotranspiration are minimal below the B horizon. What is however an excellent trace illustrating the effect of diagenesis on the carbonate, is the presence of single generation micrite in pedogenic carbonate which indicates that minimal recrystallization has occurred.

3.4 Conclusion

Arid and semi-arid regions comprise over a third of the global terrestrial environment. The lack of intense leaching by rainfall can lead to the formation of laterally extensive, meters-thick deposits of pedogenic calcium carbonate (Gile *et al.*, 1965). The carbon-cycle is critical to soil carbonate formation but the relationship is subject to large uncertainties because it is not clear precisely how much calcium is derived

from atmospheric sources compared with that from chemical weathering. Numerous authors have linked global climate change to continental weathering rates because the chemical weathering of silicate minerals consumes atmospheric CO_2 (e.g., Raymo and Ruddiman, 1992; Berner, 1991). Each mole of calcium released by silicate weathering, when combined with carbonate, acts to sequester a mole of carbon derived from photosynthetically fixed atmospheric carbon dioxide (Berner *et al.*, 1983). On the other hand, calcium derived from dissolution of calcium carbonate does not sequester any atmospheric carbon when it is reprecipitated. Globally, terrestrial carbonate sequesters about twice as much carbon as is held in the atmosphere and rivals soil organic carbon in total amount, if not in rate of carbon turnover (Eswaran *et al.*, 1993; 1995). Thus knowledge of the source of the calcium and carbon locked in these vast terrestrial deposits is critical to understanding linkages between their biogeochemical cycles (Chadwick *et al.*, 1994), depositional environments and the processes responsible for sequestration within the carbonate.

The catchments of the major Kalahari fluvial systems (Zambezi, Cunene and Kavango/Okavango) and the footwall lithologies of the Mega Kalahari Basin are dominated by Proterozoic carbonates in the northern subhumid regions (e.g. Northern Zambia, Angola and the DRC). Weathering of these lithologies has resulted in an abundance of free calcium and magnesium within the system which has been efficiently transported to the more semi-arid southern sectors of the basin by ground and surface water. In addition denudation of the southern African landscape during the Cenozoic under a range of climatic conditions meant that sedimentation within

the Kalahari sag basin was largely the result of endoreic drainage. As depositional facies and environments adapted to changing basin architecture, biotic and physico-chemical processes exploited the available cations within the system and under the right geochemical conditions produced the significant volume of intergrade carbonate which characterises the Kalahari Group. Isotopic geochemical investigation of carbonates has the ability to trace the movement of specific elements through surface systems (Graustein and Armstrong, 1983; Starinsky *et al.*, 1987; Miller *et al.*, 1993; Clow *et al.*, 1997) and thereby provide significant insight into the processes of formation and the depositional environments in which precipitation, epigenesis or diagenesis occurred.

4. METHODOLOGY AND TECHNIQUES

This chapter outlines the methodology and techniques employed within this research project. The majority of methodologies follow the rock and soil description, sampling and analysis protocols of the United States Geological Survey (USGS) and British Geological Survey (BGS). All reported units are SI relative to the universal standard if applicable. In addition all discussions regarding lithostratigraphy and chronostratigraphy adhere to the standards of the International Union of Geological Sciences, the International Commission on Stratigraphy (ICS) (http://micropress.org/stratigraphy/) and the South African Commission on Stratigraphy (SACS). References to Erathem Era, System Period, Series Epoch and Stage Age are based on the 2000 edition of the International Stratigraphic Chart (Appendix 2).

4.1 Sampling

The objective of this study was to collect intergrade carbonate sediments from a range of active geomorphic environments throughout the southern and central Kalahari in order to investigate the processes responsible for their formation and modification. A number of regions were selected due to the fact that they contained characteristic geomorphic features (Kgalagadi, Kalkweissrand and Etosha – palustrine/pan systems; Nossob/Auob/Olifants and Molopo/Kuruman Rivers – relict channel/valley and pedogenic; Okavango and Linyanti – active fluvial/alluvial; Ngami – lacustrine/palustrine).

Sampling in all of these areas was dictated by accessibility and as a result, the majority of sample sites are located on state or tribal land close to public/restricted access roads which often form transects through the regions investigated. As discussed by Nash and McLaren (2003) calcretes throughout the Kalahari have very limited exposure. As a result the majority of sections investigated and described are located within shallow quarries, prospecting and observation pits excavated by mining companies, and incised pans and drainage channels.

4.2 Mapping and Remote Sensing

A range of geological, topographic, thematic and tourist maps, orthophotos, aerial photos and satellite images at various scales were used in order to understand the relationship between the geomorphic context of chemical sediments and the processes responsible for their formation. Topographic maps and aerial photographs of South Africa and Northern Namibia (pre-1990) were obtained from the Chief Directorate of Surveying and Mapping, Mowbray, South Africa; Namibia (post-1990) from The Office of the Surveyor-General, Windhoek; Botswana from the Department of Surveys and Land, Gaborone; and for Angola the Ministério de Defesa, Instituto de Geodesia e Cartografia de Angola, Luanda and the Soviet General Staff maps available within the Bodleian Library, Oxford were used. Geological maps for South Africa were obtained from the Council for Geoscience, Pretoria; Namibia, the Geological Survey, Windhoek and Botswana the Geological Survey, Lobatse. Supplementary thematic maps of the watersheds of southern Africa (ALCOM, FAO and WWF, 1997), hydrology of the Okavango Fan (Geological Survey and Division of Hydrology, Botswana) and the 1:2 500 000 isopach map of the Kalahari Group sediments (Haddon, 1999) provided

extremely valuable information. Tourist maps and accompanying information of Botswana (Roodt, 1998) and Etosha National Park (Ministry of Environment and Tourism, Namibia) were useful for planning access and logistics.

Remote sensing imagery was obtained from a number of sources, the principal contributor being Google Earth (http://earth.google.com), MODIS (http://rapidfire.sci.gsfc.nasa.gov/), composite LANDSAT 5 images (https://zulu.ssc.nasa.gov/, http://geo.arc.nasa.gov/sge/landsat/daccess.html and http://visibleearth.nasa.gov). Additional LANDSAT 7 images were obtained from the USGS (http://landsat7.usgs.gov/index.php). SPOT 1-5 images at various resolutions (2.5, 5, 10 and 20 m) were obtained from CNES, France (http://www.spotimage.fr/home/) and combinations of LANDSAT and SPOT images were obtained from (www.sac.co.za) and (http://www.spaceimaging.com/). Low angle NASA shuttle photography (www.nasa.gov/galley/photo/) and global land cover facility using bands 4 and 5 (http://glcf.umiacs.umd.edu/data) also provided useful images. Aerial photographs also proved extremely useful for geomorphic interpretation, having a superior resolution to other types of remote-sensing imagery.

4.3 Physical and Chemical Sedimentology

4.3.1 Description

Consolidated and unconsolidated sediment samples were collected from logged profiles during August 1998, July-October 1999, September/October 2000, March/April and November-January 2001 using standard geomorphological

protocols (Goudie, 1994). Details of sample location, profile thickness, number of samples collected and geomorphic setting are shown in Appendix 3.

4.3.2 Grain Size Analysis Techniques

67 unconsolidated sediment samples were collected and analysed. 29 sediment samples were collected from a six profiles exposed along the northern shore of the Etosha Pan. An additional 29 sediment samples were collected from profiles excavated along transect across three islands (Xhamoga, Mosupatsela and Gaenga) in the permanent swamps of the Okavango. A transect of four pits corresponding to the vegetation types (at 10 m, 50 m, 75 m and 85 m from the southern perimeter of the island) were dug down to the water table from the channel bank to the centre of Xhamoga Island and sampled at 20 cm intervals down profile. On Mosupatsela Island sediment samples were collected from the 75 m pit at 20 cm intervals down profile. On Gaenga Island, only one pit was dug down to the water table on the inner side of the fringe vegetation where grass and scattered palms replaced large evergreen riparian forest. This was also sampled at 20 cm intervals. 9 samples of unconsolidated sand with carbonate grain coatings and unconsolidated powdery calcrete samples were analysed from calcrete profiles investigated within the Okavango and Ngami study areas. These grab samples were stored in air tight zip seal bags. Approximately 50 grams of the sediment was sub-sampled using the splitter. The sample to be analyzed was placed in a pre-weighed 100 ml beaker, weighed, and dried in a convection oven at 40°C so as not to destroy any clay structures. When dried, the samples were placed in a desiccator to cool and then reweighed. The decrease in weight due to water loss was taken to be the moisture content.

The samples were disaggregated on a shaking table for 15 minutes using a solution of 10% calgon (sodium hexaphosphate) in order to deflocculate the clay fraction. The solution was then wet sieved through a number 230, 63 μm (4Φ) sieve using distilled water to separate the coarse- and fine-fractions. The fine fraction was sealed in a Mason jar and reserved for analysis by CILAS laser diffraction granulometer. The coarse fraction was rewashed in tap water, reintroduced into a pre-weighed beaker, dried in the convection oven at 75°C and then reweighed. The weight of the coarse (> 63 μm) fraction is equal to the weight of the sand plus gravel. The weight of the fines (silt and clay) can also be calculated by subtracting the coarse weight from the sample weight. The coarse fraction was dry sieved at 0.25Φ intervals from -1-4Φ using a Ro-Tap shaker with the fraction retained on each sieve being weighed.

The fine fraction (< 63 μm) was analyzed using the CILAS 9100 granulometer (Shideler, 1976). To alleviate biologic or chemical changes, storage in the Mason jars prior to analysis never exceeded five days. The gravel, sand, and fine fraction data were combined, with any overlap (pan fraction for dry sieving and component > 63 μm for the granulometer) being considered error. The data were then processed using the GRADISTAT version 4.0 macro in excel (Blott, 2000). A limitation of using a laser diffraction granulometer to perform fine fraction analyses is that it has only the ability to "see" those particles for which it has been calibrated. Calibration for this study allowed determination of the distribution accurately down to 0.5 μm or 11Φ.

Size classifications are based on the method proposed by Udden (1914) and Wentworth (1922, 1929). Statistics using the GRADISTAT macro were calculated using the method of moments (Griffiths, 1967) and the inclusive graphics statistical method (Folk and Ward, 1957; Folk, 1974). Both of these are based on the nomenclature proposed by Shepard (1954). Additional methodological procedures and methods are described by Krumbein and Pettijohn (1938), Folk (1954, 1968, 1974), Galehouse (1971) or Boggs (1995).

4.3.3 Petrographic Investigation

Consolidated samples were sub-sampled for petrographic thin sections at the Department of Earth Sciences, Oxford University. Description of the petrographic properties and structures of the carbonate sediments were made using a binocular microscope as outlined by Nesse (1991) and Adams and MacKenzie (1998) using the limestone classification system of Dunham (1962) rather than that of Folk (1959, 1962), the dolomite classification system of Sibley and Gregg (1987) and the general southern African terminology of Netterberg (1980), Watts (1980), Summerfield (1982, 1983a,b,c) and Nash and Shaw (1998). The Dunham (1962) classification system assigns names according to their depositional texture. The main problem with this lies with its inability to determine when introduction of carbonate material began and where it came from (Tucker and Wright, 1990; Adams and MacKenzie, 1998). Hence, it is also impossible to determine whether the carbonate being described was introduced at the time of deposition (which only applies to lacustrine carbonates) or subsequently infiltrated a primary grainstone, as in the case of both pedogenic and non-pedogenic carbonates. The Dunham (1962) classification is, however, appropriate due to its popularity as a

simple classification which allows textural names to be prefaced by the names of the principal grain type and other textural information which relays a great deal of information about the sediment in an unambiguous fashion. In order to provide definitions for the current study a detailed atlas of structures was compiled (Appendix 1) from previous petrographic features identified within a range of terrestrial carbonates.

		Proportional % of carbonate fraction		
% Silica	% Carbonate	% Calcite	% Dolomite	Name
> 95	< 5			Pure silcrete
85 - 94.9	5.1 - 15			Impure silcrete
70 - 84.9	15.1 - 30	Dominant	Subordinant	Calc-silcrete
70 - 84.9	15.1 - 30	Subordinant	Dominant	Dolo-silcrete
50 - 69.9	30.1 - 50	> 95	< 5	Sil-calcrete
50 - 69.9	30.1 - 50	90 - 94.9	5.1 - 10	Sil-magnesian calcrete
50 - 69.9	30.1 - 50	50 - 89.9	10.1 - 50	Sil-dolo-calcrete
50 - 69.9	30.1 - 50	10 - 49.9	50.1 - 90	Sil-calc-dolocrete
50 - 69.9	30.1 - 50	< 9.9	> 90.1	Sil-dolocrete
< 50	> 50	> 95	< 5	Calcrete
< 50	> 50	90 - 94.9	5.1 - 10	Magnesian calcrete
< 50	> 50	50 - 89.9	10.1 - 50	Dolomitic calcrete
< 50	> 50	10 - 49.9	50.1 - 90	Calcitic dolocrete
< 50	> 50	< 9.9	> 90.1	Dolocrete

Table 4.1: Classification based on the proportional fabric mineralogy in grain and fabric supported chemical sediments.

The classification system of Sibley and Gregg (1987), which describes the shape of dolomite crystals, was used to explain the dolomite textures. This system places emphasis on the shape of the crystal boundary's and identifies them as non-planar (closely packed anhedral crystals with curved, lobate, serrated, or otherwise irregular intercrystalline boundaries), planar-euhedral (most dolomite crystals are euhedral rhombs) and planar-subhedral (crystals are subhedral to anhedral with straight, compromised boundaries and many crystal-face junctions) and the crystal

mosaics can be described as xenotopic, idiotopic and hypidiotopic respectively (Sibley and Gregg, 1987).

Nash and Shaw (1998) and Nash and McLaren (2003) have highlighted the gaps within the calcrete literature regarding the classification of chemical sediments at a number of levels and have made advances towards the formulation of a clear and definitive classification of calcrete, silcrete, dolocrete and intergrade sediments. A review and modification of the traditional calcrete, dolocrete and silcrete classification system is required due to the dominance of intergrade duricrusts and chemical sediments of various ages throughout the Mega Kalahari Basin. The abundance of intergrade deposits is the result of: 1) the significant range of deposit ages; and 2) the fact that near surface chemical precipitates are generally unstable over the short and medium term and under dynamic depositional, diagenetic, hydrologic, pedogenic and climatic conditions often undergo extensive and multiple phases of epigenetic modification, replacement and recrystallisation. In order to classify the chemical sediments the systems of Netterberg (1969a, 1980), Arakel and McConchie (1982), Summerfield (1983a,b,c) and Nash and Shaw (1998) which identify silcretes (pure and impure), intergrade calc-silcretes and sil-calcretes, calcretes and dolocretes were used as a foundation for an updated genetic classification system. This classification system (which has been used throughout this thesis) uses the proportional percentages of the three principal mineralogies: silica, calcite and dolomite for both fabric- and grain-supported deposits (Table 4.1) while adhering to the traditional nomenclature for limestone (Folk, 1959; Dunham, 1962), dolomite (Sibley and Gregg, 1987) and calcrete (Wright and Tucker, 1991) fabric description.

Structures and textures identified within the carbonates were based on analyses of more than 15 000 photographs of 315 thin section samples from 128 profiles investigated at the seven study locations. In line with previous petrographic analyses of carbonates (Wright and Tucker, 1991) the qualitative descriptions were intended to be used as indicators which when combined with other data would provide a series of clues to the mechanisms and processes of carbonate precipitation and subsequent modification. Nash and McLaren (2004) have used the point count method on a smaller sample population (96) to quantify the percentage of host grains, carbonate and silica cement types and porosity within Kalahari valley calcretes. Although this method can be criticised for being biased when selecting isolated components of fabrics to investigate within complex textures it may prove useful for further more detailed investigation of selected features within profiles or carbonate types.

Due to the nature of the study and issues related to the subjective nature of stain identification (Adams and MacKenzie, 1998) none of the thin sections were etched or stained with Alizarin Red S or potassium ferricyanide. This decision was taken in light of the fact that previous work on southern African calcrete mineralogy (Netterberg, 1980; Watts, 1980; Summerfield, 1982, 1983a,b,c; Nash and Shaw, 1998) had successfully identified the principal mineralogies using XRD. However, in response to the complexity and diversity of mineralogies identified within the samples it would be advantageous to use staining as a supplementary tool for micro-analysis of individual samples at a later date. In retrospect it would have been wise to use blue-dye-stained resin rather than the

colourless resin used to impregnate the porous and friable samples in order to make identification of porosity within the thin sections easier. In addition to the standard PPL and XPL used in this study, significant information could be gathered with regard to textures within the carbonates from a future cathodoluminescence based study. The abundance of Mn^{2+} and Fe^{2+} within southern African carbonates would facilitate significant variation in the luminescence intensities and thus provide insight to pore-water chemistry, precipitation mechanisms, the precipitation of diagenetic minerals (transition from oxidising to suboxic to anoxic conditions or visa versa), and help characterise generations of cement (Miller, 1988).

4.3.4 XRD

X-ray diffraction (XRD) of clay minerals is now a widely accepted method of mineral evaluation among sedimentologists and geomorphologists and has been used extensively in the Kalahari (e.g. Watts, 1980; Eitel, 2000).

The definitions of clay are slightly different in various sciences. In terms of XRD analyses clay is defined as (a) aggregates of particles finer than 2 μm, (b) adhesive substances and (c) natural inorganic materials mainly composed of silicon, aluminium, iron, magnesium, alkali-metal elements, alkaline earth elements and water. Clay minerals generally include phyllosilicates composed of sheet structures, fibrous palygorskite and sepiolite, as well as some amorphous substances. However, amorphous silica, iron oxide and alumina gels are not classified as clay minerals.

Bulk and clay mineralogy of 145 samples (Appendix 4) from the seven study locations were investigated using random powder whole rock and clay size fraction XRD analysis. The analysis was conducted at the Council for Geoscience, Pretoria, and the Agricultural Research Council, Institute for Soil Climate and Water (ARC-ISCW), Pretoria, using a Siemens D500 X-ray goniometer equipped with Cu tube, variable slit and secondary graphite monochromator. The latter eliminates K ß radiation and additionally reduces fluorescent radiation. A fine grained powder (± 10 µm) of each sample is pressed in an aluminium frame against a rough filter paper. Such random powder preparation is scanned from 2 to 65° 2Θ $Cu_{K\alpha}$ at a speed of 0.02° 2Θ steps size/sec^{-1} with generator settings of 35 kV and 25mA.

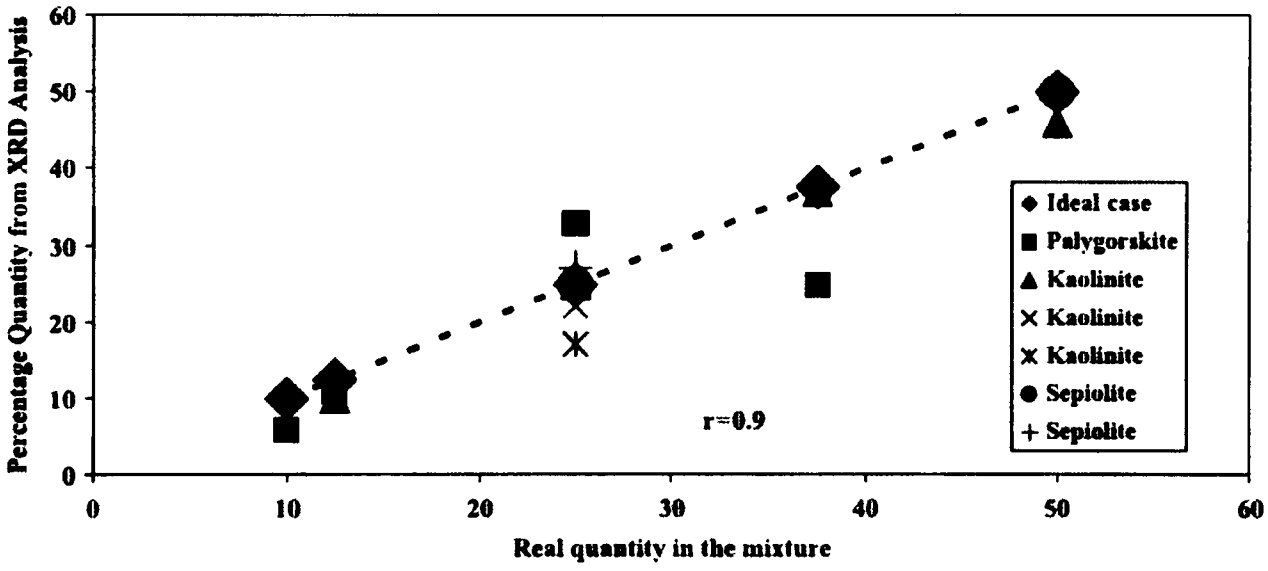


Figure 4.1: Comparison of XRD techniques for selected clay mineralogies (from Ouhadia and Yong (2003)).

The results were evaluated qualitatively using SIEMENS DIFFRAC^{Plus} software. The XRD evaluation program (EVA) allows matching with the PDF-2 Database and semiquantitive estimates are based on peak-height percentages. Ouhadia and Yong (2003) have experimentally reviewed the application of the four most

popular methods of XRD analysis, including the method used for mineral quantification purposes. They suggested that: (a) direct quantitative XRD analysis based on peak intensity or areas under the peaks is likely to cause an over- or under-estimation of the quantity of clay minerals; (b) quantitative evaluation based on only the major reflection line is likely to induce mistakes in clay mineral identification; and (c) quantitative X-ray analysis using different reflection lines of minerals that take into account the impact of clay microstructure have been shown to be the most accurate method of mineral evaluation. The most problematic clay mineralogy identified by Ouhadia and Yong (2003) was palygorskite (Fig 4.1), which is a dominant Kalahari clay mineralogy. In light of the potential over- or under-estimation of specific clay mineralogies all proportional percentages quoted are to be viewed as being semiquantitative indicators. Watts (1980) presented a slightly different and more technical description (of peak heights and reflection lines) on the XRD techniques used during his investigation of Kalahari carbonates and his motivation for the interpretation of the results includes many of the potential problems highlighted by Ouhadia and Yong (2003).

A selection of 30 X-ray diffraction traces are presented in Appendix 5.

4.3.5 Environmental Magnetic Susceptibility

Most sediments have some magnetic material in them. The type of magnetic material, its size and concentration in the sediment all affect the type of magnetic signal it gives off. The most common magnetic minerals worldwide and within the Kalahari are magnetite and haematite, both iron oxides but with different

magnetic properties. Magnetite is often found in intrusive rocks and coarse-grained sedimentary deposits like sandstone, whereas haematite typically forms as iron-rich rocks decompose within a sedimentary environment, turning red when oxidised.

Environmental mineral magnetic susceptibility measures the magnetic characteristics determined by the chemical structure of the mineral types within the sample. Unlike paleaomagnetism, which measures the sample's polarity relative to the earth's magnetic poles, mineral magnetism samples do not need to be measured *in situ*, or have their original orientation noted. Magnetism measurements are relatively fast, inexpensive, easy to make and non-destructive (the sample does have to be crushed and pulverised). The magnetic susceptibility of 96 samples (Appendix 6) from the Okavango and Ngami study areas were investigated.

The technique used in this study was to crush and pulverise a sample into a fine powder, oven dry and then pack 1 g of the sample into a small plastic cylinder. The result obtained will be a measure of the sample's ability to become magnetised. The Bartington Instruments Magnetic Susceptibility Meter is a simple instrument which can be used to scan cores using the loop or single samples using a well sensor. The well sensor was used to measure all the samples in this study. More complex instruments measure susceptibility while spinning the sample around perpendicular axes (x, y and z). However, the Bartington Instrument uses a magnetic field created by a coil surrounding the sample to induce a low frequency magnetic field. The total susceptibility of the sample is determined in either CGS

or SI units within the 1.0 or 0.1 range. Each sample was measured ten times in the following manner: 'zero' meter to remove background noise – first reading (ignore) – second 'zero' – second reading (true reading).

4.3.6 LOI Organic Carbon

The study of carbon content in sediments is a way of estimating primary productivity and the abundance of plant life. In this sense, carbon content is a proxy for past productivity and provides insight into depositional and diagenetic environments. Carbon occurs in two forms: organic and inorganic (carbonate). Organic carbon occurs as the product of photosynthesis and decomposition. Inorganic carbon comes from the dissolution and precipitation of carbonate compounds as sediments.

The organic carbon content of 30 sediments samples collected from the islands of the permanent Okavango swamps, 31 sediments samples from profiles along the northern shore of Etosha Pan and 88 crushed and pulverised carbonate samples from all seven study locations (Appendix 7) were determined by the ash-weight loss on ignition method (LOI) at 550°C in a muffle furnace (Berglund, 1986; Heiri *et al.*, 2001). Approximately 5 g of fresh sediment (FW) from each sample was placed into pre-weighed porcelain crucibles (C). The samples were then dried in an air-circulation oven at 105°C for 12 hours to drive off all the moisture. They were then cooled to room temperature in a desiccator, reweighed giving the dry-weight of sediment (DW), and then placed in a furnace at 550°C for 2 hours in order to destroy all the organic matter. As the organic matter burns, the carbon is changed to carbon dioxide (CO_2) and carbon monoxide (CO). The samples were

then allowed to cool to room temperature in a desiccator and reweighed. The percent organic matter was calculated by the difference in weight before and after heating in the oven at 550°C. Depending on the character of the sediment, various losses of volatile salts, structural and chemically bound water and ammonia will occur, which will have an effect on the final result.

LOI is a rough indication of the amount of organic matter in the sample, and the correlation with organic carbon is acceptable. Various conversion factors, such as that organic carbon represents 12/30 of the organic content ($(CH_2O)_n$), have been reported for converting loss on ignition to organic carbon (Berglund, 1986). As the factor depends on the material being analysed the use of conversion factors should be handled with care even within a single sediment profile.

4.3.7 LOI Inorganic Carbon

The allogenic, endogenic and authigenic minerals which comprise the inorganic carbon content of a sample can be measured by LOI or digest. This study used the ash-weight loss on ignition (LOI) at 1000°C method (Berglund, 1986; Goudie, 1994; Heiri *et al.*, 2001) to analyse 30 sediments samples collected from the islands of the permanent Okavango swamps, 65 sediments samples from profiles along the northern shore of Etosha Pan and 88 crushed and pulverised carbonate samples. The weighed crucible with the residual ash from the organic carbon LOI analysis (weight A) was placed in a muffle furnace for 4 hours at 1000°C. The crucible with the ignited sample was then cooled to room temperature in a desiccator and the weight of ash and crucible (weight B) determined. The inorganic carbonate content (CO_3) is equal to:

$$\frac{(A - B)}{\text{dry-weight of sediment (DW)}} \times \frac{60 \text{ (molecular weight for } CO_3)}{44 \text{ (molecular weight for } CO_2)}$$

As carbonate compounds become volatile at different temperatures, the carbonate content estimation is only a rough determination. Various conversion factors have been given by different authors, but as a general rule the ash-weight loss obtained between 550°C and 1000°C should be multiplied by 1.36 to obtain the carbonate content.

4.3.8 Electrical Conductivity

12 carbonate samples from profiles within the Okavango and 29 sediment samples from transects across the 3 islands in the permanent swamps of the Okavango were analysed for electrical conductivity (Appendix 8). In order to determine the electrical conductivity (EC) of sediment samples, 20 mg of fresh sediment or pulverised carbonate was placed into a 250 ml Erlenmeyer flask. 40 ml of deionized water was then added to the sediment in order to form a sediment/water solution which was agitated slowly on a shaking table for 2 hours in order to allow the sediment and deionized water to equilibrate. The solution was then filtered using a 0.45 μm filter and the conductivity measured on the filtered solution using a calibrated conductivity meter and electrode (http://hubcap.clemson.edu/~blpprt/).

4.3.9 pH

12 carbonate samples from profiles within the Okavango and 29 sediment samples from transects across 3 islands in the permanent swamps of the Okavango were analysed for pH. The sample's pH was determined by using a 1:1 ratio of sediment to water. 20 g of fresh sediment was weighed into a 250 ml Erlenmeyer flask. Then 20 ml of deionized water was added to produce a sediment/water solution just like for EC determination. This solution was agitated slowly on a shaking table for 2 hours in order to allow the sediment and deionized water to equilibrate. The solution was then filtered using a 0.45 μm filter and the pH value measured using a calibrated pH meter (http://hubcap.clemson.edu/~blpprt/).

4.3.10 Cations

The application of trace element analyses to carbonates requires knowledge of their solid structure and the composition of liquids which precipitate and interact with them (Dickson, 1990). Equally important to the analysis of trace elements is to determine whether precipitation has occurred in equilibrium or due to kinetic factors.

Sediment's cation exchange capacity (CEC) is a measure of its ability to provide sites for non-specific absorption of metals and metalloids. The CEC of most sediments ranges from a few to several hundred meq/100 g and far exceeds anion exchange capacity as negative rather than positive charges dominate on colloidal surfaces.

Clay minerals play a significant role in the sorption of trace elements from soil solutions, as a result of their large surface areas. However in clay poor sediments, the sorption potential of carbonates is significant and has been investigated by geochemists (e.g. Kabata-Pendias, 2004) and sedimentologists (e.g. Arakel and McConchie, 1982). The major control on trace element uptake by carbonates, often in metastable and polymorphic forms, is pH (Hall, 1998). The trace elements may be co-precipitated with the carbonates or, like Cd, may actually replace Ca^{2+} in the lattice. The greatest affinity for reaction with carbonates has been observed for Co, Cd, Cu, Fe, Mn, Ni, Pb, Sr, U and Zn (Kabata-Pendias, 2004).

In order to understand the mobility of trace elements within each of the mineralogical components a four step sequential cation extraction based on Hall (1998) was attempted with limited success rather than the elemental composition of bulk samples obtained by using XRF. The following components were investigated in 54 carbonate samples from the Okavango and Ngami study areas and the 29 sediment samples from the 3 islands investigated in the permanent swamps of the Okavango (Appendix 9):

1. Exchangeable / water soluble component: water leach
2. Carbonates (calcite) / exchangeable cations absorbed by clays and elements co-precipitated with carbonates: pH 5, 1M NH_4OAc (ammonium acetate)
3. Residual carbonates (dolomite): HCl
4. Residual silica: HF

Water leach:

1 g of finely powdered oven dried homogenised sample was weighed into a 10 ml centrifuge tube to which 5 g of Milli Q water was added. Initially the solution was swirled to mix and then agitated frequently (5-10 minutes every few hours) over the next 72+ hours using a test tube shaker. During this time the samples were kept in a hot (30-40°C) water bath. After 72+ hours the mixture was centrifuged at approximately 3000 rpm for 30 minutes. The supernatant was then withdrawn with a 1 ml syringe and filtered through a 0.2 μm syringe filter into another 10 ml centrifuge tube where it was then acidify to a pH of ~3 with 1M nitric acid. During the acidification process the solution occasionally turned cloudy. This was a result of organic (humic) acid precipitating if the pH was too low. Humic acids precipitate at pH ~1, while fulvic acids won't precipitate. Organic acids are very good receptors of 2+ metals (and calcium) due to their bond structure, therefore, if the solution turned cloudy, the sample was discarded and the procedure repeated making sure not to over acidify. 0.1 ml of indium standard was then added to 2 ml of filtered solution in a fresh centrifuge tube and the solution topped up with 1M ICP-MS grade nitric acid to weigh 5 g. The sample was then run on the ICP-MS (inductively coupled plasma mass-spectrometer) which determined the absolute quantity (in ppm or ppb) of the following elements: Li, Na, Mg, Al, K, Ca, V, Cr, Fe, Mn, Co, Ni, Cu, Zn, Rb, Sr, Ba, Th and U. Every tenth sample run was a blank (2 ml of Milli Q water was added rather than the filtered solution) and every twenty fifth sample contained a duplicate from the preceding 24 samples.

For the next stage in the sequential leach it was necessary to wash the initial residue. This residue was rinsed at least 3 times with Milli Q water, centrifuging

each time to remove the water which was then discarded. The washed residue in the centrifuge tube was then dried at 30-40°C in a clean air-circulation oven. The dried residue was then extracted and re-homogenized by grinding to a fine powder with an agate pestle and mortar.

Carbonate leach:

The preferred method of selective dissolution of the carbonate phase was the acidified acetate-buffered extraction, namely 1 M ammonium acetate at pH 5 (Hall, 1998). The buffering capacity of this solution, when used with a solid/solution ratio of 1:40, is sufficient to dissolve all the calcite in carbonate rich sediment. The method used involves 24 hours of constant agitation, at a ratio of 1:20 ($CaCO_3$:ammonium acetate), to ensure complete dissolution of the carbonate phase.

A known weight of the finely powdered sample residue from the water leach (approximately 10-20 mg of carbonate was needed so at least 50 mg of residue was used) was dissolved in 1.0 ml pH 5 1M ammonium acetate. This solution was agitated constantly for 24 hours at a constant temperature (20°C was used unsuccessfully). After 24 hours, the mixture was centrifuged at 3000 rpm for 30 minutes. Then the supernatant was withdrawn with a 1 ml syringe and filtered through a 0.2 μm syringe filter. 0.1 ml of indium standard was then added to 0.4 ml of each solution in a fresh centrifuge tube and the solution was topped up with 1 M ICP-MS grade nitric acid to weigh 2.5 g. This solution was then analysed by the ICP-MS for: Li, Na, Mg, Al, K, Ca, V, Cr, Fe, Mn, Co, Ni, Cu, Zn, Rb, Sr, Ba, Th and U. The residue was again washed 3 times in 1M ammonium acetate,

centrifuging each time, and the solid residue was then dried in a clean air-circulation oven for the third phase – reaction with HCl.

A critical problem was encountered during this second stage. The elemental levels detected by the ICP-MS were extremely low (and standard deviations extremely high). These levels were almost indistinguishable from the blank ammonium acetate samples run and it was concluded the calcite leach had failed. The most likely causes were low calcium carbonate levels (typically < 30% rather than the ~65% $CaCO_3$ of Hall (1998)), the temperature of reaction (which despite significant research has not been clearly stated in any methodology) and method of agitation. The destructive nature of the sequential leach process and the limited access to the ICP-MS meant that the process was abandoned at this stage.

The main aim of this investigation was to attempt to determine the link between the carbonate phases (dolomite and calcite), silica and intergrade fabric types with trace element composition. However, the complexity of the carbonates fabric was imitated by the geochemistry which made the results obtained from this 'bucket and spade' approach less than conclusive. The results however do show some distinctive trends and follow up analyses of specific fabric types using laser ablation ICP-MS may be more conclusive.

4.3.11 Anions

Anion analyses using liquid ion chromatography (Dionex DX500 – Peaknet 4.11 software) were conducted on a water leachate of each of the 54 carbonate samples from the Okavango and Ngami study areas and the 29 sediment samples from the

3 islands investigated in the permanent swamps of the Okavango (prepared in exactly the same way as for cation analyses – see Appendix 10).

4.3.12 Isotopes

92 carbonate samples from all seven study areas and 45 sediment samples from the 3 islands in the permanent swamps of the Okavango were analysed (Appendix 11). Samples analysed for inorganic $\delta^{12}C/^{13}C$ and $\delta^{16}O/^{18}O$ had to be pre-treated in order to remove any contaminating organic carbon. Initially any macro organic material was removed by hand. Then the samples were washed with a 30-60% NaOH.Cl (Sodium Hypochlorite) solution for 12 hours. This reaction oxidised any organic material within the sediment. On occasion it was necessary to repeat the sodium hypochlorite wash in order to remove excess organic mater. After the sample stopped reacting it was sieved at 80 μm (the fines were discarded) and the retained material was washed in deionized water and filtered at < 80 μm: using Whatman No. 41 filter paper (20 μm diameter). This wash and filter process was repeated three times. The washed filtered material collected on the filter paper was then dried on a watch glass in an air-circulation oven at 40°C. Once dry the material was cleaned off the filter paper and powdered using an agate pestle and mortar.

The methodology used to determine the inorganic $\delta^{12}C/^{13}C$ and $\delta^{16}O/^{18}O$ isotopic ratios of the authigenic carbonate (calcite and dolomite) samples using a gas-source mass spectrometry were based on the methodology of McCrea (1950) and Epstein and Meyeda (1953). Varying masses of sample (between 10 mg and 250 mg depending on the carbonate content, one needs a minimum of 10 mg of

$CaCO_3$) were loaded into sample reaction tubes and placed inside the reaction vessels containing 4 ml of anhydrous phosphoric acid. The vessels were then evacuated to > 1.0^{-4} mb, to remove atmospheric carbon dioxide and moisture, sealed and placed in a controlled temperature water bath at 25.2°C and allowed to thermally equilibrate for approximately 30 minutes. The reaction was initiated by introducing the acid into the sample reaction tubes within the sealed, evacuated vessel. The vessels were intermittently agitated to ensure the continuation of the reaction and then left for 16 hours to ensure reaction has gone to completion.

The resultant gas was cleaned cryogenically by expanding it through an acetone cold trap maintained at ~ -90°C and collected in clean dry collection vessels using liquid nitrogen. The vessels were then sealed and transferred to the VG Optima (a duel inlet gas source mass spectrometer) for analysis.

Each batch of unknown samples was run with three primary standards with known values with respect to NBS-19 and at least one secondary standard and a duplicate unknown sample.

The resultant gas values were further corrected to adjust for small levels of ^{17}O isotopes, normalized through the primary standard and corrected to the solid carbonate value using a fractionation factor (Sharma and Clayton (1965) as cited in Friedman and O'Neil, 1977) of 1.01025 for calcium carbonate at 25.2°C. All results were quoted as $\delta^{12}C/^{13}C$ and $\delta^{16}O/^{18}O$ relative to the PDB and SMOW standards.

4.3.13 C/N and $\delta^{13}C$ Organic Analysis

31 samples from the 3 islands in the permanent swamps of the Okavango were analysed for their nitrogen and organic carbon content and their $\delta^{13}C$ organic values (Appendix 12). Elemental analysers operate by flash combustion in which a sample contained within a tin capsule is dropped into a combustion reactor which is maintained at 1020°C (Mucciarone, 2003). This short flash combustion is accomplished when the tin capsule is exposed to a gas flow temporarily enriched with ultra high purity (UHP grade 4.3) oxygen (Mucciarone, 2003). The resulting oxidation raises the temperature to > 1700°C and the encapsulated sample will combust and generate one or more of the following gasses: N_xO_x, CO_2, H_2O and SO_2 depending on its composition. The machine used was setup to analyse C and N thus the N_2, CO_2 and H_2O produced in the furnace are moved through the system by an ultra pure helium (UHP grade 5.0) carrier gas. An in-line absorption trap containing anhydrous magnesium perchlorate then removed any H_2O from the carrier gas. The remaining N_2 and CO_2 gases pass through a chromatographic column and are detected based on differing retention times with a thermal conductivity detector at 190°C (Mucciarone, 2003). The elemental analyser used was coupled to a Finnigan mass spectrometer for $\delta^{13}C$ analysis of the CO_2 via a continuous flow device.

Prior to samples being run on the elemental analyser any inorganic carbon must be removed. This was achieved by adding approximately 50 ml of 5% HCl to the sample and leaving it to react overnight. If there was abundant inorganic carbon it may be necessary to add additional 5% HCl. After the reaction stopped, the residue was filtered using Whatman No. 41 filter paper and wash 3 times with

deionised water. The residue was then dried overnight at 60°C in an air-circulation oven and powdered to a fine homogeneous powder using an agate pestle and mortar. The powdered samples were then placed into glass vials, redried at 60°C overnight, and stored in a desiccator until analysed.

Prior to being analysed an exact amount of sample (at least 2.0-2.5 mg of organic carbon is required for analysis based on the organic carbon content determined by LOI at 550°C) was weighed into the small tin analysis cups. After weighing the tin cup was crushed into a pellet using a pair of tweezers ready for analysis. About 40 percent of the runs were blanks (empty tin cups) or standards (NIGL reference material), run as a means of calibrating the instrument and checking precision. Precision was always better than one standard deviation.

4.4 Hydrogeochemistry of the Okavango Alluvial Fan

Aqueous samples (surface, ground and rain water) were collected at near monthly intervals over the annual flood cycle (Appendix 13), where possible, during the period March 2001 to July 2002 from 67 sample sites throughout the Okavango alluvial fan (Appendix 14). The aim was to understand the hydrogeochemical mechanisms responsible for and quantify the relationship between active carbonate precipitation within the sediments of islands in the perennial fan and the floodplains of the seasonal fan.

4.4.1 Preparation of Containers for Aqueous Samples

Hydro-chemically clean containers were used for the collection of aqueous samples in order to minimise contamination of trace-elements. Teflon or PEP

containers were prepared using the acid-rinse methodology of the US Office of Water Quality (USOWQ) and the US National Water Quality Laboratory (USNWQL). Field rinsing is not an acceptable method of cleaning new bottles or uncapped acid-rinsed polyethylene bottles. In addition to the acid-rinse all containers and their caps were rinsed at the field site immediately prior to sample collection with the sample solution that was analyzed from that container. These rinse solutions were filtered at 0.45 μm and were either left untreated or acidified in exactly the same manner as the sample solutions. Deionised water was used for blank samples.

4.4.2 Water Sampling Protocol

Okavango channel water is well mixed vertically and laterally with respect to concentrations of target analytes, therefore water samples were collected using a combination of the single vertical at centroid-of-flow (VCF) and the nonisokinetic dip sampling methods (USGS, 2001). The VCF method aims to collect a discharge-weighted sample that represents the entire flow passing through the cross section (USGS, 2001). The centroid is the point at which discharge is equal on both sides of the point. Dip sampling involves dipping a narrow-mouthed bottle into the water body. The error introduced by dip sampling can be significant if the target analytes are sorbed onto suspended materials that are not uniformly distributed along the cross section. Care was taken to avoid collecting particulates that were resuspended as the result of bumping the sampler on the streambed.

When sampling the water, the boat was moored and stationary within the centroid of the channel. The sampler was lowered into the water body until slight contact

was made with the streambed. After contact the sampler was immediately raised at a constant rate until it reached the surface. Equipment and acid-rinsed sample bottles were first field rinsed with filtered (0.45 μm) water from the sample. The sample was then sub-sampled into bottles for anion (acidified to pH < 3 using 1M ultra pure nitric acid), cation, TDIC ($BaCO_3$ was precipitated by adding *c.* 15% of $BaCl_2$-NaOH solution to the sample and then sealing the sample vessel with the minimum of headspace) and oxygen and hydrogen isotope analysis. At the same time the temperature, pH, conductivity, alkalinity and silica (Hach colormetric test) were measured.

4.4.3 Alkalinity

Alkalinity was determination by constructing a titration curve from measurements of pH versus volume of strong acid titrant added to the sample in small increments. The endpoints for titration are taken as the inflection points on the titration curve.

Particulates can affect strong acid by dissolution, adsorption, or ion exchange and, thereby, cause anomalously high measurements (Wood, 1976). For this reason, filtration through a 0.45 μm in-line filter was necessary. Ground water usually contains far less particulate matter than surface water but it was still filtered prior to analysis. Direct sunlight can warm the sample appreciably, causing loss of carbon dioxide, thus the samples were stored in darkness at 5°C.

The procedure used was to standardize the pH meter using fresh buffer solutions of known pH. Rinse the electrode thoroughly (at least 3 times) with filtered

sample water, and adjust the temperature of the titrant to +2°C of the sample temperature. Measure and record the pH value of the freshly-collected representative sample. Then decant 50 ml of sample into a clean dry 150 ml beaker and insert the pH probe and a teflon stirring bar.

If the pH was greater than 8.3, sulfuric acid was added from the micro-dispenser. The volume delivered and pH, after allowing 15-20 seconds for equilibration, was recorded until the pH was below 8.0. Once the pH was < 8.0 additional acid was titrated rapidly until pH 5.0 was reached, recording the volume of titrant at pH 5.0. Between pH 5.0 and 4.0, acid was added slowly and the pH recorded after each addition. The pH generally stabilized around 3.

The sample's alkalinity was calculated using the USGS alkalinity calculator (http://oregon.usgs.gov/alk) which can use a range of methods (inflection point, fixed endpoint, theoretical carbonate titration curve 1 and 2, and gran function plot (http://oregon.usgs.gov/alk/methods.html)) to determine the carbonate and bicarbonate endpoints. The inflection point method which determines the carbonate and bicarbonate endpoints in the titration by finding the greatest change in the measured pH per unit volume of acid added, was used. After these equivalence points are found, the alkalinity calculator calculates the hydroxide, carbonate, and bicarbonate concentrations in the sample.

4.4.4 TDS

Often associations are made between EC of water, which is a function of the types and quantities of dissolved substances and the total dissolved solid (TDS) content.

However, there is no universal linear relation between TDS and the EC of a sample.

The TDS content of 192 surface water samples collected from the Okavango between March 2001 and July 2002 (Appendix 15) and 34 groundwater samples collected from the Okavango and Ngami area (Appendix 16) were analysed using the standard gravitational method of desiccating a known volume (~50 ml) of filtered (0.45 μm) sample water at 180°C in an air-circulation oven. After cooling in a desiccator the mass of the residue divided by the volume from which was derived is equal to the TDS in mg/l.

4.4.5 Anion and Cation Analysis of Ground and Surface Waters

Anion analysis of 13 ground water samples from the Ngami and Okavango study area and 191 surface water samples from the Okavango alluvial fan was conducted using the Dionex DX500 and Peaknet 4.11 software. The same protocol as described in section 4.3.11 was followed with samples being pre-filtered at 0.2 μm with Whatman syringe filters prior to injection into the column.

Cation analyses of the same 191 surface and 13 ground water samples (Appendix 17) were conducted using a combination of AAS (atomic absorption spectroscopy) and ICP-MS techniques. AAS was used in order to determine the approximate concentration of cations so that appropriate dilutions could be made prior to analysis on the ICP-MS.

ICP-MS samples were prepared in a similar fashion to that described in section 3.2.10. 0.2 ml of indium (internal standard) was added to a 10 ml centrifuge tube. 5 ml of sample was then added, with the total mass of sample and Indium being recorded to 2 decimal points. The total mass was then made up to 10 grams by diluting the sample with 1M ICP-MS grade nitric acid. The final mass was also recorded to 2 decimal points. Again, numerous samples were duplicated and at least 1 in 10 samples was a blank. The bulk of the analyses focussed on identifying the following elements: Li, Na, Mg, Al, K, Ca, V, Cr, Fe, Mn, Co, Ni, Cu, Zn, Rb, Sr, Ba, Th and U. In addition, a series of samples were scanned for B, Be, Y, Ag, Cd, Pb and the rare earth elements: La, Ce, Pr, Nd, Sm, Eu, Gd, Tb, Dy, Ho, Er, Tm, Yb, Lu.

4.5 Conclusion

A combination of standard descriptive geomorphic techniques, petrography, sedimentology, geochemistry, hydrochemistry and isotope geochemistry provide an impressive range of data generating techniques. When these are combined, they provide insight into mechanisms and processes of carbonate precipitation and epigenesis, hydrological flow mechanisms and the evolution of water in the Okavango alluvial fan. This information and evidence supplements existing knowledge of these processes and mechanisms and provides additional insight into critical sedimentological, geomorphological and hydrological issues within a highly sensitive environment relating to pedogenic and non-pedogenic processes of chemical sedimentation, landscape evolution, drainage reorientation and surface and ground water flow patterns within sub-basins of the Kalahari.

5. THE GEOMORPHOLOGY, PETROGRAPHY, MINERALOGY AND ISOTOPE GEOCHEMISTRY OF THE MOKALANEN FORMATION, KALAHARI GROUP AT SELECTED SITES IN THE SW KALAHARI.

5.1 Introduction

This chapter aims to provide a synthesis of previous work with new data based on the mineralogical, petrographic and geochemical analyses of samples from the Auob, Olifants, Nossob, Molopo and Kuruman Valleys (Fig 5.1). These five fluvial systems, which form a dominant geomorphic system within the SW Kalahari, can be sub-divided into a western (Auob, Olifants and Nossob Rivers) and eastern (Molopo and Kuruman Rivers) component. The catchment of the western component lies within the Precambrian geology that runs eastwards of Otjihajavara and comprises the Omieveberg range which extends into Botswana as the Ghanzi Ridge. The eastern component drains the Kaap/Ghaap Plateau (Butzer *et al.*, 1978) and the southern Botswanan Precambrian outcrops south of the Bakalahari swell near Kanye. The two sectors combine in the vicinity of Andriesvale to form the lower Molopo River.

5.2 Geomorphology

5.2.1 The Auob River Valley

The Auob River is fed by the southward draining Oanob, Usib and Skaap Rivers whose catchments lie in the Auas Mountains. Like the parallel flowing Olifants and Nossob Valleys, the upper sections of these rivers are deeply incised into the

Precambrian bedrock. The Oanob and Usib Rivers combine southwest of Rehoboth and continue southwards towards Kalkrand and Stampriet. The Skaap River similarly flows southwards through Dordabis until west of Ulenhorst where it degenerates into a series of North/South orientated pans, known as the *pannetjiesveld* (Fig 5.2). The valleys in the east (Skaap) are wider and more mature than the neighbouring drainages to the west (Oanob and Usib). NW of Stampriet the Usib and Skaap combine to form a clearly visible series of NW/SE orientated meander bends which degenerate into a series of pans after a short distance. This pan dominated region probably marks the location of the former connection between the Usib, Skaap (?) and Fish Rivers.

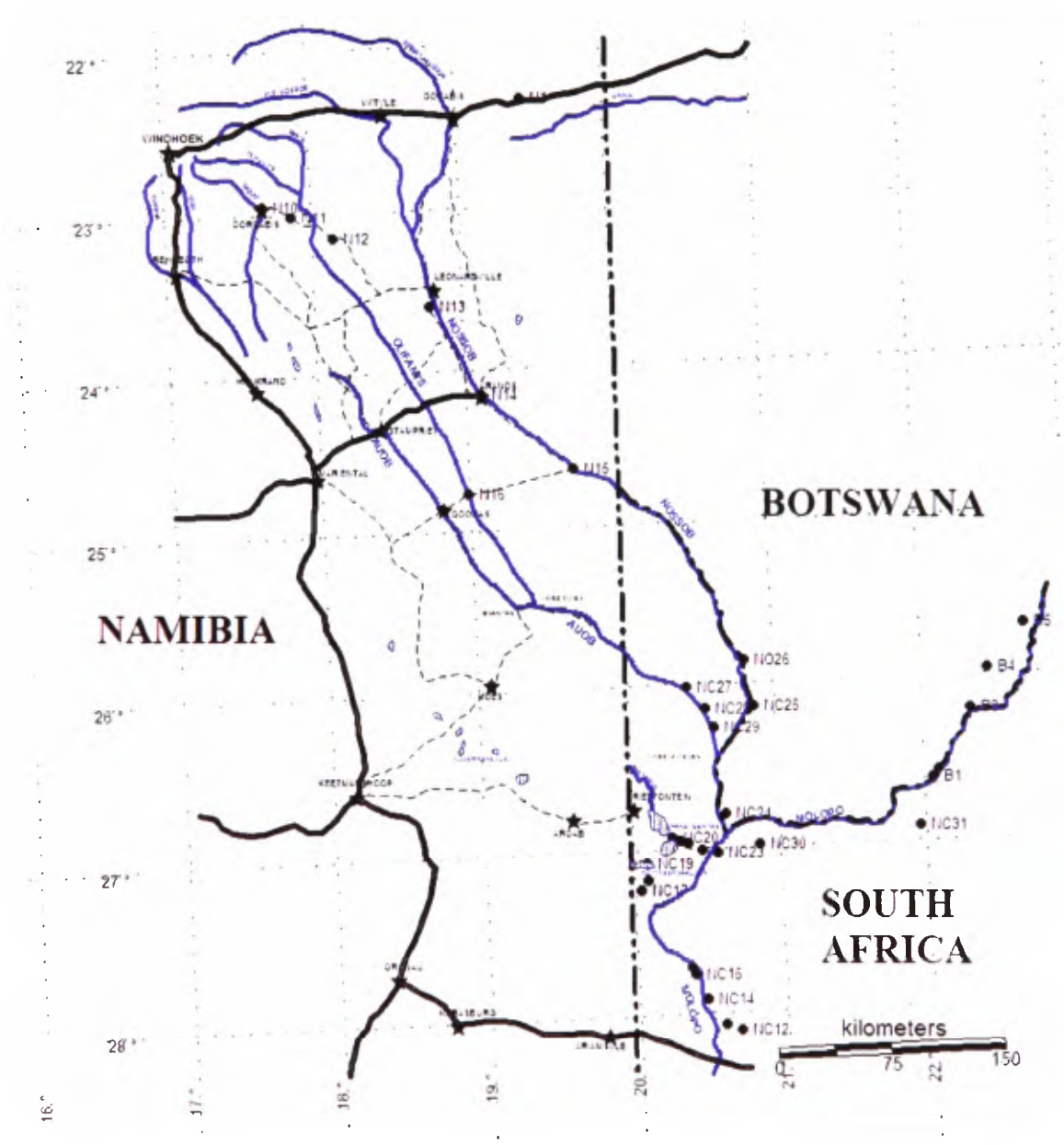


Figure 5.1: Map of the SW Kalahari showing drainages and sample sites.

South of Hoachanas the headwaters of the Auob emanate from a series of shallow artesian springs which have developed a highly pitted (evidence of sapping) dendritic drainage on the exposed carbonate cemented surface. Vogel and Van Urk (1975) calculated that the average deuterium and oxygen isotope values for groundwater are -5.28‰ and 0.48‰ respectively and radiocarbon dated this superficial phreatic aquifer at < 5000 years. These isotopic values show clear evidence of surface evaporation (Vogel and Van Urk, 1975) and therefore support the idea of localised recharge of the shallow Kalahari aquifer by infiltration of standing water, possibly from the pannetjieveld to the north. South of Lidfontein, the Auob has a well defined SSE orientated incised channel. West of Stampriet the Usib/Skaap makes a 120° turn and flows NNE to join the Auob channels near Eirup and then continues to flow SE parallel to the Olifants for another ~150 km. The lower Auob valley has a broad, flat valley which is deeply incised into the calcretised and silicified Upper Kalahari Group sediments. At Brakpan the Auob makes a sharp 90° change in direction and cuts through the 15 km wide interfluve and joins the Olifants at Tweerivier (Fig 5.3). There is no apparent physical obstruction to cause this change in direction. However, it is parallel to the Zoetfontein Fault and might be an extension of this structural lineament which may possibly account for this and some other sudden changes in direction. After this confluence, the Auob has a south-westerly orientation and continues for another 150 km before joining the Nossob at Twee Rivieren.

The significance of the Auob River to regional sedimentation and geomorphology is that it is the western most fluvial system to incise through the upper Kalahari Group sediments in the Aranos sub-basin (the most significant basin within the

SW Mega-Kalahari Basin) which have locally accumulated to > 300 m (Haddon, 1999; Haddon and McCarthy, 2005). The depositional environments, which characterised the Aranos Basin, were fed by a series of palaeo-drainages that deposited a mixture of open and closed basin fluvio-lacustrine sediments. As the basin architecture matured, the gradient decreased while at the same time piracy within the catchment caused a reduction in competence and capacity. Thus, it is highly likely that the terminal stages of deposition during the Late Miocene were characterised by a palustrine environment which underwent desiccation and stabilised with extensive pedogenesis during the Early Pliocene.

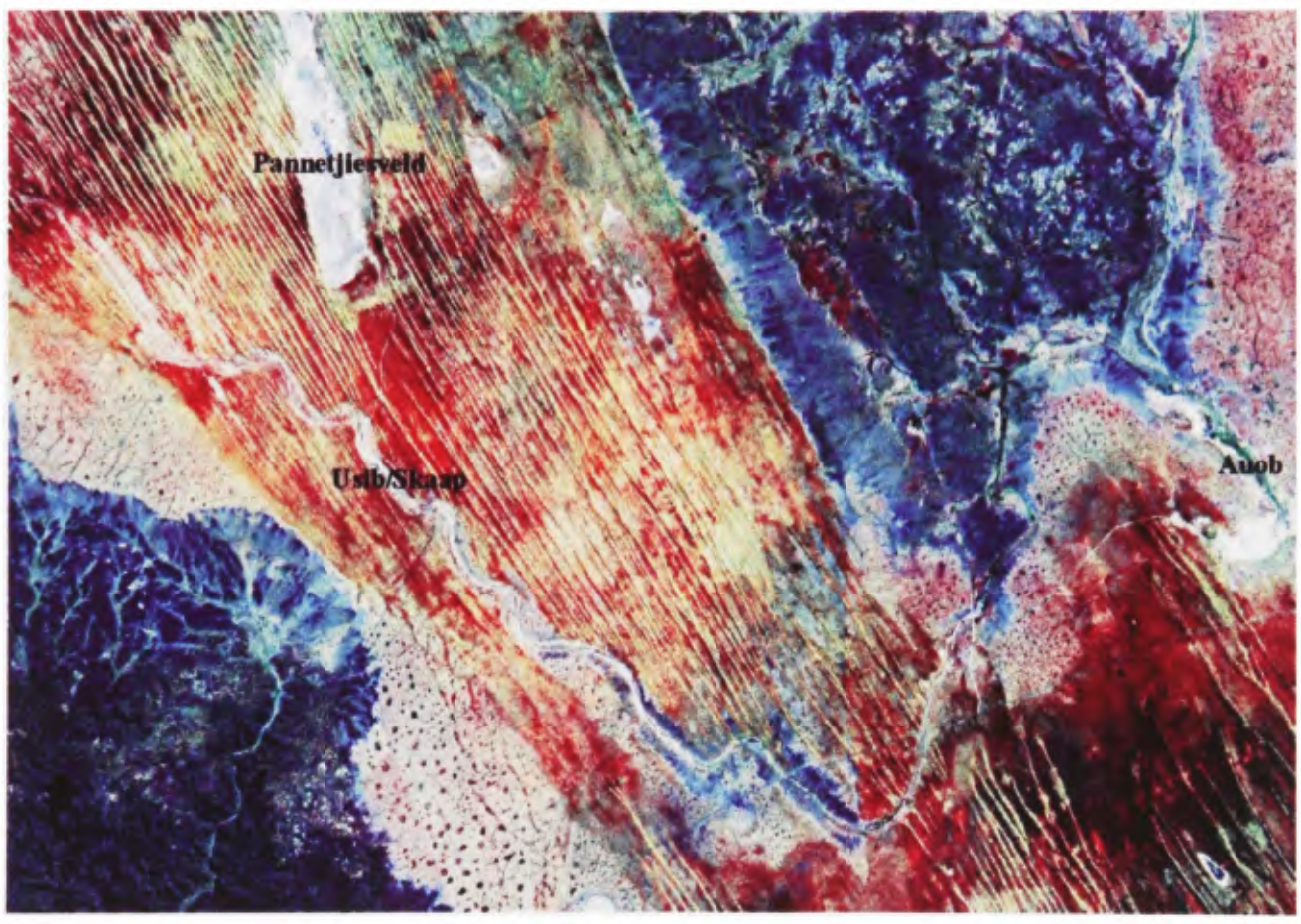


Figure 5.2: LANDSAT image of the Skaap River degenerating into the pans of the pannetjieveld and the adjacent pot-hole and incised carbonate surface among the NNW/SSE orientated linear dunes of the SW Kalahari. The Usib River to the west intersects the drainage emanating from the pannetjiesveld to form the Auob River.

The termination of deposition and initiation of incision is believed to be indicative of adjustment to Late Miocene and Early Pliocene neotectonic activity and the wetter Pliocene which energised the fluvial systems. The Oanob, Usib and Skaap Rivers, in contrast, are mostly located beyond the perimeter of the Kalahari Basin and have bedrock controlled channels which reflect limited or no sedimentation.

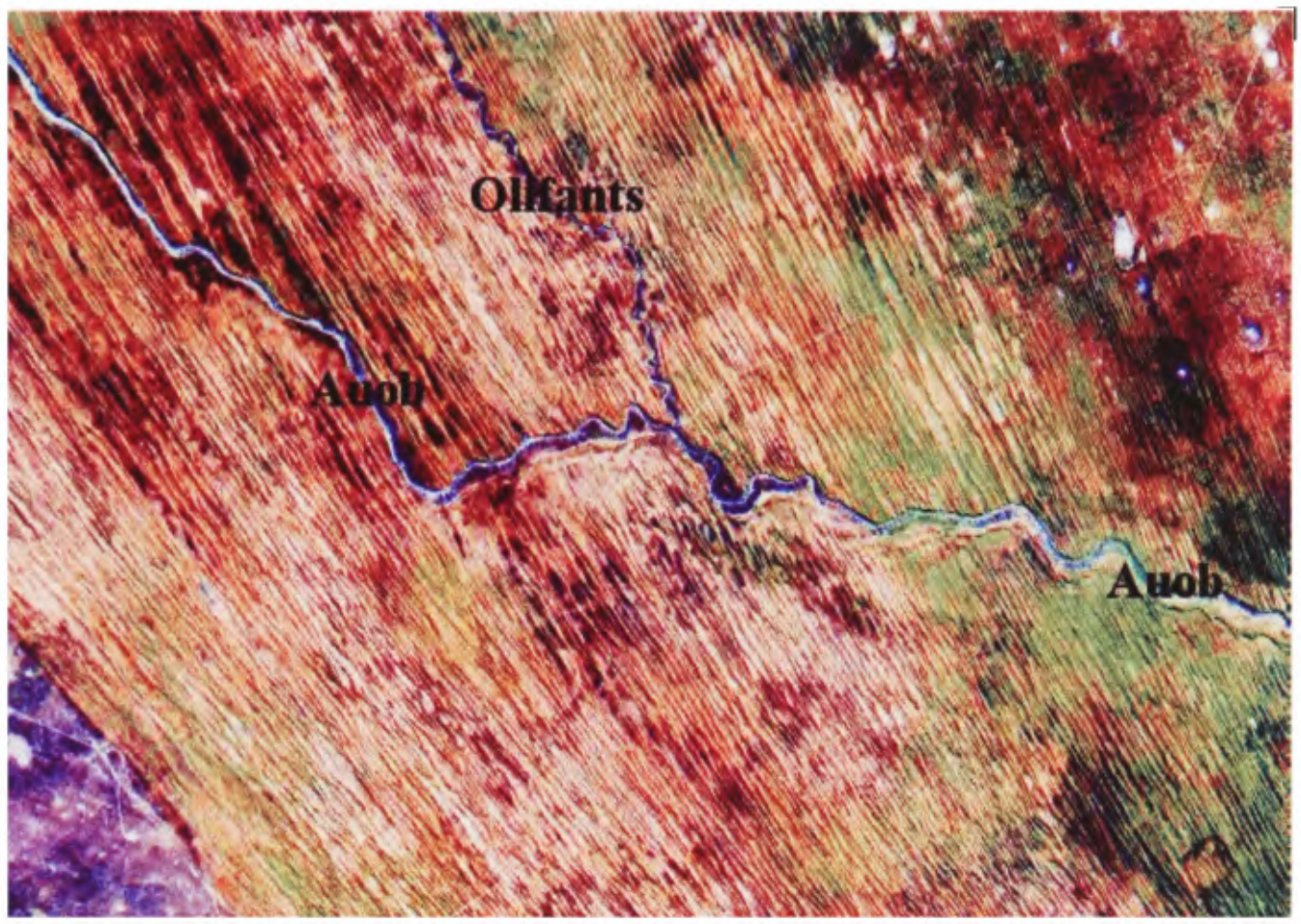


Figure 5.3: LANDSAT image of the Auob/Olifants confluence at Tweerivier.

5.2.2 The Olifants River Valley

Like the Skaap and Usib, the Olifants River's headwaters are located in the Auas Mountains. Further to the west the Seeis forms a major tributary that joins the Olifants 20 km north of Kowas. The upper Olifants is separated from the parallel flowing Skaap by the Grimmrucken and Karubeamberg. The valley in this northern section of the catchment is bedrock controlled, mature, wide and flat bottomed with shallow alluvium containing sequences of pedogenic hardpan grading into nodular and massive calcrete at depth. South of the confluence,

between the Seeis and Olifants (Fig 5.4), the Olifants flows due SSE for approximately 320 km before its confluence with the Auob at Tweerivier (Fig 5.3). The middle and lower Olifants is deeply incised into the Kalahari sediments and typically forms a wide box canyon capped by Kalahari dunes which cascade down the flanks.

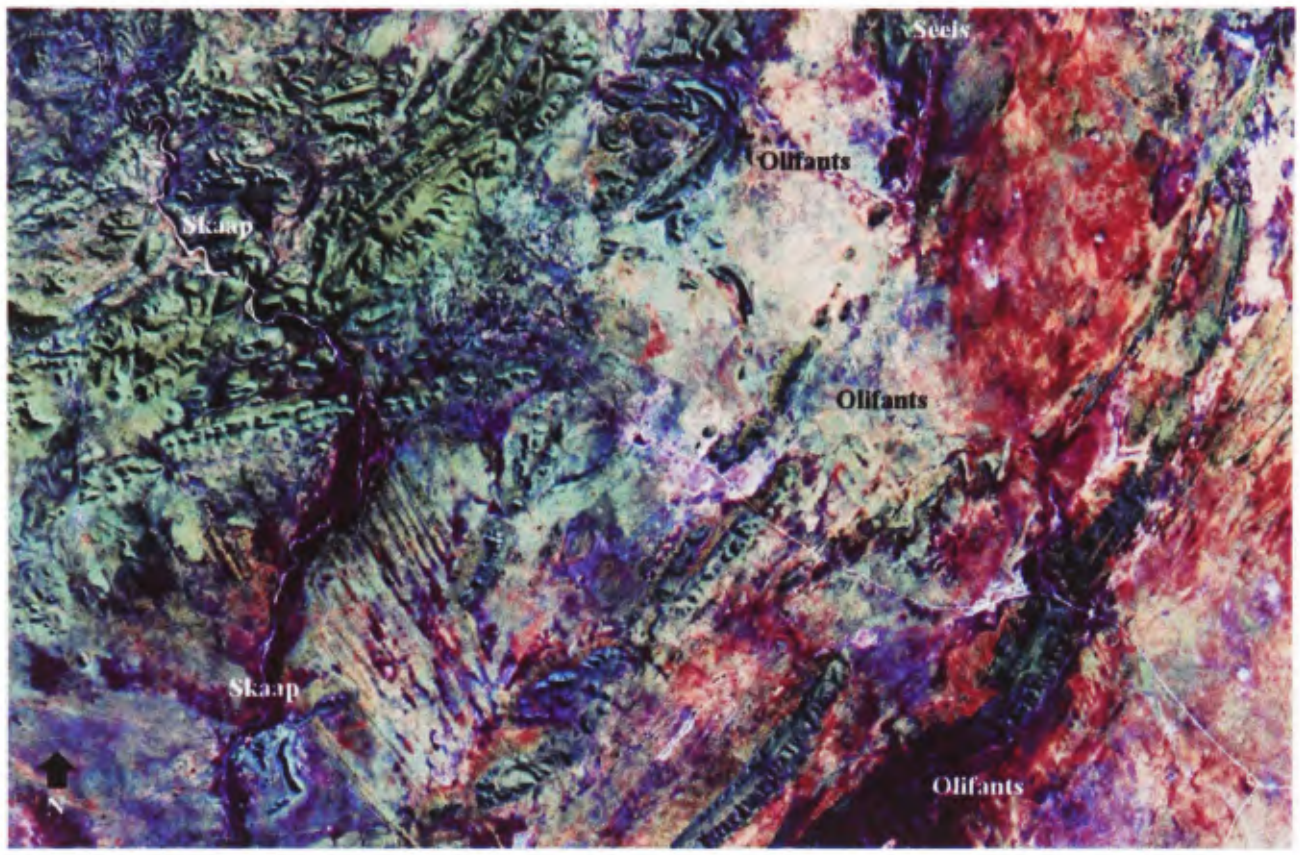


Figure 5.4: LANDSAT image of the confluence between the Olifants and Seeis Rivers and the adjacent flowing Skaap River.

5.2.3 The Nossob River Valley

Like the Olifants, the Nossob's two main tributaries (the White and Black Nossob Rivers) are located within the Auas Mountains. The White-Nossob flows as a bedrock controlled channel due east along the eastern spine of the Auas Mountains before turning southwards at Witvlei. The source of the Black-Nossob lies to the north close to the Omieveberg and flows ESE before curving southwards near Steinhausen.

The confluence of the Black and White Nossob Rivers is near Grüneberg and from this point the Nossob flows roughly SSE for almost 300 km within a broad valley incised through the Kalahari Group sediments of the Aranos Basin. At Twee Rivieren the Nossob and Auob combine and then flow southwards through a trough in the pre-Kalahari basement (the Kalahari Group sediments are significantly thicker along this corridor between the Aranos Basin and the Molopo River) for approximately another 50 km to Andriesvale where the Nossob joins the Molopo (Fig 5.5).

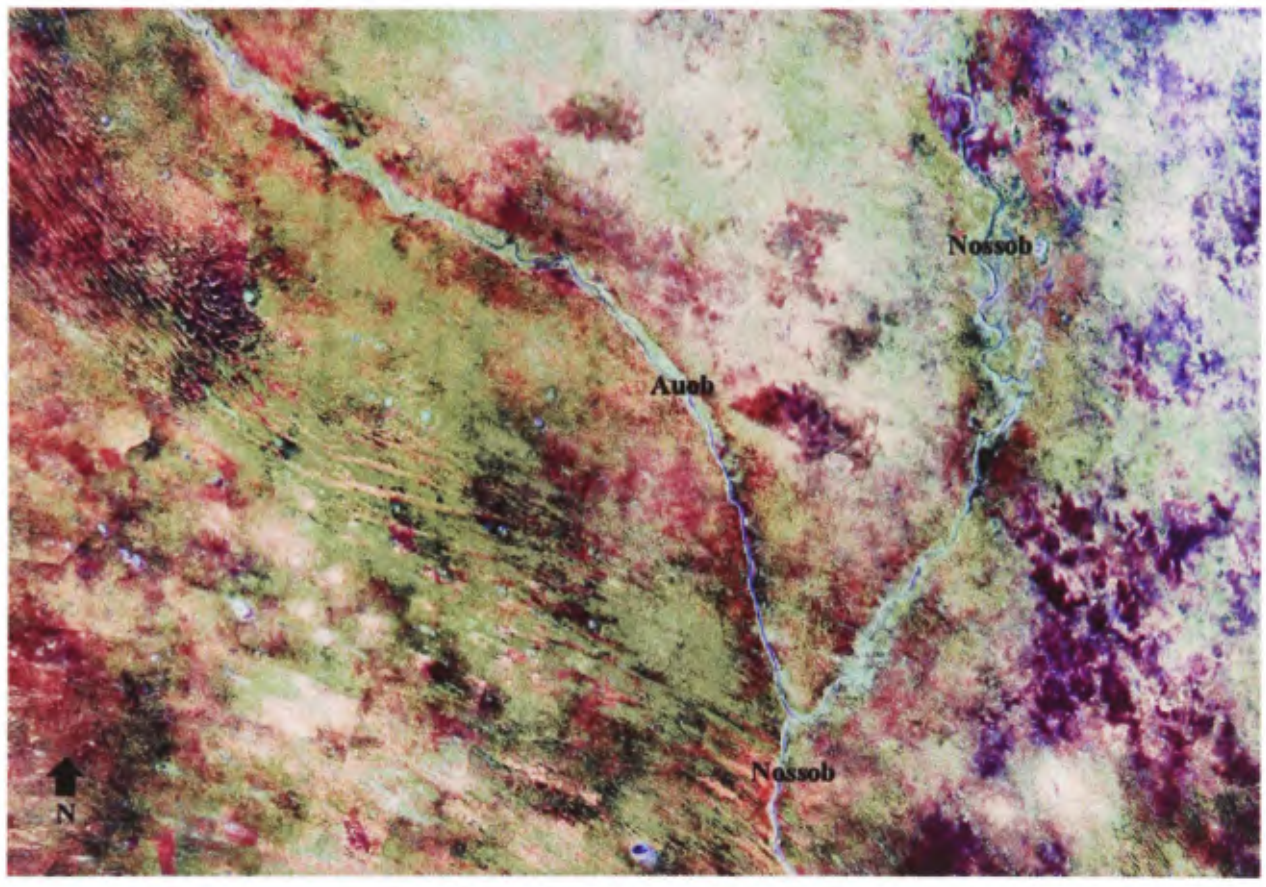


Figure 5.5: LANDSAT image of the confluence between the Auob and Nossob Rivers at Twee Rivieren.

5.2.4 The Molopo River Valley

The Molopo is a 900 km long deactivated tributary of the Orange whose catchment ranges from subhumid in the east to semi-arid and arid in the west. Work on the sediments and drainage network of the Molopo (Bootsman, 1997; 1998; Haddon, 2005) has shown the complexity of the system and the underlying

pre-Kalahari geology. The development of the Molopo drainage, like the Auob, Olifants and Nossob, is largely the result of tectonics (both large scale and localised) which was magnified by its location on the southern rim of the Kalahari Basin and resulted in a shifting of depocentres. Uplift along the Griqualand-Transvaal and Kalahari-Zimbabwe Axes (Fig 5.6) during the late Neogene (Miocene-Pliocene) (Partridge, 1997) caused the realignment of the Molopo River into its present course. Increased rainfall during the Pliocene (Tyson and Partridge, 2000; Dupont *et al.*, 2005) led to fluvial incision into the uplifted underlying sediments of the Kalahari Group and resulted in the breaching of the southern rim of the Kalahari Basin (Bootsman 1997, 1998). A return to arid conditions at the end of the Pliocene saw the cessation of flow in the lower Molopo and the mobilisation of aeolian sand.

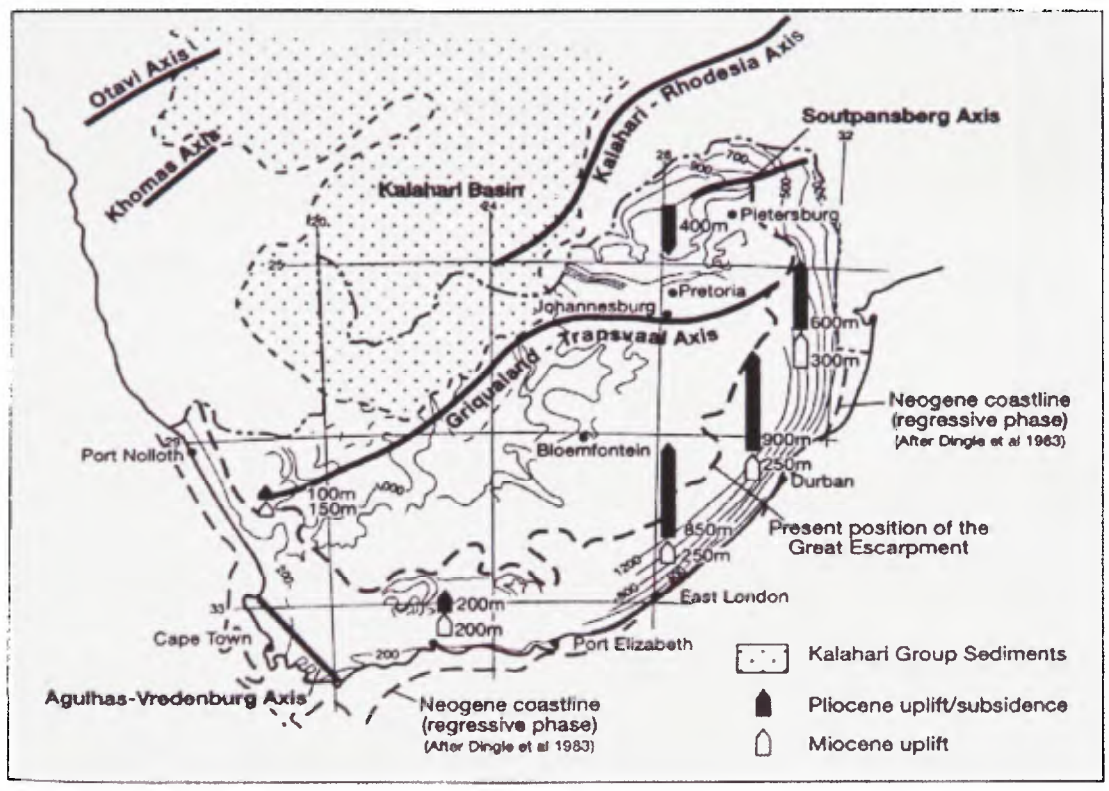


Figure 5.6: Neogene uplift within southern Africa after Partridge and Maud (2000).

The source of the contemporary Molopo comprises a number of small tributaries which drain the western margin of the Ghaap/Kaap Plateau. The Molopo initially

drains in a NW direction for approximately 240 km before swinging around to the SW near Werda in a large arc north of a local high point at 1009 m on the Kalahari Plateau associated with the Bakalahari swell (Ringrose *et al.*, 2002). For approximately the next 350 km of its course, the Molopo River drains in a SW direction until its confluence with the Nossob at Bokspit (Fig 5.7).

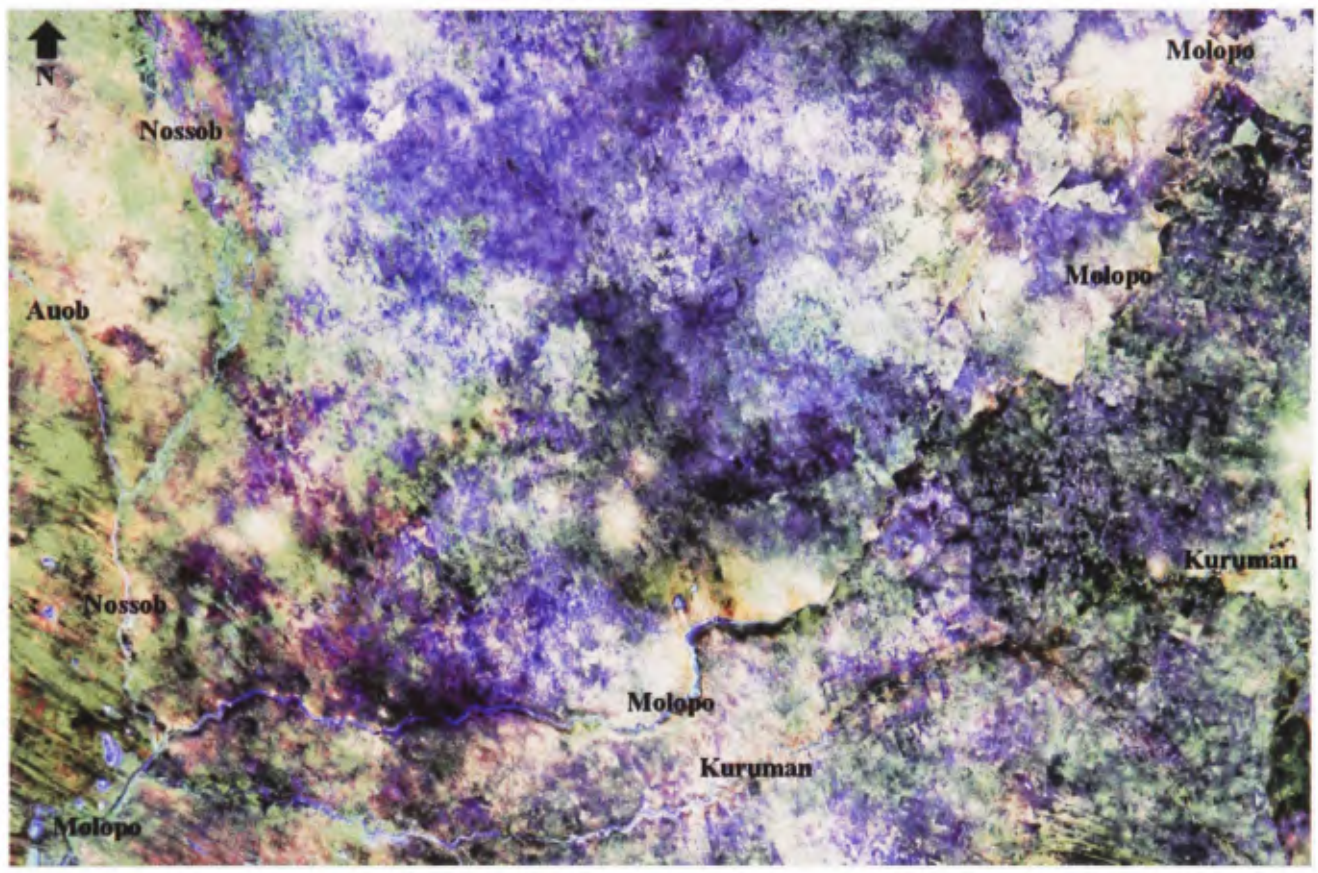


Figure 5.7: LANDSAT image of the middle and lower course of the Molopo drainage.

The geology of the drainage area can be divided into two regionally distinct groups to the west and east of Mafikeng. The eastern group consists of Ventersdorp Lavas, the Pretoria Group including the Malmani Dolomite Subgroup and the rocks of the Bushveld Basin including the Pilanesberg complex. The western group is dominated by Kalahari Group sediments, which thicken southwards towards the SW-NE orientated Moshaweng trough (Haddon, 1999). These Kalahari Group sediments reach a thickness in excess of 120 m and have been assigned to the Lonely, Goeboe Goeboe, Gordonia, Mokalanen, Eden,

Budin, Wessels and Obobogorop Formations (although not all have been approved by SACS – SACS, 1980)(Table 5.1).

Kalahari Group Sediments in South Africa				
Age	**Formal Name**	**Other Names**	**Description**	**Proposed by**
Quaternary	Lonely Formation		Soft diatomaceous limestone, up to 2m thick in river bluffs. Located along the Kuruman River and in some pans in the northern Cape.	Thomas (1981)
Quaternary	Goeboe Goeboe Formation		Brown to white sandy sediments occurring in pans in the area north of Upington, northern Cape.	Thomas (1981)
Quaternary	Gordonia Formation	Kalahari Sand	A very variable thickness of cover sands (white, yellow, brown and red) together with fossil dunes. North of Upington normally overlies calcretes of the Mokalanen Formation, elsewhere resting unconformably on various older units. Occurs north of the Orange and Vaal Rivers between 20E and 26E, with isolated outliers outside this area.	P.J. Smit (1979)
Miocene	Mokalanen Formation	Kalahari Limestone	Comprises a basal sharpstone calc-conglomerate (up to 2m thick), nodular calcrete (up to 20m thick) and an upper hardpan calcrete (up to 2m thick). Up to 48m of calcrete have been reported from boreholes. Overlies the Eden Formation or various older formations and overlain by the Gordonia Formation.	Thomas (1981)
	Eden (Sandstone) Formation	Older Kalahari Sand	Clayey calcareous sandstone with minor "grit" and conglomerate, between 20-100m thick. Overlies the Budin Formation and overlain by calcrete (Mokalanen Formation) or the Gordonia Formation. Occurs in the area north of Upington and Kuruman, cropping out in pans and along river courses.	P.J. Smit (1979)
	Budin (Clay) Formation	Kalahari Marl / Kalahari red clay	Red, calcareous gravelly clays up to 100m thick. Overlies the Wessels (Gravel) Formation and underlies the Eden (Sandstone) Formation. Confined to palaeoriver systems. Occurs in the area north of Upington and Kuruman	P.J. Smit (1979)
	Wessels (Gravel) Formation		Up to 100m of gravel and clayey gravel. Located at the base of the Kalahari Group, unconformably overlying older formations and overlain by the Budin Formation. Mainly confined to palaeovalleys in the area north of Upington and Kuruman.	P.J. Smit (1979)
Oldest (Cenozoic)	Obobogorop Formation		Gravels comprising a great variety of subangular clasts, derived from weathering of the Dwyka Group. Generally overlies Karoo Sequence strata, but in places rests on calcrete or rocks of the Nama Group. Located in the northern Cape, north of Upington.	Thomas (1981)

Table 5.1: Kalahari Group sediments in South Africa

5.2.5 The Kuruman River Valley

The Kuruman shares many of the characteristics of the parallel flowing Molopo. The upstream end of the system is perennial, fed by a series of dolomite springs, the most famous being the eye of Kuruman (Thomas and Shaw, 1991). The majority of water percolates into the stream bed only a few kilometres downstream of its source and it is only during high rainfall events that the river flows its entire length within the 'sand river' channel on the floor of the incised valley (Thomas and Shaw, 1991). Of significance to sedimentation and basin architecture in this part of the SW Kalahari, are the series of tributaries (Phepane and Moshaweng) that join the Molopo and Kuruman from the Molopo sub-basin to the north of the Morokweng impact structure (Haddon, 1999; Haddon and

McCarthy, 2005). These fluvial systems suggest that significant reorientation has occurred as the depocentres have matured.



Figure 5.8: (a) Photograph of Kalahari dunes capping the upper surface of the incised Olifants River. (b) Photograph of the profile exposed in the northern bank of the incised Auob River at site NC27.

5.3 Lithofacies of the Mokalanen Formation

Although not formally accepted by SACS, the Mokalanen Formation has been defined by Thomas (1981) as the uppermost carbonate cemented sandstone in the Northern Cape of South Africa. Visser (1957) described the same formation as the Kalahari Limestone, which he mapped into Namibia and Botswana. In keeping with both Visser (1957) and Thomas (1981), it is believed that the lithologic unit definable as the Mokalanen Formation can be mapped throughout the SW Kalahari.

Lithostratigraphic correlation within the Kalahari is extremely difficult (Thomas and Shaw, 1991) particularly due to the lack of exposure (*c.f.* Nash and McLaren, 2003). However, the steep sided valleys of the SW Kalahari provide hundreds of kilometres of nearly continuous exposures of upper Kalahari Group sediments. A range of samples belonging to the Mokalanen Formation were collected from quarry sections in the floor and walls of these valleys, which are incised 10-50 m

below the surrounding dune covered surface (Figs 5.8a and b). Kalahari Group sediments are locally highly variable in thickness (Haddon, 1999; Haddon and McCarthy, 2005) but a general sequence throughout the SW Kalahari consists of an upper hardpan unit which grades into a nodular then massive carbonate. These intergrade chemical and clastic sediments have variable dominant mineralogies (silica, calcite or dolomite), degrees of consolidation and often contain a conglomeratic member which is exposed at varying elevations within the interfluves and valley walls (Boocock and Van Straten, 1962; Watts, 1980; Thomas, 1981; Summerfield, 1982).



Figure 5.9: Photograph of the incised lower Auob River Valley.

5.3.1 Channel Carbonates

The contemporary valley sediments of the Nossob and Auob Rivers (Fig 5.9) are underlain by a laminated hardpan dolomitic calcrete. This valley hardpan has formed as a result of alteration and recrystallisation of the underlying lower sandy dolo/limestone unit of the Mokalanen Formation. The petrography is dominated by a micro-laminated micrite fabric with patches of extremely dense micrite and micrite coated detrital grains and peloids (Fig 5.10a). Within this micrite fabric are numerous rhizolith structures, channels, vugs and fractures (Fig 5.10b). Lithoclasts of the original sandy dolo/limestone, which contain etched detrital

grains within a mixed calcite and dolomite cement (Fig 5.10c), are abundant throughout the fabric. Towards the gradational base of the hardpan the detrital grain component increases as the influence of the precipitated/recrystallised dolomitic calcrete is reduced and the primary grain supported dolo/limestone fabric reasserts its dominance.

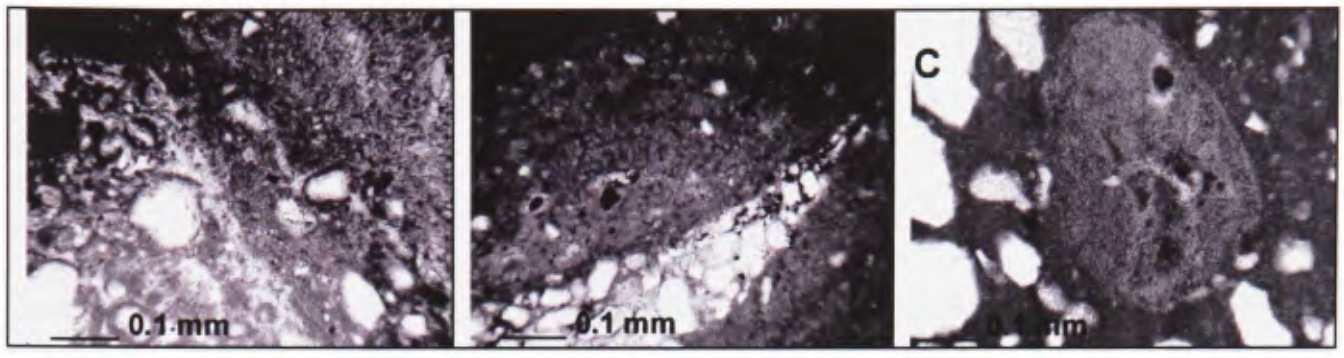


Figure 5.10: PPL thin-section photomicrographs: (a) Extremely dense micrite (upper right) and micrite coated detrital quartz grains and peloids cemented by sparmicrite (lower left) (b) cavity within the dense micrite fabric filled with detrital quartz grains cemented by a late stage micrite (c) lithoclast of the sandy dolo/limestone with small remnant detrital grains floating within the later micrite fabric with detrital quartz grains.

5.3.2 Hardpan Calcrete

The upper surface of the Mokalanen Formation consists of a hardpan calcrete which may be buried beneath a horizon of unconsolidated red/brown (limonite grain coatings) aeolian sand (Gordonia Formation in the Northern Cape of South Africa). The upper surface of the hardpan is characterised by a dense, micro-laminated micrite (Fig 5.11a), largely devoid of detrital grains or containing dispersed highly corroded or partially micritised allochems. Below the centimetre thick micro-laminated hardpan the micritic fabric becomes increasingly biogenic in character with abundant alveolar septal structures and fenestrae (Fig 5.11b). This fabric also contains numerous micrite peloids, intraclasts, rhizoliths, tubules, coated grains, pisoliths and ooids (Fig 5.11c). There is evidence of extensive

micritisation of the allochems with many of the detrital quartz grains showing distinctive etching features. Towards the base of the upper hardpan zone the micrite fabric becomes less dense and is characterised by alveolar septal structures, sparite filled vugs and micrite peloids which float within a sparmicrite cement (Fig 5.11d). With increasing depth the micrite becomes extremely patchy and a sparite fabric becomes dominant (Fig 5.11e). This transition zone is believed to demarcate the lower limit of micritisation, which is the result of near surface biological, pedogenic and crystalline precipitation/modification mechanisms. The proportional volume of detrital quartz allochems increases substantially towards the base of the profile which is grain supported (Fig 5.11f) rather than fabric supported. This change in fabric texture, degree of allochem modification and mineralogy reflects a change to the geochemical mechanisms operational at these deeper levels.

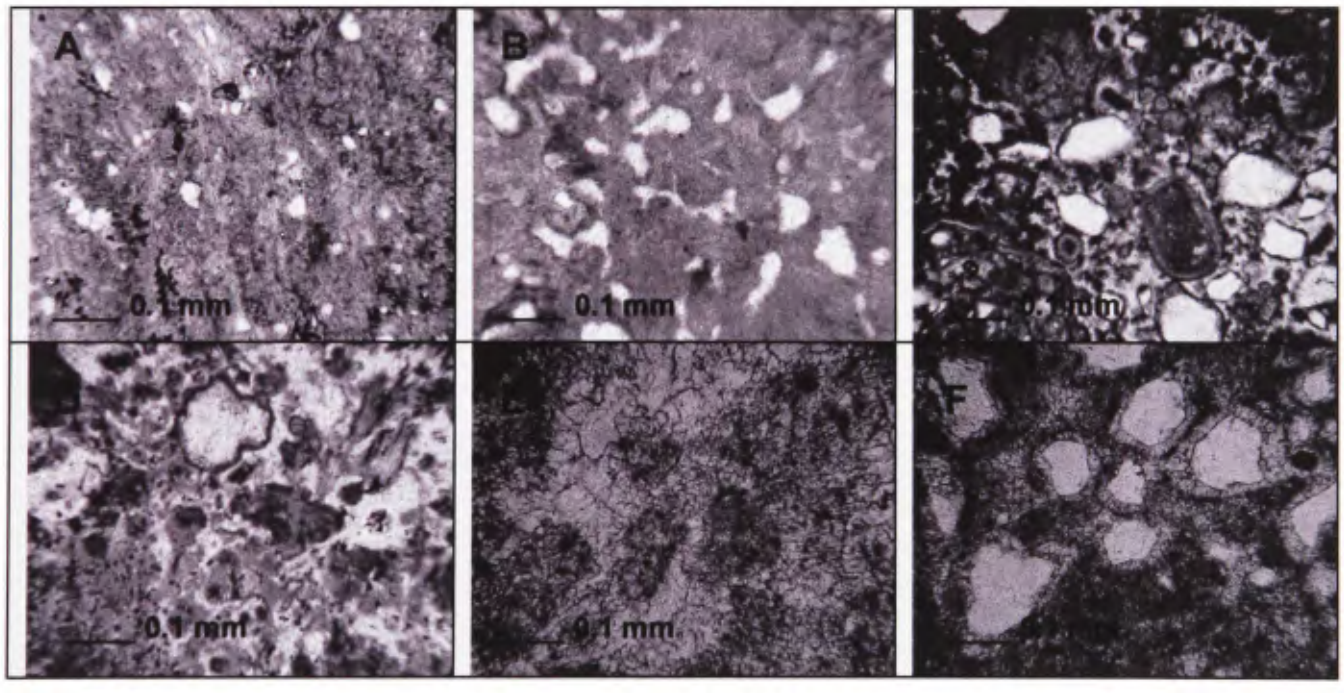


Figure 5.11: PPL thin-section photomicrographs: (a) micro-laminated micrite with dispersed floating corroded detrital quartz grains (b) fenestrae within the dense micrite fabric (c) micrite coated grains, pisoliths and ooids floating in a sparmicrite fabric (d) sparite filled vugs and micrite peloids floating within a sparmicrite cement (e) sparite

fabric with patches of sparmicrite (f) increased detrital quartz content with sparry haloes towards the base of the hardpan unit.

5.3.3 Intergrade Nodular Carbonate

The gradational boundary between the upper hardpan and the underlying nodular zone (Fig 5.12) reflects a transition from a dense micrite fabric to a less dense mixed micrite and sparmicrite fabric (Fig 5.13a). This change in fabric is reflected in the well consolidated nodular calcrete which floats in a poorly consolidated powdery matrix. Petrography reveals that the fabric of the nodules is composed of sparmicrite and sparite with limited floating, highly etched detrital grains while the powdery matrix comprises a more open fabric of micrite and sparmicrite bridge, pendant and meniscus structures, pelletal sparmicrite (Fig 5.13b) and coated detrital grains. Authigenic quartz becomes more abundant down-profile and has precipitated within fractures (Fig 5.13c), fenestrae, vugs and as fibrous grain coatings which have often partially replaced the original sparite haloes. Zones of dolomite cement are also present in association with authigenic quartz in the lower section of the horizon and reflect partial dolomitisation of the crystalline calcite fabric.



Figure 5.12: A nodular intergrade carbonate profile capped by hardpan exposed at site NC28.

Down-profile the nodules coalesce to form a moderately to well consolidated honeycomb intergrade carbonate which then grades into the massive intergrade carbonate. This gradation reflects a transition to an arenite cemented by sparmicrite, sparite crystals of various sizes, authigenic quartz and dolomite. This transition also reveals significant changes within the fabrics micromorphology which indicates a reduction in the influence of biogenic mechanisms on precipitation and the eventual dominance of pure alpha crystalline fabrics.

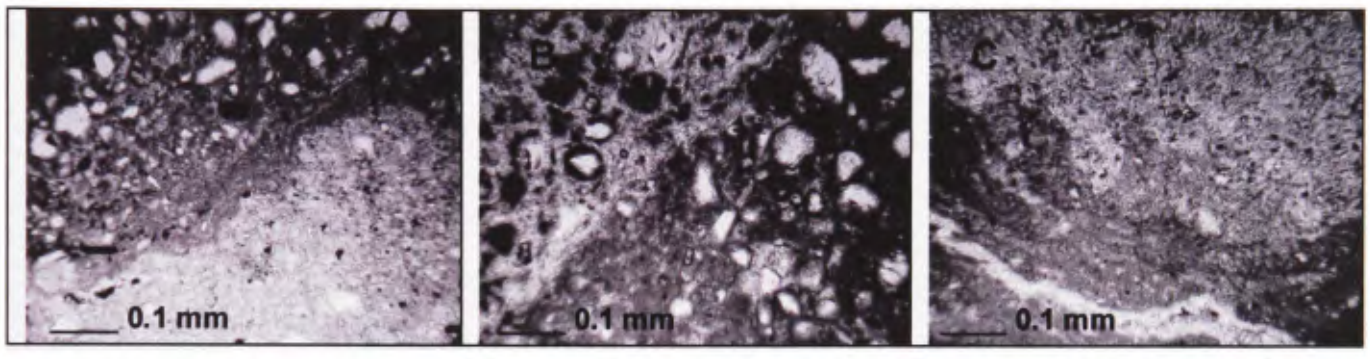


Figure 5.13: PPL thin-section photomicrographs: (a) transition from a dense micrite fabric with abundant floating detrital quartz grains to a less dense sparmicrite fabric (b) pelletal micrite and micrite coated detrital quartz grains floating in a sparmicrite fabric (c) authigenic microcrystalline quartz precipitated as fracture and vug fills within the micrite and sparmicrite fabric.



Figure 5.14: The moderately consolidated upper massive unit of the Mokalanen Formation exposed along the upper terrace of the Kuruman Valley at site NC23.

5.3.4 Massive Intergrade Carbonate

The sandy textured massive carbonate of the Mokalanen Formation can be described as a carbonate and silica cemented arenite and sub-divided into two basic units. The moderately consolidated upper massive unit (Fig 5.14) is characterised by a simple calcitic dolocrete replacement fabric consisting of coarse, crystalline dolomite, abundant authigenic silica, and sparry calcite (Fig 5.15a). Silica is typically associated with channels, fractures and vugs (Fig 5.15b), while dolomite and calcite coat the numerous floating corroded detrital grains (Fig 5.15c).

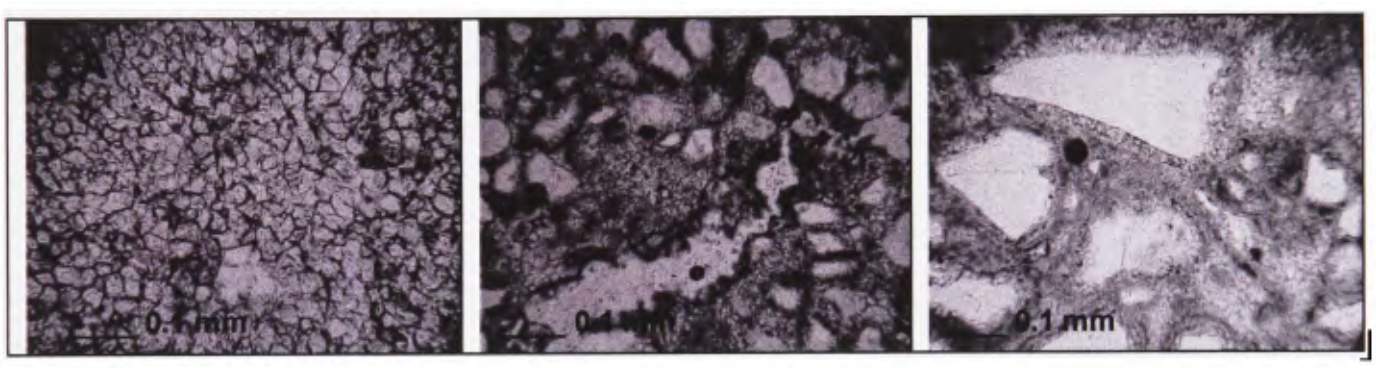


Figure 5.15: PPL thin-section photomicrographs: (a) Coarse, crystalline dolomite, authigenic silica, and sparry calcite fabric (b) authigenic silica lined vug within the sparmicrite fabric (c) dolomicrite and sparmicrite coated floating corroded detrital quartz grains

The well consolidated sandy lower massive unit can be identified by a distinct unconformity in the massive horizon (Fig 5.16), which is interpreted as a significant depositional hiatus or change in depositional environment. This unit consists of a finely crystalline, brown coloured micrite and sparmicrite fabric that has undergone partial silicification and dolomitisation and can be classified as a dolomitic calcrete. The fabric contains numerous highly etched and partially replaced floating detrital grains which show pendant structures, grain coatings and druses (Fig 5.17a). Numerous micrite peloids, glaebules (Fig 5.17b), intraclasts,

lithoclasts, biotubes, bioclasts (either disarticulated ostracods (Fig 5.17c) or diatoms), microspar filled vugs, fenestrae and fractures suggest that the sediments experienced periods of flooding, desiccation and pedogenesis prior to burial.



Figure 5.16: Photograph of the unconformity between the upper and lower sandy massive carbonate units of the Mokalanen Formations at site NC25.

At a number of locations, biotubes (Fig 5.18) have weathered out of the lower unit. These oval biotubes are filled with the same carbonate cemented sandstone as the surrounding matrix, although they appear to be slightly better cemented and as a result these delicate structures have weathered out as positive features. Two types of biotubes are exposed: the majority are root casts (rhizoliths – Klappa, 1980a) which have the inner carbonate cemented sand encased in a thin layer (~ 1 mm) of calcite. The second type comprises burrows or tap roots which lack the calcite coating layer and as a result, although the clasts are exposed as positive features, are far more fragile. The preservation of macro biogenic structures within the sediments reflects the role of evapotranspirational pumping in the precipitation of the carbonate cement.

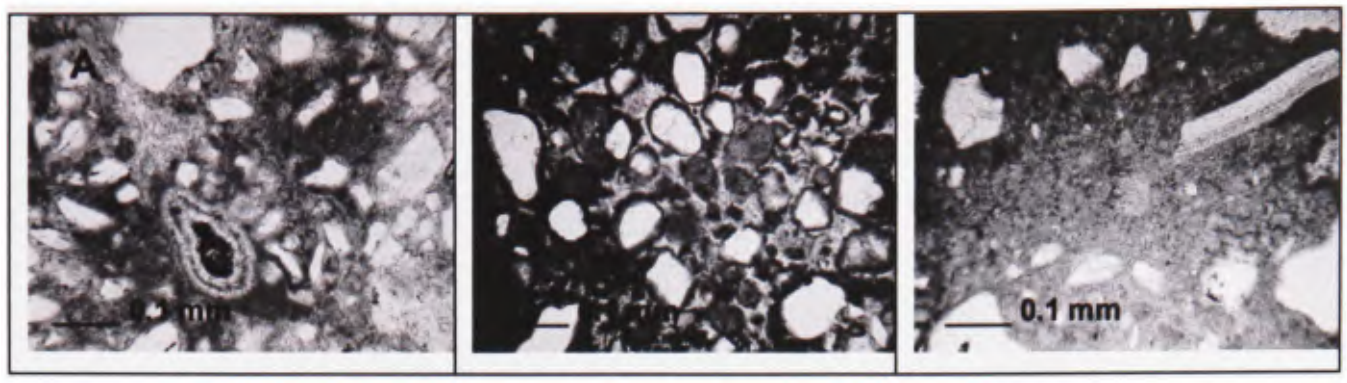


Figure 5.17: PPL thin-section photomicrographs: (a) micrite and sparmicrite fabric with numerous floating corroded detrital quartz grains and a central cavity lined with sparmicrite and micrite (b) pelletal micrite, peloids and coated detrital quartz grains floating in a sparmicrite fabric (c) bioclast (possibly a fragment of ostracod?) floating in the micrite fabric with corroded detrital quartz grains.

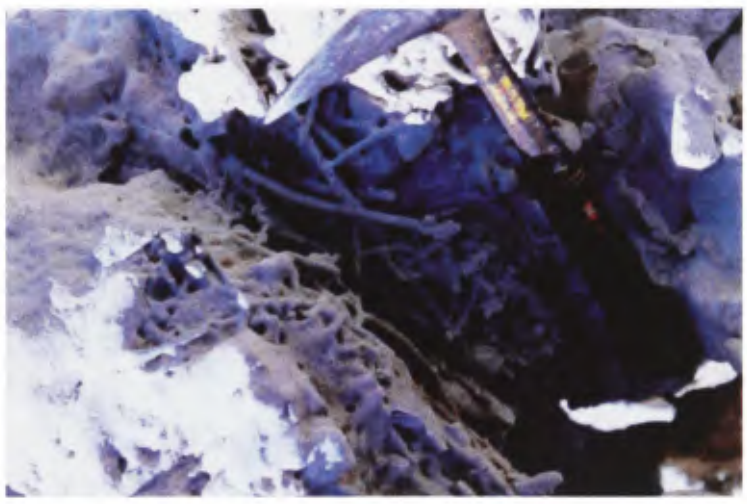


Figure 5.18: Photograph of biotubes weathered out of the carbonate at site NC25.

Both massive units contain abundant ferric iron and manganese oxides and hydroxides, often in the form of nodules (Fig 5.19) and pisoliths, along with authigenic minerals such as goethite and K-feldspar, which are believed to reflect epigenesis, modification and reprecipitation of the original fabric under a range of pH, Eh and saline conditions. The contrasting characteristics of the two massive units, a dense poorly modified lower unit and a highly recrystallised upper unit, are believed to reflect the role of fluids in cementation. If the unconformity between the units marks a depositional hiatus, when alluvial sedimentation

resumed it was continuous and the dense lower unit may have acted as a localised aquiclude which affected hydrogeochemistry and thus calcite and silica solubility.

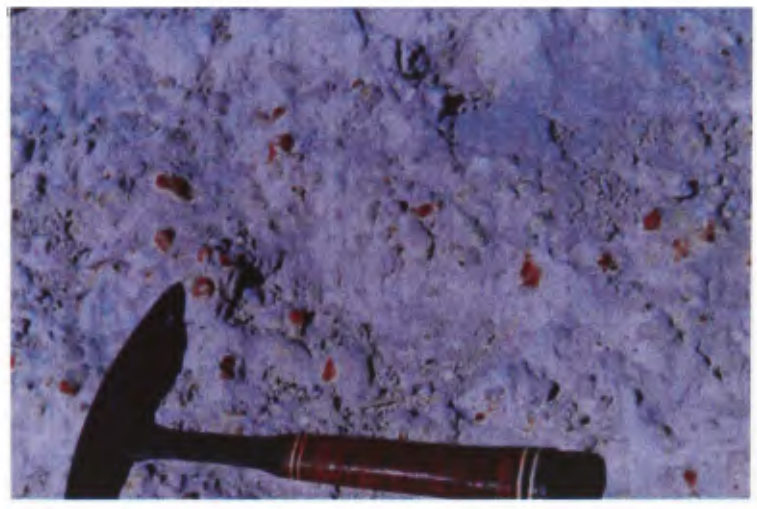


Figure 5.19: Ferric iron and manganese oxides and hydroxides nodules exposed within the upper massive intergrade carbonate.

The influence of magnesium rich saline fluids on the primary and modified fabric of the upper unit is reflected in the bulk and clay mineralogy (Table 5.2). Previous studies of Kalahari carbonates (Watts, 1980; Eitel and Blumel, 1997; Eitel, 2000) have shown that sepiolite and palygorskite clays are dominant in mature to very mature sequences and are often associated with dolomite, although the mechanism of dolomitisation is poorly understood.

It is feasible to believe that the unconformity reflects a rapid change, possibly initiated by tectonic and climatic mechanisms, from a palustrine depositional environment to a drier alluvial fan environment. The micro-structures and fine grained carbonate, which lacks the micro-lamination indicative of extensive subaerial hardpan formation, fits the model of palustrine carbonate precipitation and associated bioturbation and pedogenesis in an episodically subsiding basin as proposed by Platt (1989) and Alonso-Zarza and Calvo (2000).

	Whole Rock Analysis							< 2µm Fraction							
	Quartz	Calcite	Dolomite	Plagioclase	K-feldspar	Palygorskite	Interstratification	Quartz	Calcite	Dolomite	Mica	Palygorskite	Sepiolite	Goethite	Halloysite
NC/2000/8A	8	92	-	-	-	-	-	3	91	-	-	6	-	-	-
NC/2000/14B	30	68	-	-	-	-	2	29	9	-	9	16	36	-	-
NC/2000/23B	30	70	-	-	-	-	-	5	78	-	-	6	-	4	7
NC/2000/24B	22	74	-	-	-	4	-	10	72	-	-	10	8	-	-
NC/2000/25A	65	35	-	-	-	-	-	no < 2µm fraction analysis							
NC/2000/26A	21	67	12	-	-	-	-	no < 2µm fraction analysis							
NC/2000/27B	41	-	52	2	2	3	-	3	-	-	-	97	-	-	-
NC/2000/28B	69	20	11	-	-	-	-	no < 2µm fraction analysis							
NC/2000/29A	66	31	3	-	-	-	-	no < 2µm fraction analysis							
NC/2000/30A	30	18	58	-	-	4	-	-	87	-	-	13	-	-	-
NC/2000/30C	65	-	35	-	-	-	-	no < 2µm fraction analysis							
NC/2000/30E	75	-	19	-	6	-	-	no < 2µm fraction analysis							
NC/2000/31A	20	77	-	-	-	3	-	10	20	-	-	70	-	-	-
NC/2000/31D	64	-	31	-	-	5	-	-	10	-	-	90	-	-	-
N/2000/1A	23	75	-	-	-	-	2	no < 2µm fraction analysis							
N/2000/13A	25	75	-	-	-	-	-	no < 2µm fraction analysis							
N/2000/14A	65	35	-	-	-	-	-	no < 2µm fraction analysis							
N/2000/15A	50	39	6	-	5	-	-	no < 2µm fraction analysis							
N/2000/16B	41	31	28	-	-	-	-	no < 2µm fraction analysis							
N/2000/17B	25	39	26	-	10	-	-	no < 2µm fraction analysis							
N/2000/17C	34	57	9	-	-	-	-	no < 2µm fraction analysis							

Table 5.2: Summary of XRD analysis

5.3.5 Carbonate Cemented Conglomerate Member

A variably developed carbonate and silica cemented conglomerate member of the Mokalanen Formation is exposed at various elevations within the Auob and Nossob Valleys at sites (N13-15, N17, NC25 and NC26). The clasts of the conglomerate vary from very well/well rounded quartzite pebbles in the northern part of the basin, (Fig 5.20) which may originate for the Kamtsas and Chuos Formations, to poorly rounded sandstone clasts which produce an intra-formational conglomerate in the southern part of the basin. Thomas (1981) has described a basal sharpstone calc-conglomerate which is up to 2 m thick within the Mokalanen Formation while Summerfield (1982) and Shaw and De Vries

(1988) noted a conglomeratic silcrete, which occurred as irregular to crudely lenticular zones within the massive calcrete, and pebble beds within the Moshaweng and Letlhakeng Valleys. Based on the recorded outcrops of the conglomerate and the premise that the upper Kalahari Group has conformable gradational boundaries, there is little evidence to suggest that it can be assigned entirely to a basal unit within the Mokalanen Formation. Rather, it is believed to reflect energetic fluvial facies within the upper massive and nodular alluvial units throughout the basin. The carbonate cemented sandstone rip-up clasts of the intra-formational conglomerate support this model as they suggest that partially lithified sediment was eroded, possibly during extreme discharge events, and then redeposited within the overlying sediments possibly as the flood waters subsided and lost competence and capacity.

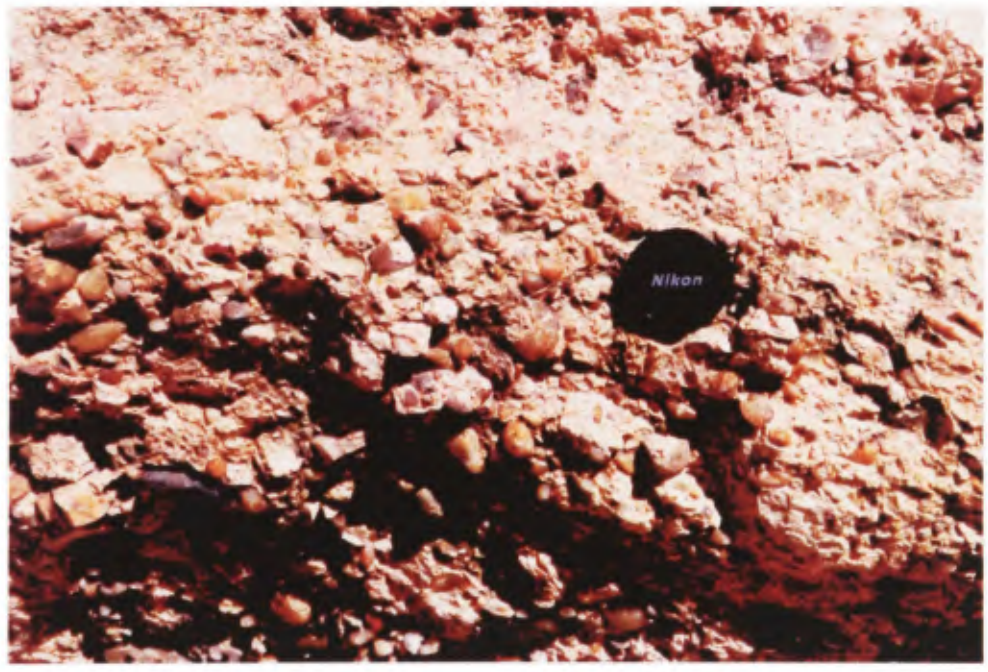


Figure 20: Photograph of well rounded quartzite clasts within the carbonate cemented conglomerate member at site N13.

The carbonate and silica cementing the conglomerate is highly variable and reflects various degrees of corrosion, recrystallisation and replacement that relates to the position of the horizon within the sequence. The majority of the

conglomerate is cemented by a mixture of crystalline calcite, dolomite and authigenic quartz, although corroded intraclasts of micrite, micritised allochems and floating micrite coated detrital quartz grains are common (Fig 5.21a), which suggest that there have been a number of stages of precipitation. The crystalline fabric is dominated by extremely well developed sparite grain coatings (Fig 5.21b) with intergranular space dominated by authigenic quartz cement and a range of dolomite crystal textures (non-planar anhedral, planar subhedral and euhedral)(Fig 5.21c).

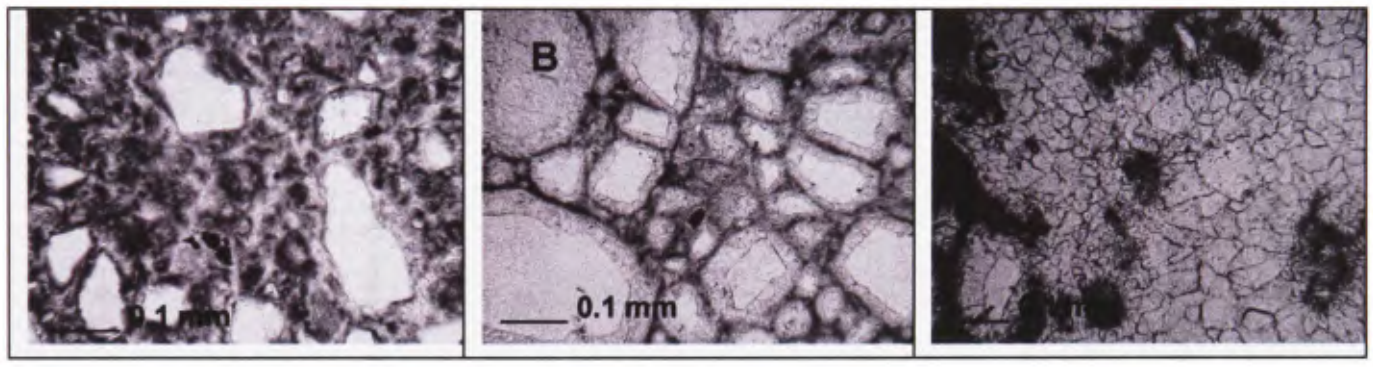


Figure 21: PPL thin-section photomicrographs: (a) detrital quartz grains with variably developed micrite grain coatings, pelletal micrite and peloids floating in a sparmicrite fabric (b) well developed sparry calcite coatings around detrital quartz grains in zones characterized by a sparmicrite fabric (c) fabric dominated by non-planar anhedral dolomite with minor authigenic silica and micrite and a single floating detrital quartz grain (lower left corner).

5.4 Isotope Geochemistry

Isotopic analysis of the dolomite at site NC27 indicated a $\delta^{13}C$ value of -3.44‰ and a $\delta^{18}O$ value of -0.94‰. This dolomite is unlikely to be representative of primary crystallisation but rather represents recrystallisation of a previous carbonate. Under these conditions the $\delta^{13}C$ value of the dolomite is generally strongly influenced by the original carbonate due to the fact that the pore-fluids involved in the recrystallisation process have low carbon contents (Tucker and

Wright, 1990, El-Sayed *et al.*, 1991). The dolomitised cement therefore believed to reflect a mixed C_3/C_4 vegetation, probably dense tree or shrub savanna which differs markedly from the contemporary C_4 dominated vegetation which consists of open savanna with occasional trees and shrubs.

Dolomite precipitated in equilibrium with calcite is approximately 3‰ to 4‰ enriched in $\delta^{18}O$ with respect to calcite. When this fractionation factor correction is applied to the $\delta^{18}O$ value it suggests that the sample was precipitated from fluids which underwent only slight evaporitic fractionation. Vogel and Van Urk (1975) recorded significantly more fractionated (0.48‰) groundwater (approximately 5000 year old) at Stampriet, which is believed to be the result of recharge emanating from the evaporitic pan system of the pannetjiesveld. In light of the minimal fractionation it is suggested that the solution from which the sil-dolocrete precipitated was recharged by infiltrating meteoric water (*cf.* Heaton *et al.*, 1983).

The use of $\delta^{18}O$ to determine the temperature of formation in dolomites is laden with problems. The main problem is the relationship between $\delta^{18}O_{water}$ and $\delta^{18}O_{dolomite}$ which is imprecisely known at the critical temperature of 15-25°C and complicated by the coexistence of dolomite and calcite (which has its own relationship between $\delta^{18}O_{water}$ and $\delta^{18}O_{calcite}$)(Land, 1980; Tucker and Wright, 1990). Thus, despite the Fritz and Smith (1970) 25-79°C fractionation equation and Friedman and O'Neil (1977) fractionation curves (using the weighted mean value of $\delta^{18}O_{SMOW}$ measured in Windhoek (-3.23‰)(IAEA, 2001)) possibly being

applicable, the calculated temperature of ~21°C using the corrected $\delta^{18}O$ value of -3.94‰ is considered too questionable, thus no direct inferences can be made.

5.5 Interpretation and Discussion

The hypothesised depositional system for the Mokalanen Formation is a sub-humid to semi-arid low gradient palustrine and alluvial fan environment which has undergone desiccation and been colonised by a mixed savanna vegetation both of which initiated pedogenic stabilisation. The conglomeratic member is believed to be an energetic fluvial (possibly distributory channels within the alluvial fan?) facies. The lithofacies, rather than the stratigraphic, context is significant as it reflects higher energy seasonal/perennial (?) palaeo-channels within the semi-arid alluvial floodplain deposits.

The widespread occurrence of authigenic palygorskite, sepiolite, K-feldspar and dolomite suggests an Mg^{2+}-rich, alkaline diagenetic and epigenetic environment is responsible for the precipitation and modification of the majority of Mokalanen Formation. The mechanisms most likely to be responsible for carbonate precipitation under high-Mg^{2+} conditions within the Kalahari are evaporation and evapotranspiration, seepage-reflux and mixing corrosion and/or precipitation/reprecipitation.

The shallow diagenetic environment experienced by the incised SW Kalahari drainages is likely to be affected by a seasonally fluctuating water table and capillary fringe, unstable wetting fronts and intense surface evaporation. As a result, solutions within the vadose zone will be subjected to salinization, thus

affecting the pH and Mg/Ca ratio of infiltrating meteoric water. The bicarbonate and carbonate content along with the Mg/Ca ratio of solutions in the vadose zone tends to be low but fluctuates seasonally due to dust fall-out and flushing by rainwater. Acidified meteoric waters in free draining sediments tend to favour silica precipitation and actively dissolve carbonaceous sediments even in Mg^{2+}-rich sediments (*cf.* Bustillo, 2001). However, if meteoric water is exposed to evaporation, the solution becomes alkaline and the pH will rise. The significance of this is the inverse solubility of silica and carbonate. Generally speaking a high pH results in carbonate precipitation and silica solution and low pH results in silica precipitation and carbonate solution. The precipitation and solution chemistry of calcite is complex but the general order of solubility dictates that the vast majority of calcite present and stable within a system is low-Mg calcite. However, in an environment such as the SW Kalahari where a sinking water-table (a result of tectonic adjustment and subsequent incision of the channels) has caused the dewatering and relocation of sediments to the capillary fringe and ultimately the vadose zone, can account for the epigenesis of the cement due to a number of silicification, calcretisation and dolomitisation events.

Recrystallisation of carbonates, silicification and associated mineralogical changes results in significant geochemical alterations. These changes commonly involve the loss of cations present within the original carbonate and gain of other trace or minor elements from the diagenetic solution. The incorporation of Fe and Mn into diagenetic low-Mg calcite or dolomite from groundwater is of particular relevance to the Kalahari. The Fe and Mn are believed to be scavenged from the Prince Albert Formation mud and siltstone, which lines the majority of the SW

Kalahari Basin. These Fe/Mn enriched carbonates provide evidence of the role played by mixing of meteoric and groundwater (*cf.* Watts, 1980; El-Sayed *et al.*, 1991) or a seepage-reflux mechanism, depending on the environmental setting, in the precipitation, corrosion and replacement of calcite by dolomite. This process is highly effective under reducing conditions below the sediment-water interface. The displacive growth characteristics and large crystal size of some dolomite is also indicative of this precipitation mechanism. The presence of abundant authigenic goethite, which precipitates from solutions enriched in iron, provides additional evidence of the phreatic mechanisms responsible for the carbonate precipitation.

However, a significant fraction of Kalahari dolomite is meteoric and associated with vadose zone precipitation. There is also no doubt that recrystallisation and stabilisation of dolomite crystals precipitated within either the phreatic or vadose zone has occurred within the upper horizons under meteoric diagenetic conditions and thus, can be used as an indicator of carbonate profile maturity as suggested by Watts (1980) and El-Sayed *et al.* (1991). This vadose zone maturity complements previous non-pedogenic carbonate studies (Mann and Horwitz, 1979; Arakel and McConchie, 1982; Arakel, 1986a,b; Wright and Tucker, 1991; Nash *et al.*, 1994a,b; Watson and Nash, 1997; Nash, 1997; Nash and McLaren, 2003) which suggest that calcretes and dolocretes formed in a phreatic setting do not develop mature profiles where carbonate decreases down-profile, but tend to be brecciated or massive in character.

Climatic conditions have a major influence on chemical cementation. Climate controls the availability of meteoric water and groundwater, its flux, temperature, and biological factors such as soil cover and type of vegetation (Tucker and Wright, 1990). Arid conditions are generally associated with slow rates of meteoric alteration due to limited infiltration and reduced soil moisture. Thus carbonates commonly accumulate slowly in the upper vadose zone as a result of evaporitic mechanisms in such environments. Arid conditions tend to result in a poorly developed capillary fringe and a phreatic zone located deep below the surface which experiences reduced rates of groundwater movement. Such conditions favour the slow precipitation of carbonate as a result of consumptive and equilibrium geochemical processes. During humid phases conditions within the vadose and phreatic zone will favour carbonate dissolution, due to increased infiltration and throughflow of neutral or acidic water, and precipitate silica instead. Thus the majority of carbonate precipitation occurs under semi-arid conditions when surface evaporation results in the concentration of ions and the resultant increase in alkalinity, but sufficient soil moisture is maintained by slowly infiltrating solutions which recharge the groundwater and maintain an active capillary fringe.

Previous investigations of geochemical cements within the Kalahari sediments have down-played the role of biogenic precipitation mechanisms in favour of physicochemical crystalline precipitation. There is abundant evidence to support the dominance of these types of precipitation mechanisms, particularly within the phreatic zone and capillary fringe. However, petrography suggests that biogenic mechanisms and pedogenesis are highly significant/dominant within the upper

vadose zone of the SW Kalahari. In line with the investigation of Nash and Smith (1998), two interrelated questions must be answered with regard to the development of carbonates within the southern Kalahari Basin. The first of these concerns the mechanisms required for the development of pedogenic and non-pedogenic carbonates within the same profile. A related question is what the presence of carbonates at a variety of positions within the landscape can tell us about the basins development and diagenetic history.

The fact that both non-pedogenic and pedogenic carbonates occur in the SW Kalahari Basin, frequently within the same profile, has a number of implications for understanding the basin's development and the age of the geochemical sediments. The main controls on carbonate formation appear to be linked to alluvial sedimentation and how the tectonically induced dynamics of this sag-basin's architecture has controlled periods of deposition, stabilisation and erosion. The deposition of the upper Kalahari Group siliciclastic sediments within a range of fluvio-palustrine environments reflects the dynamic interplay of palaeoclimatic and environmental variability, fluctuating runoff, recharge and the location and extent of the vadose and phreatic zones, basin accommodation space and general geomorphic development. Chemical sedimentation is commonly associated with such semi-arid alluvial fan systems (Khadkikar *et al.*, 1998), with the formation of carbonates being disrupted by uplift and/or incision due to increased fluvial activity or tectonic adjustments.

Based on the geomorphology of the drainage within the SW Kalahari, it is believed that the bulk of sediments exposed within the valley walls are Miocene in

age and predate the period of Pliocene fluvial incision. It is, however, impossible to determine when these sediments became carbonate and silica cemented although precipitation was probably initiated within the alluvial environment under a range of vadose and phreatic conditions.

The widespread incision of fluvial systems during the Pliocene resulted in a dramatic change to the basins hydrology, hydrogeochemistry and geochemical equilibriums. Upwarping of the southern margin of the Kalahari Basin caused sediments undergoing cementation within the phreatic zone to be gradually elevated into the capillary zone and then eventually the vadose zone. In addition, the shift from the depositional low angle alluvial fan, which probably consisted of floodplains and anastomosing channels similar to those of the contemporary Okavango and Cuvelai alluvial fans, to an erosional incised channel system resulted in extensive desiccation of the alluvial fan surface, pedogenesis and colonisation by mixed savanna vegetation.

Isotopic analysis suggests that the solution from which the carbonate precipitated was enriched in soil-derived organic carbon. However, under permanent or seasonally anoxic palustrine conditions associated with an alluvial fan complex, carbonate precipitation may have been enhanced by the contribution of CO_2 resulting from the decomposition of organic matter through the processes of bacterial sulphate reduction (BSR) and methanogenesis. Although organic-rich sediments were not detected in the upper Kalahari Group, they are frequently linked to such alluvial-palustrine carbonate sequences due to the fact that organic material is often preserved during the seasonal cycle of inundation and

desiccation. The contribution of CO_2 from organic decomposition during carbonate precipitation is usual easily identified by the very low values of $\delta^{13}C$ (around -20‰ and down to -60‰ when oxidation of methane is involved, although values far less negative (~-7‰ PDB) have been interpreted as resulting from BSR (Rouchy *et al.*, 1998; Anadon *et al.*, 1992)). However, subsequent reprecipitation under oxidising vadose conditions could have destroyed this isotopic record (Budd *et al.*, 2002).

The influence of salinity and Eh-pH on the solubility of silica and carbonate is a significant influencing factor on the diagenetic process and the resultant deposits. Within a depositional environment, geochemical changes to a fluid may cause dissolution of unstable or metastable mineralogies and their replacement by mineralogies, which are stable under the new geochemical conditions (Tucker and Wright, 1990). These diagenetic changes include replacement of high-Mg calcite by low-Mg calcite, dolomitisation and dedolomitisation, replacement of silica by carbonates and the replacement of carbonates and evaporites by silica (silicification). The interpretation of original relationships in these sediments may become complex, up to the point of being difficult to distinguish original chemical deposits from those generated at later stages. Moreover, the dynamic nature of diagenetic processes means that replacement and modification can occur repeatedly during diagenesis. The heterogeneous fabrics of the Mokalanen Formation are a direct result of harmonizing and mismatched phases of vadose and phreatic cementation along with pedogenesis.

5.6 Conclusion

The sediments of the Cenozoic Mokalanen Formation exposed in the upper 50 m of the SW Kalahari are extremely complex. Insight into the complex sedimentological and diagenetic mechanisms responsible for their formation is provided by the mineralogical components and fabric characteristics. It is believed that the chemical sediments investigated are not dormant but rather reflect corrosion, precipitation and modification processes and the abundance of a specific mineralogy and fabric attests to the longevity of the sequence and the periods during which the mechanisms driving these processes were active.

The carbonate and silica cemented sandstone deposits of the Mokalanen Formation are the result of phreatic shallow burial and vadose meteoric diagenesis along with biogenic modification and recrystallisation. This complex epigenesis and paragenesis has resulted in the sediments being characterised by gradational fabrics, which contain non-pedogenic and pedogenic calcite, dolomite and silica cements with a significant authigenic Mg-rich clay mineral and iron hydroxide (goethite) component. The non-pedogenic dolomite, silica and calcite precipitation is believed to have precipitated under reducing conditions within the capillary fringe and phreatic zone. Relocation of the sediments from the phreatic to the vadose zone as a result of a drainage incision and the associated sinking groundwater table initiated meteoric vadose diagenesis and pedogenesis under certain conditions. This new phase of diagenesis resulted in dissolution, precipitation and mineralogical transformation of the sediments within the basin. In addition, groundwater discharge from the walls of the incised valleys has had a significant influence on geochemistry and the precipitation, modification and

corrosion of chemical cements within the active and fossil seeps. Thus, the dynamic geomorphic, climatic, and hydrologic environment within the SW Kalahari has left an integrated geochemical signature on the Mokalanen Formation sediments.

6. GROUNDWATER AND PEDOGENIC MODIFICATION OF CARBONATES FROM SELECTED SITES WITHIN THE PANNETJIESVELD OF THE KALK WEISSRAND, EASTERN NAMIBIA

6.1 Introduction

The Kalk Weissrand is an extensive duricrust plain that lies ~1000 m above sea level between the Auob River and the backwasting cliffs that demarcate the western extent of the Kalahari Plateau between Keetmanshoop and Kalkrand. This potholed plain (pannetjiesveld) is exposed along the entire western length of the SW Kalahari from Kalkrand to Aroab (Fig 6.1), varying in width from a maximum of ~50 km in the south to less than 1 km in the north. The geomorphology and chemical sediments at a number of sites close to the towns of Koës and Aroab (Fig 6.2) in the southern part of this pan dominated landscape were investigated. The Aroab area is the south-western limit of the intergrade carbonate duricrust that is attributed in South African literature to the Mokalanen Formation (SACS, 1980) of the southern Kalahari. A detailed analysis of the fabrics and mineralogy associated with the Mokalanen Formation was conducted in order to understand the mechanisms responsible for precipitation, corrosion and alteration of sediments within this carbonate environment.

6.2 Lithostratigraphy and Depositional Environments

Although the Karasburg region of the SW Kalahari is structurally active and experienced considerable uplift and thrust faulting prior to the formation of the intracratonic Kalahari Basin, the basin's floor within the study area is structurally

simple and shallow (Haddon, 2001). As a result Kalahari Group sediments, which consist of a succession of Paleogene and Neogene terrestrial lacustrine, palustrine and alluvial complexes, are thin (typically less than 50 m thick in the SW pannetjiesveld (Haddon, 1999)) and the lithostratigraphy of this area is very similar to that exposed within the middle and lower sections of the Nossob and Auob River valleys to the east. This is a direct result of the eastward flowing palaeo-drainages of the Auob, Olifants, Nossob and Fish (which is believed to have previously flowed eastwards in the vicinity of Tses (Eitel *et al.* 2002)), having all contributed to the infilling of the greater Aranos sub-basin. Initially sedimentation was within a lacustrine environment which over time is believed to have evolved into a series of prograding alluvial fans and ultimately alluvial fans with large distil floodplains. This regressive sequence of low-energy lakes with low gradient ramp-type margins and ultimately alluvial fans sourced material from the uplifted basin margins and produced the detrital litharenite units which have subsequently been cemented during shallow diagenesis.

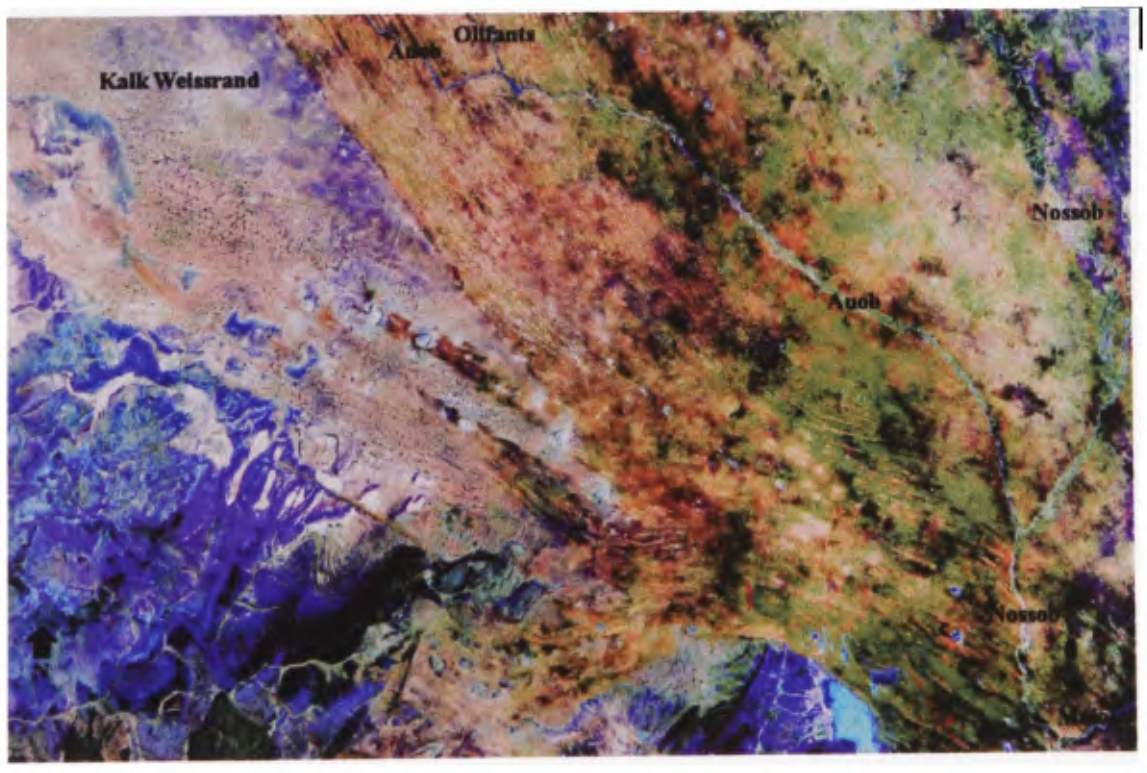


Figure 6.1: LANDSAT image of the pot-holed landscape of the Kalk Weissrand, the adjacent linear dunes of the SW Kalahari and the major drainages.

The majority of the contemporary Mokalanen Formation duricrust surface is buried beneath linear and climbing dunes of the Gordonia Formation in the vicinity of the Nossob and Auob Valleys (Bullard and Nash, 1998, 2000). The duricrust plain of the pannetjiesveld forms a predominantly dune free (Blumel *et al.*, 1998) highly indurated surface with a very poorly developed brown sandy aridisol which is sparsely vegetated with grasses and scattered *Acacia* bushes.

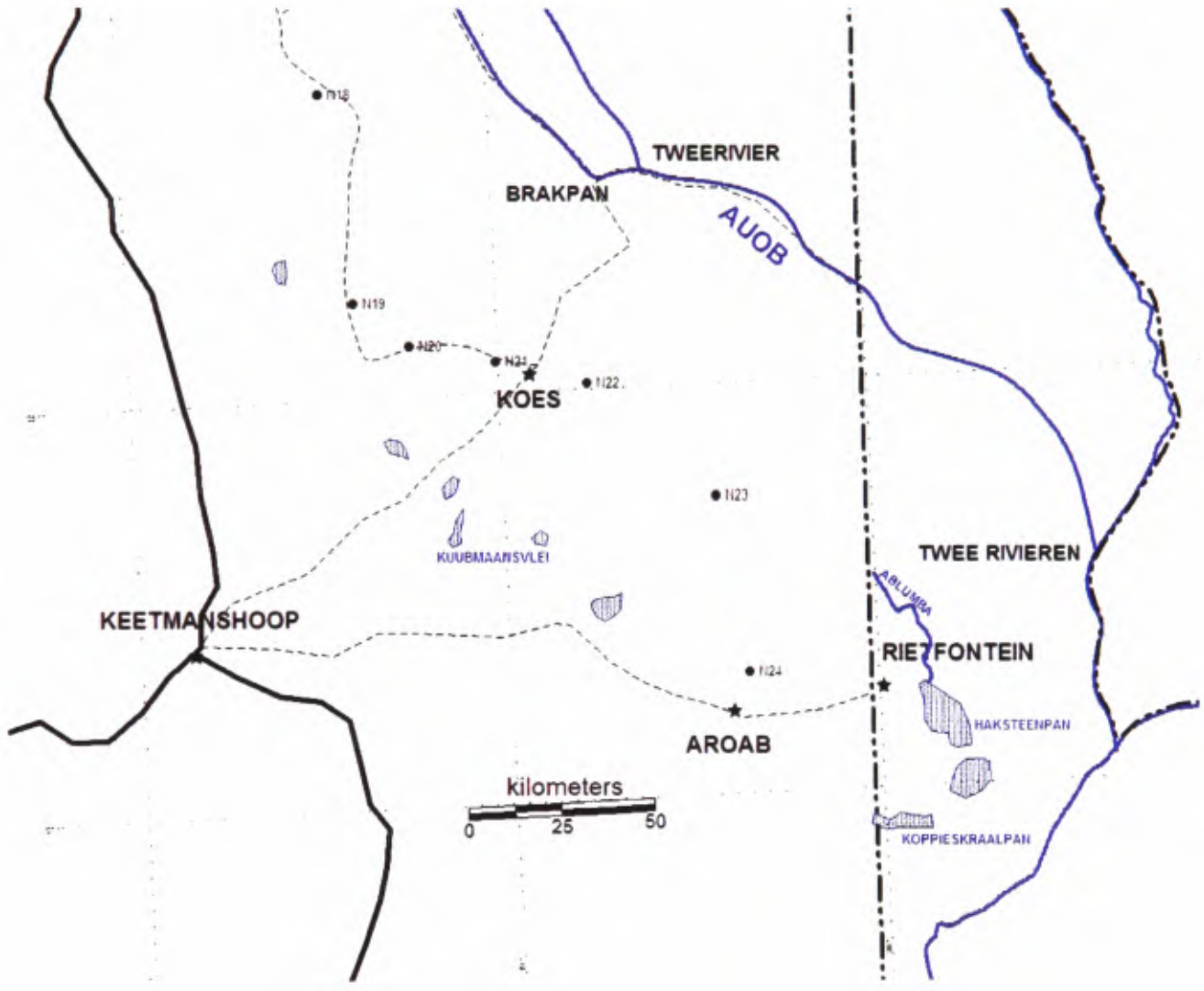


Figure 6.2: Location map of the Kalk Weissrand and sample sites.

Geomorphic evidence from the region (Partridge and Maud, 1987) suggests that the carbonate cemented duricrust surface of the SW Kalahari was formed during the Pliocene and reflects stabilisation after the termination of Kalahari Basin sedimentation. The upper carbonate is believed to be principally pedogenic, although a significant degree of modification and silicification has occurred

particularly in the pan and valley environments. Hence it is proposed that active fluvial sedimentation within the SW Kalahari Basin had all but concluded by the early Pliocene when pedogenic processes began to dominate across the stabilised Kalahari surface. Subsequent arid phases (mostly during the Late Quaternary) initiated aeolian sedimentation which formed the complex linear dunes preserved in the sandveld of the SW Kalahari. The erosion of the aeolian sediment and its replacement by the current pan dominated surface, which experiences episodic flooding, has had a significant influence on epigenesis.

6.3 Geomorphology and Hydrology

The geomorphology and hydrology of the Kalk Weissrand plain is dominated by the numerous NW-SE aligned pothole depressions, pans and their associated centripetal drainage (Fig 6.3) which are incised into the Kalahari Group and underlying Nama (Nababis Formation shale), Dwyka (shale tillite/diamictite) and Ecca (Prince Albert Formation shale) Group sediments. These depressions and the evenly spaced very subtle linear undulations, less than 0.3 m high, which separate the pan corridors, show distinct evidence of preferential alignment that corresponds extremely well with the NW-SE orientated 10-20 m high linear dunes of the main SW Kalahari sandveld (Bullard *et al.*, 1995, 1996, 1997; Bullard and Nash, 1998, 2000) located east of the pannetjiesveld. Analysis of remote sensing imagery indicates that the aligned depressions are spaced ~1 km apart which is equivalent to the spacing of the contemporary linear dune troughs in the sandveld.

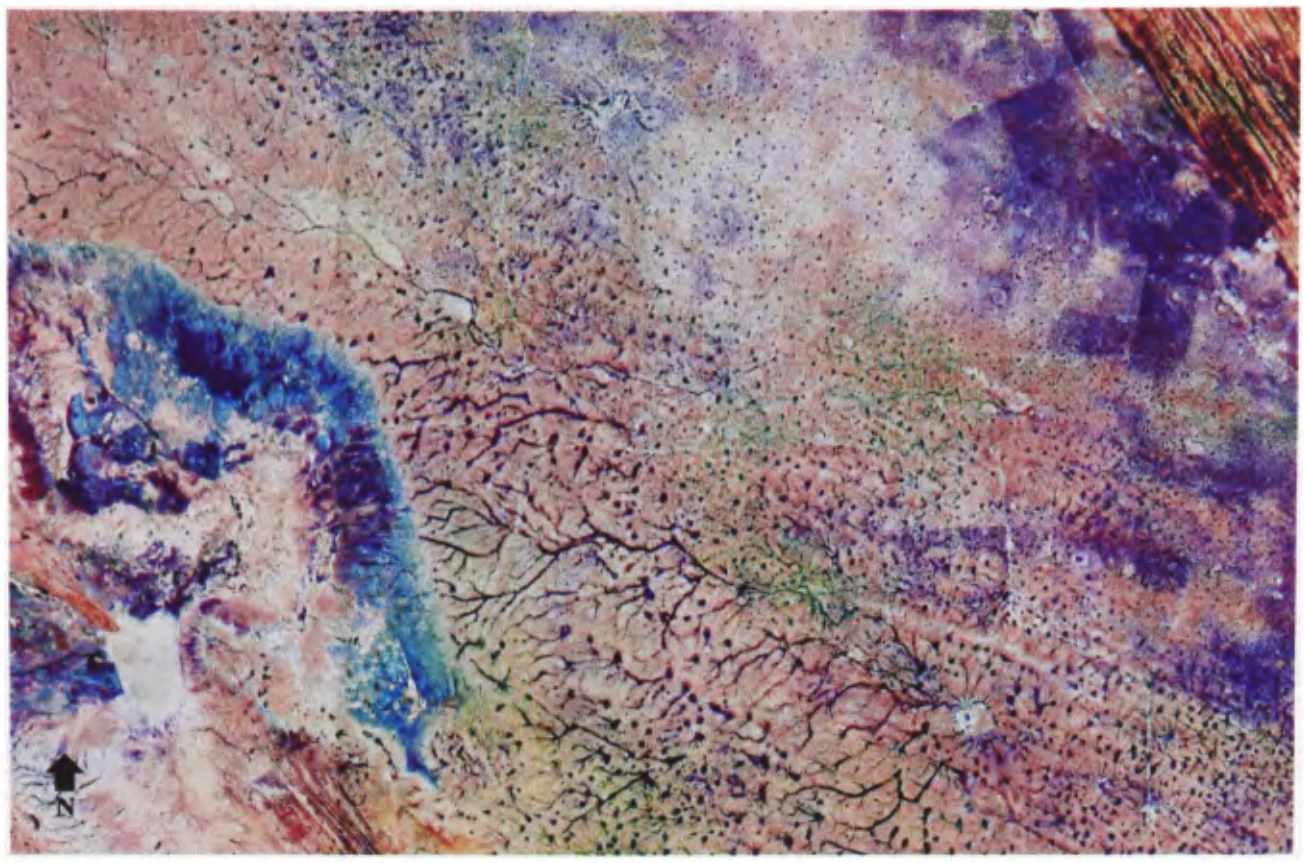


Figure 6.3: LANDSAT image of the NW/SE aligned pans with those nearest the western margin of the Kalahari Plateau characterized by incised centripetal drainage and the pothole depressions of the central pannetjiesveld.

Geomorphic evidence suggests that the presently exposed Kalahari Group duricrust plain was formerly buried beneath a more extensive sandveld which extended west of its current position. During the expanded sandveld phase, interdunal deflation within the sediment deprived aeolian environment and solution weathering initiated by seasonal ponding of water within the interdunal depressions are believed to have instigated the development of embryonic hollows within the intergrade Mokalanen Formation carbonate. A number of studies within the Kalahari (Netterberg, 1969b; Watts, 1980; Shaw and De Vries, 1988; Shaw *et al.*, 1990; Eitel, 1993; Eitel and Blumel, 1997; Shaw and Nash, 1998; Nash and McLaren, 2003; Shaw and Goudie, 2004) support a scenario of intergrade carbonate formation, alteration and dissolution within interdune corridors. Following the retreat of the sandveld to the east, as a result of sediment

starvation or climatic change (Stokes *et al.*, 1997a,b; Blumel *et al.*, 1998), the underlying duricrust surface was exposed as a very low gradient plain. The freshly exposed indurated duricrust surface contained the numerous superimposed aligned embryonic hollows which acted to focus local drainage along and into the former interdunal areas. This resulted in additional karst weathering of the carbonate (*cf.* Goudie, 1973; Balin, 2000; Twidale and Bourne, 2000) which further accentuated the hollows/dolines and resulted in the development of a local network of centripetal drainage which feeds each of the depressions which have developed into erosional pothole pans.

The Kalk Weissrand landscape shares many of the features identified in the southern High Plains of Texas and New Mexico where aligned drainage has also developed in association with a former dunefield which buried the Ogalalla Formation carbonate duricrust (Wells, 1992; Goudie and Wells, 1995). Over time the karst dolines and deflation hollows of the Kalk Weissrand have also developed into seasonal authigenic clay lined pans (Eitel and Blümel, 1997; Eitel, 2000) in a manner analogous to that proposed by Osterkamp and Wood (1987). The lack of inter-connected surface drainage suggests that the pan network acts to recharge the local groundwater in a fashion similar to that identified elsewhere within the SW Kalahari (Heaton *et al.*, 1983; Stute and Talma, 1998). Infiltration from the numerous pans is believed to play a significant role in the recharge of the shallow Kalahari Group aquifers. Groundwater from these aquifers emanates as perimeter seeps along many of the extensive pans which have developed within the Nama, Dwyka and Ecca Group sediments of the lower palaeo-Molopo catchment.

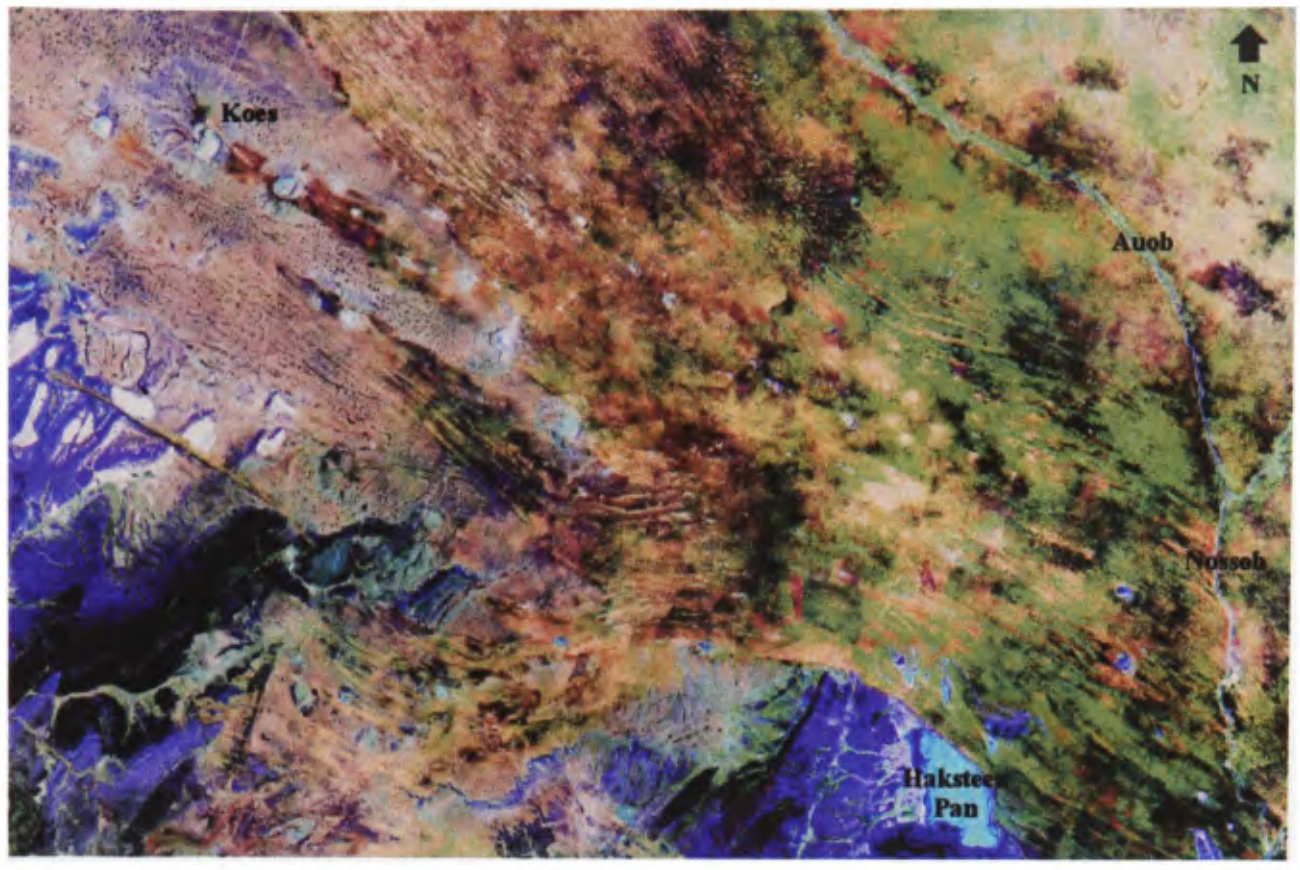


Figure 6.4: LANDSAT image of the Koes-Haksteen pan corridor.

Remnants of a palaeo-drainage are believed to be preserved as a partially buried NW-SE orientated channel network and the extremely well developed pan corridor that runs southeast from Koës through Rietfontein (Fig 6.4). These pans have a different morphology, associated lunettes on their SE perimeter and are significantly larger than the aligned karstic pans/dolines. The majority of these large pans have been excavated well below the level of the adjacent Kalahari Plateau (~80 m at Koës Pan) and have exposed the Karoo Supergroup sediments which locally form the Kalahari Basin floor. This corridor links the major pans of the region (Saulstraat Pan, Koppieskraal Pan, Uitsak Pan, Skuinskalk se Pan, Naroegas Pan, Brakpan, Soutpan, Koopan and Groot Witpan) along with the Ablumba River which terminates in the extensive 20 km by 10 km Haksteenpan on the west bank of the Molopo River.

6.4 Petrofabric and Mineralogical analysis of the Upper Makalanen Formation

Massive intergrade carbonate collected from a number of sites within the eulittoral and supralittoral zones of small pothole pans on the Kalk Weissrand plain show a series of characteristics consistent with subaerial exposure processes which have modified littoral sediments. All samples display a thin (~5 cm thick) but dense irregular but parallel laminated micrite fabric (Fig 6.5a) which may contain a number (1-2%) of very small highly corroded floating detrital grains and silica micro-nodules. This dense micrite is believed to be associated with pedogenic and biogenic micritisation and grades rapidly down-profile into a 5-10 cm thick zone characterised by larger crystals of micrite, sparmicrite and authigenic silica (Fig 6.5b). This fabric contains a wide variety of biogenic, crystalline and alteration structures, such as silica nodules with distinct edges, micrite peloids (possibly biogenic or the result of grainification), glaebules (some of which are exploded), circum-granular cracks, intraclasts, rhizoliths, brecciation features and corroded detrital grains (Fig 6.5c). A number of the detrital grains have double calcite grain coatings; an inner sparry halo around the corroded detrital grain which is then coated by a micritic lining (Fig 6.5d) which appears to be consuming the inner sparry halo and detrital grain over time to form a floating micrite peloid. Further down-profile the individual micrite peloids, silica glaebules and intraclasts (F-fabric glaebular fabric (Summerfield, 1983b)) have diffused edges (Fig 6.5e) and become less distinguishable (ghosts) as the fabric becomes devoid of structures and increasingly crystalline in texture (M-fabric massive (Summerfield, 1983b)). This gradational boundary is interpreted as reflecting the lower limit of the micritisation and its replacement by silicification and dolomitisation processes.

The lower section of the profile is characterised by a vuggy authigenic silica fabric devoid of floating detrital grains but containing solution channels, fractures, fenestrae and lenticular structures (Fig 6.5f). Silica (length-fast chalcedony and megaquartz) has filled many of these fractures, solution channels, vugs and fenestrae, although numerous unfilled structures suggest active dissolution within the profile.

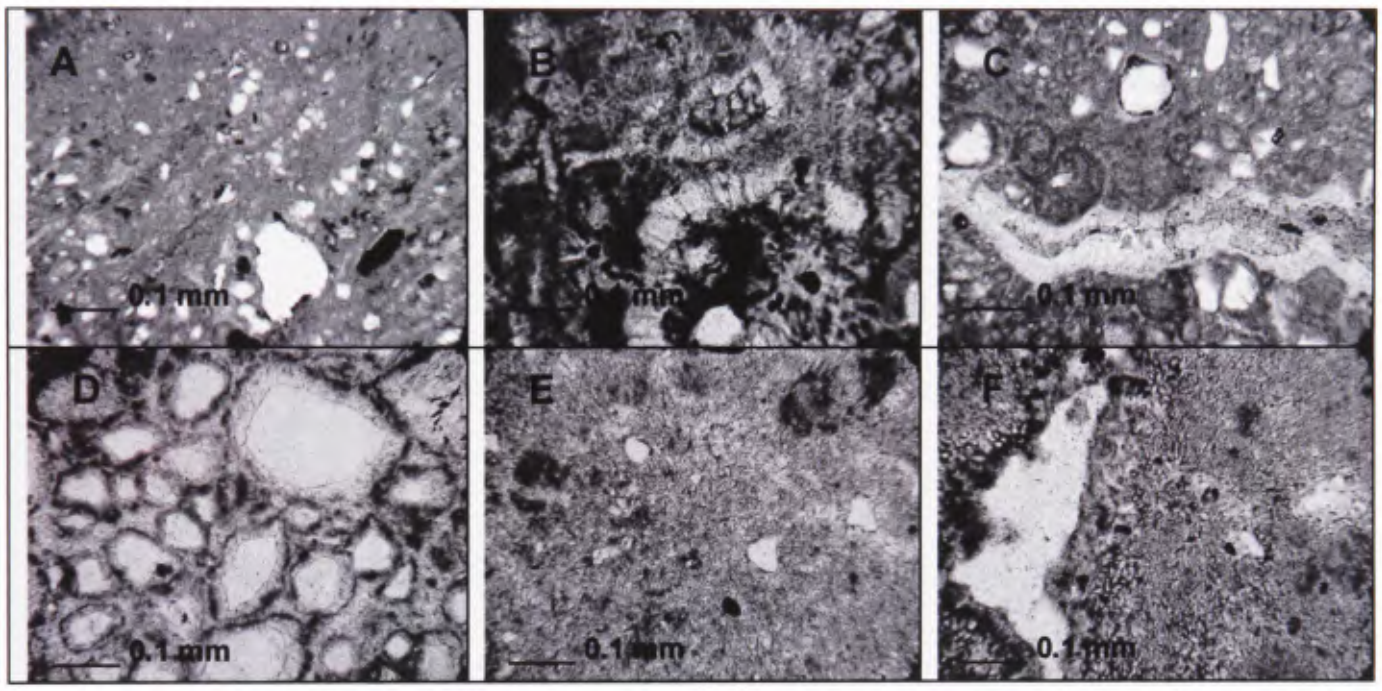


Figure 6.5: (a) Dense micrite fabric with floating highly corroded detrital quartz grains (b) complex micrite, sparmicrite and authigenic silica fabric developed 5-10 cm below the surface (c) fabric containing micrite peloids, glaebules, silica filled fracture, sparmicrite lacy fabric and numerous corroded detrital quartz grains some with micrite coatings (d) detrital quartz with a sparite (inner) and micrite (outer) grain coating (e) micrite peloids, silica glaebules and intraclasts (F-fabric glaebular fabric (Summerfield, 1983b)) have diffused edges and become less distinguishable (ghosts) as the fabric becomes devoid of structures and increasingly crystalline in texture (M-fabric massive (Summerfield, 1983b)) (f) lower vuggy authigenic micro-crystalline silica fabric devoid of floating detrital grains.

The mineralogy, although silica dominated, contains abundant euhedral calcite and dolomite crystals. The euhedral dolomite crystals within the lower silica

dominated fabric appear in some places to be undergoing dedolomitisation and replacement by sparry calcite overgrowths. This dolomite exhibits considerable iron staining which is believed to be indicative of oxidisation of the ferrous iron released during the dedolomitisation process by meteoric water percolating through the profile. The upper most samples can be broadly classified as sil-calcretes and reflect calcretisation (micritisation) of the lower impure silcrete.

6.5 Discussion

The fabrics of the upper deposits investigated are believed to be the result of partial pedogenic calcretisation of silicified sediments. These calcretisation processes have probably been initiated by the interaction of surface high pH saline pan water, meteoric water, micro-organisms and vegetation with the underlying silcrete. The carbonate rich littoral and pan sediments experience desiccation during the lengthy dry season and may be temporarily vegetated by salt tolerant grass species. This desiccation phase induces vadose carbonate diagenesis which may be appreciably magnified by the soil's micro-organisms, which can significantly contribute to processes such as sparmicritisation and micritisation. These processes and mechanisms responsible for the calcretisation of the upper sediments have been discussed by Ringrose *et al.* (2005) who argued that within similar littoral, eulittoral and supralittoral pan sediments from the Makgadikgadi sub-basin, biogenic and environmental mechanisms were responsible for surface calcretisation and sub-surface silicification. Investigations by Arenas *et al.* (1999), Bustillo and Bustillo (2000), Bustillo (2001) and Bustillo *et al.* (2002) on Palaeogene and Miocene lacustrine, palustrine and playa carbonate and silica deposits in the Madrid and Ebro Basins of Spain, have identified a number of

complementary features (nodulization, rhizoliths, fissures, vug porosity, circumgranular cementation, etc.) and primary and secondary alteration dolomitization/dedolomitization and silicification mechanisms which are applicable to the phreatic and meteoric diagenesis of the pannetjiesveld chemical deposits.

Investigation of the selected deposits suggests that silica precipitation is a result of diagenesis associated with infiltrating groundwater and phreatic zone processes during shallow burial rather than pedogenic and vadose processes which are believed to be responsible for the calcretisation. Silicification processes are believed to have altered the original detrital alluvial sediments when silica enriched pore fluids initiated cementation under conditions wetter than present. The role of the fluctuating water table, which is believed to have facilitated silica precipitation within the capillary fringe, and the later existence of the ephemeral pan network which was enriched in silica and magnesium as a result of evaporative processes, are believed to have been instrumental in the precipitation and epigenesis of the fabric. Soluble silica dissolved in this shallow groundwater has exploited the most porous sediment and resulted in its corrosion and silicification. It is also believed that primary silica precipitation as opal-CT may have occurred within the littoral, eulittoral and supralittoral sediments of permanent water bodies during initial sedimentation, where evaporitic or evapo-transpiritic concentration of silica was maximised. Due to the fact that the environment is believed to have experienced semi-arid to arid conditions throughout the majority of the Quaternary, this model for silica precipitation is believed to be only applicable to early cementation.

Despite the abundance of siliceous rocks within the catchments of the SW Kalahari, the provenance of soluble silica is generally unclear as surface and ground water samples do not indicate excessively elevated values. However, it is likely that evaporitic pumping by vegetation induced silica concentration during the initial floodplain stages (Shaw and Nash, 1998; Shaw and Goudie, 2004). A possible source of silica during the period of burial beneath the expanded sandveld may have been infiltrating meteoric water. This is believed to have corroded silica and bicarbonate as it infiltrated the dune sediments and when it accumulated in the interdune depressions evaporative and pedogenic precipitation of carbonate at the surface would have resulted in silica enrichment of the solutions which infiltrated to greater depths (*cf.* Summerfield, 1982). However, it is also believed that precipitation, alteration, corrosion or replacement of authigenic Mg-rich clays (sepiolite-smectite) associated with the pedogenic and ephemeral pan environment may have played a significant role in controlling the amount of silica available for precipitation. The precipitation of Mg-rich clays would have consumed magnesium and contributed to silica concentration in the remaining solution, while transformation of one clay type to another (smectite to sepiolite) would not significantly effect the Mg or Si cation concentration. However, the replacement of Mg-rich clays by opal-CT as a result of groundwater silicification processes (Thiry and Millot, 1987; Rayot *et al.*, 1992) would result in the enrichment of Mg in the pore water. This along with the transformation of high-Mg calcite to the more stable low-Mg calcite during diagenesis may account for Mg-enrichment associated with later stage dolomitisation and maturation of the sequence.

Petrography suggests that the upper and lower units have undergone epigenesis under different conditions and thus show a complex paragenesis. It is believed that the upper sediment has experienced solution, reprecipitation and modification within the vadose zone as a result of meteoric diagenesis and sub-aerial pedogenesis. The lower sediments by contrast have experienced epigenesis as a result of sub-surface interactions within the phreatic zone which reflect the contribution of alkaline waters from adjacent pans. Nodules, pelletal micrite and silica, rhizoliths, circumgranular cements and grainification features within the surficial deposits suggests that biogenic processes within these upper littoral, eulittoral and supralittoral pan sediments are responsible for a significant proportion of the calcite and silica precipitation. The sub-surface authigenic silica dominated fabric is far more crystalline in character and is believed to have been significantly influenced by the seasonal evaporitic pan systems whose silica rich water infiltrated the profiles via the network of fractures and solution channels. Surface and ground water processes associated with these highly alkaline pans are generally believed to induce silica mobilisation and calcite precipitation within the surface sediments and preferential calcite removal and silicification of the sediments at sub-surface locations of lower salinity and lower pH in a manner similar to that proposed by Watts (1980), Summerfield (1982, 1983a,b,c), Shaw and Nash (1998), Nash and Shaw (1998), Ringrose *et al.* (2002, 2005) and Shaw and Goudie (2004). Thus, the mature multicyclic fabrics of the cal-silcrete and impure silcrete are the result of numerous phases where either vadose or phreatic precipitation mechanisms have dominated. Most recently however, the sediments have been subjected to vadose diagenesis where mobilisation of calcite associated

with pedogenesis and meteoric water has been a significant agent in a fashion similar to the Mokalanen Formation samples investigated elsewhere in the Kalahari (Nash *et al.*, 1994a, Nash and Shaw, 1998, Nash and McLaren, 2003).

6.6 Conclusion

The cal-silcrete and impure silcrete fabrics suggest simultaneous precipitation of carbonate and silica, at differing levels within the profiles, during various stages of the landscape's evolution. Surface pedogenic cal-silcrete is likely to have been precipitated within the surface sediment while the underlying impure silcrete is associated with the deeper vadose and phreatic zones. These intergrade deposits are likely to have undergone significant alteration during the development of the Kalk Weissrand from alluvial floodplain to dunefield to exposed duricrust plain. The majority of the silcrete fabric is believed to have been precipitated within the capillary fringe and phreatic zone of the linear dunefield when the margin of the southern Kalahari erg was located west of its current position. During this period the capillary fringe would have undulated in an approximate simulation of the palaeo-dune topography and outcropped seasonally in the interdunal areas. The existence of interdune corridors characterised by seasonal pans would have played a significant role in mobilising silica rich pore water which was sourced from local quartz grain solution. The high pH and salinity of the pan environments favoured surface carbonate precipitation which resulted in additional enrichment of soluble silica. These silica rich fluids migrated down profile and then precipitated at depths where the salinity and pH were lower. Subsequent diagenetic alteration and reprecipitation of the fabric occurred as a result of changing processes linked to the retreat of the dunefield eastwards and the

dominance of surface pedogenesis and calcretisation. The reduced influence of local groundwater processes and the lowering of the capillary fringe and the phreatic zone resulted in an increased role for meteoric water in epigenesis.

7. THE RELATIONSHIP BETWEEN GEOMORPHOLOGY AND CHEMICAL SEDIMENTS AT KEY LOCATIONS IN THE KGALAGADI DISTRICT, SW BOTSWANA.

7.1 Introduction

Duricrusts form a distictive sedimentary unit of the upper stratigraphic package of the Cenozoic Kalahari Group within SW Botswana. To date very little is known about these sediments, their depositional, paragenetic and epigenetic environments and their relationship to the geomorphology of the region. These features are of significant value as stratigraphic markers when attempting to understand the sub-surface basin architecture and rates and styles of sedimentation. They can also provide significant insight to the climatic and hydrologic regimes under which precipitation and alteration has occurred.

A series of near surface intergrade chemical sediments were collected from shallow pits within Kalahari sand pedogenic (arenosol) and pan environments throughout the Kgalagadi region and investigated using an array of stratigraphic, petrographic and geochemical methods. The principle aim of this study was to investigate whether the mineralogical and geochemical characteristics of near surface sediments are in equilibrium with their contemporary physical environment or contain relict features indicative of different environmental conditions. In order to achieve this, detailed examination of pedogenic and pan hydrogeochemical processes and their influence on the mobilisation, precipitation, corrosion and alteration of the authigenic silica, carbonate and clay component of these sediments was conducted. It is hoped that this study will add contextual

information on processes and mineralogies related to specific geochemical environments within southern Africa. This information will potentially provide insight to the operational mechanisms and facilitate the elucidation of information related to the processes active within the depositional and alteration environments of similar lithologies which are preserved within the rock record without a distinct palaeogeomorphic context.

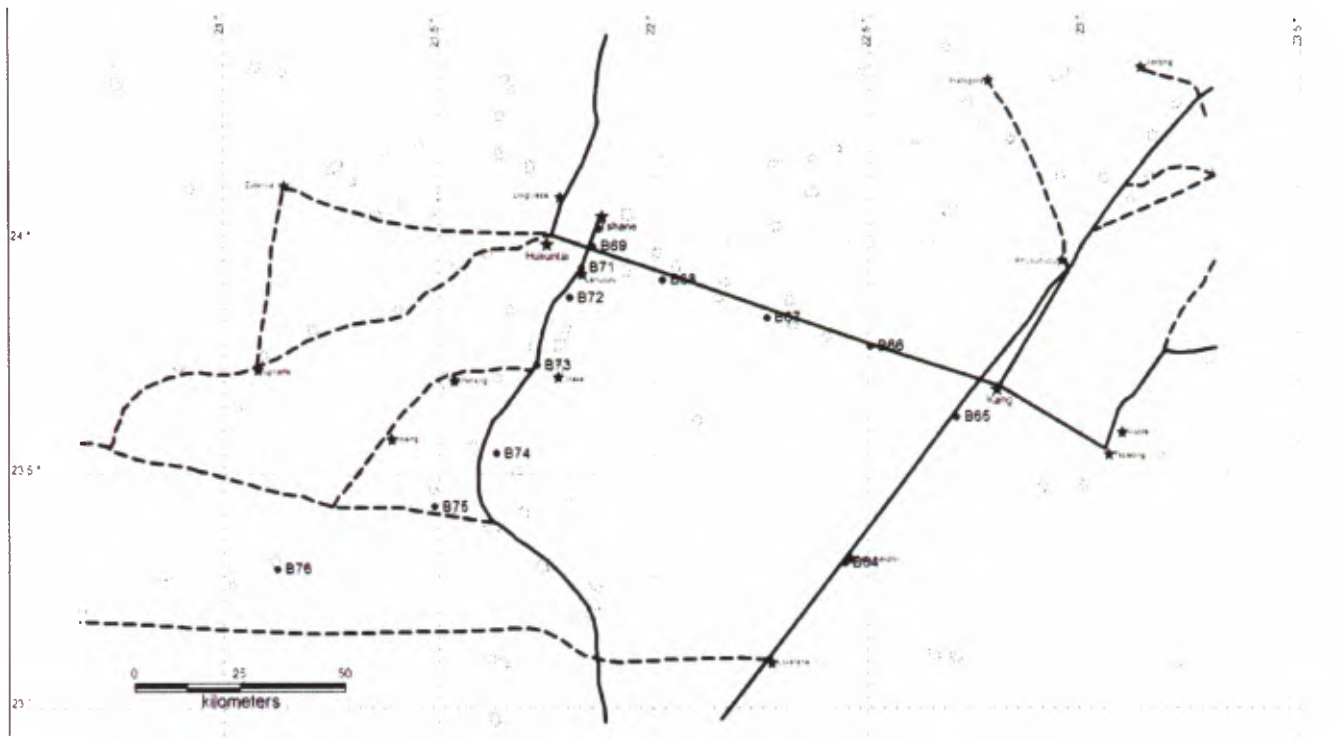


Figure 7.1: Location map of the Kgalagadi sample sites.

7.2 Physical Environment

The Kgalagadi District encompasses the entire southwestern portion of The Republic of Botswana. The area investigated is located between 23°20`S 21°05`E and 24°05`S 22°50`E and includes sixteen major pans: Letlkane, Tsatswene, Tsawe, Borema, Dimpho, Tshane, Kakwe, Katlwe, Hukuntsi, Lokgwabe, Makane, Tshotswa, Ohe, Hunhukwe, Mamasi and Konkwe along with numerous smaller (less than 100 m diameter) incipient pans (Fig 7.1).

This region is considered the most arid in Botswana with a MAP of ~350 mm and PET of ~ 1800 mm (Bhalotra, 1987). The excessively high PET means that there is seldom excess precipitation available for groundwater recharge, thus surface evaporation of ponded water and soil moisture is a dominant process.

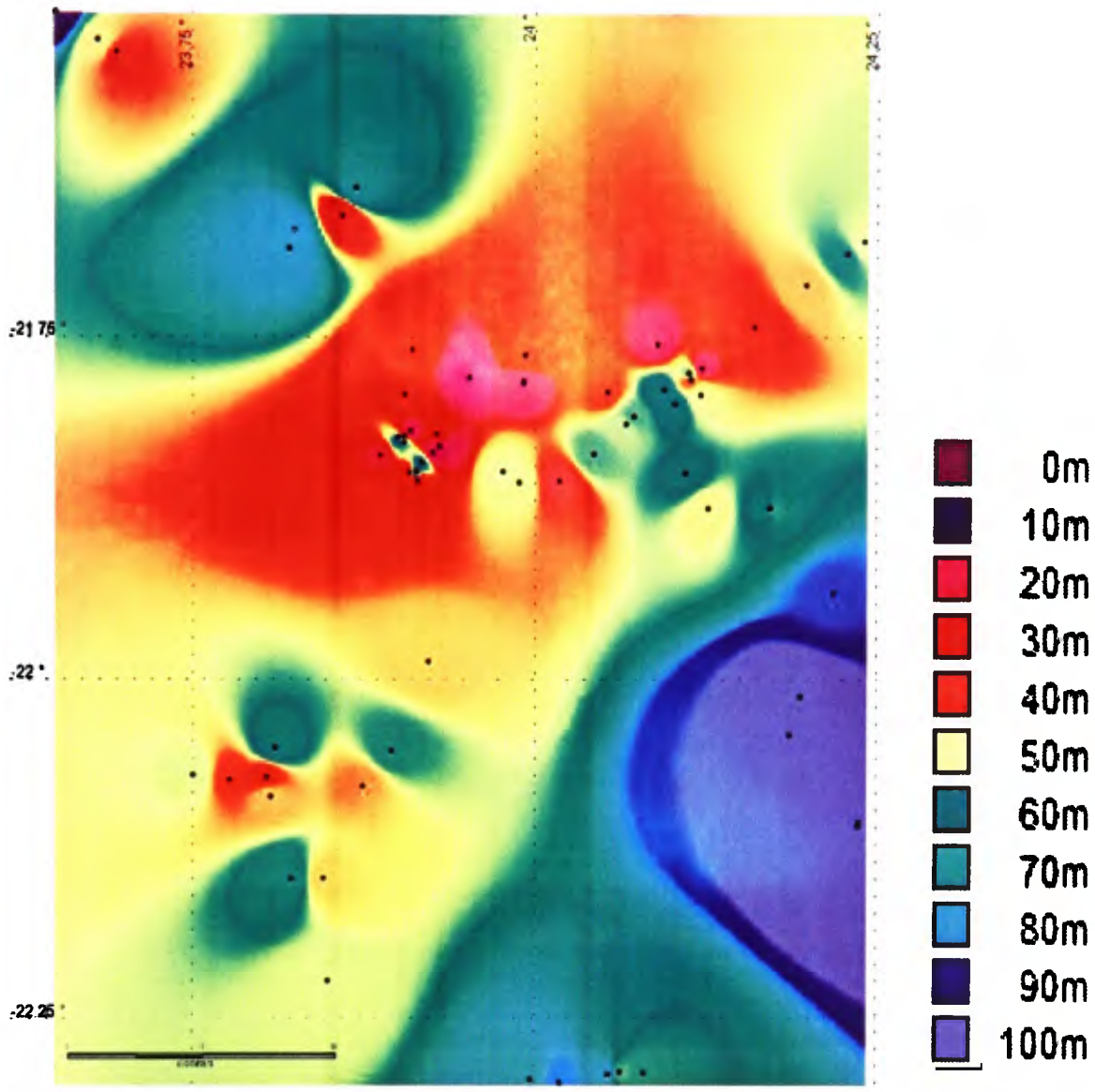


Figure 7.2: Kalahari Group Isopach map of the study area, based on BGS and WCS (1994, 1996) drill data.

The dominant surface lithologies within the study area are unconsolidated iron oxide coated aeolian sand, intergrade duricrusts and pan clays of the Kalahari Group. The thickness of Kalahari Group sediments in this area are highly variable and range between 0 and 120 m (Fig 7.2) and the lithostratigraphy is not well understood. This variability is in response to the Cenozoic infilling of the

intracontinental Mega-Kalahari sag basin (Haddon and McCarthy, 2005). The unconformity between the Cenozoic Kalahari Group and the underlying Late Paleozoic Karoo Group sediments is marked by the erosional Late Cretaceous African Surface (Partridge and Maud, 1987). Within southern Botswana (south of the Kalahari Anticline) this surface is characterised by an undulating palaeotopography consisting of a network of palaeo-channels and small sub-basins, most of which are structurally controlled troughs and synclines, which have been incised into the Mosolotsane Formation (Lebung Group, Karoo Supergroup). The Kalahari Group sediments were deposited in fluvial, alluvial fan, aeolian and fan-delta environments and are characterised by significant lateral and vertical facies variations. As a result of this variability within lithologic horizons and complex facies assemblages, the definition of sedimentary deposits as beds and formations even within sub-basins is extremely difficult and as a result the lithostratigraphy of the Kalahari Group in the southern part of the Mega-Kalahari Basin is very poorly defined (Smith, 1984; Carney *et al.*, 1994; BGS and WCS, 1994; 1996). Based on drill results from the Kgalagadi area (BGS and WCS, 1994; 1996) the characteristic lithostratigraphic package in this area consists of an immature basal conglomerate and occasional talus breccia (which are typically associated with fault bounded troughs) overlain by silt/mudstone which coarsens upwards into a subarkosic sandstone with a capping intergrade carbonate which has typically been partially silicified. This stratigraphic sequence is believed to be indicative of a slowly subsiding intracratonic sag basin setting rather than the fault bounded extensional graben hosted sequences which occur elsewhere in the Kalahari (e.g. the Okavango alluvial fan). Climatic conditions have had a marked influence on the depositional environment and have resulted in

a variable sedimentation regime: lacustrine during humid conditions, alluvial fan/fluvial during drier conditions and aeolian/evaporitic playa during arid conditions. The unconformity between the weathered Karoo and the basal Kalahari lithologies is in places distinct due to calcretisation of the uppermost Karoo sediments which probably occurred in a pedogenic environment prior to the commencement of Kalahari Group sedimentation.

Like most of the Kalahari Basin the locations investigated in this study have a dynamic hydrogeochemistry. The sparse vegetation and unconsolidated surficial Kalahari sand acts to regulate infiltration and evapotranspiration under normal conditions. However, during periods of above normal rainfall unstable wetting fronts develop which penetrate to beyond the active root zone, facilitating recharge of the relatively shallow Kalahari aquifers, 10 to 20 m below surface level (BGS and WCS, 1994; 1996; De Vries *et al.*, 2000; Kers *et al.*, 2000). Despite the widespread occurrence of low permeability indurated sediments throughout the upper Kalahari Group, recharge of the aquifers is believed to occur via infiltration through zones of increased porosity, typically faults, joints and fractures, and localised solution features. Nijsten (1995) has described these mechanisms of groundwater recharge in the confined aquifer of the Letlhakeng Botlhapatlou area in Botswana, while Van der Hoven (2005) described the generic mechanism within such sedimentary systems. Selaolo (1998) developed a general piezometric map of the Matsheng area in the Kgalagadi. This indicates that the shallow aquifers are connected and that the hydraulic gradient mimics the topography which slopes gently from the north-west towards the south-east with a

maximum gradient of 2%. Pans, which act as local drainage points, only have a localized effect on this regional hydraulic gradient.

7.3 Geomorphology

The area investigated is classified as Kalahari sandveld which consists of a flat to gently undulating (gradient 0 to 0.5%) aeolian sand covered plain with major calcrete and associated silcrete rimmed pans (De Wit and Bekker, 1990). The surficial yellowish brown to dark red coarse to fine fluvio-aeolian sands of the sandveld have been classified as a (ferralic – iron oxide/limonite rich, mostly as grain coatings around the detrital quartz) arenosol (De Wit and Nachtergale, 1990). Elevations are greatest in the north-west (~1170 m) and slope gently in a south-easterly direction to a minimum of ~1095 m south of Kakwe Pan (BGS and WCS, 1996). There are no significant regional drainage features within the area and all surficial flow is directed centripetally towards the nearest pan system.

Pans with well developed terraces and southern leeside lunettes (most pans have at least one lunette and some have coupled linear dunes on the lee of the lunette) are the dominant features throughout this landscape (Fig 7.3). Pans are generally orientated N-NE/S-SW and the pan floors, which commonly contain gleyic solonchak soils (Thomas and Shaw, 1991), are typically 2 to 5 m below the adjacent sandveld plain. The large saline pans are characterised by prominent intergrade calcrete and silcrete terraces (platforms of Lawrence and Toole (1984)) which form elevated rims above the pan floor. Various chemical sediments can be found within these pan terraces ranging from friable calcareous sand to very hard massive silcrete. Goudie (1991) and Goudie and Wells (1995) have discussed

several mechanisms of pan formation within the Kalahari. The mechanisms most likely to be active within the Kgalagadi are: disruption of surface and lateral groundwater flow, alternating groundwater levels, and periods of preferential deflation controlled by the fluctuating groundwater table and soil moisture content.

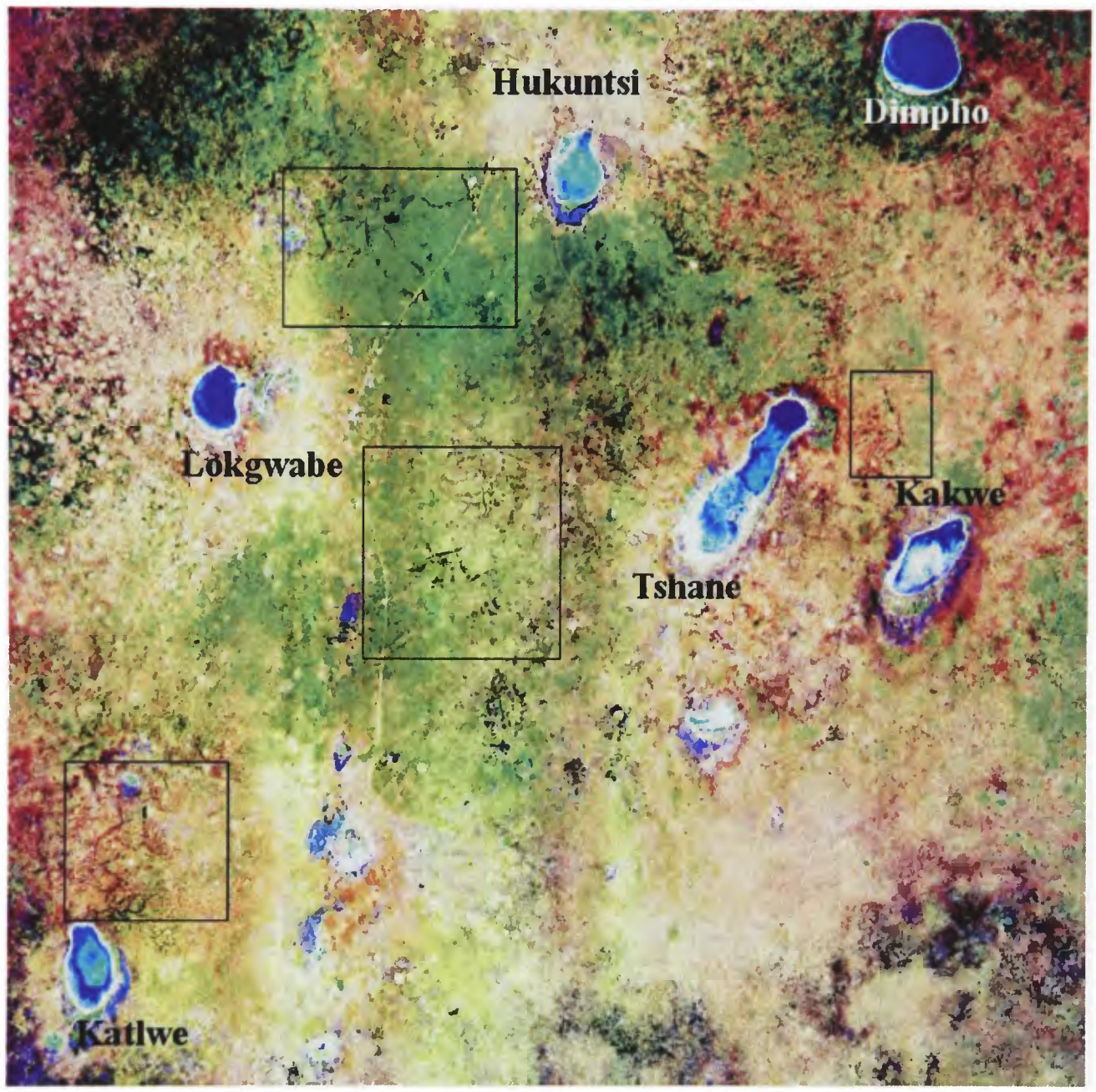


Figure 7.3: LANDSAT image of the well developed lunettes on the southern side of Kakwe Pan and the linear and curvilinear features (boxes) in the vicinity of Hukuntsi, Lokgwabe, Tshane, Kakwe and Katlwe Pans.

The non-pedogenic calcrete and silcrete terraces together with shoreline features such as bars and spits on the leeside of some pan, suggest that this landscape may

retain evidence of early lacustrine/palustrine conditions which have later been transformed to evaporitic/playa depositional environments as climatic conditions became more arid. During wetter periods, groundwater levels would have been elevated and areas are likely to have experienced prolonged periods of inundation giving rise to widespread lacustrine/palustrine sediments. This dynamic hydrogeochemical environment would have promoted the precipitation of phreatic and palustrine chemical sediments (Alonso-Zarza, 2003). Moreover under these conditions intrabasin sourced brines evolved which caused calcareous and silicious mineralisation of the entire underlying stratigraphic sequence. There is abundant evidence for wetter phases within the Kalahari during the Late Quaternary (Thomas and Shaw, 2002) and this is supported by direct observations recorded in local verbal history and historic accounts that mention the widespread occurrence of perennial fresh water springs in the area around Tshane at the time the area was settled (BGS and WCS, 1996).

Linear and curvilinear features visible on LANDSAT imagery (Fig 7.3) in the vicinity of Hukuntsi, Lokgwabe, Tshane, Kakwe and Katlwe Pans were investigated (site B71) and found to correspond with the calcrete ridges described by Mallick *et al.* (1981) and Bruno (1983). These ridges are 5 to 50 m wide, and range from tens of metres to several kilometres in length. It is believed that preferential weathering of the surrounding less indurated calcrete has resulted in the ridges standing 1 to 5 m above the surrounding landscape. A thin veneer of sand covers the ridges which are typically vegetated and thus produce very noticeable dark tones on remote sensing images. Mallick *et al.* (1981) suggested that the ridges reflect jointing and tectonic faulting within the original sheet

calcrete which underlies the entire area. It is believed that these fractures acted as conduits for groundwater circulation (*cf.* Van der Hoven *et al.*, 2005) especially during more humid periods (*c.f.* Nash *et al.*, 1998). It is believed that the fracture network allowed limited pervasive silicification (Thiry and Ribet, 1999) to occur in a similar manner to occurs around Etosha Pan. The resultant groundwater sil-calcrete thus has different characteristics to the surrounding pedogenic sheet calcrete; most notably it has a higher silica content and a mixed micrite and sparite fabric which means it was more indurated than the powdery to massive pedogenic calcrete which increases its resistance to weathering and facilitates its preservation as a positive feature on the landscape as it was denuded.

7.4 Chemical Sediments

Authigenic clay minerals, evaporites and complex intergrade dolocrete, calcrete and silcrete deposits account for a significant proportion of upper Kalahari Group sediments within the study area. It is widely accepted (Netterberg, 1969a,b, Nash *et al.*, 1994a,b, Nash and Shaw, 1998, Ringrose *et al.*, 1999, 2002 Nash and McLaren, 2003, Ringrose *et al.*, 2005) that the majority of dolocrete, calcrete and silcrete deposits are polygenetic and thus reflect formation and modification under varying conditions. They are found within a range of stratigraphic positions and are thought to have formed intermittently over an extended time period (Netterberg, 1969a, Goudie, 1983). Due to the inherent problems associated with dating silica and carbonate deposits in such environments there has been significant debate regarding the age of these precipitates. Several published calcrete ages (Thomas and Shaw, 1991) can only be considered minimum ages or must be re-evaluated due to the problems associated with the multiple phases of

reprecipitation and the recycling of detrital carbonate. It is not the aim of this study to re-evaluate the carbon dating of calcareous sediments within the Kalahari. Rather in line with the stated aim of understanding the processes of formation, alteration and replacement it is important to understand that problems associated with carbon dating these sediments are highlighted by petrographic studies which definitely prove that most Kalahari chemical sediments are multi-phase and have a complex history of epigenesis and paragenesis which is the result of pedogenic and non-pedogenic processes operating throughout the Cenozoic and continuing to occur today under specific of conditions (*cf.* Shaw *et al.*, 1990).

7.4.1 Petrographic Characteristics

7.4.1.1 Pedogenic Deposits

Pedogenic calcrete predominates throughout the study area and typically occurs as a thin hardpan which grades down-profile into a more massive calcrete beneath a 0.5 to 1.0 m thick surface veneer of red/brown Kalahari sand.

Petrographic analyses of the pedogenic samples indicate that the bulk of the consolidated sediments consist of detrital quartz forming a grain supported fabric cemented by simple inter-granular micrite precipitation structures (Fig 7.4a). The upper parts of all the profiles have been partially plugged and are forming hardpans as a result of accretionary and displacive calcretisation and selective localised silicification. Based on the diagnostic features of Machette's (1985) maturity index, the majority of the pedogenic carbonates forming within the upper sediment profile can be classified as relatively immature. At all the sites

investigated the micro-laminated hardpan at the unconformity between the calcrete and unconsolidated sand is thin and grades rapidly down-profile into a simple grainstone fabric (Fig 7.4b) which contains numerous calcite nodules/glaebules (Brewer, 1964).

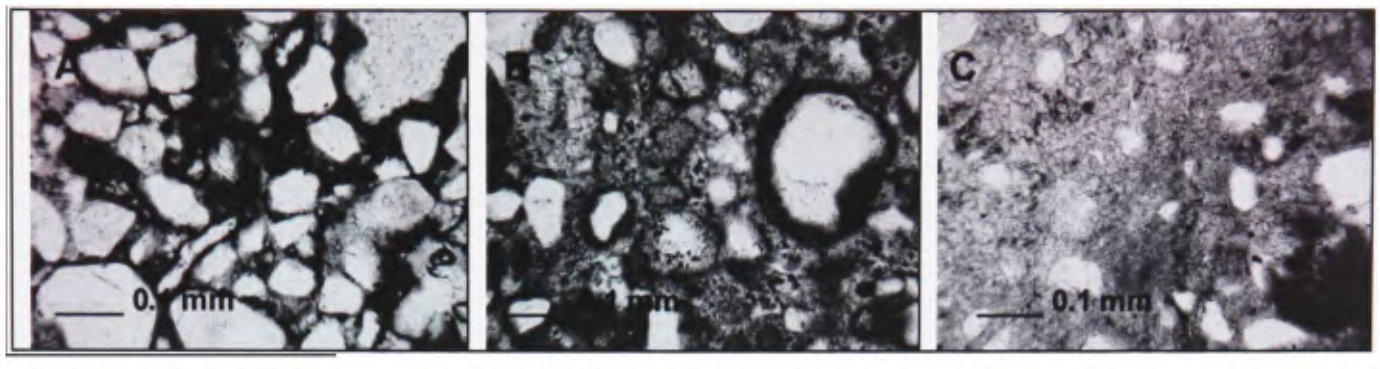


Figure 7.4: PPL thin-section photomicrographs: (a) Detrital quartz forming a grain supported fabric cemented by simple inter-granular micrite precipitation structures. (b) simple grainstone fabric containing numerous coated detrital quartz grains, pelletal micrite and glaebules (c) dispersed corroded detrital quartz grains floating in a mixed equant sparite (top left), sparmicrite (center) and micrite (lower right) fabric.

The fabrics of the upper sediments contain abundant pelletal micrite, fine grained peloids of various sizes and rhizocreations along with structures such as pendant grain coatings, meniscus bridge structures and overgrowths, which have developed around the detrital quartz grains, which show only limited evidence of corrosion. These detrital grains generally have a sub to well rounded morphology which reflects their fluvio-aeolian origin (Moore and Dingle, 1998).

The lower sections of the pedogenic profiles are characterised by late stage equant sparry and needle fibre calcite along with sparmicrite and authigenic quartz (Fig 7.4c) which has filled some of the primary and secondary pore space and fractures (most samples still have a relatively high porosity indicative of their immaturity). These lower sections of the profiles contain significantly fewer detrital quartz

grains, which suggests silica corrosion and the occurrence of floating aggregate grains suggests reworking of a primary deposit.

In line with other pedogenic environments within the Kalahari (Shaw and Goudie, 2004) within the upper horizons silica is corroded by calcite at high pH's (Flach *et al.*, 1969, Reeves, 1976, Watts, 1980 and Wang *et al.*, 1994) and the subsequent downward migration of the silica-rich solutions results in the precipitation of authigenic silica from gels in areas of higher salinity and lower pH at depth. Due to the dynamic nature of the soil water geochemistry within the vadose zone and the influence of temporary factors such as unstable wetting fronts along with longer term factors such as climate change numerous phases of precipitation-partial dissolution-reprecipitation occur at a range of depths within the profile.

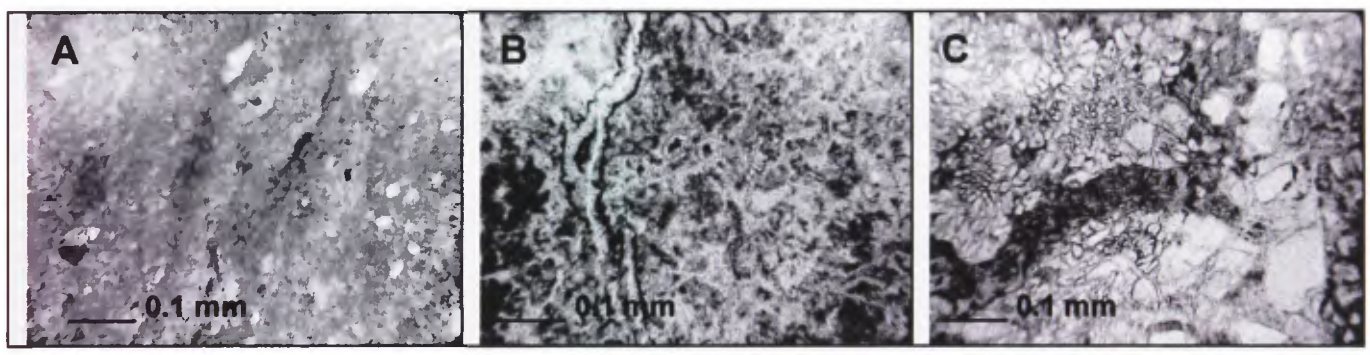


Figure 7.5: PPL thin-section photomicrographs: (a) Dense micrite fabric with sparse floating detrital quartz grains in the upper section of the ridge believed to be indicative of pedogenic micritisation (b) network of silica micro-veins and stringers within the mixed micrite and sparite fabric (c) sparite dominated fabric with a micrite filled fracture and pervasive micritisation along the margin.

7.4.1.2 Groundwater Modified Pedogenic Deposits

At site B71 a low sand covered ridge believed to be composed of intergrade sediments formed by the groundwater alteration of the primary pedogenic calcrete sheet was investigated. As discussed previously, the contrasting physical

properties of the adjacent sediments has resulted in differential weathering and the formation of inverted topography in the same fashion as occurs at Poacher's Point in the Etosha Pan (Smith and Mason, 1991). The upper ridge sediments are characterised by a dense micrite fabric (Fig 7.5a) with sparse floating detrital quartz grains. This fabric is believed to be reflective of late stage pedogenic and meteoric micritisation of the original groundwater sparite fabric and it becomes less dominant with depth and shows pervasive features along its low boundary. At depths of 0.5-1m below surface level numerous silica micro-veins and stringers (Fig 7.5b) become apparent within the sparmicrite fabric. There is abundant evidence at this depth to suggest pervasive silicification has occurred along a network of late stage secondary fractures within the original groundwater calcrete. At greater depths the fabric is dominated by an alpha fabric composed of euhedral and subhedral sparry calcite (Fig 7.5c). In places this fabric has been extensively brecciated to form sparite intraclasts which float within a later stage micrite fabric. These intraclasts show evidence of micritisation along their boundaries which is interpreted as being reflective meteoric epigenesis. The cause of the brecciation is unclear although possible mechanisms may include: 1) Compression, associated with volumetric expansion of the deposit as it matures which induces small scale folding, faulting and jointing (Watts, 1980; Netterberg, 1980); 2) Dissolution of evaporite minerals (principally halite, gypsum and anhydrite which may have precipitated from adjacent pan sourced brines infiltrating the fracture), lenses, laminations or horizons precipitated within the primary sediments which initiated additional porosity and/or produced accommodation space within horizons as a result of collapse; 3) Biomechanical (roots, burrows, etc.) disruption and fracturing.

7.4.1.3 Pedogenically Modified Groundwater Deposits

Several sediment samples were investigated from sites B68 and B69 in close proximity to the littoral zone of active pans. Profiles typically have a 0.5 to 1 m thick horizon of unconsolidated Kalahari sand which has a distinct unconformity with the underlying consolidated sediments. These consolidated sediments are at least 3 m thick (unconsolidated clastic basal sediments were not exposed at any of the sites investigated, however logs (BGS and WCS, 1996) of the area indicate sedimentary packages of consolidated calcrete and silcrete are 3 to 10 m thick and inter-spaced by unconsolidated clastic (typically quartz arenite and argillaceous quartz arenite) sediments). The consolidated sediments consist of a thin upper hardpan calcrete which grades into nodular then massive dolo/calcrete (Netterberg, 1980) and ultimately silicified cal/dolocrete containing numerous authigenic quartz nodules and stringers at depth.

The indurated sediments have a complex fabric containing abundant micrite and sparry calcite with minor dolomite and authigenic quartz in the form of length slow chalcedony, microcrystalline quartz and megaquartz. The upper hardpan sediments are characterised by a micro-laminated micrite packstone with numerous small highly corroded floating detrital grains and cryptocrystalline silica filled fractures (Fig 7.6a). The primary fabric of the upper sediments appears to have been a dense pedogenic wackestone containing abundant pelletal micrite (possibly coprolites), glaebules/peloids (Fig 7.6b) and possible rhizolith structures. Down profile the dense wackestone fabric has been disrupted by brecciation and microkarst processes which have created additional porosity. The

majority of these circum-granular cracks (Fig 7.6c), fractures, channels, fenestrae and vugs along with original pore space have been lined and filled by sparite (Fig 7.6d), sparmicrite and authigenic quartz (Fig 7.6e). Numerous angular packstone intraclasts of micrite and sparmicrite cemented moderately corroded detrital grains, float throughout this lower disrupted fabric. In places the sparmicrite fabric of the intraclasts is undergoing micritisation along the fracture network producing a chicken-wire type appearance (Fig 7.6f).

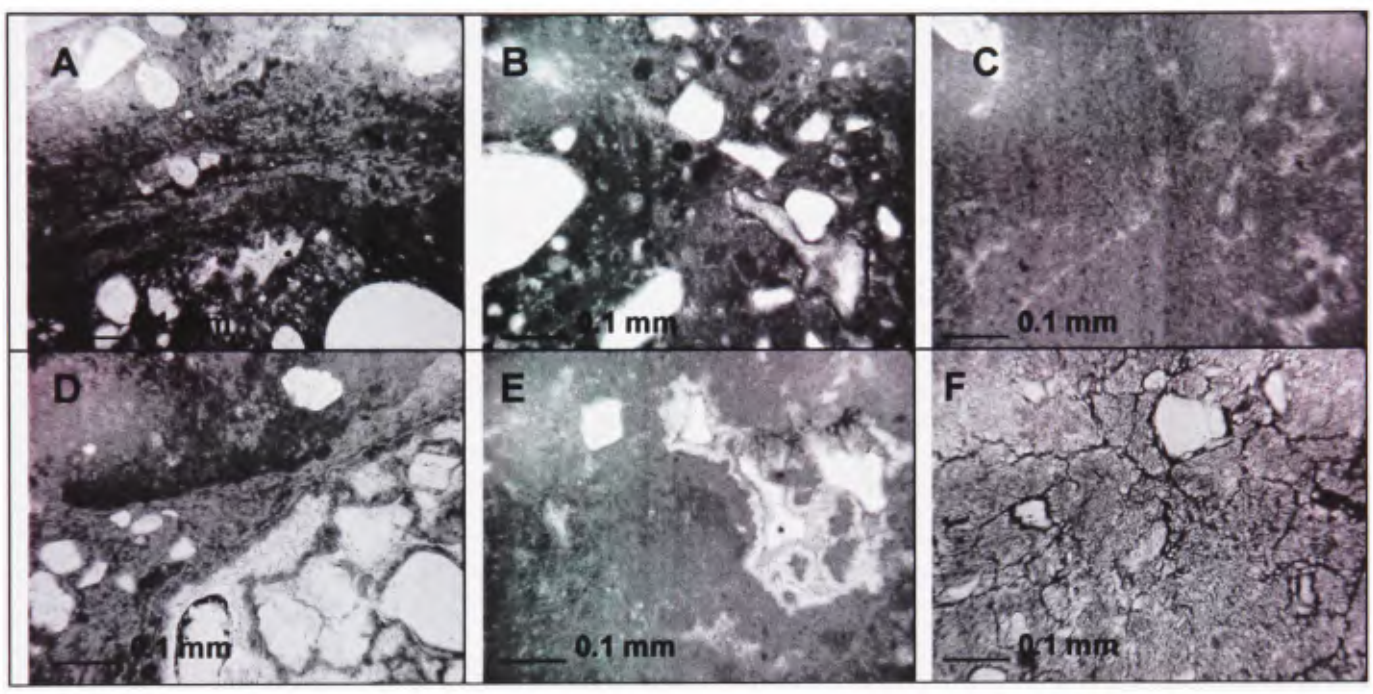


Figure 7.6: PPL thin-section photomicrographs: (a) micrite with anastomosing laminae, cryptocrystalline vug fills and floating detrital quartz grains (b) dense pedogenic wackestone containing floating detrital quartz grains, pelletal micrite and peloids with authigenic silica filled fenestrae (c) sparmicrite filled circum-granular cracks within the dense micrite fabric (d) sparite fill undergoing micritisation within the dense micrite fabric (e) authigenic silica filled vug within the dense micrite fabric (f) the sparmicrite fabric undergoing micritisation along the fracture network and around detrital grains producing a chicken-wire type appearance.

It is suggested that the beta fabric structures in the upper sediments may be associated with processes such as secondary grainification which might have occurred within freshly exposed littoral sediments during the desiccation of the

palustrine/pan environment. Subsequent burial beneath a horizon of Kalahari sand during arid phases and periods of increased aeolian activity resulted in further modification by pedogenic and vadose processes. At greater depths vadose and pedogenic processes were limited due to the influence of infiltrating saline water from the adjacent pans. Thus in the lower horizons phreatic precipitates dominated. Fluctuating hydrologic conditions will have caused changes to the unstable wetting fronts, the capillary fringe to oscillate and variations in the infiltration and through-flow of meteoric and alkaline, Mg rich ground water. These inconsistent conditions will have had a significant influence on the geochemical environment and resulted in substantial mineralogical and fabric epigenesis as a result of corrosion, replacement and recrystallisation. Evidence of dolomitisation and silicification in the lower sediments suggests that the profiles are mature and currently dominated by phreatic processes (Peterson and von der Borch, 1965; Eugster, 1967, 1969, 1980; Folk and Pittman, 1971; Eugster and Jones, 1979; Platt, 1989; Garcia-Ruiz, 1998; Thiry and Ribet, 1999; Sanz-Rubio *et al.*, 2001).

7.4.1.4 Pan Terrace Deposits

Terraces and platforms between 30 and 120 cm high are exposed at the edge of pans throughout the study area. These hardpan capped terraces are often partially buried beneath a sparsely vegetated veneer of white sand or grey brown silty sand which has deflated off the adjacent pan surface and may form lunette dunes at a distance on the leeside of the pan or merge with the red brown Kalahari sandveld. The occurrence of such well developed pan terraces is believed to be evidence of the transition from a depositional to erosional environment. Aggressive chemical

weathering in these alkaline pans is responsible for the break-down of material which is then deflated off the desiccated surface by the strong seasonal winds in this region of the Kalahari. LANDSAT images (Fig 7.7) of this area indicate that the terraces form distinct concentric pits (golf ball texture) within the low gradient landscape which are very different from the linear ridge features associated with the indurated pedogenic sediments (Fig 7.3).

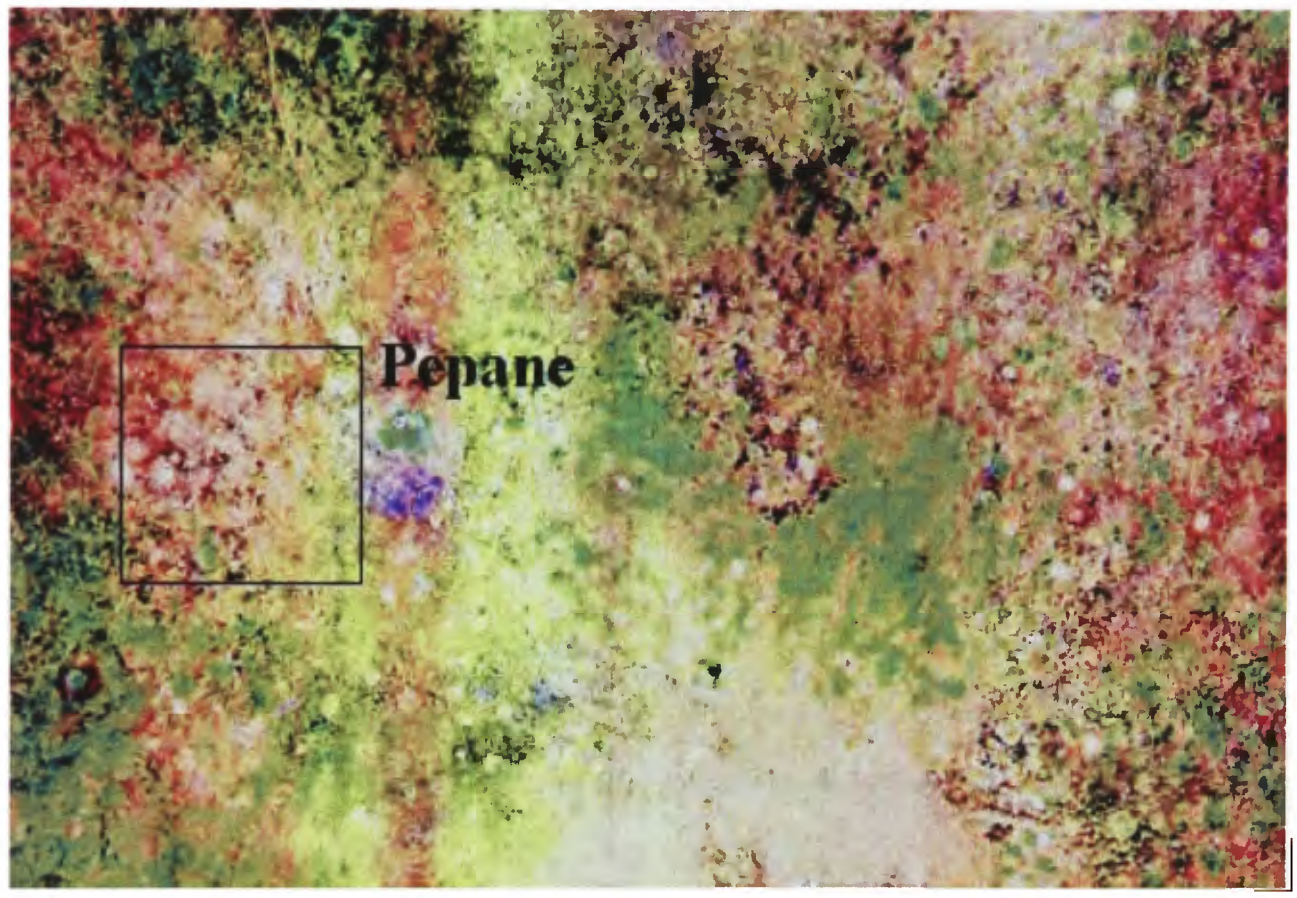


Figure 7.7: LANDSAT image of the concentric pits (box) investigated west of Pepane Pan.

Petrographic investigation of the indurated sediments (sites B70, B72, B73 and B75) reveals a moderately developed micro-laminated upper hardpan, with occasional corroded floating grains (Fig 7.8a). Down-profile the hardpan grades into a dense micrite and dolomicrite wackestone which contains floating corroded detrital quartz grains, pelletal micrite (possibly coprolites) and bioclasts (fragments of gastropod and ostracod tests, and diatoms) (Fig 7.8b). This fabric also contains features such as intraclasts, peloids/glaebules, nodules, alveolar septal fabric and micro-vugs (Fig 7.8c). Geopetally filled or partially filled

mouldic pore features (Fig 7.8d), vugs and fenestrae (which often produce a colloform surface texture due to differential weathering where exposed) are believed to be indicative of micro-karst corrosion and subsequent filling (Fig 7.8e).

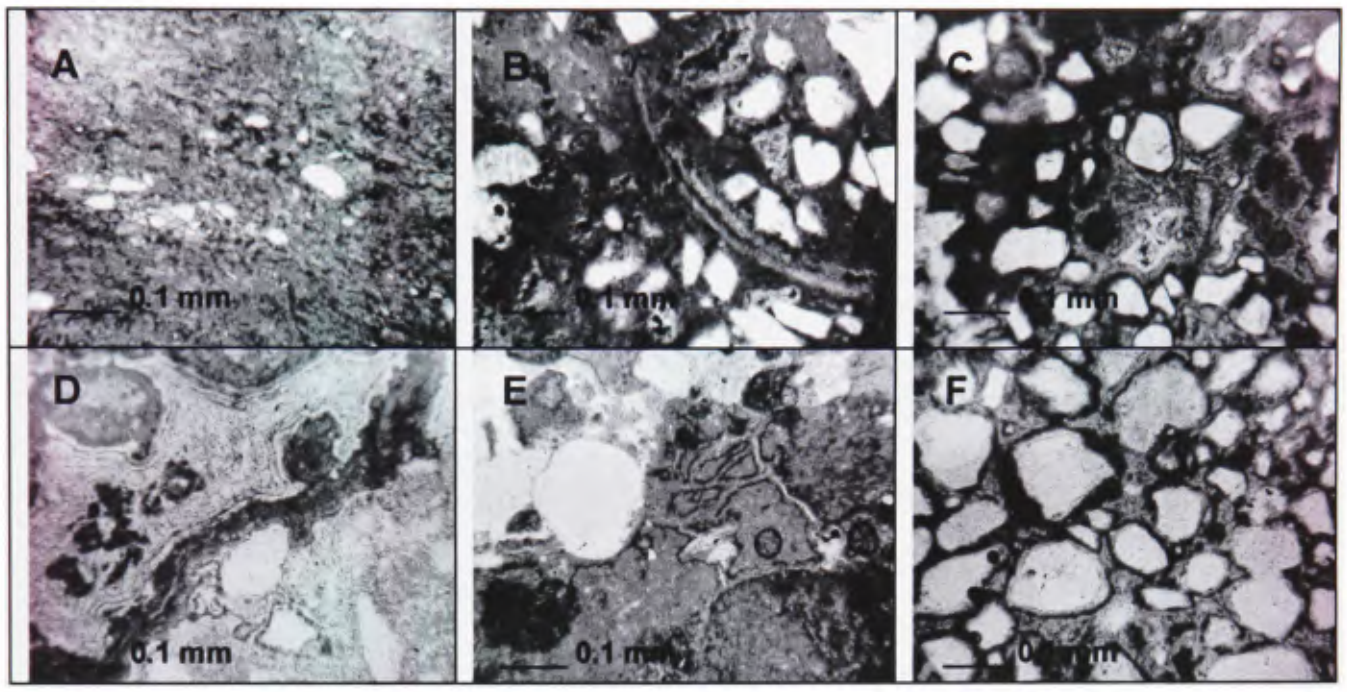


Figure 7.8: PPL thin-section photomicrographs: (a) micro-laminated micrite with occasional floating corroded detrital quartz grains (b) dense micrite and dolomicrite fabric containing floating corroded detrital quartz grains and a bioclast (center - possibly a fragment of gastropod or ostracod test) (c) an array of intraclasts, peloids/glaebules, coated detrital quartz grains, alveolar septal fabric and micro-vugs present within the micrite fabric (d) geopetal authigenic silica fill within the micrite and sparmicrite fabric (e) authigenic silica filled vug (top left) with a network of lined veinlets intruding the adjacent micrite fabric – suggestive of corrosion and replacement by silica (f) lower packstone characterized by concentric micrite grain coatings and occasional peloids floating within a sparmicrite fabric.

The sediment in the lower sections grades from a wackestone into a packstone as the fabric becomes increasingly more grain supported and shows less evidence of displacive cementation. The fabric within the lower sections is authigenic silica dominated, porous and limited to pendent and concentric grain coatings with

occasional peloids (Fig 7.8f). Some of the primary and secondary pore space has been filled by needle fibre calcite, sparmicrite, crypto-crystalline silica and dolomite.

The petrography suggests that these calcrete profiles were initially precipitated as carbonate mud within a shallow hyper-saline pan/palustrine environment (Platt, 1989; Alonso-Zarza, 2003). These palustrine fabrics subsequently underwent texturally inversion as a result of processes such as secondary grainification and pedogenic modification during desiccation events. Subsequent sub-aerial exposure and pedogenic processes (Wright and Tucker, 1991; Sanz-Rubio *et al.*, 2001) have facilitated these fine grained sediments to develop in line with Machette's (1985) stages of calcretisation. Subsequent late stage microkarst modification, dolomitisation and silicification of the original carbonate wackestone along the highly porous seepage zones at the edge of pans has resulted in additional epigenesis. Alkaline silica-rich (SiO_2 content > 250 ppm) pan and ground water with a pH value between 8.5 to 12 (*c.f.* Garcia-Ruiz, 1998) is believed to be directly responsible for the corrosion of the original calcite and the precipitation of dolomite and silica gels, which produced the secondary crypto- and micro-crystalline silica nodules, stringers and geopetal fills.

7.4.1.5 Pan Deposits

Numerous samples were collected from shallow sample pits dug into the sediment of active pans (sites B64, B74, B76). The upper pan sediments consist of laminated grey to green anoxic clays, medium to fine grained sand with dark grey clay coatings and evaporite mineral crusts (principally halite) which may have a

covering of seasonal grass. Consolidated chemical sediments are usually encountered at depths of less than 2 m. Lawrence and Toole (1984) discovered a strong correlation between pans and the occurrence of calcrete and silcrete in Botswana (Table 7.1). Butterworth (1982) has, however, questioned the relationship between the saline water conditions of the pans and precipitation mechanisms responsible for the chemical sediments in the Kgalagadi Region.

Landform	**At or near surface**	**Within 0.5 m**	**Within 1.0 m**	**Within 1.5 m**	**Within 2.0 m**	**No. of samples**
Platforms	81%	81%	86%	100%	100%	21
Pans without platform	13%	13%	29%	66%	100%	38
Depressions	0%	0%	8%	59%	93%	49
Little or no relief (grey sand)	0%	0%	5%	61%	94%	18

Table 7.1: Probability of locating calcrete adjacent to pans in the Botswana, from Lawrence and Toole (1984).

Petrographic analysis of the upper samples reveals an extremely dense wackestone fabric consisting of dark brown micrite intraclasts and peloids floating in a vuggy biege dolomicrite, micrite and sparmicrite fabric (Fig 7.9a), which reflects variations in geochemistry (redox conditions and salinity are believed to have had a strong control on the precipitation of authigenic minerals) of the solutions from which the carbonate precipitated. The fabric contains sparsely distributed corroded detrital grains and is characterised by numerous floating

bioclasts (ostracods, diatoms and fragments of gastropod tests (Lipps, 1993)), fenestrae, glaebules/peloids, intraclasts and secondary grainification structures (Fig 7.9b), such as circumgranular cracks (Hay and Wiggins, 1980; Esteban and Klappa, 1983; Platt, 1989; Wright 1990a) that are typical of pedogenically modified palustrine carbonate mud (Platt, 1989; Sanz-Rubio *et al.*, 2001) and suggests that evaporative pumping was the principal mechanism responsible for carbonate precipitation. As discussed by Wright and Tucker (1991), these palustrine or pan deposits are easily modified during subaerial exposure to resemble mature hardpan profiles. In addition numerous features such as fractures, microkarst solution channels (Fig 7.9c), voids and vugs (*cf.* Freytet and Plaziat, 1982), which are interpreted as evidence of desiccation-related secondary grainification processes and pedogenesis, have been lined or filled by later stage authigenic silica, dolomite and calcite.

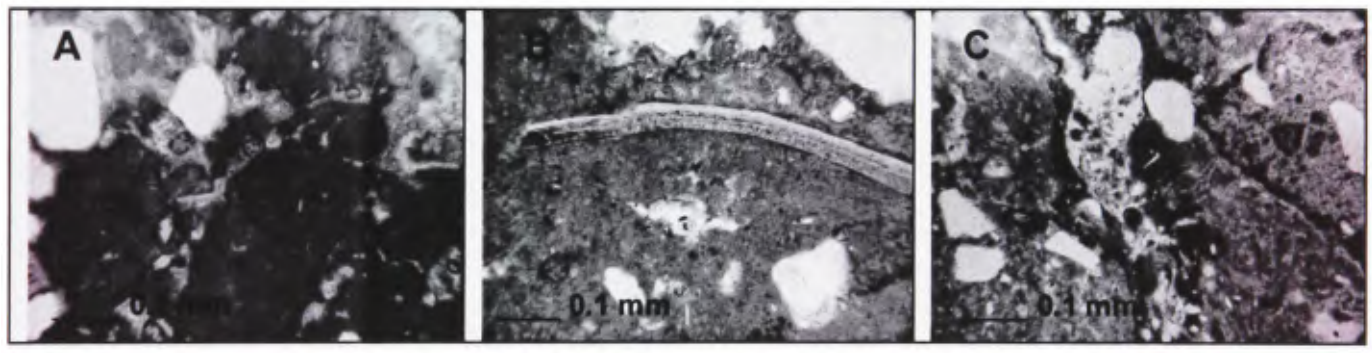


Figure 7.9: PPL thin-section photomicrographs: (a) extremely dense wackestone fabric consisting of dark brown micrite intraclasts and peloids floating in a vuggy biege dolomicrite, micrite and sparmicrite fabric (b) moderately corroded detrital quartz grains and a bioclast (possibly a fragment of ostracod test) floating in the dense micrite fabric with authigenic silica filled vugs (c) a lined and filled solution void with radial veins and lined fractures indicating the pervasive nature of the silica replacement of the original micrite fabric.

7.4.2 Mineralogy

The authigenic mineralogy of the deposits is dominated by calcite, dolomite and quartz (Table 7.2) and clearly reflects processes that operate at various levels within the profile. Within the upper profile pedogenic calcretisation, dedolomitisation and silicification associated with shallow meteoric diagenesis dominate. Analysis of the hardpan deposits indicate that the fabric consists of similar proportions of calcite and authigenic quartz. In contrast the lower profile sediments, which tend to have a distinctive green colouration, reflect the role of highly saline K and Mg enriched meteoric and ground water (the Mg/Ca ratio is highly variable in this region) in processes that favour seepage-reflux and mixing dolomitisation and silicification of the primary carbonate. XRD analyses confirm that these sediments are dominated by authigenic silica but also contain dolomite, calcite, ankerite, K-feldspar and sepiolite.

Sample	Quartz	Calcite	Dolomite	Ankerite	K-feldspar	Rutile	Altaite	Sepiolite	Hydrowoodwardite
B65	45	51	-	-	-	3	-	-	1
B66	90	10	-	-	-	-	-	-	-
B67	41	44	-	-	-	-	-	14	1
B68	8	80	-	6	-	-	-	6	-
B69	27	73	-	-	-	-	-	-	-
B70	54	46	-	-	-	-	-	-	-
B71	15	84	-	-	-	-	1	-	-
B72	24	76	-	-	-	-	-	-	-
B73	63	-	23	-	14	-	-	-	-
B74	36	24	40	-	-	-	-	-	-
B75	56	44	-	-	-	-	-	-	-
B76	21	79	-	-	-	-	-	-	-

Table 7.2: Summary of XRD analysis.

Smale (1973) attributed the green colouration of the sediments to the formation of authigenic chlorite under the highly alkaline and saline groundwater conditions associated with pans. Boocock and Van Straten (1962), Netterberg (1969a,b) and Summerfield (1982), in contrast, believe it to be the result of authigenic glauconite. However, glauconite formation is generally restricted to marine environments and, as discussed by Watts (1980), there are numerous difficulties in distinguishing glauconite/illite from chlorite in polymineralic samples such as the intergrade calcrete and silcrete of the Kalahari. But most significantly glauconite can only be associated with silcretes as authigenic glauconite and calcite are chemically incompatible (Krumbein and Garrels, 1952). Unfortunately clay fraction XRD analysis was not conducted on the samples thus it is proposed that the green colour in calcretes can be attributed to chlorite while in silcretes it can be attributed to glauconite/illite (although the formation of glauconite in terrestrial environments is still debatable).

The authigenic K-feldspar that characterises the central and lower section of profile 73 has precipitated as overgrowths on detrital grains in association with the authigenic silica fabric. Hay *et al.* (1991), Friedman (1995), Spotl *et al.* (1996), Maraschin *et al.* (2004) and Larsen and McNeal (2004) have all identified similar authigenic K-feldspar in sandstones, dolo-sandstones and carbonates within saline playa lake evaporite sequences. The mechanism of formation is believed to be hydrolysis (dissolution and replacement by clay minerals) of detrital feldspar and mica within the Kalahari sands. The K^+, H^+ and SiO_2 enriched meteoric water is then evaporitically concentrated within the pan environments and authigenic K-feldspar is precipitated at a high pH and K^+/H^+ ratio (Maraschin *et al.*, 2004). As

the pH falls and the K^+/H^+ ratio decreases as a result of consumptive precipitation, K-feldspar is replaced by palygorskite, sepiolite and smectite authogenesis.

In addition to the authigenic minerals a number of detrital minerals were identified within the Kgalagadi deposits. Of particular interest is the occurrence of rutile, hydrowoodwardite and altaite within the deposits investigated. Rutile and other titanium minerals have been identified within silicified deposits throughout southern Africa (Summerfield, 1980). The origin of rutile in the Kgalagadi and the Kalahari has traditionally been associated with the erosion and reworking of the Proterozoic igneous geology which forms the basement and outcrops throughout the Mega-Kalahari Basin (Moore and Larkin, 2001). The occurrence of hydrowoodwardite and altaite within the ridge feature deposits is of particular interest and warrants further investigation. These minerals may be associated with basement reworking or precipitation from circulating solutions along veins within the secondary carbonate.

7.5 Discussion and Conclusion

Two distinct types of carbonate have been identified within the Kgalagadi region: 1) a typical pedogenic calcrete which takes the form of a hardpan grading to moderately or well consolidated nodular to massive intergrade calcrete at depth. The typical pedogenic calcrete profile has decreasing carbonate content with depth and characterises large areas of the Kalahari Basin. The calcrete usually takes the form of a near continuous sheet between 2 to 5 m thick developed 1 to 2 m below the surface Kalahari sand. This calcrete typically contains significant silica at depth (intergrade calcrete-silcrete) and occasionally minor amounts of

late-stage dolomite in porous zones, which suggests precipitation as a result of evaporative pumping associated with temporary wetting fronts and a seasonally fluctuating capillary zone or mixing of meteoric and saline groundwater at depth.

2) Highly indurated, often intergrade, and partially reworked palustrine/pan facies carbonate. These deposits are characterised by a range of mineralogies which relate to the localised effects of hydrogeochemical interactions within these ground and surface water fed evaporitic systems. The carbonates are generally characterised by dense fine grained fabrics which often include numerous bioclasts, intraclasts (which indicate reworking of marginal deposits), desiccation induced grainification, microkarst, silicification, dedolomitisation, dolomitisation and evaporitic processes. The dense, unlaminated micrite fabrics are believed to be representative of bioturbation and carbonate deposition by a combination of biogenic and physicochemical mechanisms within the shallow, unstratified water conditions associated with ponds and pans (Platt, 1989; Alonso-Zarza, 2003). The replacement of evaporite minerals by silica and the complex fabric structures associated with grainification means that the samples could easily be confused with mature (stage 6 (Machette, 1985)) pedogenic calcretes. Platt (1989) characterises these marginal palustrine/pan facies as 'regressive' sequences that show an upward increase in the degree of pedogenic modification. This is usually incomplete and/or superimposed, reflecting the short-term climatic variation responsible for phases of desiccation and inundation. Periods of prolonged desiccation are characterised by the formation of hypersaline alkaline solutions which precipitated evaporites, authigenic clays, silica and dolomite (evaporative

(primary and replacement), seepage-reflux and mixing processes depending on the location of precipitation within the profile) sediments.

The majority of chemical sediment facies within the Kgalagadi are reflective of lacustrine/pan and phreatic precipitation and replacement processes associated with seasonal inundation, desiccation and seepage in a highly saline environment. The region has similarities with the facies associations identified, described and interpreted by Freytet (1973), Freytet and Plaziat (1982) and Platt (1989) and with the calcitisation, silicification and dedolomitisation mechanisms discussed by Arenas *et al.* (1999), Bustillo and Bustillo (2000) and Sanz-Rubio *et al.* (2001) from analogous terrestrial carbonate basins in southern Europe during the Cretaceous and Early Cenozoic.

The large scale lithostratigraphy of the Kalahari Group in the Kgalagadi region consists of numerous alternating intergrade calcrete/silcrete and inter-bedded sandstones, siltstone and clay horizons which form packages up to 50 m thick. The pedogenic duricrusts attest to periods of geomorphic stability during the Cenozoic at which time processes were active under a range of semi-arid to humid climatic conditions while the chemical sediments bear witness to a range of primary precipitation and reprecipitation processes which occurred under stable and active depositional environments. Subsequent shallow burial during renewed episodes of sedimentation within the sub-basins of the southern Mega Kalahari has initiated limited burial diagenetic alteration and recrystallisation.

The most likely depositional environment was a series of low gradient alluvial fan complexes located within the various structurally controlled sub-basins of the southern Mega Kalahari. The fluvial systems responsible for the endoreic sedimentation drained centripetally from the perimeter highlands and internal bedrock highs of the African surface along preferential drainage lines. The Karoo bedrock high beneath the Tshane area of the Kgalagadi is believed to form a significant internal watershed within the southern Kalahari, separating the Nossob (SW), Molopo (SE), Aranos (NW) and Makgadikgadi (NE) sub-basins. Based on bore-hole logs (BGS and WCS, 1994; 1996) it is believed that the basal gravel and lacustrine sediments of the Kalahari Group where never deposited in the Tshane area and only the terminal sediments (the Eden Formation sandstone and Mokalanen Formation carbonates described by Thomas (1981), Thomas *et al.* (1988) and Thomas and Thomas (1989)) associated with the laterally expansive aggrading of sedimentation within pre-Kalahari topography eventually buried the Tshane basement high. The extremely good correlation between the thickness of the Mosolotsane Formation and the Kalahari Group sediments indicates that the Karoo lithologies were probably aggressively eroded while exposed and contributed significant amounts of material to southern Kalahari sedimentation.

The clastic component of the Eden and Mokalanen Formations can be associated with channels and floodplains within a network of low gradient alluvial fans which were subject to highly variable discharge (*cf.* Alexander and Fielding, 2006). This alluvial complex would have been characterised by anabranching channels and localised palustrine environments, which influenced clastic and chemical facies (*cf.* Sehgal and Stoops, 1972; Lattman, 1973; Nickel, 1985;

Wright, 1990; Wright and Alonso Zarza, 1990; Marriott and Wright, 1993; Sanz *et al.*, 1995; Pimentel *et al.*, 1996; Wright and Marriott, 1996; Khadkikar *et al.*, 1998, 2000; Gierlowski-Kordesch, 1998; Pimentel, 2002; Aziz *et al.*, 2003; Müller *et al.*, 2004; Parcerisa *et al.*, 2005). Termination of Kalahari sedimentation was not an instantaneous event, as evidenced by the lithostratigraphy of the upper Kalahari sediments, but rather a protracted sequence of desiccation, stabilisation and erosion events, with intervening phases of renewed sedimentation, which resulted in the modification of deposits and allowed pedogenic processes to dominate and expand beyond marginal and interfluve areas.

The increasingly mesic conditions of the semi-arid Pliocene and early Pleistocene are associated with increased desiccation and ultimately the dominance of xeric vegetation within an arid aeolian environment which existed throughout the majority of the late Quaternary. Aeolian activity mobilised the abundant siliciclastic sediment and formed the Kalahari erg which in turn has undergone phases of partial pedogenesis during more humid phases, with topographic lows often being characterised by localised ponding that led to pan formation. These fluctuating climatic conditions are reflected in the most recent phases of pedogenic calcrete and the intergrade chemical sediments of the pans which attest to the dynamic geochemical environment at the various levels within the landscape.

Like the Cuvelai/Etosha system, the modern pan systems have superimposed their geomorphology and mineralogy on a series of older chemical sediments which evolved from palustrine and alluvial facies prior to burial beneath the Quaternary

Kalahari erg. During their modification and burial, these sediments experienced shallow diagenesis and recrystallisation associated with their relative position within the vadose, capillary fringe and phreatic zones and interaction with meteoric, evaporitically evolved and enriched percolating solutions, and groundwater.

The interaction of carbonate precipitation mechanisms, fluctuating climatic conditions and vadose and phreatic hydrology initially within an aggrading depositional environment which resulted in syn-sedimentary basin subsidence and subsequently within an erosional environment is responsible for the complex epigenesis, recrystallisation and alteration mineralogies which characterise the chemical sediments of the Kgalagadi region.

8. THE GEOMORPHOLOGY AND NEAR SURFACE CHEMICAL AND CLASTIC DEPOSITS ASSOCIATED WITH THE ETOSHA PAN, NORTHERN NAMIBIA

8.1 Introduction

Near surface epigenetic alteration of alluvial, palustrine and lacustrine deposits often occurs as a result of carbonate cementation (Lattman, 1973; De Ros *et al.*, 1994; Pimentel *et al.*, 1996; Khadkikar *et al.*, 1998), iron oxide remobilisation (Buurman, 1980; Pipujol and Buurman, 1994, 1997), clay diagenesis (Ingles *et al.*, 1998; Calvo *et al.*, 1999; Pimentel, 2002) and silicification (Thiry and Ribet, 1999). The occurrence of these alterations depends on four main factors: the mineralogy of the sediments, the diagenetic environment, the chemistry of the fluids interacting with the sediment, and the distance from the source area (Morad *et al.*, 2000; Parcerisa *et al*, 2005). This study aims to interpret facies assemblages and diagenetic and epigenetic processes associated with highly variable surface flow (a result of erratic rainfall within this semi-arid landscape), groundwater movement and the authigenic cementation within the Etosha Limestone of the southern Etosha Basin, Northern Namibia.

8.2 Geological Setting

The Etosha sub-basin of the Mega Kalahari Basin is bound on three sides by the Neogene Lucapa (North), Etosha-Griqualand-Transvaal (West) and Otavi-Caprivi-Mweru (South) axes of uplift. In the southern part of the sub-basin the upper Cenozoic Kalahari Group sediments are characterised by outcropping consolidated palustrine-lacustrine carbonates, sandstones and groundwater cal-

silcretes (which have been pedogenically modified in places) buried beneath alluvium and the degraded linear dunes of the reworked Quaternary erg (Shaw and Goudie, 2002). These deposits form the elevated Kalahari plateau (~1100 m above sea level) which contains the Etosha Pan and the drainages entering its northern shore from southern Angola. The preservation of this elevated surface attests to the influence of the African Superswell on the interior of southern Africa, where erosion has been minimal and the complex endoreic nature of deposition associated with the formation of sag basins within this NW sector of the Mega Kalahari Basin has dominated throughout the Cenozoic (Haddon and McCarthy, 2005).

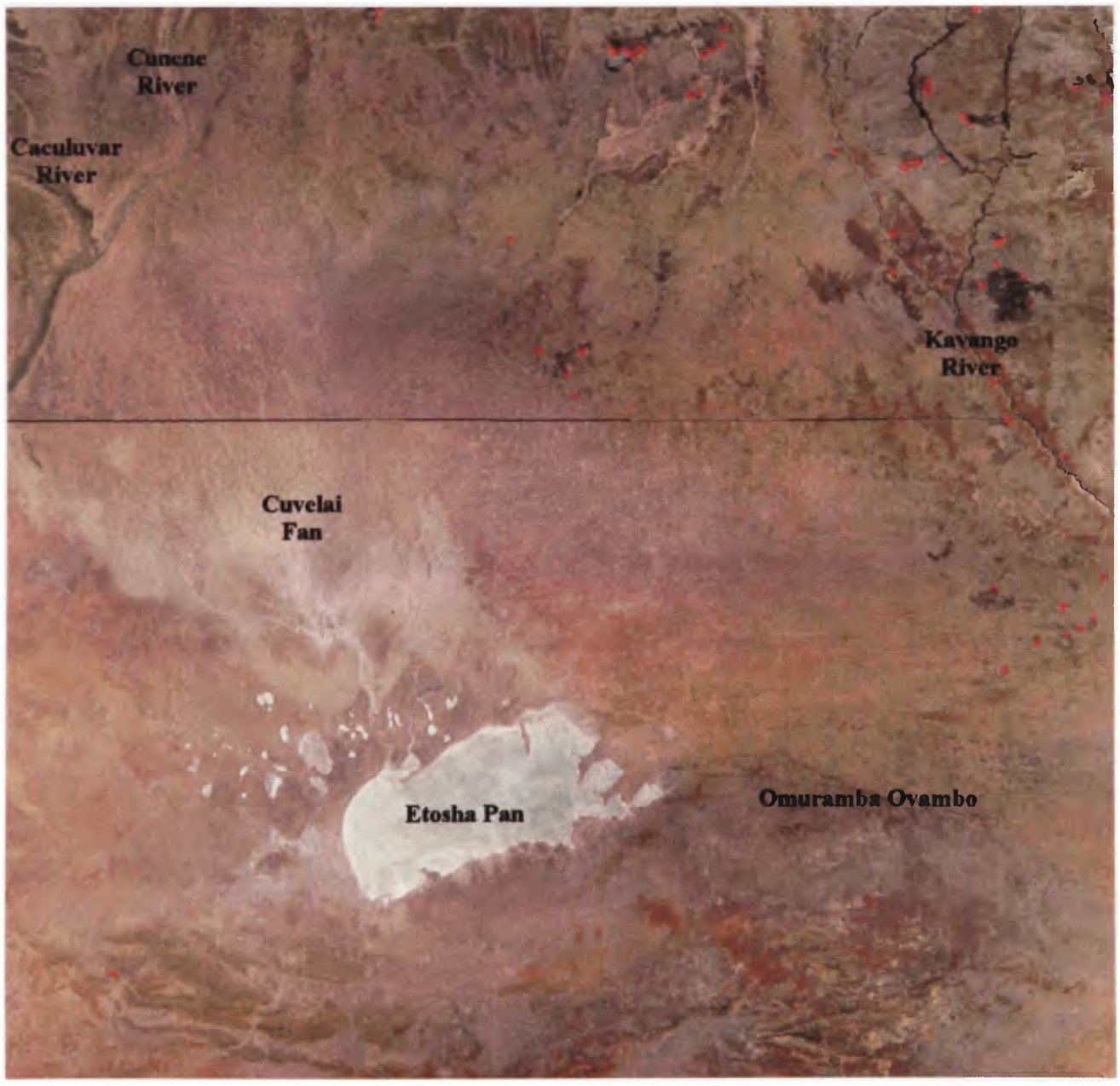


Figure 8.1: MODIS image of the Etosha Basin.

The Etosha sub-basin is filled by more than 450 m of gravels, sands, silts and clays of the Kalahari Group over a basement of Stormberg basalts and Karoo Group lithologies (Hugo, 1969; Haddon, 1999, 2001, 2005; Haddon and McCarthy, 2005). The extensive contemporary floodplain sand deposits of the palaeo Kunene/Cunene and contemporary Cuvelai alluvial fans to the north of the Etosha Pan reveal the complex and dynamic fluvio-lacustrine history which has resulted from discharge variability and modifications to the basin architecture. Palaeo-environmentally this region is extremely significant and provides a detailed record of tectonic and fluctuating climatic influence on Cenozoic depositional systems. This is especially significant in light of Africa's stable position during the last 30 Ma (Burke, 1996) when the Kalahari Group sediments in this region are believed to have accumulated.

The southern part of the sub-basin is dominated by a series of pans, of which Natukanaoka and Etosha are the largest (Fig 8.1). The central part of the sub-basin between the Cunene and Kavango Rivers is dominated by the south flowing drainages of the Etaka, Gwashuuli/Omulonga, Shalupumbi, Shilungo/Shakambebe/Cuvelai (all of which degenerate into the broad shallow anabranching/bifurcating seasonal braid-plain/floodplains known as the Oshana Region) which feed into Lake Oponono and then the Ekuma River, along with the more easterly Gwashigambo/Oshigambo and Nipele/Odila Rivers. The wetter northern part of the basin is dominated by *Miombo* and savanna woodland vegetated degraded linear dunes and dune parallel interdunal drainage (Shaw and Goudie, 2002).

8.3 Geomorphology of the Etosha Pan

The 6133 km^2 Etosha Pan complex (including the smaller adjacent pans to the east and west, commonly referred to as the Ovambo Pans Plain), is one of the largest pan systems in the world (McIntyre and Atkins, 1991). Numerous theories for the formation of the Etosha Pan have been debated. The foremost theory states that although the contemporary pan is only prone to limited seasonal inundation, the Etosha Basin was characterised by a ~45 m deep 82 000 km^2 palaeo-lake during the late Pliocene and early Pleistocene (Stuart-Williams, 1992). This palaeo-lake is believed to have formed in response to the substantial but episodic Pliocene uplift along the Etosha-Griqualand-Transvaal axis which closed the sub-basins south-western outlets. Prior to this the basins principal outlets are believed to have been located in the Starkberg and Dolomietberge area. Thus the palaeo-Cunene possibly flowed into the Atlantic Ocean via the Ohanyuna, Okawerongo and Otjovasandu into the Aap and ultimately the Hoanib River rather than its more northern contemporary course.

Although the Pliocene and Pleistocene uplift, folding and faulting along the western and south-western edge of the sub-basin reduced and ultimately closed the Hoanib-Cunene palaeo-channel and reversed the flow direction of the main channels (Omuramba Onaiso?) in the south-western sector, it also rejuvenated the coastal streams of Damaraland and Kaokoland. During the Quaternary, one of these re-energised drainages eroded through the rim of the basin and captured the lower Cunene near Ruacana. The diversion of water westwards and the subsequent adjustments to the Cunene's profile between Xangongo and Ruacana,

as evidenced by the numerous knick points, caused the palaeo-lake to gradually desiccate as it was deprived of its only perennial water source.

Throughout this period of activity along the western margin, the opposite effect was occurring to the east of the axis of uplift, where river gradients were reduced or even reversed and low energy depositional systems dominated. In this respect, it has been proposed that palaeo-lake Etosha had an eastern outlet along the Omuramba Ovambo (Stuart-Williams, 1992) which may have linked with the Okavango-Ngami-Makgadikgadi system via the Bushmanland drainage.

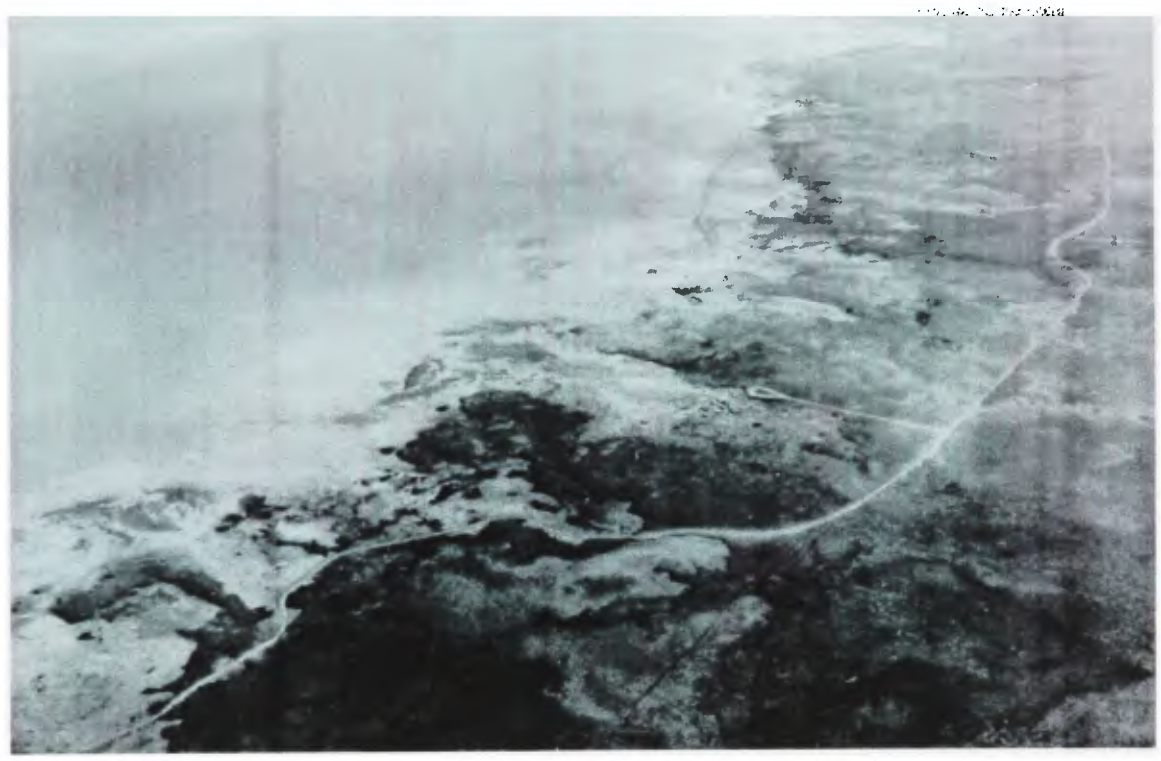


Figure 8.2: An aerial photograph of the terrace along the southern rim of Etosha Pan.

The occurrence of stromatolites (Smith and Mason, 1991) within the Poacher's Point sequence in the NE sector of the Etosha Pan alludes to the precipitation of lacustrine carbonate during the existence of palaeo-lake Etosha. This extremely well cemented exposure, which is preserved as inverted topography within the contemporary erosive system, rises ~15 m above the contemporary pan floor as a peninsula. Although isolated in this NE sector of the pan, its elevation (the pan

floor varies between 1071 m (eastern side) and 1086 m (western side) above sea level (Buch *et al.*, 1992)) corresponds well with other late Pliocene/Pleistocene lacustrine deposits in the area (pers comm. M. Hipondoka), known collectively as the 'Etosha limestone' (Rust, 1984). In addition the wide-spread occurrence of the 1100 m terrace throughout the central part of the basin (Fig 8.2) provides additional evidence for the existence of palaeo-lake Etosha.

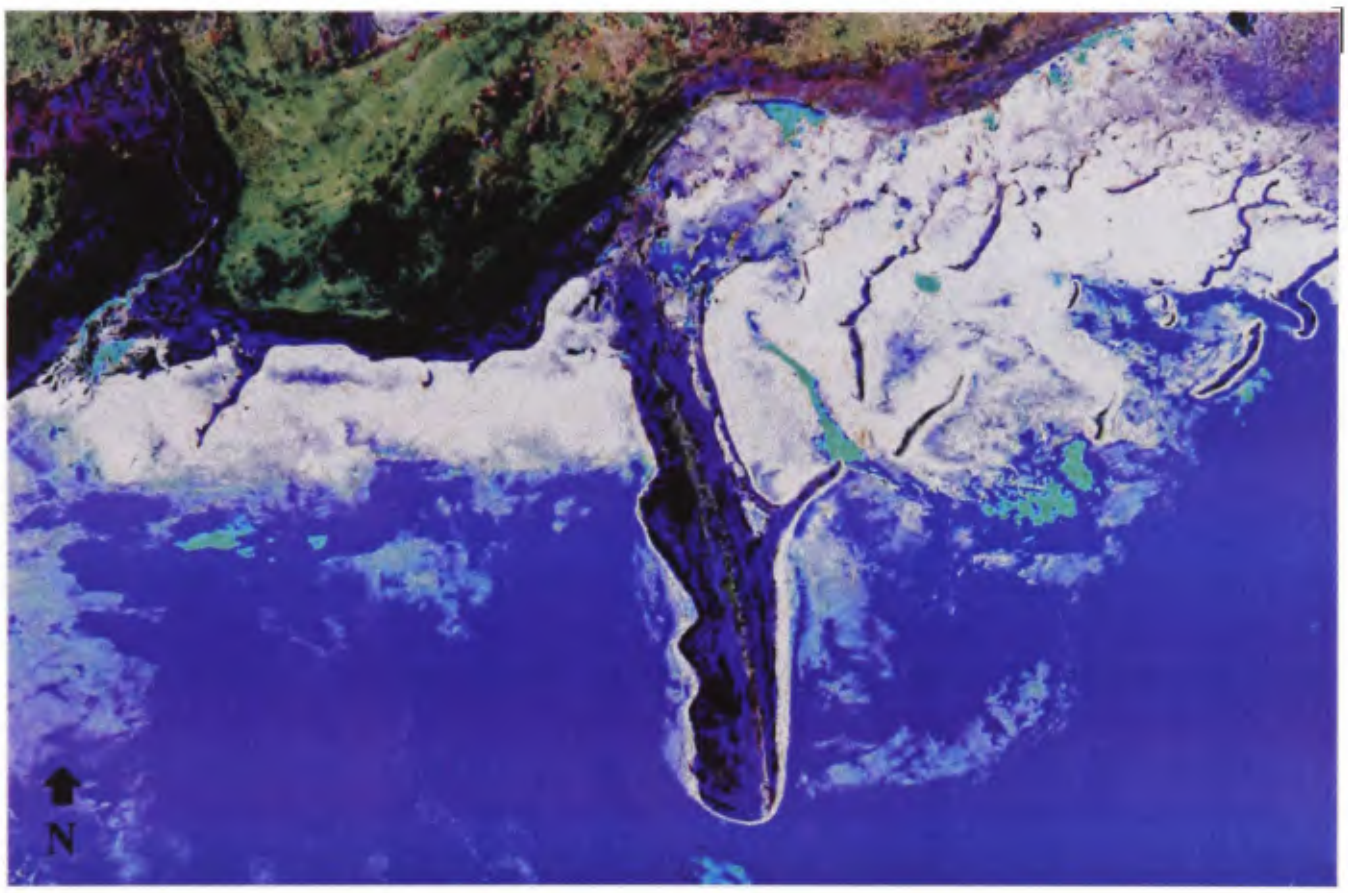


Figure 8.3: LANDSAT image of Poachers Point, the Odila River delta and the bar and peninsula features of the NE sector of Etosha Pan.

The limited evidence of strandlines (Fig 8.3) suggests that unlike the Makgadikgadi and Ngami palaeo-lakes, there has been very limited lacustrine activity within the pan during the late Quaternary. The most feasible explanation is that following the reorientation of the Cunene in the early Pleistocene the palaeo-lake slowly desiccated into a seasonal floodplain and pan network fed by the ephemeral Cuvelai, Oshigambo and Odila drainages. Thus there was a

significant reduction in competence and capacity within the system during the early Pleistocene and as a result sedimentation was curtailed and became primarily associated with flood events. The occurrence of a silicified Pleistocene vertebrate bone (pers comm.. E.R. Seiffert) lag within the upper sediments on the Oshigambo Peninsula records one such catastrophic flood event. This indicates that as the desiccating palaeo-lake contracted, so the alluvial fan and seasonal floodplains associated with the northern drainages prograded southwards, concealing the underlying lacustrine marls and clays of the lower Andoni Formation and producing a coarsening upwards sequence. Similarly reworked littoral deposits conceal the underlying lacustrine deposits to the west and NW of Ozonjuitji Mbari, NE of Andoni and SE of Kalkheuwel.

In line with Rust (1984) and Buch *et al.* (1992) the contemporary NE-SW orientated Etosha Pan is believed to be an erosional landform which has been excavated within the Etosha Limestone and Andoni Formation by continuous denudation processes operating on the playa in a seasonal rhythm. The western margin double lunettes of the Etosha Pan (dated to ~140 ka, Buch *et al.*, 1992) indicate that deposition linked to the deflation of pan material has been occurring at this location since the late Pleistocene.

The dominant seasonal cycle of inundation (summer) and subsequent desiccation of the pan promotes intense chemical weathering under alkaline conditions. During the wet season the fluvial systems in the north along with the localised centripetal drainage deposits detrital material on the pan surface. This thin surface deposit along with the perimeter Etosha Limestone and underlying Andoni

Formation then experiences intense *in situ* chemical weathering under the saline-alkaline conditions. The residual deposits are dominated by a thin veneer of corroded silt and sand impregnated with evaporate salts (halite, berlinite, thenardite and burkeite) and carbonates (calcite and dolomite) which are then eroded from the desiccated and unvegetated pan surface (Giess (1971) classified it as a saline desert) by the extensive deflation (Fig 8.4) which occurs during the dry season (winter). This cycle of weathering and erosion promotes the excavation and lateral expansion of the pan features. Borehole logs (Hugo, 1969) suggest that the intensity of *in situ* chemical alteration decreases rapidly with increasing depth. The low permeability of the Andoni clays result in a perched near surface stratified aquifer which undergoes salinization as a result of evaporitic and evapotranspiritic processes. In due course the cycle of erosion is believed to result in the coalescencing of several smaller pans following the erosion of the intervening scarps (Rust, 1984; Shaw, 1988b; Buch *et al.*, 1992).



Figure 8.4: LANDSAT image of dust blowing off NW Namibia.

The intensity of deflation and chemical weathering within the pan system is believed to have fluctuated in response to larger scale climatic variability. As a result, a number of periods of intensified erosion have been suggested by Rust

(1984) and Buch *et al.* (1992). Perhaps during the intervening (cooler?) periods when the Kalahari anticyclone was less intense and the pan surface underwent reduced deflation, a partially stabilised surface developed. This stabilised surface may then have been colonised by grass species such as *Sporobulus spicatus*, which is tolerant of high salinities (*c.f.* Hamilton *et al.*, 2001), and may have initiated pedogenesis and the associated precipitation of pedogenic calcrete within the B horizon.

The contemporary Etosha Pan is characterised by hot and semi-arid conditions with a mean annual rainfall (MAR) of ~430 mm falling during the December-April rainy season and a potential evapo-transpiration (PET) of ~3000 mm (Berry, 1973; Smith and Mason, 1991). Climatically there are three distinct seasons; hot and wet (January to April), cool and dry (May to August), and hot and dry (September to December). High wind velocities are common during the late winter (Le Roux, 1980) and it is during this period that large volumes of dust are deflated off the pan surface (Bryant, 2003).

Today Etosha Pan is subject to periodic, partial flooding during the rainy season. Direct rainfall accounts for only a small proportion of the pan's water with the majority supplied by the four seasonal rivers: the Ekuma, Oshigambo, Odila and Omuramba Ovambo, which drain into the pan from the north and east. Numerous spits and bars are evident along the northern shore of the pan and suggest very active geomorphological processes associated with periods of inundation (Fig 8.3). All four rivers flow erratically during the rainy season and, depending on their levels, flood the pan to varying degrees in a progressive clockwise direction.

In unusually dry years, the rivers may not flow at all, forming a series of disconnected pools. During these dry years, the pan holds direct rainfall only. The pan does, however, usually hold some water for a few months between January and April. Every 7-10 years, during exceptional rains, Etosha Pan is transformed into a shallow saline lake approximately one meter deep (Balfour and Balfour 1992).

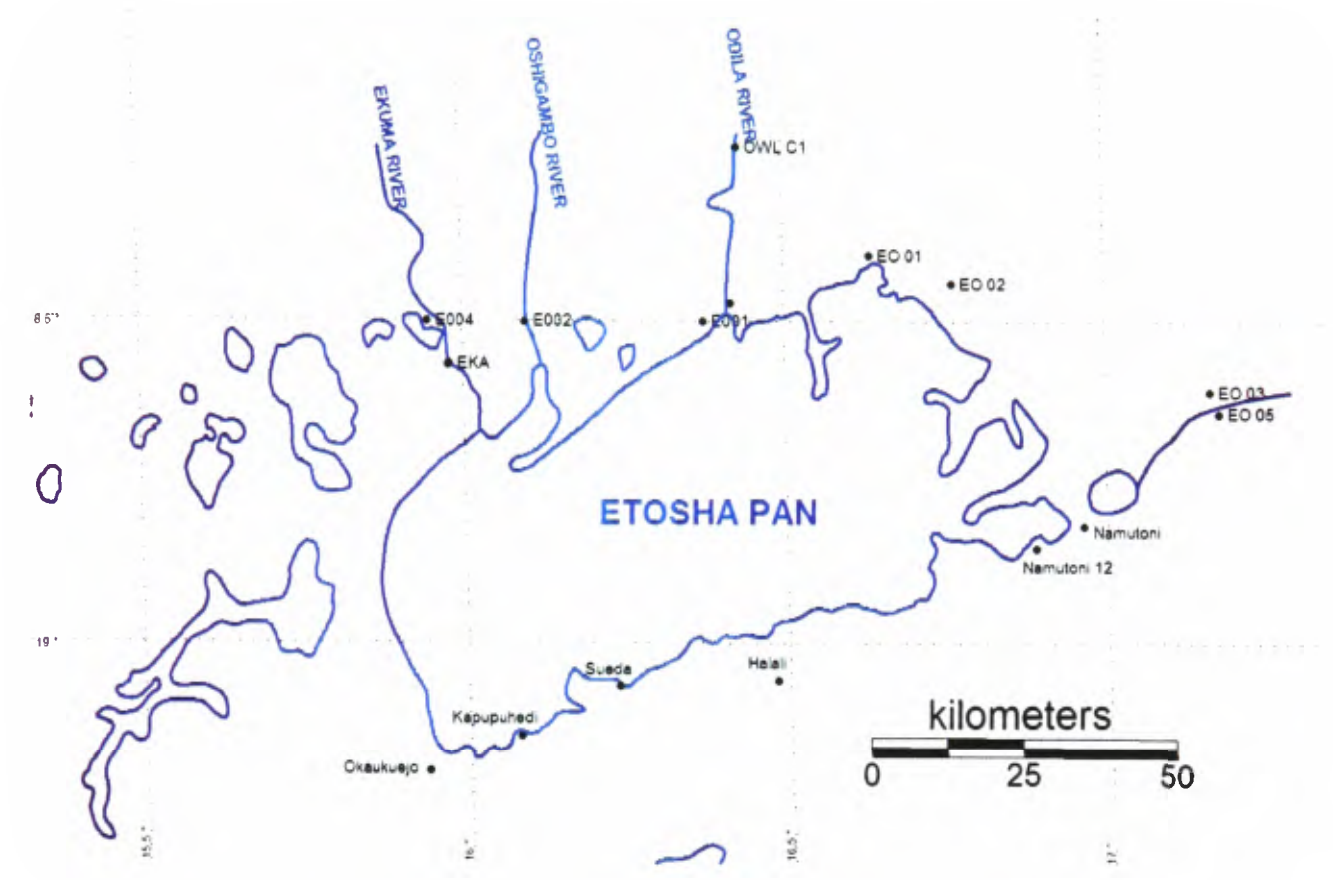


Figure 8.5: Map of Etosha indicating the location of sample sites.

Groundwater beneath the pan surface is saline with a pH between 8.8 and 10.2 and a sodium content in excess of 30,000 ppm (Le Roux, 1980). Three different types of springs (contact, water-level and artesian) are common throughout the southern Etosha sub-basin (McIntyre and Atkins, 1991). Contact springs are the most common and are found at the edge of pans where the carbonate aquifer is truncated and water seeps out above the impermeable underlying clay. Water-level springs are unreliable and occur when depressions in the surface carbonate aquifer expose the water table.

Sample	Depth	Colour	% Gravel	% Sand	% Mud	Descriptive Statistics	Textural Group	Mean (Folk & Ward Method) in microns	Median in microns
E001	0.2	10Y 5/1 Greenish Gray	0	28.4	71.6	Platykurtic, Polymodal, Coarse Skewed, Very Poorly Sorted	Slightly Gravelly Sandy Mud	33.82	24.32
E001	0.35	10Y 5/1 Greenish Gray	0	43.6	56.4	Very Platykurtic, Polymodal, Coarse Skewed, Very Poorly Sorted	Sandy Mud	42.87	31.75
E001	0.5	10Y 5/1 Greenish Gray	0.1	85.4	14.6	Very Leptokurtic, Bimodal, Very Fine Skewed, Poorly Sorted	Slightly Gravelly Muddy Sand	326.6	363.7
E001	0.75	10Y 4/1 Dark Greenish Gray	0	34.6	65.4	Very Platykurtic, Polymodal, Coarse Skewed, Very Poorly Sorted	Sandy Mud	40.38	25.43
E001	1.5	10Y 4/1 Dark Greenish Gray	0	5.5	94.5	Very Leptokurtic, Polymodal, Very Coarse Skewed, Poorly Sorted	Slightly Gravelly Mud	3.67	2.95
E001	1.75	10Y 4/1 Dark Greenish Gray	0	20.7	79.3	Leptokurtic, Polymodal, Coarse Skewed, Very Poorly Sorted	Sandy Mud	20.39	14.12
E001	2	10YR 4/2 Dark Grayish Brown	0	82.5	17.5	Very Leptokurtic, Unimodal, Very Fine Skewed, Poorly Sorted	Muddy Sand	146.9	218.8
E001	2.5	10YR 4/2 Dark Grayish Brown	0.2	80.9	18.9	Very Leptokurtic, Polymodal, Very Fine Skewed, Poorly Sorted	Slightly Gravelly Muddy Sand	132.7	211.1
E001	3	10YR 4/2 Dark Grayish Brown	0	76.4	23.5	Leptokurtic, Polymodal, Very Fine Skewed, Very Poorly Sorted	Slightly Gravelly Muddy Sand	110	201.3
E002	0.3	10YR 4/1 Dark Gray	0	83	17	Very Leptokurtic, Trimodal, Very Fine Skewed, Poorly Sorted	Muddy Sand	147.1	204
E002	0.5	10YR 4/1 Dark Gray	14.4	43.9	41.7	Mesokurtic, Polymodal, Symmetrical, Very Poorly Sorted	Gravelly Muddy Sand	100.5	112.5
E002	0.65	10YR 4/1 Dark Gray	3	41.8	55.2	Platykurtic, Polymodal, Symmetrical, Very Poorly Sorted	Slightly Gravelly Sandy Mud	39.69	36.99
E002	1	10YR 4/1 Dark Gray	18.8	31.3	49.9	Platykurtic, Polymodal, Coarse Skewed, Extremely Poorly Sorted	Gravelly Mud	109.1	63.45
E002	1.2	10YR 4/1 Dark Gray	16.8	24.1	59.1	Mesokurtic, Polymodal, Very Coarse Skewed, Extremely Poorly Sorted	Gravelly Mud	67.63	30.77
E002	1.5	5GY 5/1 Greenish Gray	14.6	30.1	55.3	Mesokurtic, Polymodal, Coarse Skewed, Very Poorly Sorted	Gravelly Mud	68.81	40.55
E002	1.75	5GY 5/1 Greenish Gray	4	46.7	49.3	Mesokurtic, Polymodal, Fine Skewed, Very Poorly Sorted	Slightly Gravelly Sandy Mud	47.26	65.52
EKA1	0.25		0	95.7	4.3	Mesokurtic, Polymodal, Symmetrical, Moderately Sorted	Sand	215.5	217.6
EKA1	0.5		0	95.1	4.9	Mesokurtic, Polymodal, Symmetrical, Moderately Sorted	Sand	207	210.6
EKA1	1		0.2	82.3	17.5	Very Leptokurtic, Trimodal, Very Fine Skewed, Poorly Sorted	Slightly Gravelly Muddy Sand	127.7	193.6
EKA1	1.5		1.6	85	13.5	Very Leptokurtic, Polymodal, Fine Skewed, Poorly Sorted	Slightly Gravelly Muddy Sand	189.1	206.7
EKA1	2		0.9	91.7	7.4	Very Leptokurtic, Polymodal, Fine Skewed, Poorly Sorted	Slightly Gravelly Sand	236.8	251.3
EKA2	0.5		0.1	94.3	5.6	Very Leptokurtic, Bimodal, Fine Skewod, Moderately Sorted	Slightly Gravelly Sand	259	272.5
EKA3	0.25		0	97.7	2.3	Leptokurtic, Bimodal, Symmetrical, Moderately Well Sorted	Sand	221.6	215.2
EKA3	0.5		0	95.9	4.1	Leptokurtic, Bimodal, Symmetrical, Moderately Sorted	Sand	195	195.8
EKA3	1		0	98.6	1.4	Leptokurtic, Bimodal, Fine Skewed, Moderately Well Sorted	Sand	301.5	316.3
EKA3	1.5		0	99	1	Leptokurtic, Unimodal, Symmetrical, Moderately Well Sorted	Slightly Gravelly Sand	361.3	352.7
EKA3	2		0.1	98.4	1.5	Mesokurtic, Trimodal, Coarse Skewed, Moderately Well Sorted	Slightly Gravelly Sand	314.9	304.1
EKA4	0.25		0.6	95.1	4.3	Very Leptokurtic, Trimodal, Symmetrical, Moderately Sorted	Slightly Gravelly Sand	256.7	249.7
EKA4	0.5		0.1	93.9	6	Very Leptokurtic, Bimodal, Fine Skewed, Moderately Sorted	Slightly Gravelly Sand	218	224

Table 8.1: Sedimentology of unconsolidated samples.

8.4 Lithological Units and Facies Assemblages

8.4.1 Unconsolidated Deposits

Fluvio-palustrine sediments were collected using a hand auger from each of the three principal drainages (Ekuma, Oshigambo and Odila) along the northern shore of Etosha Pan (Fig 8.5). Ten sample sites along two transects of the channel were investigated at the Ekuma River and one each at the Odila and Oshigambo Rivers. The geomorphology of the channels ranged from the 30 m wide simple channel of the Odila River, which was incised 1.5 m into the pan terrace, to the more complex channels of the Ekuma (Fig 8.6) and Oshigambo Rivers. The channels at these sites consisted of a mega channel ~100 m wide in each case, which was incised approximately 2-10 m into the adjacent terrace (Fig 8.7). Within the mega channel there were a number of smaller channels and eddy pools separated by 0.5 m high islands and channel bars. At all the sites investigated, samples were collected at regular intervals and lithologic unconformities to the maximum depth of penetration possible using a hand auger.



Figure 8.6: An aerial photograph of the complex channel morphology associated with the anabranching and meandering Ekuma River.

Textural analysis of the samples collected indicated that the sediments are generally poorly sorted and range between sand and sandy mud (Table 8.1). The Olida and Oshigambo Rivers have the finest textured sediments, while samples collected from the Ekuma River have a sandier texture.



Figure 8.7: Photograph of the western terrace of the Ekuma River at the old horse camp north of Etosha Pan.

Investigation of the sediments within the Odila and Oshigambo Rivers along with the northern transect across the Ekuma River suggest that these systems are actively eroding the underlying Plio-Pleistocene Andoni Formation and deposition is minimal. Thus textural analysis of the unconsolidated sediments/saprolite below the surface within the channels is believed to be reflective of sedimentation and facies assemblages associated with the Andoni Formation rather than contemporary channel deposits.

The 3 m thick channel deposits investigated at the Odila River suggests a series of sedimentary sequences (possibly cyclothems) within the green-grey marls that reflect changes to the shallow lacustrine depositional environment under varying

conditions (Fig 8.8). The lower 1 m of the profile shows a coarsening upwards sequence with a mean grain size varying from very fine to fine sand. This sequence of greyish-brown muddy sand is interpreted as being reflective of a shore face marginal lacustrine facies which experienced input of clastic terrigenous material, possibly from river generated density currents associated with episodic flood events, during a regressive lacustrine stage (*c.f.* Freytet and Plazait, 1982; Platt, 1989). At approximately 2 m below surface (m.b.s.) a distinct textural unconformity occurs. This textural unconformity marks the maximum stage of regression when the facies is fluvial (unimodal textural distribution) rather than marginal lacustrine (polymodal textural distribution). Above this level the transition to anoxic greenish-grey finer textured sediments reflects the return to marginal lacustrine and eventually deeper water more open lacustrine conditions (1.5 m.b.s.) which experience a reduced influence from terrigenous clastic material. This facies variation is believed to be the result of a lake transgression caused by either increased discharge or additional damming of the outflow point. The mechanisms driving these changes are believed to have been climatic variability and/or geomorphic/neotectonic influence on the system.

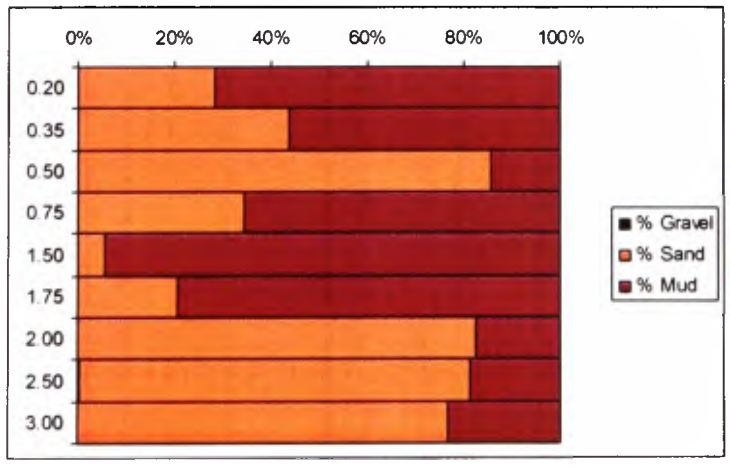


Figure 8.8: Gravel, sand and mud fraction versus depth below surface from the Odila River channel.

Between 1.5-2 m.b.s. the profile indicates a fining upwards sequence (the samples are all coarse skewed) from coarse to very fine silt, which suggests a reduced influence of clastic material input by fluvial systems along the lake margins. However, above 1.5 m.b.s. the textural profile coarsens upwards again to a maximum mean grain size (medium sand) at 0.5 m.b.s.. This suggests another regressive sequence and a return to marginal lacustrine conditions (green anoxic colouration of the sediments) which experienced a significant fluvial influence (bimodal distribution) at 0.5 m.b.s.. Above the distinct textural unconformity at 0.5 m.b.s. the profile then shows a repeat of the lower sequence with a rapid fining upwards trend, mean grain size varies from very coarse to coarse silt and all samples are coarse skewed, suggesting a return to more open lacustrine conditions.

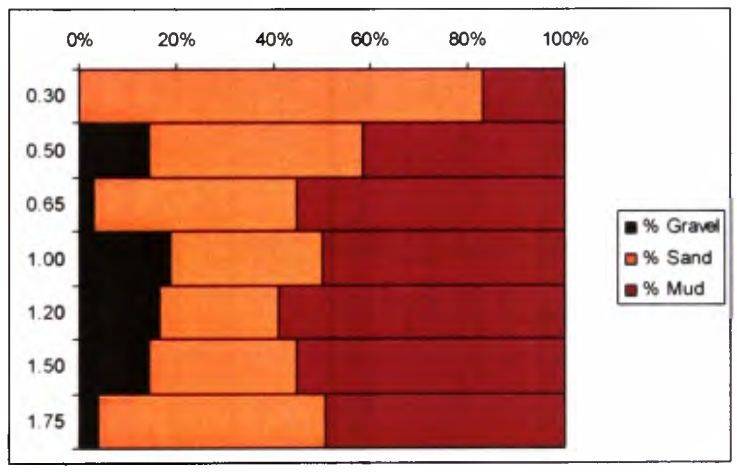


Figure 8.9: Gravel, sand and mud fraction versus depth below surface from the Oshigambo River channel.

The textural sequence at the Oshigambo River (Fig 8.9) has very similar characteristics to that investigated at the Odila River. The sequence is believed to represent an adjacent lacustrine facies or a facies continuum, although lateral correlation was not possible due to a lack of stratigraphic markers and survey data. Between 1-1.75 m.b.s. the anoxic greenish-grey to grey sediments reflect a general fining upwards sequence (mean grain sizes are all in the very fine sand

fraction). This sequence is believed to record a shift to deeper, more open lacustrine conditions and the associated reduced influence of terrigenous input linked to a transgressive lake phase from the slightly more marginal lacustrine facies at 1.75 m.b.s.. At 1 m.b.s. a minor textural unconformity records an increased terrigenous influence, probably linked to a minor regression. However, despite an initial reduction in the mean grain size (from very fine sand to very coarse silt) of the overlying sample at 0.65 m.b.s., believed to represent a partial recovery of the lake level, a general coarsening upwards sequence reflecting a lake regression is evident in the upper sediments of the profile. This coarsening upwards trend (mean grain size increases from very fine to fine sand) reflects a transition to a more marginal lacustrine facies.



Figure 8.10: Aerial photographs of the Ekuma River's birds-foot delta debouching into the Etosha Pan (a) from the south and (b) from the north.

The contemporary Ekuma River is fed by the floodplains (oshanas) of the Cuvelai alluvial fan. This system is actively eroding Kalahari palaeodunes and the Andoni Formation north of the Etosha Pan while depositing clastic material within the lower course of its channel as a large birds-foot delta where it debouches into the Etosha Pan (Fig 8.10). Significant over-grazing and increased population density within the oshanas of Ovamboland, at the heart of the Ekuma drainage, is believed to be the single most significant contributing factor to the increasing sediment

load of the lower system. By contrast the Odila and Oshigambo drainages are relatively narrow incised channels located to the east of the main population centres in Ovamboland within the well vegetated degraded linear dunes of the northern Kalahari.

A series of unpaired terraces composed of unconsolidated fluvial sand containing numerous cal-silcrete nodules near the mouth of the Ekuma River indicate the extent of recent fluvial deposition and incision. The eastern terraces occur at approximately 7.5 m above and 1-1.5 km east and 2.5 m above and 50 m east of the contemporary channel. The corresponding west bank terrace is approximately 7 m above the contemporary channel bed and forms the undercut bank of a 10 m wide side channel.

These terraces suggest that the meandering lower Ekuma River has incised into its former deposits and the underlying Andoni Formation in response to a lowering of the base-level. The mechanism responsible for this change in base-level may be Plio-Pleistocene uplift/flexure in the northern part of Etosha Pan and/or the reduced and increasingly episodic flow and the resultant receding lake levels associated with the reorientation of the Cunene River. Eastward expansion of the Ekuma has been limited due to a consolidated sandstone unit which forms the interfluve between the lower Ekuma and Oshigambo Rivers. The *Mopane* vegetated fluvial sediments of the western terrace also suggest the existence of a western palaeo-channel which may have linked to the nearby Natukanaoka Pan, although this needs further investigation.

	Whole rock analyses														< 2µm fraction analyses						
	Quartz	Analcime	Calcite	Dolomite	Plagioclase	K-feldspar	Rutile	Halite	Berlinite	Chalcopyrite	Mica	Palygorskite	Sepiolite	Interstratification	Quartz	Calcite	Dolomite	Feldspar	Mica	Palygorskite	Sepiolite
Odila River Channel (E001) - 0.75m	59	22	10		1	-	-	6	-	-	-				no < 2µm fraction analysis done						
Odila River Channel (E001) - 2.0m	97		-	-	-	1	-	2	-			-	-	-	no < 2µm fraction analysis done						
Oshigambo River Channel (E002) - 0.3m	83	6	5	-	1	-		5	-		-	-	-	-	no < 2µm fraction analysis done						
Oshigambo River Channel (E002) - 0.65m	81	13		-		-	-	1	5	-				-	no < 2µm fraction analysis done						
Oshigambo River Channel (E002) - 1.0m	80	3	11	-	-	5	-	-	-		1	-			no < 2µm fraction analysis done						
Oshigambo River Channel (E002) - 1.75m	81	18		-	-	-	-	-		1		-		-	no < 2µm fraction analysis done						
Ekuma River Channel Nodules (E003) - 0.5m	74		13	13		-	-	-			-	-	-	-	no < 2µm fraction analysis done						
Ekuma River Channel (EKA1) - 1.0m	100	-		-	-				-	-		-	-		no < 2µm fraction analysis done						
Ekuma river Channel (EKA1) - 2.0m	99				-	-	-	1	-		-	-	-		no < 2µm fraction analysis done						
Ekuma River Channel (EKA2) - Surface	19	-	-	-	-	-	-	81	-	-	-	-	-		no < 2µm fraction analysis done						
Ekuma River Channel (EKA2) - 0.3m	62	-	-	-	-	-		38	-	-	-	-	-	-	no < 2µm fraction analysis done						
Ekuma River Channel (EKA2) - 0.5m	98	-	-	-		-	2		-						no < 2µm fraction analysis done						
Ekuma River Channel (EKA3) - 2.0m	100														no < 2µm fraction analysis done						
Ekuma River Channel (EKA4) - 0.5m	100			-	-	-		-	-	-	-	-	-	-	no < 2µm fraction analysis done						
Poachers Point Nodular	46		53	-	-	-	1	-	-	-	-	-	-		no < 2µm fraction analysis done						
Poachers Point Stromatolite	19		80			-	1		-	-	-	-	-	-	no < 2µm fraction analysis done						
Andoni Formation Sandstone	48	11	14	27					-						no < 2µm fraction analysis done						
Oshigambo River Terrace (98/11)	99				-	-	1								no < 2µm fraction analysis done						
Eastern Owamboland (EO) 01	6	-	39	53	-	-	-	-	-			2			no < 2µm fraction analysis done						
Eastern Owamboland (EO) 02	44	-	16	38				-	-			-		2	31	-	33		7		29
Eastern Owamboland (EO) 03	21		1	8		-	-	-	-	-	-	-	70	-	-	-	-	-	-	3	97
Eastern Owamboland (EO) 05	25	-		75	-	-	-	-			-	-	-		no < 2µm fraction analysis done						
Okaukuejo	13	-	87	-	-	-	-	-	-	-		-			27	57			-	-	16
Kapupuhedi	8		69	23			-								no < 2µm fraction analysis done						
Sueda	7		16	77	-	-	-								no < 2µm fraction analysis done						

Namutoni 12	-		49	51		-	-			-		-			-	46	22		-		32
Ekuma/Etaka River (T1-16) - 3.5m	21		79		-	-	-	-							13	81	-		-		6

Table 8.2: Summary of XRD analysis.

The active channel of the lower Ekuma is approximately 50 m wide and bifurcates around the numerous channel bars (Fig 8.6). The contemporary channel sediments consist of a surface veneer of carbonate and evaporite minerals (Table 8.2) which grade into a thin (1-2 cm thick) clay horizon. The underlying sediment (Table 8.1) consists of a bimodal (principal mode is medium sand and the minor mode is very fine sand), moderately sorted white fluvial sand containing scattered 2-4 mm carbonate rich nodules at a depth of 0.5 m.b.s.. The bimodal distribution of the sediment is believed to reflect the highly variable discharge during flood events. In addition, late stage deposition of suspended material and illuviation of fines occurs during desiccation. At a depth of 0.6 m.b.s. the gley coloured clay of the underlying Andoni Formation is intersected and with increasing depth the sediments rapidly consolidated into a massive green coloured channel silcrete.

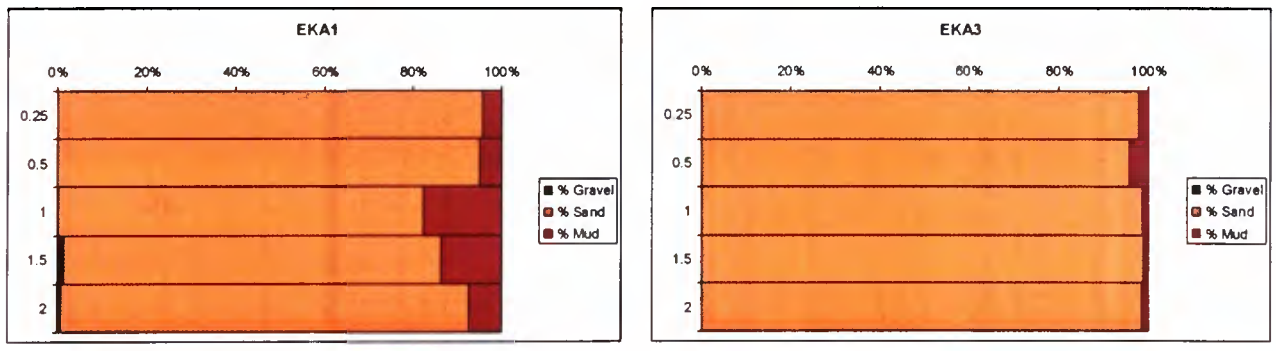


Figure 8.11: Profiles (a) EKA1 and (b) EKA2 taken along a transect across the lower Ekuma River illustrating the gravel, sand and mud fraction versus depth below surface.

A 10 m wide side channel is located at a slightly higher elevation adjacent to the bank 75 m west of the main channel bed. The 0.5 m thick sandy channel sediments, which overlie the Andoni Formation clay, are devoid of the

efflorescent salt crust and clay horizon encountered on the surface of the main channel, but are characterised by similar 2-8 mm carbonate rich nodules at depth. The textural characteristics of the sediment sampled at 0.5 m.b.s. is slightly finer but otherwise almost identical to those of the sediment sampled at the same depth in the main channel (Fig 8.11).

River	Sample	Depth	% Organic Material	% Carbonate	% Other Minerals	Comments
Odila	E001	0.20	7.32	3.37	96.63	
Odila	E001	0.35	5.28	2.83	97.17	
Odila	E001	0.50	1.33	0.95	99.05	
Odila	E001	0.75	7.31	4.64	95.36	
Odila	E001	1.50	8.19	4.70	95.30	
Odila	E001	1.75	8.70	4.83	95.17	
Odila	E001	2.00	1.98	2.01	97.99	
Odila	E001	2.50	2.39	1.90	98.10	
Odila	E001	3.00	3.75	2.42	97.58	
Oshigambo	E002	0.30	3.14	6.59	93.41	
Oshigambo	E002	0.50	2.63	6.54	93.46	
Oshigambo	E002	0.65	1.71	3.42	96.58	
Oshigambo	E002	1.00	3.36	6.85	93.15	
Oshigambo	E002	1.20	2.55	10.49	89.51	
Oshigambo	E002	1.50	3.24	5.54	94.46	
Oshigambo	E002	1.75	2.97	7.22	92.78	
Ekuma	EKA1	0.25	0.65	0.12	99.88	
Ekuma	EKA1	0.50	0.53	0.23	99.77	
Ekuma	EKA1	1.00	0.93	0.52	99.48	
Ekuma	EKA1	1.50	1.04	1.24	98.76	
Ekuma	EKA1	2.00	0.94	2.23	97.77	
Ekuma	EKA2	0.00	1.21	49.83	50.17	
Ekuma	EKA2	0.30	6.06	24.13	75.87	
Ekuma	EKA2	0.50	0.36	7.58	92.42	
Ekuma	EKA3	0.25	0.46	0.15	99.85	
Ekuma	EKA3	0.50	0.51	0.26	99.74	
Ekuma	EKA3	1.00	0.11	0.17	99.83	
Ekuma	EKA3	1.50	0.12	0.14	99.86	
Ekuma	EKA3	2.00	0.07	1.24	98.76	
Ekuma	EKA4	0.25	0.43	1.86	98.14	
Ekuma	EKA4	0.50	0.53	1.97	98.03	
Ekuma	E004A	0.15		4.53	95.47	Thermal oxidation of Fe (Red)
Ekuma	E004A	0.35		3.75	96.25	Thermal oxidation of Fe (Orange)
Ekuma	E004A	0.80		1.71	98.29	Thermal oxidation of Fe (Orange)
Ekuma	E004A	1.00		1.56	98.44	
Ekuma	E004A	1.20		1.11	98.89	
Ekuma	E004A	1.65		1.89	98.11	
Ekuma	E004A	1.80		1.99	98.01	
Ekuma	E004A	2.00		9.89	90.11	
Ekuma	E004A	2.30		12.70	87.30	
Ekuma	E004A	2.50		5.70	94.30	

Ekuma	E004B	0.30		16.02	83.98	
Ekuma	E004B	0.60		15.25	84.75	
Ekuma	E004B	1.50		7.12	92.88	
Ekuma	E004C	0.20		0.56	99.44	Thermal oxidation of Fe (Very Red)
Ekuma	E004C	0.50		1.00	99.00	
Ekuma	E004C	0.70		1.88	98.12	
Ekuma	E004D	0.10		0.06	99.94	Thermal oxidation of Fe (Orange)
Ekuma	E004D	0.40		0.09	99.91	Thermal oxidation of Fe (Orange)
Ekuma	E004D	0.65		1.04	98.96	Thermal oxidation of Fe (Orange)
Ekuma	E004D	1.00		1.07	98.93	Thermal oxidation of Fe (Orange)
Ekuma	E004D	1.50		0.90	99.10	
Ekuma	E004D	2.00		1.34	98.66	
Ekuma	E004D	2.50		0.98	99.02	
Ekuma	E004E	0.25		1.31	98.69	Thermal oxidation of Fe (Orange)
Ekuma	E004E	0.50		0.88	99.12	
Ekuma	E004E	1.00		1.63	98.37	Thermal oxidation of Fe (Orange)
Ekuma	E004E	1.30		3.66	96.34	
Ekuma	E004F	0.15		2.13	97.87	Thermal oxidation of Fe (Very Red)
Ekuma	E004F	0.30		1.72	98.28	Thermal oxidation of Fe (Very Red)
Ekuma	E004F	0.50		0.95	99.05	
Ekuma	E004F	1.00		1.70	98.30	Thermal oxidation of Fe (Orange)
Ekuma	E004F	1.50		1.64	98.36	Thermal oxidation of Fe (Orange)
Ekuma	E004F	1.80		1.18	96.82	Thermal oxidation of Fe (Orange)
Ekuma	E004F	2.50		2.78	97.22	Thermal oxidation of Fe (Orange)

Table 8.3: Summary of loss on ignition (LOI) analysis conducted on unconsolidated sediment.

The sediments collected from the channel bar separating the main and side channel shows all the characteristics of the active channel deposits. The sediments have a negligible (Table 8.3) carbonate content (< 1%) and show a general down-profile coarsening trend from fine to medium sand. Like most of the sediments sampled in the lower Ekuma, the grain size distribution is unimodal or bimodal and symmetrical to fine skewed, although the basal sample is trimodal and coarse skewed.

The 2 m eastern terrace profile of the Ekuma shows that the upper 1 m of sediments are characterised by moderately sorted medium sand while the mean sample texture below 1 m coarsens down-profile from fine to medium sand. All the samples are symmetrical to fine skewed, polymodal and show moderate to

poor sorting (Table 8.1) which suggests highly variable fluvial conditions associated with the depositional events. The lower sediments are all characterised by 2-4 mm carbonate rich nodules (Table 8.3) despite the negligible (< 2%) carbonate content of the bulk sediments.

8.4.2 Consolidated Deposits

Two distinctive types of consolidated deposits were investigated from the Etosha Pan environment. The majority of these belong to the Etosha Limestone Formation (Rust, 1984) and were collected from the consolidated surface surrounding the contemporary Etosha Pan (Fig 8.2). In addition the carbonate rich nodules and fragments associated with the unconsolidated fluvial and lacustrine Andoni Formation sediment described above were collected from the lower Oshigambo and Ekuma Rivers.

8.4.2.1 The Etosha Limestone

The southern part of the Etosha sub-basin is dominated by the outcropping or thinly covered, very well consolidated, massive, extremely low relief Etosha Limestone that extends from the Gobaubvlakte in the SE to the edge of the Kalahari plateau in the west and as far north as the Pannetjiesveld in the NW and the Andoni flats in the NE. The lithostratigraphy (Hugo, 1969) of the Etosha Basin indicates that Cenozoic deposition has occurred as a result of clastic and chemical sedimentation within both an endoreic and open basin setting. The vertical facies association consisting of unconsolidated sandy surface sediments, overlying the Etosha Limestone which in turn overlies the marls of the Andoni Formation appears to reflect the transition from open lacustrine to palustrine to

littoral to pedogenic environment, which characterised the terminal stages of deposition and surface stabilisation within the desiccating basin.

While it is highly likely that lake levels fluctuated throughout the existence of palaeo-lake Etosha, it is believed that it was not until the reorientation of the Cunene and the associated deactivation of the lakes trunk stream that carbonate precipitation dominated throughout the increasingly saline lake.

Petrography

The fabric of the Etosha Limestone exhibits many of the features typical of palustrine and shallow lacustrine limestones (Freytet and Plaziat, 1983; Bellanca *et al.*, 1992; Wright and Platt, 1995) which support deposition within an environment that experienced repeated desiccation and submergence linked to oscillating lake and groundwater levels. Brown coloured fine grained micrite and dolomicrite (Fig 8.12a), which probably precipitated from calcareous ooze deposits in a low-energy environment of varying salinity and pH, forms the primary matrix in all the samples. This fabric has been reworked by a combination of sub-aerial, pedogenic, palustrine and shallow lacustrine processes such as secondary grainification (Hay and Wiggins, 1980; Wright and Tucker, 1991), saltation and aggitation (Hay and Reeder, 1978) to produce numerous intraclasts, ooids, pseudo-ooids and peloids which float within subsequent phases of carbonate (Smith and Masson (1991) identified six phases of oncoids at Poacher's Point) and replacement silica (Figs 8.12b,c). The widespread occurrence of shell fragments (ostracods) within the fabric (Fig 8.12d) provides additional evidence of deposition within a low-energy fresh to saline shallow lacustrine or palustrine

environment.

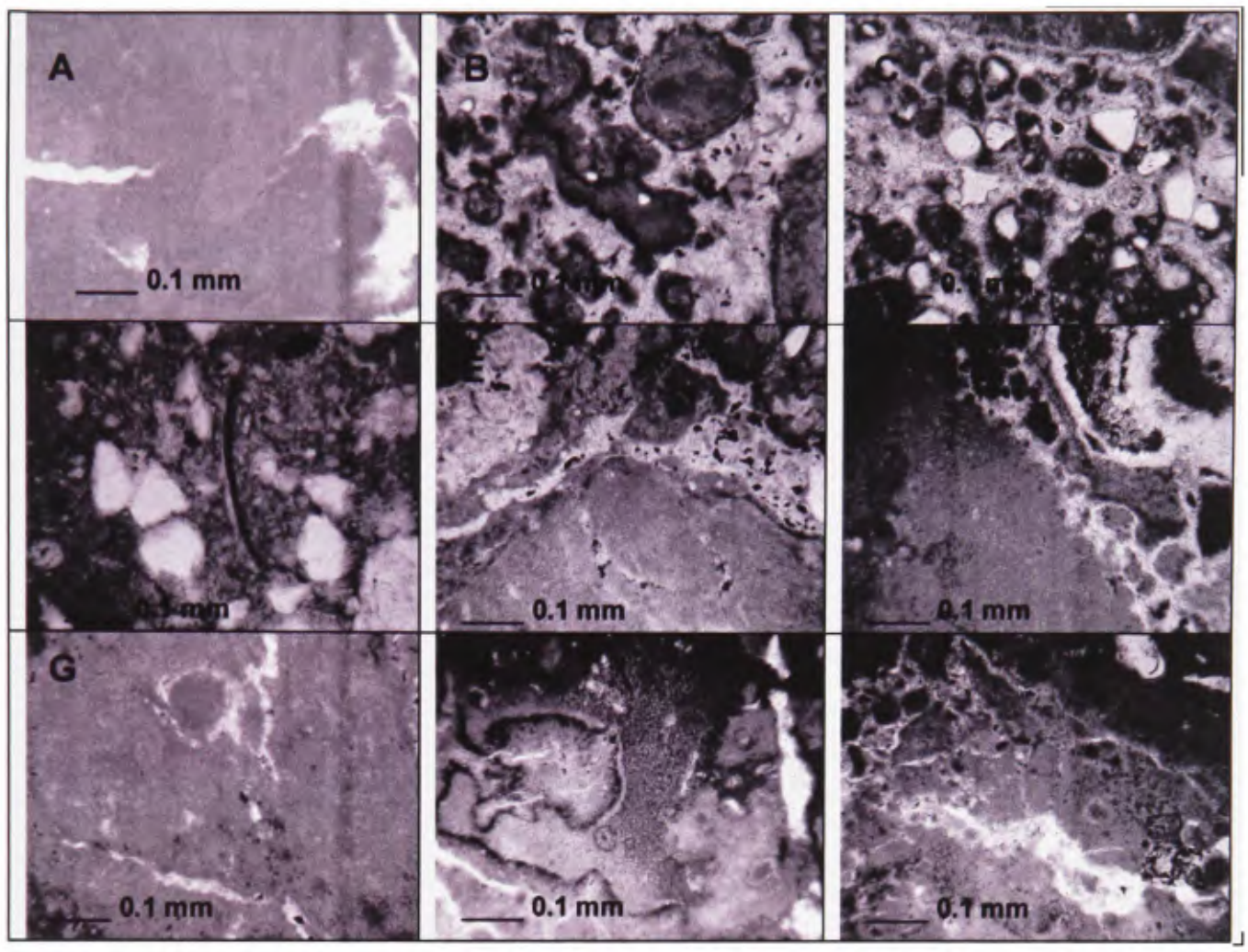


Figure 8.12: PPL thin-section photomicrographs: (a) extremely dense fine grained micrite and dolomicrite fabric with silica filled fractures (b) & (c) detrital quartz grains, intraclasts, ooids, pseudo-ooids and peloids floating within late stage carbonate and silica fabrics (d) shell fragment (possibly from an ostracod) within the micrite fabric (e) & (f) authigenic silica filled fractures, voids and fenestrae within the dense micrite and dolomicrite fabric (g) intraclast formed as a result of a circum-granular crack structure within the dense micrite and dolomicrite fabric (h) pervasive silica (i) pseudobreccia of carbonate intraclasts with silica fracture fills

Primary and secondary porosity has resulted in numerous filled and unfilled fenestrae and vugs within the fabrics (Fig 8.12e,f). In addition dewatering and pedogenic structures such as macro- and micro- brecciation, crystallaria and circum-granular cracks (Fig 8.12g) within the dense fabrics are often filled by later stage calcite (typically sparmicrite) or silica which highlights the numerous

phases of precipitation, microkarst and recrystallisation which have occurred as a result of the fluctuating hydrologic regime.

Irregularly shaped, grey to light brown coloured discordant silica nodules and stringers with discrete nongradational boundaries of varying sizes occur throughout the limestone. The distribution of the discordant silica rich nodules and stringers along with pervasive silica (Fig 8.12h), which is the most common form of silicification and may either retain the original limestone fabrics structure or form a pseudobreccia of carbonate intraclasts (Fig 8.12i), is highest in the basal unit above the Andoni clay and decreases up sequence.

Mineralogy and Diagenesis

The carbonate content of the limestone in the south of the basin varies significantly with a distinct trend of higher values (~45%) in the SW and central parts and lower values (~30%) in the SE. The carbonate mineralogy demonstrates a similar trend with samples in the SW showing abundant calcite and little or no dolomite while other samples show significant (SE) or dominant (south central) dolomite. This carbonate trend appears to be highly reflective of carbonate provenance; the south central deposits are located close to the Precambrain dolomite inselbergs at Halali which contribute considerable amounts of Mg^{2+} (the underlying Andoni clay is also believed to be an abundant source of Mg^{2+}) and dissolved carbonate to the local groundwater thus encouraging the precipitation of fine grained primary dolomite as a result of evaporitic processes or dolomitisation of the existing lacustrine calcite as a result of seepage-reflux or mixing. The increased dolomite content of samples closer to the contemporary systems sump

(Fischer's Pan) supports an evaporitic model which links evolved groundwater (Arakel, 1986) with carbonate precipitation, modification and replacement.

The majority of contemporary (and palaeo) shallow ground and surface water enters the Etosha system from the northern drainages. This is supplemented by meteoric water and localised drainage along the systems southern margin which flow northwards from the weathered Precambrian carbonate of the Otavi Hills, located between Outjo and Tsumeb. Water entering from the northern drainages has a low dissolved carbonate content which is typical of western central Kalahari fluvial systems whose catchments are dominated by acid igneous and sandstone lithologies. Thus in line with Buch and Rose (1996), it is believed that the southern drainage and groundwater are the principal source of bicarbonate and calcium carbonate within the basin. The concentration of soluble silica is also very low in the surface water, but dissolved carbonate and magnesium levels are significantly higher within the shallow groundwater. Processes of silicification as proposed by Khalaf (1988), Thiry *et al.* (1988), Arakel *et al.* (1989) and Nash and Shaw (1998) are highly active within the phreatic zone and capillary fringe due to the highly stratified aquifer which is perched above the Andoni clay.

Detrital terrigenous material and authigenic clays are sparse within the lacustrine carbonates, but the sepiolite and palygorskite clay mineralogy supports precipitation of calcite under Mg-rich brackish to saline (Jones, 1986) desiccating conditions. The occurrence of dolomite and silica are the result of primary and late-stage dolomitisation and silicification associated with the saline and Mg (Magadi-type silicification (Eugster, 1967; Heaney, 1995; Bustillo, 2001) and

evaporitic, seepage-reflux and mixing dolomitisation (Land, 1985; Tucker and Wright, 1990)) enriched groundwater.

The occurrence of pervasive microcrystalline quartz and nodules are the result of silicification of the micrite fabric by meteoric (negligible) and ground (considerable) water. The low detrital quartz and clay content of the Etosha Limestone suggests that the majority of silica is extraformational. Weathering of surface sands and silts, and corrosion of the underlying Andoni clay during shallow burial was probably the main source of silica. In line with Thiry and Ribet (1999) it is believed that the silicification process was concentrated in highly porous zones, fractures, joints and pipes where flow rates are highest. Silica would be supplied from these areas of increased flow and diffuse along crystal joints into the fabric while at the same time a reverse flow of dissolved calcite would move from the fabric towards the areas of circulating water and be discharged. The extent of diffusion and thus replacement is a function of the diffusion gradient – the greater the distance of diffusion from source the lower the rate of supply and therefore replacement. Thiry and Ribet (1999) predict that the dissolution and replacement of micrite by silica without developing additional porosity can only occur if the water flowing through the pores is close to saturation with respect to calcite.

Pervasive silicification has occurred due to the selective replacement of the micrite fabric by quartz. In order for replacement and conservation of the original fabric to occur, silica precipitation and calcite dissolution have to take place simultaneously (Thiry and Ribet, 1999). Crystallization pressure of growing

quartz crystals on neighbouring calcite crystals is the mechanism most likely to have induced this replacement (Maliva and Siever, 1988; Dewers and Ortoleva, 1990; Maliva, 1992).

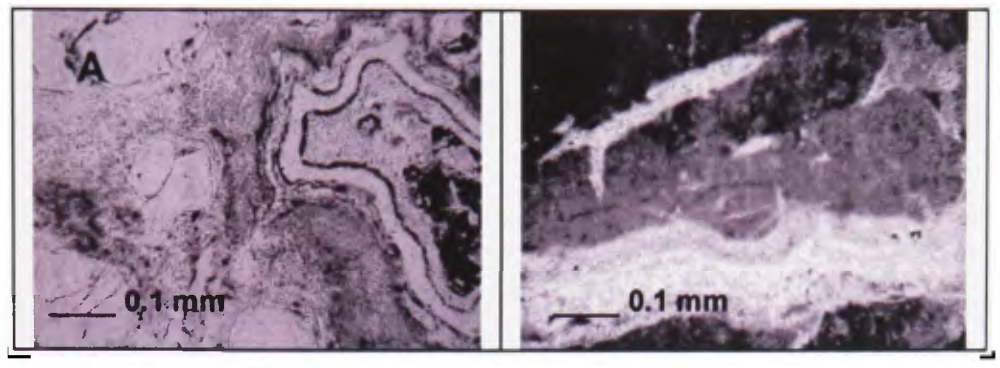


Figure 8.13: PPL thin-section photomicrographs: (a) authigenic silica void fill and silicification of the fabric with residual micrite preserved (b) crenellated authigenic fracture fill and pervasive margin with micro-veins.

Nodule growth has been complex and variable, principally as a result of the fluctuating water table, but occurred from the void wall inwards as a result of diffusive supply of silica and porewater advection. Opal, chalcedony, microquartz, small palisade quartz, inequigranular mosaics of variously sized subhedral to euhedral mega-quartz and late-stage sparite has either partially or entirely filled both primary and secondary pore space, voids and veins within the original carbonate. In line with Thiry and Ribet (1999), silicification is most pronounced where the porosity and void concentration was highest while areas with limited porosity and widely spaced disconnected voids underwent limited silicification and residual limestone zones are preserved (Fig 8.13a). Quartz growth within the voids shows both the regularly spaced crenellated (most common) (Fig 8.13b) and botryoidal ribbon (rare) patterns described by Thiry and Ribet (1999). These patterns suggest that the void fill quartz has grown directly from solution and also from recrystallisation of primary opal concretions. The limited occurrence of length-slow chalcedony, megaquartz, dolomite and calcite cemented 'cauliflower'

shaped void fillings within the palustrine limestone is believed to reflect replacement of vadose anhydrite (Tucker, 1976; Milliken, 1979; Alonso-Zarza *et al.* 2002) under hypersaline phreatic processes (Maliva, 1987).

The silicification of the Etosha Limestone occurred as a result of the through-flow of significant volumes of ground water enriched in soluble silica. The hydrodynamic conditions necessary for this flow to occur are only present along the southern margin of the basin, where there is a strong groundwater head associated with the Otavi Hills, and within the ephemeral northern drainages. Within the remainder of the basin the gradient is generally too low to support a strong hydrologic gradient so silicification is concentrated around localised topographic lows such as incised pans, waterholes/springs and drainage channels where flow rates are highest.

Stable Isotopes

Isotopic analyses (Table 8.4) of the Etosha Limestone indicated inorganic $\delta^{13}C$ values between of -3.26‰ and -0.16‰ and $\delta^{18}O$ values between -5.50‰ and -4.00‰.

The $\delta^{13}C$ values are interpreted as being indicative of a C_4 dominated vegetation with a minor and variable C_3 component. This vegetation signal suggests a mixed but grassland dominated vegetation, which complements the sweet grassveld vegetation that comprises a thin fringe around the southern margin of the pan. Further south the sand covered carbonate plain is dominated by *Mopane* and *Combretum* woodland (Le Roux, 1980; 1998) (Fig 8.14).

	Inorganic δ13C PDB	δ18O PDB
Eastern Owamboland 01	-4.69	-7.23
Eastern Owamboland 02	0.15	-5.86
Eastern Owamboland 03	-2.59	-4.43
Ekuma/Etaka River	-2.89	-6.30
Kapupuhedi	-3.26	-5.50
Namutoni 12	-0.16	-4.18
Okaukuejo	-1.57	-4.60
Oshigambo River	-2.59	-7.01
Sueda	-1.13	-4.00

Table 8.4: Summary of carbon and oxygen isotope values.

$\delta^{18}O$ values indicate meteoric solutions which have undergone limited evaporitic fractionation and cool (~15-20°C) temperatures of precipitation which support primary precipitation of calcite within either a lacustrine/palustrine or pedogenic environment rather than the highly evaporitic environment of the contemporary pan. However, despite the best attempts to only sample one carbonate phase, the complexity of the fabric means that this is probably a mixed signal which also reflects calcite recrystallisation within a pedogenic environment.

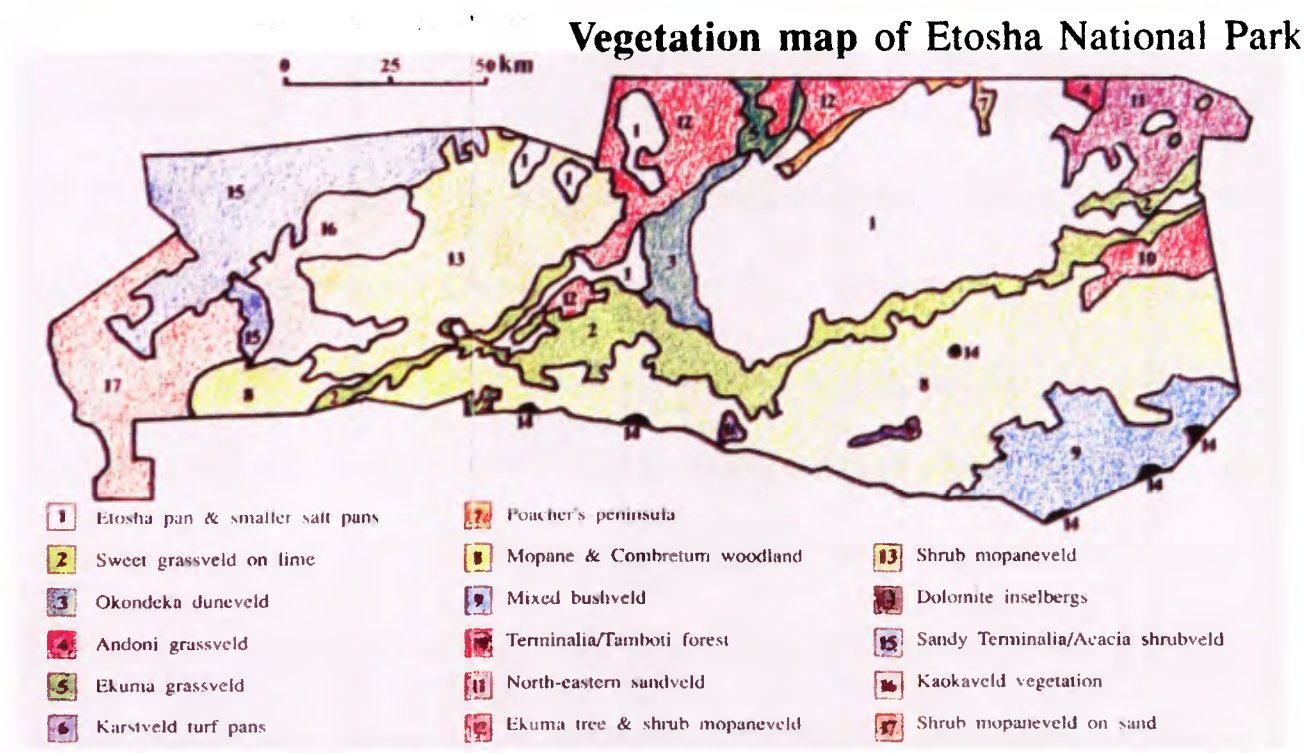


Figure 8.14: Vegetation map of Etosha National Park (Le Roux, 1980).

8.4.2.2 Andoni Formation Chemical Sediments

Silcrete and cal-silcrete fragments collected from the deflation lag on the surface of the Oshigambo River and irregularly shaped authigenic sil-calcrete nodules distributed throughout the profile of the unconsolidated sediments in the Ekuma and Oshigambo Rivers, suggest that precipitation is occurring and has occurred under a range of geochemical conditions associated with saline lacustrine and groundwater environments.

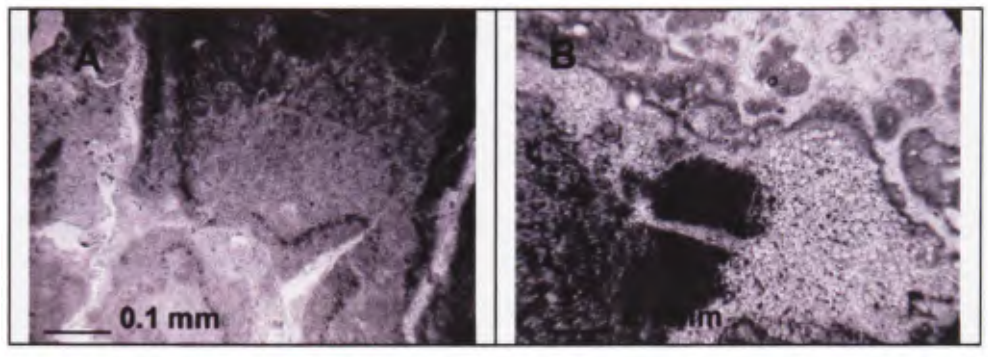


Figure 8.15: PPL thin-section photomicrographs: (a) authigenic microcrystalline quartz filled fractures with pervasive silica along the margins which have partially silicified the adjacent micrite fabric (b) a micrite intraclast with corroded edges floating within a microcrystalline silica replacement fabric.

Petrography

Petrographic investigation reveals that the fragments and nodules are wackestones containing moderately to poorly sorted floating corroded detrital silt and sand grains, and carbonate intraclasts in a mixed microcrystalline and amoeboid quartz fabric (Fig 8.15a). The majority of larger, euhedral quartz grains have an irregular shape and a dark core with abundant calcite inclusions. All the carbonate mud/micrite intraclasts have corroded edges as a result of having undergone varying degrees of silicification (Fig 8.15b). These dark carbonate intraclasts are identical to the dense dolomicrite and micrite identified in the Etosha limestone and suggest reworking of brecciated marginal lake deposits or underlying

carbonate lenses and horizons within the Andoni Formation. The occurrence of circumgranular cracks within the intraclasts indicates that they experienced limited pedogenesis prior to erosion and redeposition.

Mineralogy and Paragenesis

XRD analysis (Table 8.2) revealed dominant quartz with significant calcite and minor K-feldspar, analcime and mica. Analcime is usually found in veins and cavities in basalts or gabbros that have experienced low-grade burial metamorphism or hydrothermal activity. However, clinoptilolite and mordenite are precursors to authigenic analcime and are frequently associated with saline-lake or playa deposits in Southern Africa (Smale 1968). Buch and Rose (1996) believe that the occurrence of analcime and its mineral associations in Etosha are the result of both detrital and parautochthouous mechanisms linked to the Andoni Formation. They do not however discuss the origin of analcime within the fluvio-lacustrine Andoni Formation. It is believed that the only detrital source for analcime is either the Stormberg Lavas, which form the unconformity between the Kalahari and Karoo sediments that line the Etosha sub-basin at depths of 300-500 m (Haddon, 2001), and are thus an unlikely source, or the Etendeka igneous complex and the metamorphics of the Damara-Katanga belt. This mineral complex extends from Kaokoland northwards into Angola where it forms the escarpment and the headwaters of the Caculuvar, the main west bank tributary of the Cunene River. However, the main catchment of the Cunene lies within the central Angolan highlands, which are dominated by Precambrian and Cambrian quartzo-feldspatic paragneisses and grantoids (Burmeister, 1996). Thus, it is more likely that the analcime is authigenic and associated with the endoreic

lacustrine/palustrine/ephemeral fluvial system which became increasingly saline during desiccation of palaeo-lake Etosha. Smale (1968), Netterberg (1969c) and Watts (1980) have identified clinoptilolite within Kalahari pan sediments and it is typically associated with silcrete development (Smale, 1968). The occurrence of significant K-feldspar, which can form authigenically under similarly saline conditions, may be a source of supporting evidence.

Sample	% organic material	% carbonate	% other minerals
Eastern Owamboland 01	1.6	49.8	50.2
Eastern Owamboland 02	1.0	36.8	63.2
Eastern Owamboland 03	2.8	8.0	92.0
Kapupuhedi	3.3	48.2	51.8
Namutoni 12	7.8	29.4	70.6
Okaukuejo	3.2	44.6	55.4
Oshigambo	0.8	6.7	93.3
Sueda	3.9	43.7	56.3
Etaka/Ekuma	2.0	33.3	66.7

Table 8.5: Summary of loss on ignition (LOI) conducted on consolidated carbonates.

Studies from similar environments (Wheeler and Textoris, 1978; Wells, 1983; Arakel *et al.*, 1989) suggest that the complex geochemical processes operational within the vadose and phreatic zone of this alkaline fluvial-playa environment will result in both authigenic carbonate and silica precipitation. This is confirmed by LOI conducted on the unconsolidated sediments within the vadose zone and bulk XRD analyses of the nodules. LOI suggests fluctuating but generally moderate to low carbonate contents within the profiles (Table 8.5). This along with bulk XRD analysis (Table 8.2) of the nodules implies that carbonate precipitation as calcite and dolomite within this hypersaline and high-pH environment is secondary to silica. Carbonate precipitation appears to be occurring at the surface (as the evaporite mineral Burkeite) and within the phreatic zone as massive cal-silcrete or sil-calcrete. Evidence of massive chemical sedimentation was found within the

Ekuma and Oshigambo channels at depths of 1-1.75 m.b.s., but was not sampled due to the lack of suitable exposure. In addition in all the profiles the highest carbonate values are associated with the finest grained sediments which suggests concentration of carbonate within zones of reduced permeability and does not necessarily contradict the description of the Andoni clays as being carbonate free within the majority of the sub-basin (Buch and Rose, 1996).

Stable Isotopes

Isotopic analyses (Table 8.4) of the carbonate fraction within the sil-calcrete nodules revealed an inorganic $\delta^{13}C$ value of -2.59‰ and a $\delta^{18}O$ value of -7.01‰. The negative $\delta^{18}O$ value suggests very little or no evaporitic fractionation and suggests precipitation from groundwater which has undergone recharge from rapidly infiltrating meteoric water. The $\delta^{13}C$ value supports the interpretation of calcite precipitation from local groundwater as the value reflects a mixed but C_4 dominated vegetation, possibly shrub or tree savanna, which is typical of the vegetation in the northern part of the Etosha Pan.

8.5 Conclusion

Analyses of the Etosha sub-basin carbonates have revealed a complex sequence of fabrics and mineralogies which attest to their depositional, environmental, climatic, epigenetic and diagenetic histories. Within the indurated chemical sediments of Etosha Pan this study identified that the dominant fabric is reflective of an original palustrine carbonate mud which has undergone complex replacement and reprecipitation within both a vadose and phreatic environment. Four mineral associations were encountered within the sediments which provided

further insight to their depositional environment and diagenetic modification. These associations complement the work of Buch and Rose (1996) and can be classified as:

(1) analcime/K-feldspar and mica

(2) anaclime/K-feldspar and sepiolite

(3) expandable sheet silicate

(4) calcite and dolomite

This study along with the work of Buch and Rose (1996) supports a clear demarcation of the Etosha Pan and Ovambo-Pans-Plain deposits into:

(1) disintegrated (*in situ*) sedimentary rocks of the Andoni Formation (mineral association 1);

(2) parautochthonous sediments (mineral associations 1 and 2); and

(3) allochthonous sediments (mineral associations 1, 2, 3 and 4).

The formation of authigenic minerals in association 1 and 2 has been recorded by this and numerous other studies (Smale, 1968; Netterberg 1969c; Watts, 1980) within the evaporative pumping dominated alkaline and saline Kalahari pan environments. In line with Buch and Rose (1996), it is believed that the carbonate mineralogy is very localised and can be related to the a number of models (evaporative, seepage-reflux and mixing) which show varying influences of the Otavi Dolomite and the underlying Andoni Clay Formation on groundwater enrichment with respect to Ca^{2+}, Mg^{2+}, HCO_3^- and CO_3^{2-}. In addition the evolutionary model of groundwaters within an alluvial/playa environment (Arakel, 1986a) is considered highly applicable when explaining the occurrence of

calcite and dolomite within the northern and eastern sectors of the pan/palaeo-lake.

Analyses of the carbonate within the southern sector of the sub-basin indicates that the 'Etosha Limestone' is a terminal carbonate mud facies which is associated with the desiccation of the fluvio-lacustrine/palustrine system that filled the endoreic Etosha Basin during the Cenozoic. This carbonate facies shares many of the characteristics identified in similar lacustrine/palustrine carbonate sequences throughout the Mega-Kalahari. The transition to a low-energy depositional system and ultimately the termination/reduction in sedimentation to its current levels associated with the seasonal inundation of the pan is believed to have its origins in the capture and reorientation of the Cunene westwards towards the Atlantic during the Pleistocene which starved palaeo-lake Etosha of its principal headwaters. However, despite this critical loss of its principal headwaters and the corresponding adjustment of palaeo-lake Etosha to a new hydrological equilibrium, palaeoclimatic changes since at least the late Pliocene/early Pleistocene have also had a significant effect on the hydrology of Etosha. Quaternary desiccation of southern Africa has resulted in the fluctuation between reduced perennial and ephemeral lacustrine conditions, with an overall trend towards ephemeral conditions. The occurrence of hypersaline mineralogies (e.g. K-feldspar and analcime) in the late stage Etosha Limestone, but not in the Andoni formation, is believed to be indicative of this changing hydrology.

The stabilisation of the lacustrine/palustrine sediments by vegetation and the associated commencement of pedogenic processes also reflect the changing

hydrology and palaeoclimatic conditions. The concentration of elements such as Mg, Ca, K and dissolved silica and the related increased salinity linked to reduced inflow and recharge had a major influence on the authigenic minerals precipitated. The resultant zonation of mineralised carbonate deposits within the littoral areas has been further modified by groundwater processes of silicification and dolomitisation.

The adaptation to a new hydrological equilibrium probably had a significant effect on the geomorphology. During desiccation any significant topography on the former lake bed would have sub-divided the new system into a series of depo-centres within the topographic lows. The corresponding high ground and littoral sediments such as the gobaubvlakte and pannetjiesveld subsequently underwent pedogenic modification as a result of vadose diagenesis. In contrast the depo-centres are believed to be the embryonic pans, which when associated with the dynamic hydrology and palaeoclimate, coalesced through the processes of erosion to form the contemporary Etosha Pan and the Ovambo Pans Plain. As a result, the Etosha Pan has been transformed from a depositional to an erosional environment.

It is argued that if a palaeolake had existed during the Quaternary (Stuart-Williams, 1992) then surely significant allochthonous lacustrine sediments should be expected as all deposited material could not have been deflated during intervals of desiccation. Rather, it is proposed in line with Buch and Rose (1996) that a permanent, shallow lake existed during the evolution of the more extensive depocentre of the Etosha sub-basin throughout the Miocene and Pliocene. Petrographic analyses of the upper Andoni Clays and the lacustrine carbonates

commonly referred to as the 'Etosha Limestone' support deposition of these facies within a shrinking low-energy lacustrine environment with subsequent pedogenic and groundwater modification. Sedimentological and geomorphological evidence, along with the occurrence of stromatolites (Smith and Mason, 1991) and ooids, indicate that local wave action was a significant mechanism responsible for the reworking of sediment within the terminal shallow palaeo-lake. The deeper horizons of poorly sorted clay-rich sandstone and sandy marls containing abundant calcrete and dolocrete described by Hugo (1969) indicate that cyclothems of lacustrine and alluvial deposition have been responsible for the infilling of the greater Etosha sub-basin throughout its evolution.

9. CHEMICAL SEDIMENTS OF THE PALAEO AND ACTIVE OKAVANGO ALLUVIAL FAN, BOTSWANA: EVIDENCE FOR VARIATIONS IN THE PROCESSES OF FORMATION.

9.1 Introduction

Calcretes are important features of many drylands. They range from powdery through to massive, highly indurated types, and are produced by pedogenic and non-pedogenic processes that cause the dissolution, mobilisation and precipitation of carbonates in the near-surface environment. This paper describes, characterises and discusses possible mechanisms of formation of calcrete based on the analysis of samples collected from a range of geomorphic environments linked to the Okavango alluvial fan in north-western Botswana. These include the active and abandoned seasonal floodplains and transects across three islands within the heart of the modern active system. The term calcrete is used here to describe poorly to highly indurated calcium carbonate accumulations which have varying proportions of silica and calcium carbonate (including sil-calcrete and cal-silcrete) (see also Nash and Shaw, 1998).

The 22000 km^2 Okavango alluvial fan (Fig 9.1) is located within an incipient graben of the East African Rift system (Gumbricht *et al.*, 2001) at the heart of the Kalahari. It has acted as a dynamic repository of sedimentological information during the late Tertiary and Quaternary. Presently 96% (Dincer *et al.*, 1981) of the annual inflow

from the Okavango River, which flows south from the Angolan highlands, is lost by surface evaporation and evapotranspiration processes from the lush vegetation which covers this extensive mosaic of permanent swamps and seasonal floodplains. Water within this extremely low gradient system is distributed by a dynamic and complex interaction of vegetation and geomorphology. There has been considerable variation in flow through the Delta in both historical and Quaternary times, with the present flow regime amongst the lowest on record (Shaw, 1986, 1988). The perennial alluvial fan consists of 6000 km^2 of swamp that expands to more than 12000 km^2 (Gumbricht *et al.*, 2001) during the flood season as water inundates the seasonal floodplains between the Gumare and Thamalakane faults (Fig 9.2).

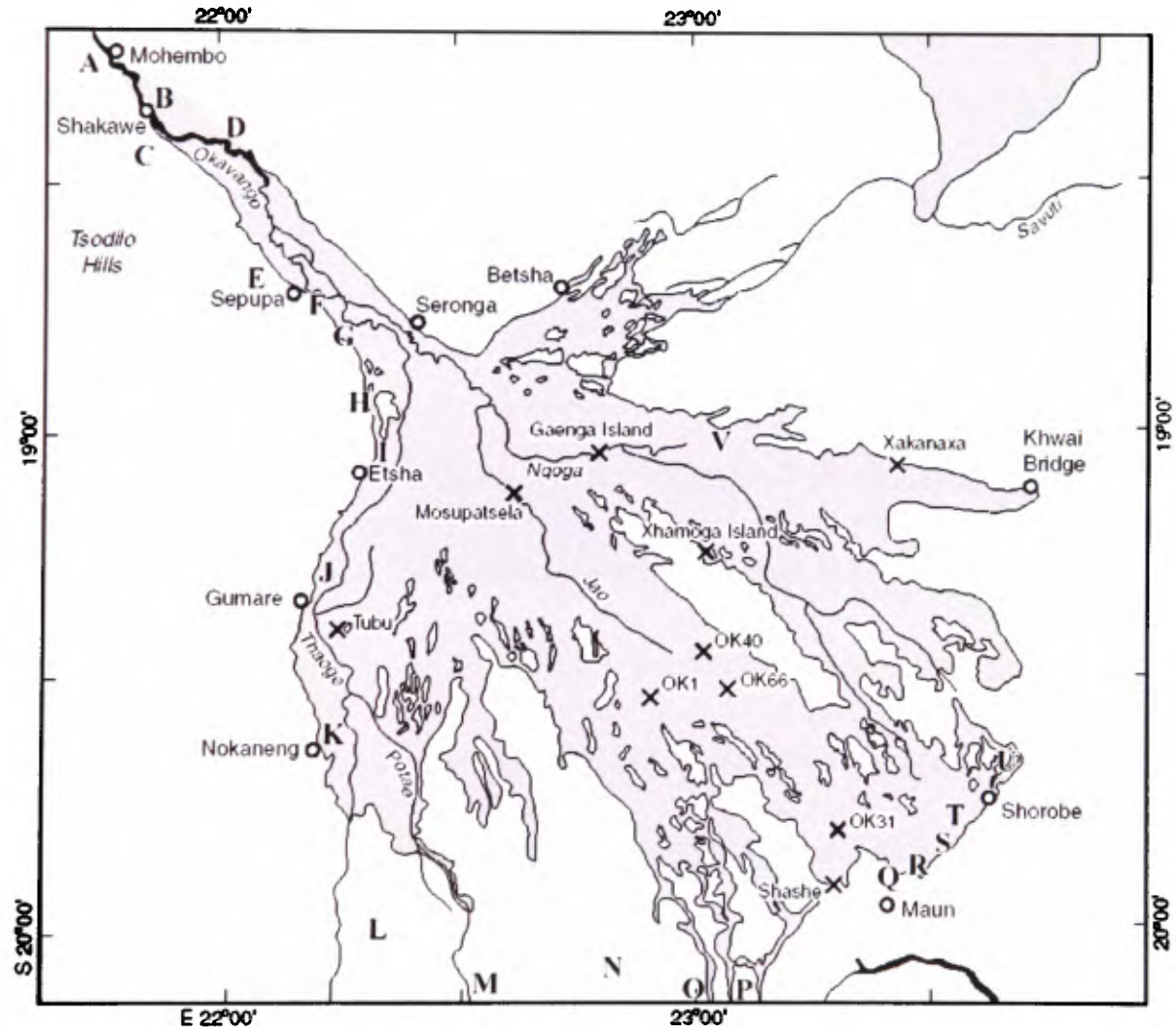


Figure 9.1: Location map of the Okavango alluvial fan in Northwest Botswana. Shaded area indicates extent of the seasonal swamps (modified from MCCARTHY et al. 1991a).

The climate is hot and dry, with annual evaporation in excess of 1860 mm and evaporation exceeding rainfall in all months of the year. Rainfall occurs in summer, mainly from December to February, and contributes approximately 30% of the total water input, with the rest supplied from the upstream catchment (Dincer *et al.*, 1987). Only 2% of inflow plus rainfall (11 x 10^9 m^3/yr and 5 x 10^9 m^3/yr, respectively) leaves the fan via the Boteti River, and a further 2% is estimated to leave through groundwater flow (Dincer *et al.*, 1981), the rest being lost by evapotranspiration. Despite the high levels of evaporation two extractive physicochemical processes are believed to account for the low salinity of the surface water (Ellery and Ellery, 1997): the concentration of salts below the multitude of islands scattered throughout the alluvial fan due to dominance of evapotranspiration (McCarthy and Ellery, 1994), and the dynamic change in distribution of water over the surface of the fan, which allows for the desiccation of vast areas and the regeneration of the soils.

The fan is situated within the Okavango sub-Basin of the Kalahari Basin, which has accumulated about 300 m of sediment since the late Pliocene or early Pleistocene (Haddon, 2000). Due to the catchment's location within the heart of the Mega Kalahari (Shaw and Goudie, 2002) the dominant sediment is medium- to fine-grained unconsolidated moderately sorted fluvially reworked siliciclastic aeolian sediment which has formed very poorly developed cyclothems within the alluvial profiles.

Over the past 30 years the geomorphology and hydrology of the fan has been well documented (e.g. Dincer *et al.*, 1987, Wilson and Dincer, 1976, Gumbricht *et al.*, 2001 and Gieske, 1996, 1997) and actively monitored by the Hydrology Division, Department of Water Affairs, Botswana. The geochemical sediments have, however, only been studied on a fairly localised scale, mostly within the terminal and eastern sectors of the system (McCarthy and Metcalfe, 1990, McCarthy *et al.*, 1986b, 1991b, 1993, McCarthy and Ellery, 1994, 1995, Shaw and Nash, 1998). The calcrete deposits of the region (Cooke, 1976) have also received relatively limited attention. Pimentel *et al.* (1996) have shown that pedogenic and groundwater calcrete deposits contained within semi-arid alluvial sequences provide a valuable tool to help improve our understanding of climatic and geomorphic controls on sedimentation.

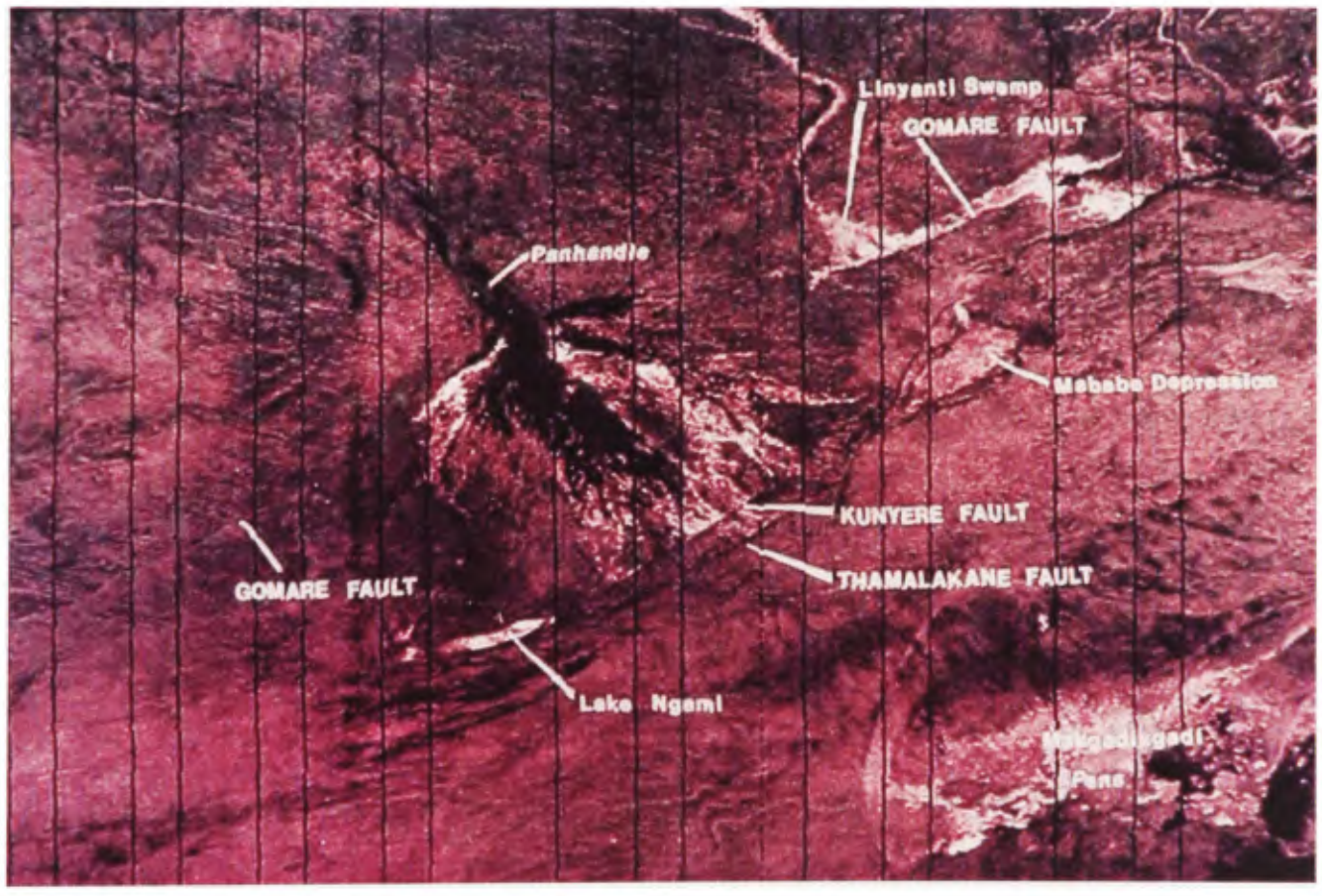


Figure 9.2: LANDSAT image of the Okavango alluvial fan showing the main faults systems of the region (Ellery and Ellery, 1997).

9.2 Clastic and Chemical Sedimentation

Modern clastic sedimentation, comprised of bedload (~170 000 t a^{-1}) and suspended load (~30 000 t a^{-1}), is presently concentrated within the Panhandle region rather than the fan itself (McCarthy *et al.*, 1986a, 1988, 1991a). Conservative mass balance calculations based on the 28 year record of daily flow volumes at Mohembo (Fig 9.1)(Dept. of Water Affairs, Botswana) and the total dissolved solids (TDS) content of water samples collected at this station over the course of the sampling period (March 2001-July 2002), indicate that as much as 440 000 tons of dissolved solids enter the Delta each year. This calculated figure for input is 10% greater than the 400 000 t a^{-1} input and ~30 000 t a^{-1} outflow proposed by McCarthy and Metcalfe (1990). In a similar manner the amount of silica entering the Okavango system at Mohembo was calculated to be approximately ~160 000 t a^{-1}. This compares with McCarthy and Metcalfe's (1990) estimate of ~135 000 t a^{-1}. Unfortunately alkalinity was not monitored throughout the sampling period and the calculated value of ~3250 t a^{-1} TDIC (total dissolved inorganic carbonate) based on only one month of monitoring data during the wet season/low flow period of December 2001 is believed to be unrealistic. McCarthy and Metcalfe (1990) calculated that ~113 000 t a^{-1} of $CaCO_3$ is accumulating on the fan as a result of ground and surface water precipitation. These calculated figures for carbonate accumulation probably have to be increased substantially due to the contributions made by airborne carbonate dust (Capo and Chadwick, 1999) sourced throughout the Kalahari (Eckardt *et al.*, 2001), rainwater (Gardner, 1972) and biogenic carbon (Salomons *et al.*, 1978).

9.3 Alluvial Carbonates

Shaw and Nash (1998) and Nash and Shaw (1998) highlighted that chemical sediments within the Kalahari are often extremely intricate and difficult to interpret due to cements being complex as a result of co-deposition of minerals, constructional and degradational processes occurring within the pedogenic zone and the post-formational near-surface diagenetic alteration of pre-existing carbonates. Vadose and phreatic zone pore waters within alluvial sequences are the main agents of this process as they undergo systematic changes in chemical composition depending upon the availability of metabolizable organic matter, Fe- and Mn-oxides/oxyhydroxides, alkalinity and the concentration of dissolved O_2 and SO_4^{2-} (Morad, 1998). These geochemical changes are likely to be at least partially imprinted within the diagenetic carbonate and hence provide a powerful tool in the recognition of the particular environment in which they precipitated (Morad, 1998). Alluvial sequences are also very important aquifers and pedogenic calcretes within the depositional sequences can, under suitable conditions, be altered during shallow burial by saline-alkaline groundwaters (Pimentel *et al.*, 1996). Within this framework of processes, the calcretes of the Okavango fan have undergone modification from pedogenic to groundwater and *vice versa* due to the dominance of one or the other process in the same manner as those described by Pimentel *et al.* (1996), due to subtle variations in controlling mechanisms that lead to shifting distributaries within the system. The carbonates contained within the sequences of the Okavango fan take many forms and are exposed in a variety of settings, from inverted topography in the lower sections of

the fan to dissected linear dunes in the northern panhandle. In most cases this study was reliant on quarries and wells for suitable exposures to log and sample.

9.3.1 Relict Interdune Calcretes

North of the Gumare fault the Okavango has incised through the linear dunes in the region known as the panhandle. Ten calcrete profiles (sites A – G) were logged and sampled (Fig 9.1) from this area. Calcrete sequences are often exposed by road cuttings or under-cutting by the Okavango River in interdune cordons or within the cores of the dunes (Fig 9.3). Brook *et al.* (1992) and Thomas *et al.* (2003) have described a lacustrine calcrete sequence from a similar environment 40 km southwest of this location at the Tsodilo Hills. The panhandle calcretes contain many of the characteristics typical of palustrine and groundwater calcrete as highlighted by Pimentel *et al.* (1996), Wright and Tucker (1991) and Alonso-Zarza (2003), including extensive Fe-Mn mottling, increasing carbonate content down profile, a range of crystal sizes, although predominantly a dense microspar crystalline matrix, etched floating quartz grains, horizontal sparite-filled vugs and significant amounts of authigenic silica, usually in the form of chalcedony in the lower parts of the sections. The concentration of authigenic silica is in line with the ideas of earlier researchers who noted the relationship between abundant authigenic silica and calcrete profiles developed due to carbonate accumulation in valley and pan type unconsolidated sediments (Netterberg, 1969, Watts, 1980, Blumel, 1982, Eitel, 1994a, Eitel and Blumel, 1997, Mees, 2002, Ringrose *et al.*, 2002). This has been the main process of carbonate accumulation within these fossil interdune areas where summer rainwater

ponded and then evaporated during the dry winter. Flach *et al.* (1969), Reeves (1976), Watts (1980) and Wang *et al.* (1994) outlined the mechanism by which etching of silicate minerals by calcite occurred at high pH in the upper levels of the profile and resulted in the subsequent downward migration of the silica-rich solutions and the resultant precipitation of authigenic silica from gels in areas of higher salinity and lower pH. Milnes and Hutton (1983) believed that increased silicification is linked to maturation within a sequence, although the point at which the silica accumulation occurs is highly variable (Watts, 1980, Nash *et al.*, 1994a,b, Nash and McLaren, 2003, Summerfield, 1982, 1983).

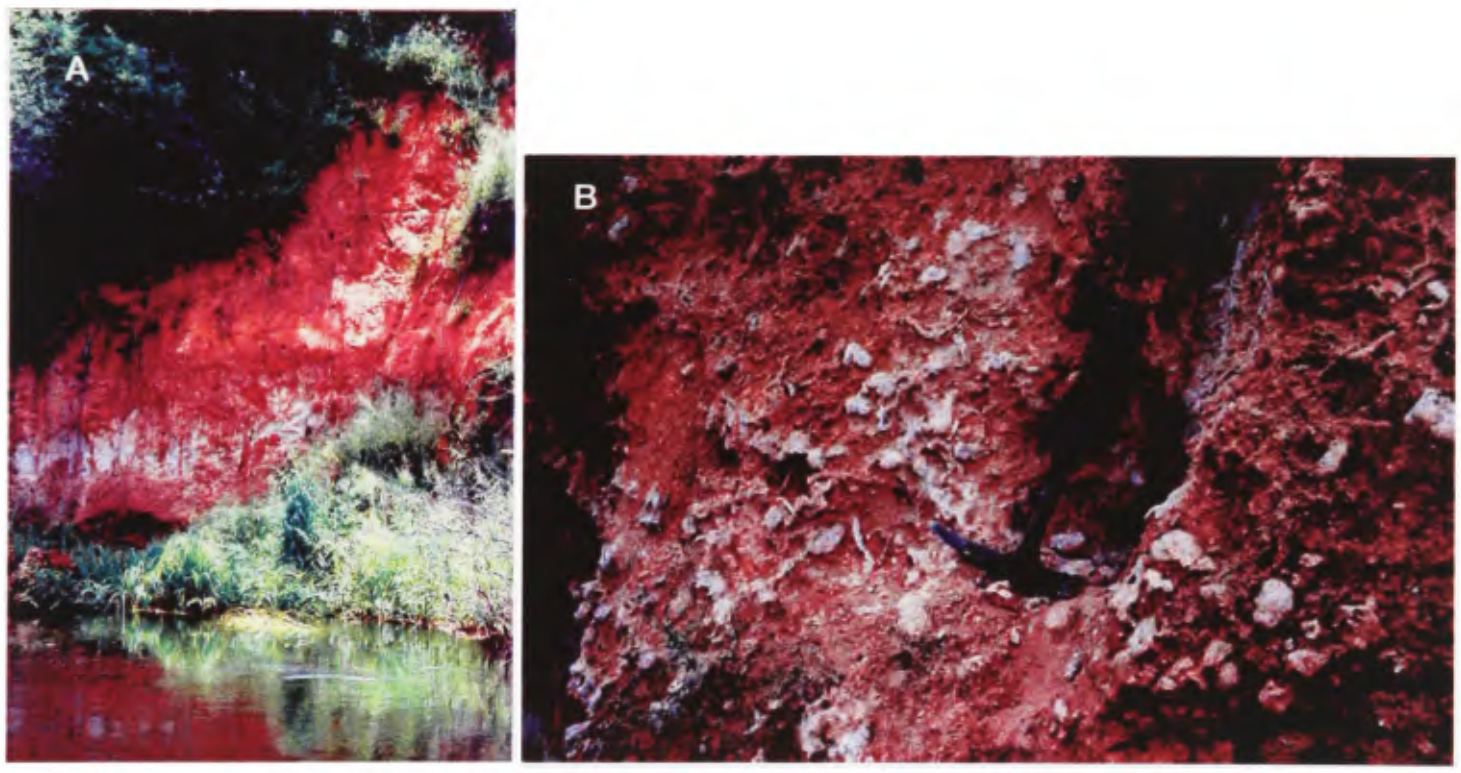


Figure 9.3: Photographs of linear dune dissected by the Okavango River. (a) Profile shows carbonate nodules formed within the aeolian sediment in the lower section. (b) Close up of calcrete nodules of various sizes and morphologies formed within the lower part of the profile.

In line with Carlisle (1980), an upper earthy zone with remnant pedogenic type features in the form of micrite glaebules and a distinct upper boundary with the modern soil were identifiable at some of the sites (sites C and E) (Fig 9.4). The lower

groundwater calcretes within these aeolian/alluvial sequences take the form of a high porosity, highly permeable, powdery type grading to nodular and in places well consolidated massive calcrete. The sequences observed in outcrops are often in excess of 5 m in thickness and the base was never exposed. Within the sequences, matrix-supported nodules, with the nodule cements containing proportionally lower carbonate and higher silica contents than the surrounding matrix, increase in size and coalesce with depth while in other profiles the opposite occurs and the nodules increase in size and coalesce up-profile.

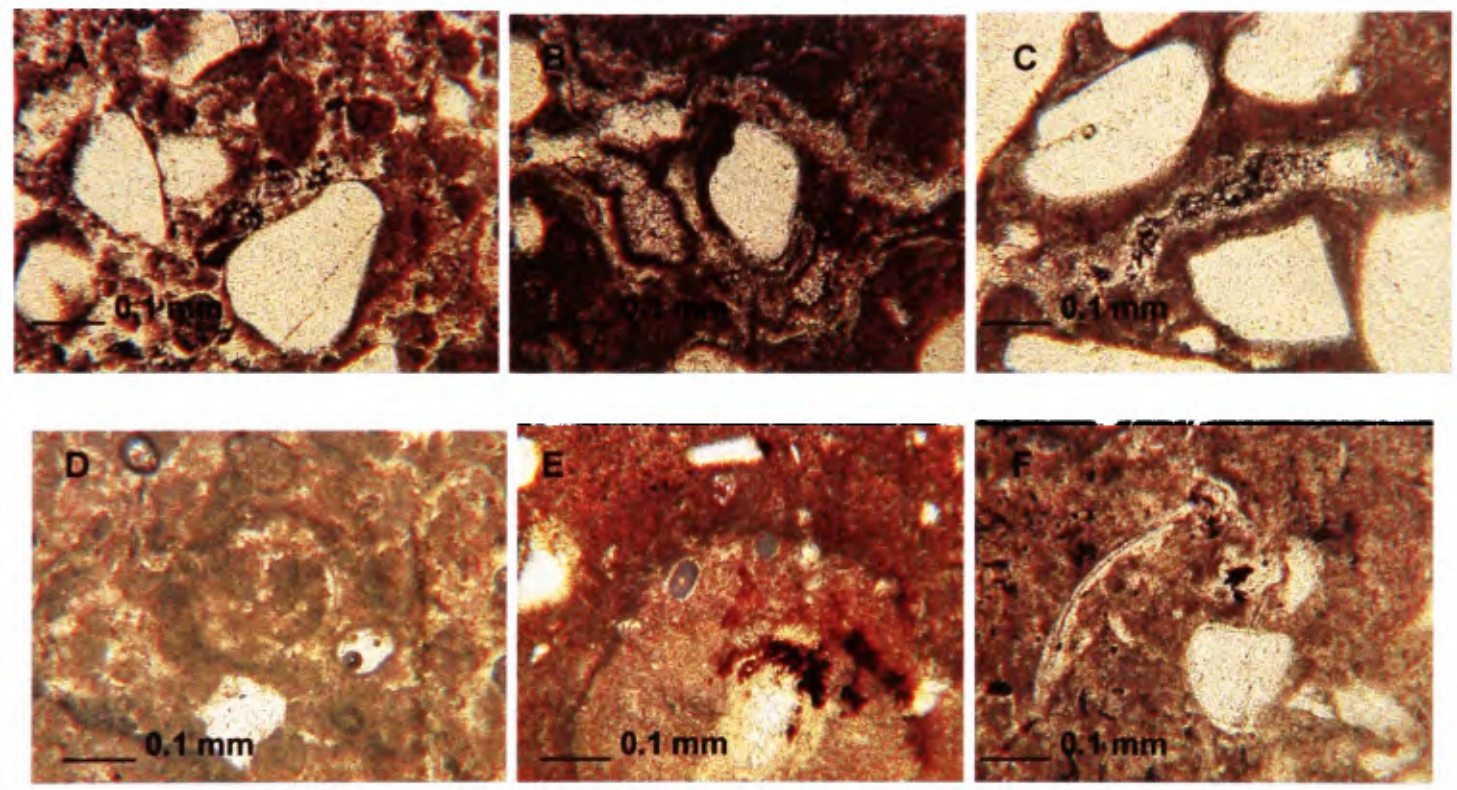


Figure 9.4: PPL thin-section photomicrographs of calcrete collected from various locations on the Okavango alluvial fan: (a) Pelletal micrite and pseudo-oolitic textured nodular calcrete at site E; (b) Complex spar fill structure with laminated micrite and authigenic quartz lining of voids within a clotted micrite fabric. Massive Fe and Mn mottled calcrete collected at site G; (c) Corroded detrital quartz grains within a micrite matrix. Void structure with spar lining and dolomite fill. Sample collected from massive poorly consolidated calcrete/dolocrete at site U; (d) Clotted micrite and sparite matrix with pseudo-oolitic and oolitic texture containing corroded detrital quartz grains. Massive nodular pedogenic

calcrete collected at site O; (e) Section through a calcrete nodule collected from the capillary fringe on Xhamoga Island showing a banded micrite fabric, Fe and Mn staining, highly corroded detrital quartz grains and authigenic silica void fills; (f) Dense micritic alpha fabric containing corroded detrital quartz grains and a skeletal shell fragment. Sample collected at site V on the seasonal floodplain.

Grain coatings (hypocoatings), dripstone cement and clay pendants (Fig 9.4), which have been identified by XRD analysis as belonging predominantly to the smectite group, were common within the calcretes. In addition significant amounts of kaolinite (profiles A, B and C), palygorskite (profiles C and E) and sepiolite (profile F) were detected (Table 9.1). In line with the clay-poor nature of Kalahari sediments, the total < 2 μm fraction within the calcretes was generally very low (< 5%) although the interdune location is thought to have resulted in local clay accumulation due to infiltration. Watts (1980) observed that montmorillonite/smectite was abundant in immature calcretes, lower portions of calcrete profiles and unaltered Kalahari sand further southeast in Botswana. Eitel (2000) also records the occurrence of smectite within Namibian calcretes and refers to the structural similarities between smectites and palygorskite and the transformation of palygorskite to smectite under more humid conditions (Paquet and Millot, 1972, Bigham *et al.* 1980). The simultaneous occurrence of palygorskite and smectite in profiles C (smectite is far more abundant) and E (in equal proportions) along with kaolinite in profile C is believed to be indicative of a transition from an arid period during which playa type conditions were dominant, to a more humid period when the fan was more extensive and feldspar dissolution and kaolinization occurred.

Sample site	Average % Carbonate	Cement type			Clay mineralogy					
		Silica	Calcite	Dolomite	Kaolinite	Smectite	Palygorskite	Sepiolite	Kaolinite + Chlorite	Interstratification
A	2%	++++	+		+	++				
B	30%	+	++++		++	++				
C	23%	+++	++		+	+++	+			
D	6%	++++	+		+	++				
E	28%	++	+++			++	++			
F	38%	++	+++			+		+++		
G	29%	++	+++				No data			
H	33%	++	+++				No data			
I	32%	++	+++			+				+++
J	36%	++	+++		+	+++				
K	47%	+	++++				No data			
L	6%	++++	+		++	++				
M	1%	++++	+		+++	+				
N	3%	++++	+		++	++	+			
O	25%	+	++++		+			++		
P	28%	++	+++					+++	++	
Q	30%	++	+++				No data			
R	33%	++	+++				No data			
S	31%	++	+++		+	++				
T	24%	++	+++		+	++++				
U	19%	+	+++	+	++	+++				
V	33%	+	++++				No detectable clay			

Table 9.1: A summary of XRD results for samples A-V. (++++) >75%, (+++) 50-74%, (++) 25-49% and (+) 0.1-24%.

Singer *et al.* (1995), Eitel (2000) and Watts (1980) identified sepiolite from southern African calcretes as being characteristic of Mg-rich alkaline environments and refer to its presence within playa-lake environments (Parry and Reeves, 1968a,b), its formation by detrital and chemical sedimentation in arid-zone soils (Reeves, 1976) as a result of neoformation in conditions of high (Mg+Si):Al ratios with a low CO_2 partial pressure (Millot, 1970, Weaver and Beck, 1977, Jones and Galan, 1988) and its formation as a result of calcite dissolution (Lacroix, 1941). Studies within the Kalahari (Eitel, 1994b, 1995, 2000, Eitel and Blumel, 1997, Watts, 1980) demonstrate that sepiolite-palygorskite clays are predominant in mature to very mature calcretes and are often associated with dolomite. Within the panhandle,

however, this is not the case as no dolomite was present within any of the profiles (C, E and F) containing sepiolite-palygorskite. If the sepiolite rich sample collected from the base of profile F is interpreted as being mature based on its clay mineralogy, its lack of distinguishing petrographic features from other massive groundwater sequences means that maturity of calcrete in this area based purely on thin section analysis must be treated with caution. Optically stimulated luminescence (OSL) dates from the Tsodilo Hills (Thomas *et al.*, 2003) and the Caprivi Strip to the north (Thomas *et al.*, 2000) show that no linear dune activity has occurred since the last glacial maximum, and that the authigenic magnesium-rich clays formed in the lower sections of the sequences due to magnesium enriched groundwaters could possibly point to a more saline arid to semi-arid phase (Calvo *et al.*, 1999). The climatic conditions of formation are a matter of considerable debate (Jones and Galan, 1988). Watts (1980) believed that sepiolite is a late stage mineral and that magnesium enrichment is caused either by the selective removal of calcium and precipitation of low-Mg calcite, thus causing an increase in the Mg/Ca ratio in the vadose waters, or alternatively due to the transformation, through dissolution-reprecipitation processes, of high-Mg calcite to low-Mg calcite and the resultant release of magnesium which enriched the vadose waters in line with Land and Epstein (1970). Watts (1980) also identified kaolinite in low quantities and believed that it is dominantly detrital and has in some cases resulted from the *in situ* weathering of feldspars, which are a component of Kalahari sediment (Moore and Dingle, 1998).

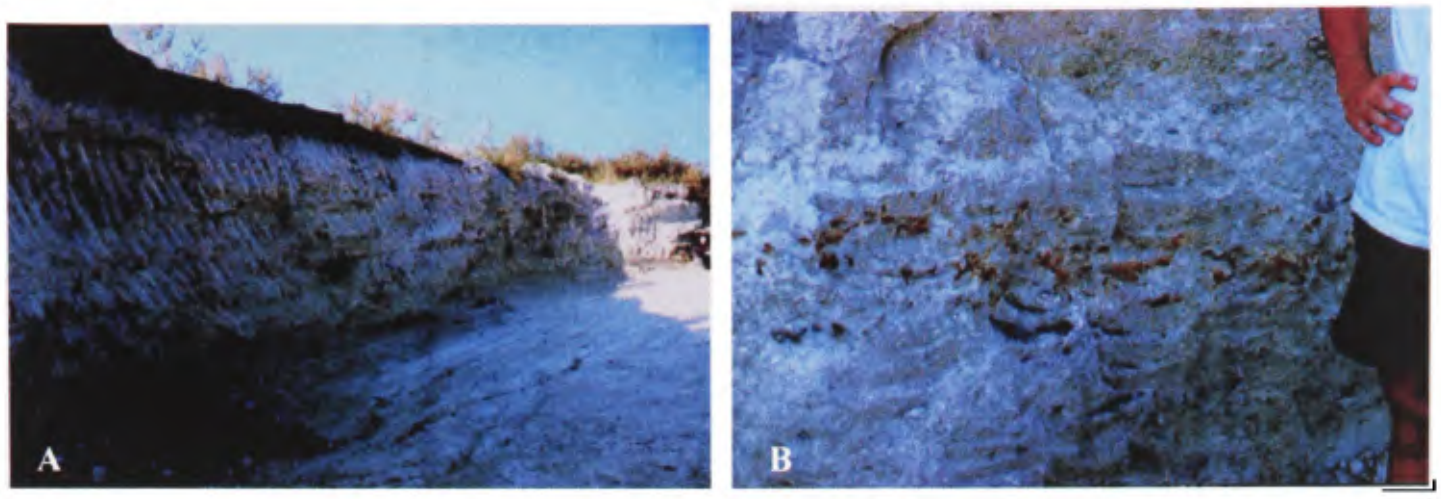


Figure 9.5: Photograph of massive groundwater calcrete profile (A) with Mn and Fe nodules and staining (B), Thamalakane Valley.

9.3.2 Calcretes of the Thamalakane Valley

South of the Gumare fault the Okavango spreads out to form vast permanent swamps and seasonal floodplains which are bounded in the southwest by the Kunyere fault and in the southeast by the Thamalakane River which runs southwest along the Thamalakane fault (Fig 9.2)(Gumbricht *et al.*, 2001). Five calcrete profiles (Q-U) were logged and sampled along the Thamalakane at the terminus of the fan and the active seasonal floodplain areas to the northwest of the river (Fig 9.1).

These profiles again show all the characteristics of groundwater calcrete. The base of the sequences was never exposed and the exposures were all in excess of 3 m and capped by a poorly developed soil approximately 0.5 to 1.0 m thick which formed above a gradational boundary. The profiles are composed principally of powdery calcrete grading down profile with increased carbonate content into nodular and then massive, nodule free, moderately to well consolidated calcrete which contains small Fe and Mn concretions and shows intense Fe- and Mn-mottling and green colouration

in the lower sections (Fig 9.5)(approximately 3.0 m, 1.5 m and 1.2 m below the surface in profiles R, S and T respectively). These features indicate reducing groundwaters at depth.

At the elbow joint of the Thamalakane and Gomoti Rivers northwest of Shorobe, the most southeast point sampled on the fan (profile U), the calcrete showed substantial dolomite (~11% by mass of total carbonates based on semi-quantitative XRD) (dolocrete is defined by Netterberg (1980) as containing more than 5% dolomite by mass of total carbonates) in relation to calcite within the lower parts of the profile (Table 9.1). Down profile the proportional percentage of calcite drops from 30% to 6% as the dolomite content increases. Near the base of the profile the calcrete (dolocrete?) becomes more friable and breaks into small pellets along type 2a and 2b fold and anticline/syncline structures as described by Watts (1977). Watts (1980) noted that dolomite occurred in two forms in most mature profiles further south in the Kalahari: firstly, as linings which may be coated by later calcite in solution channels, and secondly, as small, cloudy rhombs bunched together within the matrix. Under thin-section both of these types of dolomite appear to exist within this profile (Fig 9.4). The location of this site at the south-eastern extremity of the alluvial system (Fig 9.1) illustrates the potential evolution of the groundwaters and their resultant precipitates across the alluvial basin to develop a calcrete to dolocrete sequence based on evaporation and CO_2 loss (Arakel, 1986, Wright and Tucker, 1991). Watts' (1980) investigations also pointed to high concentrations of dolomite occurring at the capillary front at or around the groundwater table. These were believed to precipitate

as a result of the overlying vadose waters having a higher salinity and magnesium content than the underlying phreatic waters due to evaporation/evapotranspiration processes.

At all sites sampled along the Thamalakane River the < 2 μm fraction of the calcrete was dominated by smectite clays and to a lesser extent by kaolinite (Table 9.1). At the confluence of the Boro and Thamalakane Rivers (profile S) whole rock XRD and SEM analysis indicated the presence of significant amounts of kaolinized detrital mica which was absent from all of the panhandle samples and was only present in small quantities in two sites along the Thaoge and Potae Rivers (profiles L and M). The chemical weathering of detrital feldspar to kaolinite within the Kalahari sediments under humid conditions is a result of a low pressure and low temperature hydrolysis reaction (Kovda, 1964). Mica is normally associated with immature clastic sediments and its occurrence at site S is believed to be linked to sheetflood deposits which have accumulated in proximity to the Jao/Boro Channel which acts as a main distributary for suspended and bedload sediment within the system. Sediments located on the seasonal floodplains are believed to have undergone the greatest degree of weathering - hence the occurrence of kaolinite and the absence of feldspars and mica due to dissolution and replacement by carbonate cement.

9.3.3 Sandveld and Thaoge Valley Calcretes

Five calcrete profiles (L-P) were logged and samples collected from pits and profiles within the relict floodplains surrounding the Thaoge distributary and the sandveld

tongue in the southwest quadrant of the Okavango fan (Fig 9.1). The calcretes developed within this part of the floodplain show a range of features which indicate that the original groundwater calcretes have undergone a degree of pedogenic modification associated with floodplain stabilisation caused by channel avulsion during the course of the fan's history and most recently during the past century as a result of the deactivation of the Thaoge system (Shaw, 1984, 1988, Shaw *et al.*, 2003). All the calcrete sequences are developed below a distinct contact separating the overlying grey/brown alluvial soil between 1.2 and 1.5 m thick and massive powdery calcrete containing nodules of various sizes. Significantly the vegetation in this area is open mixed savanna woodland dominated by *Acacia* and *Combretum* species with a grassy understory, while the calcrete profiles investigated in the panhandle and Thamalakane areas were at all but the two northern most sites overlain by dense *Mopane* forest which thrives on the heavier textured poorly drained soils. Close to the Thaoge channel massive groundwater calcrete sequences in excess of 10 m deep have developed (Fig 9.6). Further away from the channel network calcrete profiles are far more pedogenic in character. These profiles have distinct upper surfaces, decreasing carbonate content with depth and rhizoliths in the form of calcified root casts in places. Under thin section these calcretes show micritic and microsparitic matrixes containing peloids, glaebules, pendent structures and corroded floating grains (Fig 9.4).

XRD and thin-section analysis indicated the presence of K-feldspar and kaolinite within all the calcrete samples. Smectite was present in all but one sample (profile O)

and mica was detected at two sites (profiles L and M) along the Thaoge River which complements similar immature clastic sediments located along the Boro River (profile S). At the most southerly sites (profiles O and P), located on the northern rim of the Ngami depression, the clay mineralogy of these, the most distinct pedogenic calcretes sampled, were dominated by sepiolite with lesser amounts of kaolinite and chlorite (profile P). This could be a mature calcrete, in which either smectite was transformed to sepiolite or sepiolite formed authegenically during arid to semi-arid conditions or the transition from a more humid climate. Kaolinite is more stable than smectite and hence is more resistant to weathering (Ducloux *et al.*, 2002) which explains its presence. However, as Ducloux *et al.* (2002) found, the transition to seasonal wetting and drying cycles has not induced the formation of illite from smectite but rather weathering, dissolution and the synthesis of pedogenic sepiolite and palygorskite under arid conditions in a manner similar to that outlined by Eitel (2000). Other samples within the Ngami Basin showed very similar clay mineralogies. However, as with Calvo *et al.* (1986, 1999) the sepiolite is associated with the calcrete, but there is no associated dolomite.



Figure 9.6: Photograph of an extensive calcrete sequence exposed next to the Thaoge River.

9.3.4 Islands in the Permanent Swamps of the Delta

Three islands of approximately the same size but believed to be at different stages of maturity (Xhamoga being the most immature, then Mosupatsela and Gaenga showing signs of greatest vegetational and geomorphic maturity linked to the idea of concentric migration of vegetation as an adaptation to changing chemical and physiological constraints within the island) were sampled (Fig 9.1). Xhamoga had an 85 m wide zone of fringe vegetation which was covered by large trees and undergrowth that clearly showed the transition from evergreen riparian species to the more salt tolerant species. Mosupatsela had a vegetation fringe approximately 50 m wide and Gaenga was largely devoid of vegetation except for a 10 m wide zone of fringe vegetation dominated by more salt tolerant species and a few riparian evergreen tree species. These latter two islands were also substantially flatter than Xhamoga and were characterised by a raised rim, which rose approximately 30 cm above the high water mark of the flood terrace (seasonal fluctuation in the water level of the permanent swamps is typically in the range of 10-20 cm and decreases towards the terminus of the system). This flat surface dominated the island and only at the centre was there a pan filled depression, giving the island a planed atoll shape. However, on Xhamoga the topography rises sharply from the perimeter to reach a maximum elevation of approximately 2 m above the surrounding channel and then drops towards a level equivalent to or slightly below that of the channel at the island's centre. This gave the island the distinct atoll island shape (McCarthy and Ellery, 1995). All three island centres surrounding the central pan were covered by

grass littered with dead trees, indicating that in former times the islands were heavily vegetated. On Gaenga and Mosupatsela there was evidence that during the dry winter months, an efflorescent crust of trona (sodium carbonate) covered the barren surface in the centre of the island, but due to the heavy rains much of the salt had been leached into the soil although some patches still remained.

			Sedimentology					
Sample	Colour	Description	% Gravel	% Sand	% Silt	% Clay	Mean Grain Size (micro m)	Sorting
Xhamoga A surface	10 YR 3/1	Very dark grey	0.0	73.5	25.8	0.6	184.0	Poorly Sorted
Xhamoga A 20 cm	10 YR 5/1	Grey	0.1	79.8	19.7	0.4	187.4	Poorly Sorted
Xhamoga A 40 cm	10 YR 7/2	Light grey	0.1	83.9	15.7	0.4	191.5	Poorly Sorted
Xhamoga A 60 cm	10 YR 7/1	Light grey	12.1	74.8	12.7	0.3	758.2	Poorly Sorted
Xhamoga B surface	10 YR 3/1	Very dark grey	0.0	83.5	15.5	1.1	178.2	Poorly Sorted
Xhamoga B 20 cm	10 YR 4/1	Dark grey	0.0	88.0	11.5	0.5	195.0	Poorly Sorted
Xhamoga B 40 cm	10 YR 5/1	Grey	0.0	87.1	12.0	0.9	175.7	Poorly Sorted
Xhamoga B 60 cm	10 YR 5/1	Grey	0.0	86.7	12.4	0.9	185.9	Poorly Sorted
Xhamoga B 80 cm	10 YR 6/1	Grey	0.0	87.8	11.9	0.4	184.8	Moderately Sorted
Xhamoga B 100 cm	10 YR 6/1	Grey	0.1	86.1	13.4	0.4	183.0	Poorly Sorted
Xhamoga B 120cm	10 YR 7/2	Light grey	0.0	86.1	13.5	0.4	179.7	Moderately Sorted
Xhamoga B 140 cm	10 YR 7/2	Light grey	0.0	87.3	12.3	0.4	185.7	Moderately Sorted
Xhamoga B 160 cm	10 YR 8/2	Very pale brown	0.1	81.6	17.7	0.6	170.7	Poorly Sorted
Xhamoga B 180 cm	10 YR 8/2	Very pale brown	1.2	85.9	12.5	0.4	308.1	Poorly Sorted
Xhamoga C surface	10 YR 6/1	Grey	0.0	87.5	12.2	0.3	184.6	Moderately Sorted
Xhamoga C 20 cm	10 YR 5/1	Grey	0.0	87.1	12.5	0.5	180.1	Poorly Sorted
Xhamoga C 40 cm	10 YR 6/1	Grey	0.0	88.4	11.2	0.4	188.3	Moderately Sorted
Xhamoga C 60 cm	10 YR 6/1	Grey	0.0	87.4	12.2	0.4	189.1	Moderately Sorted
Xhamoga C 90 cm	10 YR 7/2	Light grey	0.0	79.3	20.0	0.7	170.7	Poorly Sorted
Xhamoga D surface	10 YR 8/2	Very pale brown	0.0	91.9	7.9	0.2	209.8	Moderately Sorted
Xhamoga D 20 cm	10 YR 8/2	Very pale brown	0.0	89.6	10.1	0.3	183.1	Moderately Sorted

Table 9.2: A summary of Xhamoga Island's sedimentology.

In the permanent swamps, the islands, which consist of unconsolidated fluvial sand mantling the lower cemented sediments (Tables 9.2 and 9.4), tend to have either a sinuous or concentric morphology (McCarthy *et al.*, 1991a). Beneath them there is a concentration gradient in the groundwater from the island edge, which is fresh, to the

island centre, which is saline (Fig 9.7). The salinity gradient tends to be steep near the island margins but flatter near the centre. McCarthy and Ellery (1994) have shown that the transpirational demand of the riparian trees results in the lateral movement of low salinity water from the swamp channels into the island. With much of the fan surface being vegetated, actual evaporation from open water tends to be low, and transpiration is by far the dominant process of water loss. The trees and shrubs on the islands remove groundwater at a much faster rate than grasses, sedges or aquatic plants (Rogers, 1997). The roots of these trees extend below the water table and selectively remove water but actively exclude unwanted dissolved substances, thereby causing a salinity gradient. Below the fringe of riparian forest the water table is depressed below the level of the surrounding channel due to extraction. However, towards the central depression the water table rebounds due to reduced extraction and can emerge to form an active seepage zone around the central topographic low. In addition during the wet season the central pan becomes inundated with rainwater which infiltrates the sediment and amplifies the elevation of the inner island water table.

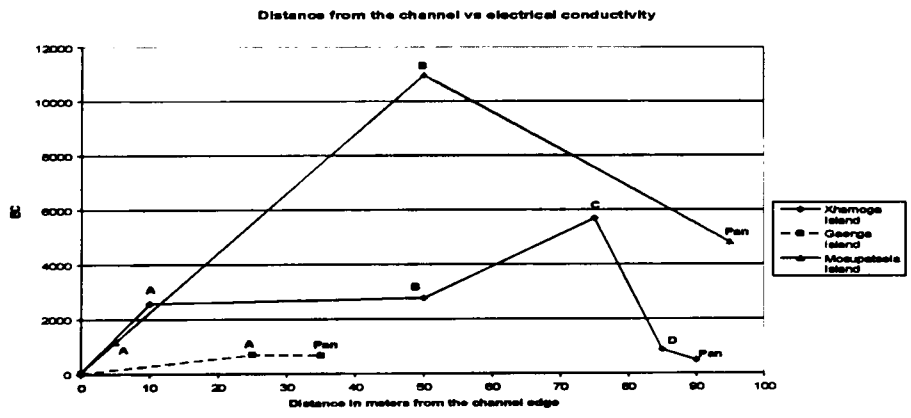


Figure 9.7: A plot of electrical conductivity in μS versus distance from the channel edge/island perimeter for each of the three islands sampled in the permanent swamps. Letters show the location of samples within the transect from perimeter to island core for each island.

					XRD						
Sample	% Organic Content	Magnetic Susceptibility (CGS/g)	% Carbonate Content	Conductivity (micro S)	Quartz	Calcite	Mica	Kaolinite	Smectite	Sepiolite	Goethite
Xhamoga A surface	9.15	3.85	3.73	2318.2							
Xhamoga A 20 cm	1.90	3.57	3.83	3146.9							
Xhamoga A 40 cm	1.18	3.48	4.64	1482.1							
Xhamoga A 60 cm	1.46	2.18	7.10	797.6	++	+++		+			
Xhamoga B surface	4.83	2.98	1.27	4829.9							
Xhamoga B 20 cm	2.29	4.95	0.86	6148.7							
Xhamoga B 40 cm	0.75	3.27	0.60	3198.8							
Xhamoga B 60 cm	0.82	4.07	0.75	2913.3	++			+++	+		+
Xhamoga B 80 cm	0.54	4.32	0.69	5095.8							
Xhamoga B 100 cm	0.46	3.98	0.97	3545.7							
Xhamoga B 120cm	0.36	3.97	0.98	2662.4	++	+	+	+++	+		
Xhamoga B 140 cm	0.37	4.10	1.26	2505.8							
Xhamoga B 160 cm	0.52	3.80	2.16	2040.5							
Xhamoga B 180 cm	0.62	1.85	3.55	2024.2	+	+++		+	+		
Xhamoga C surface	1.04	2.50	0.74	1900.1							
Xhamoga C 20 cm	0.47	1.83	0.59	3667.4							
Xhamoga C 40 cm	0.36	2.28	0.76	2962.9							
Xhamoga C 60 cm	0.49	2.97	1.12	2124.1							
Xhamoga C 90 cm	0.37	2.18	1.65	1514.5	+		+	++	+		
Xhamoga D surface	0.21	0.50	0.27	4027.4							
Xhamoga D 20 cm	0.10	0.28	0.24	816.4	++		+	++		+	

Table 9.3: A summary of Xhamoga Island's mineralogy. For XRD data (++++) >75%, (+++) 50-74%, (++) 25-49% and (+) 0.1-24%.

XRD analysis of the sediment collected from the profiles down to the water table across the three islands confirmed the presence of calcite, smectite, sepiolite, kaolinite and mica and the absence of dolomite, plagioclase and K-feldspar in any detectable quantity (Table 9.3). On Xhamoga, the most intensively sampled of the islands, the transect profiles produced a varying suit of mineralogies. As expected from the topography and the geochemistry of the fan (McCarthy *et al.*, 1991b, 1993) a down profile increase in fine grained calcite was identified and hence indicates active precipitation within the capillary fringe nearest the rim of the island (profiles A and B see Fig 9.8). Towards the centre of the island (profiles C and D see Fig 9.8) the

sediment is completely devoid of calcite. The clay mineralogies indicate another trend across the island. Kaolinite is by far the most abundant (40-50% of the clay fraction) clay mineral and is prevalent across the entire transect. However, its abundance is dramatically reduced within the capillary fringe where calcite precipitation is actively occurring (profiles A and B). This is believed to be a result of the dissolution of kaolinite and its replacement by calcite within the capillary zone. Similarly, smectite is present within all the island samples except for those collected from the centre which contain sepiolite. The formation of sepiolite within the central pan sediments may be a result of synsedimentary precipitation (Khoury *et al.*, 1982, Hay *et al.*, 1986, Mees, 2002) from the brackish (EC 490μS on the 9/12/2001) pan rather than diagenetic formation due to its absence from the sediments immediately adjacent to the central pan. Webster and Jones (1994) have shown that authigenic clay formation in lakes can be related to salinity shifts induced by evaporation. They have shown, as has Jones (1986), that precipitation of sepiolite is most likely to occur in brackish water while smectite reflects more saline lake conditions in arid to semi-arid lake systems.

			Sedimentology					
Sample	Colour	Description	% Gravel	% Sand	% Silt	% Clay	Mean Grain Size (micro m)	Sorting
Mosupatsela A 150 cm	2.5 Y 7/3	Pale yellow	1.1	82.3	16.2	0.5	310.2	Poorly Sorted
Mosupatsela B 200 cm	2.5 Y 8/1	White	0.8	64.2	34.0	0.9	239.6	Poorly Sorted
Mosupatsela C surface	10 YR 7/2	Light grey	0	95.4	4.3	0.2	241.3	Moderately Sorted
Mosupatsela C 20 cm	10 YR 8/2	Very pale brown	0	95.7	4.1	0.2	236.1	Moderately Sorted
Mosupatsela C 50 cm	10 YR 8/2	Very pale brown	0	94.7	4.8	0.4	242.7	Moderately Sorted
Gaenga surface	10 YR 7/2	Light grey	0.0	88.8	10.7	0.4	200.7	Poorly Sorted
Gaenga 20 cm	10 YR 4/1	Dark grey	0.0	93.3	6.4	0.4	221.3	Moderately Sorted
Gaenga 40 cm	10 YR 4/1	Dark grey	0.3	93.1	6.1	0.5	234.8	Moderately Sorted

Table 9.4: A summary of Gaenga and Mosupatsela Islands' sedimentology.

In support of McCarthy *et al.* (1989), near the upper surface of the root zone at 0.6 m below the surface of profile B on the crest of Xhamoga's rim, the stable iron oxyhydroxide goethite was detected in reasonably high proportions (8% of the fines fraction)(Table 9.3). The goethite is believed to have precipitated directly from the soil solution as acicular crystals within intergranular spaces.

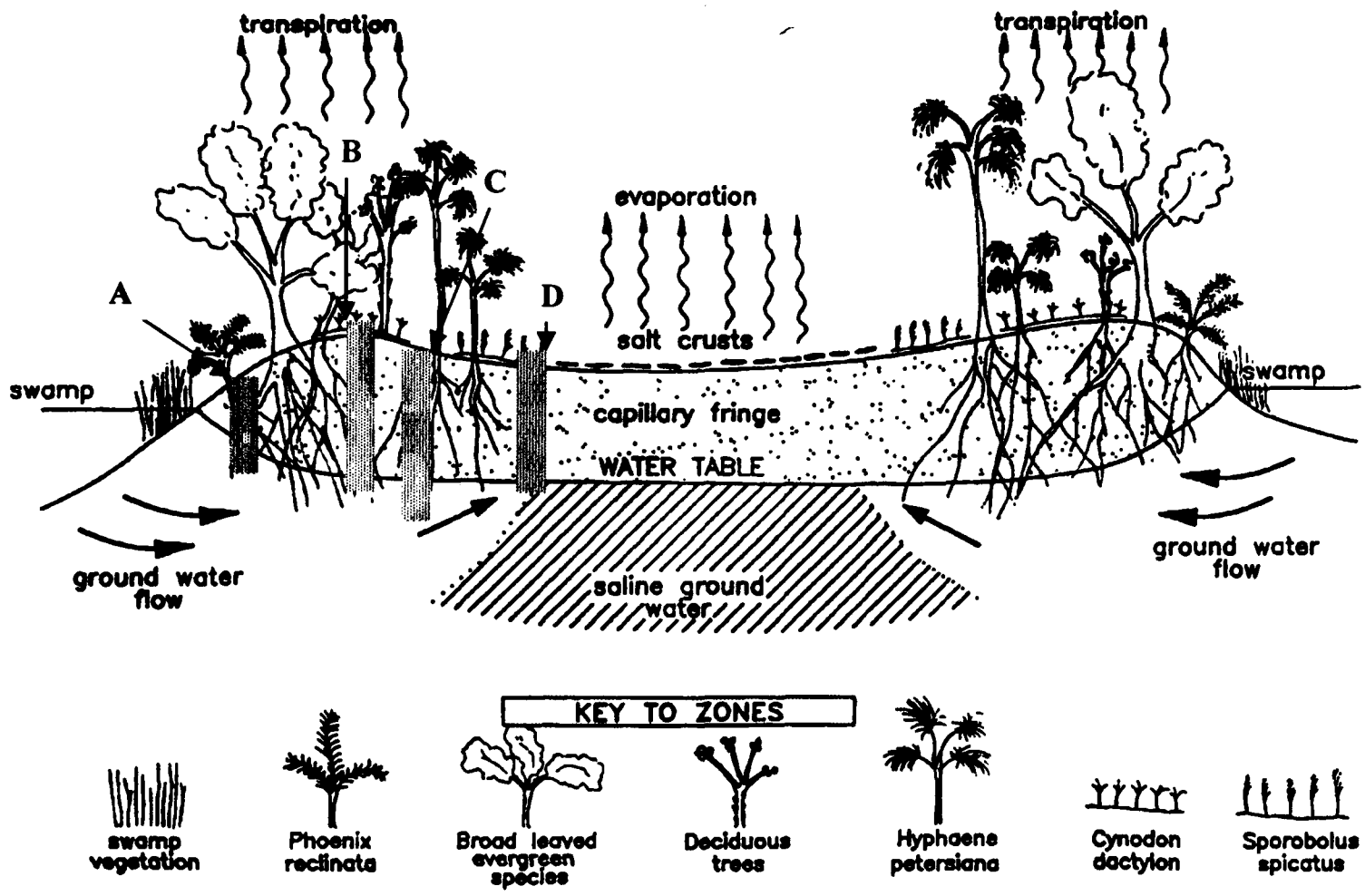


Figure 9.8: Idealised cross-section through Xhamoga Island showing the location of sample pits. Modified from Ellery & Ellery 1997.

On Mosupatsela a very similar trend to that of Xhamoga is evident. Despite the flatter topography calcite is being precipitated within the capillary fringe beneath the perimeter forest. The calcite content is highest near the inner limit of the forest and lower near the rim (Table 9.5). A similar although slightly different picture of the mineralogy develops on Gaenga where calcite is once again precipitated. However, it

does not show the distinct trend observed on Xhamoga or Mosputsela. Instead calcite is present within the entire shallow profile, indicating that the capillary fringe extends to the surface (Table 5). On both of these islands kaolinite and smectite are equally abundant and show no real trends vertically or laterally.

					XRD					
Sample	% Organic Content	Magnetic Susceptibility (CGS/g)	% Carbonate Content	Conductivity (micro S)	Quartz	Calcite	Mica	Kaolinite	Smectite	Sepiolite
Mosupatsela A 150 cm	0.34	3.82	3.22	445.7	+	++		+	++	
Mosupatsela B 200 cm	0.47	1.62	5.56	378.7	+	+++		+	+	
Mosupatsela C surface	0.10	0.83	0.10	2770.8						
Mosupatsela C 20 cm	0.07	0.97	0.09	587.9						
Mosupatsela C 50 cm	0.07	0.58	0.10	474.2						
Gaenga surface	0.93	0.50	1.71	790.5	+++	+		+	+	
Gaenga 20 cm	0.32	0.63	0.36	1541.4						
Gaenga 40 cm	0.24	0.13	0.35	2654.3	++	+	+	+	+	

Table 9.5: A summary of Gaenga and Mosupatsela Islands' mineralogy. For XRD data (++++) >75%, (+++) 50-74%, (++) 25-49% and (+) 0.1-24%.

With increasing depth the carbonate content progressively increased (Table 9.3 and 9.5) on all three islands. Towards the seasonal capillary fringe the grains show coatings of micrite and authigenic silica. Then, with increasing depth, the abundance of nodules increases. Thin-section analysis indicated that these nodules are composed of clastic quartz grains floating in a matrix of micritic calcite and authigenic silica mostly in the form of chalcedony (Fig 9.4). This is confirmed by the fact that nodules retained their integrity after complete dissolution of the carbonate cement in dilute hydrochloric acid. It is probable that varying pH conditions within the profile and capillary fringe result in authigenic silica being mobilised at high pH in the upper sections of the profile and being deposited in the lower sections due to a slight

decrease in pH associated with high levels of free CO_2 and highly saline groundwaters (Shaw and Nash, 1998, McCarthy and Ellery, 1995).

As highlighted by McCarthy *et al.* (1993) there seems to be a strong relationship between topography and calcite content, with the highest ground generally located above areas of high calcite abundance. The subsurface accumulation of calcite on the islands of the fan, and the close association of carbonate with islands suggests that a significant part of island development is a direct result of displacive calcite crystallization (Watts, 1978, McCarthy and Metcalfe, 1990). Precipitation occurs mainly within the capillary fringe directly above the laterally moving groundwater but also to a lesser degree below the water table. The cementation preferentially occurs at these topographic highs, due to groundwater being forced to rise as a result of the evapotranspirational pumping which facilitates CO_2 degassing and the common ion effect.

9.3.5 The Seasonal Floodplains

Four sites (profiles H – K) were investigated close to the Thaoge distributary on the western margin of the seasonal floodplain. The vast area that forms the seasonal swamps comprises small tree covered islands scattered throughout the broad grass and sedge covered low gradient floodplains.

The calcretes within these profiles all show the same trend down profile: a 0.5 – 1 m thick uniform grey/brown poorly developed alluvium capping showing no

stratification and varying degrees of sodicity, underlain by powdery, poorly consolidated calcrete which becomes massive and consolidated with irregular shaped nodules of increasing size with depth. The percentage of calcium carbonate increases dramatically below the alluvium and then steadily with depth. Towards the base of the sequences it reaches approximately 50% of the whole rock mineralogy in all the samples. These features, along with the crystalline alpha fabrics, are again indicative of fluctuations between processes of pedogenic and groundwater calcrete formation. The general homogeneity of the alluvium suggests that as with similar seasonally flooded low gradient semi-arid environments with micro-relief (Pal *et al.*, 2003) the formation of calcrete is associated with clay illuviation and infiltration which results in clay enrichment in the B horizon, the development of sodification and little addition of organic matter within the profile especially in low lying areas where suspended clays tend to accumulate during the wetting and drying cycles. Each seasonal cycle of inundation supplies alkali bicarbonates and carbonates due to the hydrolysis of feldspar contained within the Kalahari sand. These alkali bicarbonates and carbonates increase the level of sodium and the pH. At high pH, calcium carbonate is precipitated, although the mechanism of precipitation is believed to be induced by either the lowering of the soil CO_2 partial pressure or saturation linked to evapotranspiration. The high levels of sodium are believed to impair hydraulic conductivity at depth which results in the depletion of calcium due to calcium carbonate precipitation and the accumulation of other cations (principally magnesium). This has a direct influence on the formation of authigenic clays. The clay mineralogy of all the profiles is dominated by smectite with small quantities of

kaolinite (Table 9.1). Profile I however, showed a high level (51%) of interstratification in the clay fraction (< 2μm), which on review of the X-ray diffractograms is believed to be interstratified smectite-kaolinite. This site also has reduced quantities of smectite (15%) compared to the other sites. Pal *et al.* (1989, 2003) state that on the semi-arid Indo-Gangetic Plains smectite-kaolinite minerals result from the weathering of smectite under humid tropical conditions. Could this sequence be an indication of smectite modification and kaolinite formation under more humid conditions? The picture is, however, blurred because there has been emplacement of clay into the sandy alluvium due to the mechanisms of infiltration outlined by Matlack *et al.* (1989) and Moraes and De Ros (1990) and illuviation within the profile during its development.

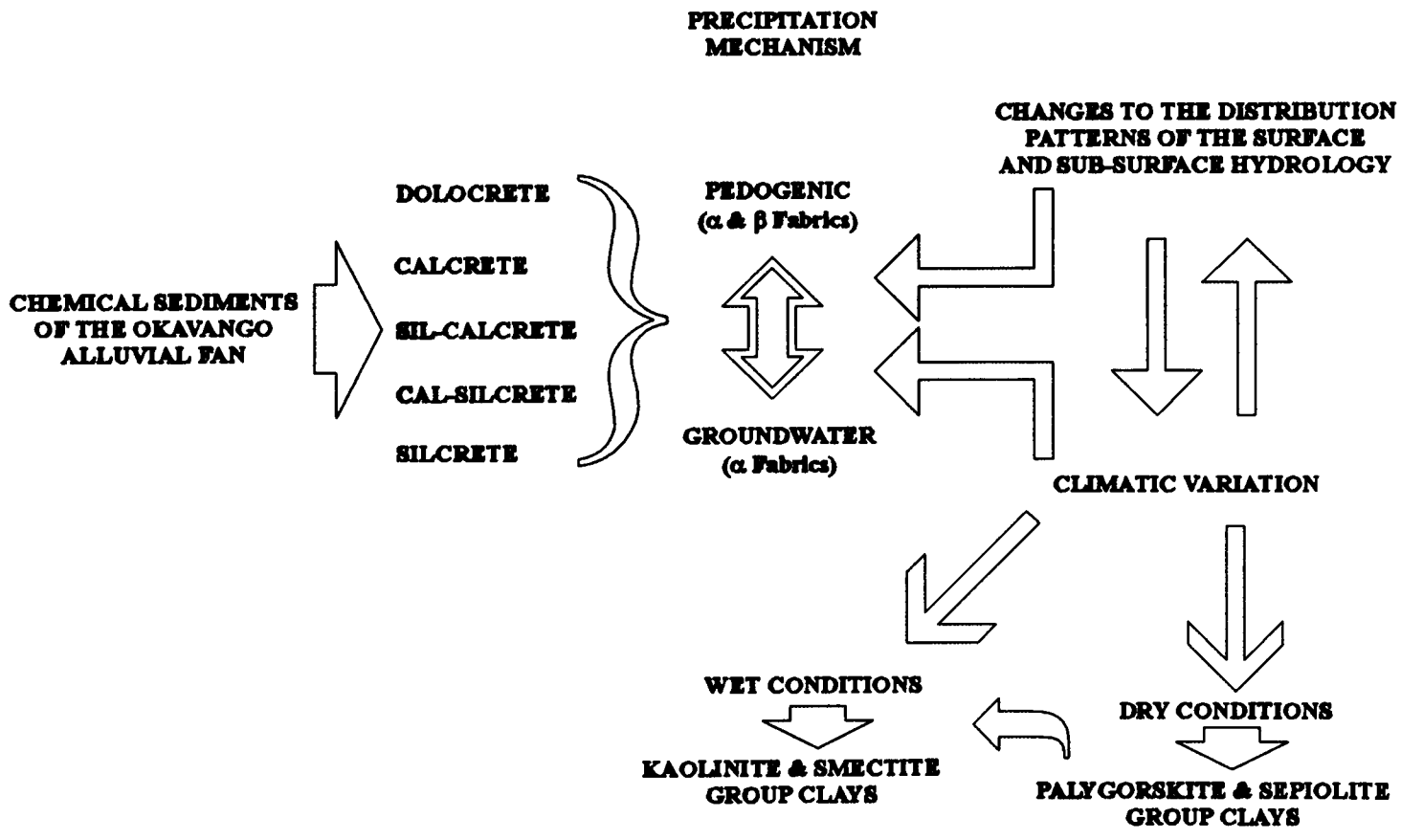


Figure 9.9: Simplified summary schematic of the processes, mechanisms and resultant mineralogies within the Okavango.

9.4 Hydro-Geochemistry

The intergrade calcrete sequences of the Okavango fan have formed mostly as a result of groundwater precipitation of calcium carbonate with later pedogenic modification (Fig 9.9). Ground and surface water analysed from a number of sites throughout the fan have indicated that the main anions are bicarbonate, chloride and sulphate while the major cations generally have low concentrations with a low (< 1) Mg/Ca ratio at all locations except the groundwater profile through Xhamoga and Mosupatsela Islands which have ratios in the range of 5:1. It is believed that this preferential enrichment of magnesium in the groundwater precipitated high Mg calcite in the form of micrite within the capillary fringe due to mechanisms of CO_2 degassing (Watts, 1980).

The contemporary groundwater geochemistry and pathways within the Okavango fan indicate that although groundwater calcrete formation has been the principal form of chemical sedimentation, the conditions under which precipitation has occurred must have varied considerably. The calcrete assemblages have shown that two distinct types of clay mineralogy exist: the majority dominated by smectite and the other dominated by sepiolite. Within the literature sepiolite dominated calcrete profiles are generally associated with magnesium rich semi-arid environments (Eitel, 2000, Eitel and Blumel, 1997, Singer *et al.*, 1995, Watts, 1980, Hay and Wiggins, 1980, Arakel, 1986, Jones and Galan, 1988, Monger *et al.*, 1991, Wang *et al.*, 1994, Calvo *et al.*, 1999). However, in environments with more than 300 mm of annual rainfall (Eitel, 2000) either smectite is formed rather than sepiolite or palygorskite (Nahon and

Ruellen, 1975, Millot *et al.*, 1977, Wang *et al.*, 1994) or palygorskite is transformed to smectite (Eitel, 2000, Paquet and Millot, 1972, Bigham *et al.*, 1980). Could this indicate that the groundwater calcretes of the Okavango formed principally during a humid phase when the alluvial fan was more extensive? Groundwaters from the Ngami Basin have Mg/Ca ratios that are not much higher than those of the Okavango system and it is believed that during periods of the Lake Makgadikgadi highstands the entire Okavango, Ngami, Boteti River, Mababe and Makgadikgadi system would have been connected (Shaw *et al.*, 2003) and substantial groundwater recharge would have occurred. This widespread shallow aquifer would have covered a far more extensive area of the fan than currently and combined with increased activity in the Okavango system the potential for groundwater calcrete formation would have been extensive.

Within the profiles the mineralogy implies palaeoclimatic variation. The occurrence of feldspar and mica in association with sepiolite could indicate that some of the calcretes (profile O in particular) formed under more arid conditions where the weathering of feldspars to kaolinite was less intense. It is proposed that these principally pedogenic calcretes represent the most recent chemical deposits of the southwestern fan and correspond to the calcretes described and dated to the period 12-10 ka BP by Cooke (1976). In profiles with an absence of plagioclase and alkali-feldspar, the sediment contains kaolinite, mica, minor playgorskite and smectite. The mica, which is believed to be detrital and linked to sheet flood deposits, has been extensively kaolinized in all of the profiles where it occurs. The near-surface

transformation (principally through hydrolysis) of detrital feldspar and mica has occurred as a result of the interaction of meteoric and ground water causing the formation of kaolinite (Morad *et al.*, 1998) during periods (either seasonal or of several years duration) of climatic variability (increased rainfall followed by drier conditions).

9.5 Conclusion

Sedimentary sequences of the Okavango fan contain groundwater and pedogenic intergrade calcretes formed through a series of near-surface processes. In the panhandle the two types of calcrete, groundwater and lacustrine, occur mostly in fossil interdune settings or within the cores of dissected linear dunes. On the fan the calcrete appears to have been formed as groundwater calcrete that in places has undergone modification via the addition of pedogenic calcrete during periods of floodplain abandonment and stabilisation. The proposed mechanism is that after floodplain abandonment, the water table subsides and calcite and authigenic silica precipitation is lowered within the profile. Over time savanna woodland colonises the floodplain and the precipitated intergrade groundwater calcrete will be added to and modified by pedogenic calcrete accumulation. The result is an *in situ* transformation from a characteristic groundwater profile to an increasingly pedogenic one which shows an overall increase in the density and amount of the carbonate up profile (Wright and Tucker, 1991). As pedogenic processes dominate, any additional carbonate accumulates below an increasingly well defined transition with the surface soil horizon. However, once the area becomes flooded again, a new cycle of

groundwater calcite and authigenic silica precipitation will replace and modify the pedogenic components of accumulation (Pimentel *et al.*, 1996). The calcrete within the sequence therefore represents an aggregate deposit of all previous cycles of floodplain inundation and abandonment. Mass-balance calculations by McCarthy and Metcalfe (1990) indicate that the quantity of chemical precipitate on the contemporary Okavango fan is at least five times that of clastic sediment. It is probable that due to the system's location within the heart of the Kalahari, chemical sedimentation has been the dominant process through the Late Pleistocene and Holocene.

10. THE GEOMORPHOLOGY AND CHEMICAL SEDIMENTS OF THE LINYANTI SYSTEM, EASTERN CAPRIVI, NAMIBIA

10.1 Introduction

The Linyanti Swamps cover approximately 1000 km^2 and form the border between the Namibian eastern Caprivi and northern Botswana (Fig 10.1). They have a complex geomorphology and are the result of neotectonic activity combined with river capture and reorientation of the Kwando (Cuando)/Mashi/Linyanti, Chobe and Zambezi Rivers and the subsequent deactivation of the Magwegqana and Savuti Channels. The position and orientation of the Linyanti is a direct result of its role within the palaeo-Makgadikgadi system and the proto-Zambezi's southerly drainage through the Mababe depression (Fig 10.2).

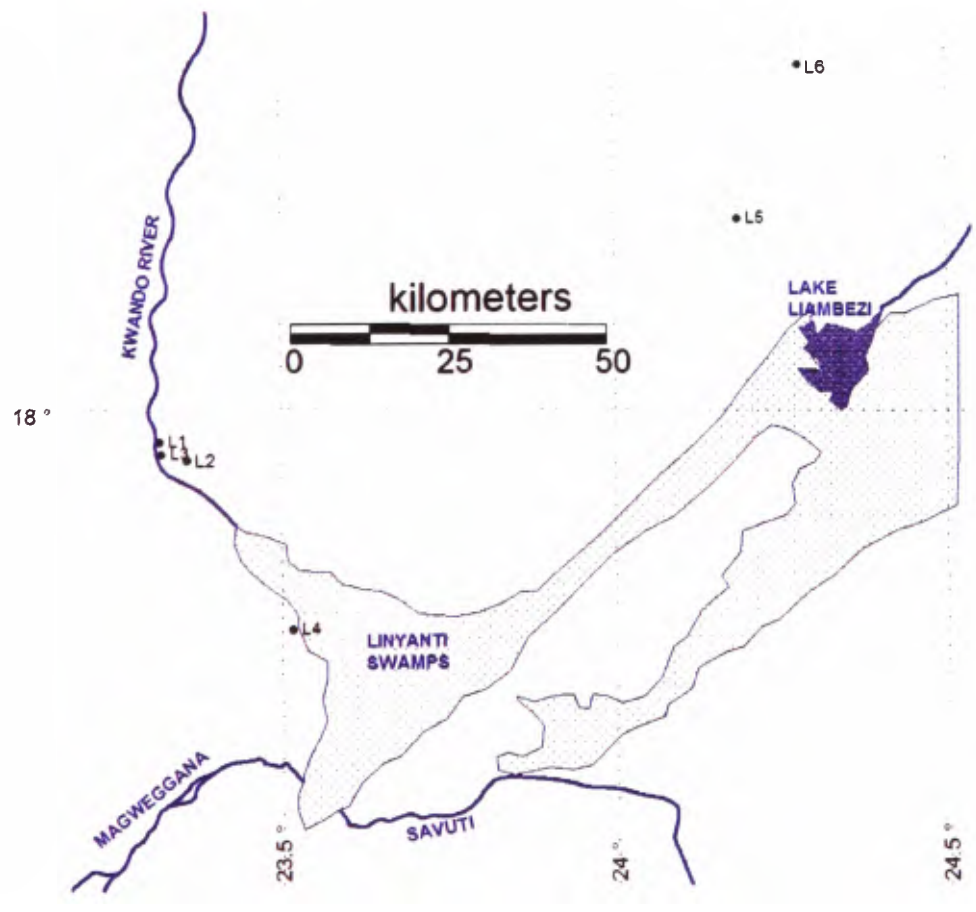


Figure 10.1: Location map of sample sites within the Linyanti Swamps.

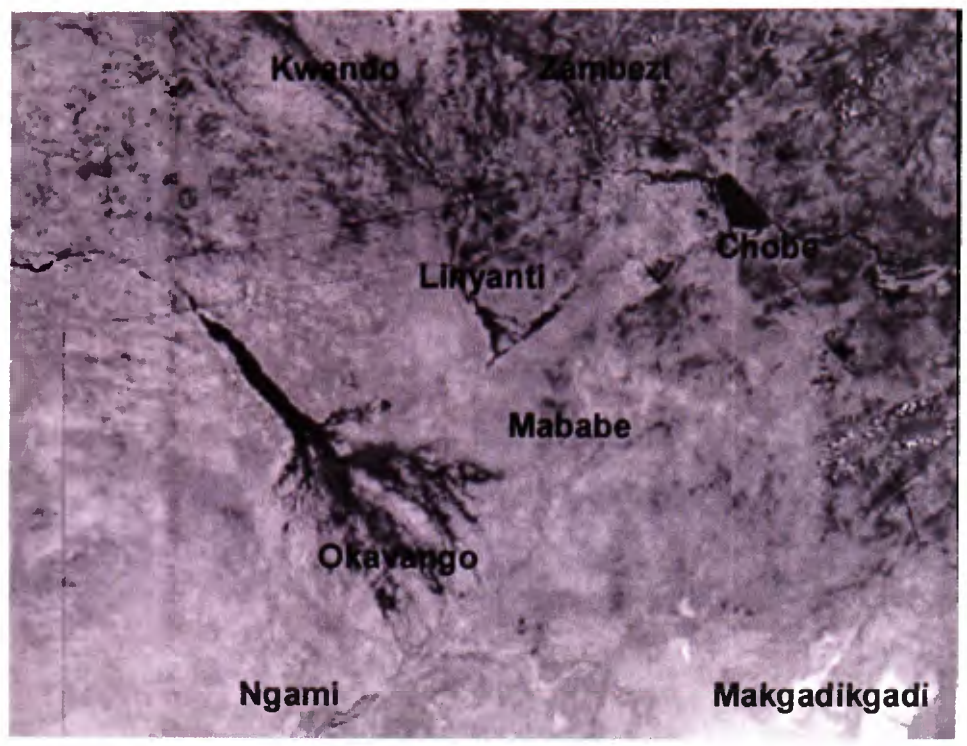


Figure 10.2: MODIS image of the Chobe-Linyanti-Okavango-Ngami-Makgadikgadi system

10.2 Geomorphology

The main body of the Linyanti Swamps forms a regionally significant tectonically controlled (the Gwembe Trough and Okavango Graben) fan, similar in morphology and orientation to that of its larger neighbour, the Okavango. Its proximal end is located at 18°17` S 23°32` E and the distal end is located along a NE/SW trending fault which corresponds to an eastern extension of the Gumare/Linyanti Fault (Orpen *et al.*, 1989; Thomas and Shaw, 1991). It is along this fault that the palaeo-Chobe/Kwando connected to the Okavango system along the Magwegqana channel (Selinda Spillway). The northeastern section of this half-graben has structural similarities to the larger southwestern part of the basin which is controlled by the Kunyere and Thamalakane faults (Fig 10.3). Deactivation of the Selinda Spillway connection between the Chobe/Linyanti system and the Okavango has its origins in Late Cretaceous uplift and later Cenozoic flexure along the Okavango-Kalahari-Zimbabwe Axis which severed

the link between the Limpopo, Okavango, Kwando and Zambezi-Luangwa systems (Gumbricht *et al.*, 2001). This reorientation of central Kalahari drainages is believed to be responsible for the formation of the endoreic drainage system which supplied the majority of sediment to the central Kalahari basin (Thomas and Shaw, 1991; Moore and Lankin, 2001). However, the uplift rejuvenated the lower Zambezi, initiating headward erosion and progressive capture of the Luangwa, upper Zambezi and Kafue Rivers (Shaw and Thomas, 1988; Thomas and Shaw, 1988; Nugent, 1990; Thomas and Shaw, 1991, Moore and Larkin, 2001; Moore and Blenkinsop, 2002).

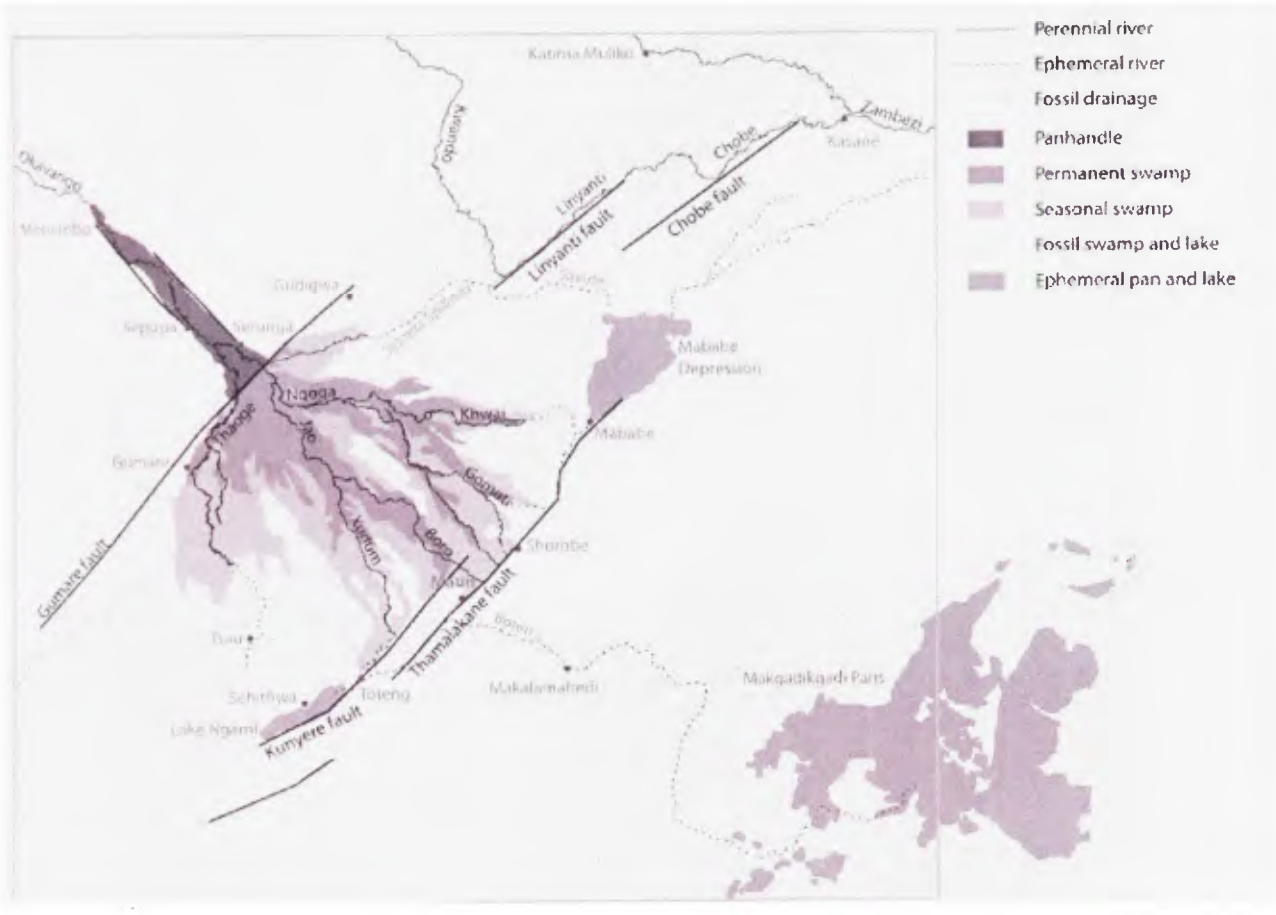


Figure 10.3: Dominant fault lineaments within the Okavango Region, from Mendelsohn and el Obeid (2004).

Extensive fluvial sand deposits are exposed southwest of Katima Mulilo. These older alluvial deposits mapped by Shaw and Thomas (1988) provide evidence to

support the existence of an extensive fluvial system flowing southwest of Katima Mulilo (Fig 10.3). The Mpandwa and the Mambova knickpoints act to demarcate the extent of the Gumare-Ngoma (southern) and Betsha-Linyanti-Katima Mulilo (north) fault lines which form the Linyanti/Chobe half-graben structure. The proximal and distal ends of the fan are constrained by this structure. In addition these deposits are believed to link with Lakes Liambezi and Lisikili to form part of the 2000 km^2 palaeo Lake Caprivi system at 936 m a.s.l. (Shaw and Thomas, 1988).

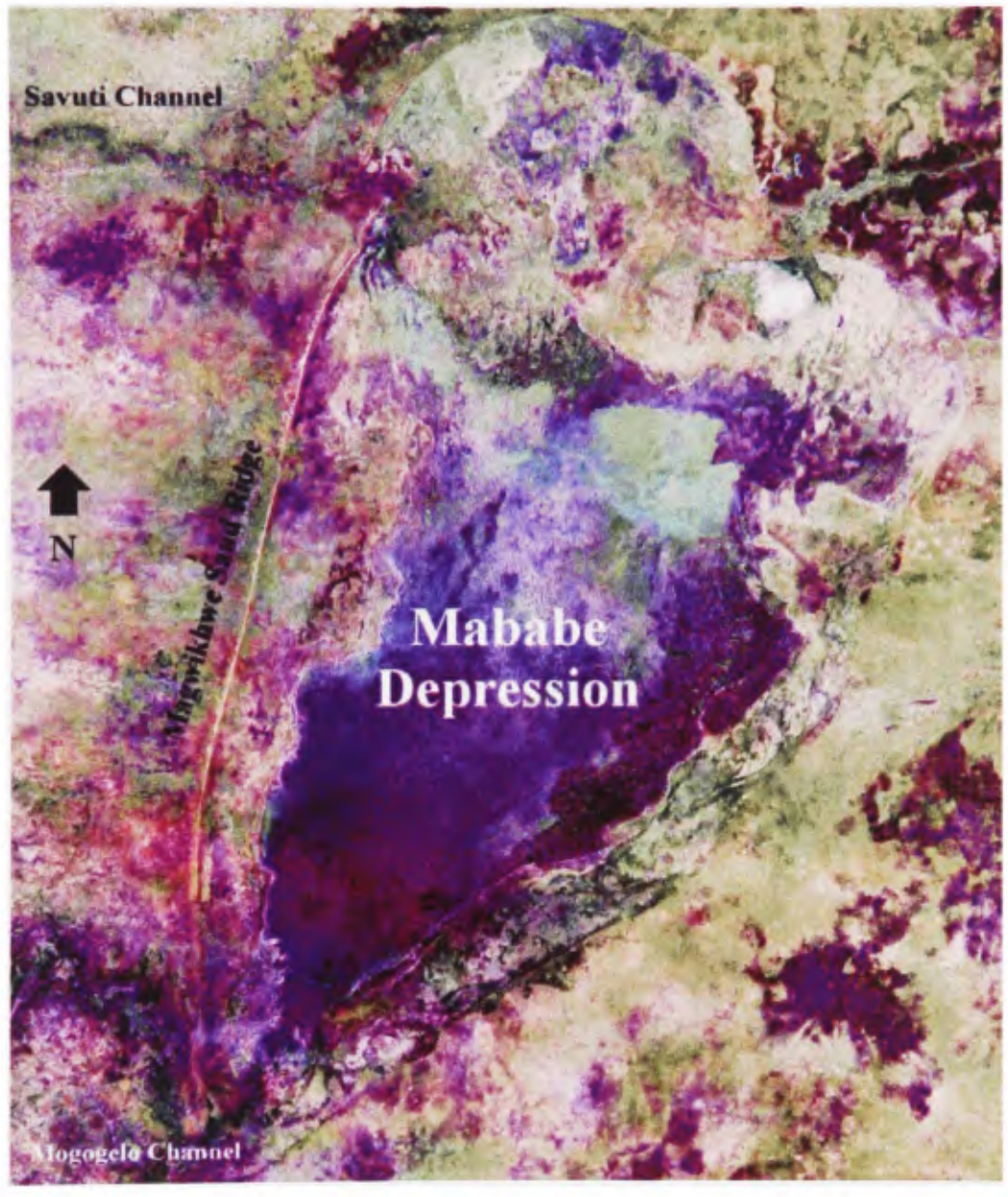


Figure 10.4: LANDSAT image of the Savuti Channel, Magwikhwe Sand Ridge, Mababe Depression and the Mogogelo Channel.

There is evidence to suggest that the Lake Caprivi/Linyanti/Chobe River system bridged the gap between the Gumare and Kunyere fault systems via the Savuti Channel and made its way southwest in the form of an extensive floodplain system within the Mababe Depression (Fig 10.4) which is orientated along the Kunyere/Thamalakane fault system. The Mababe Depression joins the present day Thamalakane River via the Mogogelo channel. The Magwikhwe sand ridge, which runs almost north/south from the Savuti Marshes to the Khwai River, is believed to be a curvilinear shoreline feature (Thomas and Shaw, 1991).

10.3 Near Surface Deposits of the Linyanti

A number of sediment samples were collected from sites along the terraces of the incised Kwando River, the edge of the floodplain at the proximal end of the Kwando alluvial fan, close to Lake Liambezi north of the Linyanti River and west of Katima Mulilo (Fig 10.1). These sites displayed a range of clastic and chemical sediments within a relatively simple lithostratigraphy.

10.3.1 Physical Characteristics of the Deposits

Detrital clastic sediments typically mantle the upper 2.5 m of the Linyanti alluvial fan. These deposits generally have very poorly developed A and B horizons and are comprised of two lithologic populations: moderately sorted, iron coated (limonite), predominately quartz, grains (typical Kalahari reworked fluvio-aeolian grains) which characterise the higher lying interfluve areas and moderately to poorly sorted, clean white or greyish brown (10YR 5/2), predominately quartz, fluvial grains which occur within the lower lying channels (*c.f.* Shaw and Thomas, 1988).



Figure 10.5: Photograph of a palaeo-channel profile exposed at site L6. An upper unconsolidated white fluvial sand horizon (containing numerous bee-eater burrows) overlies a moderately consolidated feruginised sand.

Palaeochannels within the alluvial fan which have been incised into the surrounding often partially consolidated host deposits (such as at site L6) form distinctive packages of unconsolidated sediment. These fluvial sediments often contain a number of different horizons indicative of differing sedimentation and geochemical conditions. The upper horizons are typically characterised by a poorly developed fine to medium sand textured grey alluvial soil which grades into a moderately sorted medium textured fluvial sand containing numerous mottles and pisoliths. The distinct feruginised orange colouration of the deposit is a direct result of a falling/fluctuating water table which has resulted in the oxidation of iron rich clays within the sediments (often as grain coatings) and pisoliths (Fig 10.5). The dominant feruginised medium sand is interbedded with

minor lenses and thin horizons of coarse textured clay free clean white bleached fluvial sand.

High ground within the core of the Linyanti alluvial fan (L1) is characterised by a distinct Kalahari cover which contains a 0.1 m thick pedogenic biocrust indicative of biomineralisation by soil fungi (Wright, 1986) beneath a 0.2 m thick poorly developed woodland soil. Thin section investigation reveals that this thin biocrust is characterised by numerous biogenic structures and a dominant silica beta fabric (*c.f.* Wright and Tucker, 1991).



Figure 10.6: Photograph of the down-profile increase in carbonate at site L4.

Paired terraces deposits (L4) along the lower sections of the Kwando River within the Linyanti alluvial fan are characterised by brown grey (7.5YR 4/1) grading to

brownish grey (7.5YR 5/1) unconsolidated well sorted fluvio-aeolian Kalahari sand which is rich in gastropod shells.

The transition between the upper unconsolidated clastic deposits and the lower moderately to well consolidated chemical sediments is marked by an increase in the calcium carbonate content of the material below 1.0 m (Fig 10.6). This increase in the calcium carbonate content is believed to be reflective of pedogenic mechanisms of chemical precipitation at shallow depth. However the distinct unconformity at approximately 2.5 – 3.0 m.b.s. between the powdery to moderately consolidated cal-silcrete and the moderately to highly indurated impure silcrete is believed to reflect the extent of pedogenic calcretisation of the original deposits and the role of capillary fringe and phreatic zone geochemical processes at greater depths. These processes have resulted in a lithosequence of white (10YR 8/1) powdery cal-silcrete which contains biogenic structures grading into moderately to well indurated massive crystalline brown coloured impure/pure silcrete. The upper powdery cal-silcrete typically contains numerous floating irregularly shaped cal-silcrete and impure silcrete nodules of various sizes and throughout the more consolidated cal-silcrete mega-quartz veins of various dimensions are abundant. This suggests calcification of the primary massive silcrete but the retention of later stage features such as vein fills where silica precipitated along fractures and joints which acted as conduits for enriched meteoric and phreatic water.

Geomorphic and stratigraphic evidence suggests that a palaeo-Linyanti alluvial fan and sub-basin fill sequence exists within the graben like structural controls of

the area. As channel avulsion occurred it is these older Kalahari Group sediments that have now been incised by the modern Kwando River. The result is that under current conditions the main channel is progressively migrating westwards in response to the low gradients, vegetation and lack of sediment accommodation space within this overfill sub-basin. McCarthy *et al.*, (1986a, 1988, 1991b, 1992) identified identical mechanisms which have been responsible for channel avulsion within the Okavango. Channel migration has resulted in the lowering of the water table in some parts of the fan and the subsequent localised reorientation of hydraulic gradients. This has resulted in the epigenetic modification of some chemical sediments that had been precipitated and hosted within a phreatic environment and subsequently underwent desiccation and re-equilibration within a vadose and/or pedogenic environment depending on their depth within the profile (*c.f.* Pimentel *et al.*, 1996; Shaw and Goudie, 2004).

10.3.2 Petrography

Petrographic investigation of a range of samples throughout the study area revealed that the upper consolidated cal-silcrete is a packstone characterised by a complex fabric consisting of abundant peloidal micrite (Fig 10.7a), micro- and crypto-crystalline quartz with poorly corroded floating detrital quartz grains (Fig 10.7b). Extremely well defined medium sand sized ellipsoidal peloids, possibly faecal pellets, composed of clay/silt-sized carbonate mud, ooids (Fig 10.7c) and pisoids are abundant throughout the upper samples. Samples also contain numerous calcified root hairs and rhizolith structures (mostly rhizocreations, calcified root cortex cells (possibly microcodium) (Fig 10.7d) and calcified roots),

alveolar textures indicative of root moulds (*c.f.* Klappa, 1980a) and peloids all indicative of biogenic mechanisms of precipitation.

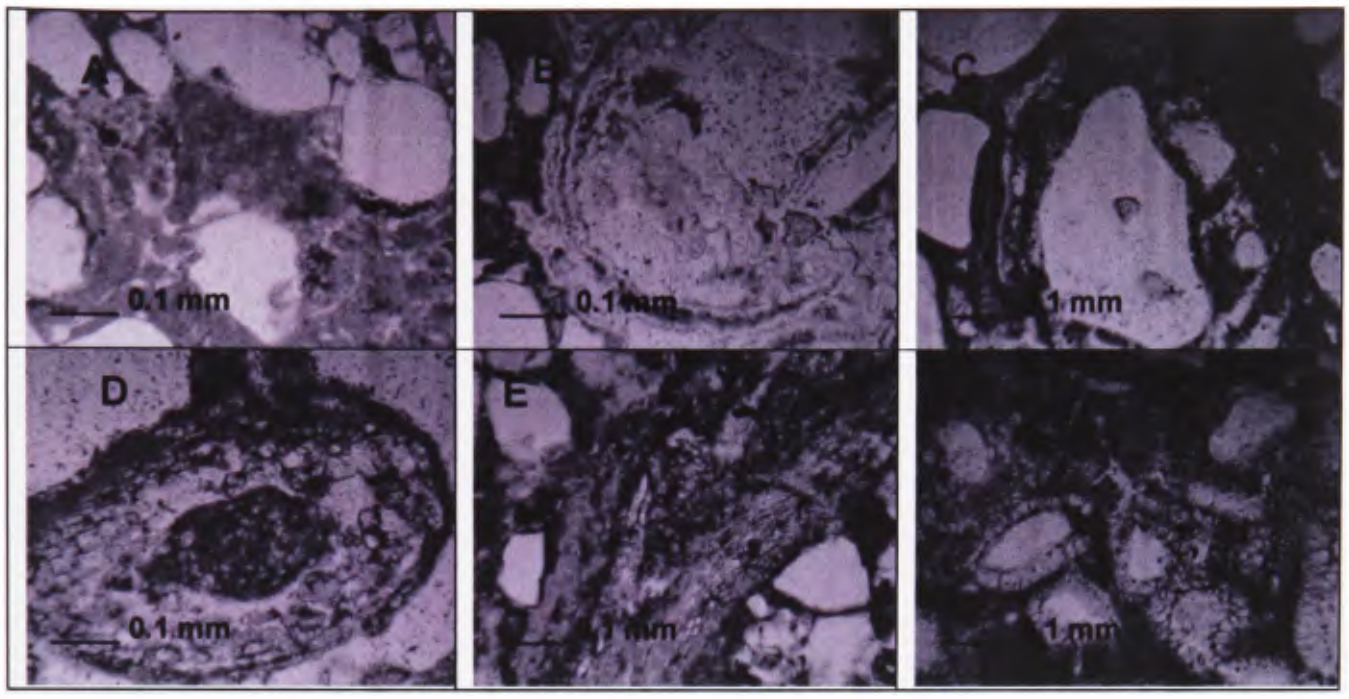


Figure 10.7: PPL thin-section photomicrographs of: (a) peloidal micrite and corroded detrital quartz grains within a lacy sparite fabric; (b) crypto-crystalline quartz with poorly corroded floating detrital quartz grains; (c) concentric laminations of micrite forming an ooid around an aggregate of detrital quartz grains; (d) calcified root cortex cells (possibly microcodium); (e) calcified root hair; (f) detrital quartz grains with very well developed sparite grain coating floating within a crystalline sparite fabric which has been partially micritised (lower left corner).

Petrography of the lower impure/pure silcrete indicates that this is a wackestone with the upper section dominated by biogenic structures such as peloids, tubules, root hairs and root petrification (Fig 10.7e) and the lower section by a crystalline texture with alpha structures (Fig 10.7f). The majority of the biogenic structures of the upper section are are preserved within an authigenic quartz fabric which is almost devoid of floating detrital grains, indicative of intense corrosion of detrital grains.

The abundance of biogenic structures within the upper cal-silcrete and impure/pure silcrete suggest precipitation within the capillary fringe of a pedogenic environment. Similar biogenic structures within cal-silcretes and impure silcretes have been documented from beneath the islands of the Okavango alluvial fan where precipitation is occurring within the root zone, capillary fringe and the phreatic zone (Shaw and Goudie, 2004).

		Whole rock analyses						< 2µm fraction analyses							
	Depth	Quartz	Calcite	Dolomite	K-feldspar	Smectite	Sepiolite	Quartz	Calcite	Feldspar	Mica	Kaolinite	Smectite	Sepiolite	Whewellite
L1 0 1m	0 10	100	-	-	-	-	-	83	-	5	-	3	9	-	-
L1b 2.0m	2.00	78	22	-	-	-	-	14	69	-	17	-	-	-	-
L1b 2.5m	2.50	80	20	-	-	-	-	-	70	-	-	5	25	-	-
L 1b 3.0m	3.00	86	14	-	-	-	-	31	27	-	-	-	42	-	-
L3 2.0m	2.00	80	19	1	-	-	-	7	69	-	-	-	24	-	-
L3 2.5m	2.50	66	34	-	-	-	-	-	-	-	-	-	-	-	18
L3 3.0m	3.00	68	32	-	-	-	-	no < 2µm fraction							
L3 3.5m	3.50	90	9	-	1	-	-	12	64	-	-	7	17	-	-
L4a 0.75m	0.75	70	30	-	-	-	-	-	89	-	-	-	-	11	-
L4a 1.0m	1.00	77	20	-	-	-	3	-	85	-	-	4	-	11	-
L4a 2.0m	2.00	97	1	-	-	2	-	20	56	-	-	24	-	-	-
L4b 1.5m	1.50	56	43	-	-	1	-	10	84	-	-	4	-	-	-
L4b 2.0m	2.00	70	30	-	-	-	-	4	93	-	-	-	3	-	-
L5 1.5m	1.50	90	9	-	-	-	1	-	64	-	-	13	-	23	-
L5 2.0m	2.00	91	8	-	-	-	-	32	-	-	-	68	-	-	-
L6 Nodules	5.00	48	52	-	-	-	-	9	86	-	-	-	-	5	-

Table 10.1: Summary of XRD analysis.

10.4 Mineralogy and Geochemistry of the Alluvial Deposits

10.4.1 XRD Mineralogy

A bulk and clay fraction XRD analysis was conducted on samples collected from the upper cal-silcrete (1.5 – 2.5 m.b.s.) and the lower impure/pure silcrete (3.0 – 3.5 m.b.s.) horizons (Table 10.1). The bulk mineralogy as determined by LOI (Table 10.2) and XRD of the uppermost cal-silcrete in all locations except site 5 (which is adjacent Lake Liambezi) corresponds well with the model of quartz

dominance with pedogenic carbonate enrichment which decreases with depth. Samples collected within the upper zone (1.0 – 2.0 m.b.s.) typically have up to 45% calcite while samples at greater depth (2.0 – 2.5 m.b.s.) are characterised by 20 – 30 % calcite (site 3 also has minor dolomite). At site 5, however, the uppermost consolidated sediments at 1.5 – 2.0 m.b.s. in the vicinity of Lake Liambezi have only 7.5 – 10% calcite which is believed to be a result of their littoral position, the near surface seasonally fluctuating water table and the desiccating nature of the system which leads to increased salinity within the local aquifer. At site L6, nodules within the lower sediments of the palaeochannel deposit reflect a 50:50 calcite and quartz mineralogy. This mineralogy is typical of nodules from similar alluvial locations within the Kalahari (Shaw and Goudie, 2004) and is believed to reflect the complex interaction of unstable wetting fronts formed by infiltrating meteoric water, evapotranspiritic and pedogenic processes operating within the upper sediments and the capillary and phreatic processes operational in the lower profile.

In contrast the clay fraction XRD reveals that micrite is the dominant < 2μm mineralogy throughout the study area. There does not appear to be any significant depth trend as samples have fluctuating values throughout the < 5.0 m vertical sections investigated. What the values do suggest is that the dominant silcrete is being calcretised in areas (particularly sites 1, 3 and 4) where the water table has dropped as a result of landscape incision. At site 5 the palustrine nature of the upper deposits (0 – 1.5 m) is evidenced by the occurrence of micrite and the absence of micro-crystalline quartz, while at depths greater than 2.0 m only micro-crystalline quartz and kaolinite were detected.

Sample	% Carbonate	% Silica	Classification
L1 0.0m	2.39	97.61	
L1 0.1m	5.27	94.73	
L1 0.2m	2.31	97.69	
L1 0.3m	2.06	97.94	
L1 0.4m	2.50	97.50	
L1 0.5m	2.06	97.94	
L1 0.6m	2.01	97.99	
L1 0.7m	2.09	97.91	
L1 0.8m	2.15	97.85	
L1 0.9m	2.00	98.00	
L1 1.0m	2.12	97.88	
L1b 2.5m	14.76	85.24	Silcrete (impure)
L1b 3.0m	14.52	85.48	Silcrete (impure)
L3 1.0m	4.64	95.36	
L3 2.0m	23.60	76.40	
L3 2.5m	14.23	85.77	
L3 2.5m	21.95	78.05	Cal-silcrete
L3 3.0m	9.44	90.56	Silcrete (impure)
L4a 0.0m	2.14	97.86	
L4a 0.2m	3.38	96.62	
L4a 0.4m	3.66	96.34	
L4a 0.6m	3.70	96.30	
L4a 0.8m	4.08	95.92	
L4a 1.0m	10.75	89.25	
L4a 1.2m	11.55	88.45	
L4a 1.4m	13.25	86.75	
L4a 1.6m	17.10	82.90	
L4a 1.8m	12.85	87.15	
L4a 2.0m	7.26	92.74	
L4b 2.0m	21.01	78.99	Cal-silcrete
L5 1.0m	10.07	89.93	
L5 1.5m	10.80	89.20	
L5 2.0m	7.11	92.89	Silcrete (impure)
L6 0.0m	1.81	98.19	
L6 0.2m	0.76	99.24	
L6 0.4m	0.68	99.32	
L6 0.6m	0.40	99.60	
L6 0.8m	0.17	99.83	
L6 1.0m	0.30	99.70	
L6 1.2m	0.22	99.78	
L6 2.0m	0.32	99.68	
L6 3.0m	0.35	99.65	
L6 4.0m	0.32	99.68	
L6 5.0m	0.62	99.38	
L6 Nodules	37.41	62.59	

Table 10.2: Summary of loss on ignition (LOI) analysis conducted on unconsolidated and consolidated sediments.

Two distinct silica and magnesium rich clay mineral groupings can be identified within the samples investigated: smectite and sepiolite. The same clay assemblages were identified within the Okavango alluvial fan (Shaw and Goudie, 2004). The majority of samples collected are characterised by smectite and kaolinite clays which suggest either alluvial deposition of smectite clays sourced from weathered basic rocks types within the Angolan catchment and/or authigenic precipitation within the poorly drained and mildly alkaline floodplain deposits under humid conditions. High Si and Mg potentials, the availability of Ca and the paucity of K are all necessary for authigenic smectite formation (Deer *et al.*, 1975; Borchardt, 1977; Wang *et al.*, 1994). In addition the poor drainage characteristic of the region is essential or else water will leach away ions (e.g. Mg) freed in alteration reactions.

The uppermost consolidated cal-silcrete samples collected from sites L4 and L5 contain sepiolite rather than smectite along with kaolinite. Like smectite, sepiolite requires alkaline conditions and high Si and Mg activities for stability (Singer and Galan, 1984; Singer, 1989). Sepiolite is typically associated with semi-arid climates and the main authigenic deposits occur as chemical sediments in shallow lakes, by the reconstitution of smectites and in calcareous soils by direct crystallization (Callen, 1984). All of these depositional and epigenetic environments exist within the Linyanti system. However it is believed that the sepiolite within the upper L4 deposits is a result of direct precipitation within the calcareous soils while at L5 the sepiolite may be a result of precipitation within littoral lacustrine deposits during a more expansive phase of Lake Liambezi.

The occurrence of kaolinite (which occurs along with both smectite and sepiolite) is believed to be related to the *in situ* weathering of feldspars (which were detected at sites L1 and L3 in minor quantities but are typically associated with Kalahari sediments (Moore and Dingle, 1998)) under acid conditions (Deer *et al.*, 1975; Swindale, 1975).

At site L3 the sample analysed at 2.5 m contained significant whewellite (hydrated calcium oxalate) which is indicative of biomineralisation within carbonates (Verrecchia, 1990; Verrecchia *et al.*, 1993). Oxalic acid is a fairly stable organic molecule typically associated with soils vegetated with trees (Braissant *et al.*, 2004) and the calcium hydroxide required for the replacement of hydrogen by calcium ions is obtained from free Ca^{2+} within the soil or from basic ground water ($H_2C_2O_4 + Ca(OH)_2 = Ca(C_2O_4).(H_2O) + H_2O$). The source of oxalic acid is undoubtedly organic and was the product of roots, actinorhizae or organic debris within the original sediments. Whewellite is typically associated with nodules and concretions within the carbonate matrix, which appears to be the case in this profile where precipitation is believed to have occurred in the capillary fringe or lower B horizon.

10.4.2 Carbon and Oxygen Isotope Analysis of the Carbonate Fraction

Interpretation of the inorganic $\delta^{13}C$ and $\delta^{18}O$ values (Table 10.3) obtained from Linyanti carbonates is difficult due to the fact that the carbonate has a mixed pedogenic and palustrine origin and thus a wide range of $\delta^{13}C$ and $\delta^{18}O$ values can occur as a result of pure evaporation, soil respiration by C_3 or C_4 plants, bacterial

sulphate reduction and methanogenesis. In addition, any meteoric epigenesis will modify the primary isotope values. Thus the isotopic value within a carbonate precipitate may be the result of any one or contributions from more than one of these sources and the influence of meteoric diagenesis may account for the loss of the primary signatures, the loss of a covariant trend between $\delta^{13}C$ and $\delta^{18}O$, or a homogenisation of values. As a guide, palustrine carbonates commonly show lower $\delta^{13}C$ and $\delta^{18}O$ values than non-pedogenically modified lacustrine carbonates (Platt, 1989; Arenas *et al.*, 1999), and greater values than adjacent carbonate soils (Wright and Alonso-Zarza, 1990; Dunagan and Driese, 1999; Tanner, 2000; Alonso-Zarza, 2003). However, this is only meaningful when there is single phase coprecipitation in adjacent lacustrine, palustrine and pedogenic environments. In light of the complex fabrics typically associated with Kalahari carbonates, the role of recrystallisation, mixing and superimposition must also be considered when interpreting the absolute values. Thus it is possible to indicate what the likely source is but almost impossible to state its exclusivity.

Sample	Depth	Inorganic δ13C PDB	δ18O PDB
L1B	2.50	-4.73	-7.63
L1B	3.00	-5.98	-8.17
L3	2.50	-5.26	-6.62
L3	3.00	-3.94	-4.83
L4	2.00	-1.94	-3.42
L5	2.00	-2.73	-1.50

Table 10.3: Summary of carbon and oxygen isotope values.

Due to the fact that there is very little stratigraphic or locational continuity to the isotopic values within the samples analysed each sample location has been interpreted separately.

At site L1, the carbonate fraction (15 – 20% $CaCO_3$) of the samples collected at 2.5 m and 3.0 m.b.s. within the cal-silcrete and impure silcrete sequence of powdery and massive horizons with gradational boundaries was analysed. The carbonate is believed to be principally pedogenic and thus the $\delta^{13}C$ values of -4.73‰ and -5.98‰ are thought to be indicative of a subtropical savanna woodland environment (Bekker and De Wit, 1991) containing both C_3 and C_4 vegetation. Using the equation derived by Wang and Zheng (1989) the proportion of C_3 vegetation is believed to be between 50% and 60% of total with a slight proportional decrease up-profile.

The extremely low $\delta^{18}O$ values of -7.63‰ and -8.17‰ suggest no significant evaporitic fractionation and are symptomatic of carbonate precipitated from directly infiltrating meteoric water. These values support the hypothesis that more depleted waters are favoured by the recharge process as a result of the seasonal effect (Sauzay, 1974) and maximum recharge is associated with high intensity rain events (Selaolo, 1998; De Vries *et al.*, 2000) which results in a 'negative shift' in the isotopic composition (Vogel and Van Urk, 1975). Based on the equation of Hays and Grossman (1991) the carbonate is likely to have precipitated under conditions slightly cooler than present.

The moderate amount (30 – 40%) of $CaCO_3$ within the cal-silcrete at site L3 returned inorganic $\delta^{13}C$ values of -5.26‰ and -3.94‰ at 2.5 m and 3 m.b.s.. These values suggest a mixed C_3/C_4 vegetation, probably savanna woodland, but the up profile trend is the opposite to L1. The basal samples point towards reduced C_3 vegetation (40 – 50%), possibly indicating drier conditions, compared

to the overlying horizon which is marginally C_3 dominated (50 – 60%). It is believed that these isotope values have not been excessively corrupted by highly negative $\delta^{13}C$ which is sometimes associated with whewellite (Zak and Skala, 1993; Hofmann and Bernasconi, 1998).

The negative $\delta^{18}O$ values of -6.62‰ and -4.83‰ suggest precipitation from infiltrating meteoric water within the vadose zone. Although the values are significantly less negative than at site L1 it is believed that infiltration occurred in a similar fashion during intense rain events with minimal evaporative fractionation. The variance within the values suggests that conditions associated with the lower horizon were slightly warmer than the upper carbonate which is less evaporitically fractionated and indicates slightly cooler conditions.

At site L4 the moderate amount of carbonate (25 – 35% $CaCO_3$) in the cal-silcrete had inorganic $\delta^{13}C$ values of -1.94‰ which has been interpreted as being indicative of a C_4 dominated environment with significant C_3 influence (>25%), possibly open tree savanna which contrasts with the modern stunted *Mopane* woodland which characterises the area. A $\delta^{18}O$ value of -3.42‰ reflects increased fractionation of the infiltrating meteoric water and is believed to be indicative of warmer and/or drier conditions.

The low carbonate (< 10% $CaCO_3$) impure silcrete samples collected from the littoral deposits at Lake Liambezi (site L5) have an inorganic $\delta^{13}C$ value of -2.73‰. The $\delta^{13}C$ value is interpreted as being indicative of a mixed but C_4 dominated (60 – 70%) vegetation, possibly open tree savanna. A $\delta^{18}O$ value of -

1.50‰ reveals a high degree of evaporitic fractionation under warm conditions. Due to the proximity of Lake Liambezi this is inferred to reflect the influence of evaporitically fractionated lake water on local groundwater recharge and the raised water table which facilitates capillary rise and evaporitic pumping.

10.5 Discussion and Conclusion

All of the sites showed distinct similarities in their lithostratigraphy: the upper 2-2.5 m of each profile comprised fluvially reworked white/grey medium to fine sand or limonite coated Kalahari sand (except for L5 where the upper 2.5 m of unconsolidated sediment consists of fine silt). This is underlain by powdery cal-silcrete grading into powdery with nodules and then massive impure silcrete which appears as horizons with varying degrees of consolidation. This sequence suggests an upward chemical facies transition from phreatic/channel silcrete precipitation to pedogenic calcrete and the calcretisation of the lower silcrete within the vadose zone as a result of desiccation.

Mineralogically, geochemically and petrographically the samples cluster into distinct groups which provide additional insight to their palaeoenvironment and mechanism of precipitation. Petrographic analyses indicated that all the samples grade from packstones to wackestones at depth and generally have a moderate detrital quartz content. These detrital grains have varying degrees of roundness and sphericity indicating their aeolian and fluvial origin and secondary corrosion. The fabric is predominantly authigenic quartz with biogenic micritised zones and spar filled vugs indicative of limited pedogenesis and micro-karst. LOI and bulk

XRD indicated that the carbonate component is typically less than 30% and the organic carbon content is negligible.

Clay mineralogy indicates three depositional environments. The dominant group, believed to be indicative of pedogenic epigenesis of fluvial/phreatic silcrete, contains abundant micrite, limited microcrystalline quartz and smectite. Of significance is the fact that whewellite was detected within the samples which indicates biogenic mechanisms of calcite precipitation (Verrecchia, 1990a; Verrecchia *et al.*, 1993). Thin-section analysis also identified numerous biogenic structures preserved within the calcite fabric indicative of pedogenesis.

The second grouping consists of fluvial/phreatic silcretes which are silica dominated, contain very little calcite and abundant kaolinite. These samples have an authigenic silica fabric rich in biogenic structures, particularly rhizoliths, which are believed to indicate the link between phreatic precipitation and chemical processes associated with evapotranspirational pumping by roots similar to those identified in the Okavango alluvial fan (Shaw and Goudie, 2004).

A third cluster of samples are associated with the fine grained littoral sediments of Lake Liambezi and contain significant amounts of sepiolite. The carbonate and sepiolite are suggestive of precipitation within a low-energy lacustrine/palustrine environment with fluctuating salinity and pH.

The majority of $\delta^{13}C$ signals imply a C_3 dominated vegetation and $\delta^{18}O$ levels symptomatic of little to no evaporitic fractionation and rapid infiltration of

meteoric water. This is believed to reflect an environment in which pedogenic calcrete precipitated principally as a result of evapotranspirational pumping and degassing by C_3 vegetation which colonised the floodplain and channels during phases of desiccation and reduced fluvial activity associated with channel avulsion. Other samples show a gradient towards more C_4 influence and increasing fractionation of water which is believed to be indicative of a shift to more open grassland vegetation and ponding of water within an active seasonal floodplain environment.

The mineralogy, geochemistry and petrology of the chemical sediments investigated within the Linyanti alluvial fan have highlighted the fact that common precipitation processes and mechanisms are operational within adjacent and similar geomorphic environments in the Kalahari. This helps facilitate and develop a better understanding of the principal processes and mechanisms of precipitation, and the linkages between geomorphic environments, hydrology, sediment provenance, vegetation and climate.

11. THE USE OF MINERALOGY, PETROGRAPHY, MAJOR ELEMENT GEOCHEMISTRY AND LIGHT STABLE ISOTOPES TO UNDERSTAND FORMATIVE PROCESSES AND DEPOSITIONAL ENVIRONMENTS OF CHEMICAL SEDIMENTS IN THE NGAMI SUB-BASIN, WESTERN CENTRAL BOTSWANA

11.1 Introduction

The Ngami Basin and in particular Lake Ngami has been the focus of extensive research (Shaw, 1985a,b, 1986a,b, 1988a; Shaw and Cooke, 1986; Thomas and Shaw, 1991; Shaw *et al.*, 2003). Although Lake Ngami is only a fraction of its former size the mineralogy and geochemistry of its deposits have facilitated elucidation of the palaeo and active processes associated with the accumulation of these sediments during the Cenozoic.

11.2 Geomorphology and Depositional Context

The Ngami sub-basin is a half graben bound by the extensional normal Kunyere fault which delineates the southern shore (Scholtz, 1975). The basin itself covers an extensive area and is reportedly filled by 400-650 m of largely unconsolidated fluvio-lacustrine sediments belonging to the Okavango Series of the Kalahari Group (Hutchins *et al.*, 1976a,b). Until recently Lake Ngami was a significant part of the Okavango-Makgadikgadi fluvial system (Shaw, 1986a, 1988a; Shaw and Cooke, 1986; Shaw *et al.*, 2003) and was fed by the anastamosing Thaoge River in the west and the Kunyere River, via the Nxaraha Valley which follows the

Kunyere fault in the east (Fig 11.1). Strandlines, lake flats and pans, with the largest in excess of 60 km long and 35 km wide, covering approximately 1800 km^2 (Thomas and Shaw, 1991) indicate the magnitude of the system.

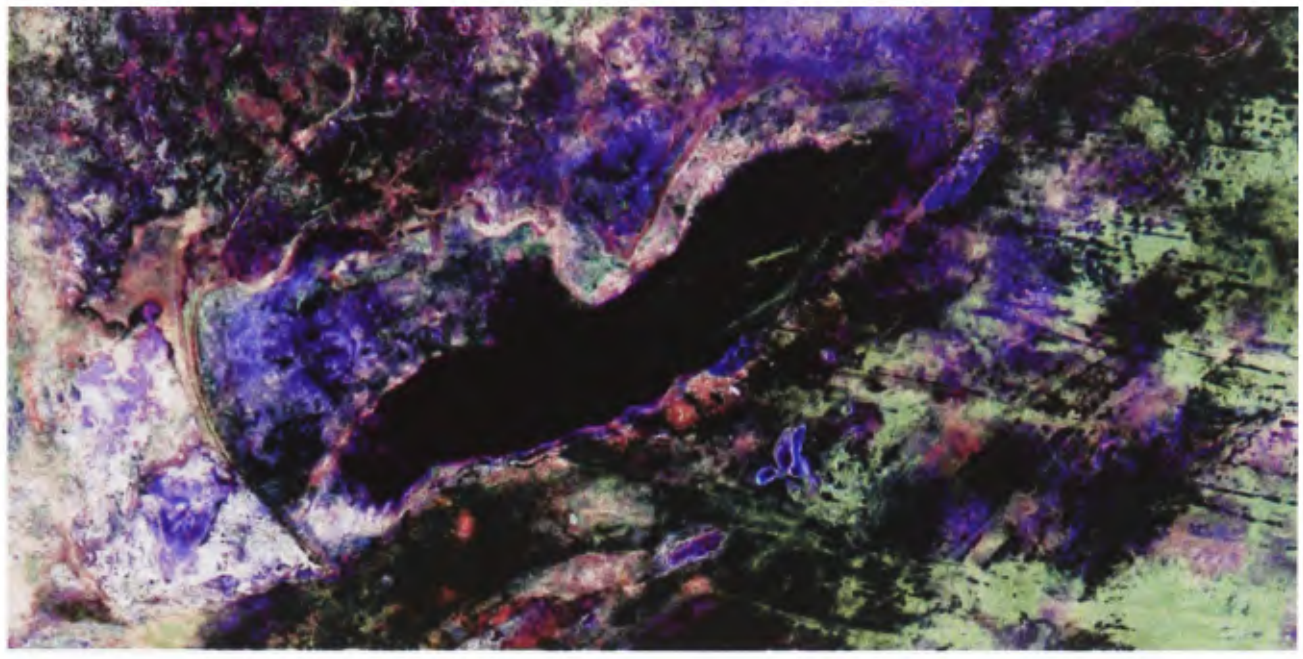


Figure 11.1: LANDSAT image of the Ngami Basin.

The linkage between the Ngami Basin and the Boteti River has been extremely dynamic. Geomorphic evidence suggests that during the most recent lake levels of 923-928 m, palaeo-lake Ngami acted as a terminal repository for water flowing down the Thaoge, the main western channel of the Okavango alluvial fan, and its point of entry (930 m) into the palaeo-lake at Setsau and Mochabeng are marked by birds-foot lacustrine deltas (Fig 11.2). The input of water to the system from the eastern tributaries of the Kunyere, principally the Xudum, via the Nxaraha Valley also drained into the 923-928 m palaeo-lake. However, during > 928 m palaeo-lake stages water from these eastern tributaries largely by-passed the palaeo-lake and entered the eastward flowing Nhabe River at Toteng (926 m). The Nhabe has an incised valley which follows the Thamalakane fault and its dimensions bear testament to the fact that it was a significant palaeo-drainage to the SW/NE over an extended period of time (Fig 11.3). In line with the neo-

tectonic activity of the area it is proposed that the dog's-leg bend in both the Thamalakane and Nhabe Rivers (Fig 11.4) prior to their confluence to form the Boteti at Dikatlhong (930 m) is the result of an extension of the parallel NW/SE faults which have resulted in the orientation of the Panhandle. It is assumed that activity along this NW/SE orientated fault system which runs through the panhandle was responsible for the effective breakout of the Boteti River through the raised scarps associated with the Kunyere and Thamalakane faults. However, there is no apparent link between the Thamalakane and Nhabe along the Thamalakane fault to prove a potential palaeo-linkage. The Boteti continues to follow this NW/SE orientation believed to be associated with the Panhadle fault system for another 60 km downstream until Makalamabedi. Neo-tectonics within the region has played a significant role in shaping the landscape, controlling hydraulic gradients and directing alluvial channels and it is believed that these processes have been instrumental in creating accommodation space within the Ngami Basin and superimposing a trellis drainage pattern in places.

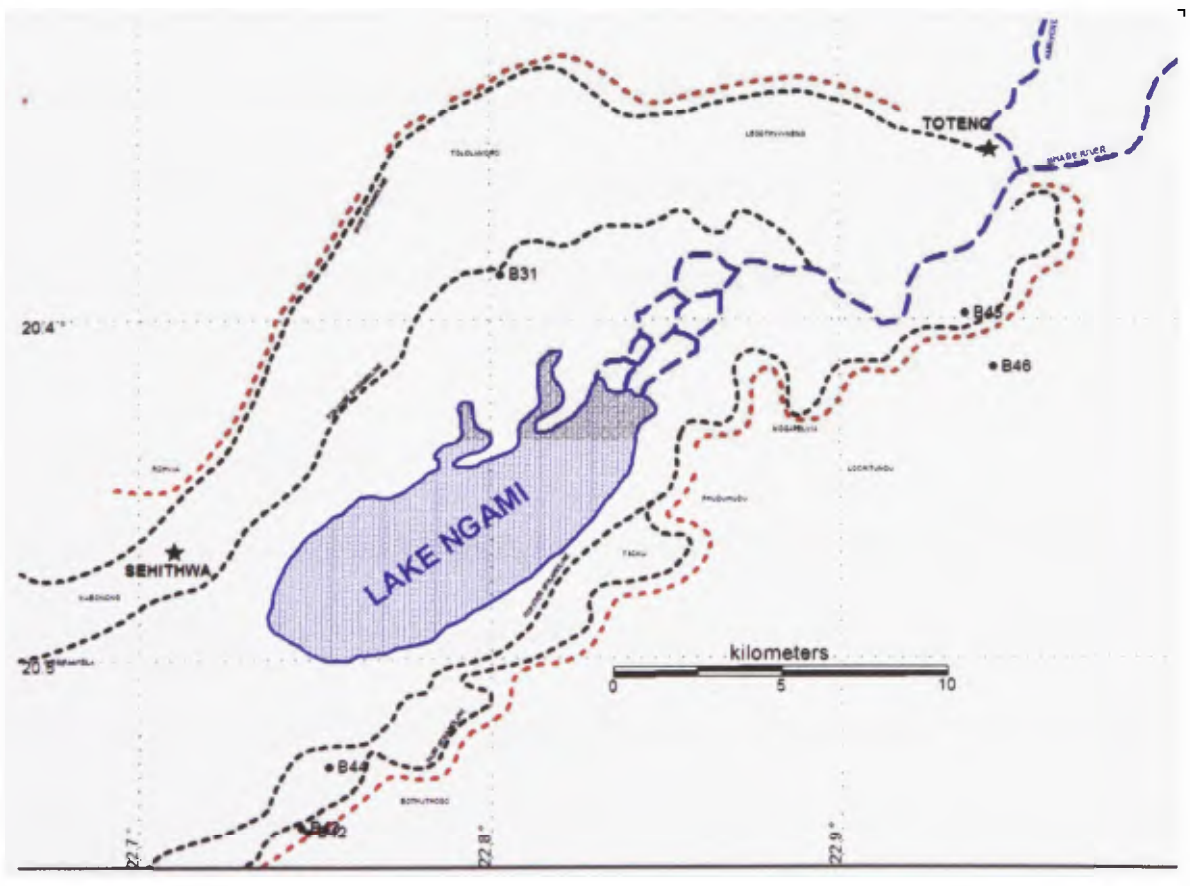


Figure 11.2: Map of Ngami Basin with sample sites and geomorphic features.

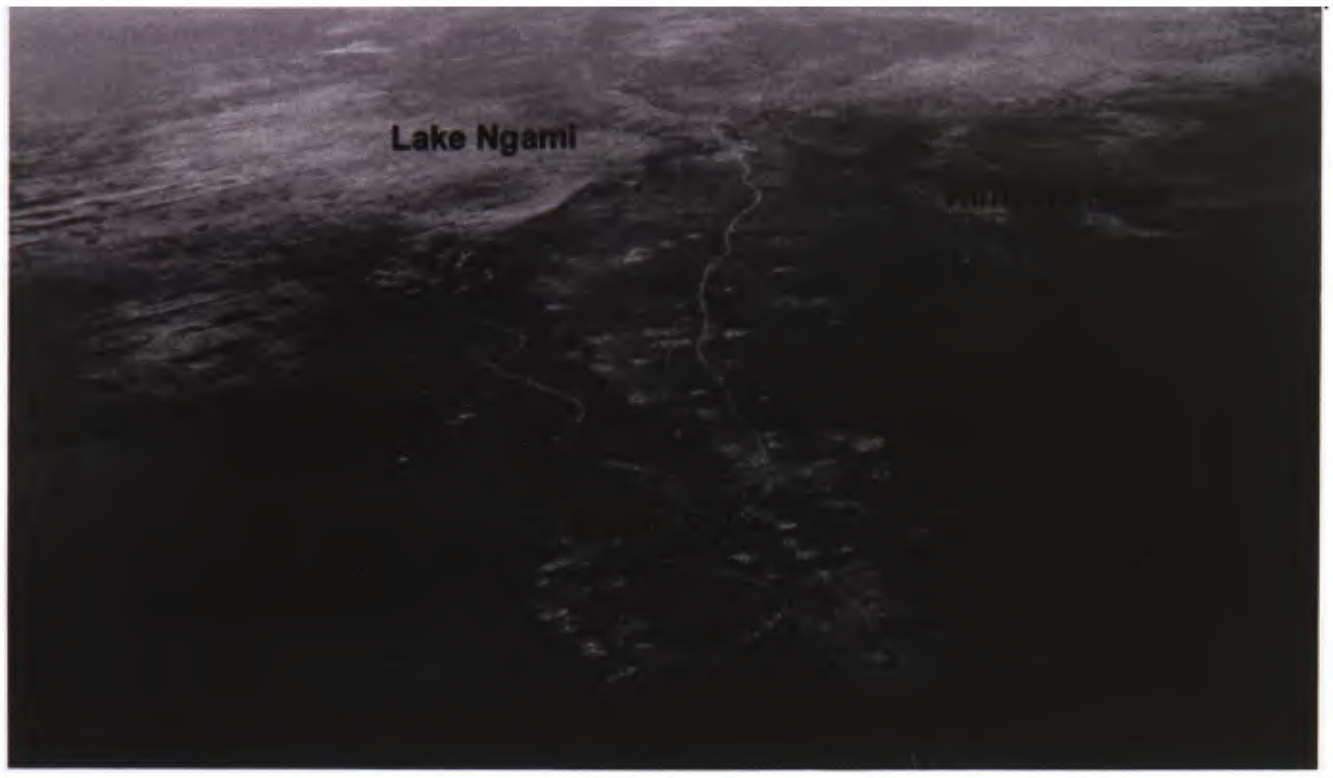


Figure 11.3: An aerial photograph of the meandering NW/SE orientated incised Nhabe River and the adjacent Kunyere River feeding into Lake Ngami.

Based simply on regional elevations it is proposed that when levels were < 930 m in palaeo-lake Ngami, Thamalakane water flowed SW down the Nhabe towards Ngami from the Dikatlhong confluence and SE along the Boteti. However, during > 930 m levels in Ngami, water flowed NE down the Nhabe combining with Thamalakane water at Dikatlhong and then flowing SE along the Boteti. Hence, the level of palaeo-lake Ngami had a significant effect on the volume of water flowing down the Boteti and entering the Makgadikgadi system.

11.3 Sedimentary Units

Six sites (Fig 11.2) were investigated and sampled from three distinct depositional features (the palaeo-lake floor at 923-928 m.a.s.l. (site B31), the 928 – 932 m.a.s.l. strandline (sites B44, B45 and B46) and the 940 – 945 m.a.s.l. strandline (site B42 and B43)) within the recorded boundary of palaeo-lake Ngami (Shaw *et al.*, 2003). Using petrography, XRD analysis of bulk and fine (< 2μm) material, LOI,

magnetic susceptibility, ICP-MS analysis of aqueous leach solutions and light stable isotope analysis of the carbonate fraction the characteristics of the sediments within each deposition environment are described and discussed below.



Figure 11.4: An aerial photograph of the confluence of the Nhabe and Thamalakane Rivers at Dikatlhong.

11.3.1 Palaeo-Lake Bed Deposits (923-928 m)

A 1.75 m deep trench east of Sehithwa on the northern Tololamoro embayment of palaeo-lake Ngami was dug exposing a 1.2 m thick brown/grey sandy soil overlying a distinct contact with what can be generally described as a massive poorly consolidated powdery sil-calcrete (Fig 11.5).



Figure 11.5: Photograph of the powdery sil-calcrete section exposed within a trench at site B31.

Mineralogy and Geochemistry

Bulk XRD (Table 11.1) analysis of the sil-calcrete sampled at 1.5 m.b.s. indicates that the mineralogy is dominated by calcite (48%) and quartz (46%) with minor K-feldspar (2%) and interstratified clays (4%). Clay fraction XRD identified abundant sepiolite (46%), micrite (40%) and kaolinite (14%). LOI (Table 11.2) suggests that the average proportional mass of carbonate for the samples analysed was 25% of total mass. The occurrence of sepiolite suggests alkaline conditions and high Si and Mg levels (Singer and Galan, 1984; Singer, 1989). A shallow desiccating Lake Ngami and the semi-arid climate is an archetypal environment for authigenic sepiolite formation. However it is also possible for the sepiolite to be associated with the reconstitution of smectites, which are abundant throughout the adjacent Okavango alluvial fan deposits (Shaw and Goudie, 2004), within calcareous soils by direct crystallization (Callen, 1984).

	Whole rock analysis							< 2µm fraction analyses					
	Quartz	Calcite	Plagioclase	K-feldspar	Mica	Palygorskite	Interstratification	Quartz	Calcite	Kaolinite	Kaolinite + Chlorite	Smectite	Sepiolite
B31 - 1.5m	46	48	-	2	-	-	4	-	40	14	-	-	46
B42 - 0.75m	7	83	-	8	-	2	-	no < 2µm fraction					
B42 - 1.2m	44	54	-	-	2	-	-	64	17	-	-	19	-
B45 - 2.0m	39	58	2	-	-	-	1	14	-	-	26	-	60

Table 11.1: Summary of XRD analysis.

Average magnetic susceptibility (Table 11.3) for the samples was recorded as 1.05 CGS. This low level of magnetism supports the conclusion based on optical microscopy that the majority of the samples consist of quartz and calcite with only

trace mafic minerals. The sediment EC determined by water leach was recorded as 458.9 μS. This moderate EC value is suggestive of significant soluble minerals being retained within the profile and suggests incomplete meteoric leaching and evaporitic concentration of salts within the vadose and capillary fringe zones.

Sample	Depth (m)	% Organic Carbon	% Carbonate	% Silica and Other Minerals
B31	1.50	2.3	25.4	74.6
B42	0.75	0.5	48.2	51.8
B43	0.00	1.2	44.1	55.9
B43	0.20	0.4	0.4	99.6
B44	0.00	0.1	0.4	99.6
B44	1.00	0.4	30.8	69.2
B44	1.50	0.4	34.9	65.1
B44	2.00	0.2	23.0	77.0
B45	0.00	1.0	29.0	71.0
B45 Matrix	1.50	1.3	25.1	74.9
B45 Nodules	1.50	1.3	33.5	66.5
B45	2.00	0.9	26.0	74.0
B46 Matrix	0.30	1.3	45.2	54.8
B46 Nodules	0.30	1.3	45.7	54.3

Table 11.2: Summary of loss on ignition (LOI) analysis.

Isotopic analyses (Table 11.4) of the inorganic carbonate revealed $\delta^{13}C$ and $\delta^{18}O$ values of 1.4‰ and 0.29‰ respectively. The $\delta^{13}C$ value is indicative of a C_4 dominated vegetation, probably open savanna grassland which contrasts with the contemporary *Acacia* woodland. The $\delta^{18}O$ value is suggestive of highly evaporitically fractionated solutions and warm temperatures which would support precipitation from a shallow water body or reprecipitation and modification of the primary carbonate due to the influence of soil moisture.

Petrography

All the samples investigated from this site can be described as poorly to moderately consolidated palustrine/pan silt/mudstone with a dominant carbonate and authigenic silica matrix. The samples are characterised by a complex micrite,

crypto- and micro-crystalline quartz fabric, containing highly corroded floating detrital grains and numerous bioclasts (principally fragments of gastropod and ostracod shell)(Figs 11.6a and b). The fabric contains numerous features such as circum-granular cracks, crypto-crystalline and manganese enriched nodules, pelletal micrite and authigenic quartz filled secondary porosity (Figs 11.6c-f) which is indicative of micro-karst and secondary grainification processes. The most likely explanation for these processes is a fluctuating pH and salinity and late stage pedogenesis.

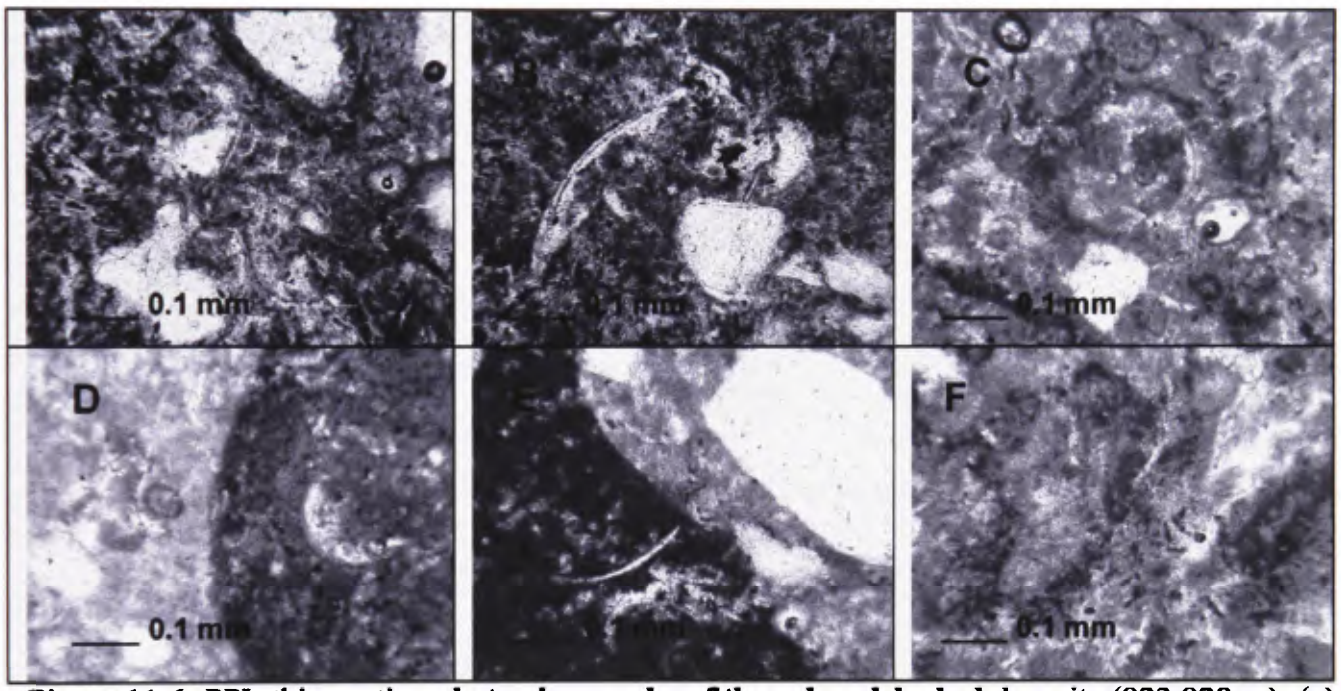


Figure 11.6: PPL thin-section **photomicrographs of the palaeo-lake bed** deposits (923-928 m): (a) highly corroded floating detrital quartz grains floating within a mixture micrite and sparmictrite fabric; (b) corroded floating detrital quartz grain and bioclast (possibly a fragment of a diatom) floating within a mixture micrite and sparmictrite fabric; (c) peliods, pelletal micrite and circum-granular crack structures within a lacy micrite and sparmictrite fabric; (d) manganese enriched micritic nodule floating within the mixed micrite and sparmicrite fabric; (e) manganese enriched micritic fabric containing a bioclast (possibly a fragment of a diatom) adjacent the mixed micrite and sparmictrite fabric containing highly corroded detrital quartz grains. Note the distinct interface between the two fabric types; (f) lacy micrite and sparmicrite fabric with authigenic silica filled secondary porosity.

Interpretation

The characteristics of the samples analysed from this site are supportive of deposition epigenesis and paragenesis associated with a desiccating embayment within palaeo-lake Ngami and the pedogenic modification of lacustrine and palustrine sediments.

11.3.2 928-932 m Strandline Deposits

Three shallow (2 – 3 m deep) quarries mined into the base of the 928-932 m strandline deposits were investigated within the eastern sector of the Ngami Basin near Toteng and the Nhabe River (Fig 11.2). Exposed sections in all three quarry sites consist of an upper surface cal-silcrete hardpan which grades down-profile into a massive powdery sil-calcrete containing green cryto-crystalline nodules of various sizes and shapes. At approximately 0.5 m.b.s. there is a gradational boundary with a grey carbonaceous silty sandstone horizon containing small calcrete nodules. At approximately 1.25 m.b.s. this horizon grades into a basal massive beige coloured sandy carbonate which becomes more consolidated with depth. Similar sequences have been described from other sites investigated within the 928-932 m strandline (Shaw *et al.*, 2003).

Mineralogy and Geochemistry

Bulk XRD (Table 11.1) analyses of the basal matrix collected at 2 m.b.s. at site B45 indicated abundant calcite (58%), quartz (39%) and minor plagioclase feldspar (2%) and interstratified clays (1%). Clay fraction XRD analyses of the basal matrix revealed abundant sepiolite (60%), significant interstratified chlorite and kaolinite (26%) and micro-crystalline quartz (14%).

At site B44 a well developed surface hardpan which grades fairly rapidly into the underlying carbonate has a LOI of 0.5% (Table 11.2) which is suggestive of a very low proportional mass of carbonate. However at sites B45 and B46 there is no hardpan developed. At these sites the massive carbonate outcrops at the surface and the LOI indicates that the proportional mass of carbonate is approximately 29%.

Magnetic Susceptibility in CGS units		
Sample	**Depth (m)**	**Average Value**
B31	1.50	1.05
B42	0.75	0.77
B43	0.00	12.93
B43	0.20	30.87
B44	0.00	1.98
B44	1.00	1.12
B44	1.50	0.78
B44	2.00	0.58
B45	0.00	5.52
B45 Matrix	1.50	1.52
B45 Nodules	1.50	3.68
B45	2.00	1.03
B46 Matrix	0.30	2.32
B46 Nodules	0.30	4.47

Table 11.3: Summary of magnetic susceptibility of consolidated and unconsolidated deposits.

At all three sites LOI suggests that the silty sandstone unit has a carbonate content of 30-35%. Down-profile at approximately 1.5 m.b.s. nodules become apparent and LOI suggests that the carbonate content of the sandy matrix ranges from 25 – 30% while the carbonate content of the nodules is slightly higher and ranges from 35 – 40%. At 2 m.b.s. LOI indicates that the proportional mass of carbonate in the matrix and nodules are very similar and range between 45 – 50%.

Magnetic susceptibility levels are higher than those recorded within the palaeo lake-bed deposits. The highest values are recorded within the surface hardpan (average 5.5 CGS) and show a general down-profile decrease (Table 11.3). At 1.5 m.b.s. the matrix has values between 2.3 – 1.5 CGS while the nodules have slightly elevated values between 4.5 – 3.7 CGS. The basal matrix and nodule samples at 2 m.b.s. have little differentiation in their values and average 1.1 CGS. The values suggest that not only do the strandline deposits record the paleaolake level and deposition within the swash-zone but that they also record the deflation of material from the desiccating lake bed. It is believed that deflation preferentially removed and mobilised material with a low specific gravity and concentrated heavy minerals such as garnet, rutile, zircon and ilmenite which accumulated in the littoral and back-shore zone as the lake level regressed. Pan lunette and back shore lacustrine dunes throughout the Kalahari (e.g. Etosha and Kgalagadi) and Australia (Murray Basin) demonstrate the same mechanical sorting processes.

Sample	Depth (m)	Inorganic δ13C PDB	δ18O PDB
B31	1.50	1.35	0.29
B42	0.75	-2.85	-6.66
B43	0.00	-4.47	-5.83
B43	0.20	-5.34	-6.99
B44	0.00	-9.89	-9.56
B44	1.00	-4.02	-4.63
B44	1.50	-3.57	-5.75
B44	2.00	-3.25	-4.90
B45	0.00	-0.53	-1.18
B45 Matrix	1.50	-3.51	-2.53
B45 Nodules	1.50	-1.71	-2.29
B45	2.00	-4.00	-2.18
B46 Matrix	0.30	0.36	-5.60
B46 Nodules	0.30	-0.67	-5.79

Table 11.4: Summary of carbon and oxygen isotope values.

Sample	Depth	Li	Na	Mg	Al	K	Ca	Fe	Mn	Sr	Ba	Th	U	Mg/Ca Ratio
		ppb	ppm	Ppm	ppm	ppm	ppm	ppm	ppm	ppb	ppb	ppb	ppb	
B42	0.75	1.89	1.44	2.71	10.68	13.34	20.68	0.00	1.09	100.00	83.81	0.32	0.81	0.13
B43	0.00	6.24	2.01	2.15	13.44	6.36	32.56	0.00	2.81	140.00	156.95	0.34	1.69	0.07
B43	0.20	3.06	2.07	2.25	70.45	9.96	33.41	0.11	12.82	123.22	548.66	0.56	0.88	0.07
B44	0.00	4.61	9.94	0.59	414.15	14.51	17.24	0.50	3.12	179.97	259.11	0.10	6.81	0.03
B44	1.00	6.69	4.27	1.34	2.66	12.32	25.87	0.00	1.78	333.96	462.56	0.12	0.69	0.05
B44	1.50	6.21	2.98	0.97	5.99	10.17	23.21	0.01	2.14	314.25	253.56	0.10	2.18	0.04
B44	2.00	6.75	6.31	0.95	180.94	12.67	20.91	0.54	7.23	248.28	149.27	0.13	4.79	0.05
B45	0.00	57.51	5.54	13.03	3.87	9.82	90.54	0.00	2.11	26648.08	100.77	0.15	9.06	0.14
B45 Matrix	1.50	45.02	-	2.15	2.23	59.90	20.12	0.00	0.33	1212.52	193.50	0.10	2.50	0.11
B45 Nodules	1.50	65.45	-	2.74	5.98	46.08	15.97	0.00	0.64	1063.82	245.12	0.09	2.88	0.17
B45	2.00	22.33	20.90	3.08	1.63	30.69	20.21	0.00	1.03	888.30	360.00	0.04	0.50	0.15
B46 Matrix	0.30	12.71	7.83	3.12	4.40	3.61	25.04	0.00	0.62	252.86	472.50	0.05	0.86	0.12
B46 Nodules	0.30	31.85	11.15	4.97	7.77	9.51	28.78	0.00	1.33	343.07	321.25	0.04	0.61	0.17

Table 11.5: Summary of major cations and principal metals detected within a water leach of consolidated and unconsolidated deposits.

Soluble and mobile cations detected in the water leach displayed fairly typical values for Kalahari carbonates (Table 11.5). Site B44, the only site with a well developed hardpan, displayed significant levels of Al and Fe and extremely low Mg concentrations. This suggests that the hardpan at this site is a true residual deposit which has been leached of its soluble cations with only the most insoluble elements remaining. In contrast at sites B45 and B46, which do not have well developed hardpans, the water leach indicated abundant soluble Mg, Ca, Sr and U in the surface carbonate and high levels of Na and K in the lower horizons with the highest levels of major and minor cations occurring within the nodules. These chemical profiles are interpreted as being reflective of deposits which have undergone very little environmental leaching within a semi-arid environment and contain abundant salts which may have precipitated *in situ* as soluble salts migrated within the upper profile as a result of infiltrating meteoric water and/or capillary rise and the evaporation of soil moisture. In addition it is believed that a

considerable volume of soluble salts have been deposited on the Ngami landscape from material deflated off the palaeo-lake surface and from the adjacent seasonal floodplains of the Okavango system.

Carbon and Oxygen Isotopes

At site B44 the upper hardpan silcrete has average $\delta^{13}C$ values of -9.98‰ and $\delta^{18}O$ values of -9.56‰ (Table 11.4). The very low carbonate content of this unit (~0.5%) means that the interpretation of these values must be conservative due to the potential for contamination. The $\delta^{13}C$ values suggest a dominant (>85%) C_3 vegetation similar to the contemporary dense savanna woodland. The $\delta^{18}O$ values are reflective of a solution that is comprised of meteoric water that experienced rapid infiltration and no significant evaporitic fractionation under cool temperatures. Rainfalls with such a negative $\delta^{18}O$ value (-10.18‰) were only recorded in this area during the heaviest convective downpours. These isotopic values when combined with the other geochemical evidence support contemporary precipitation of the hardpan silcrete under present and slightly wetter and cooler climatic conditions than present.

Analysis of near surface carbonate from sites B45 and B46 revealed $\delta^{13}C$ values between 0.36‰ and -0.53‰ for matrix material and -0.67‰ for nodules. These values suggest that although there is a -1‰ fractionation between matrix and nodule carbonate the values fairly accurately reflect the contemporary vegetation at these sites which is C_4 dominated savanna grassland with occasional C_3 shrubs. The fractionation between matrix and nodule carbonate suggests that in the upper carbonate, nodule formation could be the most recent and epigenetically mature

precipitated carbonate, thus containing detrital matrix material along with contemporary calcium carbonate. The other possibility is that the matrix carbonate, which is dominated by calcium carbonate grain coatings, is a processes that is favoured by C_4 vegetation while processes which promote nodule formation, which typically contain more complex biogenic structures, are typically associated with the roots of C_3 vegetation. These two options are not mutually exclusive and may in fact be synchronous. However the $\delta^{18}O$ value of the upper-most sample at site B45 varies significantly from the other surface samples which have very negative $\delta^{18}O$ values. At site B45 the carbonate has the most positive value of all the samples investigated. An average value of -1.18‰ suggests a significant amount of evaporitic fractionation within the solution and/or a high temperature (>20°C) at which precipitation occurred.

The grey silty sandstone and massive to nodular sandy carbonate at all the sites investigated have similar $\delta^{13}C$ values. At 1 m.b.s. values in the massive sandy carbonate average -4.02‰ while at 1.5 m.b.s. values in the sandy carbonate matrix range between -3.57‰ and -3.51‰ while the nodules, which have a slightly higher carbonate content, have values ranging between -0.53‰ and -0.67‰. At 2 m.b.s. matrix values have a much larger range and vary between -3.25‰ and -5.60‰ as do the nodules which range between -1.71‰ and -5.79‰. The reduced off-set between the matrix and nodule values (at site B46 the matrix and nodules have very similar values of -5.60‰ and -5.79‰) is believed to be the product of a number of processes. The carbonate at the deeper levels within the strandlines has a more complex epigenetic history and thus retains the signal of multiple phases of carbonate precipitation within a range of environments. These environments

have ranged from littoral lacustrine to phreatic to palustrine to vadose and pedogenic. If there was not complete dissolution and reprecipitation each of these environments would have contaminated previous detrital carbonate with its own chemical signature reflecting conditions at the time of precipitation. This is less likely to have occurred within the higher strandline sediments which have a simpler epigenetic history.

The $\delta^{13}C$ values can be interpreted to reflect a mixed vegetation with a poorly defined trend of increasing C_3 vegetation down profile. Matrix values indicate a mixed but marginally C_3 dominated vegetation which suggests a tree savanna or open shrub savanna vegetation which is common throughout this area. Nodule values, although also believed to reflect a mixed C_3/C_4 vegetation, generally suggest C_4 dominance and advocate a more open grassland or open tree savanna community especially within the upper sediments.

The $\delta^{18}O$ values of the matrix and nodule carbonate at site B44 and B46 complement each other well and range from -5.79‰ to -4.63‰. These values are representative of solutions which have undergone very slight evaporitic fractionation and are typically associated with fairly rapidly infiltrating meteoric water and warm temperatures. The $\delta^{18}O$ values of the matrix and nodule samples at site B45, however, differ markedly and range from -2.18‰ to -2.53‰. These values are significantly more fractionated and suggest increased evaporation of the solution from which the carbonate precipitated and possibly warmer temperatures. Evaporitic fractionation could have occurred within the pedogenic environment or else may reflect the role of infiltrating fractionated lake water.

The variation within the isotopic geochemistry of the carbonate at the three sites investigated suggests that the carbonate may not have been precipitated during one continuous event or necessarily under similar conditions. It is not possible to discuss when the carbonate was deposited as radiometric dating was not conducted during this investigation. It is however possible to speculate that the environments under which precipitation occurred may not have been homogenous based on the geochemical evidence provided. It is believed that despite the proximity of the sites investigated factors such as the local hydrogeochemistry and the proportion of detrital carbonate within each of the strandline deposits (which can not be determined) will have had a significant consequence on the isotopic signal and site B45 is believed to have been the most effected by exotic sources of carbonate. The most likely explanation is that the $\delta^{13}C$ values reflect a mixed TDIC signal from within the palaeo-lake and SOM during pedogenesis. Thus it is concluded that localised geochemical conditions have been very important in the development and preservation of the carbonate.

.

Petrography

Petrography of the well developed hardpan at site B44 indicates that this is a grain supported silcrete packstone composed of well sorted sub-angular to sub-round medium sand cemented by a micro-crystalline quartz fabric with small floating crypto-crystalline nodules (Fig 11.7a). Although not nearly as well developed, petrographic investigation of the surface samples at sites B45 and 46 reveals very similar fabrics (Fig 11.7b). These sediments can also be described as packstones consisting of numerous corroded detrital grains with a dense micrite (rather than

the authigenic silica that occurs at site B44) fabric which becomes highly complex, showing numerous phases of solution and replacement. In addition numerous rhizoliths and features such as micro-laminated micrite (Fig 11.7c) typical of hardpan calcrete are present. Down-profile the fabric becomes more pelletal (Fig 11.7d) with sparse floating detrital grains and is characterised by increased porosity principally in the form of vugs and fenestrae, some of which are filled with either micro- or crypto-crystalline quartz (Fig 11.7e) which suggests partial dissolution and localised silicification of the primary carbonate.

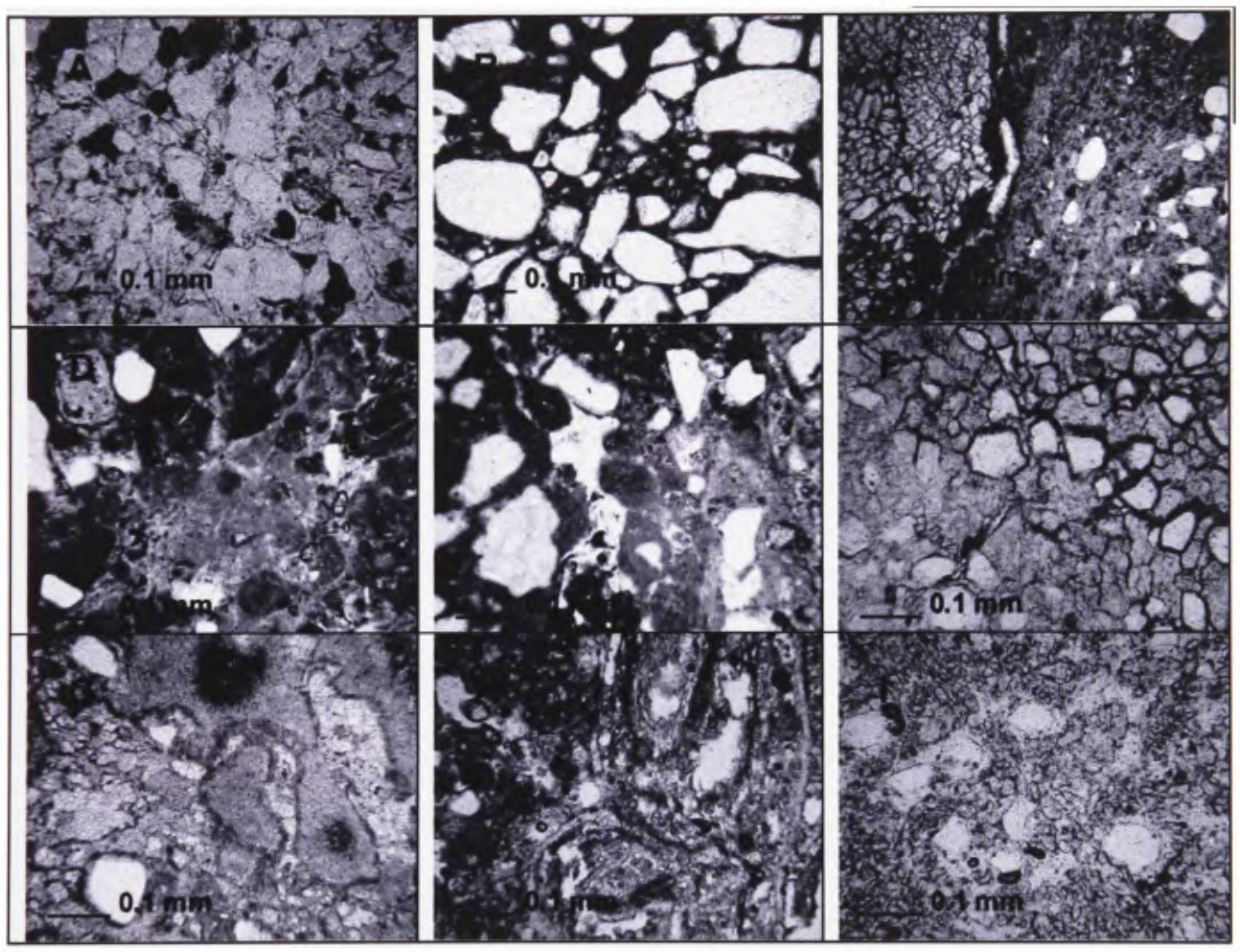


Figure 11.7: PPL thin-section photomicrographs of the 928-932 m strandline deposits: (a) grain supported silcrete packstone composed of well sorted sub-angular to sub-round medium sand cemented by a micro-crystalline quartz fabric with small floating crypto-crystalline nodules; (b) grain supported packstone with sub-round to well-rounded detrital quartz grains of various sizes cemented by micrite; (c) a rhizoliths feature consisting of calcified root cells adjacent to micro-laminated micrite containing floating detrital quartz grains; (d) dense pelletal micrite within a

sparmicrite fabric with occasional floating detrital quartz grains and manganese stained micro-nodules (top left corner); (e) micro- and crypto-crystalline silica filled fenestrae within the mixed pelletal micrite and sparmicrite fabric; (f) micrite grain envelopes around detrital quartz grains illustrate the extent of micritisation within the sparite fabric; (g) lacy fabric illustrating the dissolution and reprecipitation/replacement of the sparry calcite by micrite; (h) micrite lined and sparry calcite filled rhizolith structures (believed to be calcified root hairs); (i) sparry calcite fabric with minor crypto- and micro-crystalline quartz.

Investigation of the light grey nodules scattered throughout the upper horizons at site B45 and B46 identified the majority as being brecciated, reworked and corroded clasts of the underlying silty carbonate with a minor component being pedogenic glaebules or nodules. This suggests that significant micritisation and reworking of the underlying grey lacustrine carbonate has occurred at these sites possibly within the littoral zone during a regressive phase of the lake.

The grey coloured silty sandstone which occurs at approximately 1 m.b.s. at all the sites has an abundant sparry calcite and micro-crystalline quartz fabric which combine to produce a sil-calcrete wackestone containing numerous floating corroded detrital grains. Isolated sections of the fabric suggest micritisation processes which typically take the form of micrite grain envelopes (Fig 11.7f) around detrital grains or intraclasts. This unit grades down-profile into the poorly consolidated massive sil-calcrete wackestone which has a mixed fabric containing significant elements of the overlying sparry and micro-crystalline quartz fabric and large sections of micro-crystalline quartz fabric containing dense dark brown micrite cemented aggregate grains and peloids with scattered crypto-crystalline silica and micrite nodules. Both fabrics contain sparse corroded floating detrital

grains. The micrite fabric, although dense, contains numerous vugs and fenestrae which may be unfilled or filled with chalcedony and mega-quartz and suggest phases of dissolution. Within both units the dominant process appears to be dissolution and reprecipitation/replacement by micritisation (Fig 11.7g) of the alpha fabric sparry carbonate and gradual silicification as a result of vadose epigenesis.

The basal samples consist of a grain supported spar calcite cemented sil-calcrete wackestone. These samples share many of the overlying silty sandstone's characteristics (abundant floating moderately sorted sub-angular to sub-rounded partially corroded medium sand sized detrital grains and a dense peloidal and pisolithic micrite fabric in places) but also contain numerous sparry calcite filled rhizolith structures (mostly calcified root hairs (Fig 11.7h) and possibly charophytes), rhizocretions and occasional bioclasts believed to be ostracods. Significantly the basal fabric is dominated by a sparry calcite fabric and contains significantly less crypto- and micro-crystalline quartz (Fig 11.7i).

Interpretation

All three sites contain detrital sedimentary sequences which reflect sedimentation linked to expansion and contraction of palaeo-lake Ngami around the 928-932 m strandline. Gradational unconformities, vertical and lateral facies variations within the deposits, are suggestive of changing energy conditions and dynamic depositional environments as a result of the transition between lacustrine and palustrine sedimentation associated with transgressions and regressions. The majority of the deposits suggest both crystalline precipitation of calcite and silica

alpha fabrics within the phreatic zone and micrite mud precipitation within a littoral lacustrine and palustrine environment. Extensive bioturbation, pedogenesis and the associated meteoric micritisation, dissolution and silicification of the primary deposits is interpreted as being representative of regressive phases of palaeo-lake Ngami during its desiccation and stabilisation during depositional hiatuses.

11.3.3 940-945 m Strandline Deposits

Two sites in close proximity to each other (B42 and B43) were investigated along the 940-945 m strandline (also the footwall of the Kunyere Fault) which marks the southern limit of Ngami Basin (Fig 11.2). Shallow 1.5 to 2 m profiles of Kalahari sand (approximately 0.5 m thick) underlain by massive honeycomb calcrete (approximately 0.5 m thick) which graded into brecciated massive silcrete were exposed as a result of trenching.

Mineralogy and Geochemistry

Bulk XRD (Table 11.1) analysis of the massive honeycomb calcrete sample collected at 0.75 m.b.s. indicated a dominance of calcite (83%) with significant K-feldspar (8%), quartz (7%) and minor palygorskite (2%). At 1.2 m.b.s. bulk XRD of the brecciated silcrete indicates abundant calcite (54%) and quartz (44%) with minor mica (2%). Clay fraction XRD of the same sample identified significant micro-crystalline quartz (68%), smectite (19%) and calcite (17%). LOI (Table 11.2) suggests that the actual proportional carbonate decreases down-profile and typically ranges between 50% and 40% within the honeycomb calcrete. The basal

silcrete contains only trace carbonate (0.4%) and thus can be classified as a pure silcrete.

Soluble and mobile cation analysis indicated that the elemental composition of the profile was fairly typical for calcrete profiles within the Okavango/Ngami area (Table 11.5). The upper honeycomb calcrete indicated slightly elevated levels of potassium when compared to the underlying samples. Sodium, lithium, magnesium and calcium levels were fairly stable throughout the profile suggesting that the entire profile was subject to evaporitic processes. Of interest is the fact that the basal silcrete has significantly elevated levels of aluminium, chromium, iron, manganese, copper and barium. Nickel and rubidium levels also increase significantly within the lower honeycomb calcrete and the basal silcrete. Magnetic susceptibility (Table 11.3) complements the elemental geochemistry and shows a significant down-profile trend, increasing from 0.77 CGS in the upper honeycomb calcrete to 12.93 CGS in the lower honeycomb calcrete and 30.87 CGS in the silcrete. The elevated levels of ferrous, non-ferrous and residual elements in the lower sediments is believed to be indicative of the inclusion of residual components of the Precambrian basement geology and suggests that the basal silcrete may be the associated with a stabilised weathering profile (*c.f.* Summerfield, 1983a) which developed on the basement while the upper calcrete is far less mature and may be reflective of conditions and processes associated with the strandline.

Sample location	Date	δ18O
Maun	2/22/2001	-10.18
	3/6/2001	-5.54
	3/7/2001	-5.67
Ngami	11/28/2001	-3.04
Sepupa	3/5/2001	-2.97
Xakanaxa	2/27/2001	-7.66
	2/28/2001	-9.34
	12/8/2001	-1.42

Table 11.6: Summary of oxygen isotope values from rain samples collected.

Carbon and Oxygen Isotopes

Isotopic analyses of the upper honeycomb calcretes carbonate revealed an inorganic $\delta^{13}C$ value of -2.85‰ and a $\delta^{18}O$ value of -6.66‰ (Table 11.4). The $\delta^{13}C$ value is interpreted as reflecting a mixed but C_4 dominated (60-70%) vegetation, possibly open tree savanna which corresponds well with the current vegetation. The $\delta^{18}O$ signal is suggestive of minimal evaporitic fractionation associated with rapid infiltration of meteoric water and warm temperatures. The limited $\delta^{18}O$ records (Table 11.6) of rain at Lake Ngami, the surrounding area and the nearest GNIP site at Windhoek suggest a weighted average of -5.60‰ is typical for rain in this area, thus suggesting that the carbonate was precipitated within a pedogenic environment under slightly cooler conditions than present.

The lower honeycomb calcrete indicated inorganic $\delta^{13}C$ values of -4.47‰ and $\delta^{18}O$ values of -5.83‰. The trace carbonate of the basal silcrete has a $\delta^{13}C$ value of -5.34‰ and $\delta^{18}O$ value of -6.99‰. These values are very similar to the overlying calcrete and are suggestive of pedogenic calcretisation of the original silcrete. The $\delta^{13}C$ values of the lower horizons suggest a mixed vegetation with an equal proportion of C_3 and C_4 species, possibly dense shrub/tree savanna. The

$\delta^{18}O$ values suggest minor or no evaporitic fractionation and suggest precipitation from rapidly infiltrating meteoric water and temperatures cooler than present.

Petrography

The honeycomb calcrete horizon is a wackestone with a highly crystalline alpha fabric consisting of abundant blocky spar calcite and minor micrite and micro-crystalline quartz, mainly in the form of overgrowths and grain coatings, with highly corroded floating detrital grains (Fig 11.8a-c).

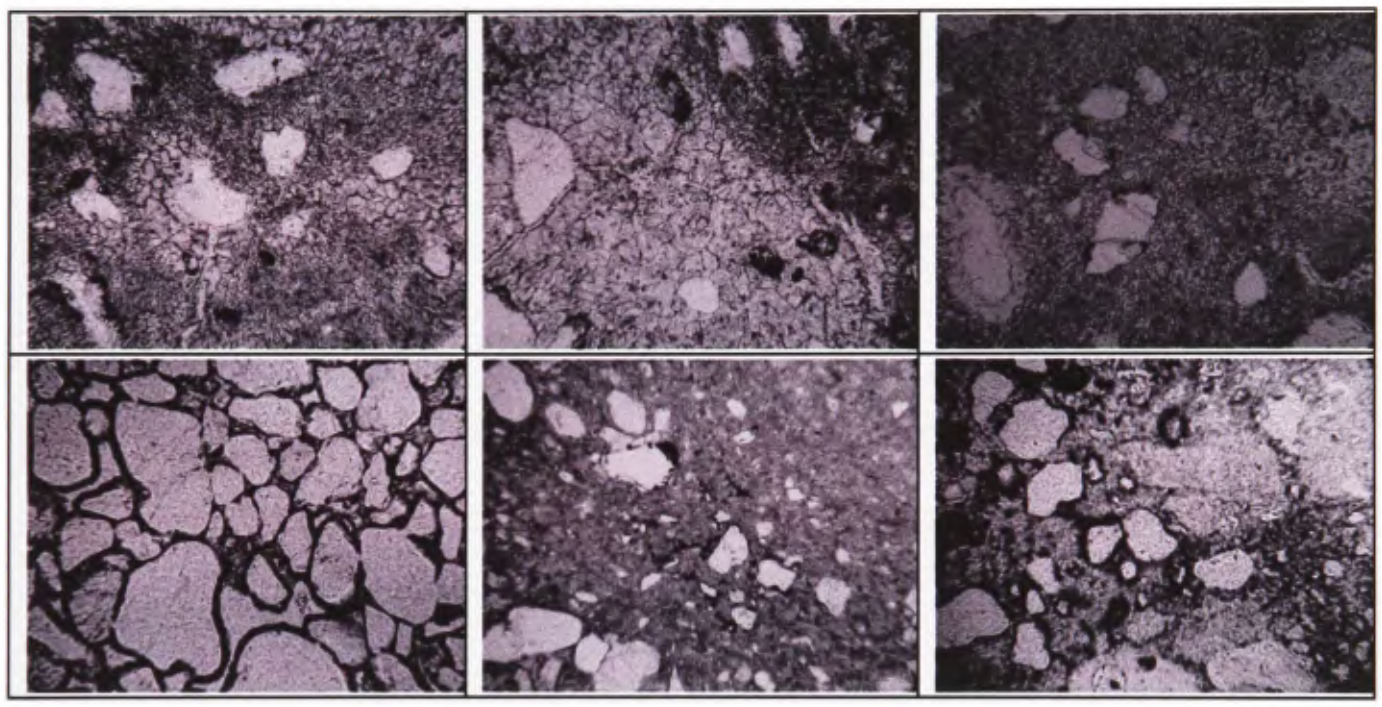


Figure 11.8: PPL thin-section photomicrographs of the 940-945m strandline deposits: (a) crystalline alpha fabric consisting of abundant blocky spar calcite and sparmicrite with corroded floating detrital quartz grains; (b) two contrasting fabrics with a distinct boundary – (left) crystalline alpha sparry calcite fabric and (right) sparmicrite and micrite fabric, both with floating corroded detrital quartz grains; (c) mixed sparry calcite and sparmicrite fabric with highly corroded floating detrital quartz grains. Some of the floating detrital grains have very well developed sparry calcite grain coatings (haloes) while other grains have poorly developed quartz overgrowths; (d) grain supported silcrete packstone with micrite rim cements around the corroded detrital quartz grains and authigenic silica filled intergranular spaces with occasional

overgrowths; (e) micro-laminated micrite containing floating detrital quartz grains; (f) complex cal-silcrete fabric consisting of an original micro-crystalline authigenic silica fabric which has been partially micritised by pervasive micrite.

The extremely hard underlying silcrete is a silica cemented packstone. The cement consists mostly of authigenic silica in the form of grain coatings and overgrowths with most primary pore space filled by micro-crystalline quartz (Fig 11.8d). In places the silcrete outcrops along the fault scarp south of Lake Ngami and a hardpan calcrete has formed as a result of calcretisation processes. The hardpan horizon is limited to approximately the upper 10 cm of the outcrop. The hardpan fabric is well developed and shows micro-laminated micrite (Fig 11.8e) with sparse highly corroded floating detrital grains. The hardpan rapidly grades into a partially calcretised cal-silcrete (matrix-supported) and then the original silcrete (grain-supported fabric). The cal-silcrete fabric is characterised by a disrupted original fabric consisting of quartz overgrowths and length-fast chalcedony rim cements and late stage pervasive micrite (Fig 11.8f). Secondary porosity is filled by a combination of micro-crystalline quartz and sparmicrite.

Interpretation

This sequence is believed to be composite and reflects a mature basal silcrete which is believed to predate the carbonate precipitation and probably formed within the weathering profile associated with the basement Precambrian geology. It is unclear what role Lake Ngami played in the formation or epigenesis of the silcrete as it lacks any significant biogenic structures suggestive of pedogenesis, but it may have been influenced by phreatic processes associated with a lake high-stand. The overlying carbonate is undoubtedly younger and is the product of

pedogenesis and meteoric processes within the vadose zone. Again there is no compelling evidence to suggest that a Lake Ngami high-stand played any role in the formation of this deposit. As a result the deposits investigated at the sites along the 940-945 m strandline are best described as a pedogenic calcrete which is actively calcretising the underlying pure silcrete within the vadose zone. Unlike the 928-932 m strandline or 923-928 m lake floor deposits there is no evidence that lake level regression or transgression and the associated facies and depositional environment changes have been preserved within these deposits or their geochemistry.

11.4 Discussion and Conclusion

The mineralogy of profiles investigated within Ngami is dominated by detrital quartz, plagioclase and K-feldspar and abundant authigenic calcite and silica. The high organic carbon content (~1-2%) of some deposits advocates a lacustrine/palustrine origin with subsequent late-stage pedogenic modification.

The clay mineralogy is dominated by sepiolite with lesser amounts of kaolinite and chlorite. The formation of sepiolite is believed to have occurred within two environments during the desiccation of the system. Initially authigenic sepiolite precipitation was associated with the brackish lacustrine/palustrine conditions. Subsequently the transition to seasonal wetting and drying cycles associated with pedogenic conditions replaced the lacustrine/palustrine conditions and pedogenic sepiolite and palygorskite, rather than smectite, formation occurred within the Mg enriched semi-arid environment (*c.f.* Eitel, 2000). However, as with Calvo *et al.* (1995, 1999) the sepiolite is associated with calcrete rather than dolomite which

suggests moderate salinities. Kaolinite is abundant throughout the Okavango region and is believed to be the stable product of the weathering (hydrolysis) of detrital feldspars within the sediment. The occurrence of interstratified kaolinite/chlorite has two possible explanations. Either the chlorite is detrital and associated with the basement metasediments which outcrop to the south and has undergone limited kaolinization or it is indicative of the transition from the humid low salinity conditions associated with a lacustrine/palustrine environment, where the hydrolysis of abundant detrital feldspars dominated, to a more saline pan environment where authigenic chlorite (Smale, 1973) and sepiolite formation dominated.

The dominance of authigenic silica, mica and smectite within the sediments associated with the 940-945 m strandline on the southern margin of the Ngami Basin suggests that these deposits may have experienced many of the processes operational within the floodplains and islands of the contemporary Okavango alluvial fan (Shaw and Goudie, 2004). However it is believed that these deposits do not retain the same depositional or environmental records as the lower 928-932 m strandline or lake bed deposits as a result of successive pedogenic overprinting.

Isotopic geochemistry of the carbonate has provided valuable information to help understand the vegetation communities present and the environments in which precipitation is believed to have occurred. Mixing of the $\delta^{13}C$ signal as a result of recrystallisation or differing precipitation mechanisms is evident within a number of the profiles investigated. Typically there is a fractionation factor between matrix and floating nodules.

As a generalisation palustrine and pan deposits tend to be characterised by a dominant C_4 vegetation, while pedogenic and phreatic environments tend to reflect mixed C_3/C_4 savanna woodland vegetation. In most cases the contemporary vegetation is in phase with the vegetation suggested by the carbon isotopes.

$\delta^{18}O$ values are highly reflective of the degree of evaporitic fractionation which is a direct result of the environment in which precipitation occurred. Highly fractionated values are reflective of evaporitic pan environments, significantly fractionated values are indicative of lacustrine and palustrine environments, moderately fractionated values suggest inhibited infiltration of meteoric water which is commonly associated with clay rich sediments or thin soils above hardpan and no fractionation indicates rapid infiltration of meteoric water which suggests sandy Kalahari pedogenic environments. The temperatures associated with the $\delta^{18}O$ values are open to interpretation due to the nature of the calculations used. However, the general trend is for a strong correlation between the vegetation, aridity and temperature (warmer/cooler and drier than present = increased C_4 dominance, contemporary conditions = mixed C_3/C_4 and warmer/cooler and wetter than present = C_3 dominance) with the overall suggestion of carbonate precipitation under cooler than present conditions.

The relationship between the type of chemical sedimentation and temperature is less apparent due to the fact that only the authigenic carbonate was analysed. Fluorination and associated isotopic analysis of the authigenic silica (not

conducted) would provide an insight into the temperatures associated with its precipitation.

A water leach of the Ngami carbonate indicates that soluble and mobile elements are fairly consistent throughout the basin and supports the premise that the influence of detrital sediments, hydrogeochemistries and external inputs such as aerosols are fairly uniform throughout the basin.

Numerous ^{14}C dates suggest carbonate precipitation/reprecipitation within the Ngami system occurred between 14620 ± 90 BP and 1460 ± 80 BP (Street and Grove, 1976; Heine, 1978, 1982, 1987; Cooke, 1984; Cooke and Verstappen, 1984; Helgren, 1984; Shaw, 1985a; Shaw and Cooke, 1986; Shaw *et al.*, 1988; Shaw and Thomas, 1988; Thomas and Shaw, 1991). There is undoubtedly older carbonate within the Ngami system and similarly mineralogy and isotope geochemistry suggests that carbonate may be actively precipitating within the contemporary environment. However, the overall suggested trend within the Ngami Basin is calcrete formation within palustrine and pedogenic environments under semi-arid conditions and a marginally drier and cooler environment than currently exists. The oxygen isotopes of most carbonates suggest rapid infiltration and recharge of soil moisture by meteoric water with very little groundwater influence (*c.f.* Shaw and Goudie, 2004). The general mixed C_3/C_4 vegetation signature of the calcrete, correlates well with the current dry savanna woodland characterised by *Acacia* and *Combretum* trees with a grassy understory which is likely to have transformed to Miombo forest during more humid periods. The Ngami silcrete is most likely to have precipitated under more humid conditions

within both the phreatic and vadose zones as a residual deposit associated with a weathered profile, direct precipitation from groundwater and within a pedogenic environment.

12. DISCUSSION AND CONCLUSION

Distinct episodes of terrestrial carbonate deposition have characterised many arid and semi-arid environments globally since the late Mesozoic. Within southern Africa the existence of the Kalahari Basin since the Mid/Late Cretaceous (De Wit, 2007) has facilitated the accumulation of the Kalahari Group sediments with a distinct chemical stratigraphy. The detailed investigation of chemical sediments formed and/or exposed within four geomorphic environments of the Kalahari (pan, alluvial/fluvial, palustrine/lacustrine and pedogenic) has contributed to the description and understanding of mechanisms and processes responsible for the precipitation, corrosion and modification of authigenic terrestrial chemical sediments over an extended time period. Chemical sediments and carbonates in particular are highly impressionable and thus often act as repositories of environmental, climatic and chemical information, although this information is often extremely complex and difficult to elucidate. Investigation of chemical sediments reveals that there are a wide range of complex and frequently over-printed mineralogies, geochemistries and petrographies which are often reflective of their depositional environment, epigenesis and paragenesis.

12.1 Depositional Environments, Palaeoenvironmental Conditions and the Relative Age of Kalahari Carbonates

The paragenesis and true age of the majority of Kalahari carbonate has been a matter of great debate since the region was first investigated. In line with Netterberg (1969b) it is believed that the majority of carbonate or Kalahari limestone as it is often referred to, is associated with the transition from

lacustrine/palustrine depositional systems to sub-aerial and vadose/meteoric epigenesis and shallow diagenesis which accompanied deposition within extensive alluvial fans. This change in depositional environment is believed to be the result of a several key factors: 1) tectonics, which modified the basin architecture and drainage orientation; 2) dynamic hydrologic conditions, which altered the competence, capacity and hydraulic characteristics of many drainages, effected groundwater recharge, hydraulic gradients and the location of shallow aquifers and the capillary fringe, which controlled the dominance of phreatic or vadose precipitation and epigenesis within the upper sediments; and 3) desiccating climatic conditions, which facilitated the colonisation and stabilisation of the sediment by plants and initiation of pedogenesis.

The termination of widespread lacustrine/palustrine deposition within the sub-basins of the Mega Kalahari is thought to have occurred during the late Miocene. Clastic sedimentation is believed to have decreased or terminated in response to a general increase in aridity during the late Miocene and early Pliocene (Zachos *et al.*, 2001a; Udeze and Oboh-Ikuenobe, 2005; Westerhold *et al.*, 2005) and a reduction in accommodation space. A number of Kalahari geomorphic features support the proposal that the Pliocene was the period during which pedogenic and non-pedogenic carbonate accumulation dominated. The most significant of these are the incised drainages throughout the Kalahari which attest to Pliocene tectonics (Partridge and Maud, 2000). Adjustment (lowering) of the phreatic zone is believed to have played a significant role in the alteration of phreatic and valley chemical sediments (Nash *et al.*, 1994a, 1998) which are predominantly composed of authigenic silica/silcrete fabrics, into carbonate with significant pedogenic

features in the upper sections. In addition to the geomorphic and tectonic control on chemical sedimentation it is widely acknowledged that the Pliocene was a period of increased aridity (Dupont *et al.*, 2005) which was characterised by a global period of carbonate accumulation. There is, however, substantial evidence throughout the southern Kalahari that there was an earlier period of landscape stability and pedogenic calcretisation of the Karoo Group sediments lining the Mega Kalahari Basin around the K/T boundary (Partridge and Maud, 1989) prior to the initiation of Kalahari sedimentation.

The complex sedimentary dynamics associated with the epigenesis, shallow diagenesis and paragenesis of Kalahari chemical sediments means that alteration, corrosion, polygenetic precipitation and replacement has blurred their palaeoenvironmental records. However, the mineralogical relationships between authigenic carbonate, silica and clays, calcite versus dolomite and sepiolite/palygorskite versus smectite/kaolinite assemblages are not only indicative of epigenetic and diagenetic mechanisms, depositional and geochemical environments but distinct inferences can also be made with respect to palaeoclimatic conditions. Thus the chemical sediments allude to a range of processes which are reflective of environmental conditions as well as the geomorphic features associated with their deposition and modification. The most obvious of these environment-process relationships is associated with moisture availability and its geochemistry within the range of environments where authigenic minerals precipitate. A solution's salinity, pH, pCO_2 and Mg/Ca ratio along with the physicochemical conditions will dictate which authigenic chemical sediment will form and thus explains why silica and carbonate frequently co-

precipitate within the same profile at different levels as a result of minor fluctuations in these critical controls. The most apparent expression of these relationships is visible within mature profiles where calcite is precipitating within the upper pedogenic horizon, dolomitisation and silicification is occurring within the capillary fringe as a result of elevated salinity and authigenic silica is precipitating within the phreatic zone. Similar relationships reflect the geochemical control on authigenic clay minerals precipitating within Mg, Ca, Si and Al enriched environments (pans and floodplains) where the controlling factor are seasonality (Wang *et al.*, 1994), humidity, pH and salinity. Recrystallisation of high-Mg calcite to low-Mg calcite is believed to be the principal source of Mg enrichment in these environments (Eitel, 2000). A general scenario detected was that under high pH (> 9.5) and highly saline conditions smectite/kaolinite clay assemblages are precipitated while reduced pH (~8.5) and lower salinity conditions favour sepiolite/palygorskite clay assemblages. A similar relationship is evident within lacustrine environments where sepiolite is reflective of brackish water conditions while smectite is indicative of high salinities and high pH. In some settings (principally the abandoned floodplains of the Okavango) both clay assemblages exist. These assemblages are proportionally dominated by sepiolite/palygorskite and are interpreted as being indicative of the transition from active floodplain environments, where smectite/kaolinite and authigenic silica with minor calcite precipitate under highly saline and alkaline conditions (typically induced by extensive evapotranspirational pumping of the shallow groundwater and capillary fringe), to the desiccated pedogenic environment where calcite precipitation and sepiolite/palygorskite precipitation dominates under lower salinity and reduced pH soil moisture conditions.

Detailed investigation of the four principal environments in which carbonates occur within the Kalahari (pan, alluvial, lacustrine and pedogenic) identified a number of distinct petrographic and mineralogical characteristics which attest to their depositional, environmental, climatic, epigenetic and diagenetic histories.

12.1.1 Pans

The indurated chemical sediments within the modern Kalahari pan environments investigated by this study revealed that the dominant fabric is reflective of a primary lacustrine/palustrine carbonate mud which has undergone complex replacement and reprecipitation within both a vadose and phreatic environment. All three pan dominated regions investigated (Etosha, Kgalagadi and the Kalkweissrand) are erosional landscapes where the pans have formed negative features within a pre-existing carbonate lithology as a result of processes outlined by Goudie (1991) and Goudie and Wells (1995). The modern pan systems have thus superimposed their geomorphology and mineralogy on these older deposits. Epigenesis of these sediments has been interpreted within the context of their relative position within the vadose, capillary fringe and phreatic zones and the sediment's interaction with meteoric, evaporitically evolved and enriched percolating solutions, and groundwater. The interaction of carbonate precipitation mechanisms, fluctuating climatic conditions and vadose and phreatic hydrology initially within an aggrading depositional environment (which resulted in syn-sedimentary basin subsidence) and subsequently within an erosional environment is responsible for the complex epigenesis, recrystallisation and alteration mineralogies which characterise these chemical sediments.

The 'Etosha Limestone' and the carbonate pan terraces of the Kgalagadi and Kalkweissrand are characterised by highly indurated, often intergrade, and partially reworked palustrine/lacustrine carbonate deposited within very similar Kalahari sub-basin environments. All of these carbonates are generally characterised by dense fine grained fabrics which often include numerous bioclasts, intraclasts, desiccation induced grainification, microkarst, silicification, dedolomitisation, dolomitisation and evaporitic structures. The dense, unlaminated micrite fabrics are believed to be representative of bioturbation and carbonate deposition by a combination of biogenic and physicochemical mechanisms associated with shallow lakes and ponds (Platt, 1989; Alonso-Zarza, 2003). The replacement of evaporite minerals by silica and the complex fabric structures associated with grainification means that these deposits can easily be confused with mature (stage 6 (Machette, 1985)) pedogenic calcretes when seen out of their depositional context within the rock record. Platt (1989) characterises these palustrine/pan facies as 'regressive' sequences that show an upward increase in the degree of pedogenic modification. This is usually incomplete and/or superimposed, reflecting the short-term climatic variation responsible for phases of desiccation and inundation. Periods of prolonged desiccation are characterised by the formation of hypersaline alkaline solutions which precipitate evaporites, authigenic clays, silica and dolomite (evaporative (primary and replacement), seepage-reflux and mixing processes depending on the location of precipitation within the profile).

Carbonate within pan environments is generally reflective of phreatic precipitation and replacement processes associated with seasonal inundation, desiccation and seepage in a highly saline environment. The region has similarities with the facies associations identified, described and interpreted by Freytet (1973), Freytet and Plaziat (1982) and Platt (1989) and with the calcitisation, silicification and dedolomitisation mechanisms discussed by Arenas *et al.* (1999), Bustillo and Bustillo (2000) and Sanz-Rubio *et al.* (2001) from analogous terrestrial carbonate basins in southern Europe during the Cretaceous and Early Cenozoic.

These deposits are characterised by a range of mineralogies which relate to the localised effects of hydrogeochemical interactions within these ground and surface water fed evaporitic systems. The cal-silcrete and impure silcrete fabrics suggest simultaneous precipitation of carbonate and silica, at differing levels within the profiles, during various stages of the landscape's evolution. Surface pedogenic cal-silcrete is believed to reflect micritisation of an original phreatic silcrete within a near surface environment while the underlying impure silcrete is associated with the deeper capillary and phreatic zones. The high pH and salinity of the pan environments favoured surface carbonate precipitation which resulted in additional enrichment of soluble silica. These silica rich fluids migrated down profile and then precipitated at depths where the salinity and pH were lower. Subsequent epigenetic and paragenetic alteration and reprecipitation of the fabric occurred as a result of changing processes linked to the dominance of surface pedogenesis. The reduced influence of local groundwater processes and the lowering of the capillary fringe and the phreatic zone resulted in an increased role for meteoric water in epigenesis.

This study has expanded the work of Buch and Rose (1996) within the Etosha Pan and Ovambo-Pans-Plain to include the Kgalagadi and Kalkweissrand pan environments. Three generalised but distinct sediment types can be identified within all these environments:

(1) disintegrated (*in situ*) calcareous sedimentary rocks;

(2) parautochthonous sediments; and

(3) allochthonous sediments

The formation of authigenic K-feldspar, mica and sepiolite has been recorded by this and numerous other studies (Smale, 1968; Netterberg 1969c; Watts, 1980) within the evaporative pumping dominated alkaline and saline Kalahari pan environments. In line with Buch and Rose (1996), it is believed that the carbonate mineralogy with pan systems is very localised and can be related to a number of models (evaporative, seepage-reflux and mixing) which show varying influences of the underlying geology on groundwater enrichment with respect to Ca^{2+}, Mg^{2+}, HCO_3^- and CO_3^{2-}. In addition the evolutionary model of groundwaters within a playa environment (Arakel, 1986a) is considered highly applicable when explaining the occurrence of calcite and dolomite.

12.1.2 Alluvial

Alluvial carbonate was investigated from three environments (Okavango, Linyanti and the SW Kalahari drainages) within the Kalahari. Sedimentary sequences of the Okavango and Linyanti alluvial fans contain groundwater and pedogenic intergrade carbonate formed through a series of near-surface processes. Carbonate

within these systems is generally immature (powdery, nodular and occasionally massive). The lithosequence is suggestive of an upward chemical facies transition from phreatic/channel silcrete precipitation to pedogenic calcrete and the calcretisation of the lower silcrete within the vadose zone as a result of desiccation. The similarity between the Okavango and Linyanti carbonates highlights the fact that common precipitation processes and mechanisms are operational within adjacent and similar geomorphic environments in the Kalahari.

Mineralogically, geochemically and petrographically the Okavango and Linyanti carbonates cluster into distinct groups which provide additional insight into their palaeoenvironments and mechanism of precipitation. Petrographic analyses indicated that all the samples grade from packstones to wackestones at depth and generally have a moderate detrital quartz content. These detrital grains have varying degrees of roundness and sphericity indicating their aeolian and fluvial origin and secondary corrosion. The fabric is predominantly authigenic quartz with biogenic micritised zones and spar filled vugs indicative of limited pedogenesis and micro-karst. LOI and bulk XRD indicates that the carbonate component is typically less than 30% and that the organic carbon content is negligible.

Groundwater and palustrine carbonate characterises fossil interdune areas and the cores of linear dunes. Within the alluvial fans the carbonate has formed as groundwater calcrete in association with silcrete, which is the dominant chemical sediment within the active fluvial environment. These deposits have then undergone pedogenic micritisation during periods of floodplain abandonment and

stabilisation. The proposed mechanism is that after floodplain abandonment, the water table subsides and calcite and authigenic silica precipitation is lowered within the profile. Over time savanna woodland colonises the floodplain and the precipitated intergrade groundwater calcrete will be added to and modified by pedogenic calcrete accumulation. The result is an *in situ* transformation from a characteristic groundwater profile to an increasingly pedogenic one which shows an overall increase in the density and amount of the carbonate up profile (Wright and Tucker, 1991). As pedogenic processes dominate, any additional carbonate accumulates below an increasingly well defined transition with the surface soil horizon. However, once the area becomes flooded again, a new cycle of groundwater calcite and authigenic silica precipitation will replace and modify the pedogenic components of accumulation (Pimentel *et al.*, 1996). The calcrete within the sequence therefore represents an aggregate deposit of all previous cycles of floodplain inundation and abandonment.

Clay mineralogy suggests at least three depositional environments within the Okavango and Linyanti. The dominant group, believed to be indicative of pedogenic epigenesis of fluvial/phreatic silcrete, contains abundant micrite, limited microcrystalline quartz and smectite. Of significance is the fact that whewellite was detected within the Linyanti samples which indicates biogenic mechanisms of calcite precipitation (Verrecchia, 1990a; Verrecchia *et al.*, 1993). The second grouping consists of fluvial/phreatic silcretes which are silica dominated, contain very little calcite and abundant kaolinite. These samples have an authigenic silica fabric rich in biogenic structures, particularly rhizoliths, which are believed to indicate the link between phreatic precipitation and chemical

processes associated with evapotranspirational pumping by roots (McCarthy *et al.*, 1993a). A third cluster of samples are associated with the fine grained littoral sediments of Lake Liambezi and the seasonal floodplains of the Okavango. These deposits contain significant amounts of sepiolite and are suggestive of precipitation within low-energy lacustrine and palustrine environments with fluctuating salinity and pH.

Mass-balance calculations by McCarthy and Metcalfe (1990) indicate that the quantity of chemical precipitate on the contemporary Okavango fan is at least five times that of clastic sediment. It is probable that due to the location of the Okavango and Linyanti within the heart of the Kalahari, chemical sedimentation has been the dominant process throughout the Late Pleistocene and Holocene.

The valley carbonates of the SW Kalahari are by contrast mature and have a more complex diagenetic and epigenetic history. The major drainages of this region have incised through the calcretised alluvium of the Mokalanen and Eden formations which underlie the unconsolidated aeolian dunes of the Gordonia formation. These deposits are characterised by non-pedogenic and pedogenic calcite, dolomite and silica cements with a significant authigenic Mg-rich clay mineral and iron hydroxide (goethite) component. The non-pedogenic dolomite, silica and calcite precipitation is believed to have precipitated under reducing conditions within the capillary fringe and phreatic zone. Relocation of the sediments from the phreatic to the vadose zone as a result of a drainage incision and the associated sinking groundwater table initiated meteoric vadose epigenesis and pedogenesis. This epigenesis resulted in dissolution, precipitation and

mineralogical transformation of the sediments within the near surface environment. In addition, groundwater discharge from the walls of the incised valleys has had a significant influence on geochemistry and the precipitation, modification and corrosion of chemical cements within the active and fossil seeps. Thus, the dynamic geomorphic, climatic, and hydrologic environment within the SW Kalahari has left an integrated geochemical signature on the Mokalanen and Eden formation deposits.

12.1.3 Lacustrine/Palustrine

Although all the sites investigated within the Kalahari by this study have depositional environments linked to palustrine conditions, the Ngami Basin was the only true lacustrine/palustrine depositional environment investigated. The mineralogy of the dense microcrystalline carbonates which characterise the basin floor and the 928-932m strandline are dominated by authigenic calcite with minor silica, plagioclase and K-feldspar. The clay mineralogy is dominated by sepiolite with lesser amounts of kaolinite and chlorite. The formation of sepiolite is believed to have occurred within two environments during the desiccation of the system. Initially authigenic sepiolite precipitation was associated with the brackish lacustrine/palustrine conditions. Subsequently the transition to seasonal wetting and drying cycles associated with pedogenic conditions replaced the lacustrine/palustrine conditions and pedogenic sepiolite and palygorskite, rather than smectite, formation occurred within the Mg enriched semi-arid environment (*c.f.* Eitel, 2000). However, as with Calvo *et al.* (1995, 1999) the sepiolite is associated with calcrete rather than dolomite which suggests moderate salinities. Kaolinite is abundant throughout the Okavango region and is believed to be the

stable product of the weathering (hydrolysis) of detrital feldspars within the sediment. The occurrence of interstratified kaolinite/chlorite has two possible explanations: (a) Either the chlorite is detrital and associated with the basement metasediments which outcrop to the south and has undergone limited kaolinization or (b) it is indicative of the transition from the humid low salinity conditions associated with a lacustrine/palustrine environment, where the hydrolysis of abundant detrital feldspars dominated, to a more saline pan environment where authigenic chlorite (Smale, 1973) and sepiolite formation dominated. The occurrence of silcrete (which has undergone very limited micritisation), mica and smectite within the sediments associated with the 940-945 m strandline on the southern margin of the Ngami Basin suggests that these deposits reflect depositional and environmental conditions that differ markedly from the lower level calcareous deposits.

Numerous ^{14}C dates suggest carbonate precipitation/reprecipitation within the Ngami system occurred between 14620 ± 90 BP and 1460 ± 80 BP (Street and Grove, 1976; Heine, 1978, 1982, 1987; Cooke, 1984; Cooke and Verstappen, 1984; Helgren, 1984; Shaw, 1985a; Shaw and Cooke, 1986; Shaw *et al.*, 1988; Shaw and Thomas, 1988; Thomas and Shaw, 1991). There is undoubtedly older carbonate within the Ngami system and similarly mineralogy and isotope geochemistry suggests that carbonate may be actively precipitating within the contemporary environment. However, the overall suggested trend within the Ngami Basin is calcrete formation within palustrine and pedogenic environments under semi-arid conditions and a marginally drier and cooler environment than currently exists. The Ngami silcrete is most likely to have precipitated under more

humid conditions within both the phreatic and vadose zones as a residual deposit associated with a weathered profile, direct precipitation from groundwater and within a pedogenic environment.

12.1.4 Pedogenic

Pedogenic duricrusts attest to periods of geomorphic stability within the Kalahari during the Cenozoic at which time processes were active under a range of semi-arid to humid climatic conditions. Pedogenic calcrete typically takes the form of a hardpan grading to moderately or well consolidated nodular to massive intergrade calcrete at depth. The typical pedogenic profile has decreasing carbonate content with depth which complements studies on pedogenic carbonates in the south-western USA (McFadden and Tinsley, 1985; Marion *et al.*, 1985; Mayer *et al.*, 1988). Pedogenic calcrete usually takes the form of a near continuous sheet between 2 to 5 m thick developed 1 to 2 m below the surface Kalahari sand. This calcrete typically contains significant silica at depth (intergrade calcrete-silcrete) and occasionally minor amounts of late-stage dolomite in porous zones, which suggests precipitation as a result of evaporative pumping associated with temporary wetting fronts and a seasonally fluctuating capillary zone or mixing of meteoric and saline groundwater at depth.

12.2 Isotope Geochemistry – Its Role in Elucidating Carbonate Precipitation and Epigenesis within the Kalahari

The isotope geochemistry of carbonates provides significant clues to depositional environments (pedogenic, phreatic or lacustrine), vegetation communities present at the time of precipitation and palaeoclimatic conditions, although reprecipitation

and the inclusion of detrital carbonate reduces the resolution of this information. The $\delta^{16}O/^{18}O$ ratios (Fig 12.1) provide definitive insight into the evolution of the solutions from which the carbonate was precipitated and the temperatures of precipitation (Hays and Grossman, 1991). Temperatures associated with $\delta^{18}O$ values are very open to interpretation due to the nature of the calculations used and have therefore been omitted from this discussion. $\delta^{18}O$ values are highly reflective of the degree of evaporitic fractionation which is a direct result of the environment in which precipitation occurred. Highly fractionated values are interpreted as being reflective of evaporitic pan environments. Significantly fractionated values are indicative of lacustrine and palustrine environments. Moderately fractionated values suggest inhibited infiltration of meteoric water which is commonly associated with clay rich sediments or thin soils above hardpan. No fractionation indicates rapid infiltration of meteoric water which suggests sandy Kalahari pedogenic environments.

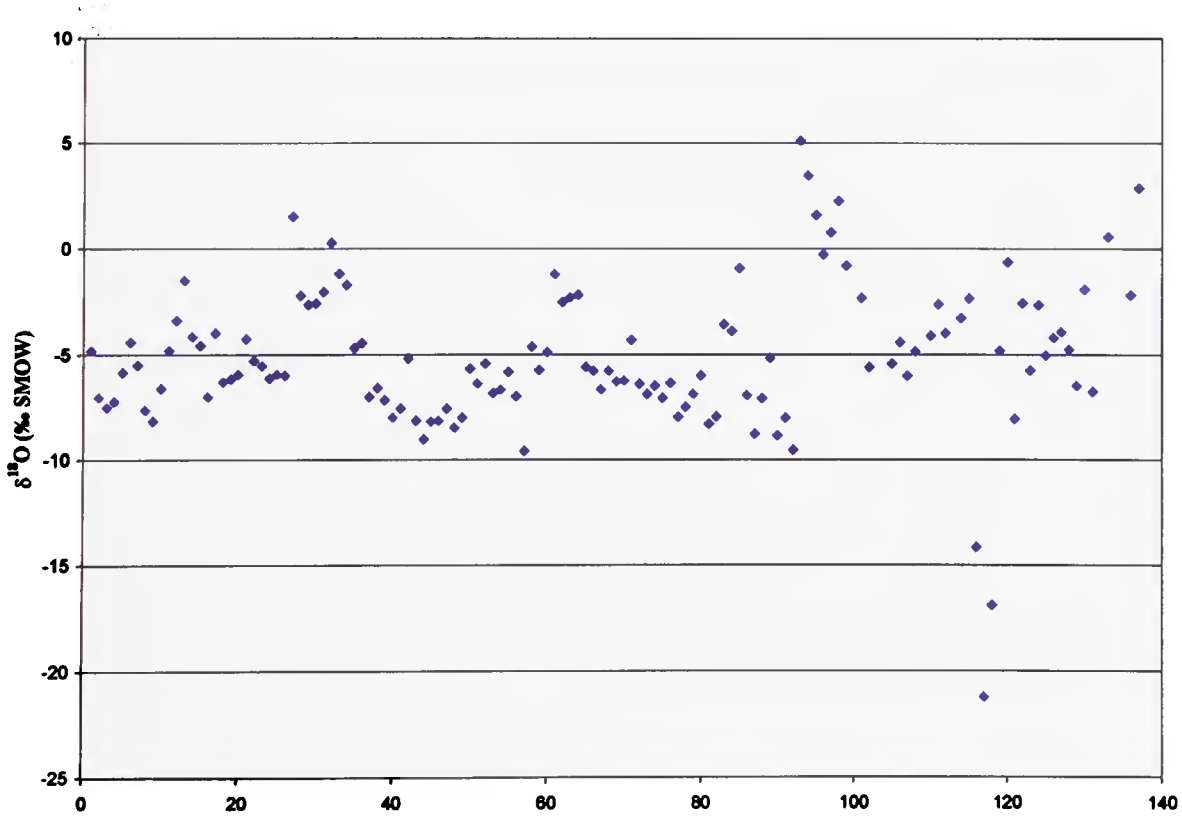


Figure 12.1: Graph of $\delta^{18}O$ values for all sediment samples analysed (sample numbers correspond with Appendix 11).

The $\delta^{12}C/^{13}C$ values (Fig 12.2) similarly suggest the proportional C_3/C_4 vegetation components (Wang and Zheng, 1989) which are reflective of geologic (*c.f.* Moore and Attwell, 1999) and palaeoenvironmental conditions: a dominance of C_4 vegetation is associated with moisture stress/drier phases and reduced atmospheric CO_2 which has characterised the Cenozoic (Cerling *et al.*, 1998), while C_3 vegetation is associated with more humid phases and elevated levels of atmospheric CO_2. The majority of the $\delta^{13}C$ values are believed to be reflective of an environment in which pedogenic carbonate precipitated as a result of evapotranspirational pumping and degassing by a mixture of C_3 and C_4 vegetation. Most of these pedogenic sequences indicate that the C_3 vegetation component is slightly less or very similar to that within the contemporary open savanna woodland which is dominant within the alluvial environments investigated. Thus it is concluded that the majority of Kalahari carbonate is precipitated within an environment that has a mixed C_3 and C_4 vegetation. The occurrence of carbonate linked with either pure C_3 or C_4 vegetation is unusual. C_3 dominant environments are interpreted as being indicative of woodland areas and riparian forests. C_4 dominant environments are believed to be reflective of more open grassland vegetation and pedogenesis probably occurred within specific geomorphic environments such as desiccated pans, lakes and floodplains. Importantly, despite this study's best efforts to analysis primary phase carbonate the influence of recrystallisation must be considered when interpreting isotope values and the link with palaeo-vegetation.

The $\delta^{18}O$ values suggest precipitation of the carbonate from cool meteoric solutions which have undergone little or no evaporitic fractionation as a result of rapid infiltration. The most likely explanation for these negative $\delta^{18}O$ values, in an environment which experiences intense evaporation, is that meteoric water associated with periods of above normal rainfall, typically linked to intense thunderstorm activity, is responsible for the formation of unstable wetting fronts which penetrate the deeper soil horizons where pedogenic calcrete precipitation occurs.

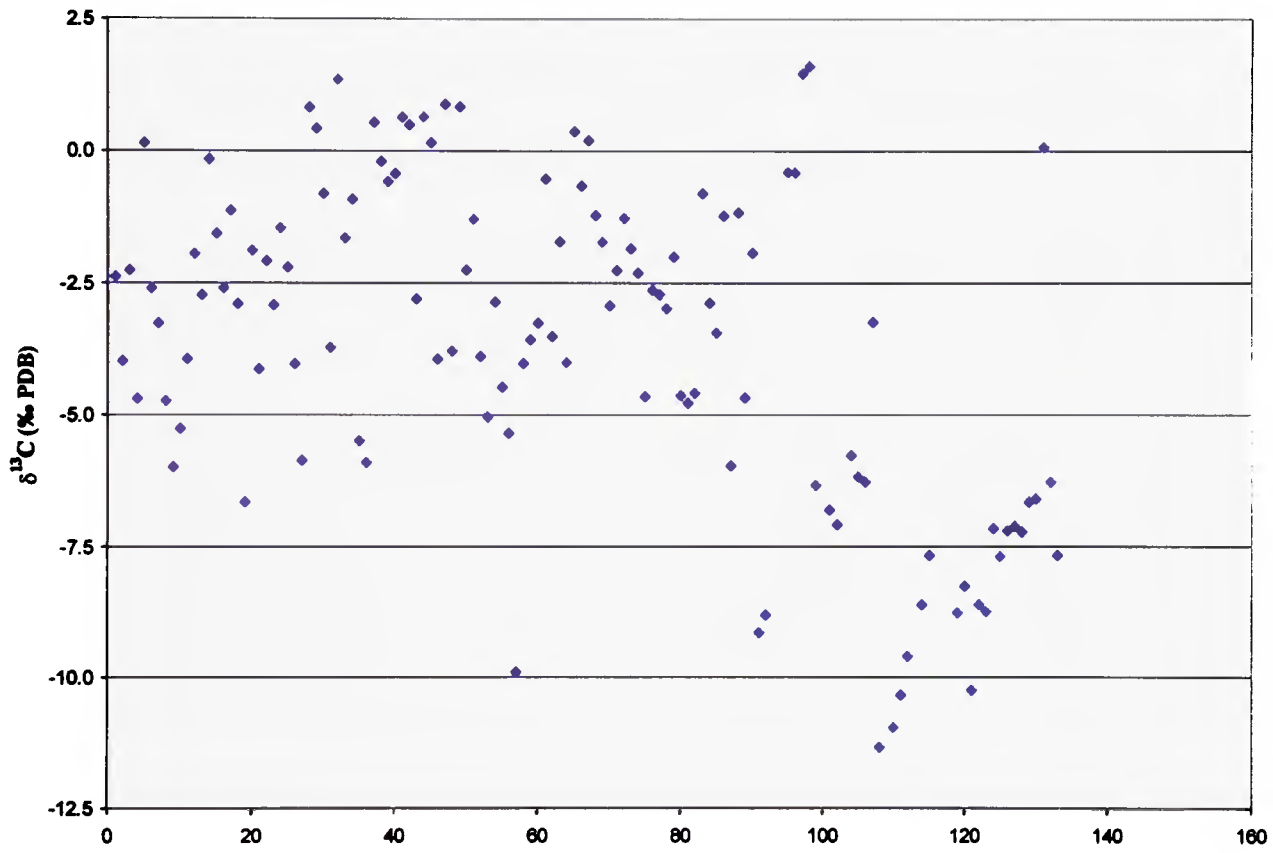


Figure 12.2: Graph of inorganic $\delta^{13}C$ values for all sediment samples analysed (sample numbers corresponds with Table 4). Pure C_4 vegetation = 1.8‰ and pure C_3 vegetation = -11.8‰.

However, the general trend is for a strong correlation between the vegetation, aridity and temperature (warmer/cooler and drier than present = increased C_4 dominance, contemporary conditions = mixed C_3/C_4 and warmer/cooler and wetter than present = C_3 dominance) with the overall suggestion of carbonate

precipitation occurred within the Kalahari under cooler and drier conditions than present.

12.3 Kalahari Chemical Sediments: Are Micro-Fabrics Linked to Paragenetic and Epigenetic Environments?

The complexity of the diagenetic history associated with mature chemical sediments within the Kalahari is believed to be responsible for the dominance of crystalline/alpha fabrics (Wright and Tucker, 1991). However, there is abundant evidence throughout the Kalahari to support the role of biogenically mediated processes of carbonate precipitation at the surface (*c.f.* Kahle, 1977), within pedogenic environments (*c.f.* Wright, 1986a; Wright *et al.*, 1988; Alonso-Zarza, 1999; Verrecchia *et al.*, 1995, 1996; Wright *et al.*, 1996) or within the capillary zone (Dunn *et al.*, 2005) where exopolysaccharide-mediated rather than photosynthesis-driven biogenic processes dominate. A key objective of this study was to investigate the occurrence of these calcareous biogenic micro-fabrics within the Kalahari and attempt to understand the mechanisms and processes responsible for their formation and preservation. The development of the carbonate microfabric can either be in equilibrium with (Bosak and Newman, 2005) or independent of biogenetic processes (Hammes and Verstraete, 2002). Investigation of the selected sites within the Kalahari has, however, highlighted the trend that due to the fragile nature of the structures within beta fabrics (Wright and Tucker, 1991) they are restricted in their preservation within mature sequences, typically as macrofeatures such as rhizoliths. Significantly to date no clear link has been detected between precipitate morphology, rhizoliths and vegetation, e.g. rhizocreations can be isotopically reflective of either C_3 or C_4

vegetation and thus don't necessarily reflect characteristic macrophyte structures (root hairs, tap roots, nodules, etc.) which initiated their precipitation. Biocrusts, hardpans and the upper sections (typically composed of powdery and nodular carbonates) of relatively modern calcretes which have not undergone excessive recrystallisation also display abundant biogenic micro-structures.

12.3.1 Biogenic Processes

The cool dry and reduced atmospheric CO_2 conditions associated with the Neogene induced an evolutionary transition from the humid forest, which had dominated since the Mesozoic, to savanna woodland and grassland (Cerling *et al.*, 1977, 1997, 1998). This evolutionary process resulted in the dominant savanna tree species being legumes which form root nodules containing symbiotic mycorrhizae bacteria. The mycorrhizae-infected root systems are responsible for biogeochemical acquisition of both water and nutrients (Hogberg, 1989). Mycorrhizas act to reduce interspecific competition by capturing resources not available to other plants, and by increasing the competitive advantages of the mutualistic plant species (Stock *et al.*, 1997). Besides their role in nutrient acquisition, a network may exist in the soil of arbuscular mycorrhizal hyphae. This hyphal network, in conjunction with a continuous lateral root system can function to maintain tight nutrient cycling patterns (Pankow *et al.*, 1991), improve soil structure (Miller and Jastrow, 1990) and initiate the precipitation of biogenic crusts (Kahle, 1977) and laminar and rhizogenic calcretes (Wright *et al.*, 1988, 1995) which often contain needle-fibre calcite (Wright, 1984; Phillips and Self, 1987; Verrecchia and Verrecchia, 1994) and spherulites (Verrecchia *et al*, 1995, 1996; Wright *et al.*, 1996). Of particular significance is that within savanna

communities leguminous trees don't perform nitrogen fixation. This is performed by nodulated leguminous forbs or by free-living bacteria and soil surface crusts of cyanobacteria (Zietsman *et al.*, 1988). Empirical observations of root distributions (Scholes, 1988; Scholes and Walker, 1993) show that the rooting depth separation between trees and grass is real but slight. Grass root density exceeds tree root density to a depth of nearly 1 m. Trees and grasses both have most of their roots in the top 40 cm of the soil, since in semi-arid climates water seldom penetrates below this depth in significant quantities as the PET greatly exceeds MAP throughout the Kalahari. However, there are sporadic periods during which recharge of the deeper horizons occurs. This generally constitutes 1-2% of MAP under current conditions (Mazor, 1982; Selaolo, 1998; De Vries *et al.*, 2000). This relationship between infiltration of meteoric water and root density is extremely significant to biogenically induced pedogenic carbonate precipitation which tends to occur in the middle to lower B horizon of soil profiles. Although tree and grass communities share many processes they have very different physiologies which have been linked to preserved biogenic structures within Mediterranean carbonates (Klappa, 1978a,b, 1979a,b, 1980a,b, 1983) but as discussed earlier this study was unable to differentiate between tree and grass biogenic structures successfully.

Vegetation patchiness in arid regions may be exacerbated by the lack of a permanent mycorrhizal population which has a coincidental effect on the precipitation of biogenic but not necessarily crystalline carbonate in the vadose zone. In the Kalahari, where grass growth is interrupted by the long dry season, infection of the new season's grass occurs only from spores (Veenendal *et al.*,

1992). Spore numbers decrease if drought or disturbance prevents plant growth as illustrated by the lower mycorrhizal propagule numbers on bare dunes compared to vegetated dunes in the southern Kalahari (Allsopp cited in Stock *et al.*, 1997).

It is thought that during the Quaternary the combined climatic factors of aridity and low atmospheric CO_2 levels acted to reduce the C_3 component within the savanna communities. The associated increase in the C_4 component, possibly with an associated increase in the non-perennial C_4 component, probably played a significant role in the mobility of the surface sediment (A and upper B horizons) which became mobilised as the Kalahari erg. This disturbance/disruption along with the reduced vegetation, severely affected arbuscular mycorrhizal populations and thereby excluded or minimised the role played by biogenic processes in the resolution and reprecipitation of arid phase Kalahari vadose carbonates. Similarly during warm and humid climatic phases associated with increased atmospheric CO_2, it is proposed that the available moisture initiated increased biogenic carbonate precipitation. Thus a continuum of dominant fabric types is proposed for the Kalahari: semi-arid, low biomass, C_4 dominated and high levels of environmental disturbance/disruption = crystalline (alpha) to sub-humid, high biomass, high proportion of C_3 vegetation and stable environment = biogenic (beta). This can be integrated into a matrix with the more traditional (but often disputed) climatic conditions associated with chemical sediment precipitation: hyper-arid = gypcrete, arid/semi-arid = dolo/calcrete and >750mm/sub-tropical/tropical = silcrete/ferricrete.

It is believed that the difference in epigenesis and paragenesis accounts for the differing abundance of biogenic structures within Kalahari carbonates when compared to Mediterranean carbonates rich in biogenic structures (*c.f.* Klappa, 1978a,b, 1979b, 1980a,b, 1983). Thus, although all near surface carbonates experience geomycology, the effects of vadose and sub-aerial epigenesis and shallow burial diagenesis which initiate numerous cycles of solution, reprecipitation and modification result in the dominance of robust crystalline/alpha fabrics (Chadwick and Nettleton, 1990) within mature carbonates and 'passive' cementation associated with beta fabrics (Wright and Tucker, 1991) within immature carbonates.

12.4 A Holistic Lithostratigraphy within the Kalahari

Duricrusts form a significant part of the Kalahari Group lithostratigraphy and investigation of the processes and mechanisms responsible for their formation has to been seen within the context of their depositional environment and the development of the Kalahari Basin. Research and insight on sedimentation within the Kalahari Basin is limited (e.g. Bootsman, 1997, 1998; Haddon, 1999, 2000, 2001; Haddon and McCarthy, 2005; De Wit, 2007) with the southern sector of the basin being the only region where enough information is available to attempt a synthesis with the aim of defining the lithostratigraphy and identifying possible formations.

The development of the southern rim of the Kalahari Basin occurred towards the end of the Cretaceous as a result of continental down-warping (Smit 1977; Gould *et al.* 1987; Thomas and Shaw, 1991; Bootsman, 1997, 1998; Haddon and

McCarthy, 2005). However, it was uplift along the Griqualand-Transvaal Axis during the early Miocene which is believed to have had the most significant effect on sedimentation in the southern sag basin of the Kalahari. The various sub-basins, Aranos/Nossob in the south-west and the Molopo Basin in the south-east, are believed to have become regionally significant depocentres during this phase of Neogene tectonic activity. Evidence for the Miocene initiation of sedimentation within these sub-basins, rather than in the Late Cretaceous as proposed by Bootsman (1997, 1998), is based on the lack of duricrusts older than the Late Miocene within the sedimentary sequences of the southern Kalahari. There is, however, evidence of the basal gravels of the Obobogorop and Wessels formations lying unconformably upon calcrete remnants and weathered Dwyka and Nama Group sediments (Thomas, 1981). Therefore if the Wessels and Budin formations had been accumulating within the southern Kalahari sub-basins during the Late Cretaceous and Early Palaeocene as suggested, they would contain a number of well developed duricrust sequences correlating with the global and southern African Palaeocene duricrust sequences associated with aridification at the K/T boundary (Gassaway 1988; Partridge and Maud, 1989) and not rest unconformably upon weathered calcrete remnants, conglomerate and basement saprolite. Rather it is proposed in line with De Wit *et al.* (2000) that during the early stages of the Kalahari Basin's development, the Late Cretaceous climate was changing from warm and humid to more arid (Tyson and Partridge, 2000). The result of this was that the deeply weathered mantles of the African Surface (Partridge and Maud, 1987) developed on the basement Karoo Geology were at least partially preserved despite widespread erosion in southern Africa during the Maastrichtian (Dingle *et al.* 1983). It was on these deeply weathered profiles that

the duricrusts, principally calcretes and silcretes of the Palaeocene developed. Then during the more mesic Eocene and Oligocene and principally the subtropical Early Miocene (24-15 Ma) the duricrust armoured profiles of the Cretaceous saprolite (African Surface) were eroded by the Post-African I cycle. This material was deposited in offshore deposits (Dingle *et al.* 1983) and within the depocentres of the southern Kalahari as the basal gravel conglomerate known as the Obobogorop formation (Thomas, 1981). Poorly sorted structureless fluvial gravel valley infill horizons are characteristic of basal Kalahari Group sediments throughout the Mega-Kalahari Basin (Rogers, 1936; Hugo, 1969; Gould *et al.*, 1987) and attest to periods of energetic fluvial erosion.

The gravels and clay gravels of the Wessels and Budin formations (Thomas 1981; Thomas *et al.* 1988; Behr, 1989; Thomas and Thomas 1989), which also contain eroded remnants of the African surface material, were initially deposited within a low-energy system restricted to the pre-Kalahari palaeo-valleys (Haddon, 2001). These depositional facies took advantage of the topography which had been back-tilted and eroded during the Paleogene. Later as deposition and down-warping continued, deposition occurred within a palustrine/lacustrine environment (*c.f.* Alonso-Zarza *et al.*, 1992a,b; Alonso-Zarza and Calvo, 2000). It is believed, based on the coarsening upwards cyclothems and facies assemblages, that deposition within this low energy fluvial and lacustrine environment changed to the higher energy floodplain and fluvial sediments of the Eden and Mokalanen formations. These poorly sorted sediments are characterised by Mg-rich clays, red coloured iron coated (limonite) grains indicative of vadose oxidation and calcareous (calcite and dolomite) cementation, which supports a semi-arid alluvial

fan/floodplain depositional environment (Alexander and Fielding, 2006), and mixed phreatic and vadose diagenesis (Pimentel *et al.*, 1996).

The textural change from the Budin to the Eden formation is believed to be not only due to aridification during the Middle and Late Miocene (De Wit *et al.*, 2000; Westerhold *et al.*, 2005), which resulted in more flashy seasonal fluvial systems and enhanced physical weathering, but also to the change in the geometry of the depocentre. Reduced back-tilting and down-warping tectonic activity caused the pre-Kalahari topography to be infilled and thus resulted in the expansion of sedimentation into the greater basin. Eastward expansion of the palaeo-Molopo's catchment into areas of higher precipitation and similar headward erosion by its tributaries during the Miocene may have resulted in the capture and reorientation of other neighbouring systems. This increased fluvial activity would have had major implications for the system's competence and capacity which would have supplemented regional climatic change (Westerhold *et al.*, 2005).

It is believed that the denudational processes of the Post-African I cycle during the Palaeogene and Early Neogene resulted in the erosion of the African Surface, exposing the pre-Kalahari topography of the basement Karoo and Nama Group sediments. Early Miocene uplift along the Griqualand-Transvaal Axis, combined with wetter climatic conditions during the same period, were the principal mechanisms responsible for the orientation of the palaeo-Molopo and the commencement of sedimentation. The cumulative result was that the basal Kalahari Group sediments in the southern Kalahari were deposited initially within

the pre-Kalahari topography controlled valleys/sub-basins as a basal conglomerate which fined-upwards into a lacustrine deposit. This sequence then coarsens-upwards (Budin-Eden-Mokalanen formations) which reflects increasingly energetic seasonal fluvial systems which expanded as aggrading alluvial fans beyond the pre-Kalahari topography into the greater depocentre of the southern Kalahari Basin.

Based purely on the facies and lithostratigraphy of the various formations it is proposed that the Wessels formation gravels and overlying Budin formation clays accumulated during the Early Miocene. The transition from the warm and humid Early Miocene to the drier and cooler conditions of the Middle and Late Miocene in southern Africa is attributed to climate forcing responding to fluctuations in the amplitude of eccentricity and obliquity (Westerhold *et al.*, 2005) in phase with the world-wide long-term cooling and the resultant late Miocene glacial events in the high latitudes believed to be a result of the buildup of the East Antarctic Ice Sheet (Zachos *et al.*, 2001a,b). Within the Kalahari Group sediments this palaeo-climatic and resultant environmental change is evidenced by the increasing gravel (a common principal component of Miocene fluvial deposits) and sand component which implies increased physical weathering and a waning detrital clay content which is indicative of chemical weathering of bedrock within the catchment. The facies variation up-profile also indicates an evolution within the drainage from closed lacustrine to playa to open high energy fluvial floodplain. This is believed to be the result of expansion of the depocentre into the surrounding Kalahari Basin as a result of termination of Miocene upwarping along the Griqualand-Transvaal Axis which controlled the sub-basin's architecture (Fig 58). The increase in

oxidised haematite/limonite along with the increasing carbonate, dolomite and sepiolite/palygorskite contents of the Budin, Eden and Mokalanen formations is believed to be indicative of semi-arid conditions and seasonal desiccation.

Increasing desiccation within the system during the Middle and Upper Miocene is reflected by the gradational boundary between the clay rich Budin formation and the overlying sandier textured Eden formation. The sediments of the Eden formation were deposited under sporadic flow conditions principally as sheetflood deposits within an anastomosing system (horizons showing cross-bedding have been described by Thomas (1981)) which indicate a high energy fluvial system operating under arid and semi-arid climatic conditions (Alexander and Fielding, 2006). The sediments bear witness to the increased physical weathering and mixed phreatic and vadose chemical cementation. The overlying Mokalanen formation consists of three units: a dolo/calc-conglomerate, a nodular grading to massive calcitic dolomite/dolomite (also referred to incorrectly (according to the classification system of Adams *et al.* (1984)) as the sandy limestone (dolomite is the dominant cement as a result of calcite replacement) units) and an upper hardpan calcrete (Thomas, 1981; Johnson, 1994).

Carbonate cemented 'limestone' formations cap the Kalahari Group sediments not only in the southern part of the Kalahari Basin but also in the northwestern part of the basin as the 'Etosha limestone' (Buch *et al.*, 1992). This is indicative of the widespread decline and ultimate termination of fluvial sedimentation, although it is highly unlikely this occurred as a synchronised event. It was followed by stabilisation and pedogenesis within the basin under predominantly semi-arid

climatic conditions. If one assumes that sedimentation ceased within the southern Kalahari towards the end of the Neogene the average rate of Kalahari Group accumulation within the southern basin was extremely low (in the region of approximately 20 mm ka^{-1}).

This pluvial phase, unlike the almost tropical conditions that prevailed during the Early Miocene, was wet enough to support open savanna vegetation. It was during this period that the majority of pedogenic calcretes are believed to have formed. This initiation of calcrete formation supports the proposals of Watts (1980) for episodic calcrete formation in the southern Kalahari since the Pliocene and the four major episodes of calcrete formation (Pliocene, Mid-Pleistocene, Upper Pleistocene and Late Pleistocene to Recent times) proposed by Netterberg (1980). The timing for the initiation of groundwater carbonate cementation within the Kalahari Group sediments is far less apparent. It is believed that the carbonate rich groundwater associated with the Malmani dolomites played a significant role in the initial calcite cementation and later dolomitisation of the Eden and Mokalanen sandstone sequences during the Miocene. The lowering of the groundwater table in the vicinity of the Malmani dolomites as a result of the Late Miocene/Pliocene diastrophic uplift along the Griqualand-Transvaal axis (Mayer, 1973) would have had a substantial effect on the hydrochemistry of the Molopo system and the transition from phreatic cementation to vadose epigenesis and cementation within the Kalahari sediments.

In line with the SACS approved lithostratigraphy of the Karoo Basin, which underlies the majority of the Mega Kalahari Basin and extends from South Africa

northwards into Namibia and Botswana, it is recommended that the proposed lithostratigraphy of Kalahari Group sediments in the Northern Cape (Table 7) be applied to equivalent lithologies and be supplemented with new formations and members throughout the basin with any necessary revisions to type-sections. The most apparent application of this lithotype is the Mokalanen formation which can be mapped over a vast area of the central and southern Kalahari. It is strongly believed that despite the complexity of Kalahari Group sequence stratigraphy, if the lithostratigraphy is mapped in a holistic and detailed manner then a far better understanding of facies assemblages, depositional and palaeoenvironments can be achieved. The present regionalised lithostratigraphies often reflect nothing more than lateral facies assemblages, i.e. members, of formations mapped elsewhere. The construction of a clearer lithostratigraphy, which can then be supplemented on a regional scale by investigation of chrono- and bio-stratigraphies, is undoubtedly the first step to understanding Kalahari sequence stratigraphy.

12.5 Conclusion

The chemical sediments of the Kalahari Basin cover an extensive area from South Africa to the DRC (Shaw and Goudie, 2002) and characterise a range of geomorphic environments. Investigation has revealed that despite the diversity of environmental and depositional settings the processes responsible for precipitation, epigenesis and paragenesis of these sediments are fairly uniform under semi-arid conditions. A combination of the location of precipitation and geochemical parameters dictates the characteristics of the chemical sediments. Exploration of phreatic, fluvial channel and saline pan environments has indicated that authigenic silica precipitation is dominant while desiccated lacustrine and

palustrine sediments suggest the dominance of calcite precipitation. The epigenesis of desiccated former phreatic and pan sediments indicates that calcretisation and dolomitisation are the dominant processes principally as a result of increased vadose and pedogenic diagenesis.

Pedogenic sequences within the Kalahari have formed within low productivity, low biomass and water stressed environments. However, it is apparent that despite differences from other vadose and pedogenic environments microbial and biogeochemical activity within the Kalahari is far more significant than preserved structures suggest. It is suggested that the complex and typically intergrade mineralogical assemblages encountered within these depositional environments are not always a direct result of purely physicochemical reactions, although it is highly probable that these are dominant. This study has indicated that the role of biotic processes in carbonate precipitation appears to be linked not only to cool semi-arid climatic conditions but also to particular savanna biomes, with increased C_3 vegetation supporting pedogenic calcrete precipitation.

Identification of the vegetation communities contributing SOM and CO_2 at the time of carbonate precipitation indicated that periods of pedogenic carbonate accumulation are associated with mixed C_3/C_4 savanna vegetation that generally shows higher levels of C_3 vegetation than most of the contemporary communities associated with carbonate deposits. This suggests increased precipitation associated with higher levels of atmospheric CO_2 and cooler climatic conditions, although there is abundant evidence to suggest contemporary vadose carbonate precipitation at a number of sites.

13. REFERENCES

Adams, A.E. and MacKenzie, W.S. 1998. A colour atlas of carbonate sediments and rocks under the microscope. Manson Publishing, London, 180 pp.

Adams, A.E., MacKenzie, W.S. and Guilford, C. 1984. Atlas of sedimentary rocks under the microscope. Longman, London, 104 pp.

Adams, S., Titus, R., Pietersen, K., Tredoux, G., Harris, C. 2001. Hydrochemical characteristics of aquifers near Sutherland in the western Karoo, South Africa. *Journal of Hydrology*, **241**: 91-103.

Alemaw, F., Ashworth, J.M. and Hughes, D. 2003. Hydrology of the Okavango Delta (Summary), Water Resources Consultants (Pty) Ltd.

Alexander, J. and Fielding, C.R. 2006. Coarse-grained floodplain deposits in the seasonal tropics: towards a better facies model. *Journal of Sedimentary Research*, **76**: 539– 556.

Allen, B.L. 1985. Micromorphology of Aridsols. In: Soil Micromorphology and Soil Classification (Eds L.A. Douglas and M.L. Thompson), No. 15, pp. 197-216. Soil Science Society of America Special Publication.

Allen, J.R.L. 1974. Sedimentology of the Old Red Sandstone (Siluro-Devonian) in the Clee Hills area, Shropshire, England. *Sedimentary Geology*, **12**: 73-167.

Allsopp, N. and Stock, W.D. 1995. Relationships between seed reserves, seedling growth and mycorrhizal responses in fourteen related shrub (Rosidae) from a low nutrient environment. *Functional Ecology*, **9**: 248-54.

Alonso-Zarza, A.M. 1999. Initial stages of laminar calcrete formation by roots: examples from the Neogene of central Spain. *Sedimentary Geology*, **126**: 177-191.

Alonso-Zarza, A.M. 2003. Palaeoenvironmental significance of palustrine carbonates and calcretes in the geological record. *Earth-Science Reviews*, **60**: 261-298.

Alonso-Zarza, A.M. and Calvo, J.P. 2000. Palustrine sedimentation in an episodically subsiding basin: the Miocene of the northern Teruel Graben (Spain). *Palaeogeography, Palaeoclimatology, Palaeoecology*, **160**: 1 –21.

Alonso-Zarza, A.M., Calvo, J.P. and Garcia del Cura, M.A. 1992. Palustrine sedimentation and associated features - grainification and pseudo-microkarst - in the Middle Miocene (Intermediate Unit) of the Madrid Basin, Spain. *Sedimentary Geology*, **76**: 43– 61.

Alonso-Zarza, A.M., Silva, P.G., Goy, J.L. and Zazo, C. 1998. Fan-surface dynamics and biogenic calcrete development: Interactions during ultimate phases of fan evolution in the semiarid SE Spain (Murcia). *Geomorphology*, **24**: 147-167.

Amundson, R.G., Chadwick, O.A., Sowers, J.M. and Doner, H.E. 1989. The stable isotope chemistry of pedogenic carbonates at Kyle Canyon, Nevada. *Soil Science Society of America Journal*, **53**: 201-210.

Anadon, P., Rosell, L. and Talbot, M.R. 1992. Carbonate replacement of lacustrine gypsum deposits in two Neogene continental basins, eastern Spain. *Sedimentary Geology*, **78**: 201-216.

Anadon, P., Utrilla, R. and Vazquez, A. 2000. Use of charopyte carbonates as proxy indicators of subtle hydrological and chemical changes in marl lakes:

example form the Miocene Bicorb Basin, eastern Spain. *Sedimentary Geology*, **133**: 325– 347.

Andersson, L., Gumbricht, T., Hughes, D., Kniveton, D., Ringrose, S., Savenije, H., Todd, M., Wilk, J. and Wolski, P. 2003. Water flow dynamics in the Okavango River Basin and Delta - A prerequisite for the ecosystems of the Delta. *Physics and Chemistry of the Earth*, **28**: 1165-1172.

Arakel, A.V. 1982. Genesis of calcrete in Quaternary soil profiles, Hutt and Leeman lagoons, Western Australia. *Journal of Sedimentary Petrology*, **52**: 109-125.

Arakel, A.V. 1986a. Evolution of calcrete in palaeodrainages of the Lake Napperby area, central Australia. *Palaeogeography, Palaeoclimatology, Palaeoecology*, **54**: 283-303.

Arakel, A.V. 1986b. Silicification of calcrete in palaeodrainage basins of the Australian arid zone. *Australian Journal of Earth Sciences*, **36**: 73-89.

Arakel, A.V. 1991. Evolution of Quaternary duricrusts in Karinga Creek drainage system, central Australian groundwater discharge zone. *Australian Journal of Earth Sciences*, **38**: 333-347.

Arakel, A.V. and McConchie, D. 1982. Classification and genesis of calcrete and gypsite lithofacies in palaeodrainage systems of inland Australia and their relationship to carnotite mineralisation. *Journal of Sedimentary Petrology*, **52**: 1149-1170.

Arakel, A.V. and Cohen, A. 1991. Deposition and early diagenesis of playa glauberite in the Karinga Creek drainage system, Northern Territory, Australia. *Sedimentary Geology*, **70**; 41-59.

Arakel, A.V. and Hongjun, T. 1994. Seasonal evaporite sedimentation in desert playa lakes of the Karinga Creek drainage system, central Australia. Sedimentology and geochemistry of modern and ancient saline lakes. Special Publication SEPM (Society for Sedimentary Geology), **50**.

Arakel, A.V., Jacobson, G., Salehi, M. and Hill, C.M. 1989. Silicification of calcrete in palaeodrainage basins of the Australian arid zone. *Australian Journal of Earth Sciences*, **36**: 73-89.

Arenas, C., Alonso-Zarza, A.M. and Pardo, G. 1999. Dedolomitization and other early diagenetic processes in Miocene lacustrine deposits, Ebro Basin (Spain). *Sedimentary Geology*, **125**: 23-45.

Arkley, R.J. 1963. Calculation of carbonate and water movement in soil from climatic data. *Soil Science*, **96**: 239-248.

Badiozamani, K. 1973. The Dorag dolomitisation model: application to the Middle Ordovician of Wisconsin. *Journal of Sedimentary Petrology*, **43**: 965-985.

Bailey, C.L. 1994. The distribution and Functioning of Rhizosheaths among South African Grass Species. MSc Thesis, University of the Witwatersrand, Johannesburg.

Bal, L. 1975. Carbonate in soils: a theoretical consideration on, and proposal for its fabric analysis. I and II. *Netherlands Journal of Agricultural Science*, **23**: 163-176.

Balfour, D. and Balfour, S. 1992. Etosha. Struik Publishers, Cape Town, South Africa.

Bauer, P., Thabeng, G., Stauffer, F. and Kinzelbach, W. 2004. Estimation of the evapotranspiration rate from diurnal groundwater level fluctuations in the Okavango Delta, Botswana. *Journal of Hydrology*, **288**: 344-355.

Baver, L.D., Gardner, W.H. and Gardner, W.R. 1972. Soil Physics. Wiley, New York.

Beerling, D.J. and Royer, D.L. 2002. Fossil plants as indicators of the Phanerozoic global carbon cycle. *Annual Review of Earth and Planetary Sciences*, **30**: 527-556.

Beetz, P.F.W. 1934. Geology of South West Angola, between Cunene and Lunda Axis. *Transactions of the Geological Society of South Africa*, **36**: 137-176.

Behr, S.H. 1989. The thickness of the Kalahari Group sediments in the proto-Molopo River basin. In: Abstract 9th Biennial SASQUA Conference, 22, Durban.

Beier, J.A. 1987. Petrographic and geochemical analysis of caliche profiles in a Bahamian Pleistocene Dune. *Sedimentology*, **34**: 991-998.

Bekker, R.P. and De Wit, P.V. 1991. Contribution to the vegetation classification of Botswana., FAO/UNDP Soil Mapping and Advisory Services, Gaborone.

Berglund, B.E. 1986. Handbook of Holocene palaeoecology and palaeohydrology. Wiley.

Berner, R.A. 1991. A model for atmospheric CO2 over Phanerozoic time. *American Journal of Science*, **291**: 339-376.

Berry, C. 1991. Trees and Shrubs of the Etosha National Park. Directorate of Nature Conservation, Windhoek, Namibia.

Berry, H.H., Stark, H.P. and van Vuuren, A.S. 1973. White Pelicans Pelecanus onocrotalus breeding on the Etosha Pan, South West Africa, during 1971. *Madoqua*, **1**: 17-31.

Bhalotra, Y.P.R. 1987. Climate of Botswana, Part II: Elements of climate 1, 2 and 4., Department of Meteorological Services, Gaborone.

Birkeland, P.W. 1984. Soils and Geomorphology. Oxford University Press, New York.

Blank, H.R. and Tynes, E.W. 1965. Formation of caliche in situ. *Geological Society of America Bulletin*, **76**: 1387-1392.

Blokhuis, W.A., Pape, T. and Slager, S. 1968. Morphology and distribution of pedogenic carbonate in some Vertisols of the Sudan. *Geoderma*, **2**: 173-200.

Blott, S. 2000. GRADISTAT: A Grain Size Distribution and Statistics Package for the Analysis of unconsolidated Sediments by Sieving or Laser Granulometer. Version 4.0. Surface Processes and Modern Environments Research Group, Department of Geology, Royal Holloway, University of London., London.

Blumel, W.D. 1979. Zur Struktur, Reliefgebundenheit und Genese sudwestafrikanischer und sudostspanischer Kalkkrusten. *Zietscrift fur Geomorphologie N.F. Suppl. Bd.*, **36**: 154-167.

Blumel, W.D. 1982. Calcretes in Namibia and SE-Spain: relations to substratum, soil formation and geomorphic factors. In: Aridic Soils and Geomorphic Processes (Ed D. Yaalon), 1, pp. 67-82. Catena Supplement.

Blumel, W.D., Eitel, B. and Lang, A. 1998. Dunes in southeastern Namibia: evidence for Holocene environmental changes in the southwestern Kalahari

based on thermoluminescence data. *Palaeogeography, Palaeoclimatology, Palaeoecology*, **138**: 139-149.

Boggs, S.J. 1995. Principles of Sedimentology and Stratigraphy. Prentice-Hall, Inc., New Jersey.

Bohacs, K.M., Carroll, A.R., Neal, J.E. and Mankiewicz, P.J. 2000. Lake-basin type, source potential, and hydrocarbon character: an integrated-sequence-stratigraphic – geochemical framework. In: Lake Basins through Space and Time. (Eds E.H. Gierlowski-Kordesch and K.R. Kelts), 46, pp. 3 –34. AAPG Studies in Geology, Tulsa, OK.

Boocock, C. and Van Straten, D.J. 1962. Notes on the geology and hydro-geology of the central Kalahari, Bechuanaland Protectorate. *Transactions of the Geological Society of South Africa*, **5**: 125-171.

Bootsman, C.S. 1997. On the evolution of the upper-Molopo Drainage. *South African Geographical Journal*, Special Edition: 83-92.

Bootsman, C.S. 1998. The evolution of the Molopo drainage. Unpublished Ph.D., University of the Witwatersrand, Johannesburg.

Bosak, T. and Newman, D.K. 2005. Microbial kinetic controls on calcite morphology in supersaturated solutions. *Journal of Sedimentary Research*, **75**: 190-199.

Bothma, J.P. and De Graaf, G. 1973. A habitat map of the Kalahari Gemsbok National Park. *Koedoe*, **16**: 181-188.

Bourke, M.C. and Pickup, G. 1999. Fluvial form variability in arid central Australia. In: Varieties of Fluvial Form. (Eds A.J. Miller and A. Gupta). John Wiley and Sons, Chichester.

Braissant, O., Chailleau, G., Aragno, M. and Verrecchia, E.P. 2004. Biologically induced mineralization in the tree Milicia excelsa (Moraceae); its causes and consequences to the environment. *Geobiology*, **2**: 59-66.

Brehm, U., Gorbushina, A. and Mottershead, D. 2005. The role of microorganisms and biofilms in the breakdown and dissolution of quartz and glass. *Palaeogeography, Palaeoclimatology, Palaeoecology*, **219**: 117-129.

Brewer, R. 1964. Fabric and Mineral Analysis of Soils. Wiley, New York, 470 pp.

Brewer, R. 1972. The basis of interpretation of soil micromorphological data. *Geoderma*, **8**: 81-95.

Brewer, R. 1976. Fabric and mineral analyses of soils. Wiley & Sons, New York, 470 pp.

British Geological Survey and Wellfield Consulting Services 1994. Matsheng area groundwater investigation (TB 10/2/12/92-93). Technical report T3: inventory report, Botswana.

British Geological Survey and Wellfield Consulting Services 1996. Matsheng area groundwater investigation - final report.

Brook, G.A., Cowart, J.B. and Marais, E. 1996. Wet and dry periods in the southern African summer rainfall zone during the last 330 kyr from speleothem, tufa and sand dune age data. *Palaeoecology of Africa*, **24**: 147-158.

Brown, C.N. 1956. The origin of caliche on the Northeastern Llano Estacado, Texas. *The Journal of Geology*, **64**: 1-14.

Bruno, S.A. 1983. Pan genesis in the southern Kalahari. In: The proceedings of a seminar on the mineral exploration of the Kalahari October 1980. (Eds D.G.

Hutchins and A.P. Lynam), Bulletin 29, pp. 261-277. Geological Survey Department, Lobatse, Botswana.

Bryant, R.G. 2003. Monitoring hydrological controls on dust emissions: preliminary observations from Etosha Pan, Namibia. *The Geographical Journal*, **169**: 131-141.

Buch, M.W. and Rose, D. 1996. Mineralogy and geochemistry of the sediments of the Etosha Pan Region in northern Namibia: a reconstruction of depositional environment. *Journal of African Earth Sciences*, **22**: 355-378.

Buch, M.W., Rose, D. and Zoller, L. 1992. A TL-calibrated pedostratigraphy of the western lunette dunes of Etosha Pan/northern Namibia: Palaeoenvironmental implications for the last 140 ka. *Palaeoecology of Africa*, **23**: 129-147.

Budd, D.A., Pack, S.M. and Fogel, M.L. 2002. The destruction of paleoclimatic isotopic signals in Pleistocene carbonate soil nodules of Western Australia. *Palaeogeography, Palaeoclimatology, Palaeoecology*, **188**: 249-273.

Bull, W.B. 1997. Discontinuous ephemeral streams. *Geomorphology*, **19**: 227-276.

Bullard, J.E. and Nash, D.J. 1998. Linear dune pattern variability in the vicinity of dry valleys in the southwest Kalahari. *Geomorphology*, **23**: 35-54.

Bullard, J.E. and Nash, D.J. 2000. Valley-marginal sand dunes in the south-west Kalahari: Their nature, classification and possible origins. *Journal of Arid Environments*, **45**: 369-383.

Bullard, J.E., Thomas, D.S.G., Livingstone, I. and Wiggs, G.F.S. 1995. Analysis of linear sand dune morphological variability, southwestern Kalahari Desert. *Geomorphology*, **11**: 189-203.

Bullard, J.E., Thomas, D.S.G., Livingstone, I. and Wiggs, G.F.S. 1997. Dunefield activity and interactions with climatic variability in the southwest Kalahari Desert. *Earth Surface Processes and Landforms*, **22**: 165-174.

Burford, E.P., Fomina, M. and Gadd, G.M. 2003a. Fungal involvement in bioweathering and biotransformation of rocks and minerals. *Mineral Magazine*, **67**: 1127-1155.

Burford, E.P., Kierans, M. and Gadd, G.M. 2003b. Geomycology: fungi in mineral substrata. *Mycologist*, **17**: 98-107.

Burmeister Consulting 1996. Prefeasibilty Report for the Epupa Dam Scheme, Namibian Department of Water Affairs, Windhoek.

Bustillo, M.A. and Bustillo, M. 2000. Miocene silcretes in argillaceous playa deposits, Madrid Basin, Spain: petrological and geochemical features. *Sedimentology*, **47**: 1023-1037.

Bustillo, M.A., Arribas, M.E. and Bustillo, M. 2002. Dolomitization and silicification in low-energy lacustrine carbonates (Paleogene, Madrid Basin, Spain). *Sedimentary Geology*, **151**: 107-126.

Butterworth, J.S. 1982. The Chemistry of Mogatse pan - Kgalagadi District. Unpublished Report JSB/14/82, Botswana Geological Survey, Lobatse.

Butzer, K.W., Stuckenrath, R., Bruzewicz, A.J. and Helgren, D.M. 1978. Late Cenozoic paleoclimates of the Gaap Escarpment, Kalahari margin, South Africa. *Quaternary Research*, **10**: 310-339.

Cabrera, L. and Saez, A. 1987. Coal deposition in carbonate-rich shallow lacustrine systems: the Calaf and Mequinenza sequences (Oligocene, eastern Ebro Basin, NE Spain). *Journal Geological Society London*, **144**: 451–461.

Callen, R.A., Wasson, R.J. and Gillespie, R. 1983. Reliability of radiocarbon dating of pedogenic carbonate in the Australian arid zone. *Sedimentary Geology*, **35**: 1-14.

Callot, G., Guyon, A. and Mousain, D. 1985. Inter-relations entre aiguilles de calcite et hyphes myceliens. *Agronomie*, **5**: 209-216.

Calvet, F. 1982. Constructive micrite envelopes developed in vadose continental environments in Pleistocene eolianites of Mallorca (Spain). *Acta. Geologica Hispanica*, **17**: 169-178.

Calvet, F. and Julia, R. 1983. Pisoids in the calcite profiles of Tarragona, north-east Spain. In: Coated Grains (Ed T.M. Peryt), pp. 456-473. Springer-Verlag, Berlin.

Calvo, J.P., Jones, B.F., Bustillo, M., Fort, R., Alonso-Zarza, A.M. and Kendall, C. 1995. Sedimentology and geochemistry of carbonates from lacustrine sequences in the Madrid Basin, Central Spain. *Chemical Geology*, **123**: 173–191.

Calvo, J.P., Blanc-Valleron, M.M., Rodriguez-Arandia, J.P., Rouchy, J.M. and Sanz, M.E. 1999. Authigenic clay minerals in continental evaporitic environments. Special Publication International Association of Sedimentologists 27, 129–151 pp.

Canaveras, J.C., Sanchez-Moral, S., Calvo, J.P., Hoyos, M. and Ordonez, S. 1996. Dedolomites associated with karstification: an example of early dedolomitization in lacustrine sequences form the tertiary Madrid basin, Central Spain. *Carbonates and Evaporites*, **11**: 85– 103.

Candy, I. 2002. Quaternary climate change and landform development in southeast Spain: U-series dating of calcretes. PhD, University of Reading, Reading, UK.

Candy, I., S., B., Sellwood, B.W. and Rowan, J.S. 2003. Calcrete profile development in Quaternary alluvial sequences, southeast Spain: implications for using calcretes as a basis for landform chronologies. *Earth Surface Processes and Landforms*, **28**: 169-185.

Capo, R.C. and Chadwick, O.A. 1999. Sources of Strontium and Calcium in desert soil and calcrete. *Earth and Planetary Science Letters*, **170**: 61-72.

Carlisle, D. 1983. Concentration of uranium and vanadium in calcretes and gypcretes. In: Residual Deposits (Ed R.C.L. Wilson), pp. 185-195. Geological Society of London Special Publication No. 11, London.

Carney, J.N., Aldiss, D.T. and Lock, N.P. 1994. The geology of Botswana., Bulletin 37. the Director, Geological Survey Department, Lobatse, Botswana.

Carroll, A.R. and Bohacs, K.M. 1999. Stratigraphic classification of ancient lakes: balancing tectonic and climatic controls. *Geology*, **27**: 99-102.

Castañeda, C., Herrero, J. and Casterad M.A. 2005. Facies identification within the playa-lakes of the Monegros Desert, Spain, from field and satellite data. *Catena*, **63**: 39-63.

Cecil, C.B. 1990. Paleoclimate controls on stratigraphic repetition of chemical and siliciclastic rocks. *Geology*, **18**: 533-536.

Cerling, T.E. 1984. The stable isotope composition of modern soil carbonate and its relationship to climate. *Earth and Planetary Science Letters*, **71**: 229-240.

Cerling, T.E. 1991. Carbon dioxide in the atmosphere: evidence from Cenozoic and Mesozoic paleosols. *American Journal of Science*, **291**: 377-400.

Cerling, T.E. 1999. Stable carbon isotopes in palaesol carbonates. In: Palaeoweathering, Palaeosurfaces and Related Continental Deposits (Eds M. Thiry and R. Simon-Coincon), Special publication No. 27 of the International Association of Sedimentologists, pp. 43-60. Blackwell Science, Oxford.

Cerling, T.E. and Hay, H.L. 1986. An isotope study of palaeosol carbonates from Olduvai Gorge. *Quaternary Research*, **25**: 63-78.

Cerling, T.E. and Quade, J. 1993. Stable Carbon and Oxygen isotopes in soil carbonates. In: Climate Change in Continental Isotopic Records, Geophysical Monograph 78, pp. 217-231. American Geophysical Union.

Cerling, T.E., Hay, R.L. and O'Neil, J.R. 1977. Isotopic evidence for dramatic climatic changes in East Africa during the Pleistocene. *Nature*, **267**: 137-138.

Cerling, T.E., Quade, J., Wang, Y. and Bowman, J.R. 1989. Carbon isotopes in soils and palaeosols as ecology and palaeoecology indicators. *Nature*, **341**: 138-139.

Cerling, T.E., Wright, V.P. and Vanstone, S.D. 1992. Further comments on using carbon isotopes in palaeosols to estimate the CO2 content of the palaeo-atmosphere. *Journal of the Geological Society*, **149**: 673-676.

Cerling, T.E., Harris, J.M., MacFadden, B.J., Leakey, M.G., Quade, J., Eisenmann, V. and Ehleringer, J.R. 1997. Global vegetation change through the Miocene-Pliocene boundary. *Nature*, **389**: 153-158.

Cerling, T.E., Ehleringer, J.R. and Harris, J.M. 1998. Carbon dioxide starvation, the development of C4 ecosystems, and mammalian evolution. *Philosophical Transactions of the Royal Society of London Series B Biological Sciences*, **353**: 159-171.

Chadwick, O.A. and Nettleton, W.D. 1990. Micromorphological evidence of adhesive and cohesive forces in soil cementation. In: Soil Micromorphology: A Basic and Applied Science (Ed L.A. Douglas), Developments in Soil Science No. 19. Elsevier, Amsterdam.

Chadwick, O.A., Hendricks, D.M. and Nettleton, W.D. 1987. Silica in duric soils. I. A depositional model. *Soil Science Society of America Journal*, **51**: 975-982.

Chatupa, J.C. and Direng, B.B. 2000. Distribution of trace and major elements in the -180 + 75 mm and -75 mm fractions of the sandveld regolith in northwest Ngamiland, Botswana. *Journal of African Earth Sciences*, **30**: 515-534.

Clarke, J. 2003. The occurrence and significance of biogenic opal in the regolith. *Earth-Science Reviews*, **60**: 175-194.

Clow, D.W., Mast, M.A., Bullen, T.D. and Turk, J.T. 1997. Strontium 87/strontium 86 as a tracer of mineral weathering reactions and calcium sources in an alpine/subalpine watershed, Loch Vale, Colorado. *Water Research*, **33**: 1335-1351.

Cohen, A.S. 1982. Palaeoenvironments of root casts from the Koobi Formation, Kenya. *Journal of Sedimentary Petrology*, **52**: 401-414.

Coleman, M.L., Sheperd, T.J., Durham, J.J., Rouse, J.E. and Moore, G.R. 1982. Reduction of water with zinc for hydrogen isotope analysis. *Analytical Chemistry*, **54**: 993-995.

Cooke, H.J. 1975. The palaeoclimatic significance of caves and adjacent landforms in Western Ngamiland, Botswana. *Geographical Journal*, **141**: 430-444.

Cooke, H.J. 1976. The palaeogeography of the Middle Kalahari of northern Botswana. In: Proceedings of the Symposium on the Okavango Delta and its Future Utilisation, pp. 21-28. The Botswana Society, Gaborone.

Cooke, H.J. 1984. The evidence from northern Botswana of Late Quaternary climatic change. In: Late Cainozoic Palaeoclimates of the Southern Hemisphere. (Ed J.C. Vogel), pp. 265-78. Balkema, Rotterdam.

Cooke, H.J. and Verstappen, H.T. 1984. The landforms of northern Botswana, with a consideration of the chronology of the evolution of Lake palaeo-Makgadikgadi. *Zeitschrift fur Geomorphologie*, **28**: 1-19.

Craig, H. 1953. The geochemistry of the stable carbon isotopes. *Geochimica et Cosmochimica Acta*, **3**: 53-92.

Craig, H. 1961. Standards for reporting concentrations of deuterium and oxygen-18 in natural waters. *Science*, **133**: 1833.

Craig, H. 1965. The measurement of oxygen isotope paleotemperatures. In: Stable Isotopes in Oceanographic Studies and Paleotemperatures. (Ed V.E. Tongiorgi), pp. 161-182. Laboratorio di Geologia Nucleare, Pisa.

Cronberg, G., Gieske, A., Martins, E., Nengu, J.P. and Stenström, I.-M. 1995. Hydrobiological studies of the Okavango Delta and the

Kwando/Linyanti/Chobe River, Botswana. *Botswana Notes and Records*, **27**: 151-226.

Dames, J.F. 1991. The distribution of Vesicular Arbuscular Mycorrhizal Fungi in the Savanna Region of Nylsvley Nature Reserve in Relation to Soil Fertility Factors. MSc Thesis, University of the Witwatersrand, Johannesburg, RSA.

Das, A., Krishnaswami, S. and Bhattacharya, S.K. 2005. Carbon isotope ratio of dissolved inorganic carbon (DIC) in rivers draining the Deccan Traps, India: Sources of DIC and their magnitudes. *Earth and Planetary Science Letters*, **236**: 419–429.

De Deckker, P. and Last, W.M. 1988. Modern dolomite deposition in continental, saline lakes, western Victoria, Australia. *Geology*, **16**: 29-32.

De Ros, L.F., Morad, S. and Paim, P.S.G. 1994. The role of detrital composition and climate on the diagenetic evolution of continental molasses: evidence from the Cambro-Ordovician Guaritas Sequence, southern Brasil. *Sedimentary Geology*, **92**: 197–228.

De Vries, J.J., Selaolo, E.T. and Beekman, H.E. 2000. Groundwater recharge in the Kalahari, with reference to paleo-hydrologic conditions. *Journal of Hydrology*, **238**: 110-123.

De Wet, C., Yocum, D.A. and Mora, C. 1998. Carbonate lakes in closed basins: sensitive indicators of climate and tectonics: an example from the Gettysburg Basin (Triassic), Pennsylvania, USA. Role of Eustasy, Climate and Tectonism in Continental Rocks. Society of Economic Paleontologists and Mineralogists Special Publication, 59: 191–209.

De Wit, M. 2007. The Kalahari Epeirogeny and climate change: differentiating cause and effect from core to space. *South African Journal of Geology*, **110**: 367-392.

De Wit, M.C.J. 1981. A Geophysical and Geological Interpretation of part of the Diamondiferous Gravels on the Farm Grasfontein (356 JP), West of Bakerville. Unpublished M.Sc., University of Pretoria, RSA.

De Wit, M.C.J., Marshall, T.R. and Partridge, T.C. 2000. Fluvial Deposits and Drainage Evolution. In: The Cenozoic of Southern Africa. (Eds T.C. Partridge and R.R. Maud), pp. 55-72. Oxford University Press, Oxford.

De Wit, P.V. and Bekker, R.P. 1990. Explanatory note on the land systems map of Botswana., FAO/UNDP Soil Mapping and Advisory Services, Gaborone.

De Wit, P.V. and Nachtegaele, F.O. 1990. Explanatory note on the soil map of the Republic of Botswana., FAO/UNDP, Soil Mapping Advisory Service, Botswana.

Deines, P. 1980. The isotopic composition of reduced organic carbon. In: Handbook of Environmental Isotope Geochemistry. (Eds P. Fritz and J.C. Fontes), Vol. 1: The Terrestrial Environments, A, pp. 329-406. Elsevier, Amsterdam.

Delwiche, C.C. 1975. The geobiology of calcium. *Communications in Soil Science and Plant Analysis*, **6**: 207-218.

Deutz, P., Montanez, I.P., Mack, G.H. and Monger, H.C. 1995. Should stable isotope values of pedogenic carbonates be used in paleoclimatic reconstructions? The effects of diagenesis on the geochemistry of pedogenic carbonates. In: Annual Convention Program, 4. American Association of Petroleum Geologists.

Deutz, P., Montanez, I.P., Monger, H.C. and Morrison, J. 2001. Morphology and isotope heterogeneity of Late Quaternary pedogenic carbonates: Implications for paleosol carbonates as paleoenvironmental proxies. *Palaeogeography, Palaeoclimatology, Palaeoecology*, **166**: 293-317.

Dickson, J.A.D. 1990. Carbonate mineralogy and chemistry. In: Carbonate Sedimentology. (Eds M.E. Tucker and V.P. Wright), pp. 284-312. Blackwell Science Ltd, Oxford.

Dincer, T., Hutton, L.G. and Kupee, B.B.J. 1981. Study, using stable isotopes of flow distribution, surface- groundwater relations and evaportranspiration in the Okavango Swamp, Botswana. I.A.E.A. Proc., Ser. SII/AUB/493: 3-26.

Dincer, T., Child, S. and Khupe, B. 1987. A simple mathematical model of a complex hydrologic system - Okavango Swamp, Botswana. *Journal of Hydrology*, **93**: 41-65.

Dingle, R.V., Siesser, W.G. and Newton, A.R. 1983. Mesozoic and Tertiary Geology of Southern Africa. Balkema, Rotterdam.

Dogramaci, S.S. and Herczeg, A.L. 2002. Strontium and carbon isotope constraints on carbonate-solution interactions and inter-aquifer mixing in groundwaters of the semi-arid Murray Basin, Australia. *Journal of Hydrology*, **262**: 50-67.

Donner and Lynn 1989. Carbonate, Halide, Sulfate, and Sulfide Minerals. In: Minerals in Soil Environments (Eds J.B. Dixon and S.B. Weed) 2 edn, Number 1 in the Soil Science Society of America Book Series. Soil Science Society of America, Madison, Wisconsin, USA.

Drummond, C.N., Patterson, W.P. and Walker, J.C.G. 1995. Climatic forcing of carbon–oxygen isotopic covariance in temperate-region marl lakes. *Geology*, **23**: 1031-1034.

Du Toit, A.L. 1926. The Mier country. *South African Geographical Journal*, **9**: 21-6.

Du Toit, A.L. 1933. Crustal movement as a factor in the geographical evolution of South Africa. *South African Geographical Journal*, **16**: 3-20.

Du Toit, A.L. 1954. The Geology of South Africa. Oliver and Boyd, Edinburgh.

Dunagan, S.P. and Driese, S.G. 1999. Control of terrestrial stabilization on late Devonian palustrine carbonate deposition: Catskill Magnafacies, New York, U.S.A. *Journal of Sedimentary Research*, **69**: 772–783.

Dunham, R.J. (Ed), 1962. Classification of carbonate rocks according to depositional texture. (Ed W.E. Ham), Classification of carbonate rocks., Memoir 1. American Association of Petroleum Geologists, 108-121 pp.

Dunn, A.M., Silliman, S.E., Dhamwichukorn, S. and Kulpa, C.F. 2005. Demonstration of microbial transport into the capillary fringe via advection from below the water table. *Journal of Hydrology*, **306**: 50-58.

Dupont, L.M., Donner, B., Vidal, L., Perez, E.M. and Wefer, G. 2005. Linking desert evolution and coastal upwelling: Pliocene climate change in Namibia. *Geology*, **33**: 461-464.

Durand, J.H. 1959. Les sols rouges et les croutes en Algerie., Etude generale no. 7. Direction de l'hydraulique et de l'equipement rural, Birmandreis, Algerie, 188 pp.

Eckardt, F.D., Washington, R. and Wilkinson, J. 2001. The origin of dust on the West Coast of Southern Africa. *Palaeoecology of Africa*, **27**: 207-219.

Ehleringer, J.R., Cerling, T.E. and Helliker, B.R. 1997. C4 photosynthesis, atmospheric CO2, and climate. *Oecologia*, **112**: 285-299.

Ehleringer, J.R., Buchmann, N. and Flanagan, L.B. 2000. Carbon isotope ratios in below ground carbon cycle processes. *Ecological Applications*, **10**: 412-422.

Eitel, B. 1993. Kalkkrustengenerationen in Namibia: Carbonatherkunft und genetische Beziehungen. *Die Erde*, **124**: 85-104.

Eitel, B. 2000. Different amounts of pedogenic palygorskite in South West African Cenozoic calcretes: Geomorphological, paleoclimatical and methodological implications. *Zietscrift fur Geomorphologie N.F.*, **121**: 139-149.

Eitel, B. and Blumel, W.D. 1997. Pans and dunes in the southwestern Kalahari (Namibia): Geomorphology and evidence for Quaternary paleoclimates. *Zietscrift fur Geomorphologie N.F.*, **111**: 73-95.

Eitel, B., Blumel, W.D. and Huser, K. 2002. Environmental transitions between 22 ka and 8 ka in monsoonally influenced Namibia - A preliminary chronology. *Zietscrift fur Geomorphologie N.F.*, **126**: 31-57.

Ekart, D.D., Cerling, T.E., Montanez, I.P. and Tabor, N.J. 1999. A 400 million year carbon isotope record of pedogenic carbonate: implications for paleoatmospheric carbon dioxide. *American Journal of Science*, **299**: 805–827.

Elbersen, G.W.W. 1982. Mechanical replacement processes in mobile soft calcic horizons; their role in soil and landscape genesis in an area near Mérida, Spain. Doctoral Thesis, Wageningen, The Netherlands.

Ellery, K. and Ellery, W.N. 1997. Plants of the Okavango Delta. A field guide. Tsaro Publishers, Durban, 225 pp.

Ellery, W.N., Ellery, K., McCarthy, T.S., Cairncross, B. and Oelofse, R. 1989. A peat fire in the Okavango Delta, Botswana, and its importance as an ecosystem process. *African Journal of Ecology*, **27**: 7-21.

Ellery, K., Ellery, W.N. and Verhagen, B.T. 1992. The distribution of C-3 and C-4 plants in a successional sequence in the Okavango Delta. *South African Journal of Botany*, **58**: 400-402.

Ellery, W.N., Ellery, K. and McCarthy, T.S. 1993a. Plant distribution on islands in the Okavango Delta: determinants and feed back interactions. *African Journal of Ecology*, **31**: 118-134.

Ellery, W.N., Ellery, K., Rogers, K.H., McCarthy, T.S. and Walker, B.H. 1993b. Vegetation, hydrology and sedimentation processes as determinants of channel form and dynamics in the northeastern Okavango Delta, Botswana. *African Journal of Ecology*, **31**: 10-25.

Ellery, W.N., McCarthy, T.S. and Dangerfield, J.M. 1998. Biotic factors in mima mound development: evidence from the floodplains of the Okavango Delta, Botswana. *International Journal of Ecology and Environmental Sciences*, **24**: 293-313.

Ellery, W.N., McCarthy, T.S. and Smith, N.D. 2003. Vegetation, hydrology, and sedimentation patterns on the major distributary system of the Okavango Fan, Botswana. *Wetlands*, **23**: 357-375.

El-Sayed, M.I., Fairchild, I.J. and Spiro, B. 1991. Kuwaiti dolocrete: petrology, geochemistry and groundwater origin. *Sedimentary Geology*, **73**: 59-75.

Epstein, S. and Meyeda, T.K. 1953. Variations of the 18O/16O ratio in natural waters. *Geochimica et Cosmochimica Acta*, **4**: 1315-1326.

Esteban, M. 1976. Vadose pisolite and caliche. *The American Association of Petroleum Geologists Bulletin*, **60**: 2048-2057.

Esteban, M. and Klappa, C.F. 1983. Subaerial exposure environment. *Memoir of the American Association of Petroleum Geologists*, **33**: 1-54.

Eugster, H.P. 1967. Hydrous sodium silicates from Lake Magadi, Kenya; precursors of bedded chert. *Science*, **157**: 1177-1180.

Eugster, H.P. 1969. Inorganic bedded cherts from the Magadi area, Kenya. *Continental Mineralogy and Petrology*, **22**: 1-33.

Eugster, H.P. 1980. Lake Magadi, Kenya, and its precursors. In: Developments in Sedimentology: Hypersaline Brines and Evaporitic Environments (Ed A. Nissenbaum), 28, pp. 195-232. Elsevier.

Eugster, H.P. and Jones, B.F. 1979. Behaviour of major solutes during closed-basin brine evolution. *American Journal of Science*, **279**: 609-631.

Fedoroff, N., Country, M.A., Lacroix, E. and Oleschko, K. 1994. Calcitic accretion on indurated volcanic materials (example of tepetates, Altiplano, Mexico). In: Proceedings of the XVth World Congress of Soil Science, 6A, pp. 459–472, Acapulco.

Flach, K.W., Nettleton, W.D., Gile, L.H. and Cady, J.G. 1969. Pedocementation: induration by silica, carbonates, and sesquioxides in the Quaternary. *Soil Science*, **107**: 442-453.

Folk, R.L. 1954. The distinction between grain size and mineral composition in sedimentary rock nomenclature. *Journal of Geology*, **62**: 344-359.

Folk, R.L. 1959. Practical petrographic classification of limestones. *American Association of Petroleum Geologists, Bulletin*, **43**: 1-38.

Folk, R.L. 1962. Spectral subdivision of limestone types. In: Classification of carbonate rocks. (Ed W.E. Ham), Memoir 1, pp. 62-84. American Association of Petroleum Geologists.

Folk, R.L. 1968. Petrology of Sedimentary Rocks. Hemphill Publishing Company, Austin, Texas, 170 pp.

Folk, R.L. 1974. Petrology of sedimentary rocks. Hemphill Publishing Company, Austin, Texas, 182 pp.

Folk, R.L. and Ward, W.C. 1957. Brazos River bar: a study in the significance of grain size parameters. *Journal of Sedimentary Petrology*, **27**: 3-26.

Folk, R.L. and Pittman, J.S. 1971. Length-slow chalcedony: a new testament for vanished evaporites. *Journal of Sedimentary Petrology*, **41**: 1045-1058.

Folk, R.L. and Siedlecka, A. 1974. The 'schizohaline' environment: its sedimentary and diagenetic fabrics as exemplified by Late Paleozoic rocks of Bear Island, Svalbard. *Sedimentary Geology*, **11**: 1-15.

Freytet, P. 1973. Petrology and paleoenvironment of carbonated continental deposits with a particular reference to Upper Cretaceous and Lower Eocene of Languedoc (southern France). *Sedimentary Geology*, **10**: 25-60.

Freytet, P. and Plaziat, J.C. 1982. Continental carbonate sedimentation and pedogenesis - Late Cretaceous and Early Tertiary of southern France. *Contributions to Sedimentology*, **12**: 213pp.

Freytet, P. and Verrecchia, E.P. 2002. Lacustrine and palustrine carbonate petrography: an overview. *Journal of Paleolimnology*, **27**: 221–237.

Friedman, E. and O'Neil, J. 1977. Data of Geochemistry, 6th edn. Compilation of stable isotope fractionation factors of geological interest. US Geol. Survey Prof. Pap. 440-KK.

Friedman, G. 1995. Discussion on vitrinite reflectivity and the structure and burial history of the Old Red Sandstone of the Midland Valley of Scotland. *Journal of the Geological Society*, **152**: 196.

Fritz, P. and Smith, D.G.W. 1970. The isotopic composition of secondary dolomite. *Geochemica et Cosmochimica Acta*, **34**: 1161-1173.

Galehouse, J.S. 1971. Sedimentation analysis. In: Procedures in Sedimentary Petrology (Ed R.E. Carver). John Wiley and Sons, Inc., New York.

Garcia-Ruiz, J.M. 1998. Carbonate precipitation into alkaline silica-rich environments. *Geology*, **26**: 843-846.

Gardner, L.R. 1972. Origin of the mormon mesa caliche, Clark County, Nevada. *Geological Society of America Bulletin*, **83**: 143-156.

Garstang, M., Ellery, W.N., McCarthy, T.S., Scholes, M.C., Scholes, R.J., Swap, R.J. and Tyson, P.D. 1998. The contribution of aerosol- and water-borne nutrients to the functioning of the Okavango Delta ecosystem, Botswana. *South African Journal of Science*, **94**: 223-229.

Gassaway, J.S. 1988. Silcrete-Palaeocene marker beds in the Western Interior. *Geological Society of America Abstracts*, **21**: 379.

Gierlowski-Kordesch, E.H. 1998. Carbonate deposition in an ephemeral siliciclastic alluvial system: Jurassic Shuttle Meadow Formation, Newark Supergroup, Hartford Basin, USA. *Palaeogeography, Palaeoclimatology, Palaeoecology*, **140**: 161–184.

Gieske, A. 1996. Modelling surface outflow from the Okavango Delta. *Botswana Notes and Records*, **28**: 165-192.

Gieske, A. 1997. Modelling outfiow from the Jao/Boro River system in the Okavango Delta, Botswana. *Journal of Hydrology*, **193**: 214-239.

Giess, W. 1971. A preliminary vegetation map of South West Africa. *Dintera*, **4**: 1-114.

Gigout, M. 1960. Sur le genese des croutes calcaires pleistocene en Afrique du Nord. *C.R. Somm. Soc. Geol. Fr.*, 42-43.

Gile, L.H. 1961. A classification of ca horizons in soils of a desert region, Dona Ana County, New Mexico. *Soil Science Society of America Proceedings*, **25**: 52-61.

Gile, L.H. 1977. Holocene soils and soil-geomorphic relations in a semi-arid region of southern New Mexico. *Quaternary Research*, **7**: 112-132.

Gile, L.H. and Grossman, R.B. 1979. The Desert Project Soil Monograph. U.S. Department of Agriculture Soil Conservation Service, Washington, DC.

Gile, L.H., Peterson, F.F. and Grossman, R.B. 1965. The K horizon: a master soil horizon of carbonate accumulations. *Soil Science*, **99**: 74-82.

Gile, L.H., Peterson, F.F. and Grossman, R.B. 1966. Morphological and genetic sequences of carbonate accumulations in desert soils. *Soil Science*, **100**: 347-360.

Gile, L.H., Hawley, J.W. and Grossman, R.B. 1981. Soils and geomorphology in the Basin and Range area of southern New Mexico - Guidebook to the Desert Project., 39. N.M. Bur. Mines Mineral. Res. Mem.

Goldstein, R.H. 1988. Paleosols of Late Pennsylvanian strata, New Mexico. *Sedimentology*, **35**: 777-803.

Goudie, A.S. 1972a. A regional bibliography of calcrete. In: Food, Fiber and the Arid Lands (Eds W.G. McGinnies, B.J. Goldman and P. Paylore), pp. 421-437, Arizona.

Goudie, A.S. 1972b. On the definition of calcrete deposits. Zietscrift *fur Geomorphologie N.F.*, **16**: 464-468.

Goudie, A.S. 1973. Duricrusts in Tropical and Subtropical Landscapes. Clarendon Press, Oxford.

Goudie, A.S. 1983. Calcrete. In: Chemical Sediments and Geomorphology (Eds A.S. Goudie and K. Pye), pp. 93-131. Academic Press, London.

Goudie, A.S. 1991. Pans. *Progress in Physical Geography*, **15**: 221-237.

Goudie, A.S. (Ed), 1994. Geomorphological techniques, 2nd edn. Routledge, London.

Goudie, A.S. 1996. Organic agency in calcrete development. *Journal of Arid Environments*, **32**: 103-110.

Goudie, A.S. 2005. The drainage of Africa since the Cretaceous. *Geomorphology*, **67**: 437-456.

Goudie, A.S. and Wells, G.L. 1995. The nature, distribution and formation of pans in arid zones. *Earth-Science Reviews*, **38**: 1-69.

Gould, D., Rathbone, P.A. and Kimbell, G.S. 1987. The Geology of the Molopo Farms Complex, Southern Botswana., 23. Bulletin Geological Survey of Botswana, Lobatse, 178 pp.

Graustein, W.C. and Armstrong, R.L. 1983. The use of strontium-87/strontium-86 ratios to measure atmospheric transport into forested watersheds. *Science*, **219**: 289-292.

Griffiths, J.C. 1967. Scientific methods and analysis of sediments. McGraw Hill, New York, 508 pp.

Grove, A.T. 1969. Landforms and climatic changes in the Kalahari and Namib. *Geographical Journal*, **135**: 191-212.

Guler, C. and Thyne, G.D. 2004. Hydrologic and geologic factors controlling surface and groundwater chemistry in Indian Wells-Owens Valley area, southeastern California, USA. *Journal of Hydrology*, **285**: 177-198.

Gumbricht, T., McCarthy, T.S. and Merry, C.L. 2001. The topography of the Okavango Delta, Botswana, and its tectonic and sedimentological implications. *South African Journal of Geology*, **104**: 243-264.

Gumbricht, T. and McCarthy, T.S. 2003. Spatial patterns of islands and salt crusts in the Okavango Delta, Botswana. *South African Geographical Journal*, **85**: 164-169.

Gumbricht, T., McCarthy, J. and McCarthy, T.S. 2004a. Channels, wetlands and islands in the Okavango Delta, Botswana, and their relation to hydrological and sedimentological processes. *Earth Surface Processes and Landforms*, **29**: 15-29.

Gumbricht, T., Wolski, P., Frost, P. and McCarthy, T.S. 2004b. Forecasting the spatial extent of the annual flood in the Okavango delta, Botswana. *Journal of Hydrology*, **290**: 178-191.

Gumbricht, T., McCarthy, T.S. and Bauer, P. 2005. The micro-topography of the wetlands of the Okavango Delta, Botswana. *Earth Surface Processes and Landforms*, **30**: 27-39.

Haddon, I.G. 1999. Isopach map of the Kalahari Group. 1: 2500000. Council for Geoscience, South Africa (on behalf of SADC), Pretoria.

Haddon, I.G. 2000. Kalahari Group Sediments. In: The Cenozoic of Southern Africa. (Eds T.C. Partridge and R.R. Maud), pp. 173-181. Oxford University Press, Oxford.

Haddon, I.G., 2001. Sub-Kalahari Geological Map. 1: 2500000. Council for Geoscience, Pretoria, South Africa.

Haddon, I.G., 2005. The sub-Kalahari geology and tectonic evolution of the Kalahari Basin, southern Africa. Unpublished PhD thesis, University of the Witwatersrand, South Africa, 343pp.

Haddon, I.G. and McCarthy, T.S. 2005. The Mesozoic–Cenozoic interior sag basins of Central Africa: The Late-Cretaceous–Cenozoic Kalahari and Okavango basins. *Journal of African Earth Sciences*, **43**: 316–333.

Hall, G.E.M. 1998. Analytical perspective on trace element species of interest in exploration. *Journal of Geochemical Exploration*, **61**: 1-19.

Hamilton, E.W. III, McNaughton, S.J. and Coleman, J.S. 2001. Molecular, physiological, and growth responses to sodium stress in C4 grasses from a soil salinity gradient in the Serengeti ecosystem. *American Journal of Botany*, **88**: 1258–1265.

Hammes, F. and Verstraete, W. 2002. Key roles of pH and calcium metabolism in microbial carbonate precipitation. *Reviews in Environmental Science and Biotechnology*, **1**: 3-7.

Harrington, G.A. and Herczeg, A.L. 2003. The importance of silicate weathering of a sedimentary aquifer in arid central Australia indicated by very high $^{87}Sr/^{86}Sr$ ratios. *Chemical Geology*, **199**: 281-292.

Harrison, C.C. and Shaw, P.A. 1995. Bacterial involvement in the production of silcretes? *Bulletin Institut Oceanographique, Monaco*, **14**: 291-295.

Harrison, R.S. 1977. Caliche profiles: indicators of near-surface subaerial diagenesis, Barbados, West Indies. *Bulletin of Canadian Petroleum Geology*, **25**: 123-173.

Hay, R.L. and Reeder, R.J. 1978. Calcretes of Olduvai Gorge and the Ndolanya Beds of Northern Tanzania. *Sedimentology*, **25**: 649-673.

Hay, R.L. and Wiggins, B. 1980. Pellets, ooids, sepiolite and silica in three calcretes of the south-western United States. *Sedimentology*, **27**: 559-576.

Hay, R.L., Guldman, S.G., Matthews, J.C., Lander, R.H., Duffin, M.E. and Kyser, T.K. 1991. Clay mineral diagenesis in core KM-3 of Searles Lake, California. *Clays and Clay Minerals*, **39**: 84-96.

Hays, P.D. and Grossman, E.L. 1991. Oxygen isotopes in meteoric calcite cements as indicators of continental paleoclimate. *Geology*, **19**: 441-444.

Heaton, T.H.E., Talma, A.S. and Vogel, J.C. 1983. Origin and history of nitrate in confined groundwater in the western Kalahari. *Journal of Hydrology*, **62**: 243-62.

Heine, K. 1978. Radiocarbon chronology of Late Quaternary lakes in the Kalahari, southern Africa. *Catena*, **5**: 6-17.

Heine, K. 1982. The main stages of the Late Quaternary evolution of the Kalahari region, southern Africa. *Palaeoecology of Africa*, **15**: 53-76.

Heine, K. 1987. Zum alter Jungquartarer seespiegelschwankungen in der Mittleren Kalahari, Sudliches Afrika. *Palaeoecology of Africa*, **18**: 73-101.

Hoffe, B., Wright, J.A., Piper, D.P. and McMullan, S.R. 1991. Deep seismic evidence of late middle Proterozoic rifting along the Kalahari Line, western Botswana. *Tectonophysics*.

Hofmann, B.A. and Bernasconi, S.M. 1998. Review of occurrences and carbon isotope geochemistry of oxalate minerals: implications for the origin and fate of oxalate in diagenetic and hydrothermal fluids. *Chemical Geology*, **149**: 127-146.

Högberg, P. 1989. Root symbioses of trees in savannas. In: Mineral Nutrients in Tropical Forest and Savanna Ecosystems. (Ed J. Procter), pp. 121-36. Blackwell, Oxford.

Högberg, P. and Piearce, G.D. 1986. Mycorrhizas in Zambian trees in relation to host taxonomy, vegetation type and successional patterns. *Journal of Ecology*, **74**: 775-85.

Holmgren, K. and Shaw, P. 1997. Palaeoenvironmental reconstruction from near-surface pan sediments; an example from Lebatse Pan, Southeast Kalahari, Botswana. *Geografiska Annaler. Series A: Physical Geography,* **79**: 83-93.

Hugo, P.J. 1969. Stratigraphic test boreholes: Owamboland, Ministry of Mines and Energy, Geological Survey, Namibia.

Hutchins, D.G., Hutton, S.M. and Jones, C.R. 1976a. The geology of the Okavango Delta. Proceedings of the Symposium on the Okavango Delta and its Future Use. Botswana Society, Gaborone, 15-19 pp.

Hutchins, D.G., Hutton, L.G., Hutton, S.M., Jones, C.R. and Loenhert, E.P. 1976b. A summary of the Geology, Seismicity, Geomorphology and Hydrogeology of the Okavango Delta. Botswana Geological Survey Department Bulletin, 7, 27 pp.

Hutton, L.G. and Dincer, T. 1976. Chemistry and stable isotope composition of the Okavango Delta waters, UNDP/FAO BOT/71/506. Tech Note 23, Gaborone, Botswana.

Jacobson, G., Arakel, A.V. and Yijian, C. 1988. The central Australian groundwater discharge zone: evolution of associated calcrete and gypcrete deposits. *Australian Journal of Earth Sciences*, **35**: 549-565.

Jaillard, B., Guyon, A. and Maurin, A.F. 1991. Structure and composition of calcified roots, and their identification in calcareous soils. *Geoderma*, **50**: 197–210.

James, N.P. 1972. Holocene and Pleistocene calcareous crust (caliche) profiles: criteria for subaerial exposure. *Journal of Sedimentary Petrology*, **42**: 817-836.

Jenny, H. and Leonard, C. 1939. Functional relationships between soil properties and rainfall. *Soil Science*, **38**: 363-381.

Jiamao, H., Keppens, E., Tungsheng, L., Paepe, R. and Wenying, J. 1997. Stable isotope composition of the carbonate concretion in loess and climate change. *Quaternary International*, **37**: 37-43.

Johnson, M.R. (Ed), 1994. Lexicon of South African Stratigraphy. Part 1: Phanerozoic Units. Council for Geoscience, South Africa., Pretoria, 56 pp.

Jones, B. and Ng, K.-C. 1988. The structure and diagenesis of rhizoliths from Cayman Brac, British West Indies. *Journal of Sedimentary Research*, **58**: 457-467.

Jones, B. and Squair, C.A. 1989. Formation of peloids in plant rootlets, Grand Cayman, British West Indies. *Journal of Sedimentary Research*, **59**: 1002-1007.

Jones, B., Pleydell, S.M. and Ng, K.-C. 1989. Formation of poikilotopic calcite-dolomite fabrics in the Oligocene-Miocene Bluff Formation of Grand

Cayman, British West Indies. *Bulletin Canadian Petroleum Geology*, **37**: 255-265.

Kabata-Pendias, A. 2004. Soil-plant transfer of trace elements--an environmental issue. *Geoderma*, **122**: 143-149.

Kahle, C.F. 1977. Origin of subaerial Holocene calcareous crusts: role of algae, fungi and sparmicritisation. *Sedimentology*, **24**: 413-435.

Kano, K. and Taguchi, K. 1982. Experimental study on the ordering of Opal-CT. *Geochemical Journal*, **16**: 33-41.

Kanthack, F.E. 1921. Notes on the Kunene River, southern Angola. *Geographical Journal*, **107**: 321-335.

Kelly, E.F., Amundson, R.G., Marino, B.D. and DeNiro, M.J. 1991. Stable carbon isotope composition of carbonate in Holocene grassland soils. *Soil Science Society of America Journal*, **55**: 1651-1658.

Kelts, K.R. and Hsu, K. 1978. Freshwater carbonate sedimentation. In: Lakes—Chemistry, Geology, Physics. (Ed A. Lerman), pp. 295– 323. Springer, New York, NY.

Kelts, K.R. and Talbot, M.R. 1990. Lacustrine carbonates as geochemical archives of environmental change and biotic– abiotic interactions. In: Ecological Structure and Function in Large Lakes. (Eds M.M. Tilzer and C. Serruya), pp. 290– 317. Science and Technology Publishers, Madison, WI.

Kendall, T.A. and Martin, S.T. 2005. Mobile ions on carbonate surfaces. *Geochimica et Cosmochimica Acta*, **69**: 3257-3263.

Kers, B.A.M., Spriensma, J.J., Meijer, H.A.J., Venema, R., Streurman, H.J., v.d. Plicht, J. and Obakeng, O. 2000. IH-02 GRES II 1995-1997, Vrije Universiteit, Amsterdam.

Khadkikar, A.S., Merh, S.S., Malik, J.N. and Chamyal, L.S. 1998. Calcretes in semi-arid alluvial systems: formative pathways and sinks. *Sedimentary Geology*, **116**: 251-260.

Khadkikar, A.S., Chamyal, L.S. and Ramesh, R. 2000. The character and genesis of calcrete in Late Quaternary alluvial deposits, Gujarat, western India, and its bearing on the interpretation of ancient climates. *Palaeogeography, Palaeoclimatology, Palaeoecology*, **16**: 239-261.

King, L.C. 1963. South African Scenery: a Textbook of Geomorphology. Oliver and Boyd, Edinburgh.

Kirkham, D. and Powers, W.L. 1972. Advanced Soil Physics. Wiley-Interscience, New York.

Klappa, C.F. 1978a. Morphology, composition and genesis of Quaternary calcretes from the western Mediterranean: a petrographic approach. Ph.D., University of Liverpool, Liverpool, UK.

Klappa, C.F. 1978b. Biolithogenesis of Microcodium: elucidation. *Sedimentology*, **25**: 489-522.

Klappa, C.F. 1979a. Lichen stromatolites: criterion for subaerial exposure and a mechanism for the formation of laminar calcrete (caliche). *Journal of Sedimentary Petrology*, **49**: 387-400.

Klappa, C.F. 1979b. Calcified filaments in Quaternary calcretes: organo-mineral interactions in the subaerial vadose environment. *Journal of Sedimentary Petrology*, **49**: 955-968.

Klappa, C.F. 1980a. Rhizoliths in terrestrial carbonates: classification, recognition, genesis and significance. *Sedimentology*, **27**: 613-629.

Klappa, C.F. 1980b. Brecciation textures and tepee structures in Quaternary calcrete (caliche) profiles from eastern Spain: the plant factor in their formation. *Geological Journal*, **15**: 81-89.

Klappa, C.F. 1983. A process-response model for the formation of pedogenic calcretes. In: Residual Deposits (Ed R.C.L. Wilson), Special Publication No 11, pp. 211-220. Geological Society of London.

Knoop, W.T. and Walker, B.H. 1984. Interactions of woody and herbaceous vegetation in a southern African savanna. *Journal of Ecology*, **73**: 235-53.

Knox, G.F. 1977. Caliche profile formation, Saldanha Bay (South Africa). *Sedimentology*, **24**: 657-674.

Krah, M., McCarthy, T.S., Annegarn, H. and Ramberg, L. 2004. Airborne dust deposition in the Okavango Delta, Botswana, and its impact on landforms. *Earth Surface Processes and Landforms*, **29**: 565-577.

Krauskopf, K.B. and Bird, D.K. 1995. Introduction to geochemistry. McGraw-Hill, Inc., New York.

Krumbein, W.C. and Pettijohn, F.J. 1938. Manual of Sedimentary Petrology. Appleton, Century, and Crofts, Inc., New York, 549 pp.

Krumbein, W.C. and Garrels, R.M. 1952. Origin and classification of chemical sediments in terms of pH and oxidation-reduction potentials. *Journal of Geology*, **60**: 1-33.

Krumbein, W.E. and Giele, C. 1979. Calcification in a coccoid - cyanobacterium associated with the formation of desert stromatolites. *Sedimentology*, **26**: 593-604.

Kump, L.R., Brantley, S.L. and Arthur, M.A. 2000. Chemical Weathering, Atmospheric CO2, and Climate. *Annual Review of Earth and Planetary Sciences*, **28**: 611-667.

Lancaster, I.N. 1974. Pans of the southern Kalahari. *Botswana Notes and Records*, **6**: 157-169.

Lancaster, I.N. 1978. Composition and formation of southern Kalahari pan margin dunes. *Zeitschrift fur Geomorphologie N.F.*, **22**: 148-69.

Lancaster, I.N. 1981. Palaeoenvironmental implications of fixed dune systems in southern Africa. *Palaeogeography, Palaeoclimatology, Palaeoecology*, **33**: 327-46.

Lancaster, I.N. 1988. Development of linear dunes in the south western Kalahari, Southern Africa. *Journal of Arid Environments*, **14**: 233-44.

Lancaster, N. 1986. Pans in the southwestern Kalahari: a preliminary report. *Palaeoecology of Africa*, **17**: 59-68.

Land, L.S. 1980. The isotopic and trace element geochemistry of dolomite: the state of the art. In: Concepts and Models of Dolomitization (Eds D.H. Zenger, J.B. Dunham and R.L. Ethington), 28, pp. 87-110. Spec. Publ. Soc. econ. Paleont. Miner.

Lange, J. 2005. Dynamics of transmission losses in a large arid stream channel. *Journal of Hydrology*, **306**: 112-126.

Larsen, D. and McNeal, D. 2004. Factors controlling authigenic mineralogy in the Plio-Pleistocene Lake Tecopa beds, southeastern California, USA. *Geological Society of America Abstracts with Programs*, **36**: 472.

Lattman, L.H. 1973. Calcium carbonate cementation of alluvial fans in Southern Nevada. *Geological Society of America Bulletin*, **84**: 3013-3028.

Lattman, L.H. and Lauffenburger, S.K. 1974. Proposed role of gypsum in the formation of caliche. *Zeitschrift fur Geomorphologie N.F. Suppl. Bd.*, **20**: 140-149.

Lawrence, C.J. and Toole, T. 1984. The location, selection and use for bituminous road construction in Botswana. Transport and Road Research Laboratory, Department of Transport, TRRL Laboratory Report 1122, Crowthorne.

Lawson, M.P. and Thomas, D.S.G. 2002. Late Quaternary lunette dune sedimentation in the southwestern Kalahari desert, South Africa: luminescence based chronologies of aeolian activity. *Quaternary Science Reviews*, **21**: 825-836.

Le Roux, C. 1998. Road Map of the Etosha National Park. Ministry of Environment and Tourism, Windhoek, Namibia.

Le Roux, C.J.G. 1980. Vegetation Classification and Related Studies in the Etosha National Park. D.Sc. (Agric) thesis, University of Pretoria, Pretoria, RSA.

Lee, S.Y. and Gilkes, R.J. 2005. Groundwater geochemistry and composition of hardpans in southwestern Australian regolith. *Geoderma*, **126**: 59-84.

Leistner, O.A. 1967. The plant ecology of the southern Kalahari. Memoirs of the Botanical Survey of South Africa, 38.

Lipps, J.H. 1993. Fossil Prokaryotes and Protists. Blackwell Scientific Publications, Boston, 342 pp.

Liu, B., Phillips, F.M., Elmore, D. and Sharma, P. 1994. Depth dependence of soil carbonate accumulation based on cosmogenic ^{36}Cl dating. *Geology*, **22**: 1071-1074.

Liu, B., Phillips, F.M., Hoines, S., Campbell, A.R. and Sharma, P. 1995. Water movement in desert soils traced by stable isotopes, Cl, chlorine-36, southern Arizona. *Journal of Hydrology*, **168**: 91-110.

Liu, B., Phillips, F.M. and Campbell, A.R. 1996. Stable carbon and oxygen isotopes of pedogenic carbonates, Ajo Mountains, southern Arizona: implications for paleoenvironmental change. *Palaeogeography, Palaeoclimatology, Palaeoecology*, **124**: 233-246.

Londry, K.L. and Des Marais, D.J. 2003. Stable Carbon Isotope Fractionation by Sulfate-Reducing Bacteria. *Applied and Environmental Microbiology*, **69**: 2942-2949.

Machel, H.G. 2001. Bacterial and thermochemical sulfate reduction in diagenetic settings – old and new insights. *Sedimentary Geology*, **140**: 143-175.

Machette, M.N. 1985. Calcic soils of the south-western United States. *Geological Society of America Special Paper* 1-21.

Mack, G.H. and James, W.C. 1992. Calcic paleosols of the Plio–Pleistocene Camp Rice and Palomas Formations, southern Rio Grande rift, USA. *Sedimentary Geology*, **77**: 89– 109.

Mallick, D.I.J., Habgood, F. and Skinner, A.C. 1981. A geological interpretation of Landsat imagery and air photography of Botswana. Overseas Geology & Mineral Resources, 56. Institute of Geological Sciences, London, 36 pp.

Mann, A.W. and Deutscher, R.L. 1978. Genesis principles for the precipitation of carnotite in calcrete drainages in Western Australia. *Economic Geology*, **73**: 1724-1737.

Mann, A.W. and Horwitz, R.C. 1979. Groundwater calcrete deposits in Australia. Some observations from Western Australia. *Journal of the Geological Society of Australia*, **26**: 293-303.

Maraschin, A.J., Mizusaki, A.M.P. and De Ros, L.F. 2004. Near-Surface K-Feldspar Precipitation in Cretaceous Sandstones from the Potiguar Basin, Northeastern Brazil. *The Journal of Geology*, **112**: 317-334.

Marion, G.M., Schlesinger, W.H. and Fonteyn, P.J. 1985. Caldep: a regional model for soil CaCO3 (caliche) deposition in south western deserts. *Soil Science*, **139**: 468-481.

Marion, G.M., Introne, D.S. and Cleve, K.V. 1991. The stable isotope geochemistry of CaCO3 on the Tanana River floodplain of interior Alaska, U.S.A.: composition and mechanisms of formation. *Chemical Geology* (Isotope Geoscience Section), **86**: 97-110.

Marshall, T.R. 1990. The Nature, Origin, and Evolution of the Diamondiferous Gravels of the South-Western Transvaal. Unpublished Ph.D., University of the Witwatersrand, RSA.

Mayer, J.J. 1973. Morphotectonic development of the Harts River valley in relation to the Griqualand-Transvaal axis and the Vaal and Molopo Rivers. *Transactions of the Geological Society of South Africa*, **76**: 183-193.

Mayer, L., McFadden, L.D. and Harden, J.W. 1988. Distribution of calcium carbonate in desert soils: a model. *Geology*, **16**: 303-306.

Mazor, E. 1982. Rain recharge in the Kalahari - a note on some approaches to the problem. *Journal of Hydrology*, **55**: 137-144.

Mazor, E., Verhagen, B.T., Sellschop, J.P.F., Jones, M.T., Robins, N.E., Hutton, L. and Jennings, C.M.H. 1977. Northern Kalahari ground waters:

hydrologic isotopic and chemical studies at Orapa, Botswana. *Journal of Hydrology*, **34**: 203-234.

McCarthy, T.S. 1992. Physical and biological processes controlling the Okavango Delta - a review of recent research. *Botswana Notes and Records*, **24**: 57-86.

McCarthy, T.S. and Metcalfe, J. 1990. Chemical sedimentation in the semi-arid environment of the Okavango Delta, Botswana. *Chemical Geology*, **89**: 157-178.

McCarthy, T.S. and Ellery, W.N. 1994. The effect of vegetation on soil and ground water chemistry and hydrology of islands in the seasonal swamps of the Okavango Fan, Botswana. *Journal of Hydrology*, **154**: 169-193.

McCarthy, T.S. and Ellery, W.N. 1995. Sedimentation on the distal reaches of the Okavango Fan, Botswana, and its bearing on calcrete and silcrete (ganister) formation. *Journal of Sedimentary Research*, **A65**: 77-90.

McCarthy, T.S., Ellery, W.N., Rogers, K.H., Cairncross, B. and Ellery, K. 1986a. The roles of sedimentation and plant growth in changing flow patterns in the Okavango Delta, Botswana. *South African Journal of Science*, **82**: 579-584.

McCarthy, T.S., McIver, J.R. and Cairncross, B. 1986b. Carbonate accumulation on islands in the Okavango Delta, Botswana. *South African Journal of Science*, **82**: 588-591.

McCarthy, T.S., Stanistreet, I.G., Cairncross, B., Ellery, W.N., Ellery, K., Oelofse, R. and Grobicki, T.S.A. 1988. Incremental aggradation on the Okavango Delta-Fan, Botswana. *Geomorphology*, **1**: 267-278.

McCarthy, T.S., McIver, J.R., Cairncross, B., Ellery, W.N. and Ellery, K. 1989. The inorganic chemistry of peat from the Maunachira channel-swamp system, Okavango Delta, Botswana. *Geochemica et Cosmochimica Acta*, **53**: 1077-1089.

McCarthy, T.S., McIver, J.R. and Verhagen, B.T. 1991a. Groundwater evolution, chemical sedimentation and carbonate brine formation on an island in the Okavango Delta swamp, Botswana. *Applied Geochemistry*, **6**: 577-595.

McCarthy, T.S., Stanistreet, I.G. and Cairncross, B. 1991b. The sedimentary dynamics of active fluvial channels on the Okavango Fan, Botswana. *Sedimentology*, **38**: 471-487.

McCarthy, T.S., Ellery, W.N. and Stanistreet, I.G. 1992. Avulsion mechanisms on the Okavango fan, Botswana: the control of a fluvial system by vegetation. *Sedimentology*, **39**: 779-795.

McCarthy, T.S., Ellery, W.N. and Ellery, K. 1993a. Vegetation induced subsurface precipitation of carbonate as an aggradational process in the permanent swamps of the Okavango (Delta) fan, Botswana. *Chemical Geology*, **107**: 111-131.

McCarthy, T.S., Ellery, W.N. and Stanistreet, L.G. 1993b. Lakes of the north eastern region of the Okavango Swamps, Botswana. *Zietscrift fur Geomorphologie N.F.*, **37**: 273-294.

McCarthy, T.S., Franey, N.J., Ellery, W.N. and Ellery, K. 1993c. The use of SPOT imagery as an aid to the study of environmental processes in the wetlands of the Okavango Delta, Botswana. *South African Journal of Science*, **89**: 432-436.

McCarthy, T.S., Green, R.W. and Franey, N.J. 1993d. The influence of neo-tectonics on water dispersal in the northeastern regions of the Okavango swamps, Botswana. *Journal of African Earth Sciences*, **17**: 23-32.

McCarthy, T.S., Bloem, A. and Larkin, P.A. 1998a. Observations on the hydrology and geohydrology of the Okavango Delta. *South African Journal of Geology*, **101**: 101-117.

McCarthy, T.S., Ellery, W.N. and Bloem, A. 1998b. Some observations on the geomorphological impact of hippopotamus (Hippopotamus amphibius L.) in the Okavango Delta, Botswana. *African Journal of Ecology*, **36**: 44-56.

McCarthy, T.S., Ellery, W.N. and Dangerfield, J.M. 1998c. The role of biota in the initiation and growth of islands on the floodplain of the Okavango alluvial fan, Botswana. *Earth Surface Processes and Landforms*, **23**: 291-316.

McCarthy, T.S., Cooper, G.R.J., Tyson, P.D. and Ellery, W.N. 2000. Seasonal flooding in the Okavango Delta, Botswana - Recent history and future prospects. *South African Journal of Science*, **96**: 25-33.

McCarthy, J.M., Gumbricht, T., McCarthy, T., Frost, P., Wessels, K. and Seidel, F. 2003. Flooding Patterns of the Okavango Wetland in Botswana between 1972 and 2000. *Ambio*, **32**: 453-457.

McCrea, J. 1950. On the isotope chemistry of carbonates and a paleotemperature scale. *Journal of Chemistry and Physics*, **18**: 849-857.

McFadden, L.D. and Tinsley, J. 1985. Rate and depth of pedogenic-carbonate accumulation in soils: formulation and testing of a compartment model. Geological Society of America Special Paper No. 203: 23-42.

McFarlane, M.J. 1975. A calcrete from the Namanga-Bissel area of Kenya. *Journal of the Geographical Society of Kenya*, **1**: 31-43.

McFarlane, M.J., Eckardt, F.D., Ringrose, S., Coetzee, S.H. and Kuhn, J.R. 2005. Degradation of linear dunes in Northwest Ngamiland, Botswana and the implications for luminescence dating of periods of aridity. *Quaternary International*, **135**: 83-90.

McIntyre, C. and Atkins, S. 1991. Guide to Namibia and Botswana. Chalfont, St. Peter, England.

McKenzie, J.A. 1985. Carbon isotopes and productivity in the lacustrine and marine environment. In: Geochemical Processes in Lakes. (Ed W. Stumm), pp. 99– 118. Wiley, New York, NY.

Mees, F. 1999. The unsuitability of calcite spherulites as indicators of subaerial exposure. *Journal of Arid Environments*, **42**: 149-154.

Mees, F. 2002. The nature of calcareous deposits along pan margins in eastern central Namibia. *Earth Surface Processes and Landforms*, **27**: 719–735.

Mendelsohn, J. and el Obeid, S. 2004. Okavango River - The flow of a lifeline. Struik Publishers, Cape Town, 176 pp.

Merry, C.L., Heister, H., Barry, M., Ellery, W.N., McCarthy, T.S., Ruther, H. and Sternberg, H. 1998. GPS heighting in Okavango Delta. *Journal of Surveying Engineering*, **124**: 145-155.

Miller, E.K., Blum, J.D. and Friedland, A.J. 1993. Determination of soil exchangeable-cation loss and weathering rates using Sr isotopes. *Nature*, **362**: 438-441.

Miller, J. 1988. Cathodoluminescence microscopy. In: Techniques in sedimentology. (Ed M.E. Tucker), pp. 174-190. Blackwells, Oxford.

Miller, R.M. and Jastrow, J.D. 1990. Hierarchy of root and mycorrhizal fungal interactions with soil aggregation. *Soil Biology and Biochemistry*, **22**: 579-84.

Millot, G. 1970. Geology of Clays. Springer-Verlag, New York.

Millot, G., Nahon, D., Paquet, H., Ruellan, A. and Tardy, Y. 1977. L' Eprgenie calcaire des roches silicatees dans les encroutements carbonates en pays subaride; Antiatlas, Maroc. *Sciences Geologiques Bulletin*, **30**: 129-152.

Monger, H.C., Daugherty, L.A., Lindermann, W.C. and Liddell, C.M. 1991. Microbial precipitation of pedogenic calcite. *Geology*, **19**: 997-1000.

Moore, A.E. and Dingle, R.V. 1998. Evidence for fluvial sediment transport of Kalahari sands in central Botswana. *South African Journal of Geology*, **101**: 143-153.

Moore, A.E. and Attwell, C.A.M. 1999. Geological controls on the distribution of woody vegetation in the central Kalahari, Botswana. *South African Journal of Geology*, **102**: 350-362.

Moore, A.E. and Larkin, P.A. 2001. Drainage evolution in south-central Africa since the breakup of Gondwana. *South African Journal of Geology*, **104**: 47-68.

Moore, A.E. and Blenkinsop, T. 2002. The role of mantle plumes in the development of continental-scale drainage patterns: The southern African example revisited. *South African Journal of Geology*, **105**: 353-360.

Morad, S. 1998. Carbonate cementation in sandstones: distribution patterns and geochemical evolution. In: Carbonate Cementation in Sandstone: distribution patterns and geochemical evolution. (Ed S. Morad), Spec. Publ. int. Ass. Sediment. 26, pp. 1-26. Blackwell Scientific Publications, Oxford.

Morad, S., Ketzer, J.M. and De Ros, L.F. 2000. Spatial and temporal distribution of diagenetic alterations in siliciclastic rocks: implications for mass transfer in sedimentary basins. *Sedimentology*, **47**: 95-120.

Mount, J.F. and Cohen, A.S. 1984. Petrology and geochemistry of rhizoliths from Plio-Pleistocene fluvial and marginal lacustrine deposits, East Lake Turkana, Kenya. *Journal of Sedimentary Petrology*, **54**: 263-275.

Mucciarone, D.A. 2003. Stanford University Stable Isotope Laboratory, On-line Manual, Carlo Erba NA 1500 Elemental Analyzer, Stanford University.

Nahon, D. and Ruellan, A. 1975. Les accumulations de calcaires sur les marnes Eocene de la Falaise de Thies (Senegal). Mise en evidence des phenomenes d'epigenie. In: Colloque: Types de Croutes Calcaires et Leur Repartition Regionale. (Ed T. Vogt), pp. 7-11, Strasbourg.

Naiman, Z., Quade, J. and Patchett, P.J. 2000. Isotopic evidence for eolian recycling of pedogenic carbonate and variations in carbonate dust sources throughout the southwest United States. *Geochimica et Cosmochimica Acta*, **64**: 3099-3109.

NamPower 2004. Technical report on the pre-feasibility study for the Popa Falls Hydro Power Project, Windhoek.

Nash, D.J. 1996. On the dry valleys of the Kalahari: Documentary evidence of environmental change in central southern Africa. *Geographical Journal*, **162**: 154-168.

Nash, D.J. 1997. Groundwater as a geomorphological agent in drylands. In: Arid Zone Geomorphology: Process, Form and Change in Drylands (Ed D.S.G. Thomas), pp. 319-348. John Wiley, Chichester.

Nash, D.J. and Shaw, P.A. 1998. Silica and carbonate relationships in silcrete-calcrete intergrade duricrusts from the Kalahari of Botswana and Namibia. *Journal of African Earth Sciences*, **27**: 11-25.

Nash, D.J. and Smith, R.F. 1998. Multiple calcrete profiles in the Tabernas Basin, southeastern Spain: their origins and geomorphic implications. *Earth Surface Processes and Landforms*, **23**: 1009-1029.

Nash, D.J. and McLaren, S.J. 2003. Kalahari valley calcretes: their nature, origins, and environmental significance. *Quaternary International*, **111**: 3-22.

Nash, D.J. and McLaren, S.J. 2005. Geochemical Sediments and Landscapes. Blackwell, London.

Nash, D.J., Shaw, P.A. and Thomas, D.S.G. 1994a. Duricrust development and valley evolution - process-landform links in the Kalahari. *Earth Surface Processes and Landforms*, **19**: 299-317.

Nash, D.J., Thomas, D.S.G. and Shaw, P.A. 1994b. Siliceous duricrusts as palaeoclimatic indicators: evidence from the Kalahari Desert of Botswana. *Palaeogeography, Palaeoclimatology, Palaeoecology*, **112**: 279-295.

Nash, D.J., Meadows, M.E., Shaw, P.A., Baxter, A.J. and Gieske, A. 1997. Late Holocene sedimentation rates and geomorphological significance of the Ncamasere Valley, Okavango Delta, Botswana. *South African Geographical Journal*, **79**: 93-100.

Nash, D.J., Shaw, P.A. and Ullyott, J.S. 1998. Drainage-line silcretes of the Middle Kalahari: An analogue for Cenozoic sarsen trains? *Proceedings of the Geologists' Association*, **109**: 241-254.

Nash, D.J., Meadows, M.E. and Gulliver, V.L. 2005. Holocene environmental change in the Okavango Panhandle, northwest Botswana. *In press*.

Negra, C., Ross, D.S. and Lanzirotti, A. 2005. Soil Manganese Oxides and Trace Metals: Competitive Sorption and Microfocused Synchrotron X-ray Fluorescence Mapping. *Soil Science Society of America Journal*, **69**: 353-361.

Nesse, W.D. 1991. Introduction to optical mineralogy. Oxford University Press, Inc., Oxford, 335 pp.

Netterberg, F. 1969a. Ages of calcretes in Southern Africa. *The South African Archeological Bulletin*, **24**: 88-92.

Netterberg, F. 1969b. The interpretation of some basic calcrete types. *The South African Archeological Bulletin*, **24**: 117-122.

Netterberg, F. 1969c. The geology and engineering properties of South African calcretes. Ph.D., University of Witwatersrand, Johannesburg, RSA.

Netterberg, F., 1978. Dating and correlation of calcretes and other pedocretes. *Transactions of the Geological Society of South Africa*, **81**: 379–391.

Netterberg, F. 1980. Geology of southern African calcretes. 1. Terminology, description, macrofeatures and classification. *Transactions of the Geological Society of South Africa*, **83**: 255-283.

Nettleton, W.D. and Peterson, F.F. 1983. Aridisols. In: Pedogenesis and Soil Taxonomy. II. The Soil Orders (Eds L.P. Wilding, N.E. Smeck and G.F. Hall), pp. 165-215. Elsevier, Amsterdam.

Nickel, E. 1985. Carbonates in alluvial fan systems, an approach to physiography, sedimentology and diagenesis. *Sedimentary Geology*, **42**: 83–104.

Nijsten, G.-J. 1995. Recharge in the Eastern Botswana Kalahari. Groundwater Flow Studies in the Letlhakeng - Botlhapatlou area, GRES-II project, Department of Geological Survey, Lobatse, Botswana.

Nordenstam, B. 1970. Notes on the flora and vegetation of Etosha Pan, South West Africa. *Dintera*, **5**: 3-6.

Nugent, C. 1990. The Zambezi River: tectonism, climatic change and drainage evolution. *Palaeogeography, Palaeoclimatology, Palaeoecology*, **78**: 55-69.

Okujeni, C.D., Ackon, P., Baugaard, W. and Langa, N. 2005. Controls of element dispersion in aeolian sand and calcrete-dominated regolith associated with gold mineralization in the Kraaipan greenstone belt, South Africa. Geochemistry: *Exploration, Environment, Analysis*, **5**: 223-231.

Orpen, J.L., Swain, C.J., Nugent, C. and Zhou, P.P. 1989. Wrench-fault and half-graben tectonics in the development of the Palaeozoic Zambezi Karoo basins in Zimbabwe - the 'Lower Zambezi' and 'Mid-Zambezi' basins respectively - and regional implications. *Journal of African Earth Sciences*, **8**: 215-229.

Ouhadia, V.R. and Yong, R.N. 2003. Impact of clay microstructure and mass absorption coefficient on the quantitative mineral identification by XRD analysis. *Applied Clay Science*, **23**: 141-148.

Pankow, W., Boller, T. and Wienken, A. 1991. The significance of mycorrhizas for protective systems. *Experientia*, **47**: 391-4.

Paquet, H. and Millot, G. 1972. Geochemical evolution of clay minerals in the weathered products and soils of Mediterranean climates. Proceedings of the International Clay Conference Madrid: 199-203.

Parcerisa, D., Gomez-Gras, D. and Trave, A. 2005. A model of early calcite cementation in alluvial fans: Evidence from the Burdigalian sandstones and limestones of the Valles-Penedes half-graben (NE Spain). *Sedimentary Geology*, **178**: 197-217.

Parry, W.T. and Reeves, C.C.J. 1968a. Clay mineralogy of pluvial lake sediments, southern High Plains, Texas. *Journal of Sedimentary Petrology*, **38**: 516-529.

Parry, W.T. and Reeves, C.C.J. 1968b. Sepiolite from pluvial Mound Lake, Lyn and Terry Counties, Texas. *American Mineralogist*, **53**: 984-993.

Partridge, T.C. 1997. Cainozoic environmental change over Southern Africa, with special emphasis on the last 20 000 years. *Progress in Physical Geography*, **21**: 3-22.

Partridge, T.C. and Maud, R.R. 1987. Geomorphic evolution of southern Africa since the Mesozoic. *South African Journal of Geology*, **90**: 179-208.

Partridge, T.C. and Maud, R.R. 1989. The end-Cretaceous event: new evidence from the southern hemisphere. *South African Journal of Science*, **85**: 428-430.

Partridge, T.C. and Maud, R.R. 2000. Macro-Scale Geomorphic Evolution of Southern Africa. (Eds T.C. Partridge and R.R. Maud), pp. 3-18. Oxford University Press, Oxford.

Partridge, T.C. and Scott, L. 2000. Lakes and Pans. In: The Cenozoic of Southern Africa (Eds T.C. Partridge and R.R. Maud), pp. 145-161. Oxford University Press, Oxford.

Partridge, T.C., Scott, L. and Hamilton, J.E. 1999. Synthetic reconstructions of southern African environments during the Last Glacial Maximum (21-18 kyr) and the Holocene Altithermal (8-6 kyr). *Quaternary International*, **57/58**: 207-214.

Pearson, P.N. and Palmer, M.R. 2000. Atmospheric carbon dioxide concentrations over the past 60 million years. *Nature*, **406**: 695-699.

Pendall, E.G., Harden, J.W., Trumbore, S.E. and Chadwick, O.A. 1994. Isotopic Approach to Soil Carbonate Dynamics and Implications for Paleoclimatic Interpretations. *Quaternary Research*, **42**: 60-71.

Peterson, M.N.A. and von der Borch, C.C. 1965. Chert: modern inorganic deposition in a carbonate-precipitating locality. *Science*, **149**: 1501-1503.

Phillips, S.E. and Self, P.G. 1987. Morphology, crystallography and origin of needle-fibre calcite in Quaternary pedogenic carbonates of South Australia. *Australian Journal of Soil Research*, **25**: 429-444.

Phillips, S.E., Milnes, A.R. and Foster, R.C. 1987. Calcified filaments: an example of biological influences in the formation of calcrete in South Australia. *Australian Journal of Soil Research*, **25**: 405-428.

Pierrehumbert, R.T. 2004. High levels of atmospheric carbon dioxide necessary for the termination of global glaciation. *Nature*, **429**: 646-649.

Pimentel, N.L.V. 2002. Pedogenic early diagenetic processes in Palaeogene alluvial fan lacustrine deposits from the Sado Basin (S Portugal). *Sedimentary Geology*, **148**: 123–138.

Pimentel, N.L., Wright, V.P. and Azevedo, T.M. 1996. Distinguishing early groundwater alteration effects from pedogenesis in ancient alluvial basins: examples from the Palaeogene of southern Portugal. *Sedimentary Geology*, **105**: 1-10.

Platt, N.H. 1989. Lacustrine carbonates and pedogenesis: sedimentology and origin of palustrine deposits from the Early Cretaceous Rupelo Formation, West Cameros Basin, North Spain. *Sedimentology*, **36**: 665-684.

Platt, N.H. and Wright, V.P. 1992. Palustrine carbonates and the Florida Everglades; towards an exposure index for the fresh-water environment. *Journal of Sedimentary Research*, **62**: 1058-1071.

Pokrovsky, O.S., Golubev, S.V. and Schott, J. 2005. Dissolution kinetics of calcite, dolomite and magnesite at 25°C and 0 to 50 atm pCO_2. *Chemical Geology*, **217**: 239-255.

Quade, J., Cerling, T.E. and Bowman, J.R. 1989a. Development of Asian monsoon revealed by marked ecological shift during the latest Miocene in northern Pakistan. *Nature*, **342**: 163-166.

Quade, J., Cerling, T.E. and Bowman, J.R. 1989b. Systematic variations in the carbon and oxygen isotopic composition of pedogenic carbonate along elevated transects in the southern Great Basin, United States. *Geological Society of America Bulletin*, **101**: 464-475.

Quade, J. and Cerling, T.E. 1990. Stable isotopic evidence for a pedogenic origin of carbonates in trench 14 near Yucca Mountain, Nevada. *Science*, **250**: 1549-1552.

Rabenhorst, M.C., Wilding, L.P. and West, L.T. 1984a. Identification of pedogenic carbonates using isotope and microfabric analyses. *Soil Science Society of America Journal*, **48**: 125-132.

Rabenhorst, M.C., Wilding, L.P. and Girdner, C.L. 1984b. Airborne dusts in the Edwards Plateau region of Texas. *Soil Science Society of America Journal*, **48**: 621-627.

Rabenhorst, M.C., West, L.T. and Wilding, L.P. 1991. Genesis of calcic and petrocalcic horizons in soils over carbonate rocks. In: Occurrence, Characteristics, and Genesis of Carbonate, Gypsum, and Silica

Accumulations in Soils. (Ed W.D. Nettleton), 26, pp. 61-74. SSSA Special Publication.

Rahner, S., Amiel, A., Ronen, D. and Magaritz, M. 1991. The scavanging effects of sand coated by iron hydroxide in phreatic aquifers. In: Abstracts of the Proceedings of the 2nd International Symposium on Environmental Geochemistry, Uppsala, Sweden.

Ranson, M.D. and Bidwell, O.W. 1990. Clay movement and carbonate accumulation in Ustolls of central Kansas, USA. In: Soil Micromorphology: a Basic and Applied Science. (Ed L.A. Douglas), 19, pp. 417-423. Developments in Soil Science.

Ravelo, A.C., Andreasen, D.H., Lyle, M., Olivarez Lyle, A. and Wara, M.W. 2004. Regional climate shifts caused by gradual global cooling in the Pliocene epoch. *Nature*, **429**: 263-267.

Raymo, M.E. and Ruddiman, W.F. 1992. Tectonic forcing of late Cenozoic climate. *Nature*, **359**: 117-122.

Read, D.J. 1991. Mycorrhizas in ecosystems. *Experientia*, **47**: 376-91.

Read, J.F. 1974. Calcrete deposits and Quaternary sediments, Edel Province, Shark Bay, Western Australia. *Memoir of the American Association of Petroleum Geologists*, **22**: 250-282.

Reeves, C.C.J. 1970. Origin, classification and geologic history of caliche on the Southern high plains, Texas and New Mexico. *Journal of Geology*, **78**: 352-362.

Reeves, C.C.J. 1976. Caliche, origin, classification, morphology and uses. Estacado Books, Lubbock, Texas, 233 pp.

Reeves, C.C. 1983. Pliocene channel calcrete and suspen-parallel drainage in West Texas and New Mexico. In: Residual Deposits (Ed R.C.L. Wilson), Special Publication No. 11, pp. 179-183. Geological Society of London, London.

Reeves, C.V. 1972. Rifting in the Kalahari? *Nature*, **237**: 95-96.

Retallack, G.J. 2001. A 300-million-year record of atmospheric carbon dioxide from fossil plant cuticles. *Nature*, **411**: 287-290.

Ribet, I. and Thiry, M. 1990. Quartz growth in limestone: example from water-table silicification in the Paris Basin. *Chemical Geology*, **84**: 316-319.

Ringrose, S., Downey, B., Genecke, D., Sefe, F. and Vink, B. 1999. Nature of sedimentary deposits in the western Makgadikgadi basin, Botswana. *Journal of Arid Environments*, **43**: 375-397.

Ringrose, S., Kampunzu, A.B., Vink, B.W., Matheson, W. and Downey, W.S. 2002. Origin and palaeo-environments of calcareous sediments in the Moshaweng dry valley, southeast Botswana. *Earth Surface Processes and Landforms*, **27**: 591-611.

Ringrose, S., Huntsman-Mapila, P., Kampunzu, A.B., Downey, W., Coetzee, S., Vink, B., Matheson, W. and Vanderpost, C. 2005. Sedimentological and geochemical evidence for palaeo-environmental change in the Makgadikgadi subbasin, in relation to the MOZ rift depression, Botswana. *Palaeogeography, Palaeoclimatology, Palaeoecology*, **217**: 265-287.

Rogers, A.W. 1936. The surface geology of the Kalahari. *Transactions of the Royal Society of South Africa*, **24**: 57-80.

Rogers, K.H. 1997. Freshwater wetlands. In: Vegetation of southern Africa (Eds R.M. Cowling, D.M. Richardson and S.M. Pierce), pp. 322-47. Cambridge University Press, Cambridge.

Roodt, V. 1998. The Shell Tourist Map of Botswana. Shell Oil Botswana, Gaborone.

Rosen, M.R. and Holdren, G.R. 1986. Origin of dolomite cement in Chesapeake Group (Miocene) siliciclastic sediments: an alternative model to burial dolomitization. *Journal of Sedimentary Petrology*, **56**: 788-798.

Rossinsky, V., Wanless Jr., H. and Swart, P.K. 1992. Penetrative calcretes and their stratigraphic implications. *Geology*, **20**: 331–334.

Rouchy, J.M., Taberner, C., Blanc-Valleron, M.M., Sprovieri, R., Russell, M., Pierre, C., Di Stefano, E., Pueyo, J.J., Caruso, A., Dinares, J., Gomis-Coll, E., Cespuglio, G., Wolff, G., Ditchfield, P., Santisteban, C., Pestrea, S., Combourieu-Nebout, N., Santisteban, S. and Grimalt, J.O. 1998. Sedimentary and diagenetic markers of the restriction in a marine basin: the Lorca basin (SE Spain) during the Messinian. *Sedimentary Geology*, **121**: 23-55.

Rouchy, J.M., Taberner, C. and Peryt, T.M. 2001. Sedimentary and diagenetic transitions between carbonates and evaporites. *Sedimentary Geology*, **140**: 1-8.

Ruellan, A. 1968. Les horizons d'individualisation et d'accumulation du calcaire dans les sols du Maroc. Transactions of the 9th International Conference of Soil Science. Adelaide, Australia, 4: 501-510.

Ruellan, A. 1970. Les sols a profil calcaire differencie des plaines de la basse Moulouya. Doctoral, University of Strasbourg, 302 pp.

Rust, U. 1984. Geomorphic evidence of Quaternary climatic changes in Etosha, South West Africa/Namibia. In: Late Cainozoic Palaeoclimates of the Southern Hemisphere. (Ed J.C. Vogel), pp. 279-286. Balkema, Rotterdam.

Rust, U., Schmidt, H. and Dietz, K. 1984. Palaeoenvironments of present day arid south western Africa, 30,000-5,000 BP: results and problems. *Palaeoecology of Africa*, **16**: 109-148.

Rutherford, M.C. 1984. Relative allocation and seasonal phasing of woody plant components in a South African savanna. *Progress in Biometeorology*, **3**: 200-21.

South African Commission on Stratigraphy (SACS) 1980. Stratigraphy of South Africa. Part I: Lithostratigraphy of the Republic of South Africa, SWA/Namibia and the Republics of Bophuthatswana, Transkei and Venda., Handbook 8. Geological Society of South Africa, Pretoria.

Salomons, W. and Mook, W.G. 1976. Isotope geochemistry of carbonate dissolution and reprecipitation in soils. *Soil Science*, **122**: 15-24.

Salomons, W., Goudie, A.S. and Mook, W.G. 1978. Isotopic composition of calcrete deposits from Europe, Africa and India. *Earth Surface Processes and Landforms*, **3**: 43-57.

Sanz, M.E., Alonso-Zarza, A.M. and Calvo, J.P. 1995. Carbonate pond deposits related to semi-arid alluvial systems: examples from the Tertiary Madrid Basin, Spain. *Sedimentology*, **42**: 437–452.

Sanz, E., Hoyos, M., Calvo, J.P. and Rouchy, J.M. 1999. Nodular anhydrite growth controlled by pedogenic structures in evaporite lake formations. *Sedimentary Geology*, **125**: 195–203.

Sanz-Rubio, E., Sanchez-Moral, S., Canaveras, J.C., Calvo, J.P. and Rouchy, J.M. 2001. Calcitization of Mg-Ca carbonate and Ca sulphate deposits in a continental Tertiary basin (Calatayud Basin, NE Spain). *Sedimentary Geology*, **140**: 123-142.

Sarg, J.F. 2001. The sequence stratigraphy, sedimentology, and economic importance of evaporite–carbonate transitions: a review. *Sedimentary Geology*, **140**: 9-34.

Sauzay, G. 1974. Sampling of lysimeters for environmental isotopes of water. In: Techniques in Groundwater Hydrology, 2, pp. 61. IAEA, Vienna.

Sawula, G. and Martins, E. 1991. Major ion chemistry of the lower Boro River, Okavango Delta, Botswana. *Freshwater Biology*, **26**: 481-493.

Schefub, E., Schouten, S., Jansen, J.H.F. and Sinninghe Damsté, J.S. 2003. African vegetation controlled by tropical sea surface temperatures in the mid-Pleistocene period. *Nature*, **422**: 418-421.

Schlesinger, W.H. 1985. The formation of caliche soils of the Mojave Desert, California. *Geochimica et Cosmochimica Acta*, **49**: 57-66.

Scholes, R.J. 1988. The Responses of Three Savannas on Contrasting Soils to Removal of the Woody Component., University of the Witwatersrand, Johannesburg, RSA.

Scholes, R.J. and Walker, B.H. 1993. An African Savanna: Synthesis of the Nylsvley Study. Cambridge University Press, Cambridge.

Scholtz, C.H. 1975. Seismicity, Tectonics and Seismic Hazard of the Okavango Delta. UNDP/FAO Bot/71/506 Project Report, Gaborone.

Selaolo, E.T. 1998. Tracer studies and groundwater recharge assessment in the eastern fringe of the Botswana Kalahari. The Letlhakeng-Botlhapatlou area, Vrije Universiteit, Amsterdam.

Semeniuk, V. 1986. Calcrete breccia floatstone in Holocene sand developed by storm-uprooted trees. *Sedimentary Geology*, **48**: 183-192.

Semeniuk, V. and Meagher, T.D. 1981. Calcrete in Quaternary coastal dunes in south western Australia: a capillary rise phenomenon associated with plants. *Journal of Sedimentary Petrology*, **51**: 47-68.

Shafiqual Alam, M., Keppens, E., Paepe, R. and 168. 1997. The use of oxygen and carbon isotope compositions of pedogenic carbonates from Pleistocene palaeosols in NW Bangladesh, as palaeoclimatic indicators. *Quaternary Science Reviews*, **16**: 161-168.

Shaw, A.I. and Goudie, A.S. 2002. Geomorphological evidence for the extension of the Mega-Kalahari into south-central Angola. *South African Geographical Journal*, **84**: 182-194.

Shaw, A.I. and Goudie, A.S. 2004. Chemical sediments of the palaeo and active Okavango alluvial fan, Botswana: evidence for variations in the processes of formation. *Zietscrift fur Geomorphologie N.F.*, **136**: 89-112.

Shaw, P.A. 1984. A historical note on the outflow of the Okavango Delta system. *Botswana Notes and Records*, **16**: 127-130.

Shaw, P.A. 1985a. Late Quaternary landforms and environmental change in northwest Botswana: the evidence of Lake Ngami and the Mababe Depression. *Transactions of the Institute of British Geographers N.S.*, **10**: 333-346.

Shaw, P.A. 1985b. The desiccation of Lake Ngami: an historical perspective. *Geographical Journal*, **151**: 318-326.

Shaw, P. 1986a. The palaeohydrology of the Okavango delta - some preliminary results. *Palaeoecology of Africa*, **17**: 51-8.

Shaw, P. 1986b. Geomorphic evidence for the Late Quaternary palaeoclimates of the middle Kalahari of northern Botswana. *Catena*, **13**: 349-59.

Shaw, P. 1988a. After the flood: the fluvio-lacustrine landforms of northern Botswana. *Earth Science Reviews*, **25**: 449-456.

Shaw, P.A. 1988b. Lakes and Pans. In: The Geomorphology of Southern Africa. (Eds B.P. Moon and G.F. Dardis), pp. 120-140. Southern Book Publishers, Johannesburg.

Shaw, P.A. and Cooke, H.J. 1986. Geomorphic evidence for the late Quaternary palaeoclimates of the middle Kalahari of northern Botswana. *Catena*, **13**: 349-359.

Shaw, P.A. and De Vries, J.J. 1988. Duricrust, groundwater and valley development in the Kalahari of south-east Botswana. *Journal of Arid Environments*, **14**: 245-254.

Shaw, P.A. and Thomas, D.S.G. 1988. Lake Caprivi: a Late Quaternary link between the Zambezi and middle Kalahari drainage systems. *Zietscrift fur Geomorphologie N.F.*, **32**: 329-337.

Shaw, P.A. and Nash, D.J. 1998. Dual mechanisms for the formation of fluvial silcretes in the distal reaches of the Okavango Delta Fan, Botswana. *Earth Surface Processes and Landforms*, **23**: 705-714.

Shaw, P.A., Cooke, H.J. and Perry, C.C. 1990. Microbialitic silcretes in highly alkaline environments: some observations from Sua Pan, Botswana. *South African Journal of Geology*, **93**: 803-808.

Shaw, P.A., Cooke, H.J. and Thomas, D.S.G. 1988. Recent advances in the study of Quaternary landforms in Botswana. *Palaeoecology of Africa*, **19**: 15-26.

Shaw, P.A., Thomas, D.S.G. and Nash, D.J. 1992. Late quaternary fluvial activity in the dry valleys (mekgacha) of the Middle and Southern Kalahari, southern Africa. *Journal of Quaternary Science*, **7**: 273-281.

Shaw, P.A., Bateman, M.D., Thomas, D.S.G. and Davies, F. 2003. Holocene fluctuations of Lake Ngami, Middle Kalahari: chronology and responses to climatic change. *Quaternary International*, **111**: 23-35.

Shepard, F.P. 1954. Nomenclature based on sand-silt-clay ratios. *Journal of Sedimentary Petrology*, **24**: 151-158.

Shi, N., Dupont, L.M., Beug, H.-J. and Schneider, R. 2000. Correlation between vegetation and southwest Africa and oceanic upwelling in the past 21,000 year. *Quaternary Research*, **54**: 72-80.

Shi, N., Schneider, R., Beug, H.-J. and Dupont, L.M. 2001. Trade wind variation during the last 135 kyr: evidence from pollen spectra in eastern South Atlantic sediments. *Earth and Planetary Science Letters*, **187**: 311-321.

Shideler, G.L. 1976. A comparison of electronic particle counting and pipette techniques in routine mud analysis. *Journal of Sedimentary Petrology*, **42**: 122-134.

Siesser, W.G. 1973. Diagenetically formed ooids and intraclasts in South African calcretes. *Sedimentology*, **20**: 539-551.

Singer, A. 1979. Palygorskite in sediments: detrital, diagenetic or neoformed: a critical review. *Geoogische Rundschau*, **68**: 996-1008.

Singer, A. and Norrish, K. 1974. Pedogenic palygorskite occurrences in Australia. *American Mineralogist*, **59**: 508-517.

Smale, D. 1968. The occurrence of clinoptilolite in pan sediments in the Nata area, Northern Botswana. *Transactions of the Geological Society of South Africa*, **71**: 147-152.

Smale, D. 1973. Silcretes and associated silica diagenesis in Southern Africa and Australia. *Journal of Sedimentary Petrology*, **43**: 1077-1089.

Smit, P.J. 1974a. Explanatory notes, geological map 2522 Bray, 1:250 000 Geological Series, Geological Survey, Pretoria.

Smit, P.J. 1974b. Explanatory notes, geological map 2622 Morokweng, 1:250 000 Geological Series, Geological Survey, Pretoria.

Smit, P.J. 1977. Die Geohidrologie in die Opvanggebied van die Moloporivier in die Noordelijke Kalahari. Unpublished Ph.D., University of the Orange Free State, Bloemfontein, RSA.

Smith, A.M. and Mason, T.R. 1991. Pleistocene, multiple-growth, lacustrine oncoids from the Poacher's Point Formation, Ethosa Pan, northern Namibia. *Sedimentology*, **38**: 591-599.

Smith, G.A., Wang, Y., Cerling, T.E. and Geissman, J.W. 1993. Comparison of a paleosol-carbonate isotope record to other records of Pliocene-early Pleistocene climate in the western United States. *Geology*, **21**: 691-694.

Smith, N., McCarthy, T.S., Ellery, W.N., Merry, C.L. and Ruther, H. 1997. Avulsion and anastomosis in the panhandle region of the Okavango Fan, Botswana. *Geomorphology*, **20**: 49-65.

Smith, R.A. 1984. The lithostratigraphy of the Karoo Supergroup in Botswana. A report on the geophysical and geological results of follow-up drilling to the Aeromagnetic Survey of Botswana. Bulletin Series, 26. Geological Survey Deparment, Lobatse.

Smith, T.M. and Goodman, P.S. 1986. The effect of competition on the structure and dynamics of Acacia savannas in southern Africa. *Journal of Ecology*, **74**: 1031-44.

Smith, T.M. and Grant, K. 1986. The role of competition in the spacing of trees in a Burkea africana-Terminalia sericea savanna. *Biotropica*, **18**: 219-23.

Soil Survey Staff 1975. Soil taxonomy: a basic system of soil classification for making and interpreting soil surveys. USDA-SCS Agricultural Handbook No. 436. US Government Printing Office, Washington, DC, 754 pp.

Solano-Acosta, W. and Dutta, P.K. 2005. Unexpected trend in the compositional maturity of second-cycle sand. *Sedimentary Geology*, **178**: 275-283.

Solomon, S.T. and Walkden, G.M. 1985. The application of cathodoluminescence to interpreting the diagenesis of an ancient calcrete profile. *Sedimentology*, **32**: 877-896.

Spotl, C., Kralik, M. and Kunk, M.J. 1996. Authigenic feldspar as an indicator of paleo-rock/water interactions in Permian carbonates of the northern calcareous alps, Austria. *Journal of Sedimentary Research*, **66**: 139-146.

Stalker, A.D. 1983. Aha Hills prospecting licence 39/80. Final report, Billiton Botswana (Pty) Limited, Gaborone.

Stanistreet, I.G. and McCarthy, T.S. 1993. The Okavango Fan and the classification of subaerial fan systems. *Sedimentary Geology*, **85**: 115-133.

Stanistreet, I.G., Cairncross, B. and McCarthy, T.S. 1993. Low sinuosity and meandering bedload rivers of the Okavango Fan: channel confinement by vegetated levees without fine sediment. *Sedimentary Geology*, **85**: 135-156.

Starinsky, A., Bielski, M., Ecker, A. and Steinitz, G. 1987. Tracing the origin of salts in groundwater by Sr isotope composition (the crystalline complex of the southern Sinai, Egypt). *Isotope Geoscience*, **1**: 257-267.

Stock, W.D., Allsopp, N., Heyden, F.v.d. and Witkowski, E.T.F. 1997. Plant form and function. In: Vegetation of southern Africa (Eds R.M. Cowling, D.M. Richardson and S.M. Pierce), pp. 376-96. Cambridge University Press, Cambridge.

Stokes, S., Thomas, D.S.G. and Washington, R. 1997a. Multiple episodes of aridity in southern Africa since the last interglacial period. *Nature*, **388**: 154-158.

Stokes, S., Thomas, D.S.G. and Shaw, P.A. 1997b. New chronological evidence for the nature and timing of linear dune development in the southwest Kalahari Desert. *Geomorphology*, **20**: 81-93.

Stratten, T. 1979. The origin of the diamondiferous alluvial gravels in the south-western Transvaal. Geological Society of South Africa, Special Publication: 219-228.

Street, F.A. and Grove, A.T. 1976. Environmental and climatic implications of late Quaternary lake-level fluctuations in Africa. *Nature*, **261**: 385-390.

Stuart-Williams, V. 1992. Etosha: third largest lake in the world. In: Oshanas, Sustaining People, Environment and Development in Central Owambo, Namibia. (Eds A. Marsh and M. Seely), pp. 1-13. Desert Research Foundation of Namibia, Windhoek.

Summerfield, M.A. 1978. The Nature and Origin of Silcrete with Particular Reference to Southern Africa. Unpublished D.Phil., University of Oxford, Oxford, UK.

Summerfield, M.A. 1981. Nature and occurrence of silcrete, southern Cape Province, South Africa. School of Geography, University of Oxford Research Paper, 28.

Summerfield, M.A. 1982. Distribution, nature and genesis of silcrete in arid and semi-arid southern Africa. In: Catena Supplement (Ed D.H. Yaalon), 1, pp. 37-65.

Summerfield, M.A. 1983a. Petrography and diagenesis of silcrete from the Kalahari Basins and Cape coastal zone, Southern Africa. *Journal of Sedimentary Petrology*, **53**: 895-909.

Summerfield, M.A. 1983b. Silcrete as a palaeoclimatic indicator. *Palaeogeography, Palaeoclimatology and Palaeoecology*, **41**: 65-80.

Summerfield, M.A. 1983c. Silcrete. In: Chemical Sediments and Geomorphology. (Eds A.S. Goudie and K. Pye), pp. 59-91. Academic Press, London.

Sutcliffe, J.V. and Parks, Y.P. 1989. Comparative water balances of selected African wetlands. *Hydrological Science Journal*, **34**: 49-62.

Talbot, M.R. 1990. A review of the palaeohydrological interpretation of carbon and oxygen isotopic ratios in primary lacustrine carbonates. *Chemical Geology*, **80**: 261–279.

Talbot, M.R. and Kelts, K. 1990. Paleolimnological signatures from carbon and oxygen isotopic ratios in carbonates from organic rich lacustrine sediments. In: Lacustrine Exploration: Case Studies and Modern Analogues. (Ed B.J.

Katz), 50, pp. 99– 112. American Association Petroleum Geologist Memoir, Tulsa, OK.

Talma, A.S. and Netterberg, F. 1983. Stable isotope abundances in calcretes. In: Residual Deposits: Surface Related Weathering Processes and Materials. (Ed R.C.L. Wilson), 11, pp. 221– 233. Geological Society London, Special Publication, Blackwell, Oxford.

Tanner, L.H. 2000. Palustrine – lacustrine and alluvial facies of the (Norian) Owl Rock Formation (Chinle Group), Four Corners Region, Southwestern U.S.A: implications for late Triassic paleoclimate. *Journal of Sedimentary Research*, **70**: 1280– 1290.

Thiry, M. and Ribet, I. 1999. Groundwater silicification in Paris Basin limestones; fabrics, mechanisms and modelling. *Journal of Sedimentary Research*, **69**: 171– 183.

Thomas, D.S.G. 1984. Ancient ergs of the former arid zones of Zimbabwe, Zambia and Angola. *Transactions of the Institute of British Geographers N.S.*, **9**: 75-88.

Thomas, D.S.G. and Shaw, P.A. 1988. Late Cainozoic drainage evolution in the Zambezi basin: Geomorphological evidence from the Kalahari rim. *Journal of African Earth Sciences*, **7**: 611-618.

Thomas, D.S.G. and Shaw, P.A. 1991. The Kalahari Environment. Cambridge University Press, Cambridge, 284 pp.

Thomas, D.S.G., Nash, D.J., Shaw, P.A. and Van der Post, C. 1993. Present day lunette sediment cycling at Witpan in the arid southwestern Kalahari Desert. *Catena*, **20**: 516-527.

Thomas, D.S.G., Stokes, S. and Shaw, P.A. 1997. Holocene aeolian activity in the southwestern Kalahari Desert, southern Africa: significance and relationships to late-Pleistocene dune-building events. *The Holocene*, **7**: 273-281.

Thomas, D.S.G., O'Connor, P.W., Bateman, M.D., Shaw, P.A., Stokes, S. and Nash, D.J. 2000. Dune activity as a record of late Quaternary aridity in the Northern Kalahari: new evidence from northern Namibia interpreted in the context of regional arid and humid chronologies. *Palaeogeography, Palaeoclimatology, Palaeoecology*, **156**: 243-259.

Thomas, D.S.G. and Shaw, P.A. 2002. Late Quaternary environmental change in central southern Africa: new data, synthesis, issue and prospects. *Quaternary Science Reviews*, **21**: 783-797.

Thomas, D.S.G., Brook, G., Shaw, P.A., Bateman, M., Haberyan, K., Appleton, C., Nash, D., McLaren, S. and Davies, F. 2003. Late Pleistocene wetting and drying in the NW Kalahari: an integrated study from the Tsodilo Hills, Botswana. *Quaternary International*, **104**: 53-67.

Thomas, M.A. 1981. The geology of the Kalahari in the northern Cape Province (areas 2620 and 2720). MSc. unpublished, University of the Orange Free State, Bloemfontein, RSA.

Thomas, R.J. and Thomas, M.A. 1989. The geology of the Noenieput area. Explanation of sheet 2720, scale 1:250 000, Geological Survey, Department of Mineral and Energy Affairs, RSA.

Thomas, R.J., Thomas, M.A. and Malherbe, S.J. 1988. The geology of the Nossob and Twee Rivieren areas. Explanation of sheets 2520 and 2620, scale 1:250 000., Geological Survey, Department of Mineral and Energy Affairs, RSA.

Tooth, S. 1999. Floodouts in Central Australia. In: Varieties of fluvial form. (Eds A.J. Miller and A. Gupta), pp. 219-247. John Wiley and Sons, Chichester.

Tooth, S. 2000. Downstream changes in dryland river channels: the Northern Plains of arid central Australia. *Geomorphology*, **34**: 33-54.

Tucker, M.E. and Wright, V.P. 1990. Carbonate Sedimentology. Blackwell Science, Oxford.

Tyson, P.D. 1999. Late-Quaternary and Holocene palaeoclimates of southern Africa: A synthesis. *South African Journal of Geology*, **102**: 335-349.

Tyson, P.D. and Partridge, T.C. 2000. Evolution of Cenozoic Climates. In: The Cenozoic of Southern Africa. (Eds T.C. Partridge and R.R. Maud), pp. 371-387. Oxford University Press, Oxford.

Udden, J.A. 1914. Mechanical composition of clastic sediments. *Bulletin of the Geological Society of America*, **25**: 655-744.

Udeze, C.U. and Oboh-Ikuenobe, F.E. 2005. Neogene palaeoceanographic and palaeoclimatic events inferred from palynological data: Cape Basin off South Africa, ODP Leg 175. *Palaeogeography, Palaeoclimatology, Palaeoecology*, **219**: 199-223.

Urbano, L.D., Person, M.A. and Hanor, J. 2000. Groundwater-lake interactions in semi-arid environments. *Journal of Geochemical Exploration*, **69-70**: 423-427.

USGS 2001. Collection of water samples. In: U.S. Geological Survey TWRI Book 9, pp. 24-55. U.S. Geological Survey.

Valero Garces, B. and Gisbert, J. 1992. Shallow carbonate lacustrine facies models in the Permian of the Aragon– Bearn Basin (Western Spanish-French Pyrenees). *Carbonates and Evaporites*, **7**: 94– 107.

Van der Hoven, S.J., Solomon, D.K. and Moline, G.R. 2005. Natural spatial and temporal variations in groundwater chemistry in fractured, sedimentary rocks: scale and implications for solute transport. *Applied Geochemistry*, **20**: 861-873.

Van Houten, F.B.V. 1973. Origin of red beds: a review, 1961-1972. *Annual Review of Earth and Planetary Science*, **1**: 39-61.

Veenendal, E.M., Monnaapula, S.C., Gilika, T. and Magole, I. 1992. Vesicular-arbuscular mycorrhizal infection of grass seedlings in a degraded semi-arid savanna in Botswana. *New Phytologist*, **121**: 477-85.

Verrecchia, E.P. 1990. Litho-diagenetic implications of the calcium oxalate-carbonate biogeochemical cycle in semiarid calcretes, Nazareth, Israel. *Geomicrobiology Journal*, **8**: 87-99.

Verrecchia, E.P. 1996. Morphometry of microstromatolites in calcrete laminar crusts and a fractal model of their growth. *Mathematical Geology*, **28**: 87-109.

Verrecchia, E.P. and Verrecchia, K.E. 1994. Needle-fibre calcite: a critical review and a proposed classification. *Journal Sedimentary Research*, **A64**: 650-664.

Verrecchia, E.P. and Le Coustumer, M.N. 1996. Occurrence and genesis of palygorskite and associated clay minerals in a Pleistocene calcrete complex, Sde Boqer, Negev Desert, Israel. *Clay Minerals*, **31**: 183-202.

Verrecchia, E.P., Dumont, J.L. and Rolko, K.E. 1990. Do fungi building limestones exist in semi-arid regions? *Naturwissenschaften*, **77**: 584-586.

Verrecchia, E.P., Dumont, J.L. and Verrecchia, K.E. 1993. Role of calcium oxalate biomineralization by fungi in the formation of calcretes: a case

study from Nazareth, Israel. *Journal of Sedimentary Petrology*, **63**: 1000-1006.

Verrecchia, E.P., Freytet, P., Verrecchia, K.E. and Dumont, J.L. 1995. Spherulites in calcrete laminar crusts: biogenic CaCO3 precipitation as a major contributor to crust formation. *Journal of Sedimentary Research*, **A65**: 690-700.

Verrecchia, E.P., Freytet, P., Verrecchia, K.E. and Dumont, J.L. 1996. Spherulites in calcrete laminar crusts: biogenic CaCO3 precipitation as a major contributor to crust formation. Reply. *Journal of Sedimentary Research*, **A66**: 1041-1044.

Vogel, J.C. and Van Urk, H. 1975. Isotopic composition of groundwater in semi-arid regions of southern Africa. *Journal of Hydrology*, **25**: 23-36.

Walker, B.H. 1985. Structure and function of savanna: an overview. In: Ecology and Management of the World's Savannas (Eds J.H. Tothill and J.J. Mott), pp. 350-3. Australian Academy of Science, Canberra.

Walker, B.H. and Noy-Meir, L. 1982. Aspects of the stability and resilience of savanna ecosystems. In: Ecology of Tropical Savannas (Eds B.J. Huntley and B.H. Walker), pp. 556-609. Springer-Verlag, Berlin.

Walker, T.R. 1960. Carbonate replacement of detrital crystalline silicate minerals as a source of authigenic minerals in sedimentary rocks. *Bulletin of the Geological Society of America*, **71**: 145-152.

Walker, T.R. 1967. Colour of recent sediments in tropical Mexico: a contribution to the origin of the red beds. *Bulletin of the Geological Society of America*, **78**: 917-920.

Walker, T.R. and Honea, R.M. 1969. Iron content of modern deposits in the Sonoran Desert: a contribution to the origin of red beds. *Bulletin of the Geological Society of America*, **80**: 535-594.

Walter, H. 1971. Ecology of Tropical and Subtropical Vegetation. Oliver and Boyd, London.

Wang, Y. and Zheng, S. 1989. Paleosol nodules as Pleistocene paleoclimatic indicators, Luochuan, P.R. China. *Palaeogeography, Palaeoclimatology, Palaeoecology*, **76**: 39-44.

Wang, Y., Nahon, D. and Merino, E. 1994. Dynamic model of the genesis of calcrete replacing silicate rocks in semi-arid regions. *Geochimica et Cosmochimica Acta*, **58**: 5131-5145.

Wasilenkoff, J.M. 1988. Exploration results of the Kalahari Geophysical project 1987-1988, Botswana, Africa Petro-Canada International Assistance Corporation report for Department of Geological Survey, Lobatse, Botswana.

Watson, A. and Nash, D.J. 1997. Desert crusts and varnishes. In: Arid Zone Geomorphology: Process, Form and Change in Drylands (Ed D.S.G. Thomas), pp. 69-107. John Wiley, Chichester.

Watts, N.L. 1977a. Pseudo-anticlines and other structures in some calcretes of Botswana and South Africa. *Earth Surface Processes and Landforms*, **2**: 63-74.

Watts, N.L. 1977b. A comparative study of some Quaternary, Permo-Triassic and Siluro-Devonian calcretes. Ph.D., University of Reading, Reading, UK.

Watts, N.L. 1978. Displacive calcite: evidence from recent and ancient calcretes. *Geology*, **6**: 699-703.

Watts, N.L. 1980. Quaternary pedogenic calcretes from the Kalahari (southern Africa): mineralogy, genesis and diagenesis. *Sedimentology*, **27**: 661-686.

Weaver, C.E. and Beck, K.C. 1977. Miocene of the S.E. United States: a model for chemical sedimentation in a peri-marine environment. *Sedimentary Geology*, **17**: 1-234.

Webb, J.A. and Bennetts, D.A. 2003. Groundwater evolution within a catchment affected by dryland salinity, southeastern Australia. *Abstracts with Programs - Geological Society of America,* **35**(6): 565

Wellington, J.H. 1938. The Kunene River and Etosha Plain. *South African Geographical Journal*, **20**: 21-32.

Wellington, J.H. 1939. The Greater Etosha Basin. *South African Geographical Journal*, **21**: 47-48.

Wells, N.A. 1983. Carbonate deposition, physical limnology and environmentally controlled chert formation in Paleocene – Eocene Lake Flagstaff, Central Utah. *Sedimentary Geology*, **35**: 263– 296.

Wentworth, C.K. 1922. A scale of grade and class terms for clastic sediments. *Journal of Geology*, **30**: 377-392.

Wentworth, C.K. 1929. Method of computing mechanical composition of sediments. *Geological Society of America Bulletin*, **40**: 771-790.

West, L.T., Wilding, L.P. and Hallmark, C.T. 1988. Calcius-tolls in central Texas: II Genesis of calcic and petrocalcic horizons. *Soil Science Society of America Journal*, **53**: 1731-1740.

Westerhold, T., Bickert, T. and Rohl, U. 2005. Middle to late Miocene oxygen isotope stratigraphy of ODP site 1085 (SE Atlantic): new constrains on

Miocene climate variability and sea-level fluctuations. *Palaeogeography, Palaeoclimatology, Palaeoecology*, **217**: 205-222.

White, F. 1983. The vegetation of Africa, a descriptive memoir to accompany the UNESCO/AETFAT/UNSO Vegetation Map of Africa (3 Plates, Northwestern Africa, Northeastern Africa, and Southern Africa, 1:5,000,000). UNESCO, Paris.

Wiggs, G.F.S., Thomas, D.S.G., Livingstone, I. and Bullard, J.E. 1995. Dune mobility and vegetation cover in the southwest Kalahari desert. *Earth Surface Processes and Landforms*, **20**: 515-530.

Wilbert, J. 1962. Croutes et encroutements calcaires au Maroc. *Al Awamia*, **3**: 175-192.

Wilson, B.H. 1973. Some natural and man-made changes in the channels of the Okavango Delta. *Botswana Notes and Records*, **5**: 132-153.

Wilson, B.H. and Dincer, T. 1976. An introduction to the hydrology and hydrography of the Okavango delta. In: Proceedings of the Symposium on the Okavango Delta and its Future Utilisation., pp. 33-48. Botswana Society, Gaborone.

Winland, H.D. 1968. The role of high-Mg calcite in the preservation of micrite envelopes and textural features of aragonite sediments. *Journal of Sedimentary Petrology*, **38**: 1320-1325.

Winland, H.D. 1969. Stability of calcium carbonate polymorphs in warm, shallow seawater. *Journal of Sedimentary Petrology*, **39**: 1579-1587.

Wood, W.W. 1976. Guidelines for collection and field analysis of groundwater samples for selected unstable constituents. Techniques of Water Resources Investigations of the United States Geological Survey, Book 1. USGS.

Worden, R.H., Ruffell, A.H. and Cornford, C. 2000. Palaeoclimate, sequence stratigraphy and diagenesis. *Journal of Geochemical Exploration*, **69-70**: 453-457.

Wright, D.T. 1999. The role of sulphate-reducing bacteria and cyanobacteria in dolomite formation in distal ephemeral lakes of the Coorong region, South Australia. *Sedimentary Geology*, **126**: 147-157.

Wright, V.P. 1983. A rendzina from the early Carboniferous of South Wales. *Sedimentology*, **30**: 159-179.

Wright, V.P. 1984. The significance of needle-fibre calcite in a Lower Carboniferous paleosol. *Geological Journal*, **19**: 23-32.

Wright, V.P. 1986. The role of fungal biomineralization in the formation of early Carboniferous soil fabrics. *Sedimentology*, **33**: 831-838.

Wright, V.P. 1989. Terrestrial stromatolites and laminar calcretes: a review. *Sedimentary Geology*, **65**: 1-13.

Wright, V.P. 1990a. Syngenetic formation of grainstones and pisolites from fenestral carbonates in pertidal settings: discussion. *Journal of Sedimentary Petrology*, **60**: 309-310.

Wright, V.P. 1990b. Estimating rates of calcrete formation and sediment accretion in ancient alluvial deposits. *Geological Magazine*, **127**: 273-276.

Wright, V.P. 1990c. A micromorphological classification of fossil and recent calcic and petrocalcic microstructures. In: Soil Micromorphology: A Basic and applied Science (Ed L.A. Douglas), Developments in Soil Science, Vol. 19, pp. 401-407. Elsevier, Amsterdam.

Wright, V.P. 2005. Calcretes. In: Geochemical Sediments and Landscapes. (Eds D.J. Nash and S.J. McLaren). Blackwells, London.

Wright, V.P. and Wilson, R.C.L. 1987. A terra-rosa like complex from the Upper Jurassic of Portugal. *Sedimentology*, **34**: 259-273.

Wright, V.P. and Robinson, D. 1988. Early Carboniferous floodplain deposits from South Wales; a case study of the controls on Palaeosol development. *Journal of the Geological Society*, **145**: 847-857.

Wright, V.P. and Alonso Zarza, A.M. 1990. Pedostratigraphic models for alluvial fan deposits; a tool for interpreting ancient sequences. *Journal of the Geological Society*, **147**: 8-10.

Wright, V.P. and Tucker, M.E. 1991. Calcretes. Reprint Series Volume 2 of the International Association of Sedimentologists, 2. Blackwell Scientific Publications, Oxford.

Wright, V.P. and Marriott, S.B. 1993. The sequence stratigraphy of fluvial depositional systems: the role of floodplain sediment storage. *Sedimentary Geology*, **86**: 203–210.

Wright, V.P. and Sandler, A. 1994. A hydrogeological model for the early diagenesis of Late Triassic alluvial sediments. *Journal of the Geological Society*, **151**: 897-900.

Wright, V.P. and Marriott, S.B. 1996. A quantitative approach to soil occurrence in alluvial deposits and its application to the Old Red Sandstone of Britain. *Journal of the Geological Society*, **153**: 907-913.

Wright, V.P., Platt, N.H. and Wimbledon, W.A. 1988. Biogenic laminar calcretes: evidence of calcified root-mat horizons in paleosols. *Sedimentology*, **35**: 603-620.

Wright, V.P., Platt, N.H., Marriott, S.B. and Beck, V.H. 1995. A classification of rhizogenic (root formed) calcretes, with examples from the Upper Jurassic-

Lower Cretaceous of Spain and Upper Cretaceous of southern France. *Sedimentary Geology*, **100**: 143-158.

Wright, V.P., Beck, V.H., Sanz-Montero, M.E., Verrecchia, E.P., Freytet, P., Verrecchia, K.E. and Dumont, J.-L. 1996. Spherulites in calcrete laminar crusts; biogenic CaCO 3 precipitation as a major contributor to crust formation; discussion and reply. *Journal of Sedimentary Research*, **66**: 1040-1044.

Wright, V.P., Alonso-Zarza, A.M., Sanz, M.E. and Calvo, J.P. 1997. Diagenesis of Late Miocene micritic lacustrine carbonates, Madrid Basin, Spain. *Sedimentary Geology*, **114**: 81– 95.

Yaalon, D.H. 1981. Pedogenic carbonates in aridic soils - magnitude of the pool and annual fluxes. In: Abstracts: International Conference on Aridic Soils, pp. 94, Jerusalem.

Yaalon, D.H. 1988. Calcic horizon and calcrete in Aridic soils and paleosols: progress in the last twenty two years. Soil Science of Society of America Agronomy Abstract.

Zachos, J.C., Flower, B.P. and Paul, H. 1997. Orbitally paced climate oscillations across the Oligocene/Miocene boundary. *Nature*, **388**: 567-570.

Zachos, J.C., Pagani, M., Sloan, L., Thomas, E. and Billups, K. 2001a. Trends, rhythms, and aberrations in global climate 65 Ma to present. *Science*, **292**: 686-693.

Zachos, J.C., Shackleton, N.J., Revenaugh, J.S., Palike, H. and Flower, B.P. 2001b. Climate response to orbital forcing across the Oligocene-Miocene boundary. *Science*, **292**: 274-278.

Zak, K. and Skala, R. 1993. Carbon isotopic composition of whewellite (CaC2O4.H2O) from different geological environments and its significance. *Chemical Geology*, **106**: 123-131.

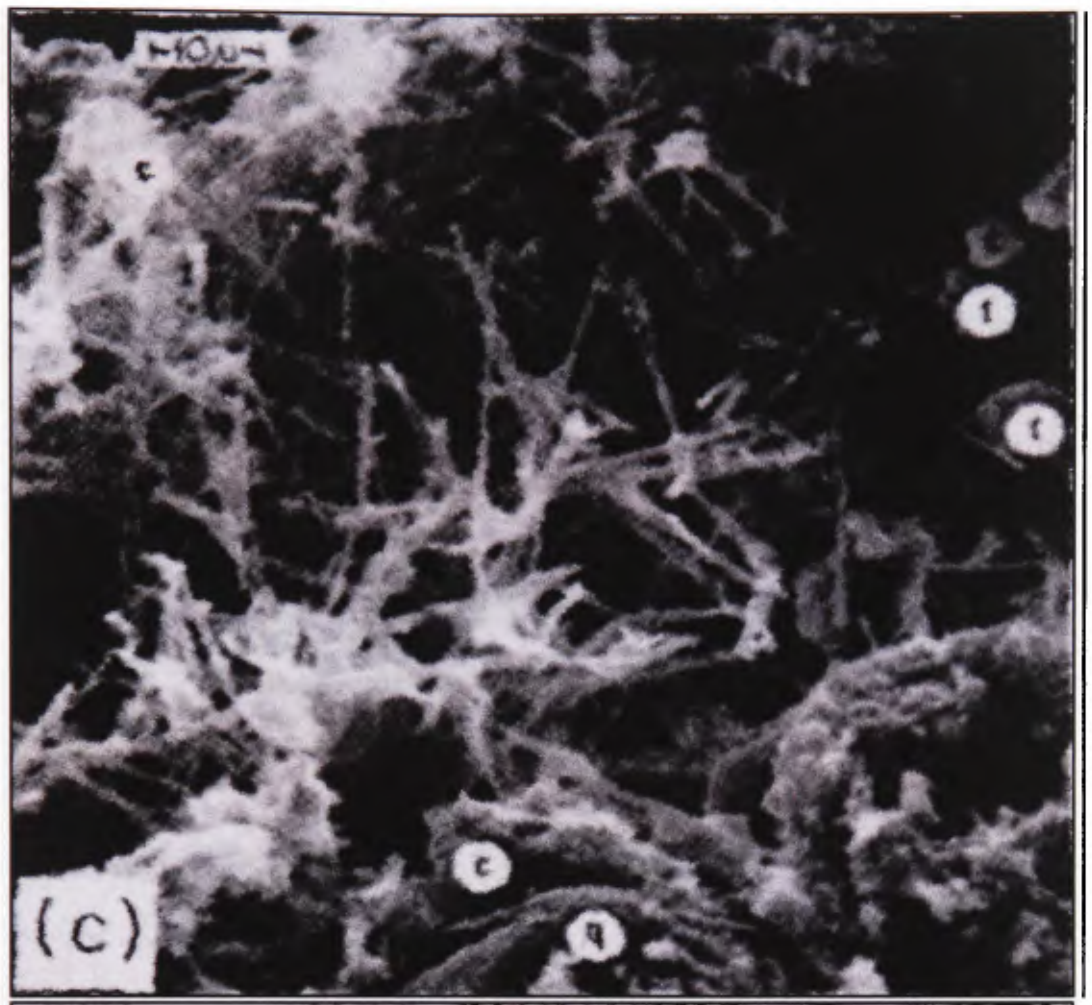
Zietsman, P.C., Grobbelaar, N. and van Rooyen, N. 1988. Soil nitrogenase activity of the Nylsvley Nature Reserve. *South African Journal of Botany*, **54**: 21-7.

14. APPENDICES 1-17

Appendix 1: Atlas of micro-structures within terrestrial carbonates.

GEOCHEMICAL / CRYSTALLINE STRUCTURES

Acicular calcite (Needle like)

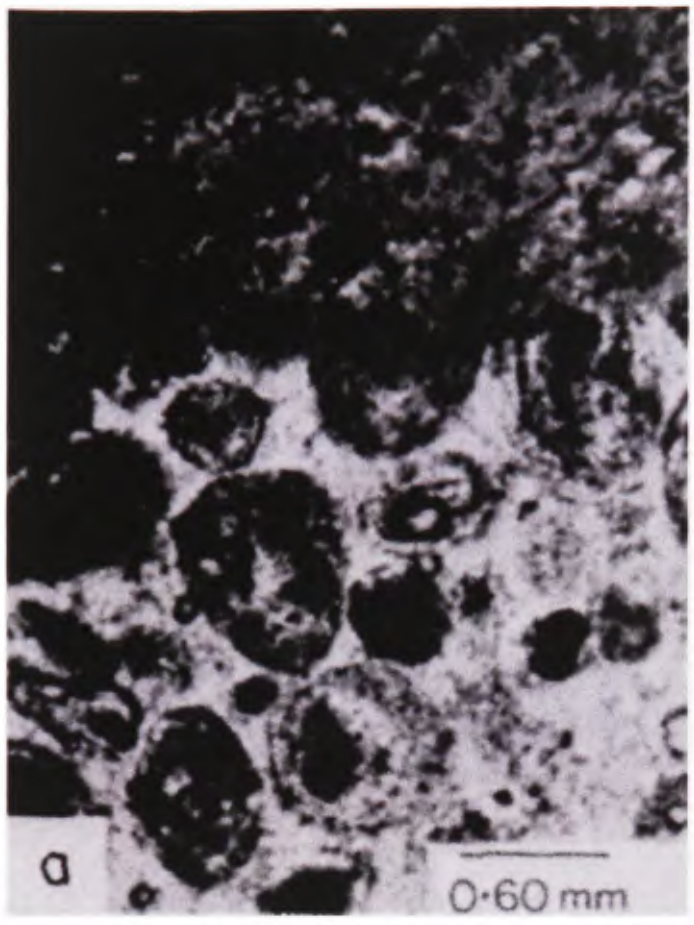


SEM photograph showing a **void filled** with an interlocking network of **acicular fibres**. A quartz grain (q) with an irregular **micritic coating** (c) occurs in the foreground. **Tubules** (t) are present to the right. (Knox, `77)

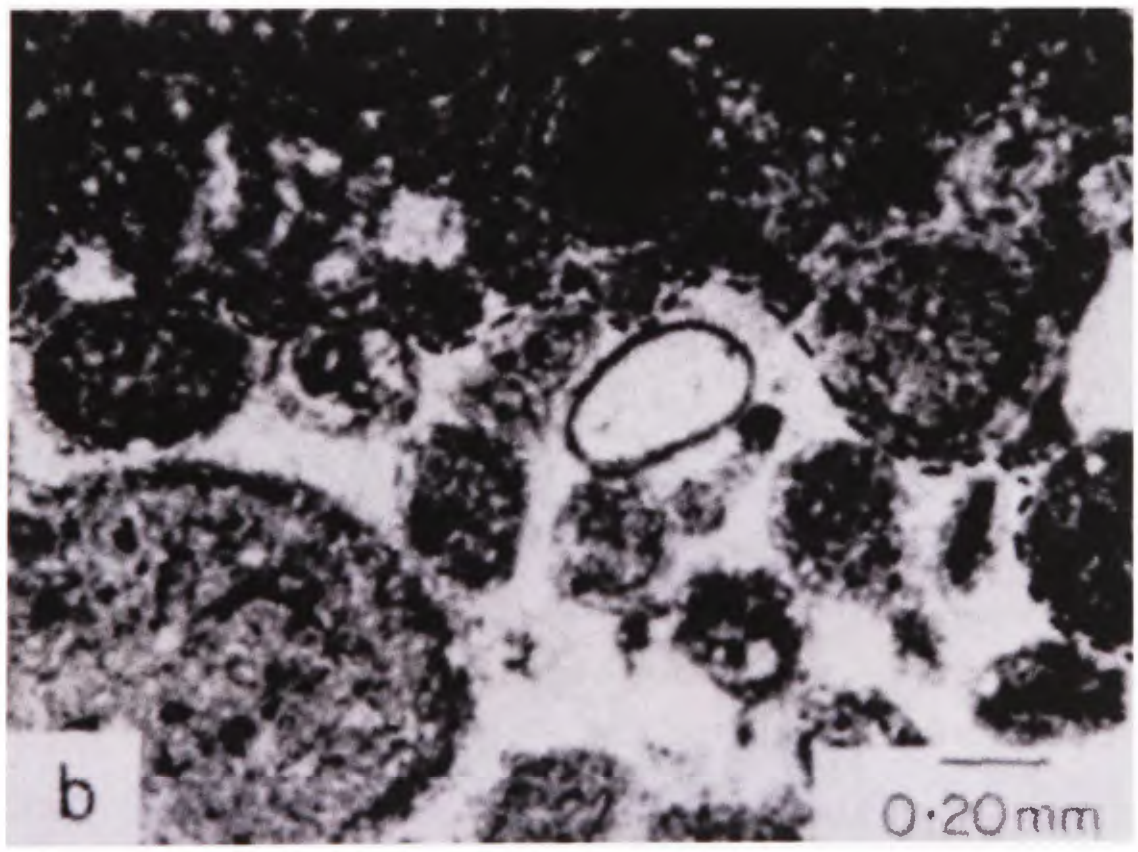


SEM view of interlocking **acicular fibres** bound together by **membraneous coatings**. Note the furrow running down the fibres. (Knox, `77)

Allochems



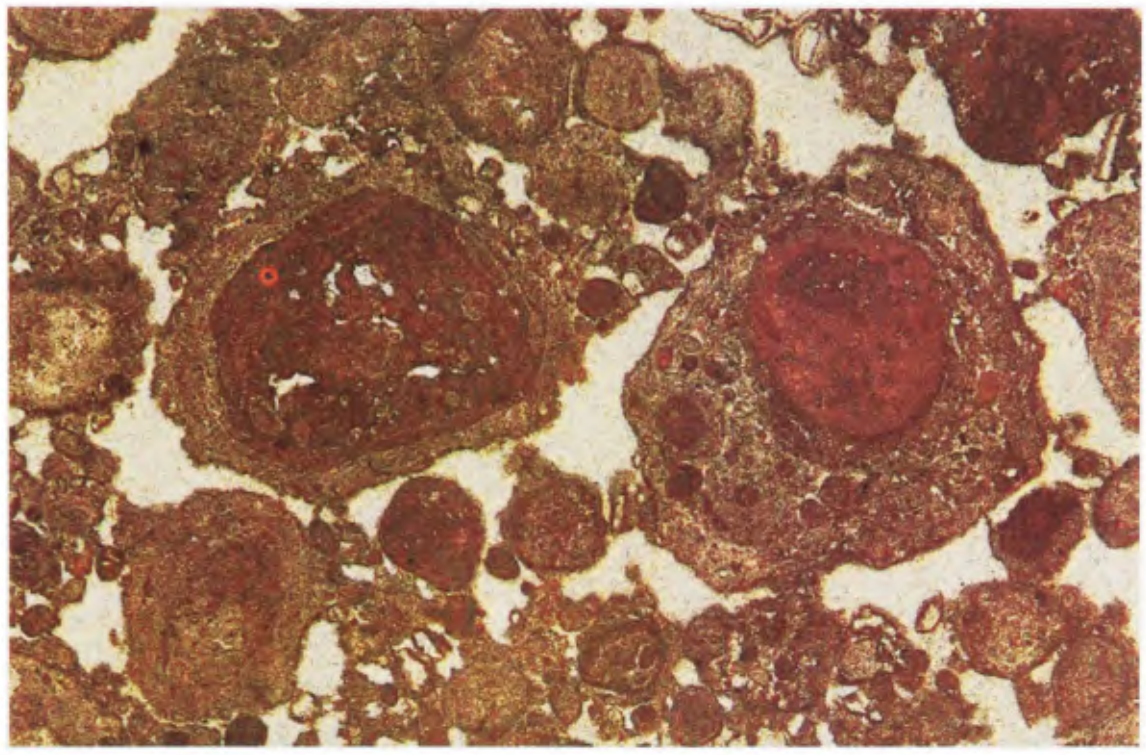
Thin section, plane light. Zone of alteration in the topmost portion of the Miami Limestone in contact with calcareous crust showing **micritisation** of **allochems** and **sparmicritisation** of **sparry calcite cement** (faintly visible between **allochems**). (Kahle, `77)



Thin section, plane light. Contact (dashed) between Miami Limestone and overlying calcareous crusts. Note relics of **allochems** and of **sparry calcite cement** from the Miami Limestone in the calcareous crusts. (Kahle, `77)

Aggregate Grains

An aggregate grain is formed when two or more originally separate particles become cemented together by micrite (Adams and MacKenzie, 1998).

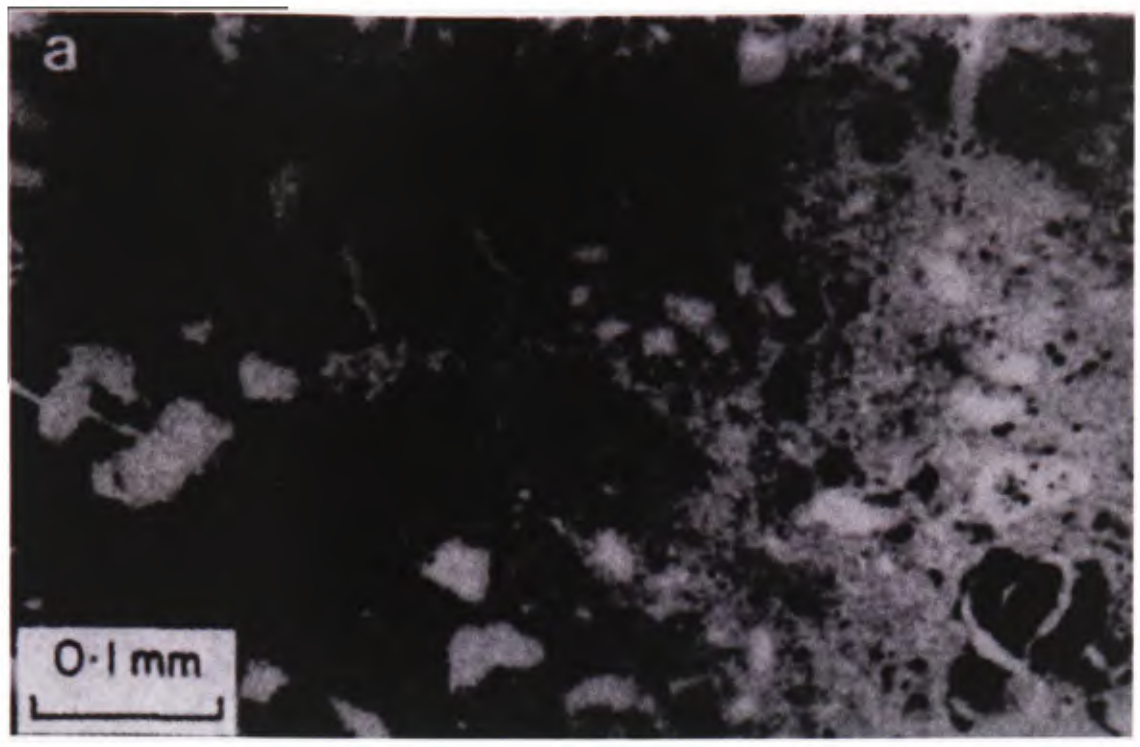


Complex **aggregate grains** showing evidence of *in situ* growth, at least during the later stages of their formation, with smaller grain enveloped in the coatings of larger ones and bridging sediments between grains or groups of grains (Adams and MacKenzie, `98)

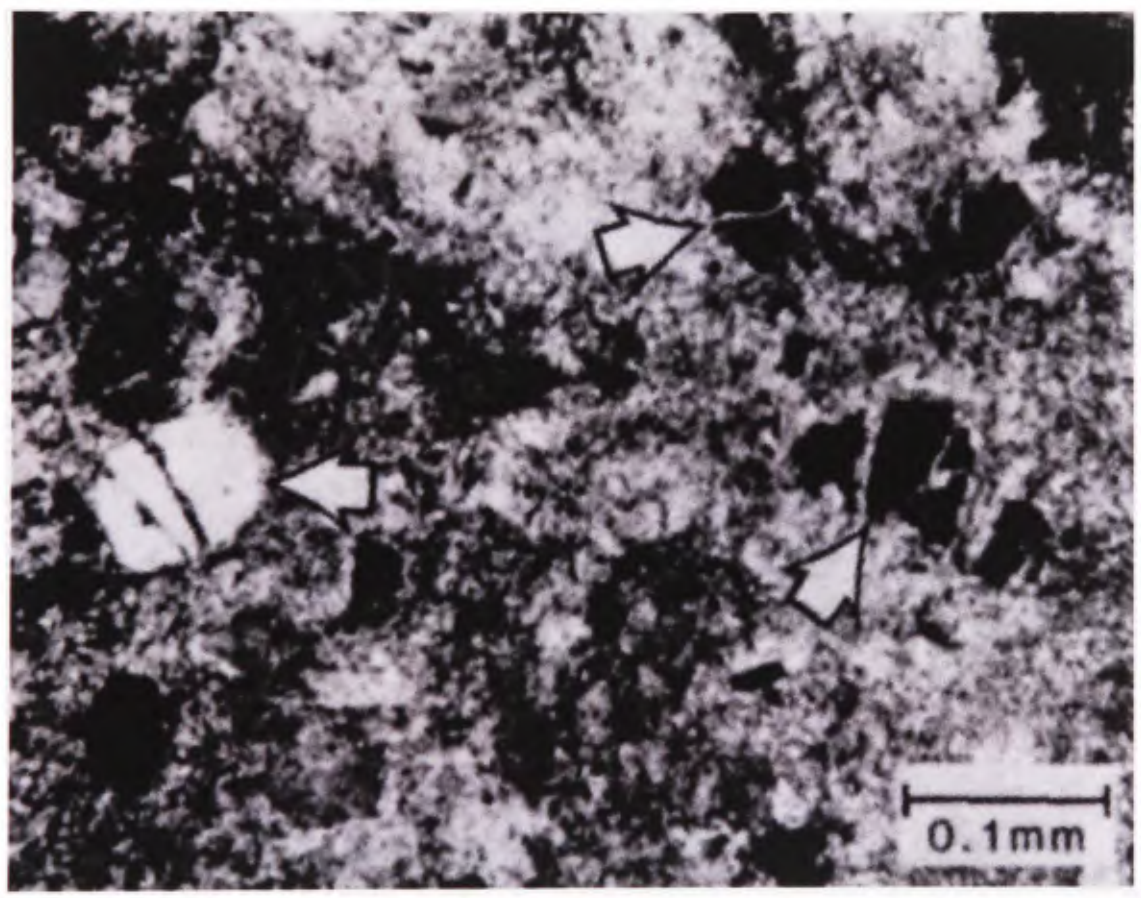
Brecciation



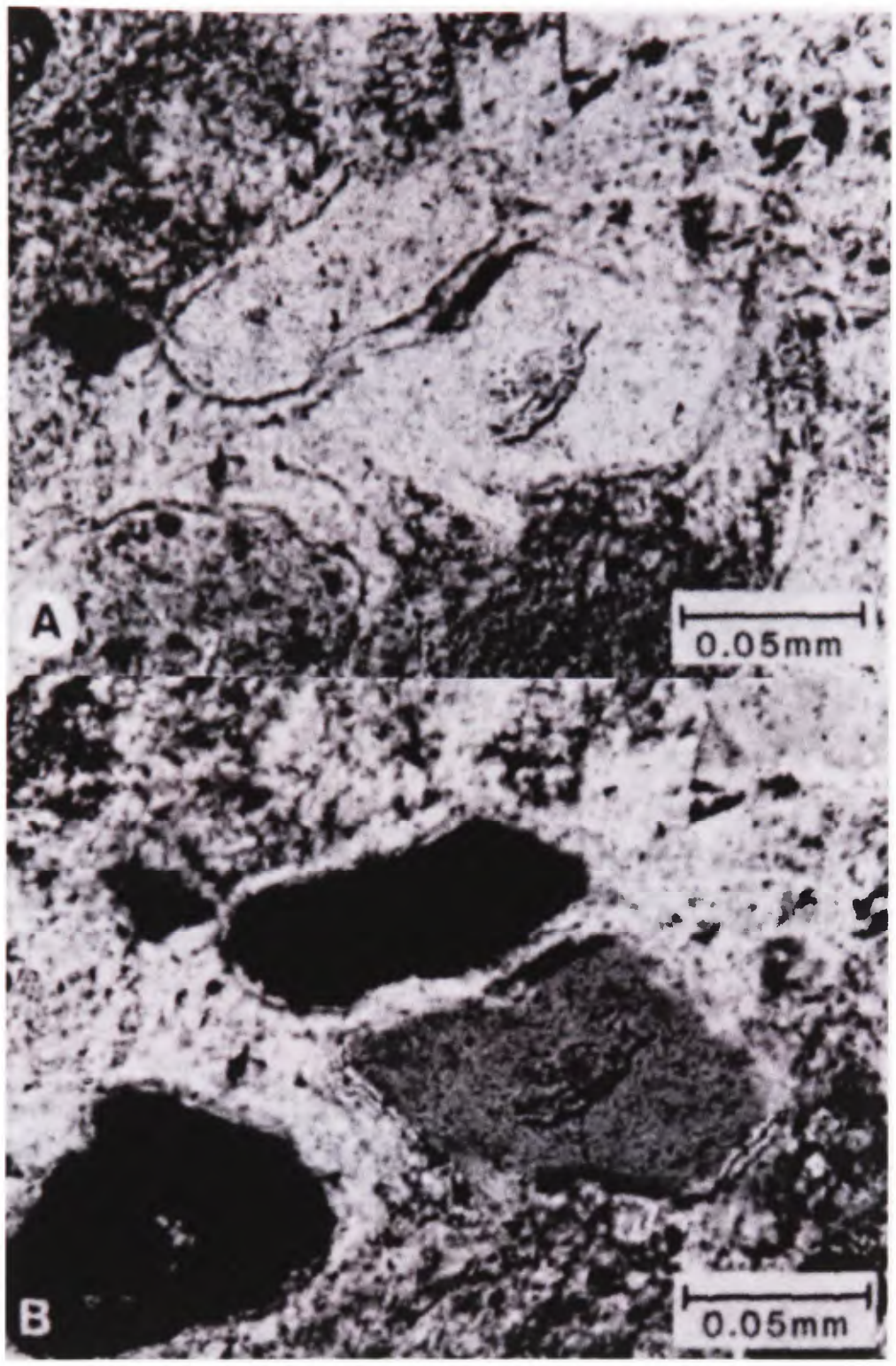
Brecciated detrital quartz grains with matching outlines. Fracturing attributed to **displacive growth** of calcite. Thin section, crossed nicols. Scale bar represents 50 μm. (Tandon & Narayan, `81)



Thin section of typical clotted micrite with glaebules (one with concentric structure) and floating quartz grains. Calcite viens have cut the glaebules and surrounding sediment at different stages. (Tandon & Friend, `89)



Thin section photo taken under crossed polars showing several **fractured / brecciated** quartz grains (arrows) 'floating' in a calcite matrix. (Buczynski & Chafetz, `87)

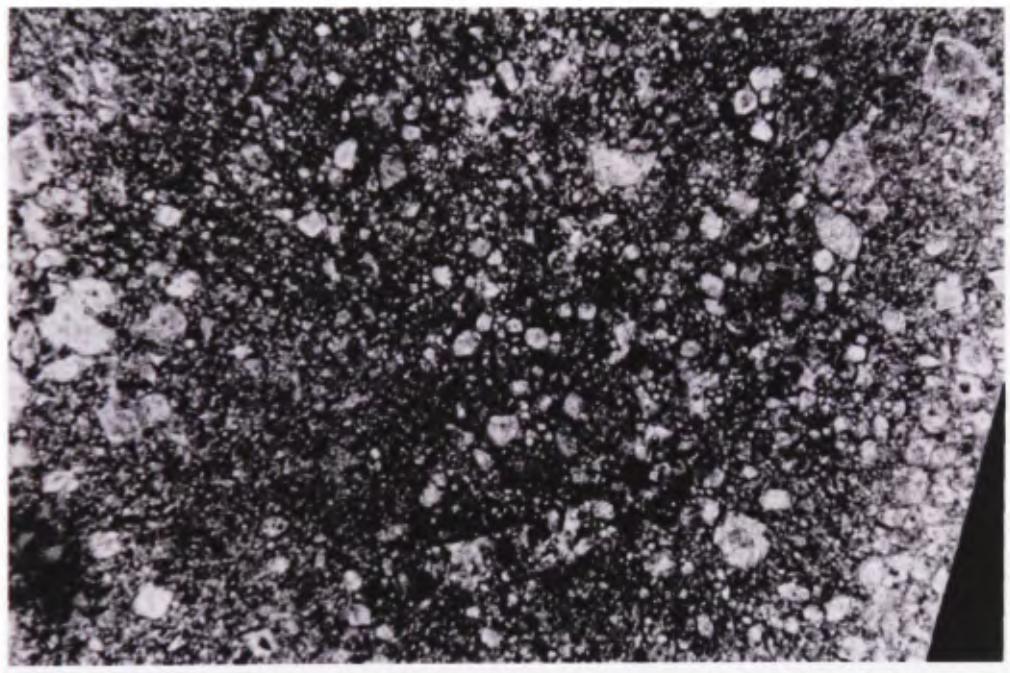


Photos of a **broken** quartz grain in calcite cement displaying an essentially perfect 'jigsaw-puzzle fit' of the two pieces. The pieces have undergone some **rotation** relative to each other and **lateral movement** away from each other. The **rotation** is indicated by the difference in crystallographic orientation displayed by the two pieces when viewed through crossed polars (B). (A) and (B) show the same field of view through plane light and crossed polars, respectively. (Buczynski & Chafetz, `87)

Calcite



SEM close-up of **calcite crystals** encrusting tubules. (Beier, `87)



Solution rounded **calcite crystals**. Primary crystals had a rhombic habit. Larger crystals average 50 μm in diameter. Lower Carboniferous, Llanelly Formation, South Wales. (Wright)

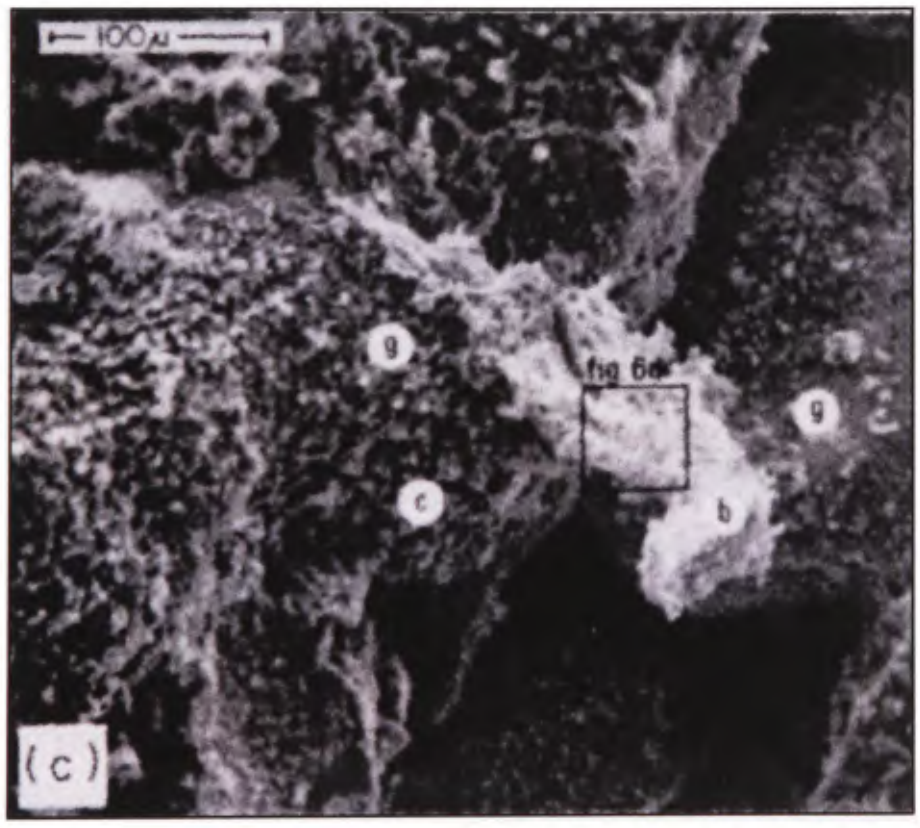


Densely crystalline **calcite** fabric (crystic plasmic fabric). Average crystal size is 10 μm. Lower Carboniferous, Llanelly Formation, South Wales. (Wright)

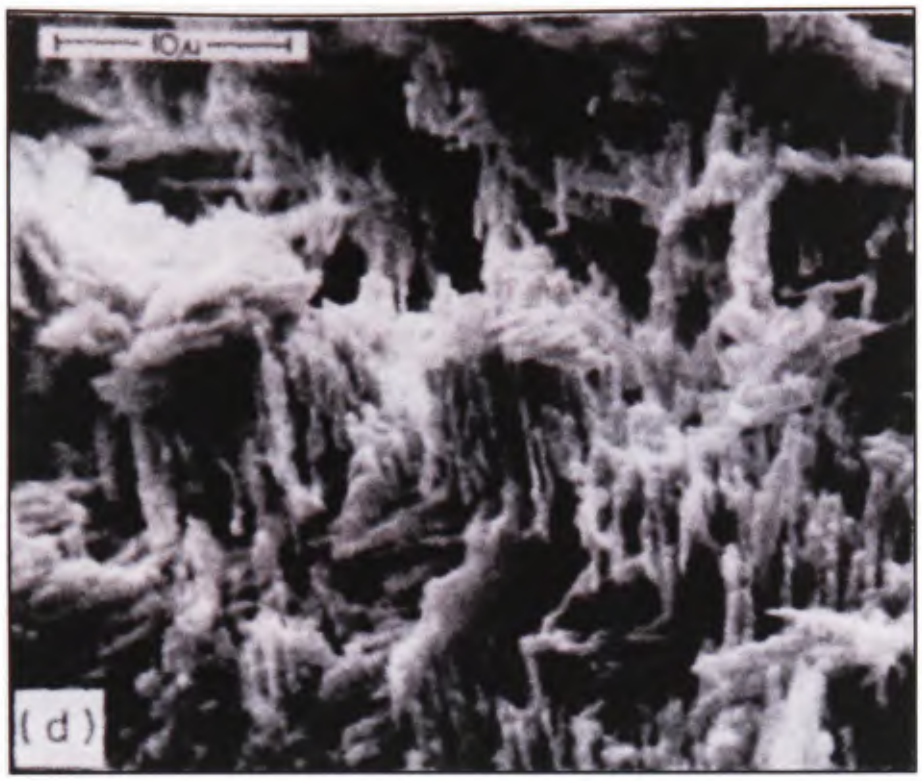
Cement



Calcerenite in which contacts owing to **vadose compaction** occur (c). **Micritic bridge** (b) and **meniscus structures** (m) are present between grains. Considerable **primary pore space** (ϕ) is visible. (Knox, `77)



SEM photograph of a **bridge structure** (b) extending between grains (g). The latter are partly covered by a **drusy calcite** (c). (Knox, `77)



Close-up SEM photograph of **bridge structures** (see square 6c), which consist of regular bundles of **acicular fibres** orientated in two planes. The size of individual fibres is approximately 10 μm. (Knox, `77)

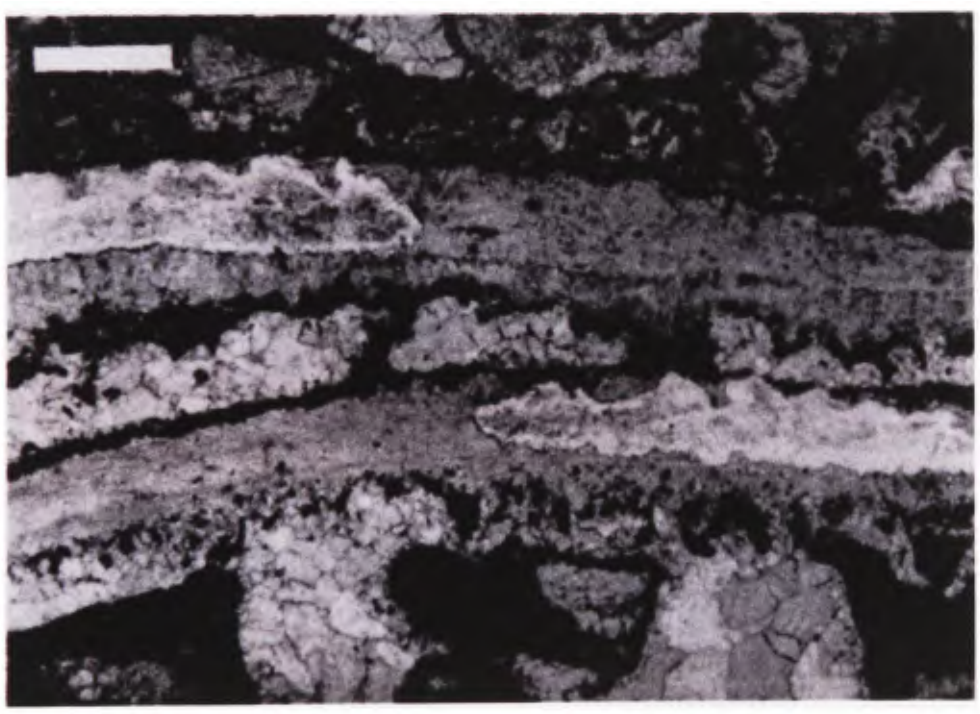
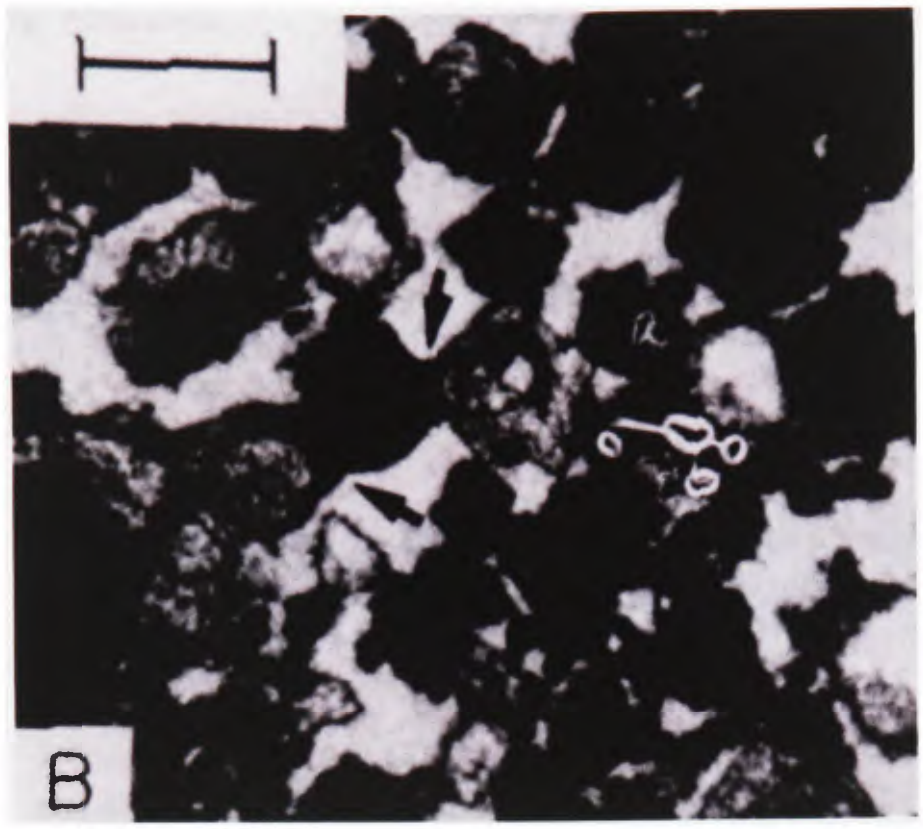
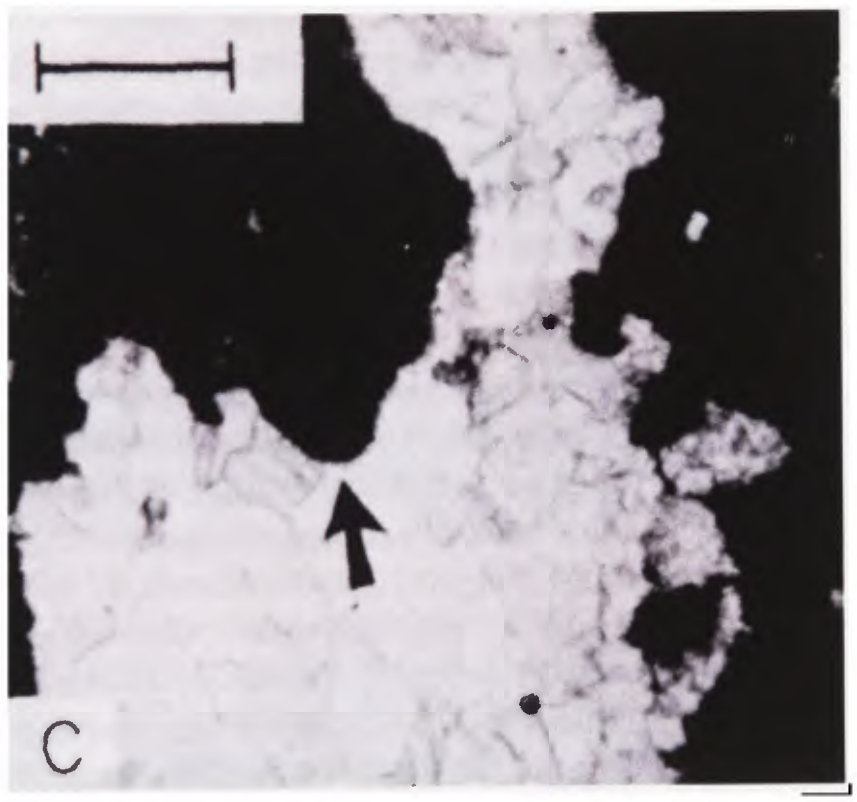


Photo showing possible examples of **vadose cement** and sediment. Shell fragments are partly **silicified**. Scale bar represents 0.5 mm. (Adams, `80)



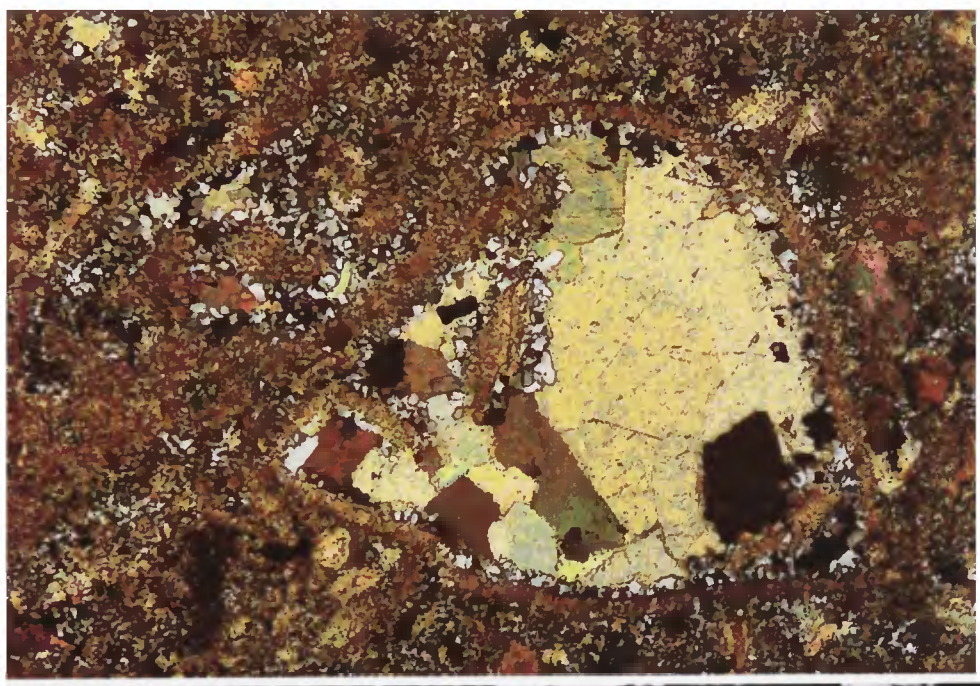
Peloids (sediment grains) coated by fine spar. Note the meniscus-like thickenings (arrowed). Scale bar is 0.5 mm long. (Wright, `83)

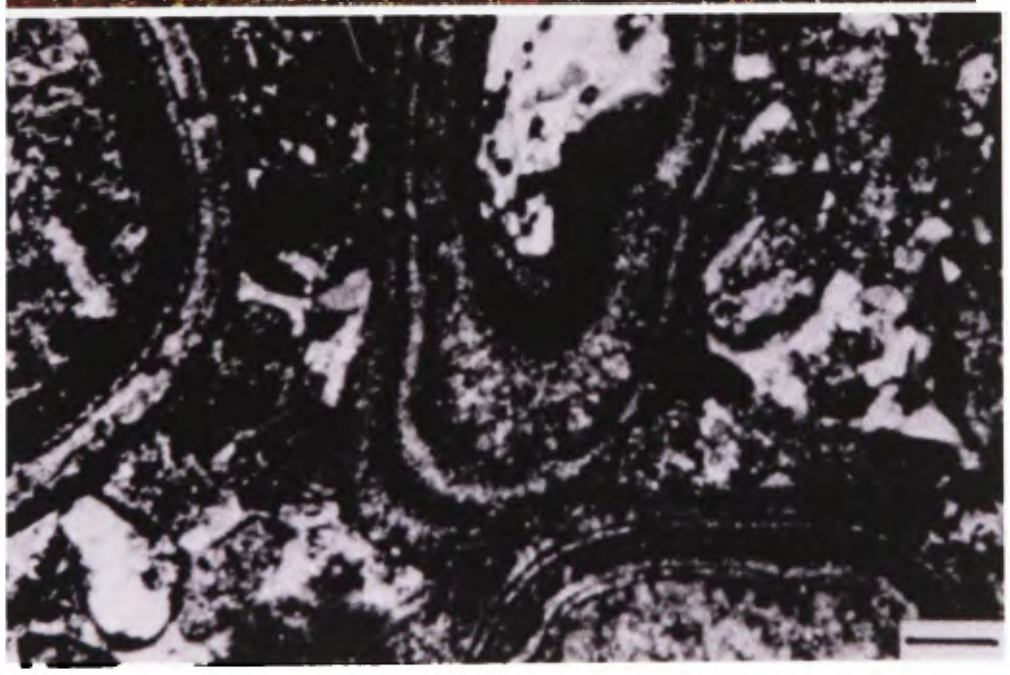


Gravitational 'cement' (arrowed) composed of very fine spar. Scale bar is 0.5 mm long. (Wright, `83)

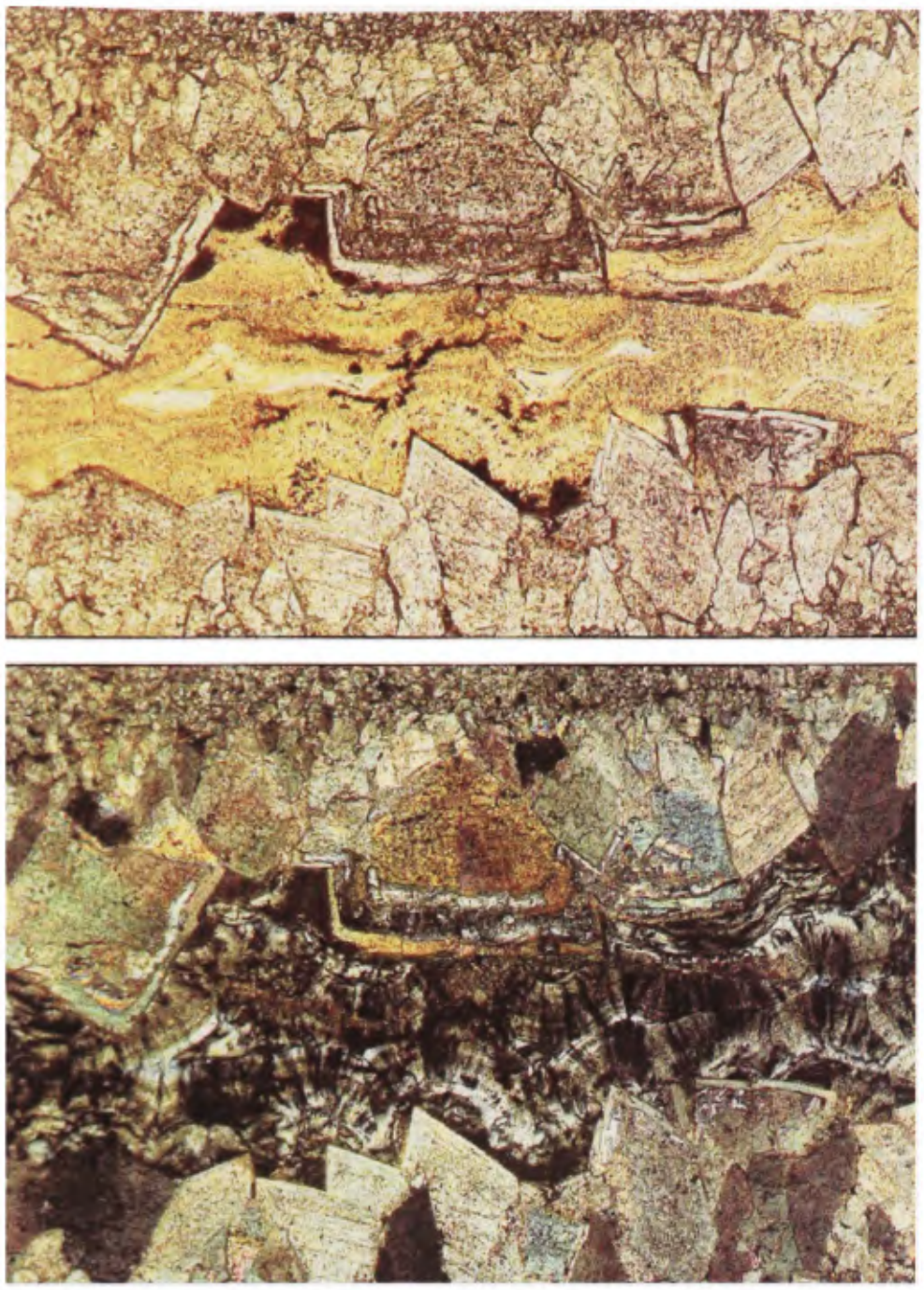


An early **quartz cement** within a fractured ostracod shell (Adams and MacKenzie, `98).

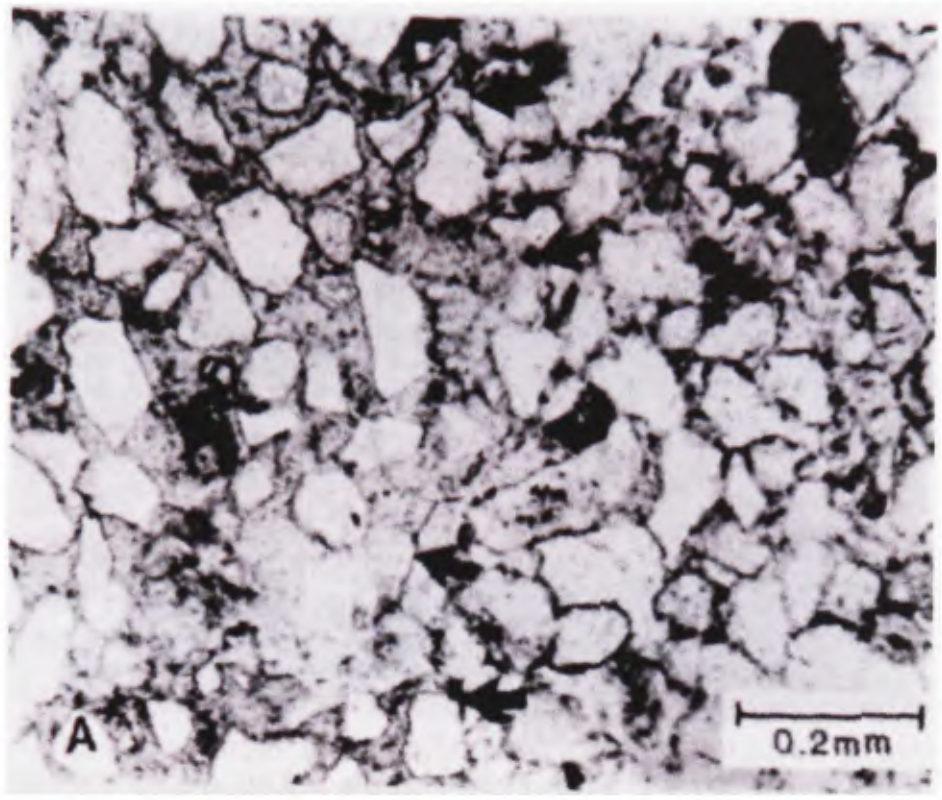


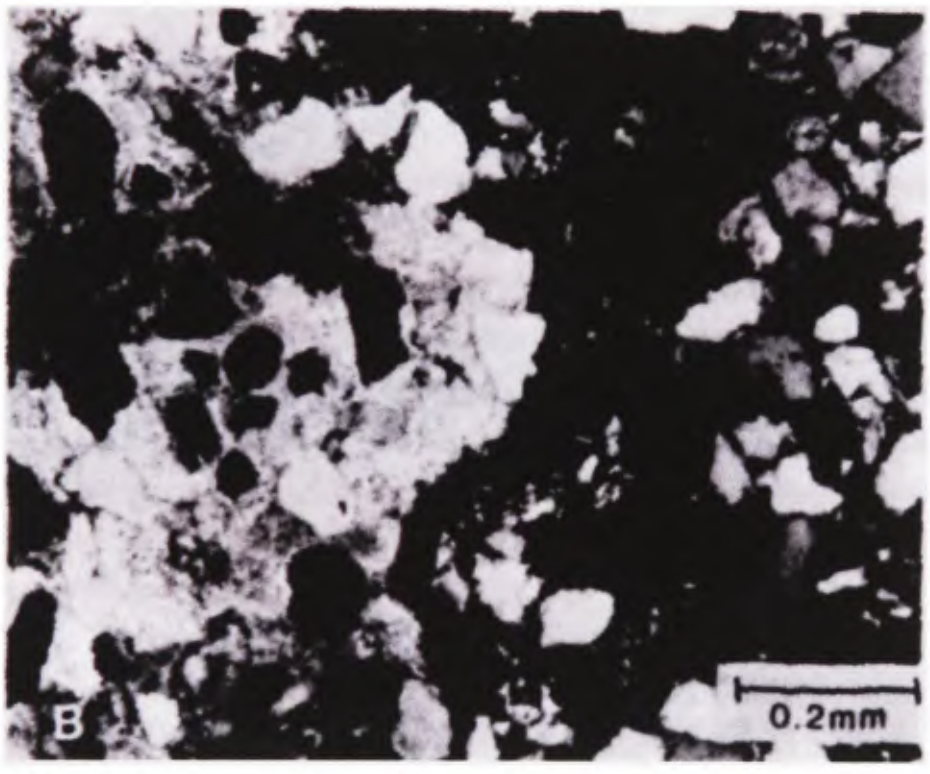


Pisolite showing typical **'dripstone' cement** indicative of **vadose cementation.** Calcrete conglomerate. Thin section, crossed nicols. Scale bars represent 200 μm. (Tandon & Narayan, `81)



The variety of silica forming fibrous growths with a rounded botryoidal outline is **chalcedony**. Here it has filled a fracture in a dolomite. There is also some (replacive?) quartz within the dolomite crystals close to the chalcedony. The quartz is transparent in the view taken with PPL (upper), in contrast to the cloudy dolomite, but is best seen in the view taken with XPL where the first-order interference colours of the quartz contrast with the high-order colours of the dolomite (Adams and MacKenzie, `98).

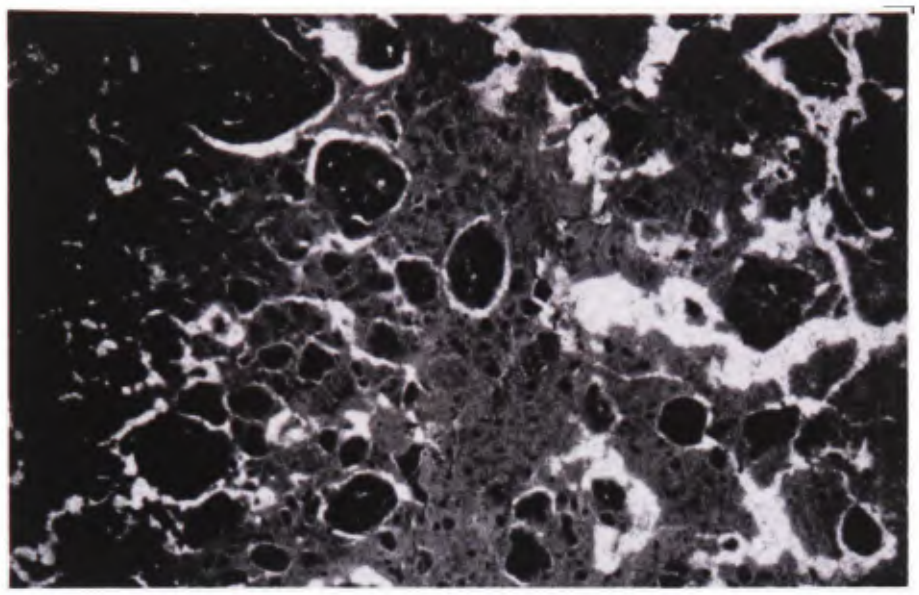




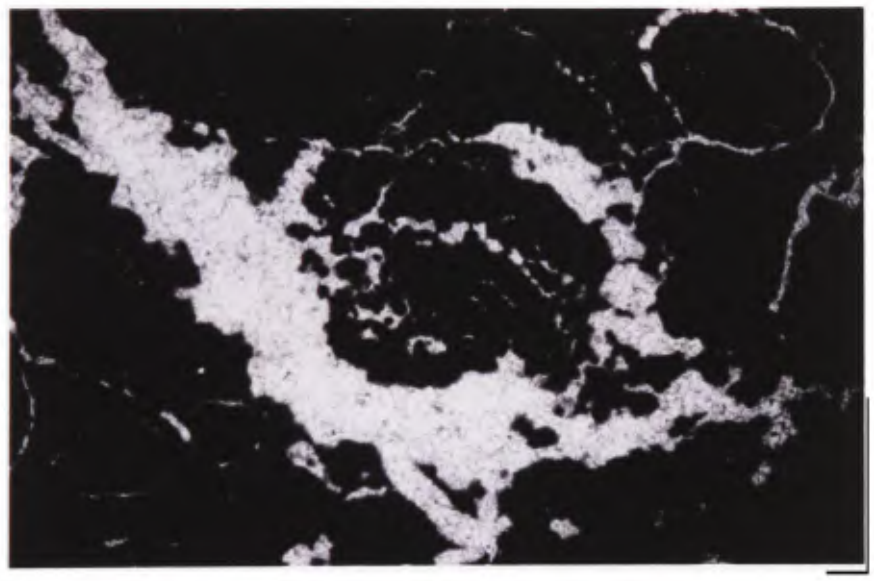
The left half of this pair of photos (A = plane light, B = crossed polars) is **calcite-cemented** and the right half is 'normal', non-calcite-cemented sandstone. The contact between the two areas runs essentially vertically through the centre of the field of view (arrows). The expanded, **open fabric** of the framework grains is readily apparent in the calcite-cemented area when compared with the non-calcite-cemented area. The light area in (B) is poikilotopic calcite cement. (Buczynski & Chafetz, `87)

Circum-granular cracks

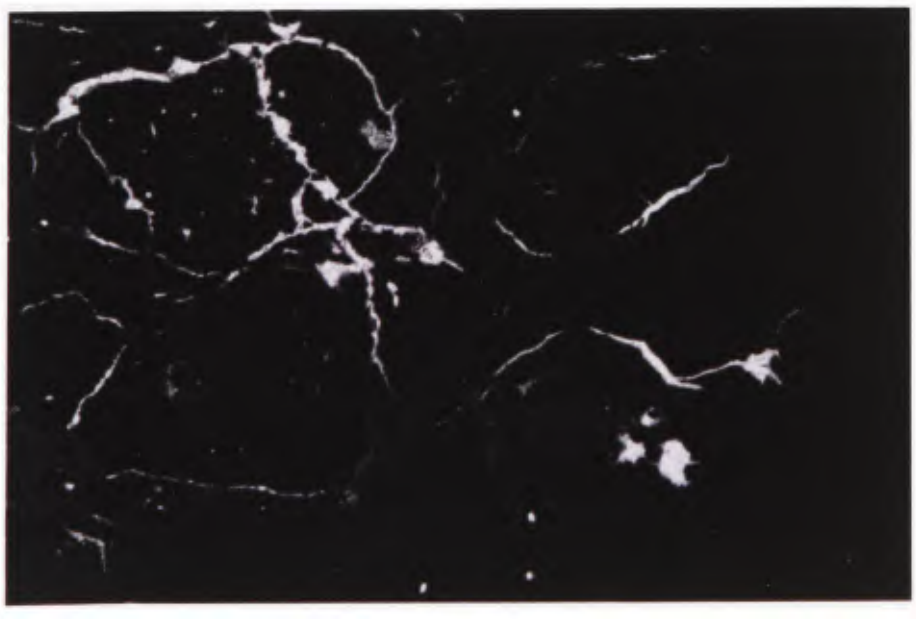
'**Glaebules**' defined by spar-filled **circum-granular 'cracks'** (probably **crystallaria**). This is a very common feature of palaeosols, especially calcretes. Some spar-rims may form by neomorphism or by displacive growth of calcite, but most commonly the veins show 'passive' cement fabrics and centripetal fabrics.



'Glaebules' defined by spar-filled **circum-granular 'cracks'** (probably **crystallaria**). Field of view is 6 mm wide. Lower Carboniferous, South Wales. (Wright)



'Glaebules' defined by spar-filled **circum-granular 'cracks'** (probably **crystallaria**). Field of view is 6 mm wide. Lower Carboniferous, South Wales. (Wright)



Dense **micritic** fabric with irregular planes (probably originally **crystallaria**). Note **circumgranular** form. Lower Carboniferous, Llanelly Formation, South Wales. (Wright)

Compactional Textures

A number of micro-textures combined with the mineralogy can be used to determine the diagenetic history of chemical sediments. The order of different cement generations, any dissolution, compaction and fracturing during deposition and later burial can be deduced to a greater or lesser degree.

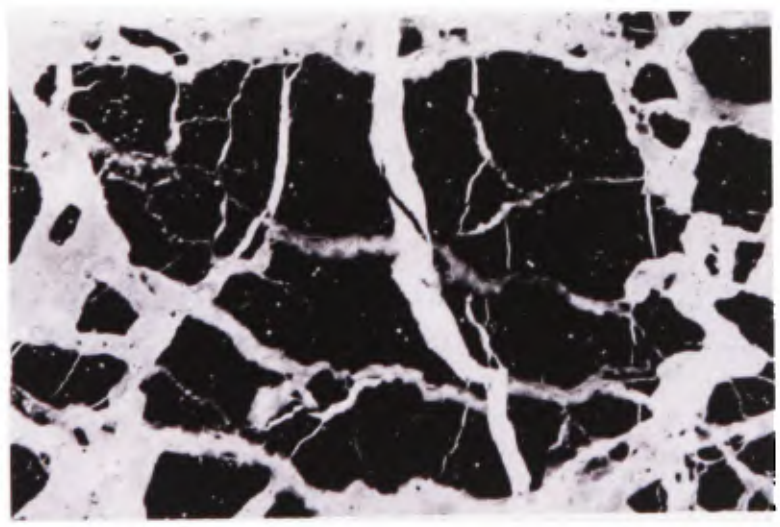


This is a thin section of a brecciated nodular chert. The chert matrix (m) has been heavily fractured then resealed by later very fine, cryptocrystalline chert (c). The framboidal pyrite (p) is only present within and surrounded by the matrix chert and must therefore predate this or was formed at the same time. The resealed fractures stop where the nodule meets the sandstone (s), this suggests the sediment was not fully silicified at the time the chert nodules were fractured, being more ductile to compactional deformation than the brittle nodule.

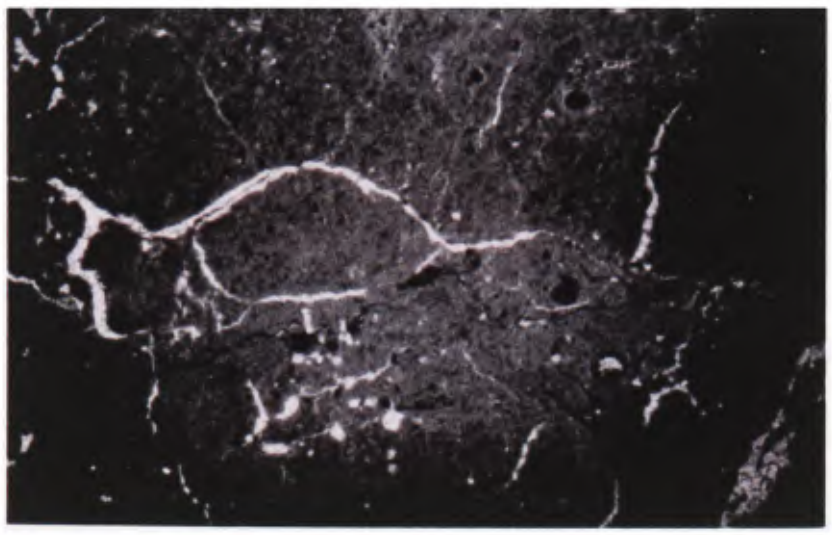
Brecciated nodular chert showing chert matrix (**m**) with scattered framboids of pyrite (**p**). Fractures resealed by later cryptocrystalline chert (**c**) have not affected the intercalated sediment (**s**) (scale bar = 300μm).

Crystallaria

Planes (cracks) are common in soils and palaeosols and are called crystallaria if filled by pedogenic crystalline material. The planes commonly result from drying and are often irregular in form.

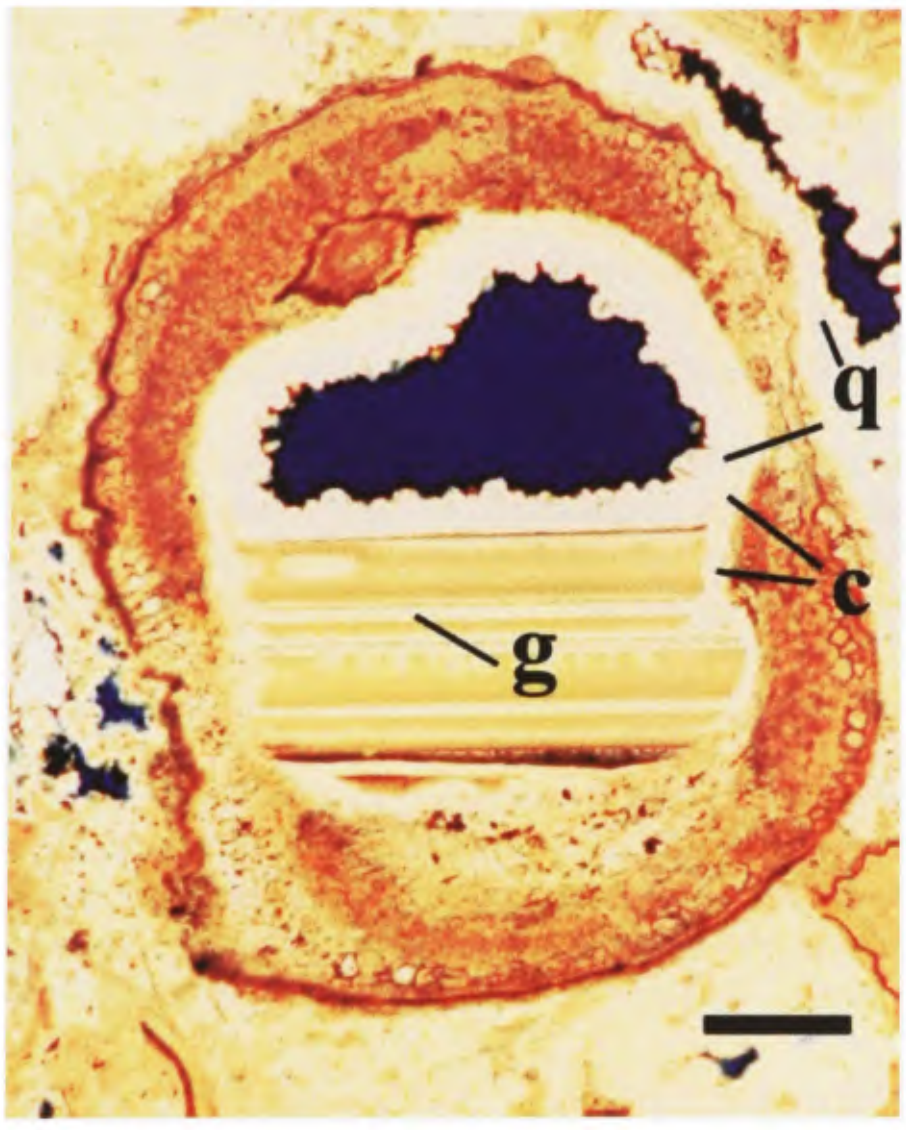


Complex **multi-fracture crystallaria**. Field of view approx. 6 mm. Lower Carboniferous, Llanelly Formation, South Wales. (Wright)



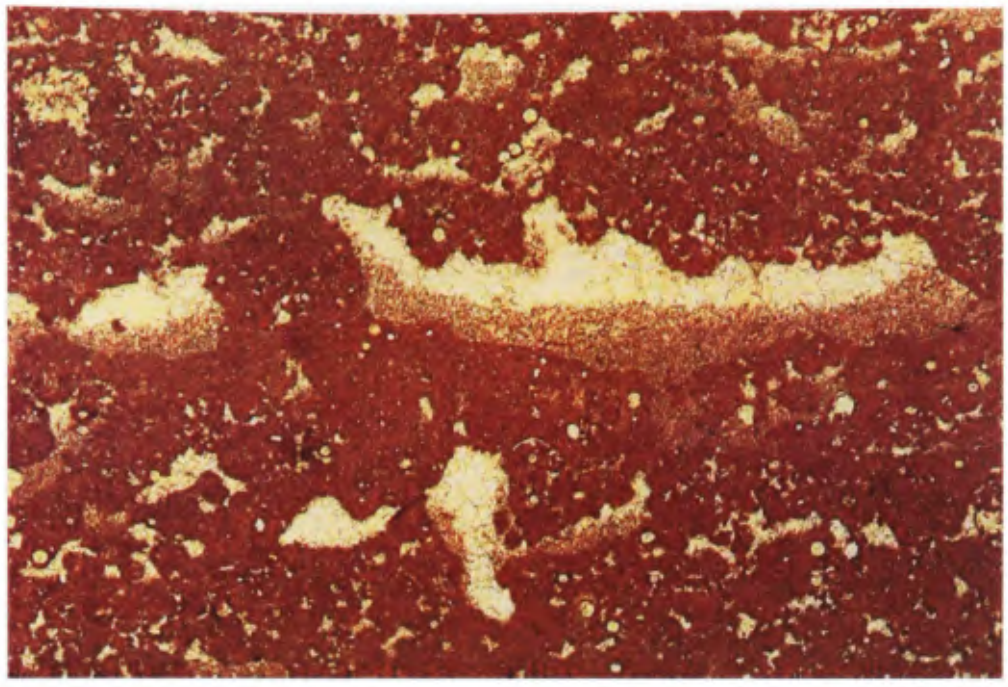
Irregular planes (crystallaria?). Field of view is 2 mm wide. (Wright)

Geopetal Textures



Geopetal layers tend to form by the accumulation of very fine infiltrated organic and detrital material as a layer within voids in sediment, such as in the hollow straws of plant stems. Similarly, in carbonates and chert beds geopetal layers may also form from successive generations of calcite or silica cement. They are perhaps most common in the vuggy to massive sediments.

Geopetal layers (**g**) in a straw of *Aglaophyton major*, denoting the image is the correct 'way-up'. Notice also earlier 'straw-lining' overlay of chert cement (**c**) and the later generation of quartz cement (**q**) lining the remaining void space after the geopetal fill (scale bar = 1mm).



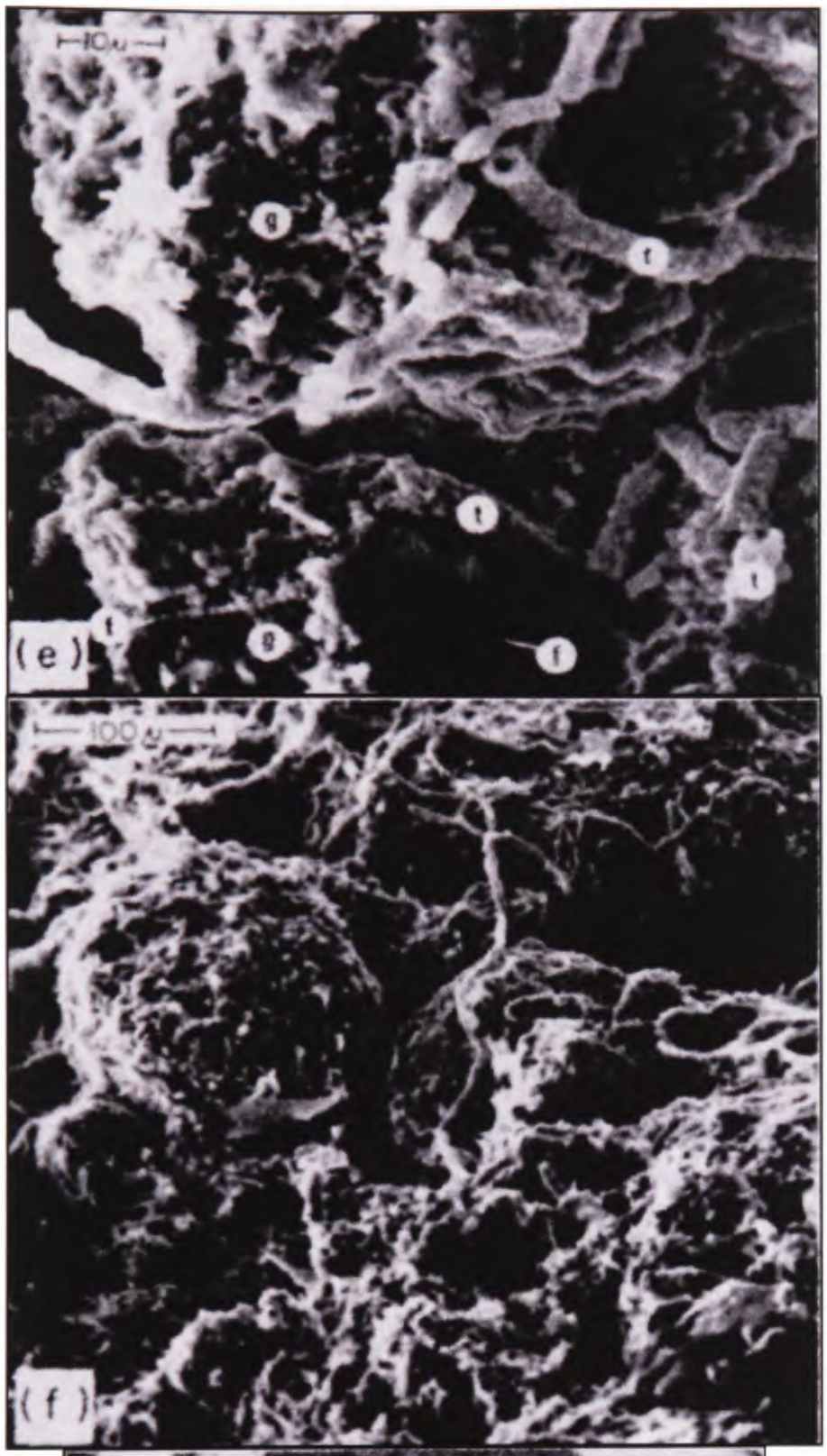
Laminoid fenestrae with geopetal fill – Fenestrae rich, some laminar, sediment. The fenestrae are filled with a mixture of silt-sized sediment and cement. The sediment rest on the base of the fenestrae and was deposited after the enclosing carbonate mud (Adams and MacKenzie, '98).

Grain coatings

A common feature of many chemical sediments are coated grains. Numerous different names and definitions have been used for coated grains (Peryt, 1983) with classification systems being based on size, shape, regularity of concentric laminations, presence of obvious biogenic structures and, often, an interpretation of their origin (Adams and MacKenzie, 1998). Within soils various types of coatings occur in (clay coats, carbonate, gypsum, iron, etc.). These are generally known as cutans in the soil literature. Coated grains usually comprise a well-defined nucleus, surrounded by a coating of calcareous material, usually fairly fine-grained, called the cortex (Adams and MacKenzie, 1998). In a number of cases the cortex is at least partially laminated.

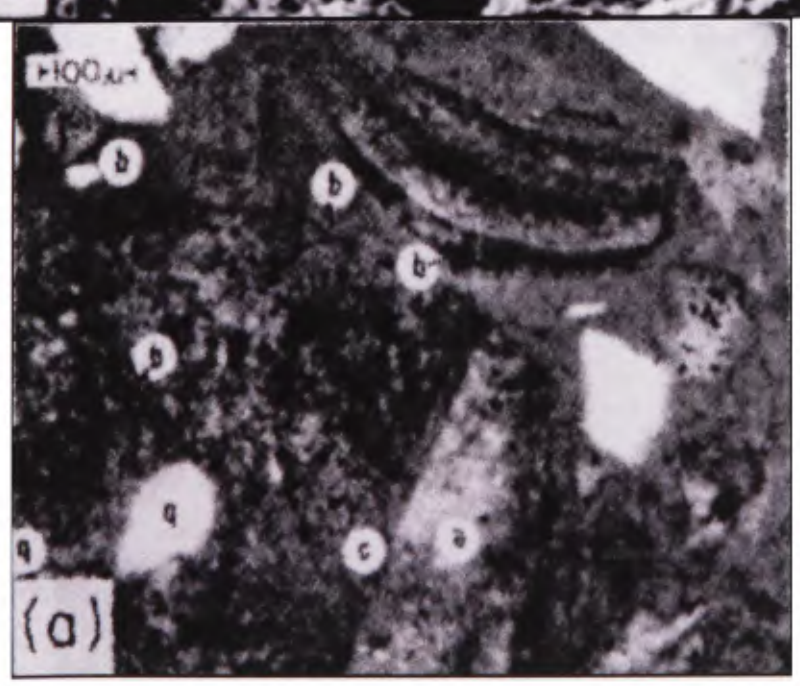
Carbonate coatings in calcretes are usually micritic and may be multi-layered to form ooids or pisoids. Typically such coats are irregular in thickness with meniscus or gravitational thickenings (microstalactitic) or with bumps and thread-like outcrops. Due to the fact that coated grains of similar appearance can form in different environments, the descriptive classification system of Tucker and Wright (1990) has been used, rather that other systems which relie on an interpretation of mode of formation and origin.

Like a number of other depositional structures within carbonate sedimentology, there exists a degree of discrepancy between what is known for modern and recent environments and what appears in the more ancient geological record. Detailed work on Quaternary calcretes in Spain and South Africa has shown that the coats are in part biogenic, formed by the calcification of various micro-organisms (especially fungi).

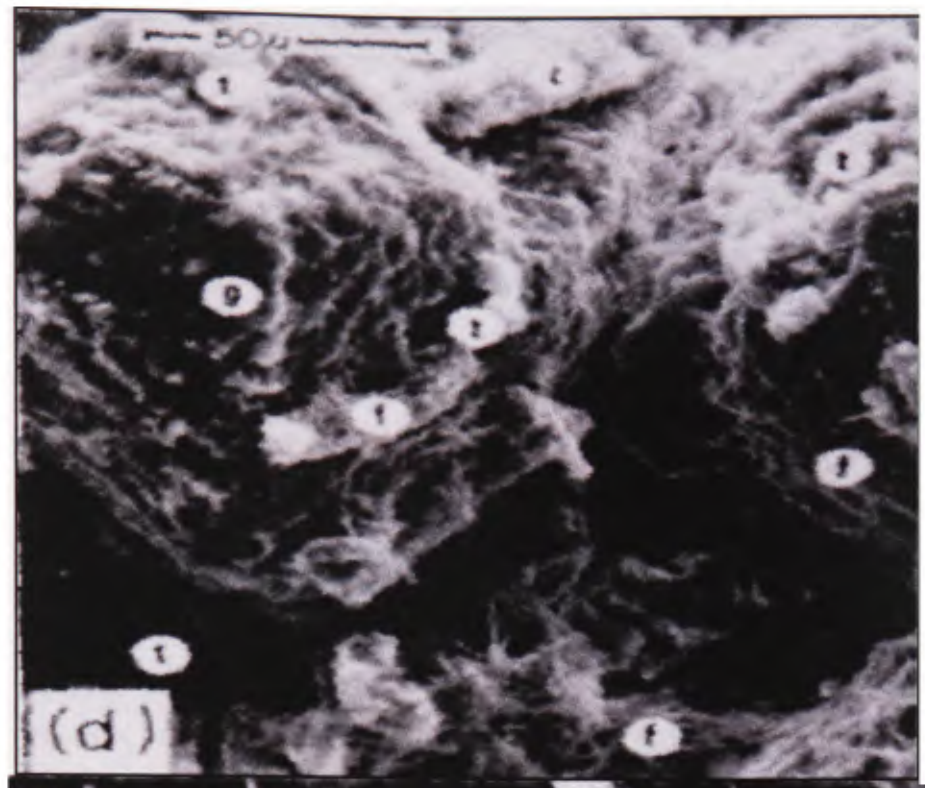


SEM photograph showing the outline of **coated grains** (g) in which the coatings consist of aggregates of **tubules** (t) and some **fibres** (f) and **micritic calcite.** (Knox, `77)

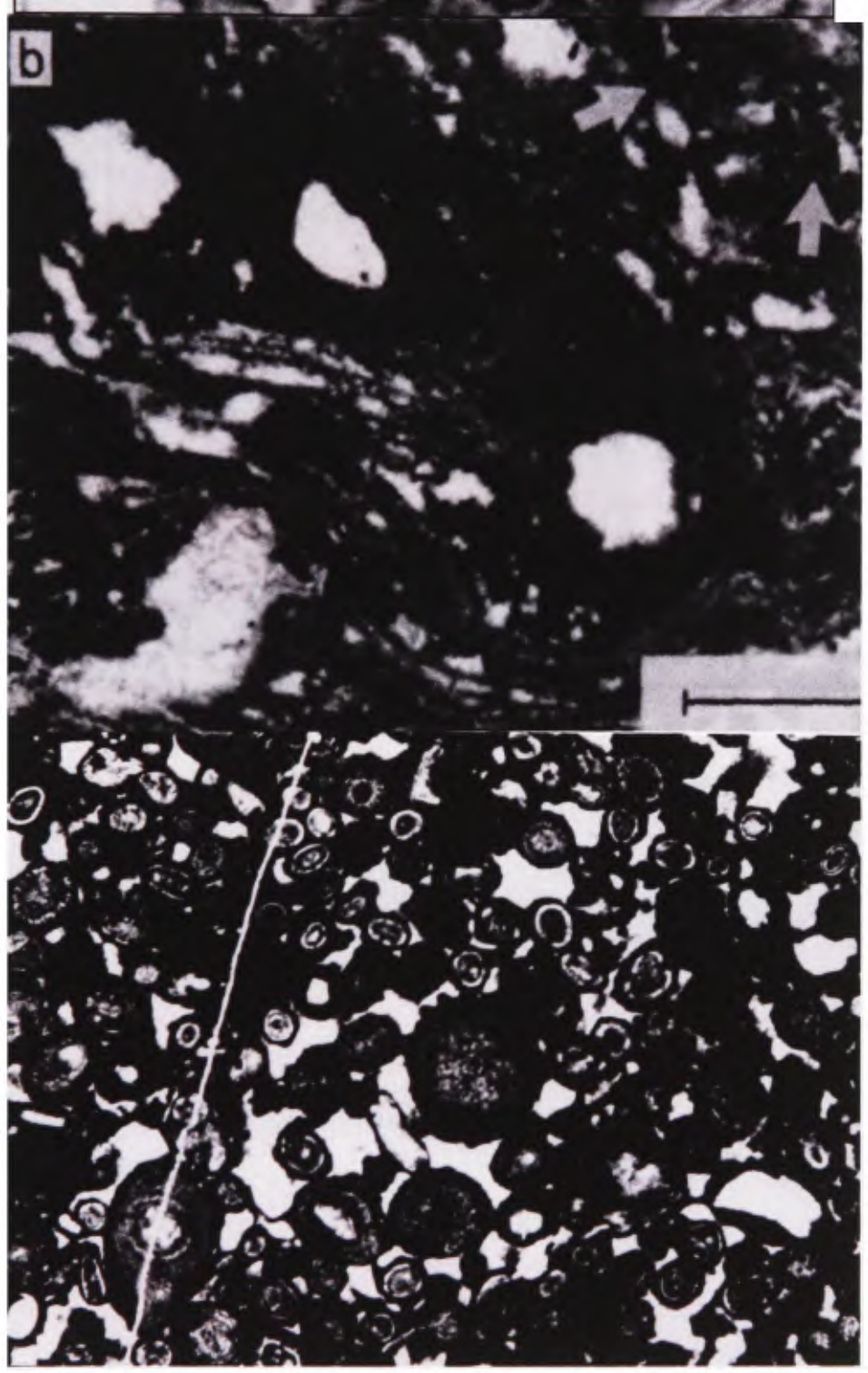
SEM photograph exhibiting **coated grains** in which the coatings consist mainly of **tubules** and **micrite**. Some of the tubules may continue for some distance, following a winding course between coated grains. (Knox, `77)



Composite-coated grain with other coated grains. The composite grain contains quartz (q) and a **bioclastic allochem** (a). The latter with the coating (c) shows an irregular fibre riddled with **borings**. A second coated grain also exhibits **borings** (b) in the micritic coating. Micrite has filled the **intraparticle space** and this too has a few **borings**. (Knox, `77)



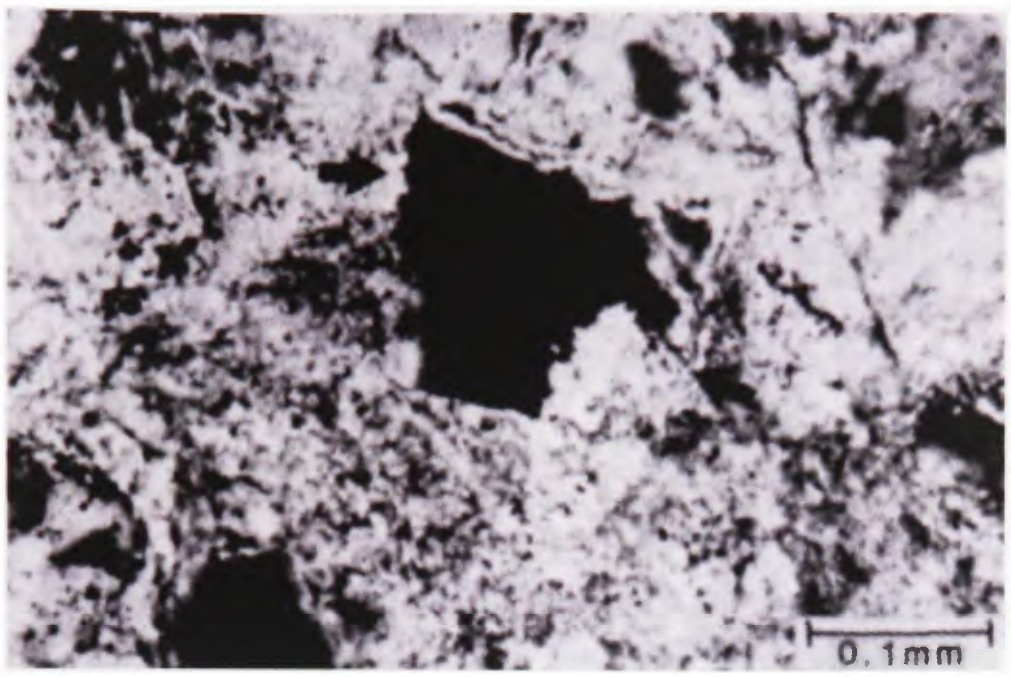
SEM photograph exhibiting **coated grains** (g) in which the coatings are made up of **tubules** (t) and tangential networks of **acicular fibres.** (Knox, `77)



Thin section of laminar calcrete from Miskin. Detail of microfabric, showing the dark **micritic** coating around the cylinders (transverse sections of tubes) and the crudely micro-laminar structure of the matrix. A small **pellet** concentration is arrowed. Scale bar represents 0.5 mm. (Wright et al., `88)

Grain coats in a calcretised **oolitic** grainstone. Note the irregular **thickenings** and **outgrowths**. Field of view is 10 mm wide. (Wright)

Grain Replacement



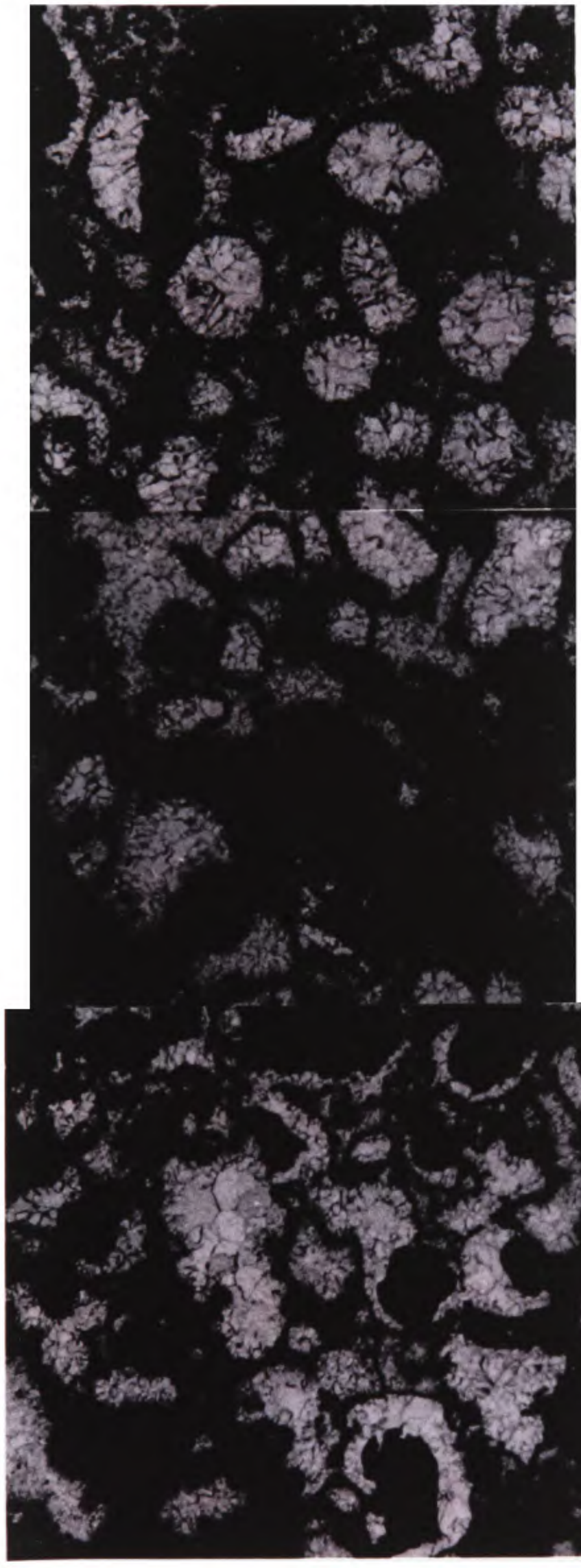
Many grains show evidence of having been partially **replaced**. Thin section photo, showing crenulated, irregular boundaries are characteristic of replaced grains (arrows). Under crossed-polars. (Buczynski & Chafetz, `87)

Intraclasts

Intraclasts are irregularly-shaped grains that form by syndepositional erosion of partially lithified sediment. Examples include carbonate mud that is torn up from littoral lakes sediments during storms and hardened desiccated mud flake conglomerate produced by reworking of desiccated sediments (e.g. playa and seasonal floodplain environments). Intraclasts can also be produced by reworking of consolidated sediments within the depositional environment.

Lacy Fabric

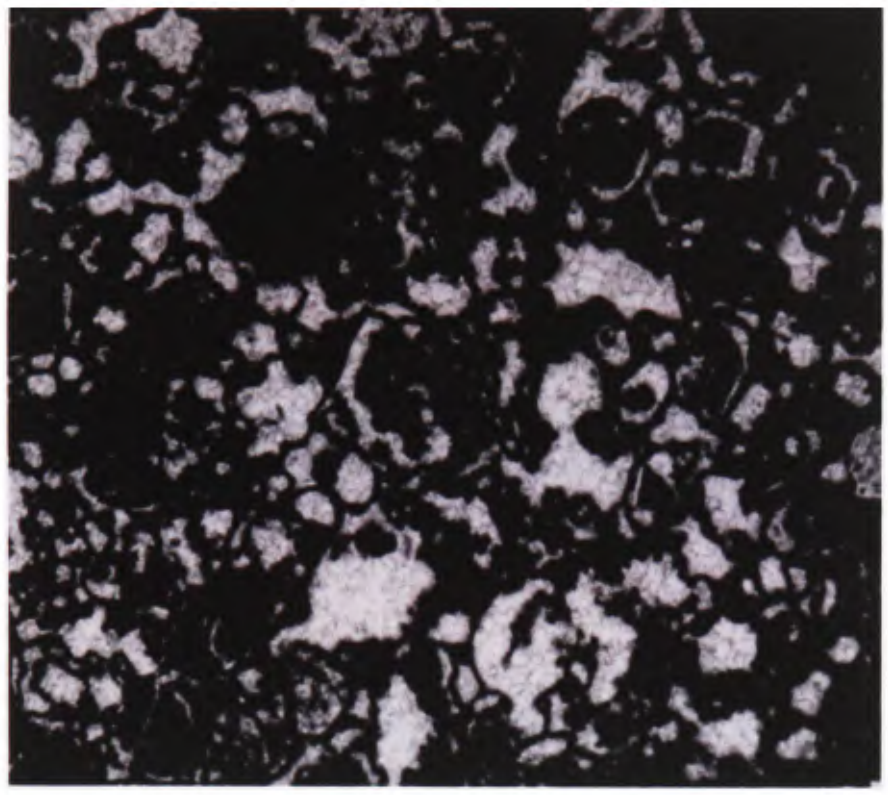
This is an unusual 'porosity' type developed in some paleosols and could be mistaken for alveolar-septal fabric. It consists of a network of micritic spheres which are filled by spar or partially replaced allochems. It is believed that this forms by the dissolution of grains after coating by constructive micrite envelopes (cutans, calcans or calcitans). The result is a void defined by the pedogenic coating which is later filled by spar cement. Where the sediment consists of well sorted uniform shaped grains the resulting structure is simple but where the grains were irregular in shape, size and packing, a more complex fabric results.



Lacy fabric – the voids are after the dissolution of medium sand sized peloids. Lower Carboniferous. (Wright)

Lacy fabric – the voids are after the dissolution of medium sand sized peloids. Lower Carboniferous. (Wright)

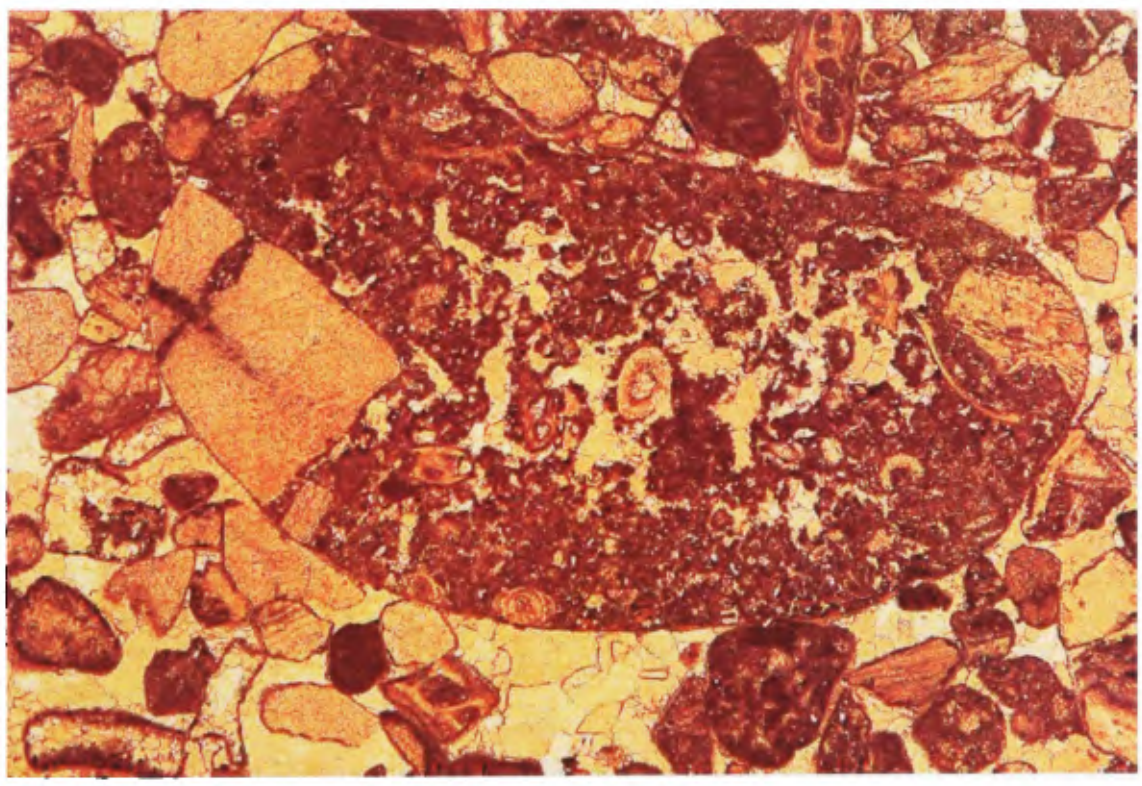
Lacy fabric – the voids are after the dissolution of medium sand sized peloids. Lower Carboniferous. (Wright)



Lacy fabric – the voids are after the dissolution of medium sand sized peloids. Lower Carboniferous. (Wright)

Lithoclasts

Lithoclasts or extraclasts are irregular fragments of carbonate that have been eroded and transported from outside of the immediate basin of deposition. The clast boundary cuts across cement and particles in the fragment, reflecting its well-indurated nature. Lithoclasts are indicative of processes that rip-up, abrade, subaerially eroded and transport pieces of previously lithified carbonates.

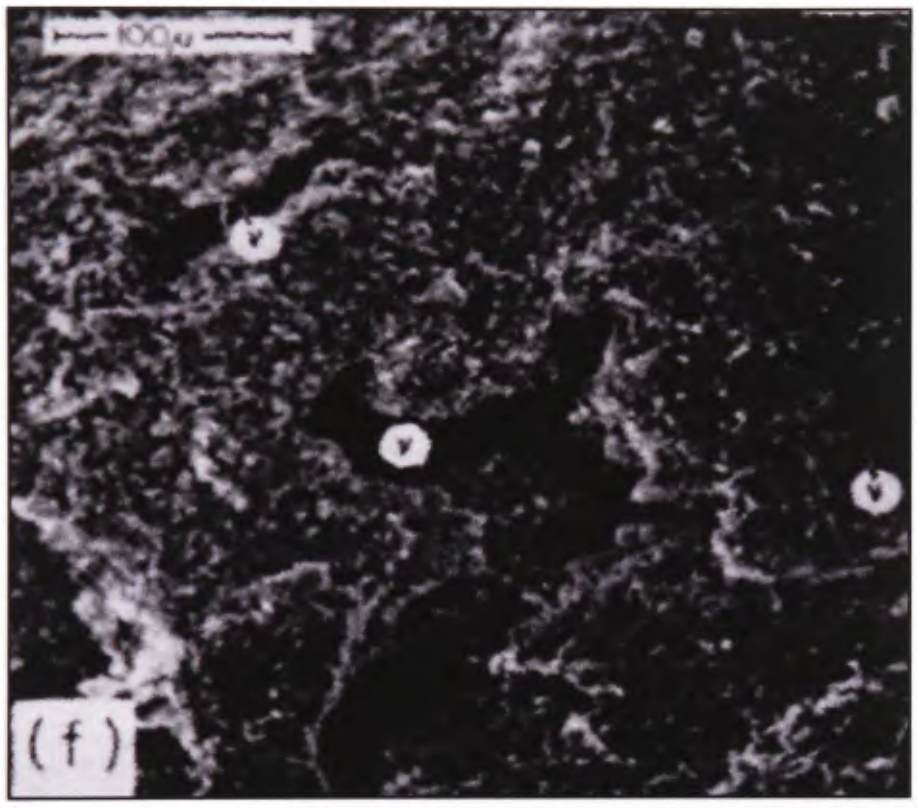


Lithoclast – a lithoclast cemented in a bioclastic grainstone. The grain must have been lithified at the time of reworking to allow the rounding of the echinoderm fragment seen at the left-hand end of the clast. It is also a more carbonate mud-rich lithology than the grainstone in which it is now incorporated (Adams and MacKenzie, 98).

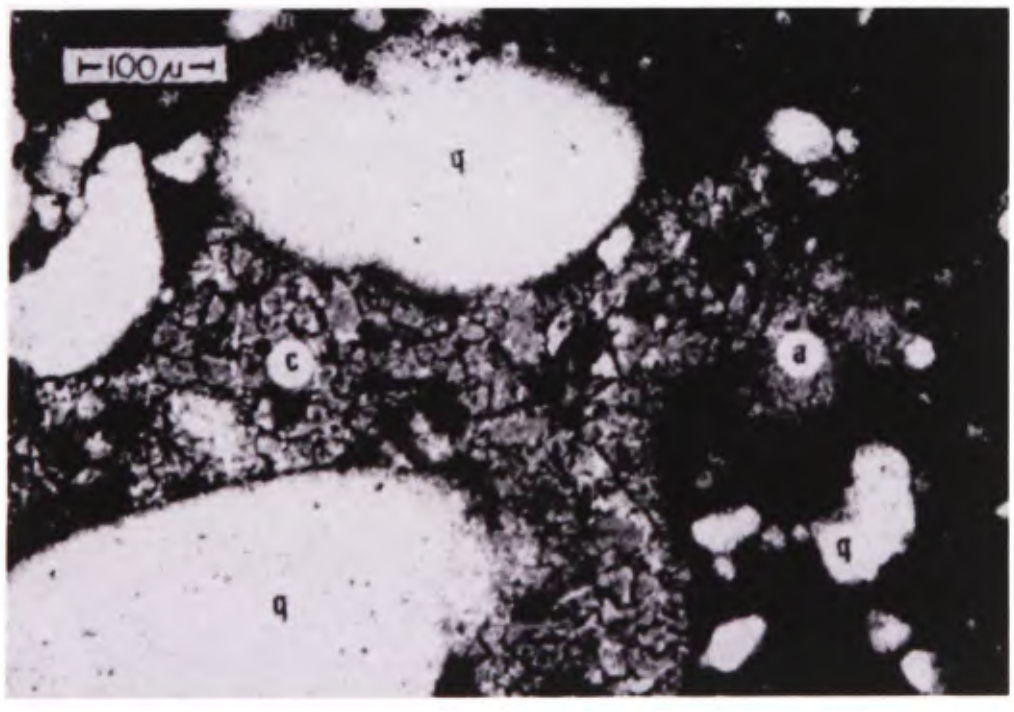
Micrite

A large volume of any carbonate is usually composed of micrite. Because of the small size of the grains or crystals in the micrite, identification of their origin is difficult to impossible. The grain size boundary between sand and mud that is used by geologists for carbonates varies: for instance, Dunham (1962) puts it at 0.02 mm and Folk (1962) 0.004 mm.

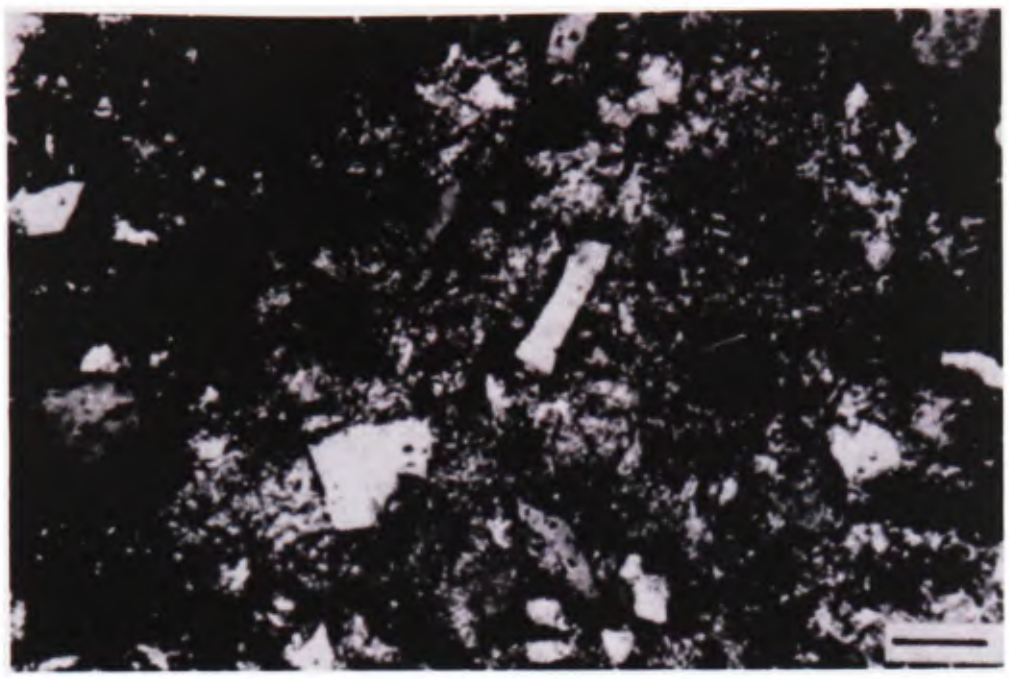
Micrite may be precipitated chemically or biochemically, derived from the abrasion of pre-existing calcium grains, or form during disintegration of calcareous green algae.



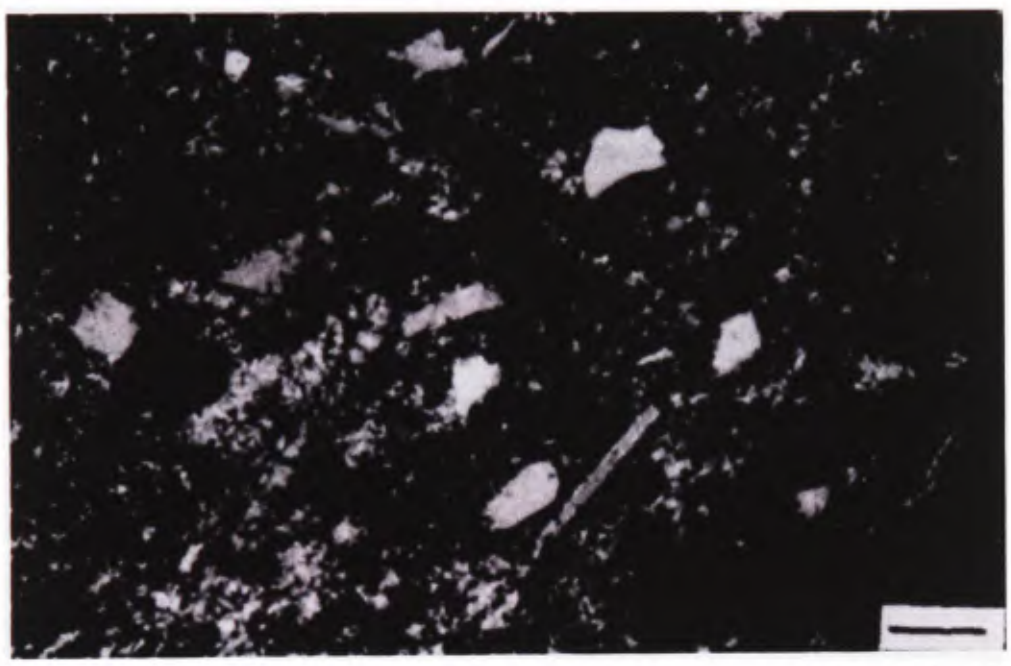
SEM view of the surface of an indurated caliche (calcrete) which consists of a microcrystalline aggregate of micritic calcite. A few voids (v) occur which may be lined by microspar calcite. (Knox, `77)



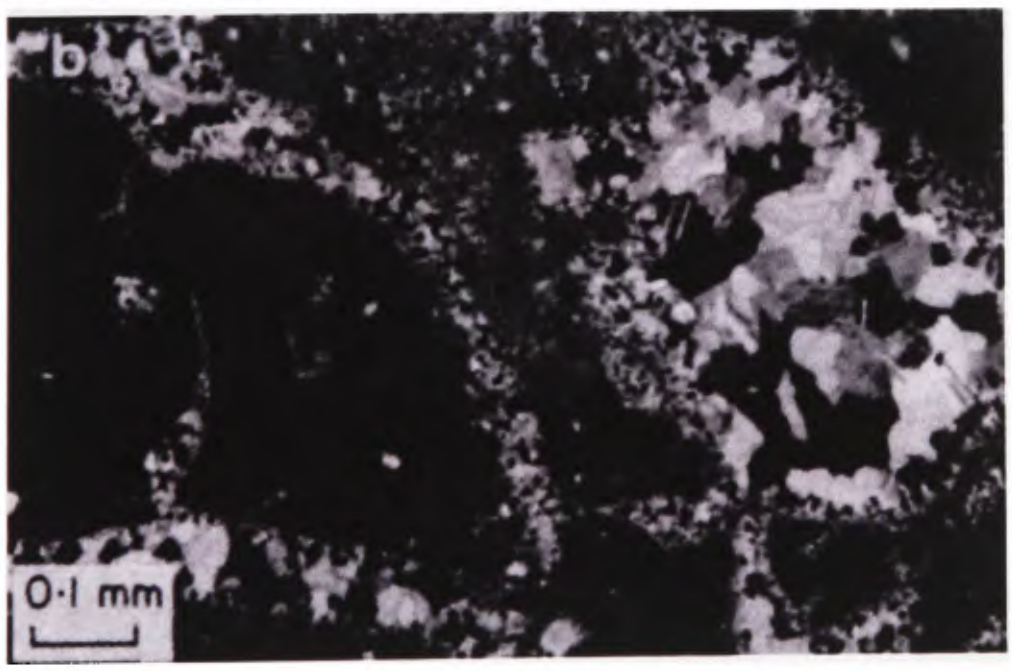
SEM photo. **Microspar calcite** (c) filling a **void** within a **microcrystalline micrite** containing **detrital** quartz **grains** (q) and carbonate **allochems** (a). (Knox, `77)



Cornstone showing a **secondary mud-support** fabric. The dark patches are **authigenic ferruginous glaebules** – Fe-oxide stained **micritic** masses. Thin section, crossed nicols. Scale bar represents 50 μm. (Tandon & Narayan, `81)



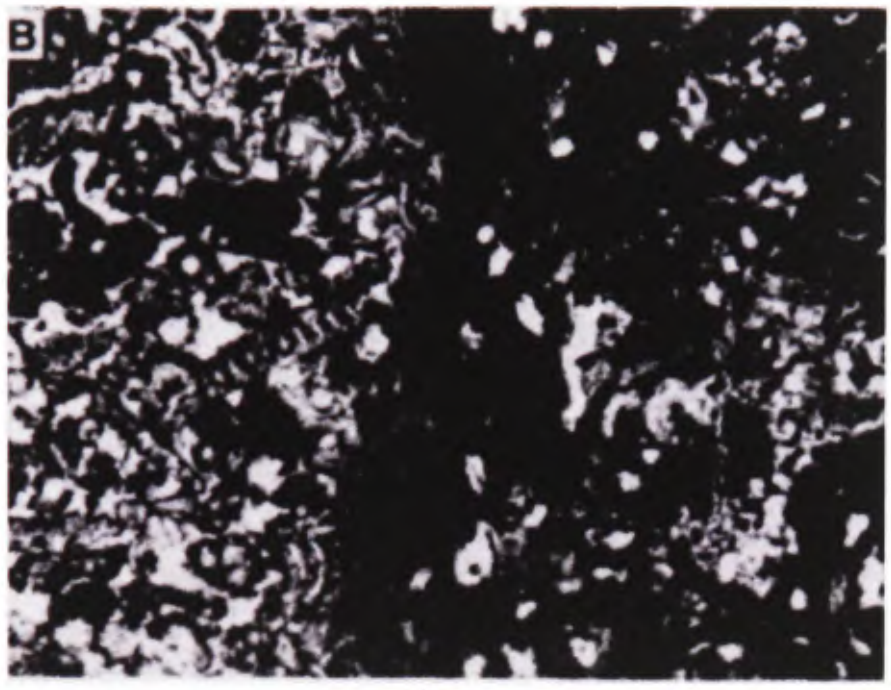
Recent nodular calcrete displaying typical **mud-support fabric.** Corroded **detrital grains** floating on a **micritic matrix.** Thin section, crossed nicols. Scale bar represents 50 μm. (Tandon & Narayan, `81)



Thin section of **clotted micrite** showing **vein fills, fenestrae** and patches of **spar** and **microspar.** (Tandon & Friend, `89)

Micritisation

Micritization (real or apparent) is a common feature in calcretes where host rock is progressively 'replaced' by a dense crystalline calcrete matrix (crystic plasmic fabric). Some micritization results from the activities of endolithic micro-organisms, especially fungi. Most, however, is probably due to fine scale dissolution and reprecipitation where the host is/was limestone. In mud-rocks both displacive and replacive processes operate which can even result in extrusive diapirism of the matrix as it is displaced.



Thin section photo of the outer edge of a **rhizomorph** showing **micritization** of the host grainstone toward the centre of the rhizomorph. (Beier, `87)

Epigenesis - Recrystallisation or Inversion

Epigenesis merely denotes changes to a precipitate brought about by a different mechanism. The main processes are:

1. Textural and crystalline inversion, whereby calcite changes to dolomite, the two minerals remaining in essential contact (in sediments nearly always with a thin water-film allowing ion-transport between host and replacer).
2. True "recrystallisation" where calcite of a particular crystal size, shape, or orientation, may be either aggrading or degrading.
3. Strain-recrystallisation whereby a strained calcite lattice transforms to a mosaic of new unstrained calcite crystals.

The term "recrystallisation" has been used in the past for almost any method which explains the formation of sparry calcite in carbonates, even for simple phreatic cementation. Solution-cavity fill, where a large gap in time of in space separates the solution of one type of carbonate and precipitation of another type, is not considered epigenesis; it is no different than simple cementation.

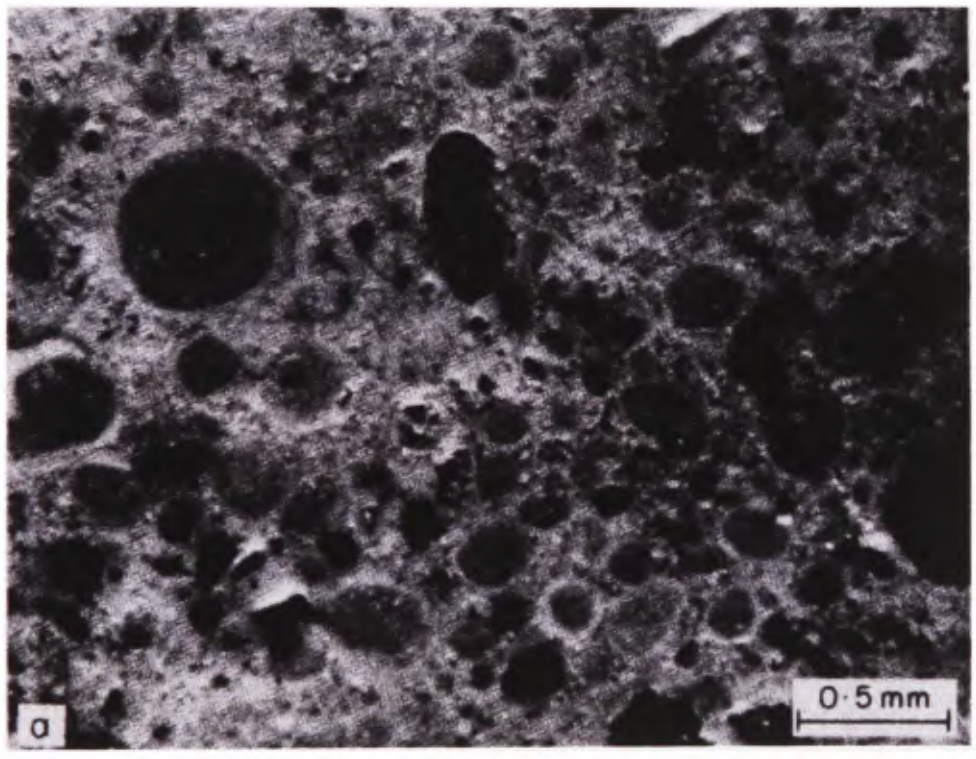
Of the processes grouped under epigenesis, recrystallisation of carbonate mud to microspar and the inversion of calcite to dolomite are probably the most important and easiest to identify.

Ooids

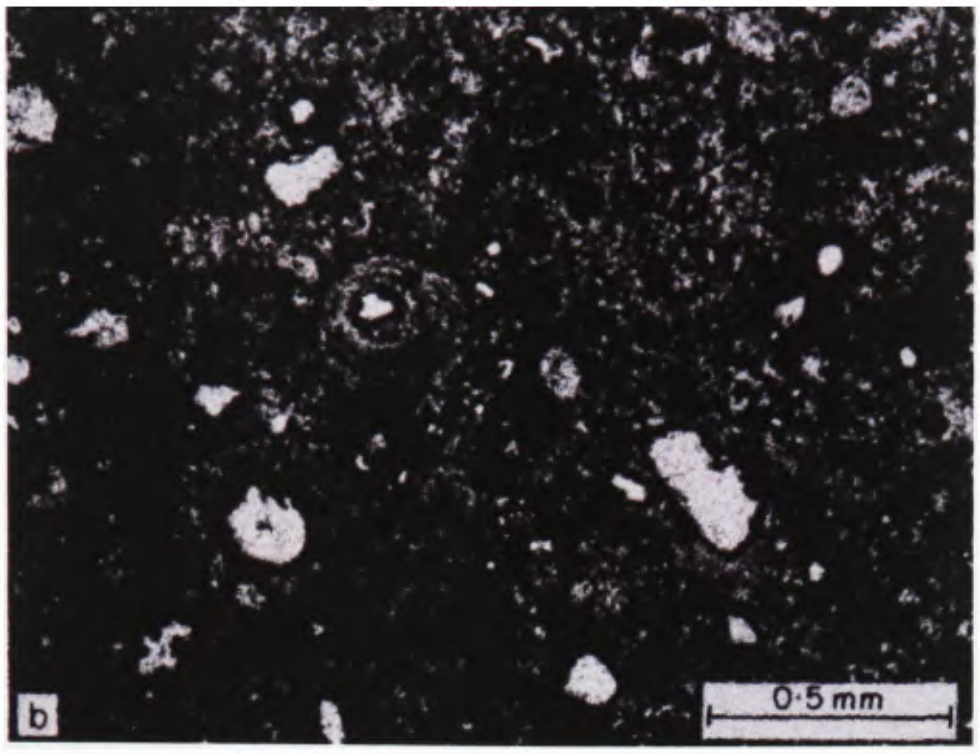
Adams and MacKenzie (1998) define ooids and pisoids as being spherical or ellipsoidal coated grains with a nucleus surrounded by a cortex of which at least the outer part is smoothly concentrically laminated. Obvious biogenic structures should be at most a minor component of the cortex. Ooids are < 2 mm in diameter, pisoids > 2 mm. In older literature the terms oolith and pisolith are used to describe the same features. However, the terms oolitic for a sediment containing ooids, and oolite for a sediment dominated by ooids, are still used (Adams and MacKenzie, 1998).

Most ooids and pisoids are calcareous, but there are numerous examples of grains fulfilling the specifications of ooids and pisoids despite having non-calcareous cortices. The best southern African examples of these are oolitic ironstones in which the cortices comprise various iron minerals.

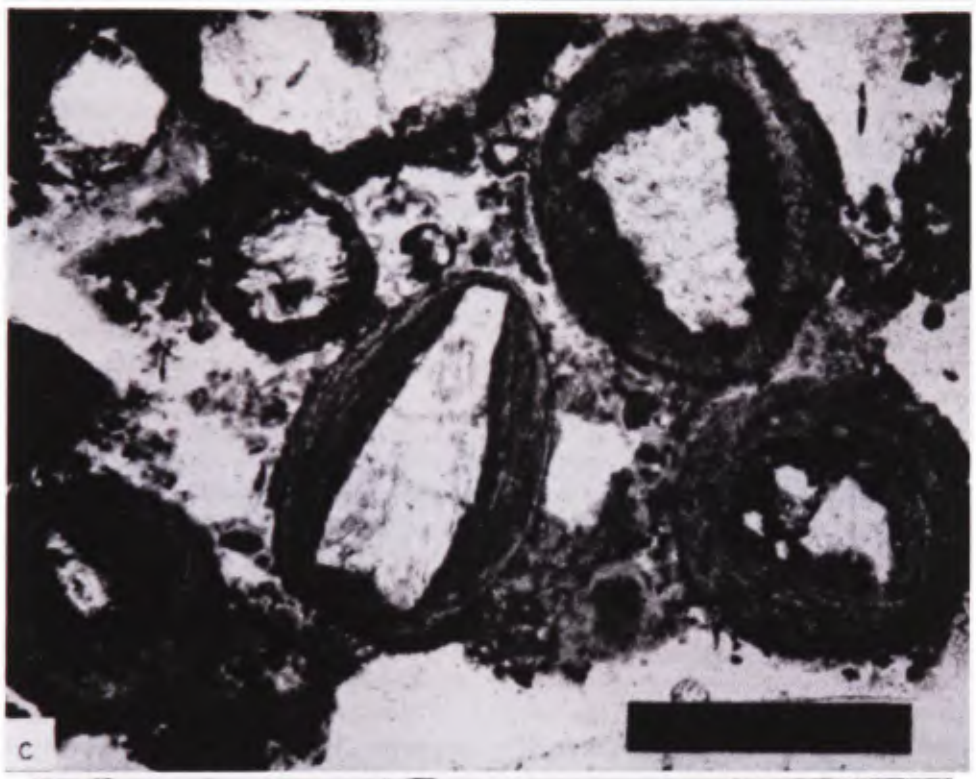
Ooids demonstrate a variety of cortical structures and mineralogies which depend on their age, mode of formation and diagenesis.



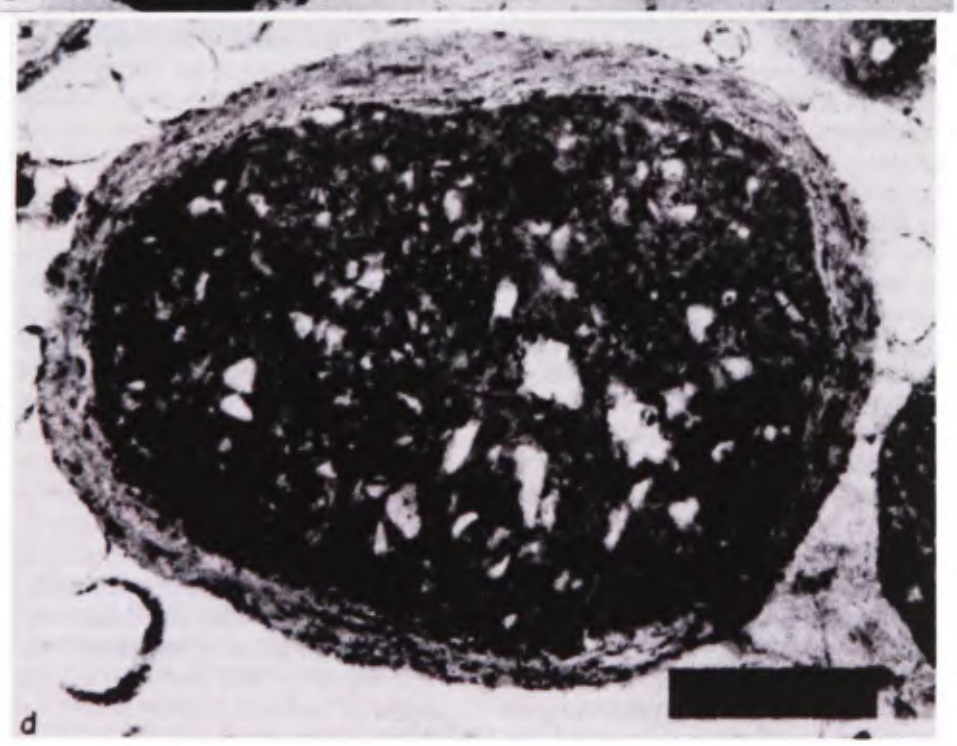
Oolitic texture in a massive calcrete from Tanzania. Photo of a polished surface in reflected light. The centers of the ooids appear dark. The fabric is grain supported by the ooids. (Hay & Reeder, `78)



An acetate peel of massive calcrete from Tanzania in transmitted light. An **ooid with concentric layers of micrite** is visible in the center of the photo. (Hay & Reeder, '78)



Ooids from the calcrete near Wickieup, USA. **Ooid coatings** consist of calcite and opal. These coatings thin over the corners of the angular nucleus of the central ooid. Ooids lie in a patchy matrix of crumb aggregates. Scale bar is 0.5 mm. (Hay & Wiggins, `80)



An **ooid with a pelletal nucleus** from the Argus Range, USA calcrete. The nucleus is sandy, sepiolite micrite, and the ooid coating consists largely of sepiolite. Scale bar is 0.5 mm. (Hay & Wiggins, `80)

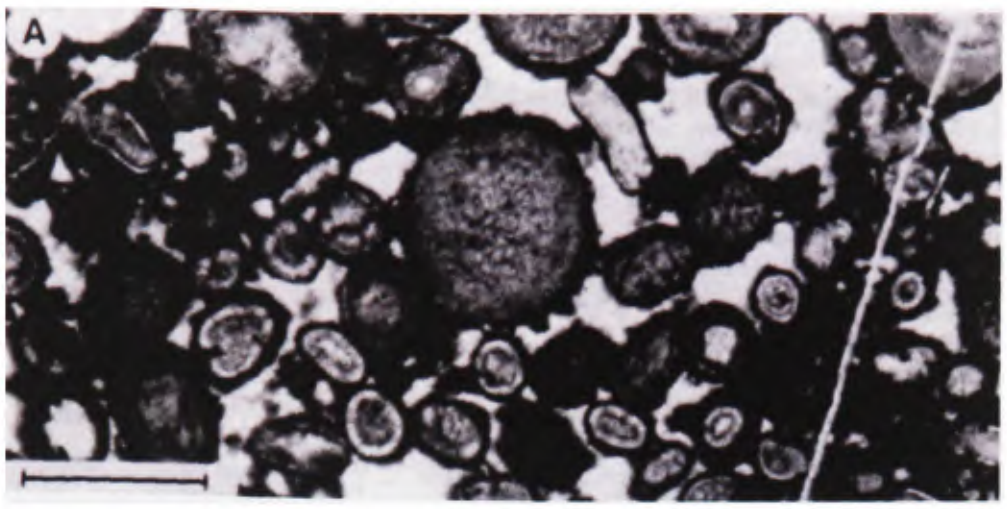
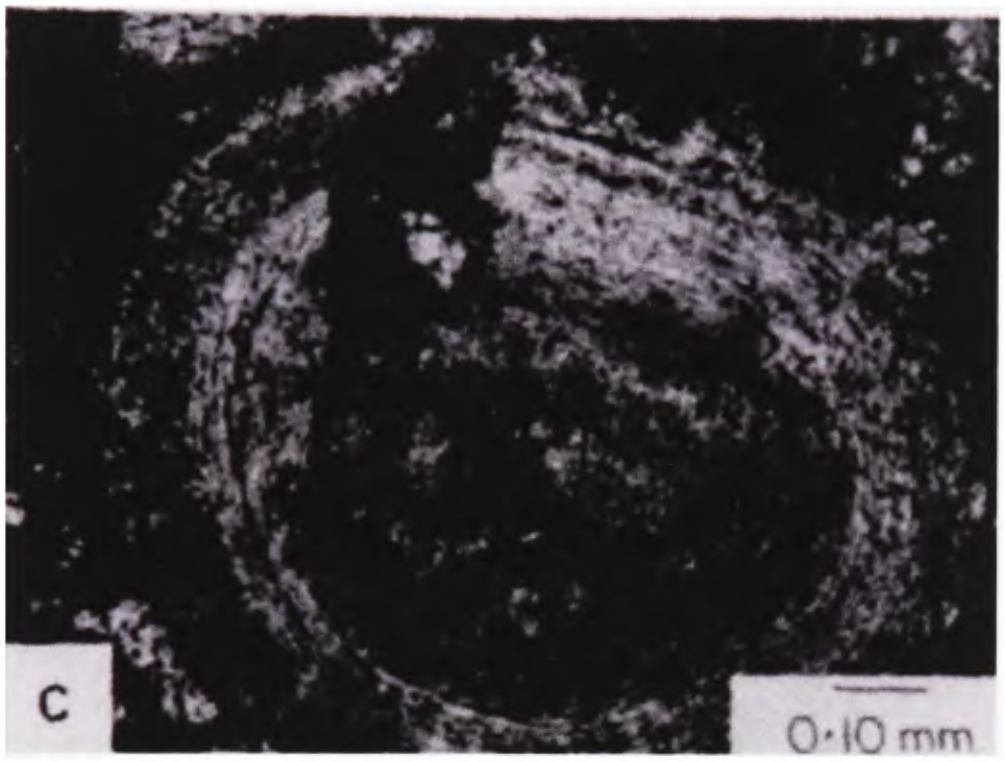
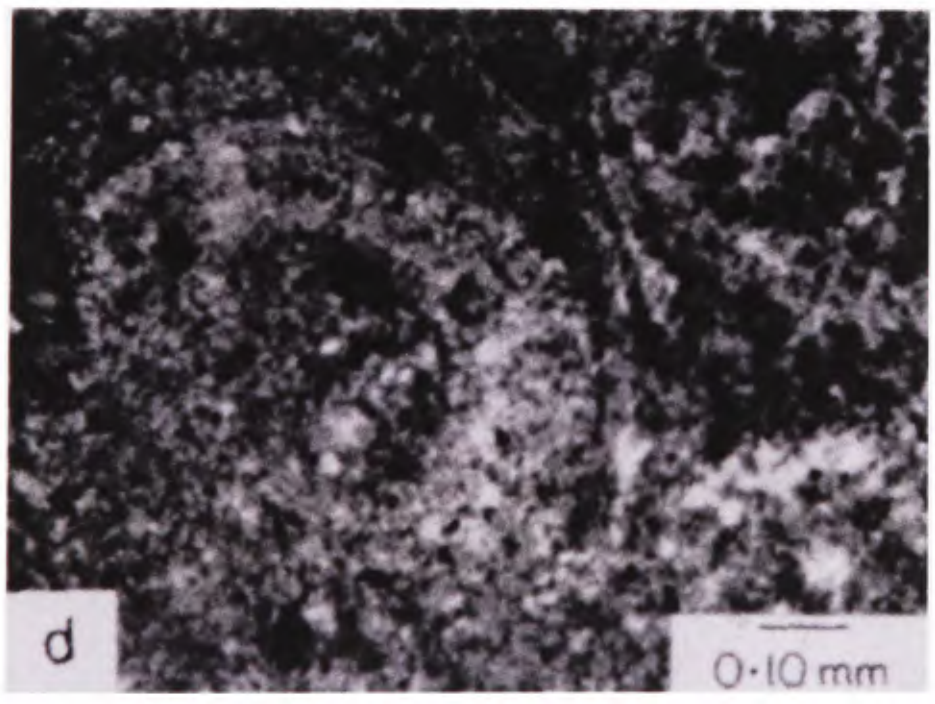


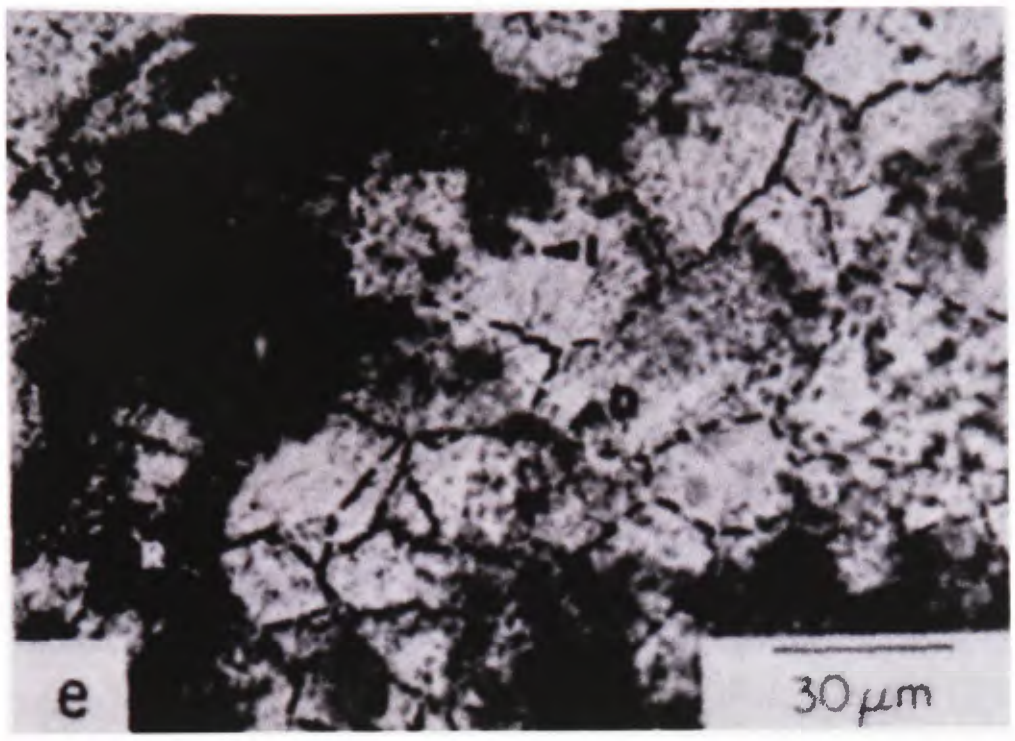
Photo of grain coats from the Heatherland Geosol at Miskin. **Oolitic** grainstone with **micritised ooids** coated by dark **micrite** showing irregular thickness around the **ooids**. **Protuberances** occur on some grains (e.g. large ooid in the **centre**). Scale bar represents 750 μm. (Wright, `86)



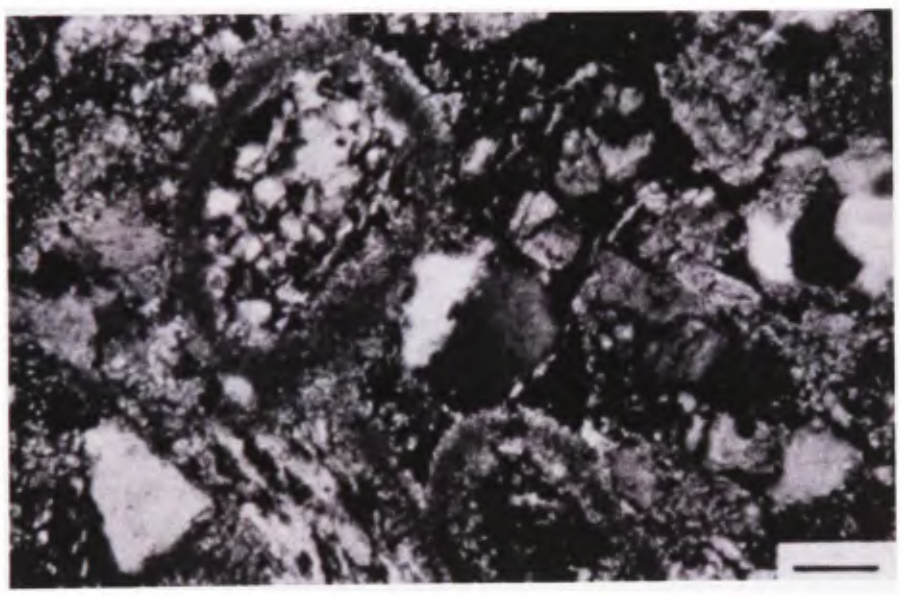
Thin section, plane light. Relict of **allochem** from the Miami Limestone in calcareous crust. Note merging of **micrite** created by **micritisation** of **allochem** with **micrite** making up the matrix surrounding calcareous crust. **Ooid** contains numerous **endolithic fungi**. (Kahle, `77)



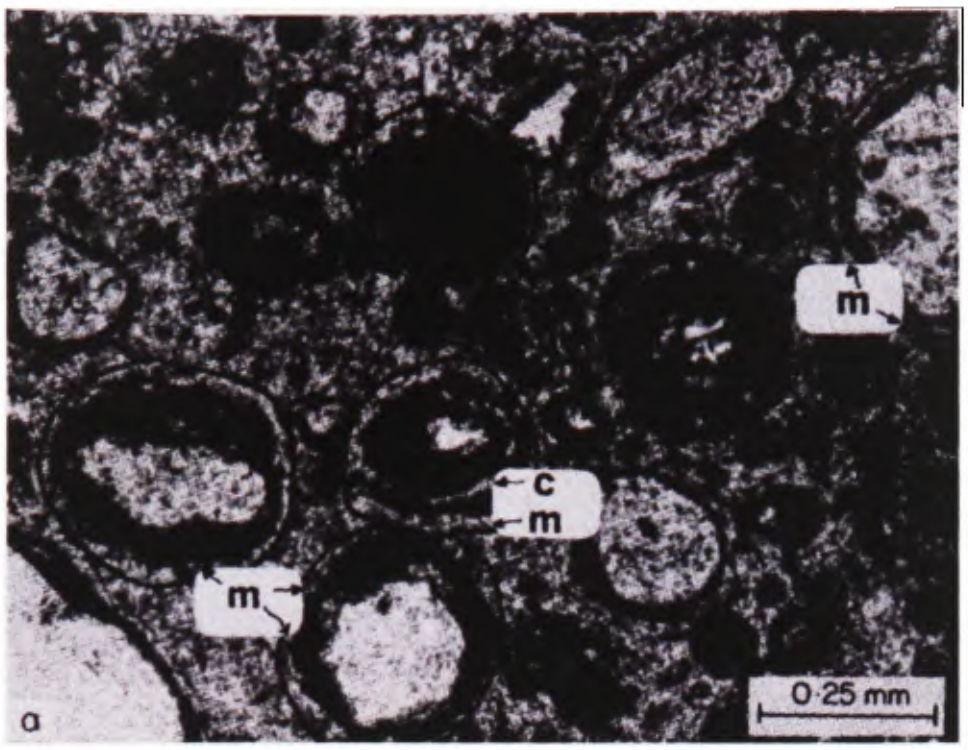
Thin section, plane light. 'Ghosts' of **ooids** from the Miami Limestone in calcareous crusts. (Kahle, `77)



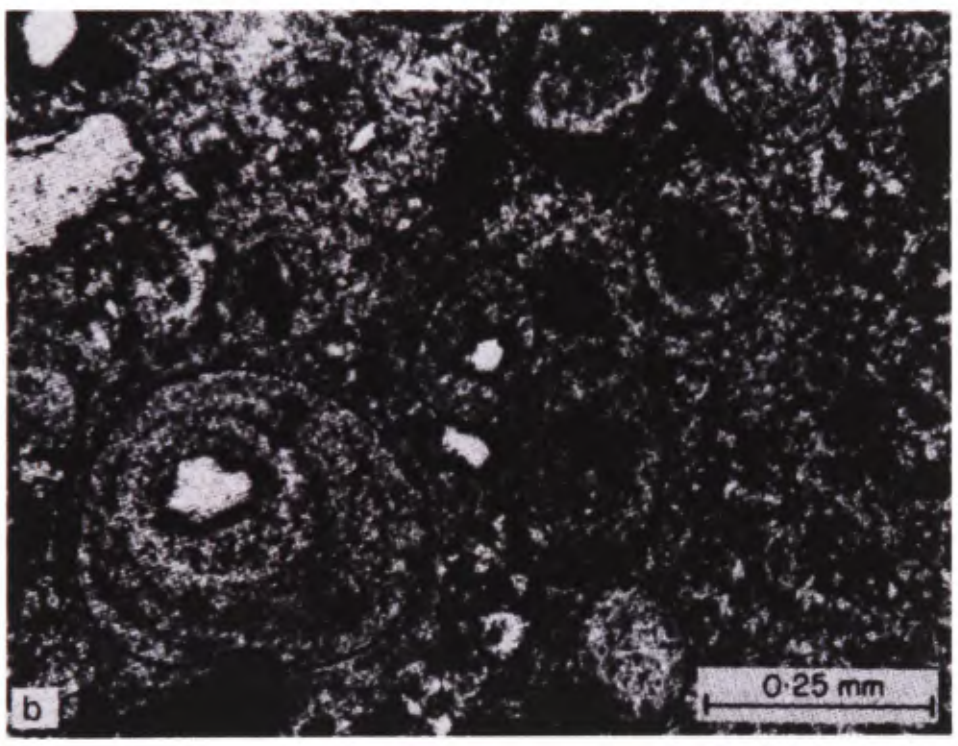
Thin section, plane light. Portion of **ooid** rim that has undergone **aggrading recrystallization**. Miami Limestone. Boundaries of crystals of **sparry calcite** indicated by dashed lines. The intrusion of patches of **micrite** into crystals of **sparry calcite** (I), patches of **micrite** that cross-cut such crystals and their boundaries (D), and the presence of rhomboid-shaped patches of **micrite** (R) indicate that **sparmicritisation** occurred after **aggrading recrystallisation**. (Kahle, `77)



Micritic ooids developed in cornstone. Note the fuzzy **laminae**. Thin section, crossed nicols. Scale bar represents 50 μm. (Tandon & Narayan, `81)



Pseudo-ooids and oolitic textures illustrated by acetate peels of the massive calcrete at the base of the Ndutu Beds Tanzania. This photo depicts an early stage in the formation of pseudo-ooids in which micrite (light) is replacing clay (dark) at the margin of (m) and in the concentric zones (c) of pelletoid clay coats. (Hay & Reeder, `78)



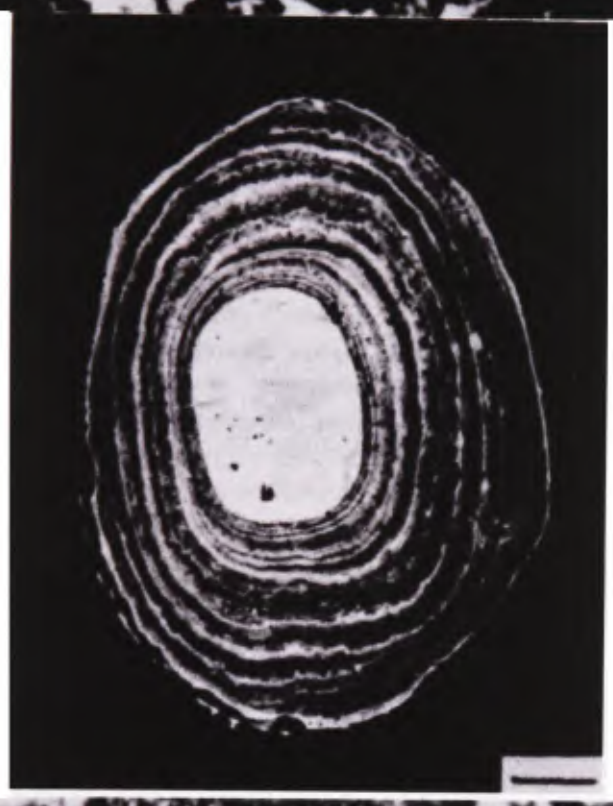
Pseudo-ooids and oolitic textures illustrated by acetate peels of the massive calcrete at the base of the Ndutu Beds Tanzania. This photo depicts a late stage in the replacement of clay coated ooids. The original grain outlines are indicated by inked lines. (Hay & Reeder, `78)

Pisoids

Smoothly laminated grains > 2 mm in diameter are far less common than ooids and form in more specialized environments. It is generally believed that pisoids do not form as a result of carbonate layer accretion while in suspension. As such, it is widely believed that the majority of pisoids grow in part within the sediment where there is no restriction on size.



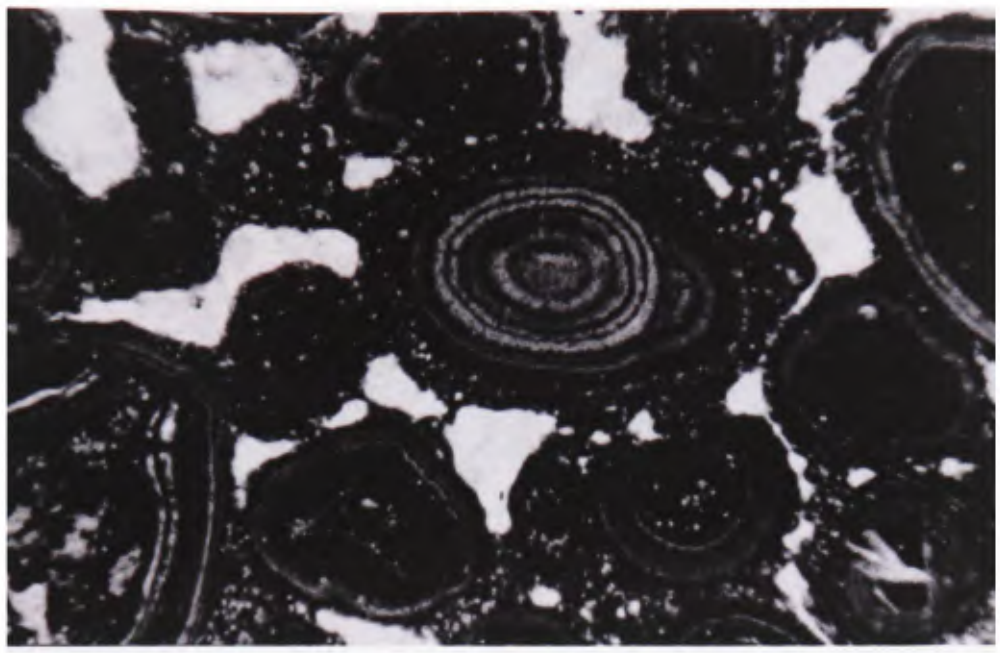
Thin section, crossed nicols. **Pisoid** calcrete conglomerate. Note the **stylolitic** seam in the lower left corner. Scale bar represents 200 μm. (Tandon & Narayan, `81)



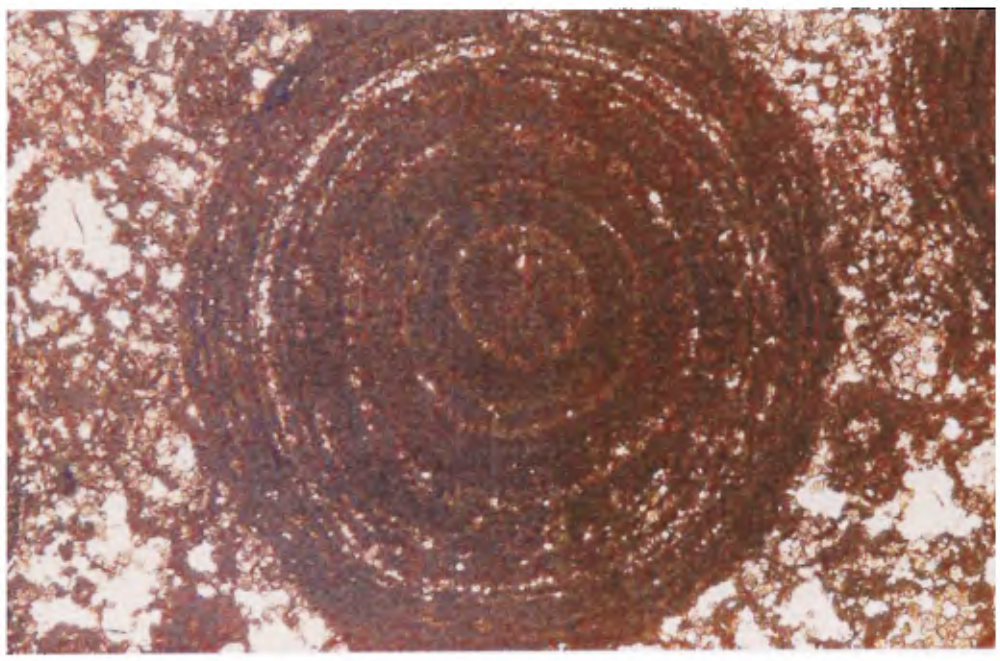
A large **pisoid** from a calcrete conglomerate showing more than 20 distinct **laminations**. Negative print from an acetate peel. Scale bar represents 1 cm. (Tandon & Narayan, `81)



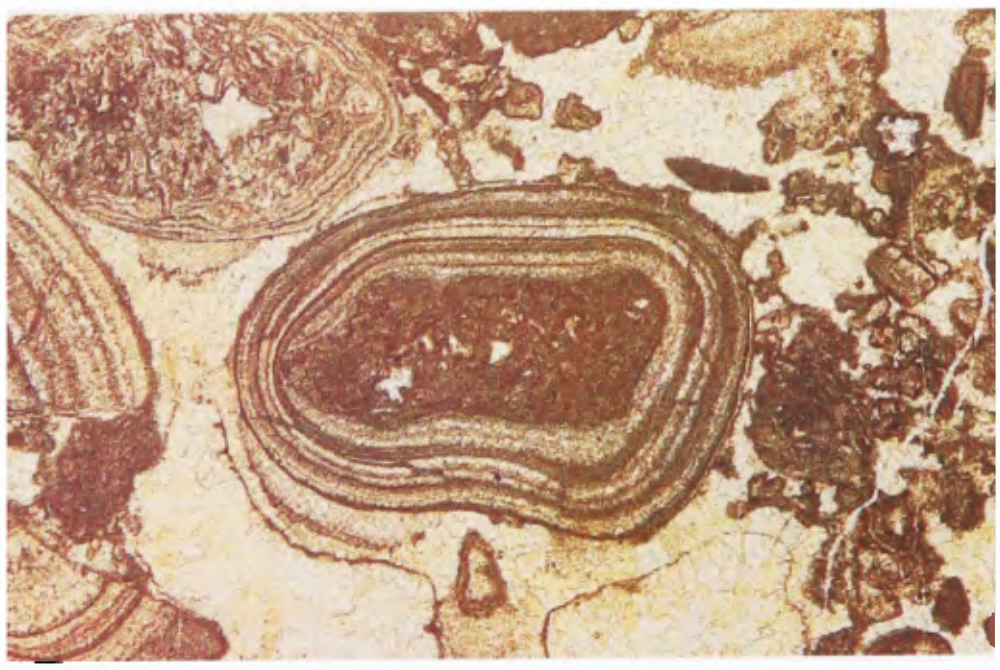
Smaller pisoid penetrating into the rind of a larger pisoid. Note the bending and breaking of laminae of the larger pisoid due to the pressure exerted by the smaller pisoid. Thin section, crossed nicols. Scale bar represents 50 μm. (Tandon & Narayan, `81)



The photo shows '**vadose**' **pisoids** from the Carboniferous near Calgary. They have a strong radial fabric and probably formed in a supratidal setting. Many show fractures which have been solution enlarged. Some pisoids have nucelii of fractured forms. The sediment received a pedogenic overprint when the dolomitic coatings were formed. The coatings exhibit bridge structures connecting the coats which is a very common pedogenic feature. (Wright)



A dolomitised **pisoid** showing smooth concentric laminations (Adams and MacKenzie, `98).

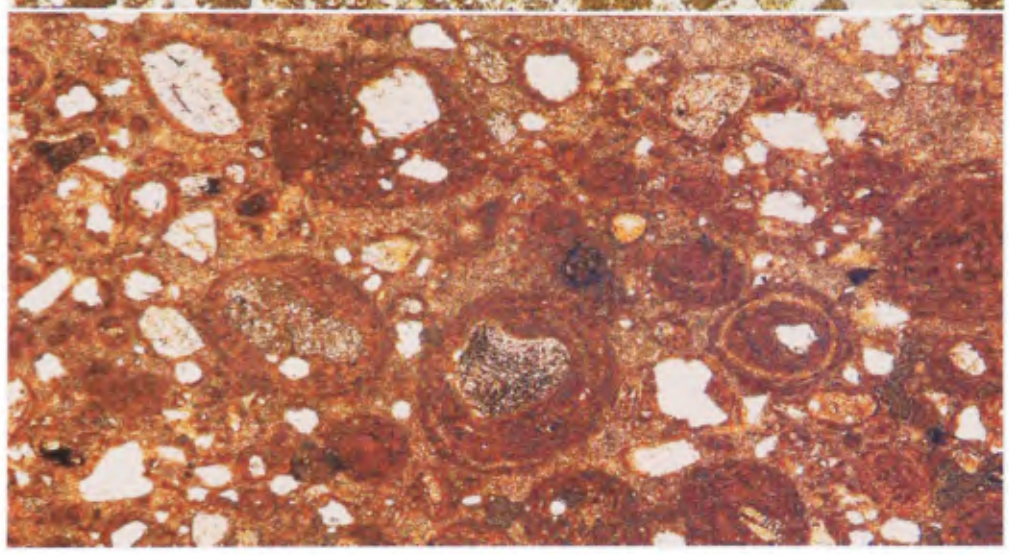


A **pisoid** showing evidence of having been cemented within the vadose zone, with early cement present on the undersurface of the grain and absent from the upper surface, but does not show clear evidence of preferential downward growth, a characteristic of vadose pisoids (Adams and MacKenzie, `98).

Oncoids are coated grains in which the calcareous cortex is less smoothly laminated than in the case of ooids and pisoids, with irregular laminae overlapping and are often not entirely concentric (Adams and MacKenzie, 1998). Oncoids are often irregular in shape, may have poorly defined nucleus and may contain biogenic structures. Oncoids are >2 mm in diameter; grains of this type <2 mm in diameter are known as micro-oncoids.

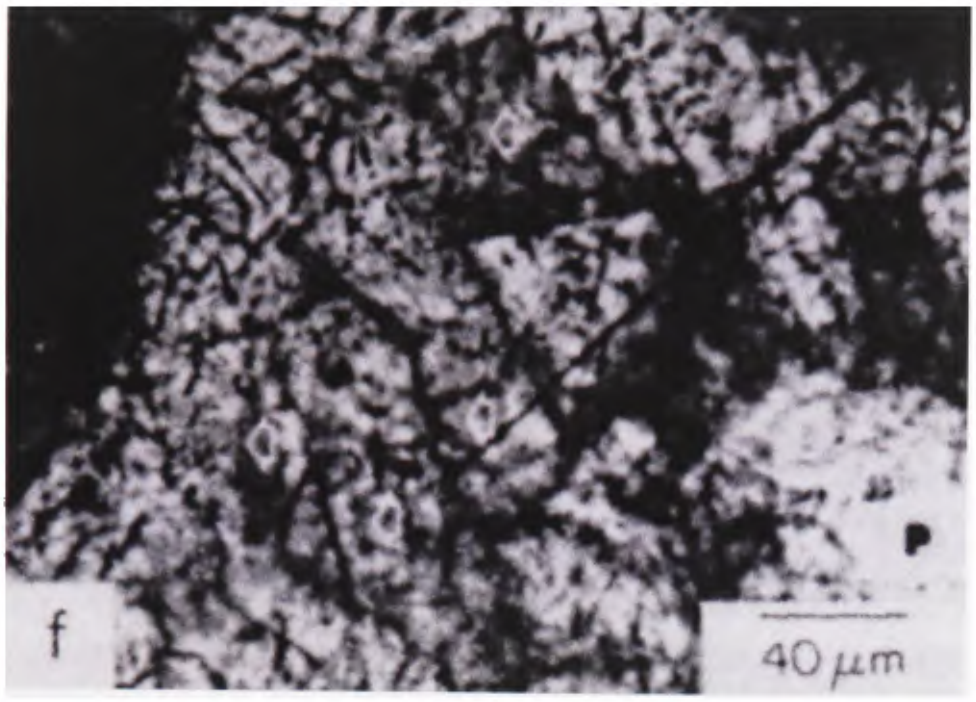


A freshwater limestone containing an **oncoid**. The nucleus is indistinct, but the concentric laminations and the rather irregular outer surface of the grain are clear (Adams and MacKenzie, `98).

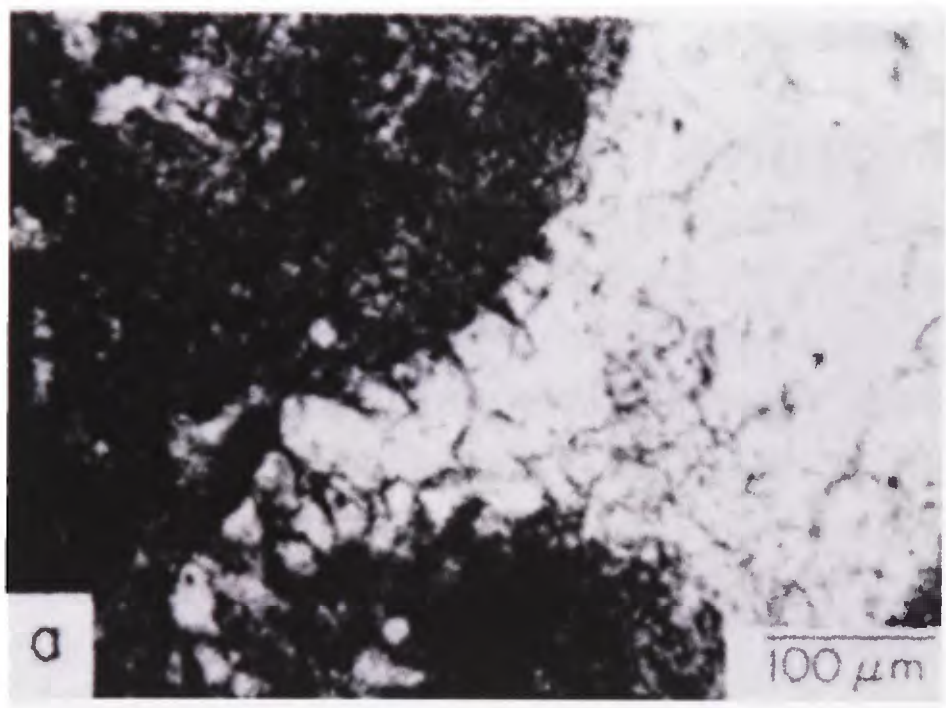


Micro-oncoids formed in paleosols as a result of microbial processes (Adams and MacKenzie, `98).

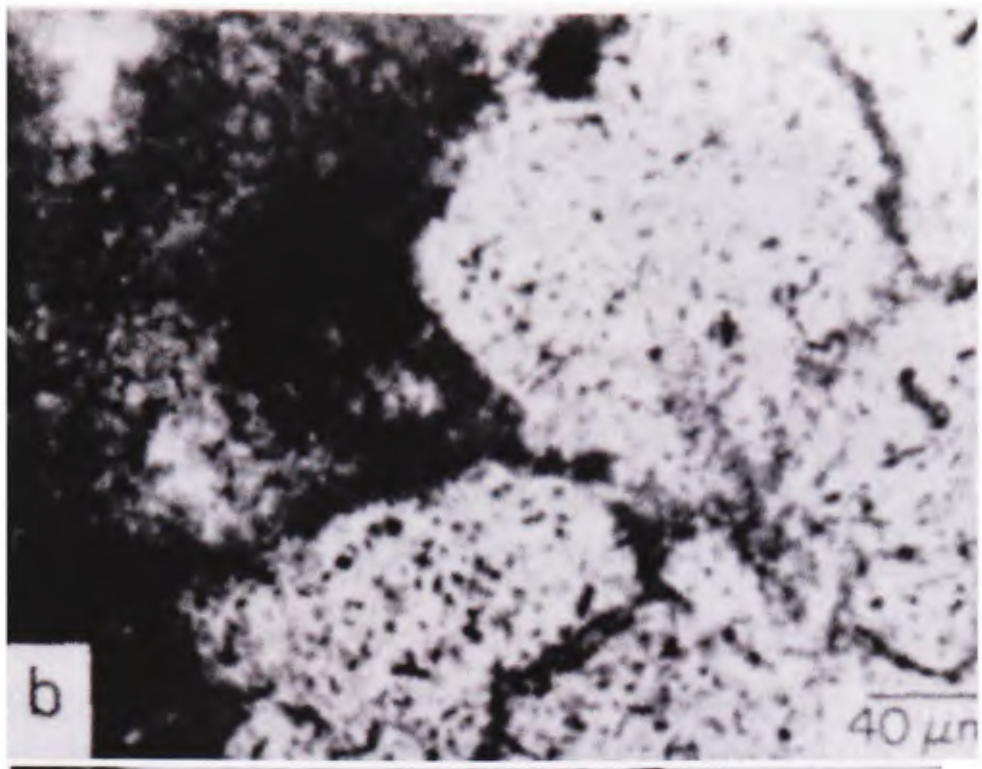
Sparmicrite



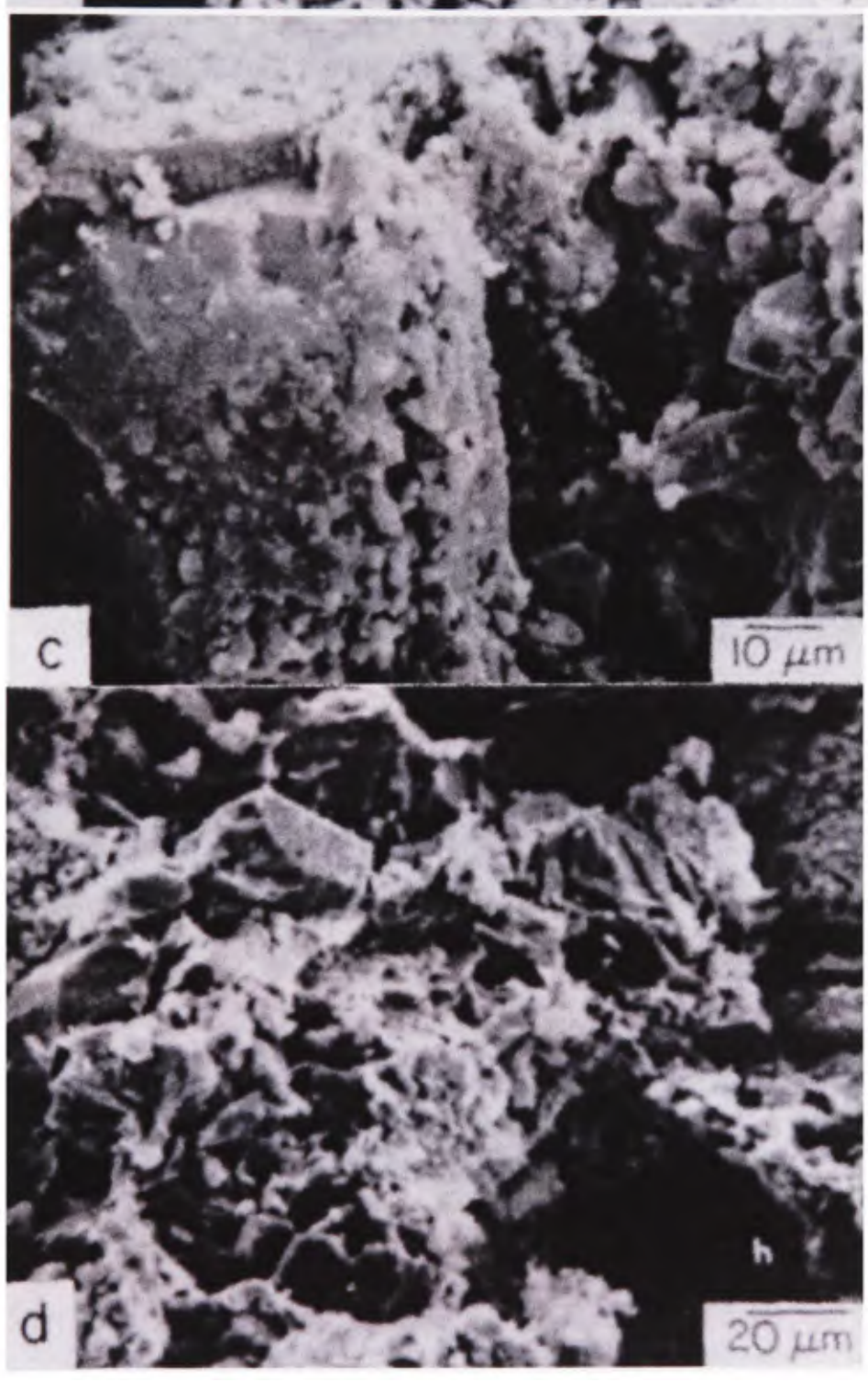
Thin section, plane light. **Sparmicritisation** concentrated primarily along the boundaries of crystals of **sparry calcite cement**. Miami Formation. Portions of some crystals (arrows) show a brown discolouration. **Fungal endoliths** appear as dark lines some of which branch. (P) is a pore. (Kahle, `77)



Incipient **sparmicritisation** represented by 'spikes' of **micrite** extending away from calcareous crusts along the boundaries of **sparry calcite** cement in the Miami Limestone (near center). The 'spikes' of **micrite** grade into a more advanced stage of **sparmicritisation** represented by crystals of **sparry calcite** enveloped by **micrite** (lower left) that grade, in turn, into a patch of **sparmicrite** in the Miami Limestone (bottom center). (Kahle, `77)

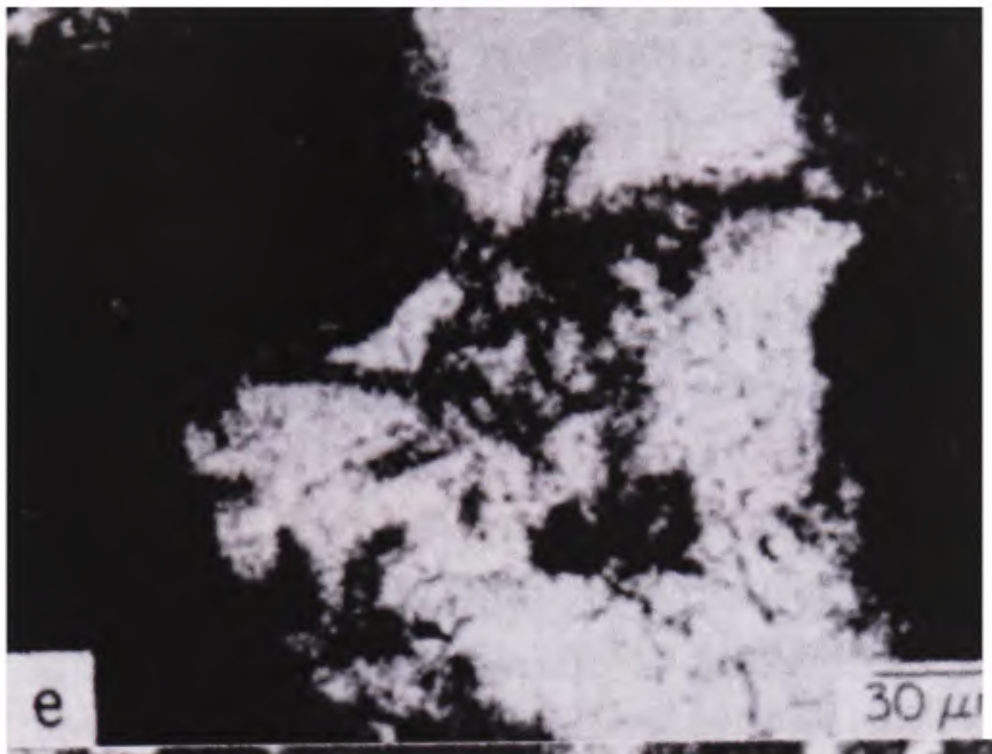


Thin section, plane light. Calcareous crusts on left and Miami Limestone on right. Nearly complete **sparmicritisation** of a former crystal of **sparry calcite** cement in the Miami Limestone (triangular area of **micrite** left of center). Note areas of **sparmicritisation** along the boundaries of crystals of **sparry calcite** and projecting away from the former into the center of the latter. **Fungal endoliths** appear as dashes or dashed lines. (Kahle, `77)

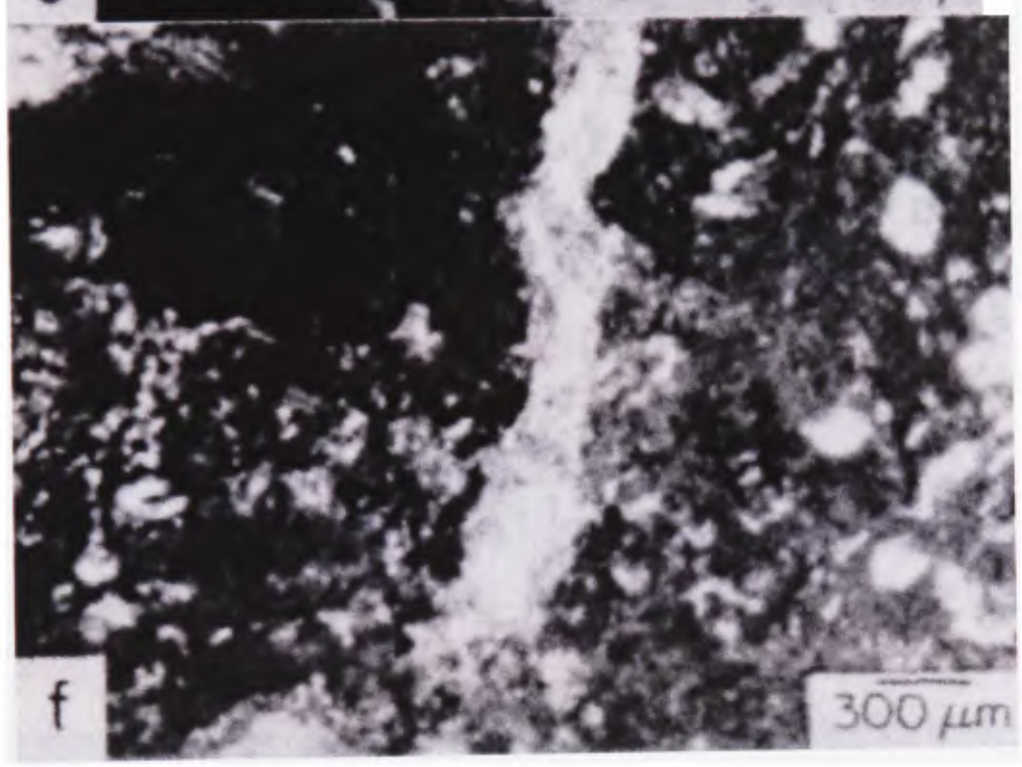


SEM photo. Crystals of **sparry calcite cement** that have undergone partial **sparmicritisation** in the alteration zone in the Miami Limestone. (Kahle, `77)

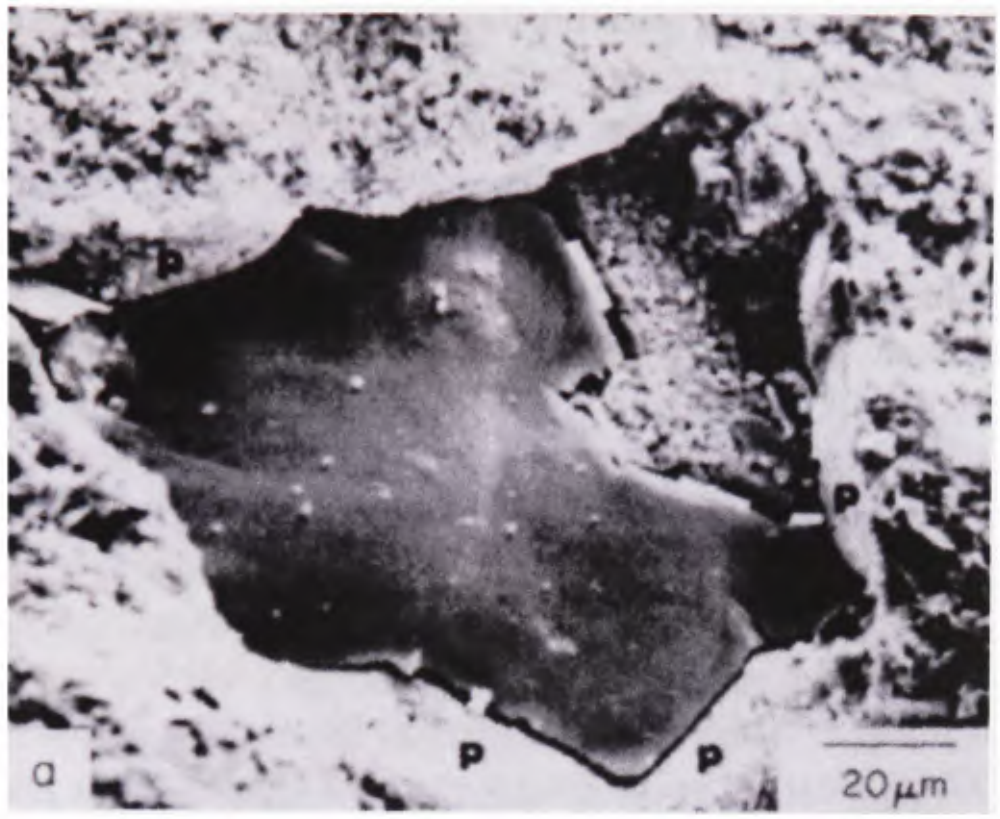
SEM photo. Crystals of **sparry calcite cement** that have undergone partial **sparmicritisation** in the alteration zone in the Miami Limestone. Hole (H) is a possible algal boring. (Kahle, `77)



Thin section, plane light. Pore within calcareous crusts that were filled by **sparry calcite cement** and then subsequently bored by fungi. Each of the finger-like areas of **sparmicrite** contains one or more **fungal endoliths** aligned parallel or sub-parrallel to the length of the 'finger'. The **sparmicrite** occurs within or directly adjacent to the **endoliths**. (Kahle, `77)



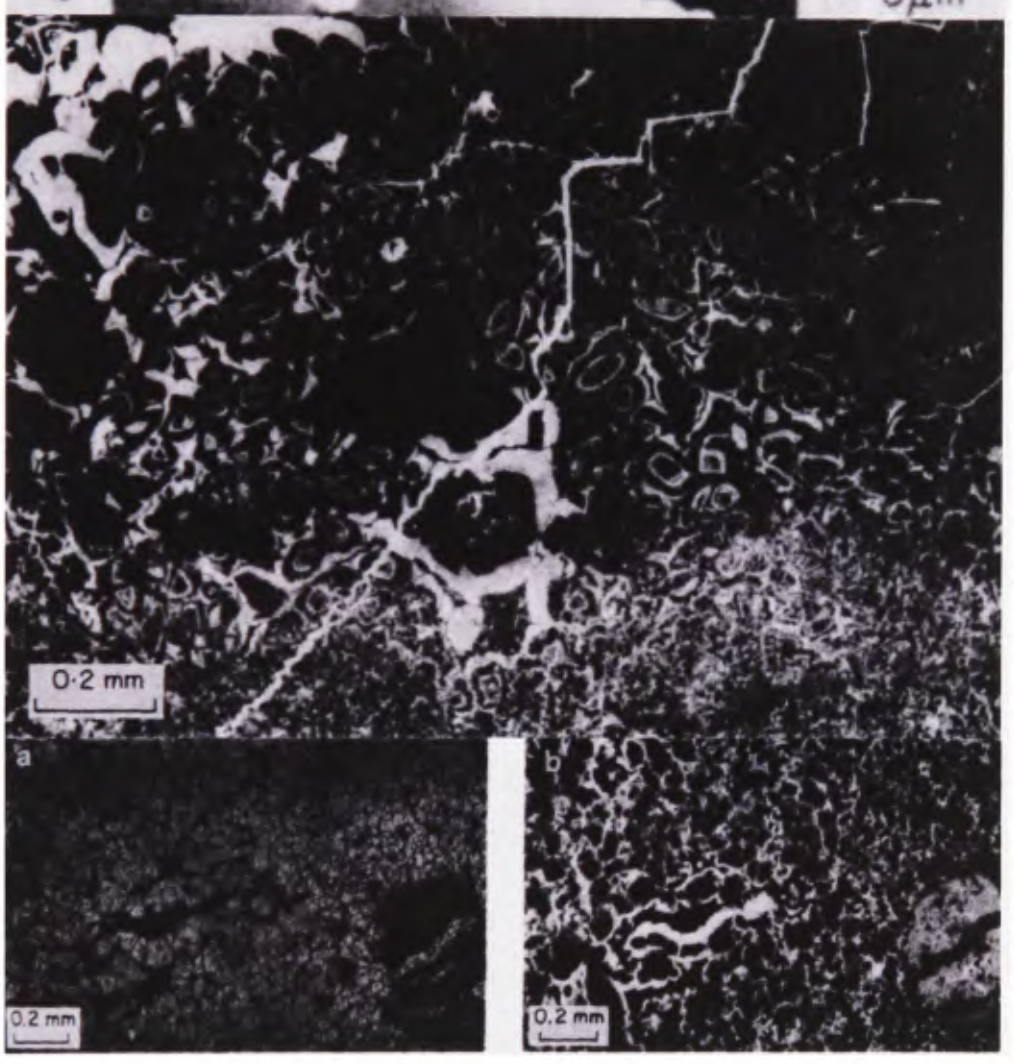
Thin section, plane light. Fracture within crust that contains a mixture of **sparry calcite cement** and **sparmicrite**. All areas of **sparmicrite** contain abundant **fungal endoliths**. Such **endoliths** are absent or few in number in the **sparry cement**. (Kahle, `77)



SEM photo. Relict crystal of **sparry calcite cement** from the Miami Limestone in calcareous crust. A portion of the crystal has undergone **sparmicritisation** (area outlined by dashed line). Crystal is located about 50 μm above the contact between the Miami Limestone and overlying crust. **Sparmicritisation** of this crystal is interpreted to have involved a semi-continuous process of concomitant dissolution-precipitation whereby a dissolution 'front' followed by a zone in which backfilling occurred in the form of **micrite** precipitation, moved part way through the crystal. The planar surfaces (P) above the crystal surface appear to be the walls of a mold. This mold may have formed by dissolution of a portion of the crystal shown or by way of dissolution of another crystal that occurred above the crystal shown. (Kahle, `77)



SEM photo. Close-up of the central portion of A above.

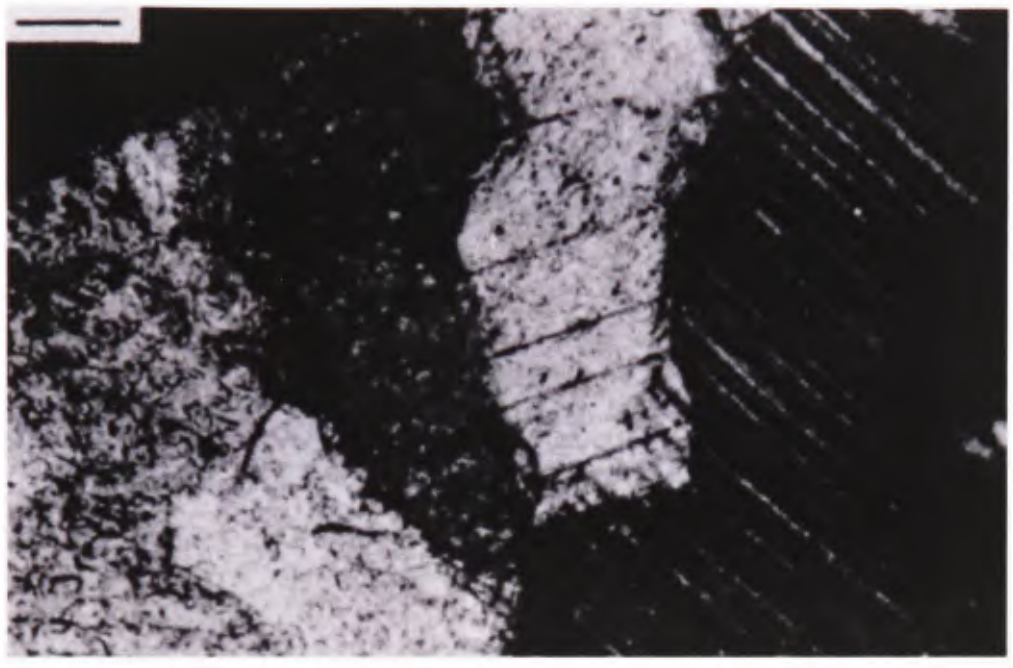


Cathodoluminescence photo. The central part and most of the upper part of the area are formed by spar, showing peripheral growth of the crystals. Micrite below and above shows replacement of the micrite fabric by spar-sized crystals, presumably by solution and precipitation about certain centres in the micrite. (Tandon & Friend, `89)

Plane-polarised light (a) and cathodoluminescene

Sparry Calcite

A mosaic of crystals larger than those of micrite (Bathurst, 1975). For neomorphic microspar mainly in the size class 4-10 μm and pseudospar mainly in the size class 10-50 μm. Other terms frequently encountered in the literature refer to specific arrangements of silt-sized crystals: drusy spar implies spar lining a cavity, while flowerspar is applied to relatively elongated (bladed) crystals that occur in bunches at regular intervals.



Sparry calcite cement from the case-hardened conglomerate showing well-developed **cleavage** and straight, **intercrystalline boundaries**. Thin section, crossed nicols. Scale bar represents 200 μm. (Tandon & Narayan, '81)

Voids

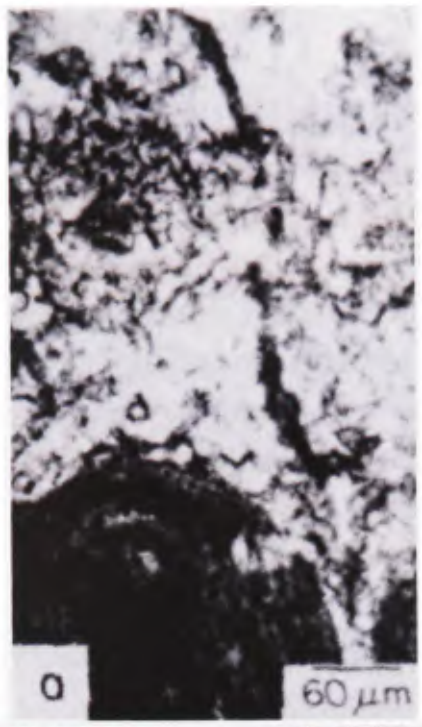
Druse – a cavity in a rock or mineral vein into which euhedral crystals of the minerals forming the rock or vein project.



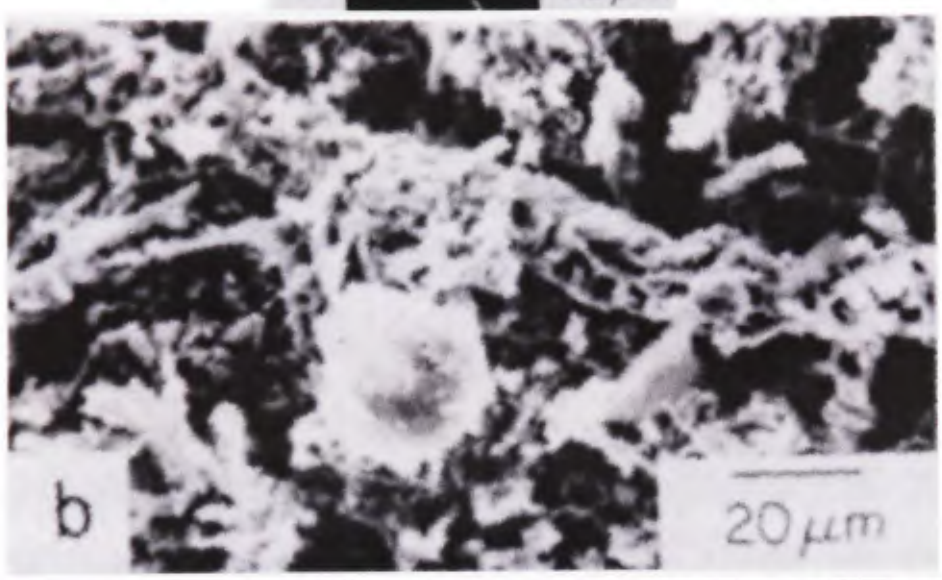
Aeolian calcarenite in which the centres of some **bioclastic allochems** are leached leaving a **micritic margin**. A **drusy calcite** (c) lines these **intraparticle voids** (v). A thin **micritic coating** (m) covers most of the grains. **Primary pore space** is considerable (ϕ). (Knox, '77)

BIOLOGICAL

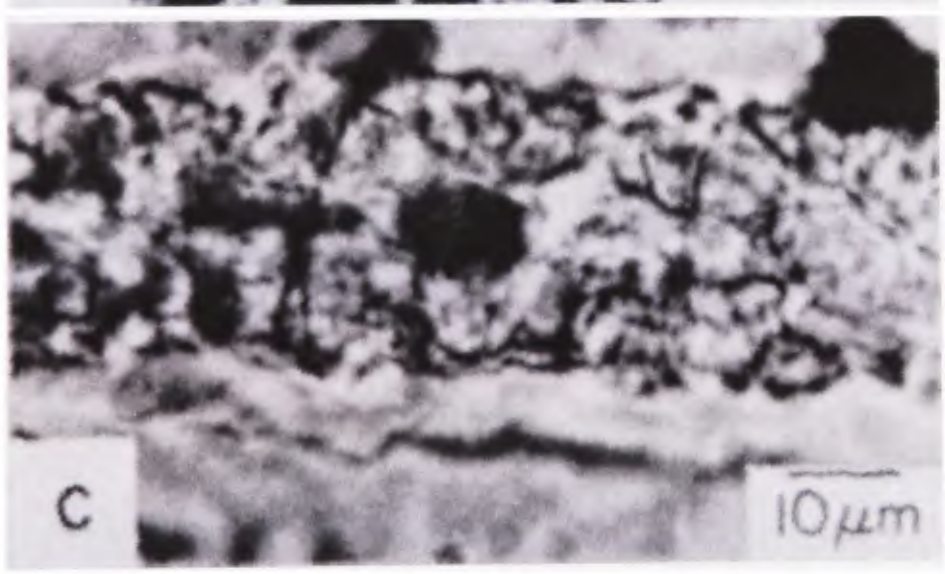
Algae



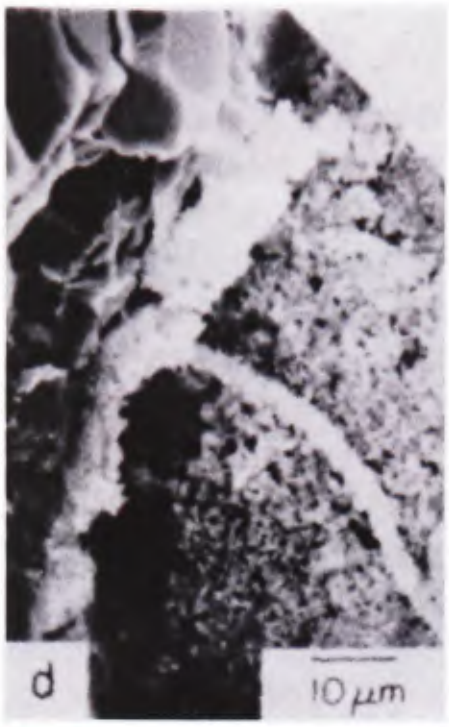
Thin section, plane light; longitudinal and cross-sectional views of **endolithic algae** calcified by **calcite micrite** in **sparry calcite** cement. Miami Limestone. (Kahle, `77)



SEM photo. **Endolithic algae** calcified by calcite. Miami Limestone. (Kahle, `77)



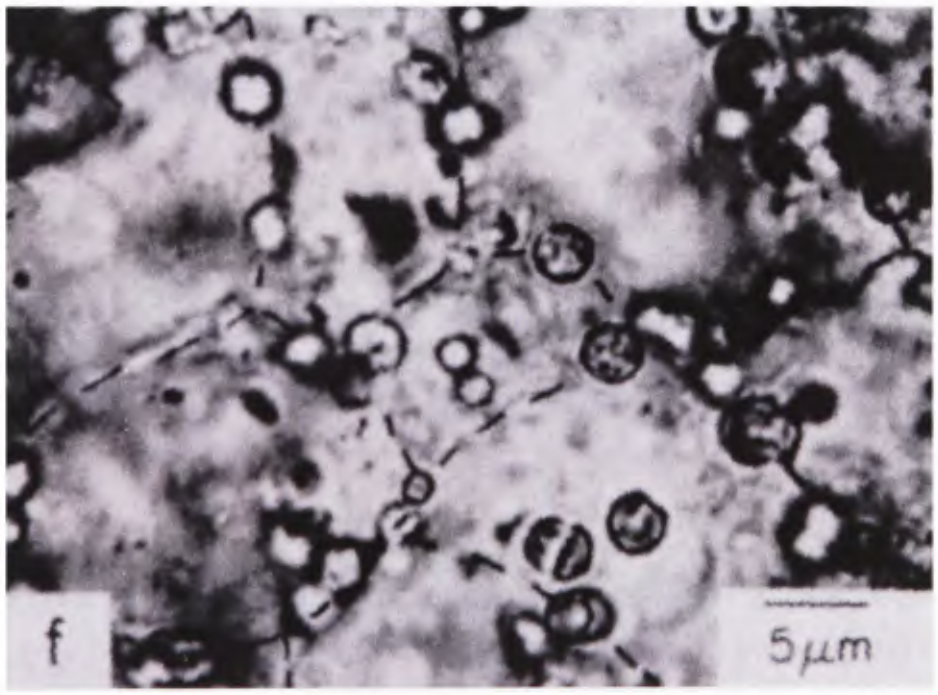
Thin section, plane light. **Endolithic algae** calcified by calcite. Miami Limestone. (Kahle, `77)



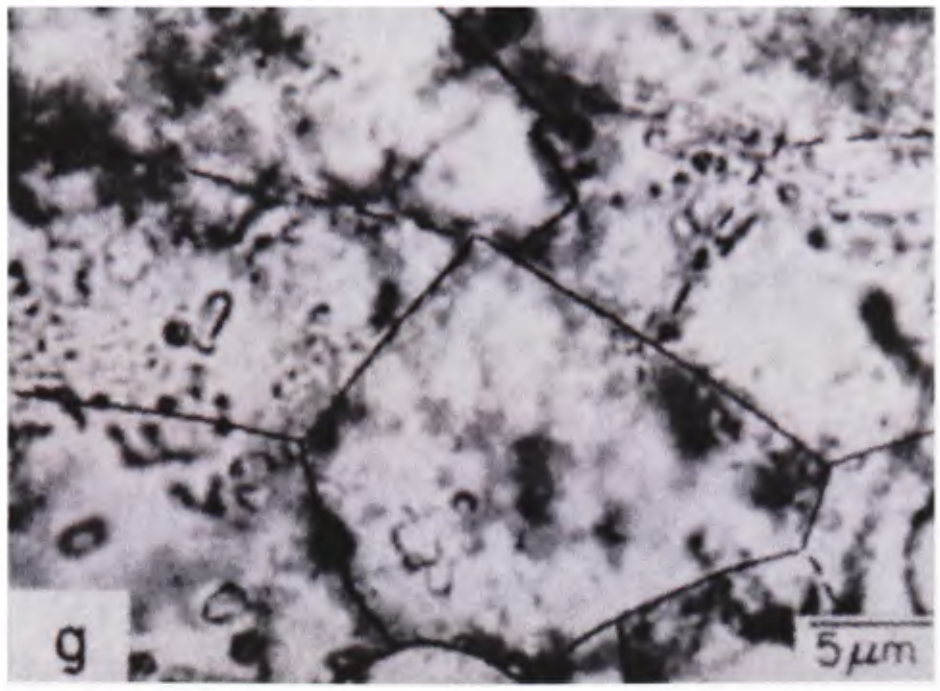
SEM photo. **Chasmolithic algae** (upper right to lower left) calcified by **aragonite battons**. A possible **chasmolithic fungi**, also calcified by battons, extends from the lower right towards the upper left. Miami Limestone. (Kahle, `77)



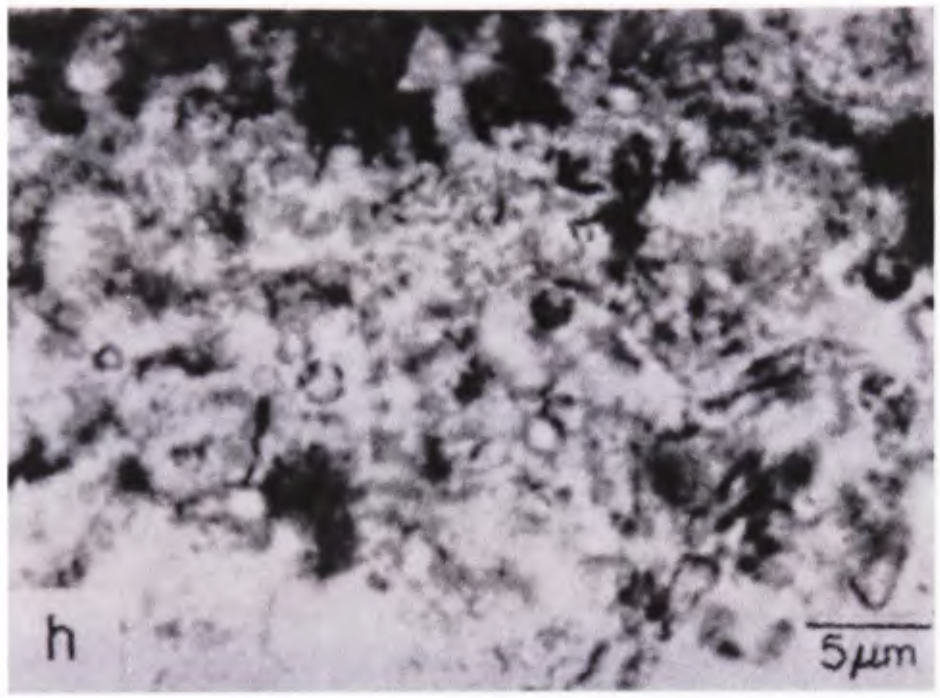
SEM photo. **Algal endolith** of unknown composition in a matrix of **micrite calcite.** Calcareous crusts. **Boring** in lower left was presumably made by the same type of algae. Smaller 2-3 μm **borings** in upper right are interpreted to be of fungal origin. (Kahle, `77)



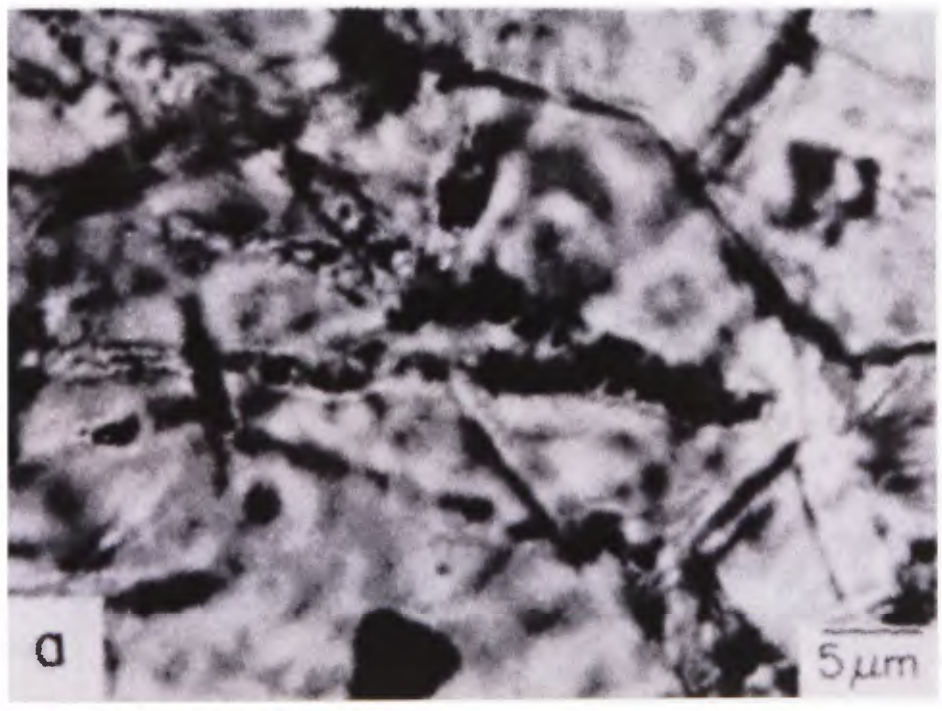
Thin section, plane light. **Treppelithic unicellular algae** concentrated along the boundaries (dashed lines) of crystals of **sparry calcite** cement. Miami Limestone. (Kahle, `77)



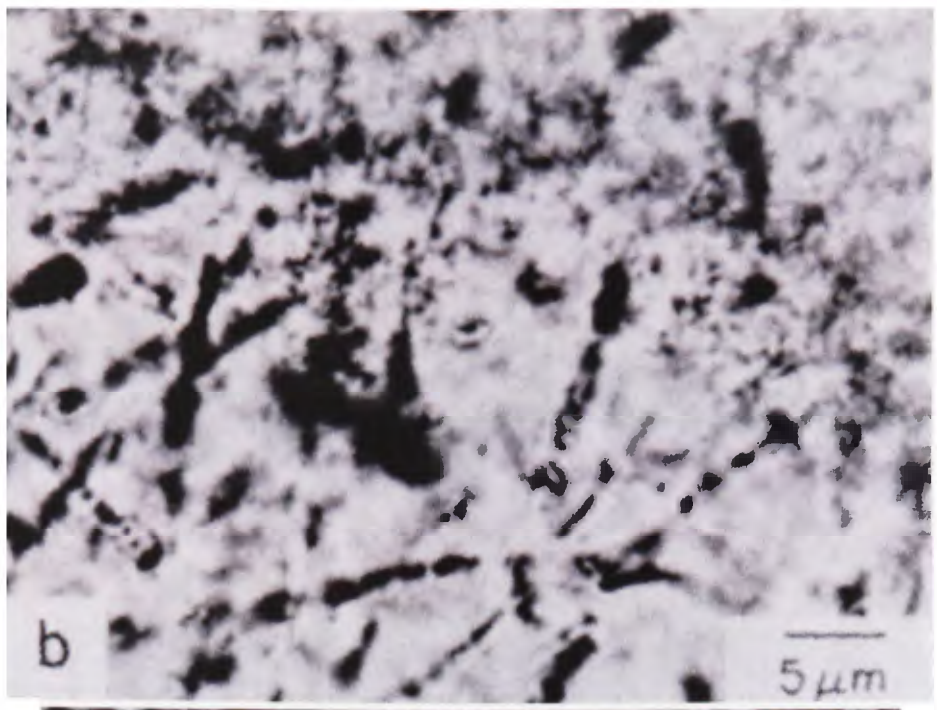
Thin section, plane light. Degraded **treppelithic algae** associated with the degrading recrystallization of crystals of **sparry calcite** cement to **micrite (sparmicritisation).** Miami Limestone. Boundaries of cement crystals where known are shown by solid lines and by dashed lines where approximate. (Kahle, `77)



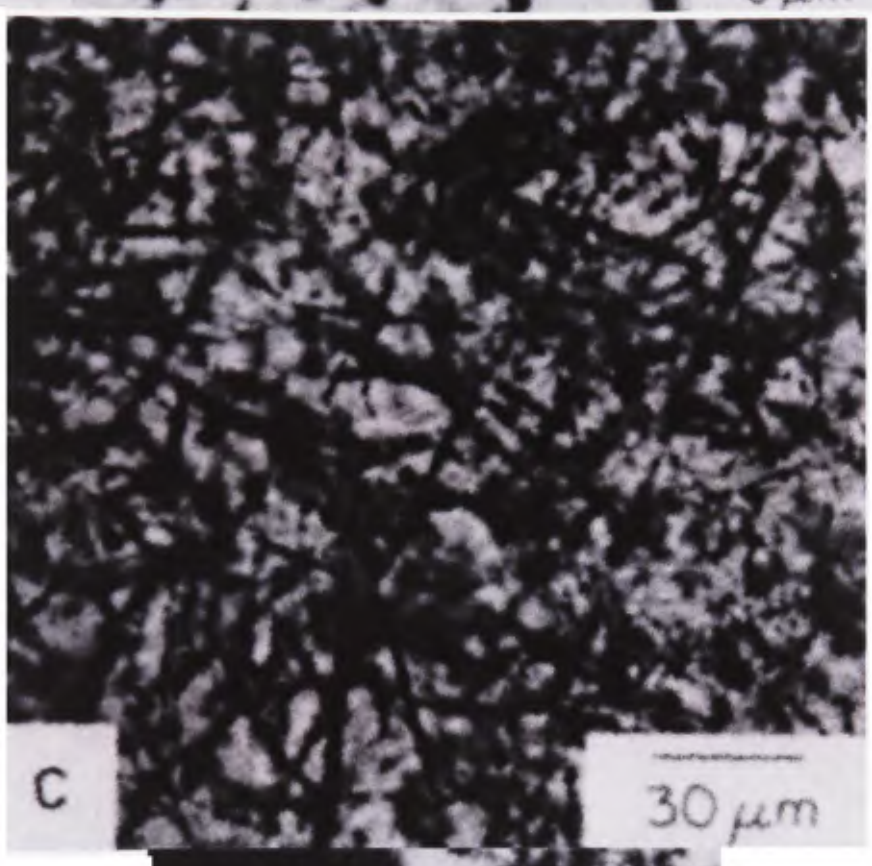
Thin section plane light. Traces of **treppelithic algae** within calcareous crusts. (Kahle, `77)



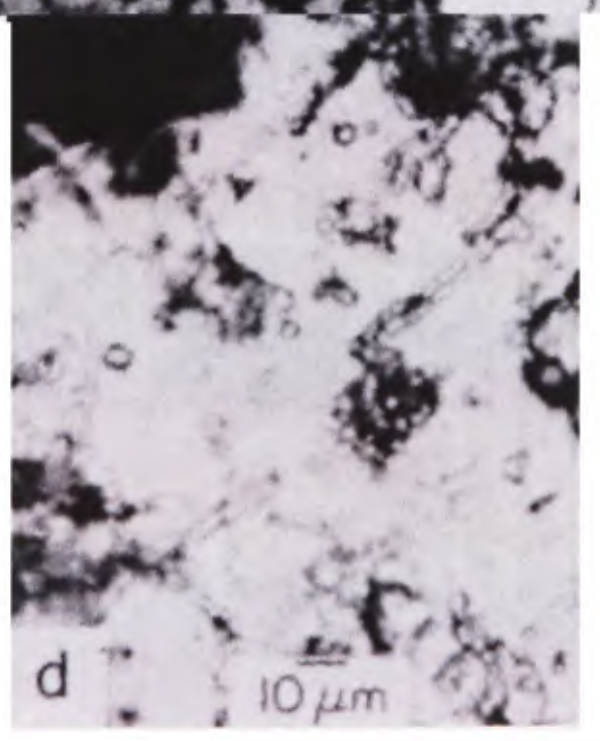
Thin section, plane light. **Fungal endoliths** in crystals of **sparry calcite** cement. Miami Limestone. (Kahle, `77)



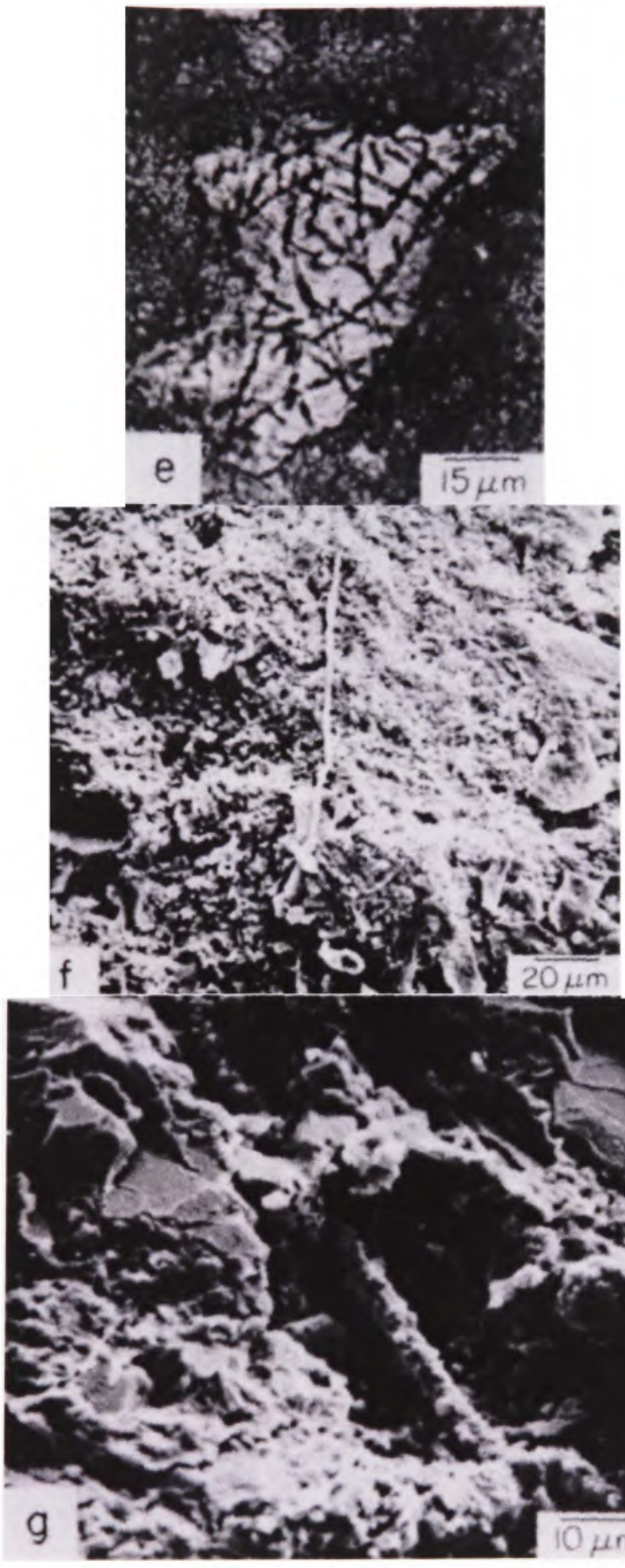
Thin section, plane light. **Fungal endoliths** in **sparry calcite** cement in the Miami Limestone (bottom) and (faintly visible) in calcareous crusts (top). (Kahle, `77)



Thin section, plane light. **Fungal endoliths** (appear as dark lines) and **fungal borings** (appear as light lines) in **sparry calcite** cement. Miami Limestone. The somewhat mottled appearing areas in portions of the photograph, as along the top, are areas of brown discolouration often associated with **fungal structures** in crystals of **sparry calcite** cement. (Kahle, `77)



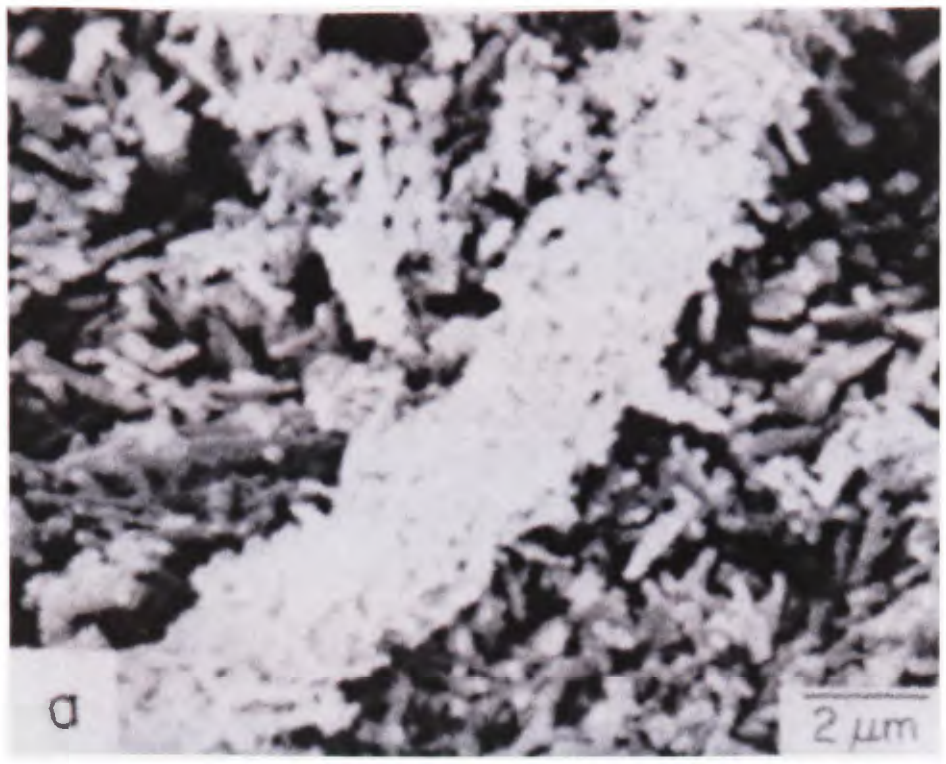
Thin section, plane light. **Endolithic fungal filaments** preserved in situ in the interior of an **allochem.** Miami Limestone. (Kahle, `77)



Thin section, plane light. **Endolithic fungi** with possible **conidia** or **sporangia** in **sparry calcite** cement. Calcareous crusts. Note **sparmicritisation** adjacent to some of the **endoliths** and the faint traces of **endoliths** in the **micrite** surrounding the former **pore space**. (Kahle, `77)

SEM photo. **Chasmolithic fungi** of unknown composition in calcareous crusts. Note corroded relicts of **sparry calcite** cement from the Miami Limestone. (Kahle, `77)

SEM photo. Combined **chasmolithic** and **endolithic fungi** calcified by calcite **micrite**. Calcareous crusts. Note corroded relics of **sparry calcite** cement from the Miami Limestone. (Kahle, `77)



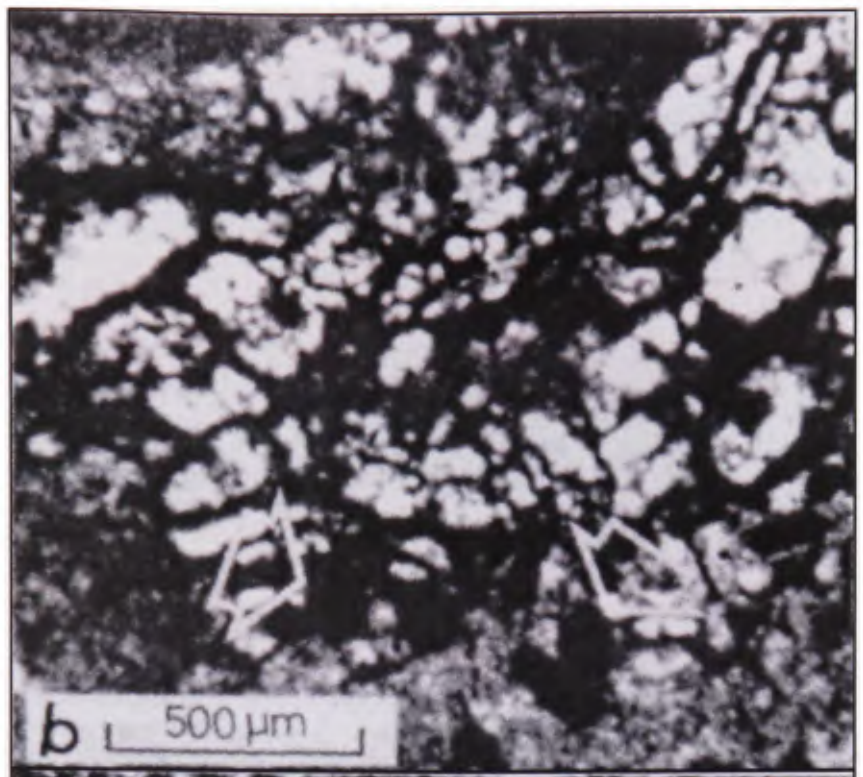
SEM photo. **Chasmolithic fungi** calcified by **aragonite battons**. The walls of the pore (upper left and lower right) are lined by cement made up of **battons** identical to those which calcify the **endolithic fungi**. Miami Limestone. (Kahle, '77)

Alveolar-septal structures

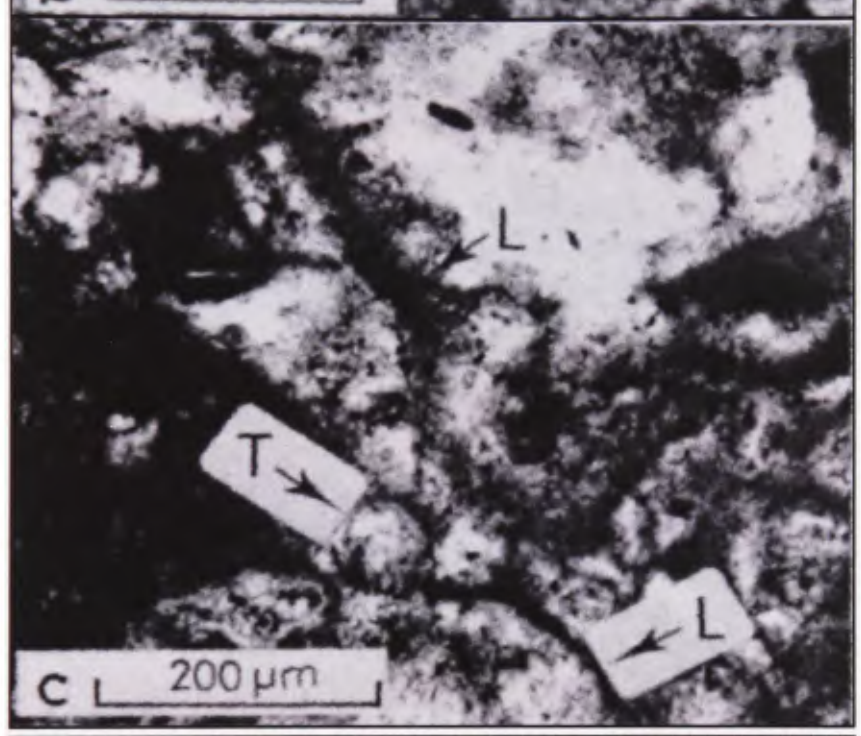
An alveolar texture is characterised by irregular, bifurcating, arcuate micritic septae. However the term 'alveolar' is already used in soil science for a type of fabric resembling irregular fenestrae (birdseyes). It has been suggested the 'alveolar texture' be replaced with 'alveolar-septal structure' to avoid confusion. Whatever term is used, it is a form of rhizocretion (root calcification). However several problems exist over its origin.

1) What creates the septae? Perhaps they represent the collapsed parts of the root coating or are calcified collapsed root-hairs?
2) The root origin is obvious when the structure occurs in a root-like tubule but it also occurs as an irregular network in larger irregular pores. One fine variant of this latter type represents calcified fungal hyphae.

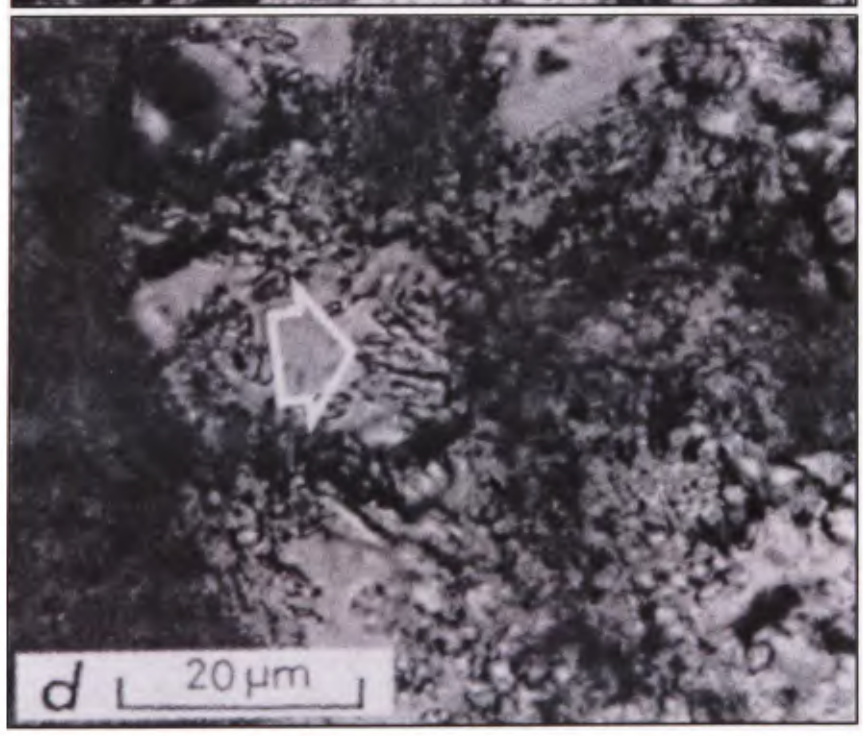
Needle-fibre calcite is common in the septae which suggests that calcification was in part fungally induced. It has recently been suggested that the structure represents collapsed, calcified fungal root sheaths (endomyccorhizae fungi). Such sheaths are very common and are a symbiotic root-fungi association.



Alveolar texture consisting of ramifying **micritic walls.** White areas are **root moulds.** Black **peloids** (arrows), composed of **cryptocrystalline calcite,** are interpreted as **calcified faecal pellets.** Thin section, PPL. (Klappa, `80)



Detail of (b) above showing transverse sections (T) and longitudinal sections (L) through **micritic cylinders.** Thin section, PPL. (Klappa, `80)



Detail of **micritic wall** shown in (c) above. Wall is composed of **micron-sized calcite needles** (*cf.* tangential needle fibres; James, 1972). Arrow points to **columnar calcite crystals** which have their long axes perpendicular to needle calcite walls. Thin section, polarizers at 45^0. (Klappa, `80)

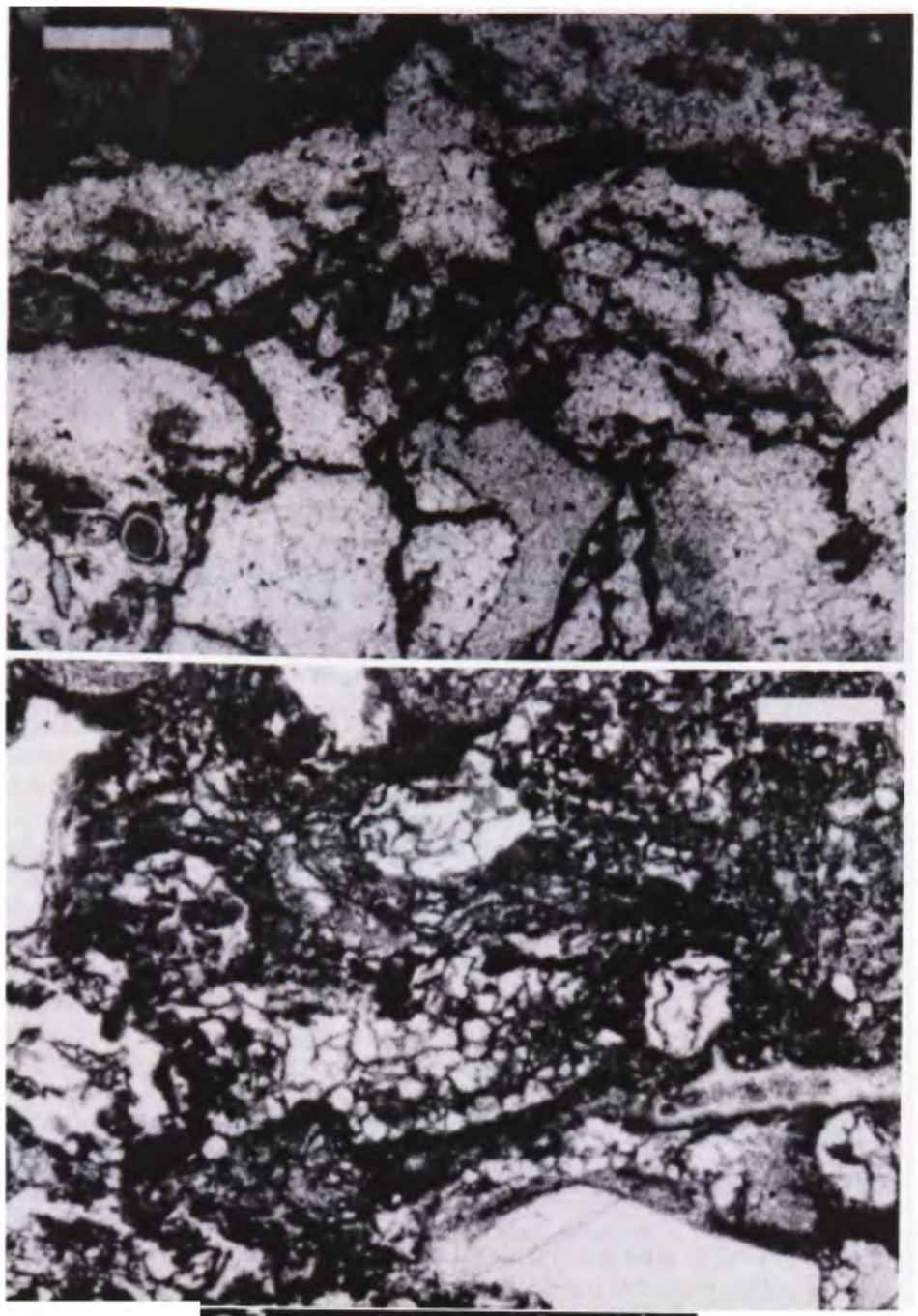
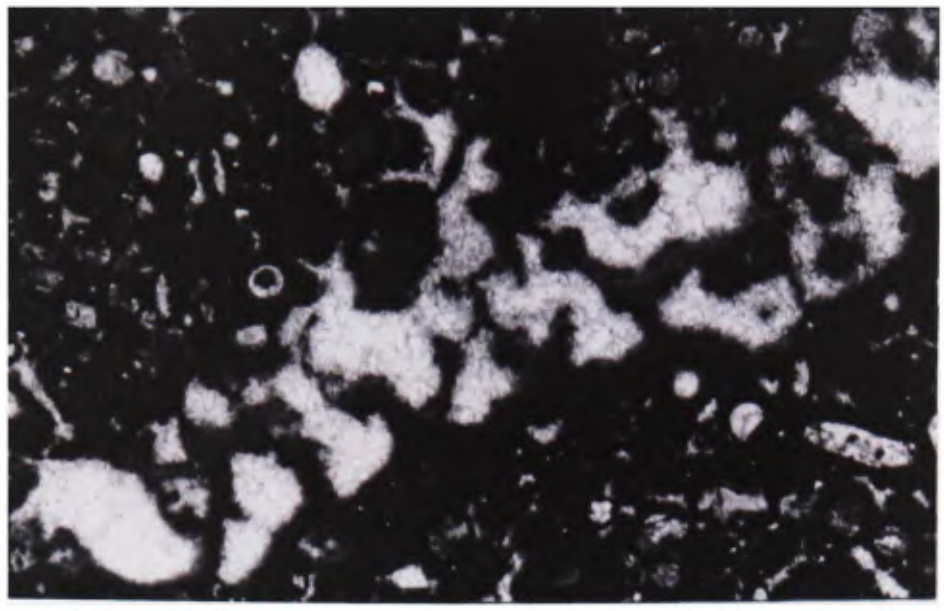


Photo showing irregular **spar-filled voids** separated by a network of **micrite** walls. Interpreted as **alveolar texture** formed by the deposition of fine-grained carbonate around decaying **rootlets**. Scale bar represents 0.5 mm. (Adams, `80)

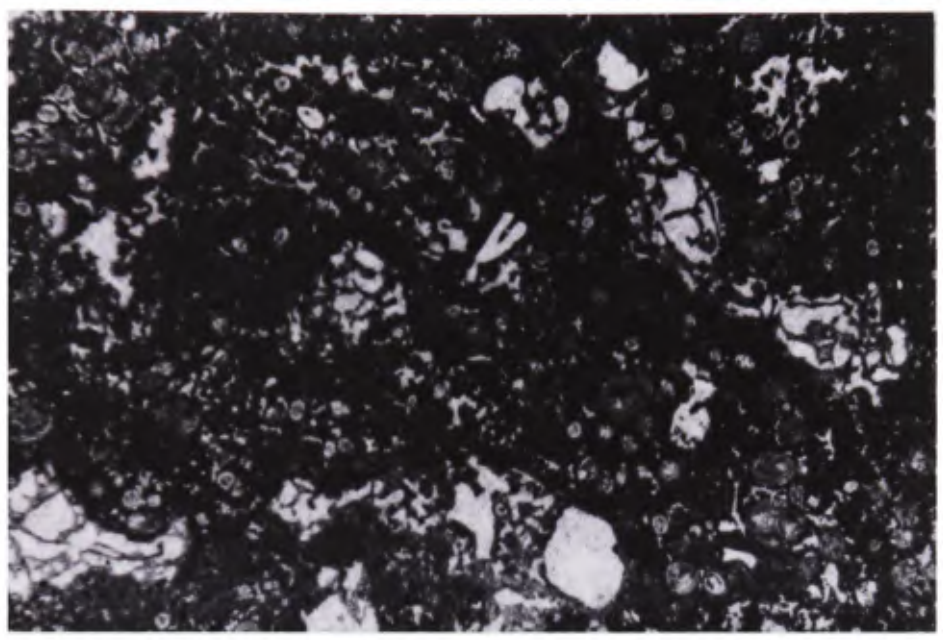
Photo showing well-developed **alveolar texture** from immediately below laminar unit. Scale bar represents 0.5 mm. (Adams, `80)



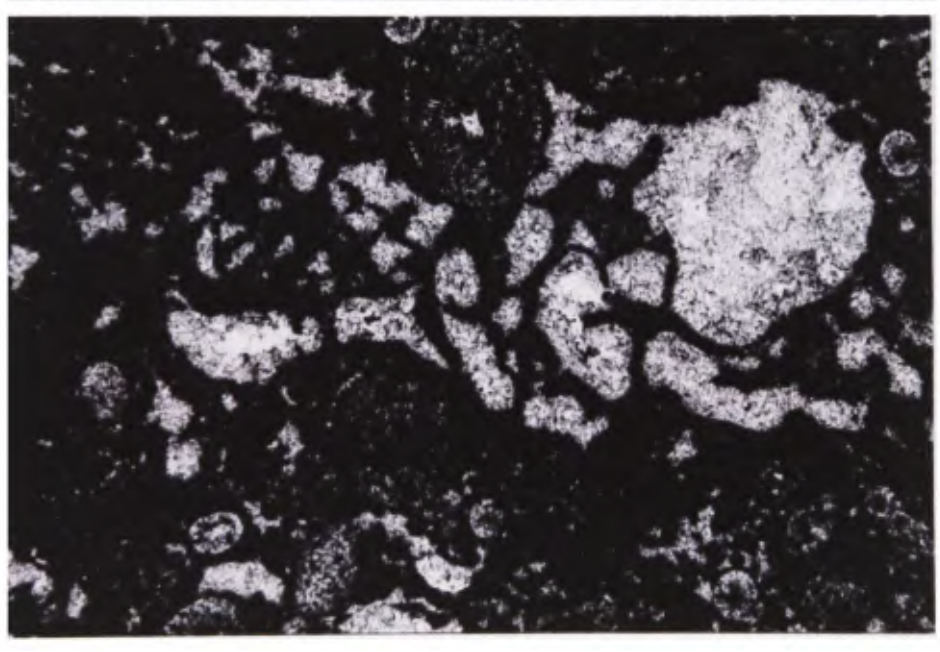
Photo of an **alveolar-septal structure** from the Heatherslade Geosol at Three Cliffs Bay. Scale bar represents 0.75 mm. (Wright, `86)



Diagonal, bifurcating micrite **alveolar-septal structures.** (Wright)



Alveolar-spetal structure in a diagenetic packstone. (Wright)



Close-up of an **alveolar-spetal structure** which is composed of **needle-fibre calcite.** (Wright)

Bioclasts

Ostracods

Ostracods have two valves, usually less than 1 mm in diameter, that may be smooth or ornamented. The valves are joined along a hinge and overlap slightly, so that in section the shell is asymmetric. Some smooth-shelled forms have calcified projections on the shell that point inward. Although quite variable in microstructure, the shells usually have fine prismatic structure.



A group of complete **ostracods** in cross-section. The two valves can be seen, and in a number of cases, the characteristic overlap of one valve by another is also seen (Adams and MacKenzie, '98).

A carbonate mudstone in which the only visible bioclasts are disarticulated and sometimes fragmented **ostracods**, some of which have been fractured during compaction (Adams and MacKenzie, '98).

Molluscs

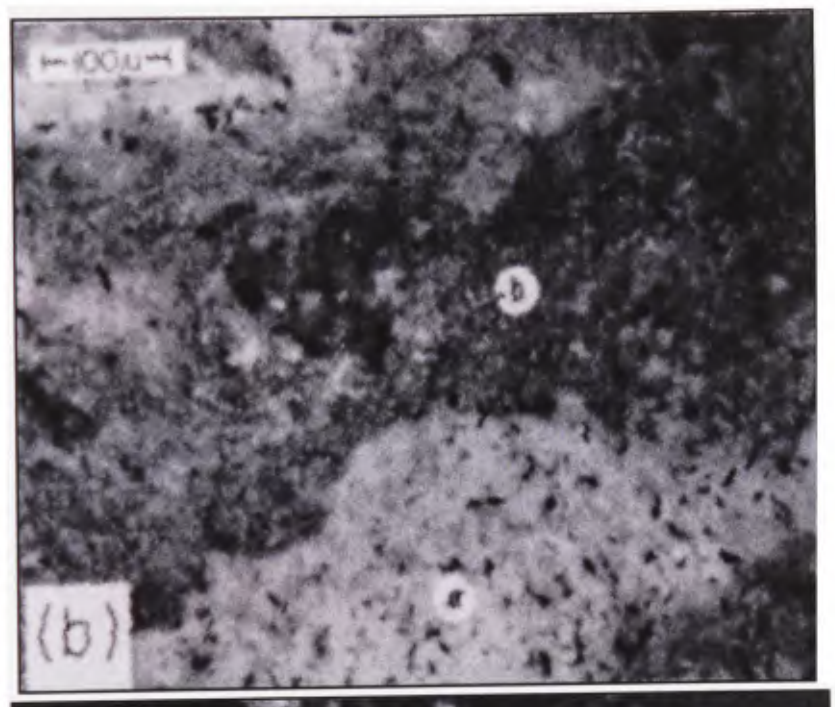
Gastropods are the most significant molluscs in terrestrial sequences. Molluscs can be recognized by their shell shape and multilayered wall structures. Broken pieces of fine mollusk debris may not be recognized as such because the fragments are commonly leached and infilled or replaced by calcite spar. Shell growth is environmentally controlled; thin shells typify quiet-water or cold environments whereas thick shells occur in higher-energy environments. The shells are primarily aragonite or may be a mixture of aragonite and calcite; thus,

their manner of preservation is variable. In shells with mixed mineralogies, the outer layers are commonly calcitic and the inner layers are commonly aragonitic.

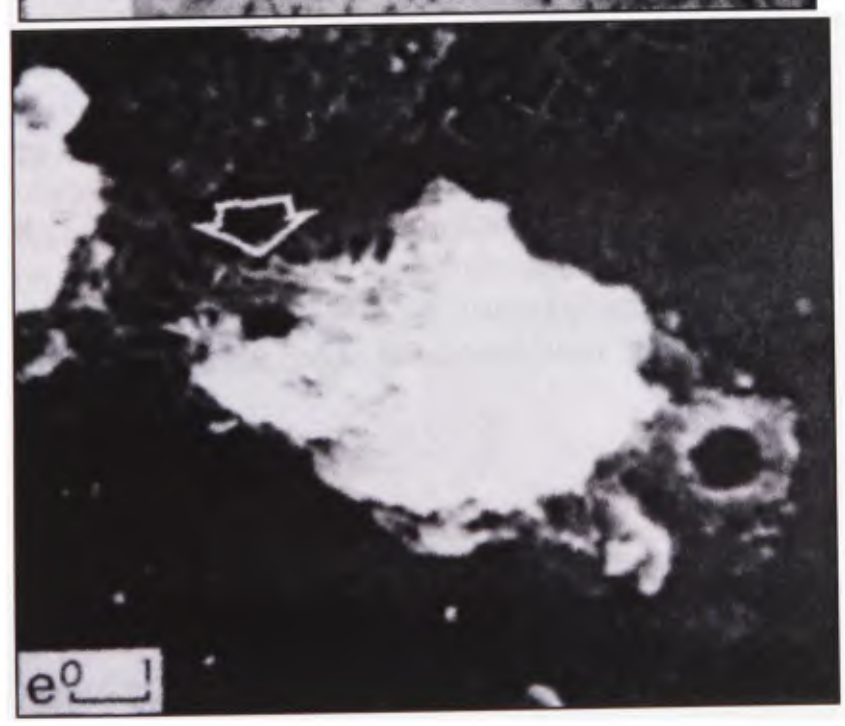
Cyanobacteria

Stromatolites are layered structures formed by cyanobacteria and carbonate sediment. Cyanobacteria typically form mats composed of filaments and carbonate. The carbonate may be precipitated through photosynthesis or trapped as grains washed onto the mat. The cyanobacteria tend to form colonies. They form crinkly banding in soil concretions or calcrete which exhibits horizontal banding, spherical growths and heads. Occasionally algae infest the surface of grains and form an envelope of micrite. This envelope represents an alteration or addition to the perimeter of the grain. The alteration replaces the organised grain fabric with disorganized micrite in two steps: (1) the boring activity of the algae with dissolution of the grain followed by (2) reprecipitation or trapping of calcium carbonate in the void.

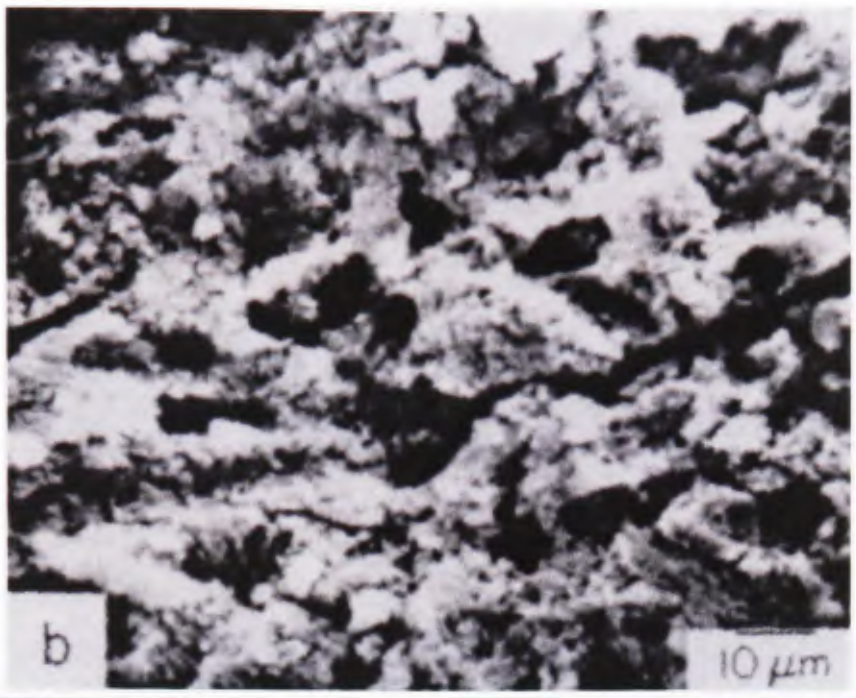
Borings



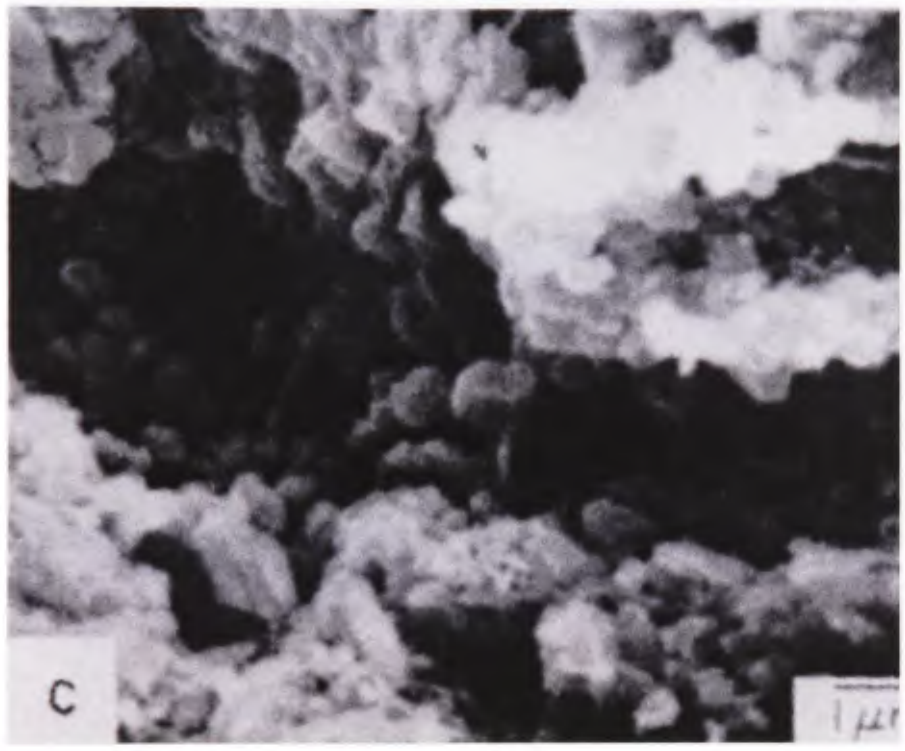
Micrite from within a funnel-shaped body riddled with irregular **borings** (b) or build up of **tubules**. Some **pore space** occurs (ϕ). (Knox, '77)



Surface of '**bored**' wall showing 1.0 μm diameter **cylinderical pores** surrounded by **fibrillar mat** (arrow). The latter is interpreted as disaggregated plant cell wall material. (Klappa, '78)

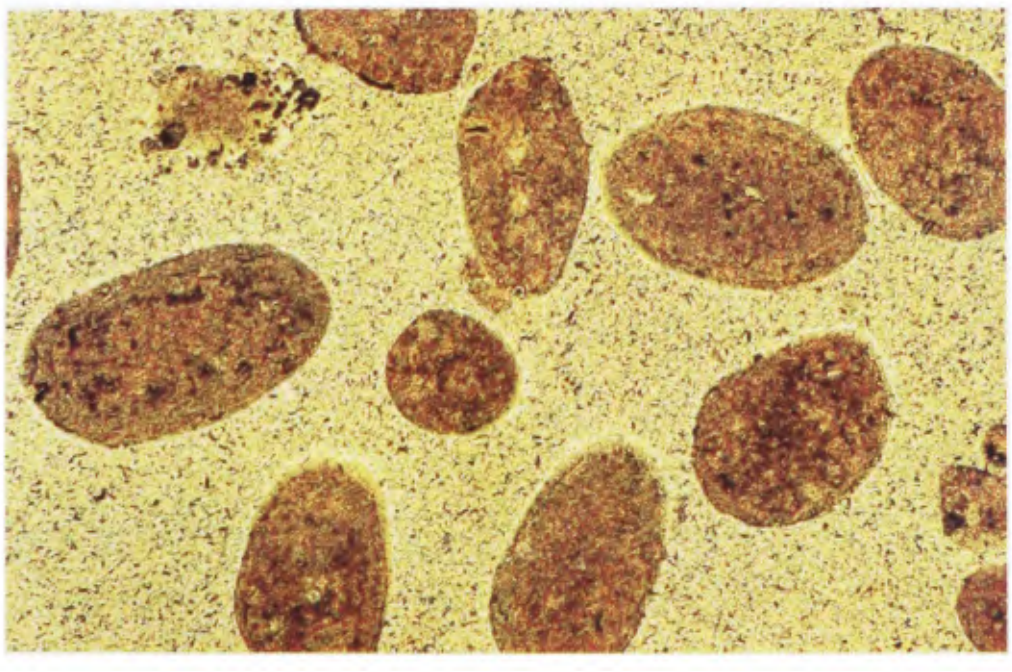


SEM photo. Fungal borings in calcareous crusts. (Kahle, `77)

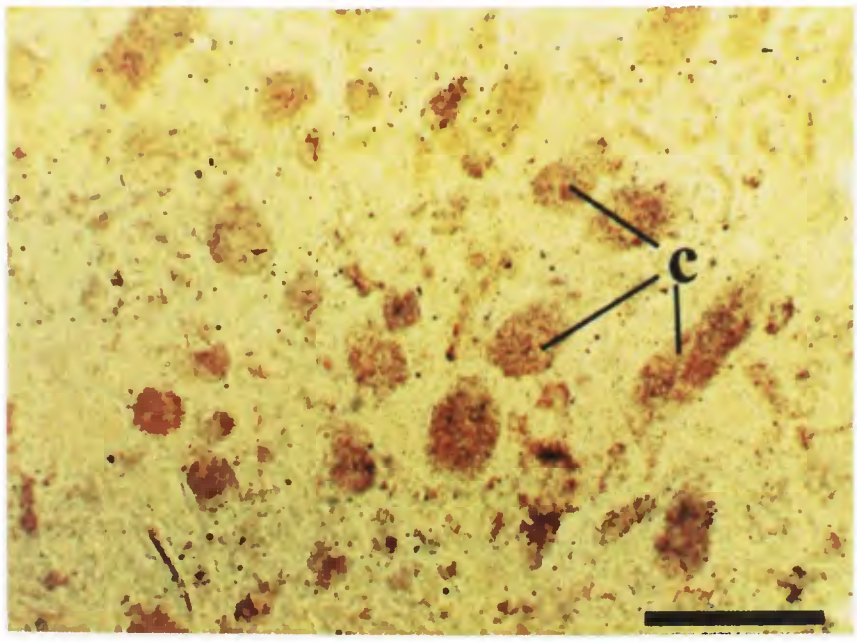


SEM photo. **Fungal borings** partially lined with crystals of **calcite micrite** in a crystal of **sparry calcite** cement. Miami Limestone. (Kahle, `77)

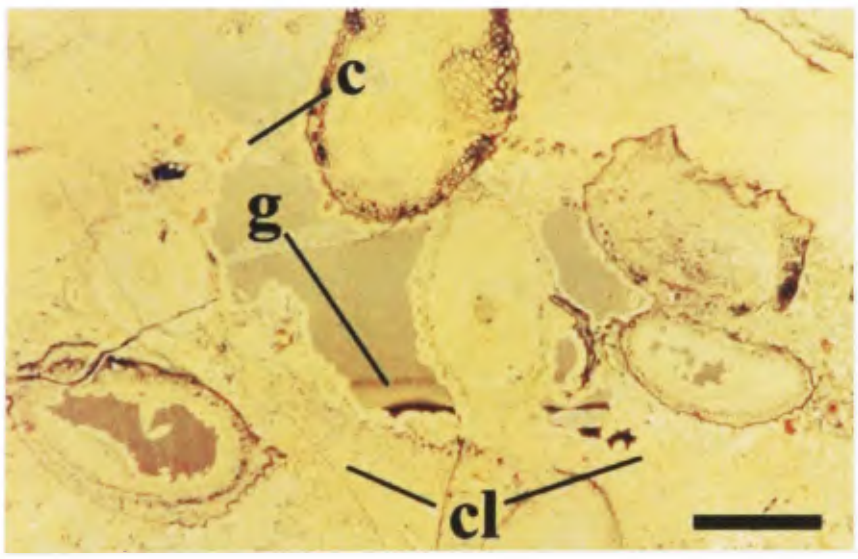
Coprolites



Mud pellets, probably faecal in origin, show the typical ellipsoidal shape and, in addition to the clay-sized carbonate mud which makes up the bulk of them, they include slightly larger particles and are stained brown by organic matter (Adams and MacKenzie, `98).



The amorphous, organic-rich, ellipsoidal, elongate and spherical bodies are fossilised faecal pellets, termed **coprolites**. It is most likely that the bed this sample came from was deposited in an aquatic setting, perhaps a pond or ephemeral body of water. These features, at least at this scale, are rarely preserved in terrestrial settings. Secondly, it is likely that the silicification of this deposit was very early because the coprolites are not squashed and compacted together, in fact there is a very open 'framework' between the pellets. These coprolites were probably produced by small crustaceans (scale bar = 500μm).

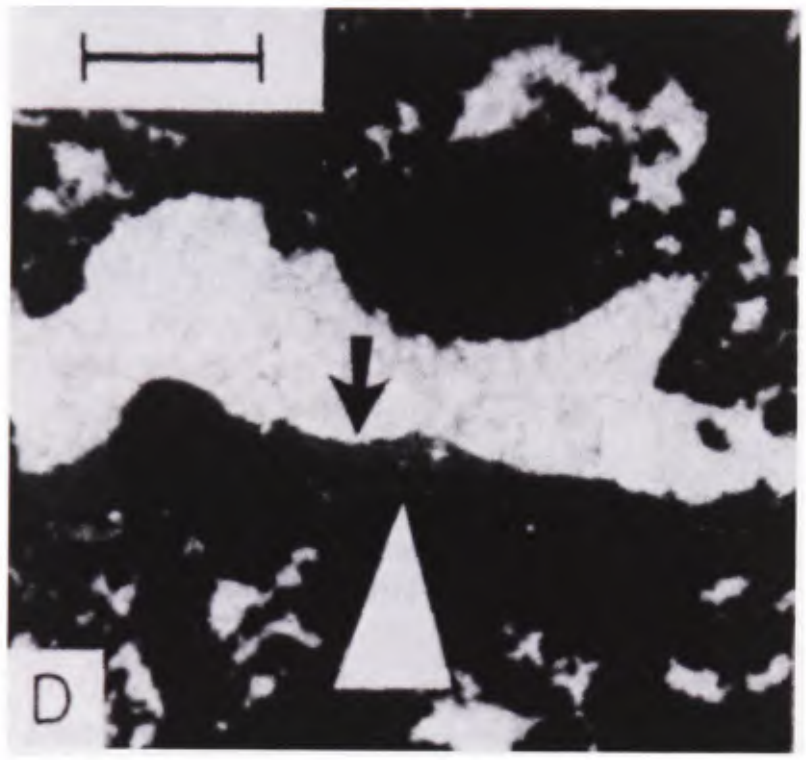


Coprolites often occur together within a fine meshwork of filaments (fungal and/or cyanobacterial), unicells and aggregated fine amorphous organic material forming an open, loose, plexus-like matrix that often binds and coats floral and faunal remains, giving the chert or carbonate a 'clotted' appearance in thin section (cl). Often associated with this texture are fossils of aquatic biota such as charophyte algae and branchiopod crustaceans, though remains of terrestrial plants and arthropods may also be common.

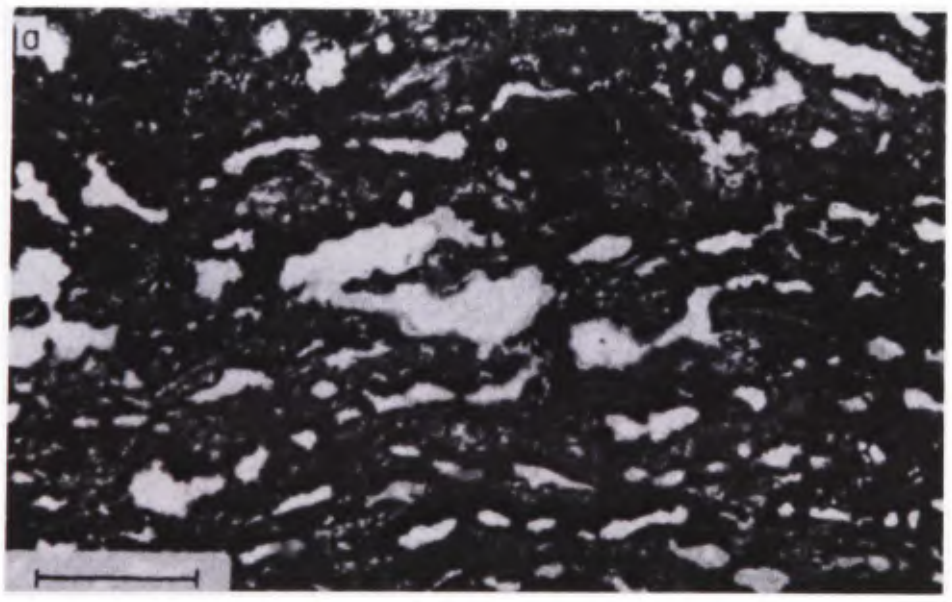
This distinctive **clotted chert texture** is directly comparable to **mulm**, the amorphous organic material that is often found in modern freshwater ponds (Anderson & Trewin 2003; Trewin *et al.* 2003). The presence of this texture indicates that silicification or calcification occurred in an aquatic setting with no desiccation prior to preservation, since desiccation would have led to the collapse and degradation of these fine, open organic mesh-works.

Fenestrae

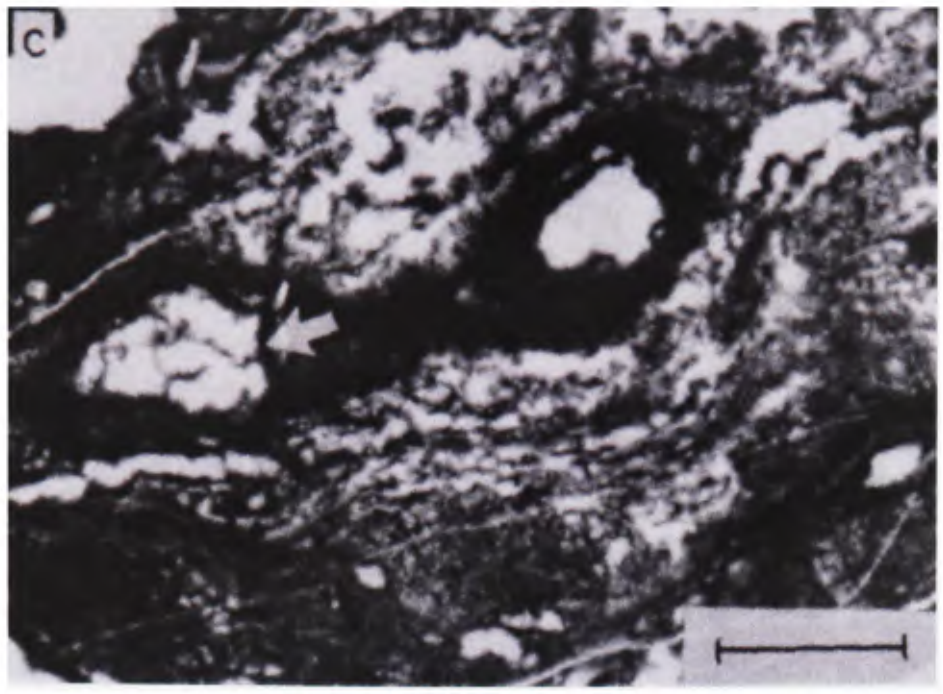
Many laminar calcretes are highly fenestral and have crudely biogenic, microstructures. These often cover dense calcrete horizons and probably represent calcified root-mats (horizontal root systems). As the underlying horizons become plugged the roots spread out horizontally, tapping perched water. Progressive calcification leads to the formation of a crudely laminar layer with numerous root-tubule holes (fenestrae). Alveolar-septal structures also occur. This is another mechanism of forming laminar calcretes which usually represented dense precipitates on plugged (petrocalcic) horizons or apparently can form by the calcification of lichens and other microbial crusts.



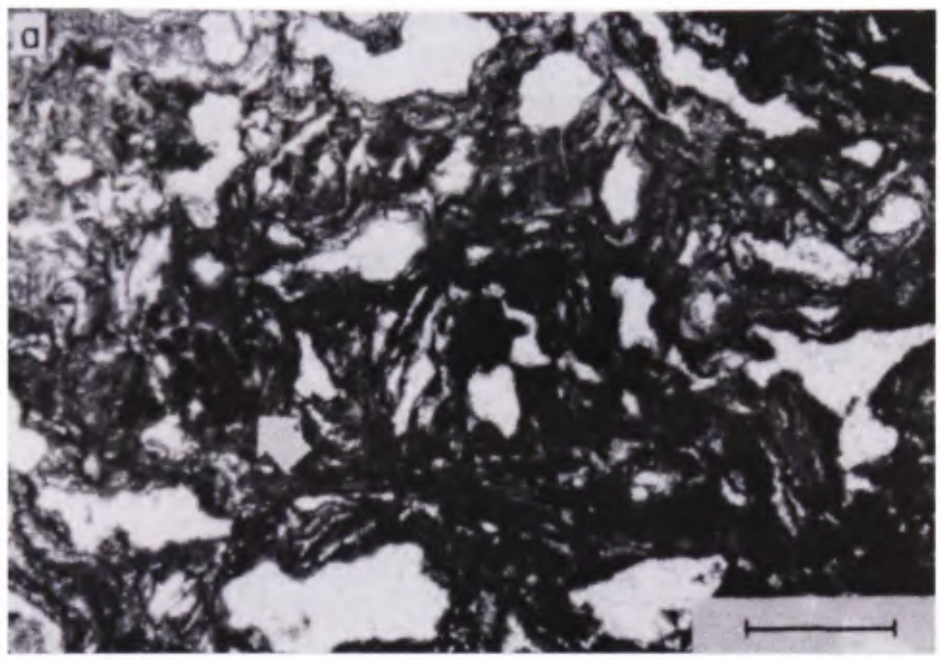
Irregular fenestra with a clay-lined bottom (white arrow) overlain by **geopetal crystal** silt (black arrow). Scale bar is 0.5 mm long. (Wright, '83)



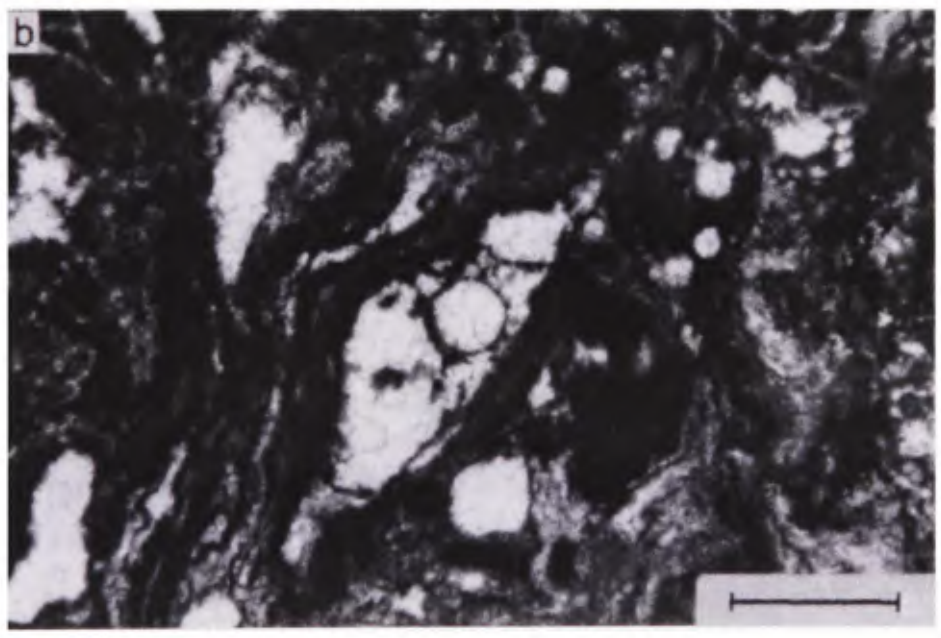
Thin section of laminar calcrete from Miskin. Highly **fenestral fabric**. The long axes of the cylindrical **fenestrae** are subparallel to the base of the horizon. Note the larger irregular **calcite-filled vugs**. Scale bar represents 2.5 mm. (Wright et al., '88)



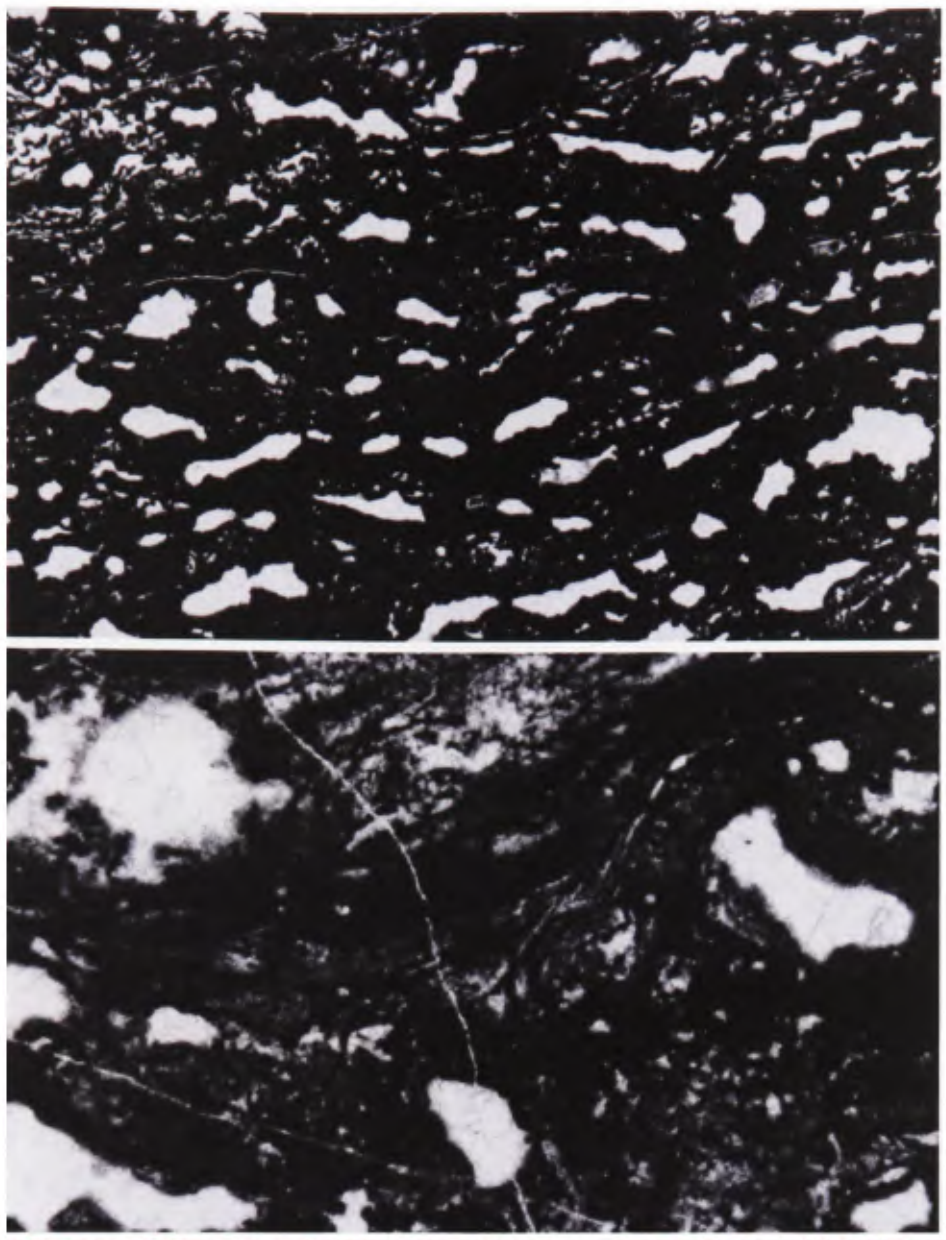
Thin section of laminar calcrete from Miskin. Note dark **micritic** coatings around the **spar-filled cylindrical fenestrae,** passing into the crudely micro-laminar zone. **Alveolar septal fabric** (arrowed) occurs within a **micrite-rimmed tubule,** and the diffuse fabric representing **alveolar-septal structure** above the two **micrite-coated** cylinders. Scale bar represents 0.5 mm. (Wright et al., `88)



Thin section of laminar calcrete from Senora de Brezales Formation. Irregular and cylindrical **fenestrae** surrounded by **micro-laminar micrite**. Note cluster of **pellets** (arrowed). Scale bar represents 1 mm. (Wright et al., `88)

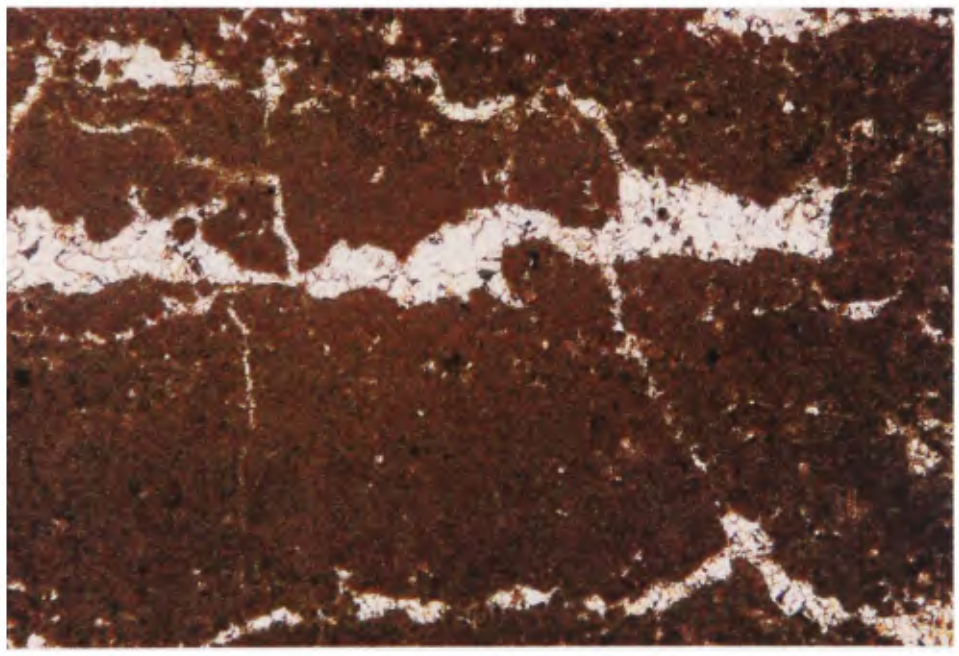


Thin section of laminar calcrete from Senora de Brezales Formation. **Irregular spar-filled fenestrae** and **micro-laminar micrite.** Note **micritic cylinder** within one of the pores. This probably represents the light calcification of the outer margin of a rootlet or root hair. Scale bar represents 0.5 mm. (Wright et al., `88)



Laminar-fenestral calcrete crust. (Wright)

Close-up showing the **lamellar, biogenic fabric** interpreted as being formed by calcified root mats. (Wright)



Laminoid fenestrae – a cement filled fenestrae parallel with bedding are associated with subvertical fractures which are probably filled desiccation cracks (Adams and MacKenzie, `98).

Filaments



Micritic filaments (arrowed) extending from coatings and connecting grains. Identical fabrics have been described from Quaternary calcrete formed by **micro-organisms.** Heatherslade Geosol at Miskin. Scale bar represents 0.5 mm. (Wright, `86)

Micritic filaments (arrowed), as above, extending from coatings and connecting grains. Heatherslade Geosol at Miskin. Scale bar represents 0.5 mm. (Wright, `86)

Micritic filaments (arrowed), as above, extending from coatings and connecting grains. Heatherslade Geosol at Miskin. Scale bar represents 0.5 mm. (Wright, `86)

Laminae

Laminar calcretes are of two basic types:

1) Biogenic – e.g. subaerial stromatolites and licen stromatolites and root rock.
2) Abiogenic

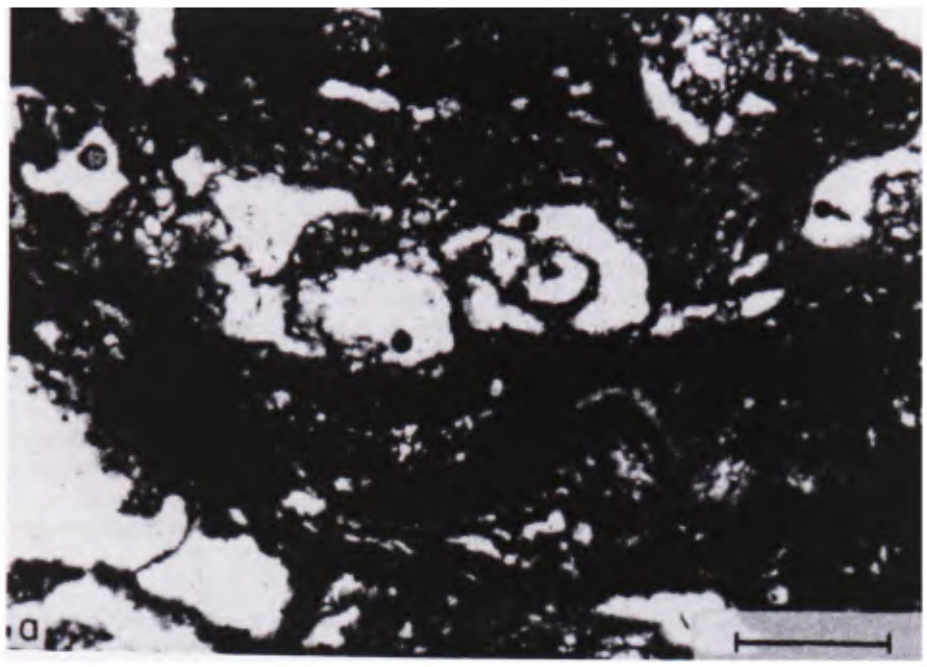
The latter commonly occur in mature calcrete profiles due to 'ponding' of water on the upper surface of the plugged horizon (petrocalcic horizon). They also form on lithified bedrock and typically have a dense micritic structure.



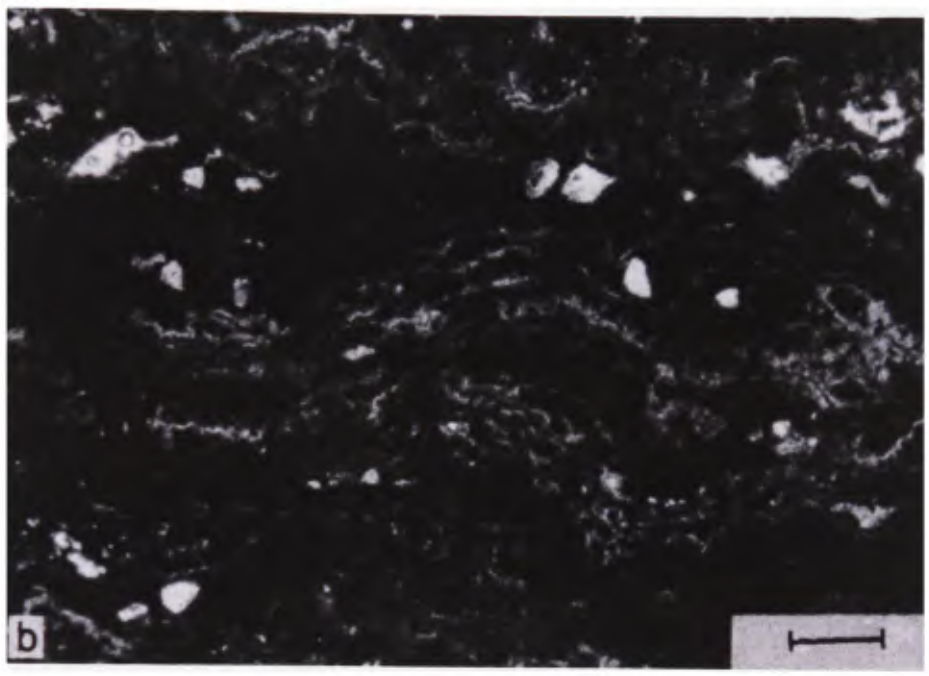
Cherts and carbonates displaying irregular, sub-parallel, wavy to crenulated laminations on a sub-millimetre to centimetre scale, consisting of variable thicknesses of stacked chert laminae with fine sandstone partings. Plants, if at all present, are confined to specific bands. Locally fine organic detritus including spores and fossilised cyanobacteria may be preserved within the laminae.

This particular texture most probably originated by deposition from successive inundations by silica-rich waters, with periods of silica precipitation occasionally interrupted by the influx of detrital material.

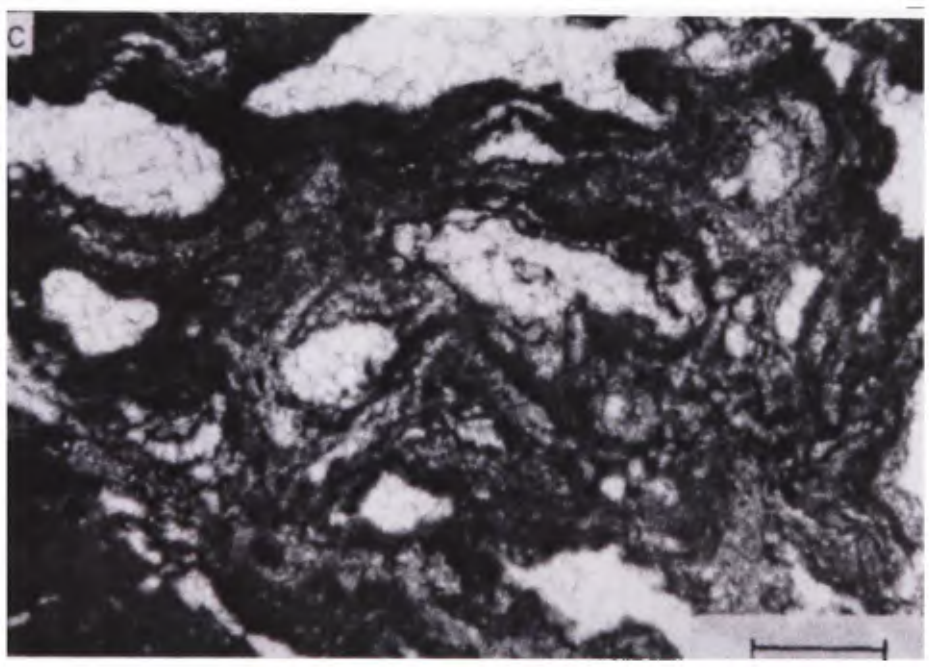
Right: Tabular bed of laminated chert showing wavy and crenulated laminae of chert (**c**) with fine sandstone partings (**s**). Notice also the syn-sedimentary fracturing and brecciation in this bed (**f**).



Thin section of the town Gardens Member laminar calcrete. **Porous, micro-laminar microfabric** showing fine **tubular** and large irregular **pores** (some with a crude **septal structure** resembling **alveolar-septal structure**) set in a **micro-laminar matrix.** Scale bar represents 0.5 mm. (Wright et al., `88)



Thin section of the town Gardens Member laminar calcrete. Dense **micritic laminae** forming layers several millimeters thick. Scale bar represents 0.5 mm. (Wright et al., `88)



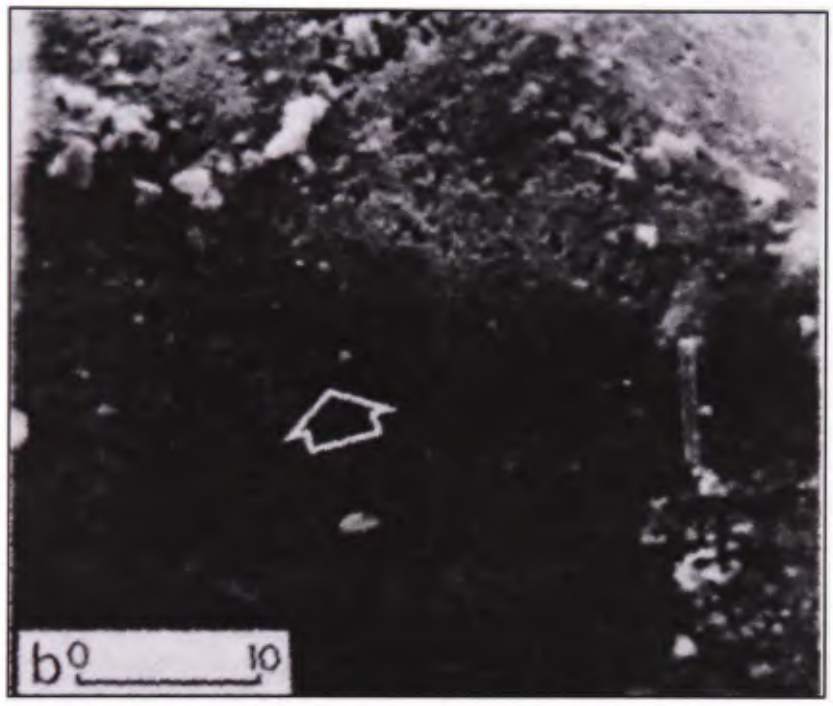
Thin section of laminar calcrete from Senora de Brezales Formation. **Micro-laminar micrite fabric.** Scale bar represents 0.5 mm. (Wright et al., `88)

Microcodium

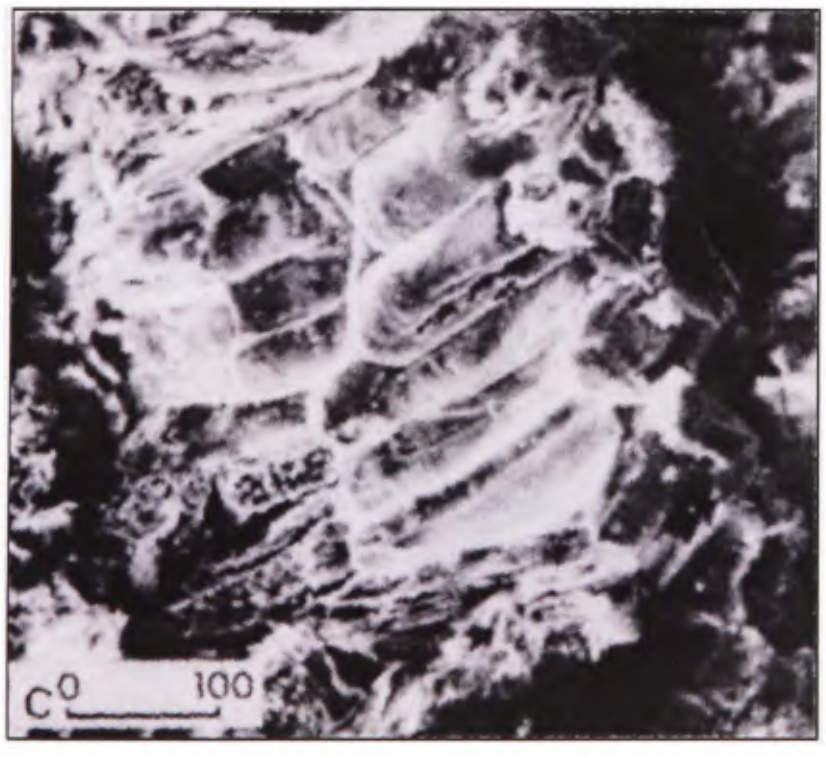


SEM photomicrographs of Recent ***Microcodium*** aggregates and grains. Loose sediment mounts, Cieza, S.E. Spain.

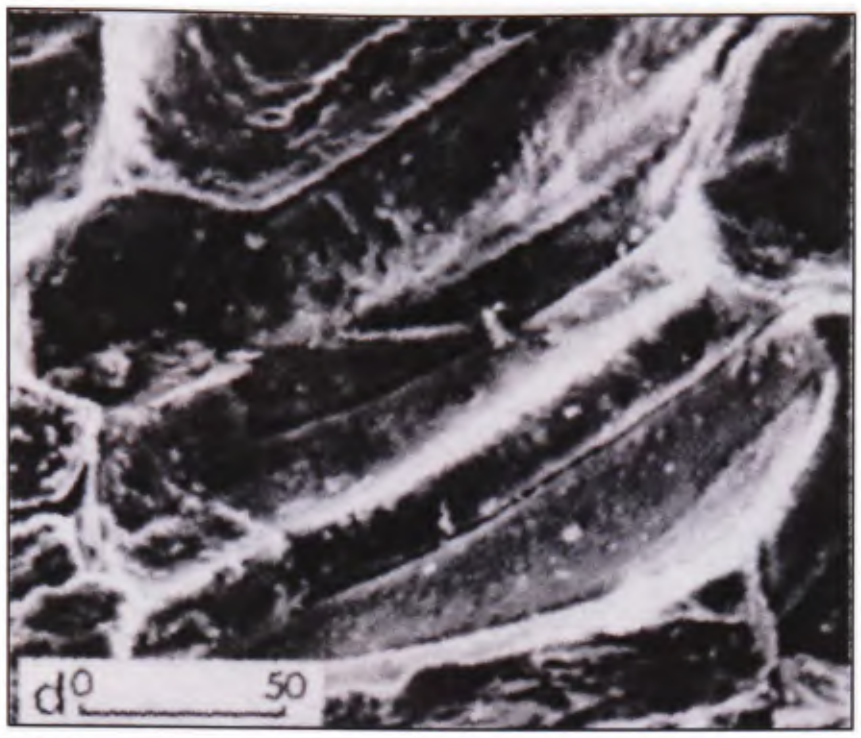
Ellipsoidal ***Microcodium*** aggregate with grains showing interference growth boundaries. (Klappa, `78)



Enlargement of (a), showing surface detail. Note pore pattern and presence of subsurface channels (arrow). (Klappa, `78)



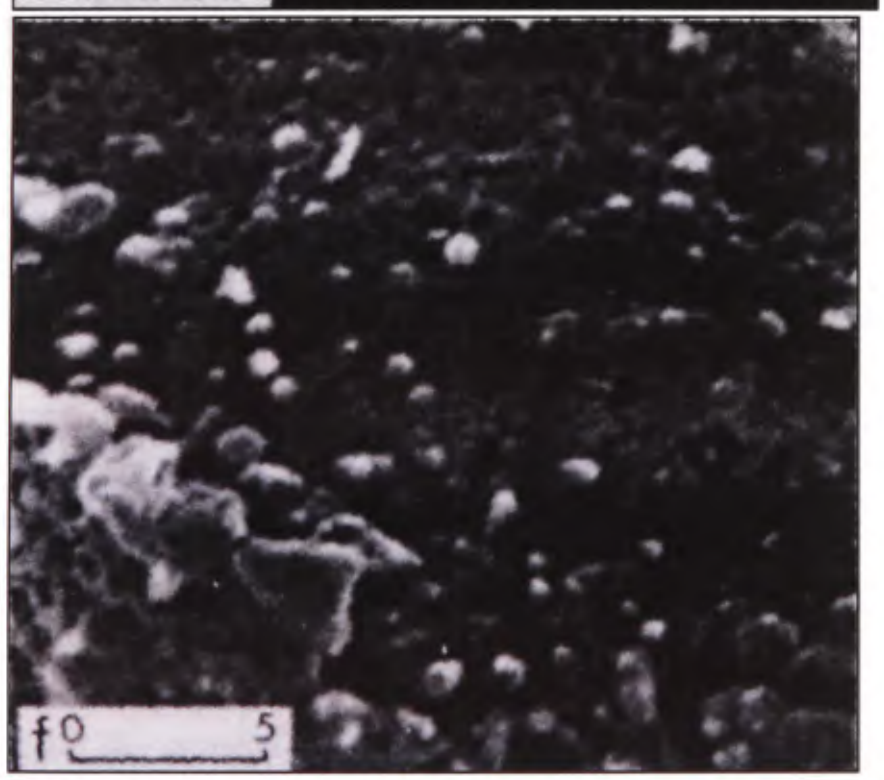
Elongate *Microcodium* aggregate with grains in concentric layers. (Klappa, `78)



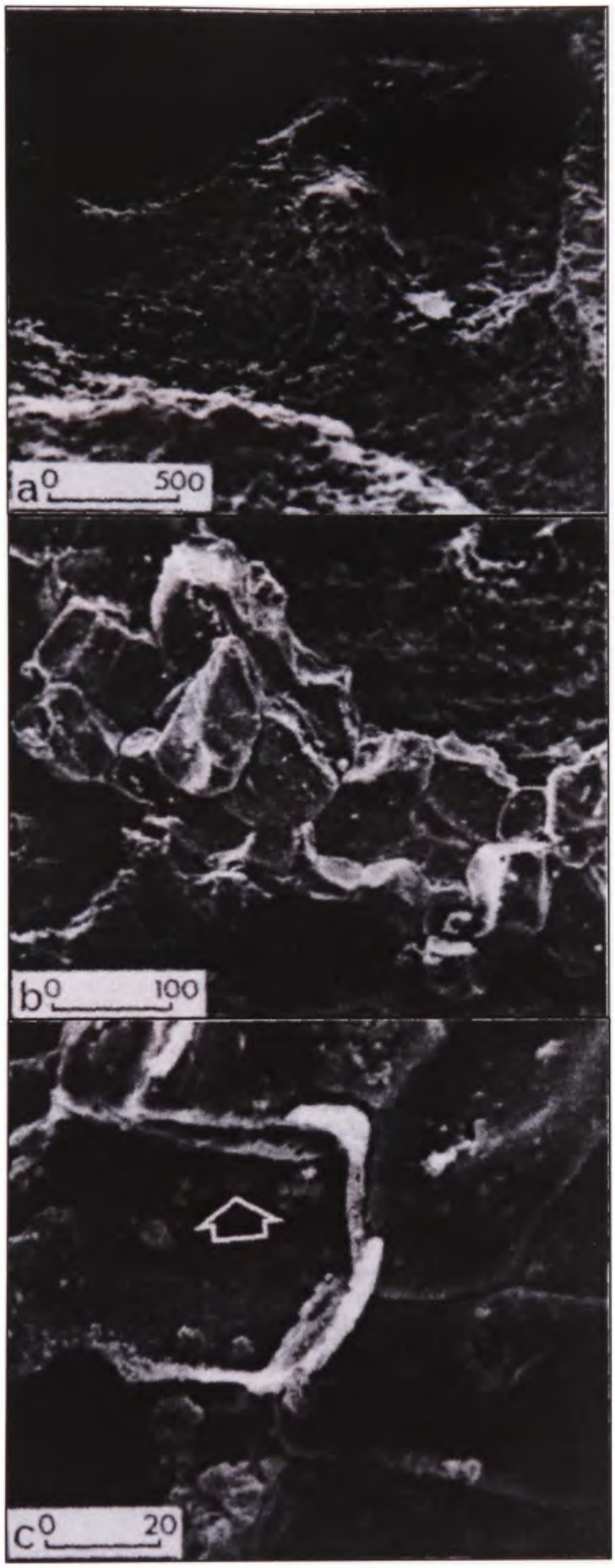
Enlargement of (c), showing grain surface concavities and naturally etched ***Microcodium*** grains. (Klappa, `78)



Single ***Microcodium*** grain with concave faces. Note subsurface **tubular** networks with tube diameters of 1.0 μm or less (arrow). (Klappa, `78)



Detail of (e), showing **protuberances** on surface of naturally etched ***Microcodium*** grain. Scale in μm. (Klappa, `78)



SEM photomicrographs of Recent ***Microcodium*** grains. Untreated surface samples, Cieza, S.E. Spain.

Surface of dolomite **lithoclast** fragment with pitted channels due to the corroding action of ***Microcodium***. (Klappa, `78)

Linear aggregate of ***Microcodium*** grains within surface channel of dolomite **lithoclast**. (Klappa, `78)

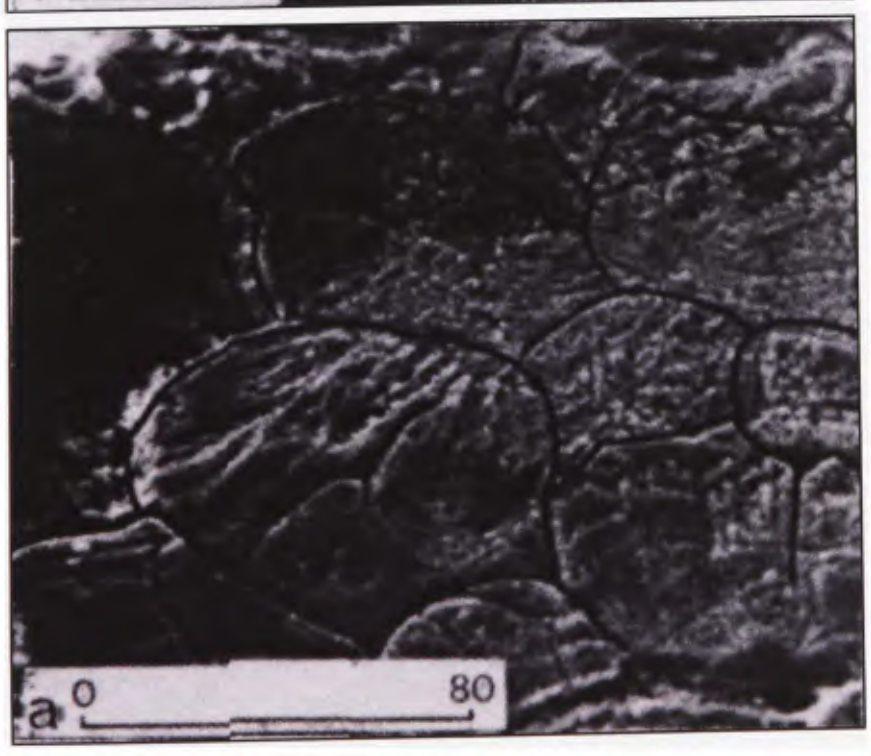
Enlargement of (b), showing **intragranular protuberances** (arrow) within a completely dissolved (natural) ***Microcodium*** grain. (Klappa, `78)



Detail of (c). Lower surface is partially etched wall. Aerial fungal hypha is probably post-cavity formation. **Residual intragranular structures** are arrowed. (Klappa, `78)

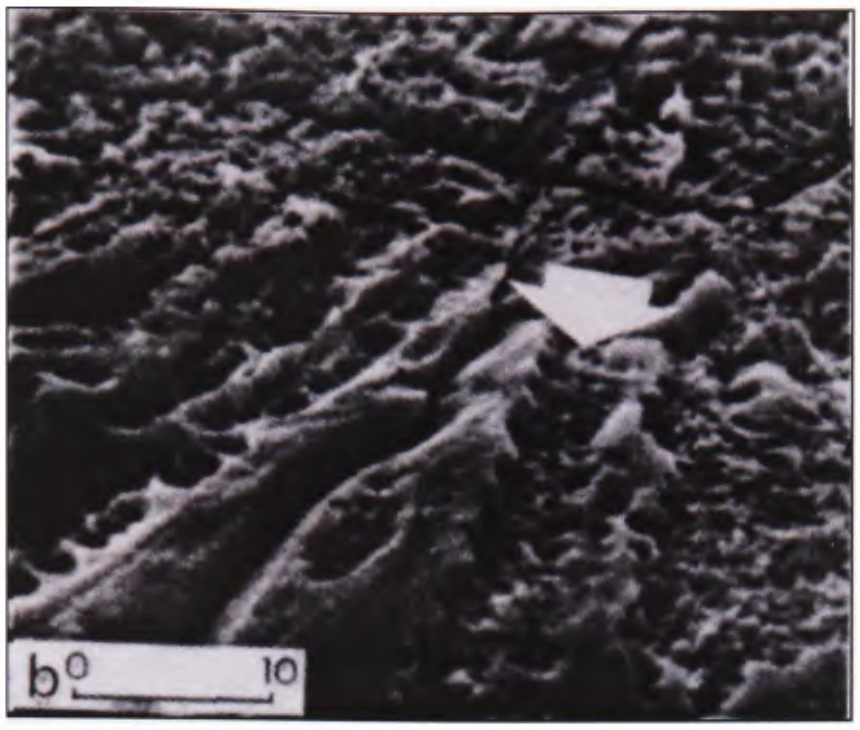


Naturally etched *Microcodium* grain showing **anastomosing subsurface (originally) tubes**, 1.0 μm diameter. Scale in μm. (Klappa, `78)

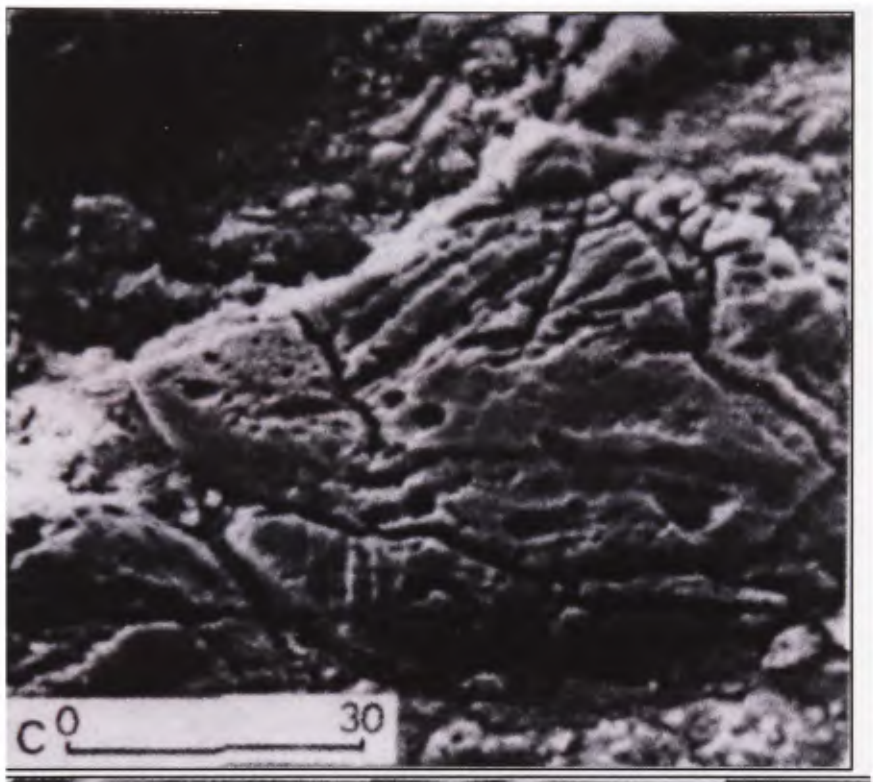


SEM photomicrographs of polished and etched rock samples from a calcified *terra-rossa* soil. Pleistocene, Ibiza.

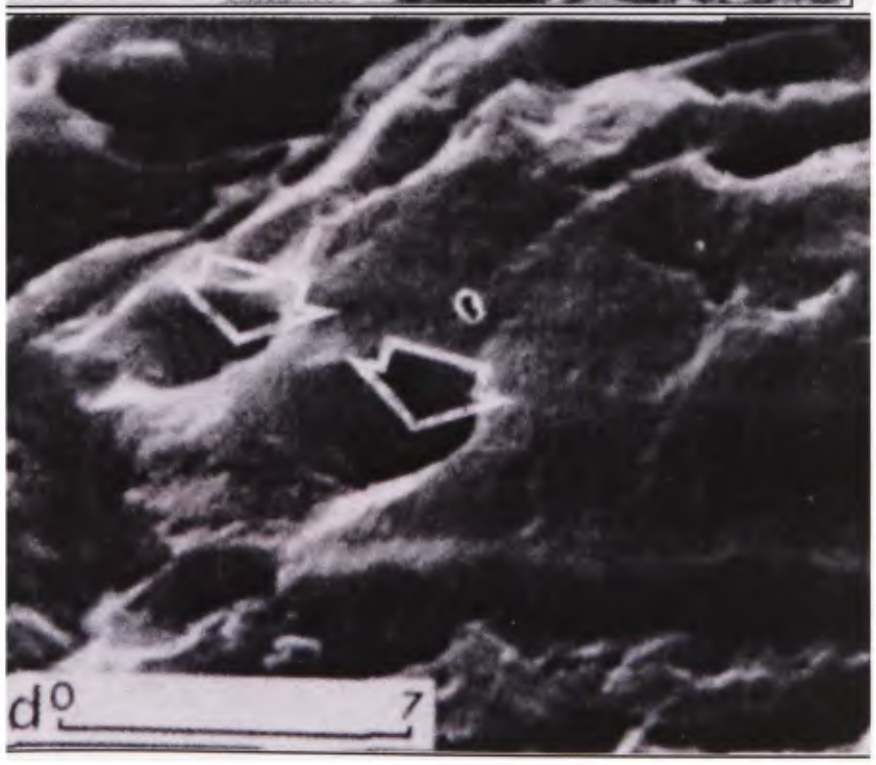
Isodiametric *Microcodium* grains with convex and concave boundaries. Individual grains have been outlined in ink. (Klappa, `78)



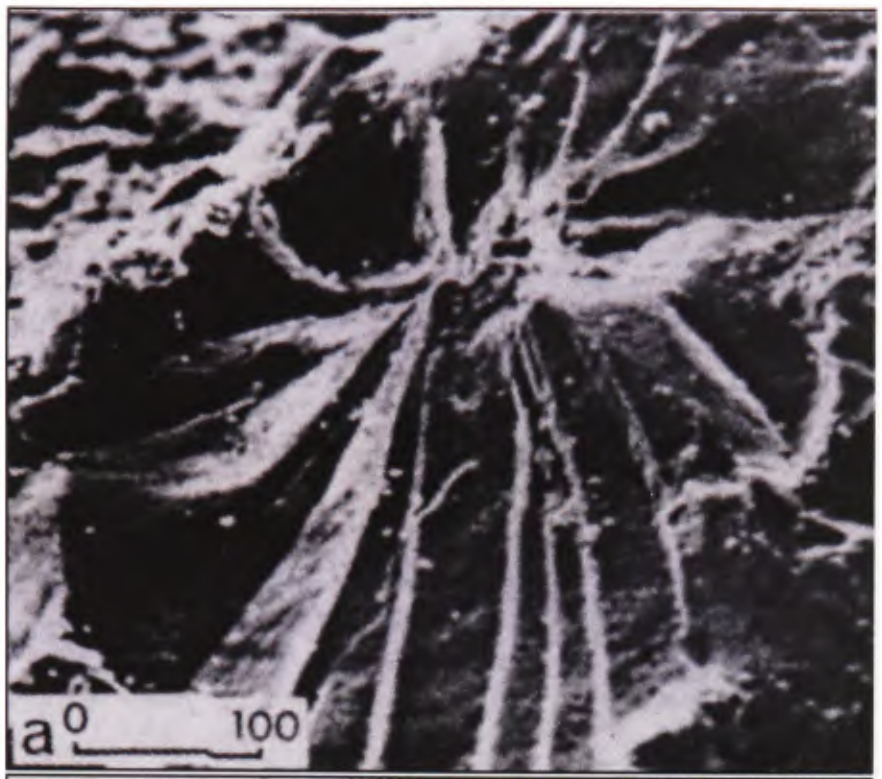
Detail of (a), showing **linear pore pattern** (accentuated by etching in dilute HCL acid) indicated by arrow. (Klappa, `78)



Single ***Microcodium*** grain showing **cracks** and **tubular pores**. (Klappa, `78)

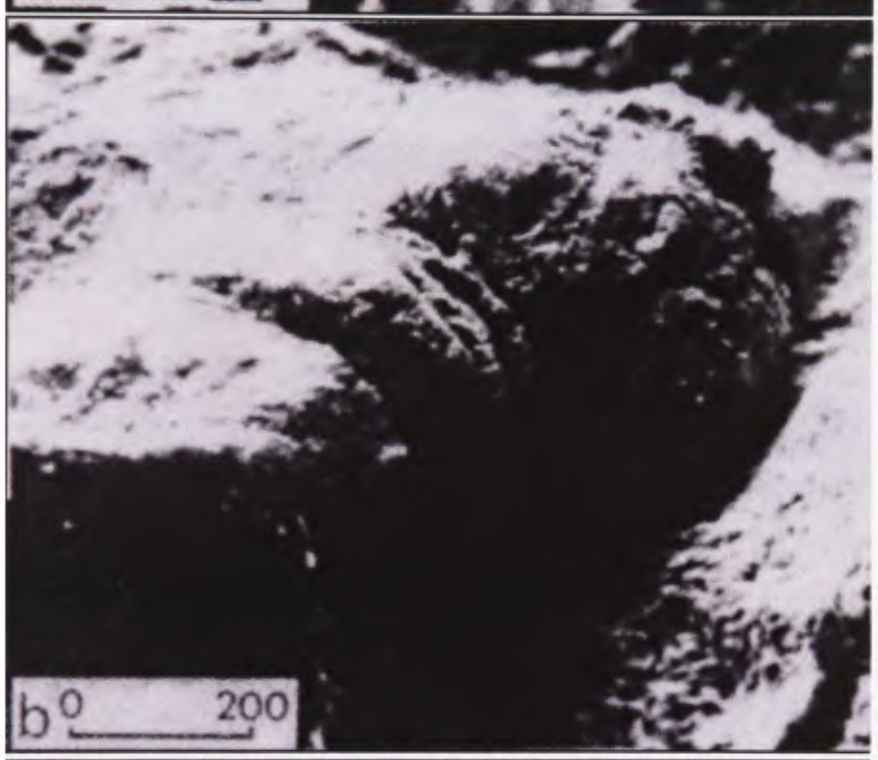


Detail of (c), indicating presence **of filamentous structures** (tips just visible) within **tubular pores**. Scale in µm. (Klappa, `78)

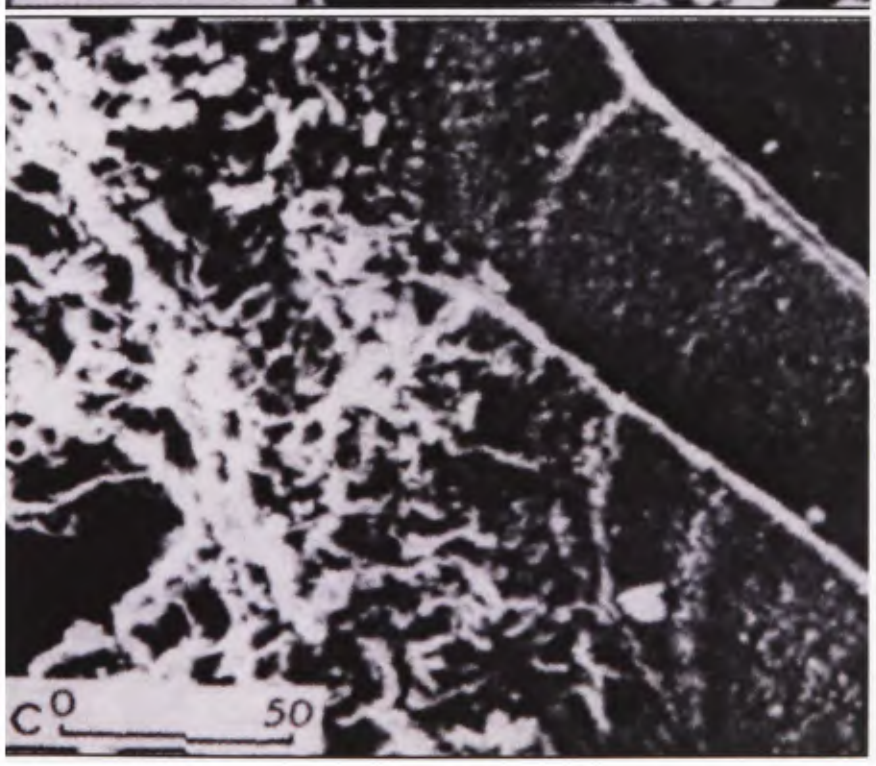


SEM photomicrographs of fractured samples from the Eocene of northeastern Spain and southern France.

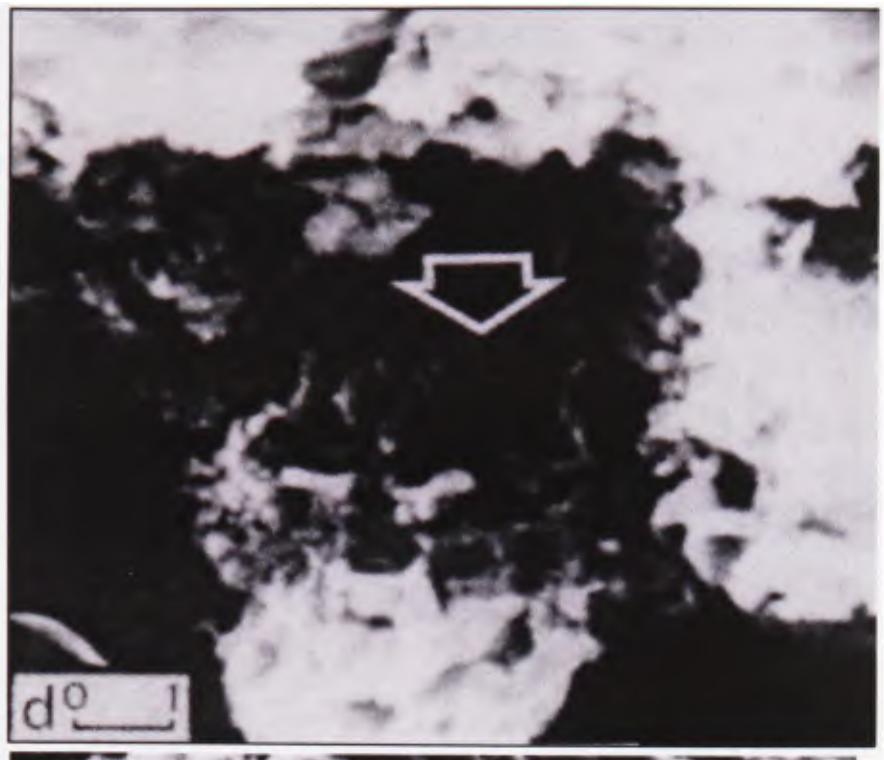
Transverse section of ***Microcodium*** cylinder composed of **radiating petal-like prisms.** (Klappa, '78)



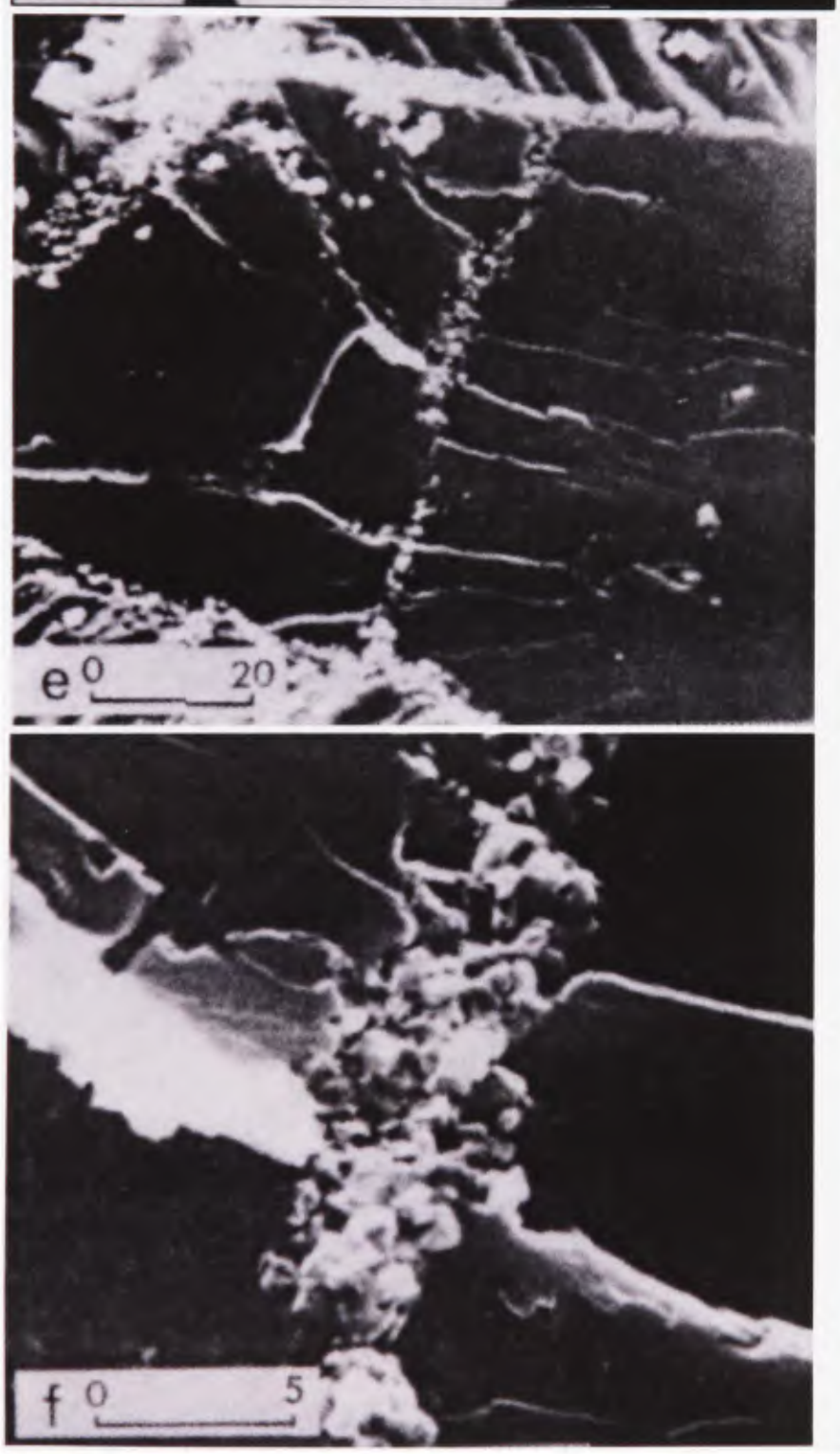
Oblique section of cylinder with **constrictions or disc-like structures.** Cylinder axis lies NE-SW in photomicrograph. (Klappa, '78)



Contact between ***Microcodium*** grains (right) and **calcisiltite matrix** (left). Concentric bands within ***Microcodium*** grains may be trapped insoluble residues at successive growth fronts. (Klappa, '78)

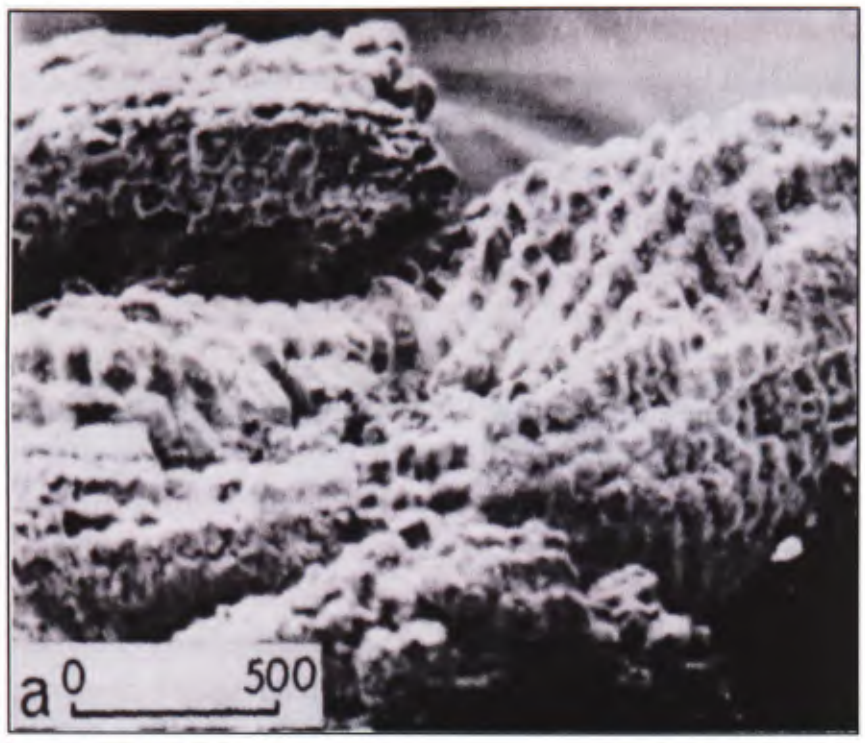


Detail of (c) at junction. Note **micro-honeycombed structure** (arrow) at periphery of ***Microcodium*** grain. (Klappa, `78)



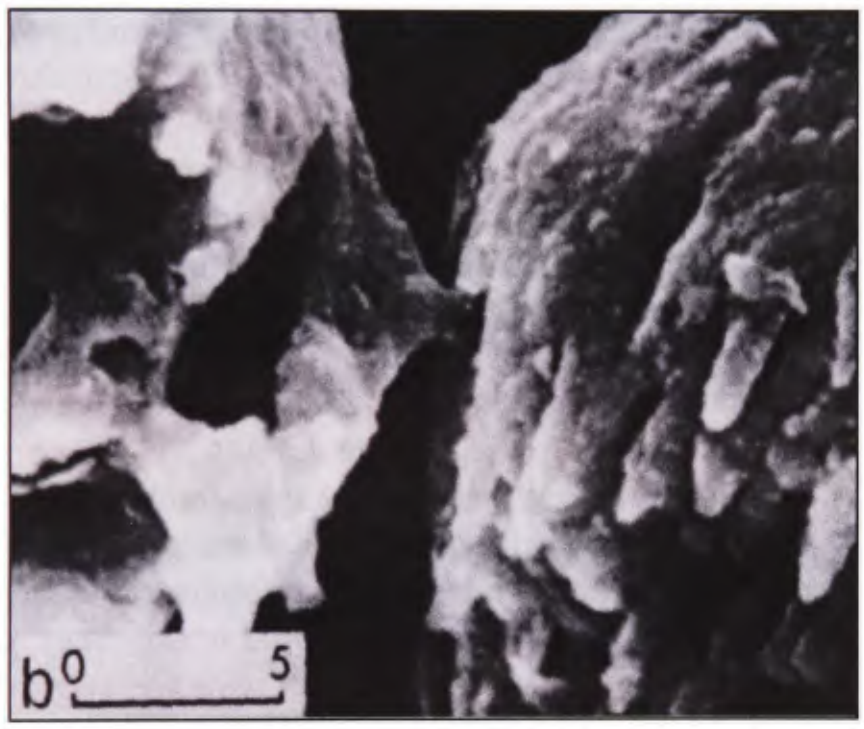
Walls between and within ***Microcodium*** grains consisting of **porous clay-sized aggregates.** (Klappa, `78)

Enlargement of (a). Scale in μm. (Klappa, `78)



SEM photomicrographs of Pleistocene *Microcodium*, Ibiza.

Partially collapsed **rod of *Microcodium***, resembling a 'corn on the cob'. **Isodiametric grains** which constitute the rod similarly show signs of deflation. (Klappa, `78)



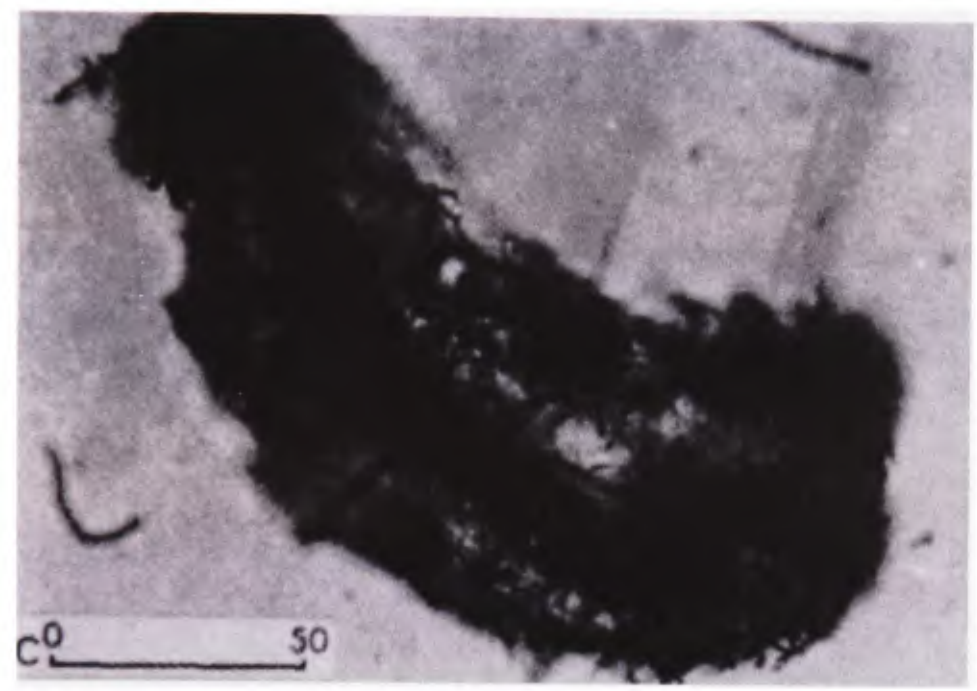
Detail of surface features in (a), revealing presence of **filamentous structures** within, and traversing across, ***Microcodium*** grains. Scale in μm. (Klappa, `78)



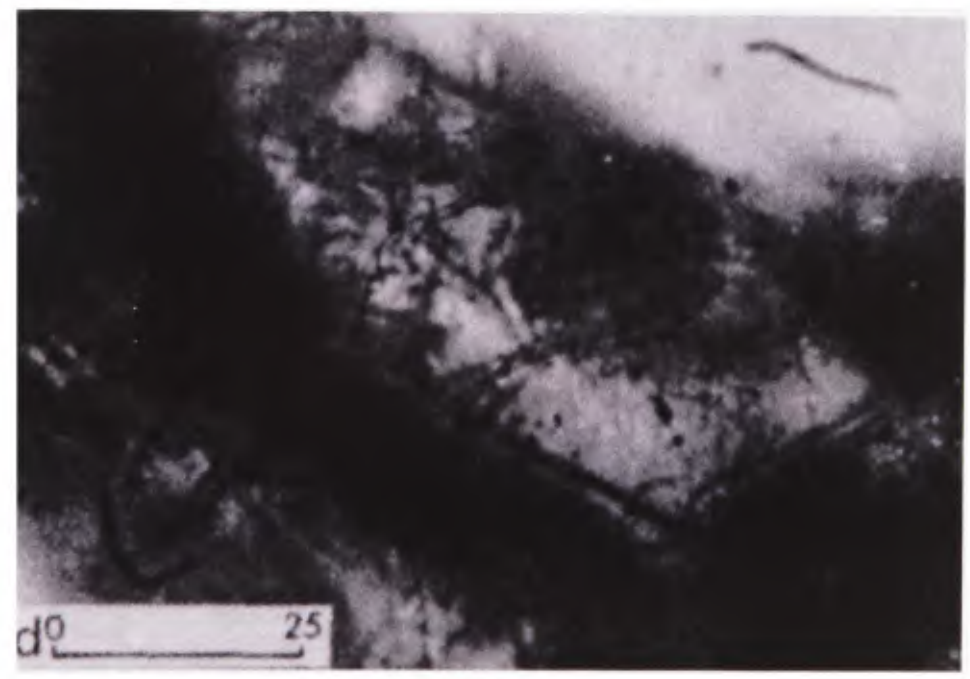
Petrographic details of internal structures of Recent **Microcodium** grains from Cieza, Spain. Elongate **Microcodium** grain displaying a radial-fibrous calcite fabric. Note discrete peripheral nucleus for part of radial-fibrous calcite (arrow). (Klappa, `78)



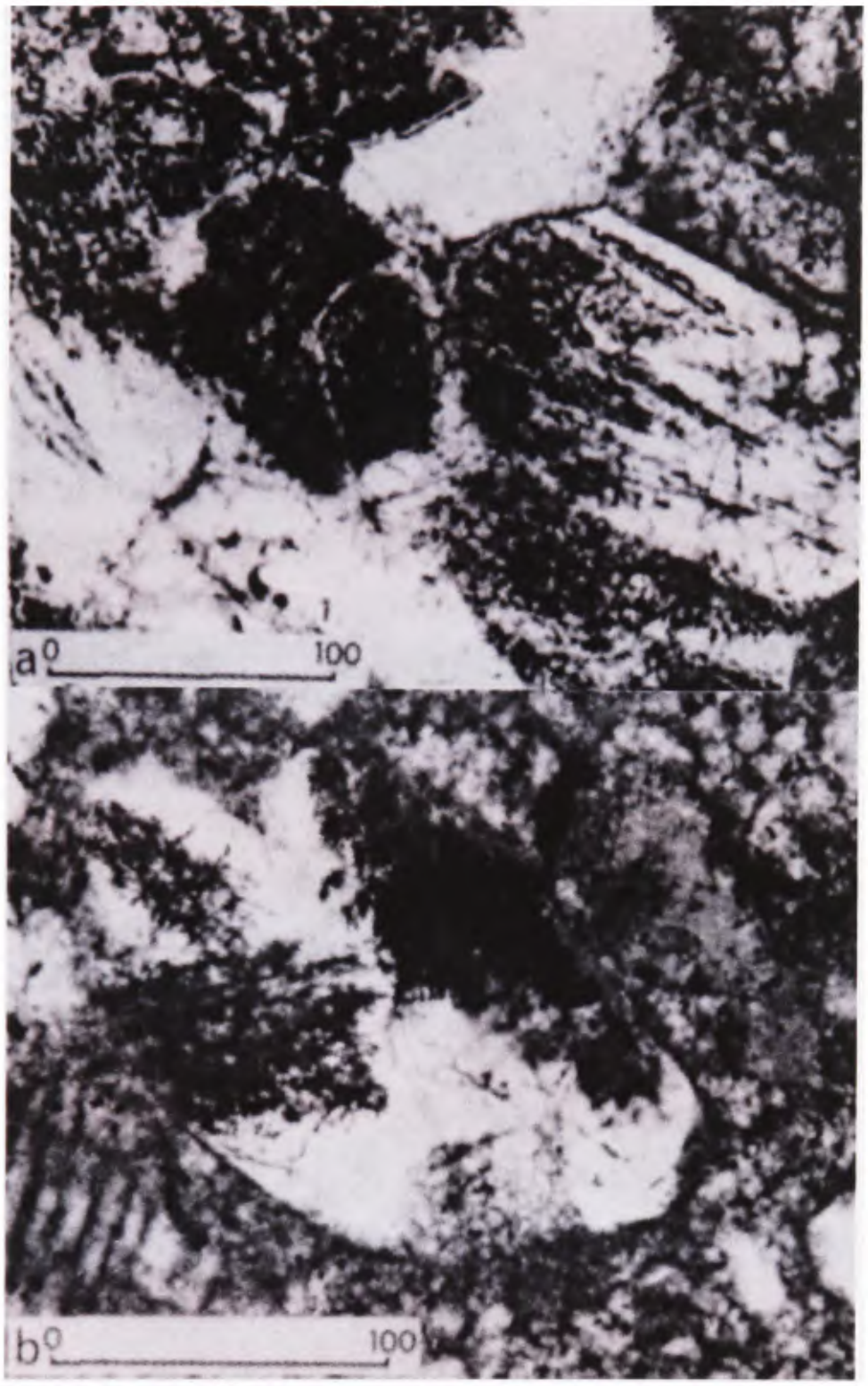
Petrographic details of internal structures of Recent **Microcodium** grains from Cieza, Spain. **Microcodium** grain consisting of bundles of radial-fibrous calcite. (Klappa, `78)



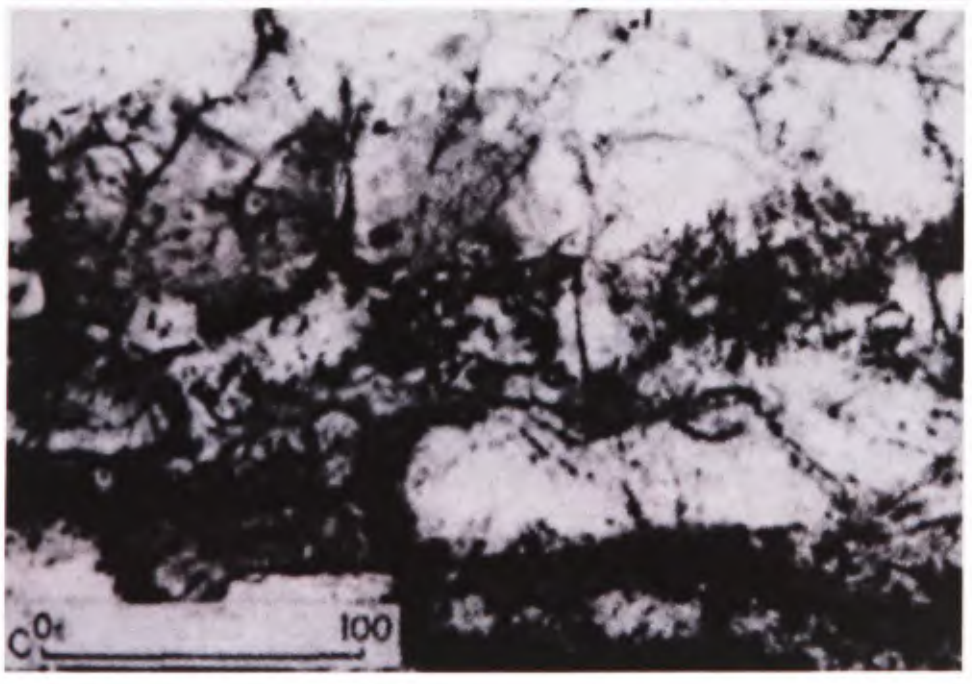
Petrographic details of internal structures of Recent **Microcodium** grains from Cieza, Spain. Central tubular structure (10 μm diameter) and smaller tubular pores. (Klappa, `78)



Petrographic details of internal structures of Recent **Microcodium** grains from Cieza, Spain. Enlargement of (c). Scale in μm. (Klappa, `78)

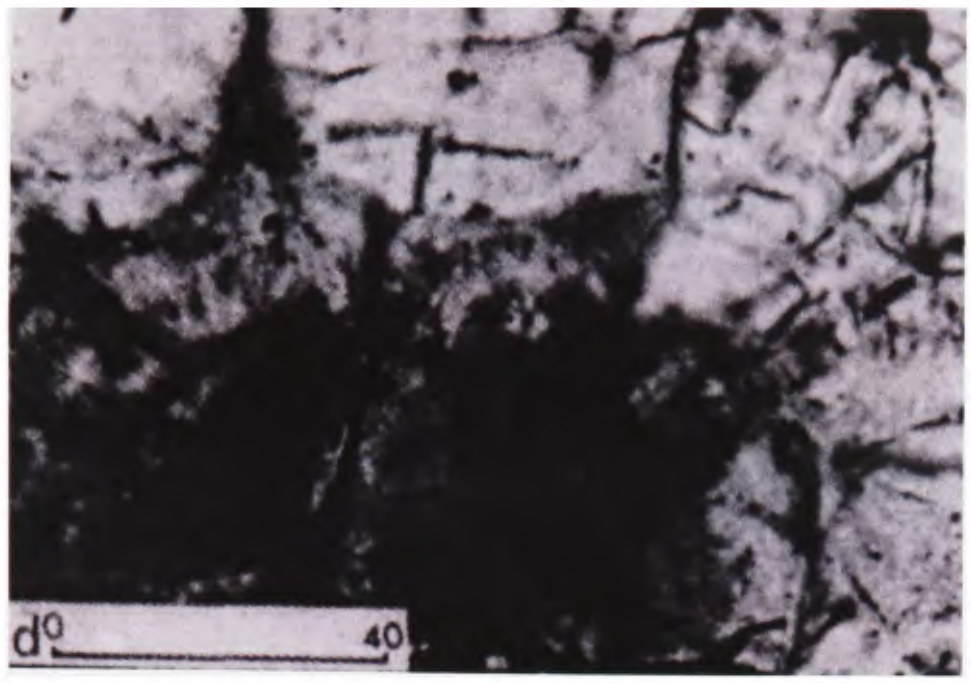


Thin section from the Pleistocene of Ibiza. Plane light. **Microcodium** aggregate composed of apparently overlapping prismatic grains (due to interference growth) with linear pore patterns (dark areas). (Klappa, `78)

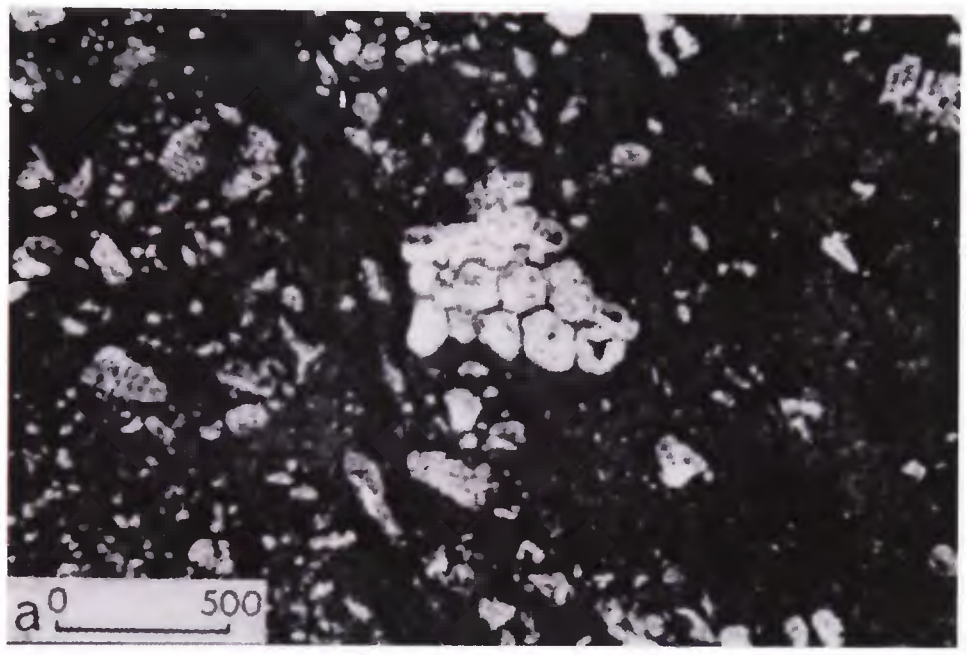


Thin section from the Pleistocene of Ibiza. Plane light. Single detrital **Microcodium** grain with irregular ('wiggly') tubular pores radiating from periphery. Note: (i) **re-entrant** at top; and (ii) partial **micritization** at base. Grain to lower left is a partially **micritized** coralline algal fragment. (Klappa, `78)

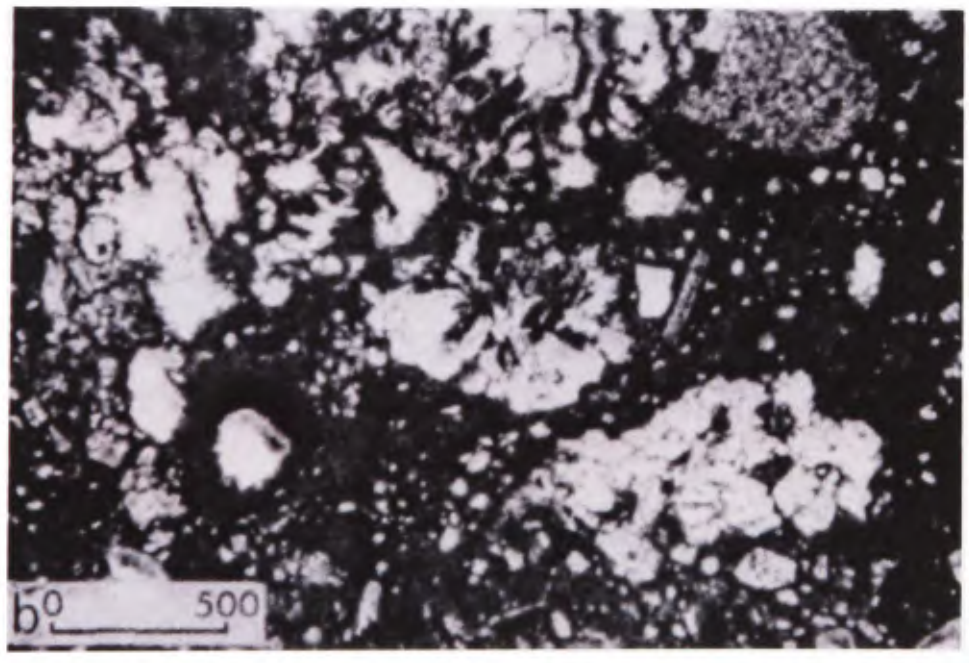
Thin section from the Pleistocene of Ibiza. Plane light. Part of **Microcodium** aggregate stained with Alizarin red S and potassium ferricyanide. **Radial-fibrous fabric** has taken up stain (red, indicating non-ferroan calcite), whereas grains or parts of grains with uniform extinction have remained unstained. (Klappa, `78)



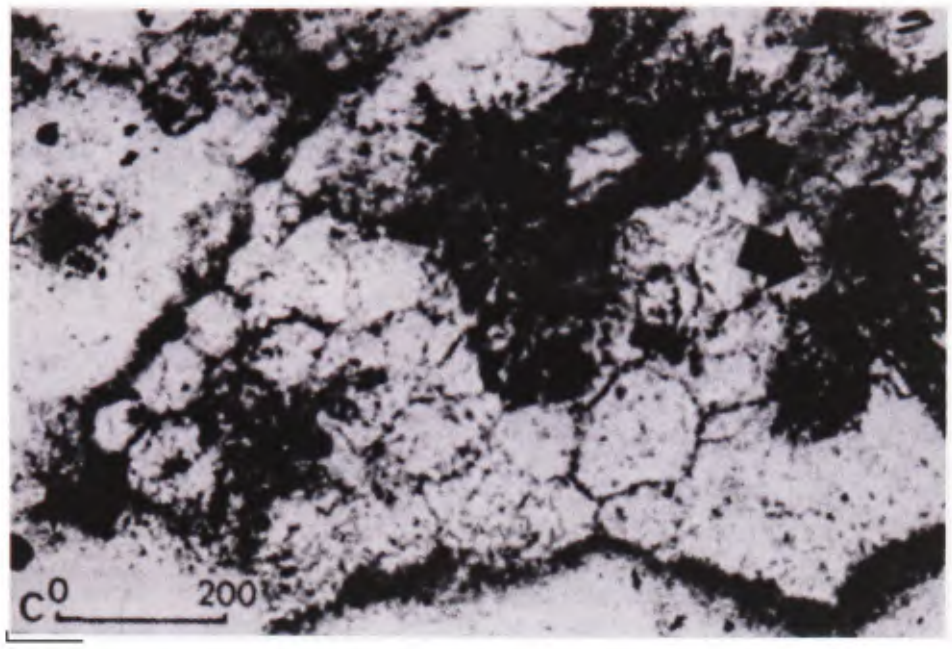
Thin section from the Pleistocene of Ibiza. Plane light. Detail of (c) above. Shows stained **radial-fibrous calcite** (lower half) and unstained **monocrystalline calcite** (upper half). Scale in μm. (Klappa, `78)



Thin section from Pleistocene deposits, Ibiza, plane light. Fragmented, detrital aggregate consisting of **isodiametric Microcodium** grains 'floating' in a **calcisiltite matrix**. (Klappa, `78)



Thin section from Pleistocene deposits, Ibiza, plane light. In situ **Microcodium** grains with dark **inclusions** or **pores** (cf. 'shell-residue micrite of Alexandersson, 1972). (Klappa, `78)

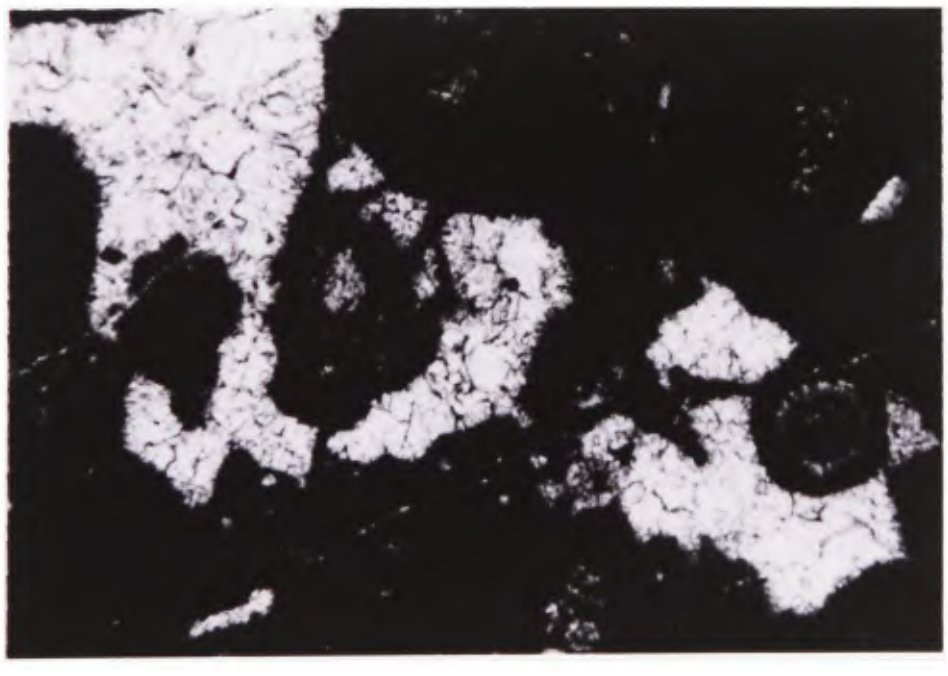


Thin section from Pleistocene deposits, Ibiza, plane light. Detail of (b) above, showing dark inclusions radiating from discrete nuclei (arrows). Scale in μm. (Klappa, '78)

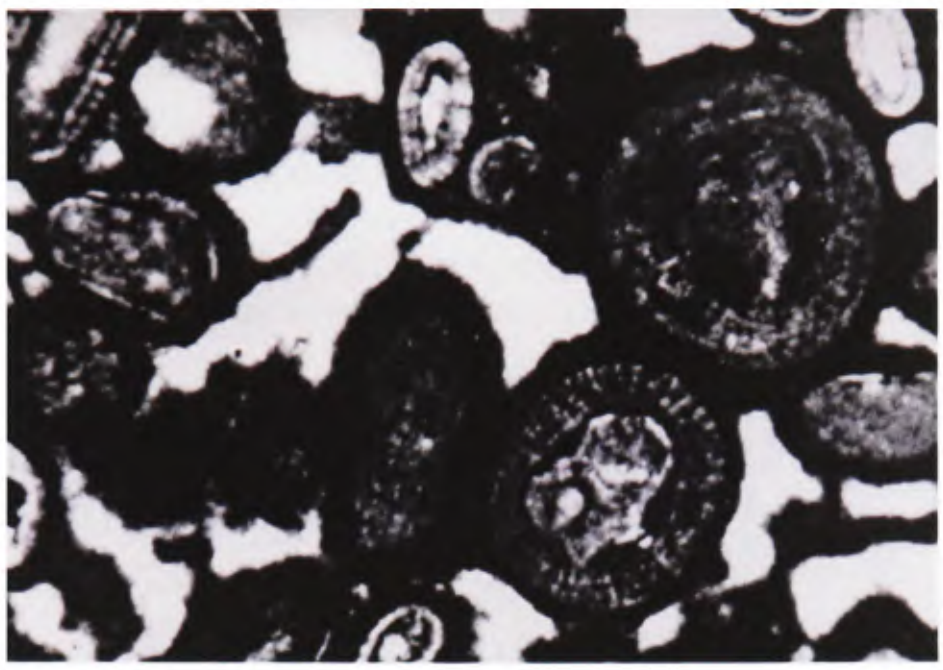
Mycelia

In present day soils, fungal networks (mycelia) pervade the soil fabric. Some fungi calcify to form a variety of textures, including needle-fibre calcite. In many cases threads arise from and connect irregular micrite coats on ooids. Work on Spanish Quaternary calcretes has shown that fungi are important in forming both the micritic grain coats and the threads.

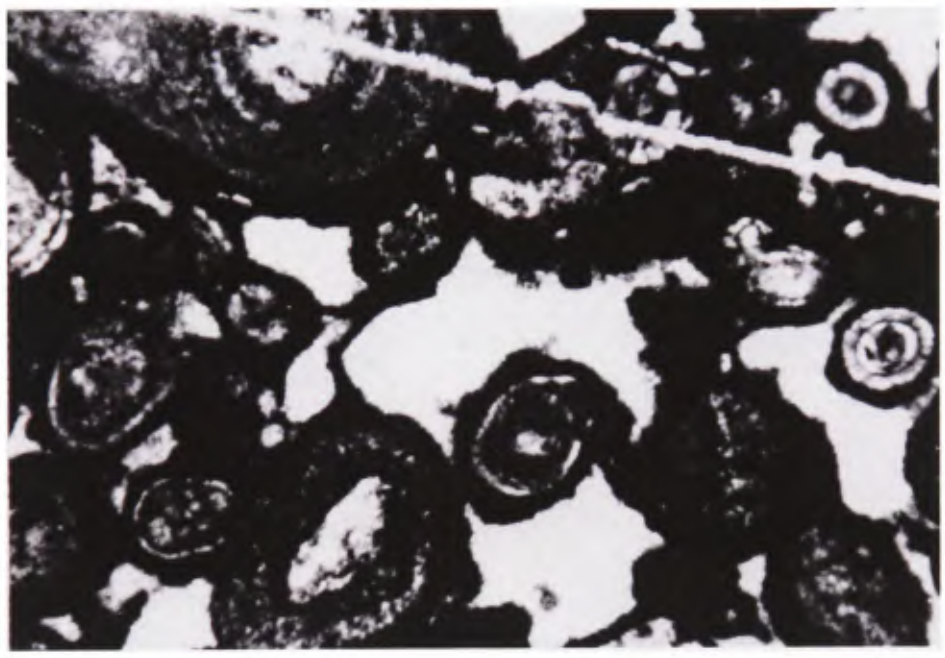
These threads can form networks which could be mistaken for alveolar-septal structures but since both are probably in-part fungal they actually constitute two end-members. In the case of the threads, the fungi occurred as loose networks between grains while in the case of alveolar-spetal structures the fungi occupied root tubules. The septae average only 20 μm in width while associated alveolar-septae average 60 μm.



Mycelia from the Heatherslade geosol, Lower Carboniferous, Cardiff. (Wright)



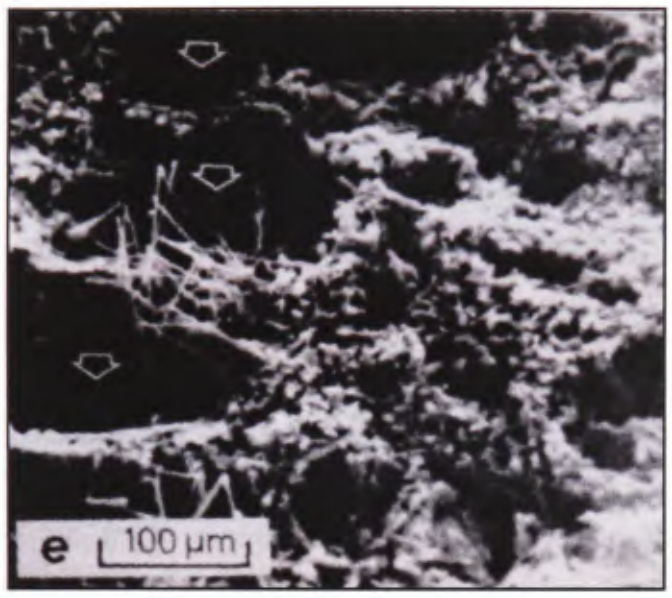
Mycelia from the Heatherslade geosol, Lower Carboniferous, Cardiff. (Wright)



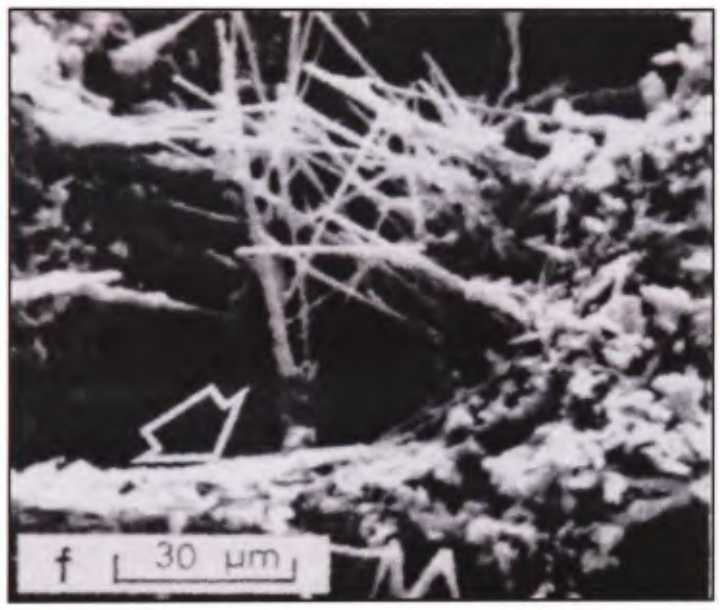
Mycelia from the Heatherslade geosol, Lower Carboniferous, Cardiff. (Wright)

Needle-Fibre Calcite

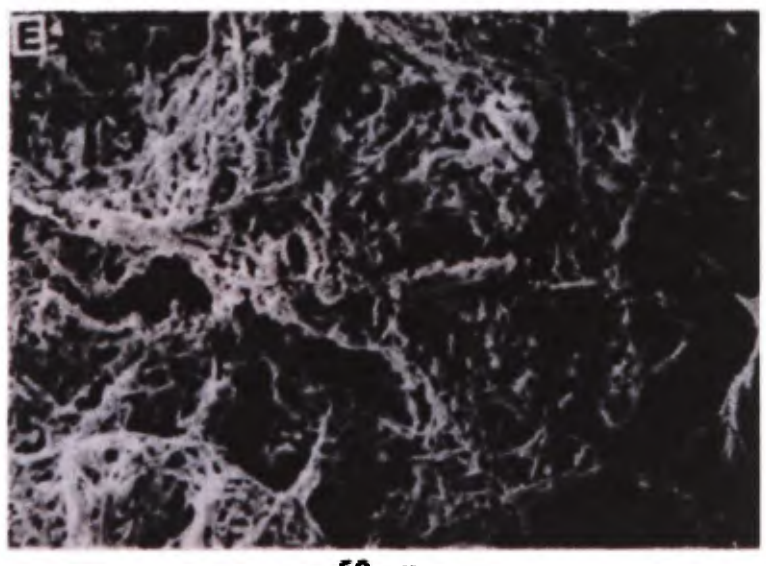
Thin elongated calcite crystals with a diameter of up to 5 µm which have mainly grown along one axis, ranging in size from 10-300 µm are reported by James (1972) for calcareous crusts. He distinguishes furthermore between long randomly orientated needle fibres which may form felt-like mats and the shorter tangentially orientated needle fibres which often coat particles.



Cylinders composed of **calcite needles** oriented tangentially with respect to the surface of the cylinders but random with respect to the long axes of the cylinders. **Tubular voids** (arrows) are root moulds. SEM. Location: Tarragona, NE Spain. (Klappa, `80)



Detail of (e) above. **Needle calcite** wall has a **banded fibrous fabric** when viewed in transverse section and a **hyphantic fibrous fabric** when viewed in longitudinal section. Equant **microcrystalline calcite** precipitated on needle wall (arrow) leads to thickening of wall.SEM. (Klappa, `80)



SEM photo of **tangential needle-fibre calcite** crystals which also coat grains inside **pisolites** and may have a fungal origin. (Beier, `87)



SEM close-up of **tangential needle-fibre calcite** crystals shown in (E) above. (Beier, `87)

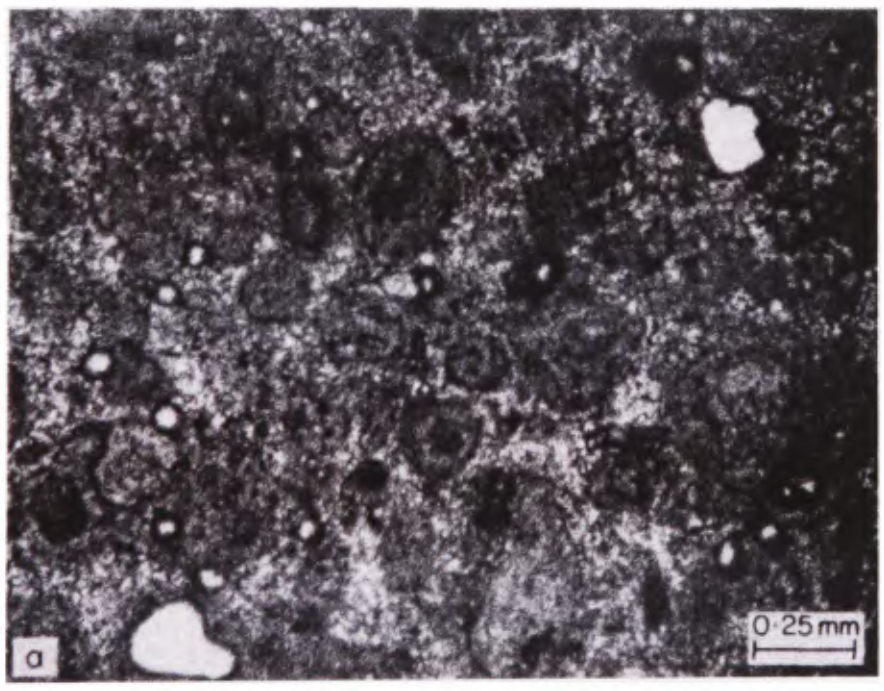
Pelletal Micrite

Many carbonates contain peloids (sand-sized micritic grains). They are especially common in calcretes developed on limestones. They are most abundant in the upper parts of profiles and usually been regarded as micro-nodules (glaebules) but appear to mostly represent calcified faecal pellets.

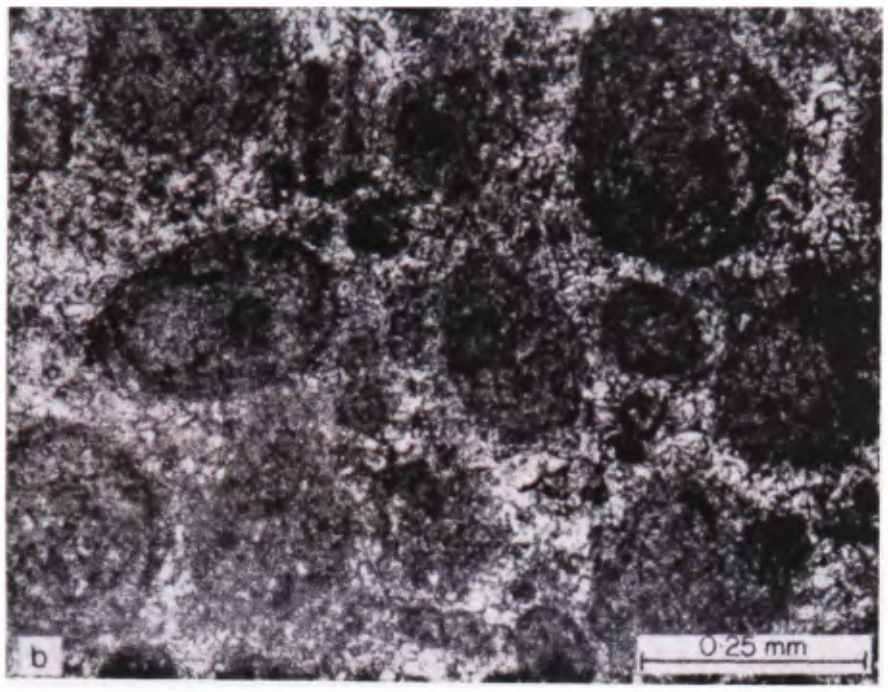
In paleosols such pellets can be recognised by several features:

1) they may occur within burrow-structures
2) they occur in dense clusters with a high degree of sorting
3) they are well-rounded, spherical to elliptical.

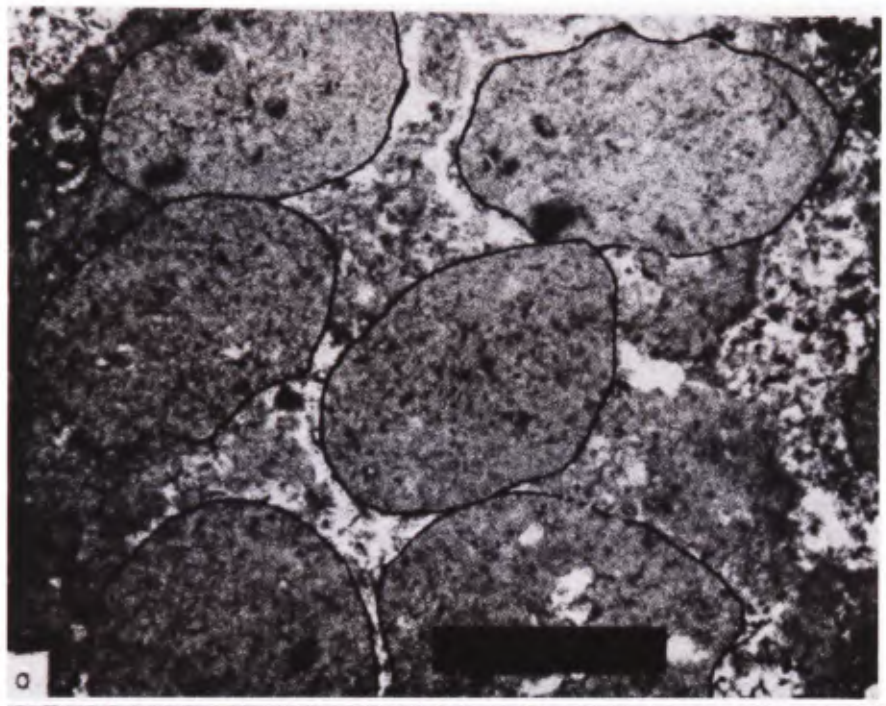
Most pellets decay, a process known as 'ageing' in the soil literature and can aggregate into dense masses.



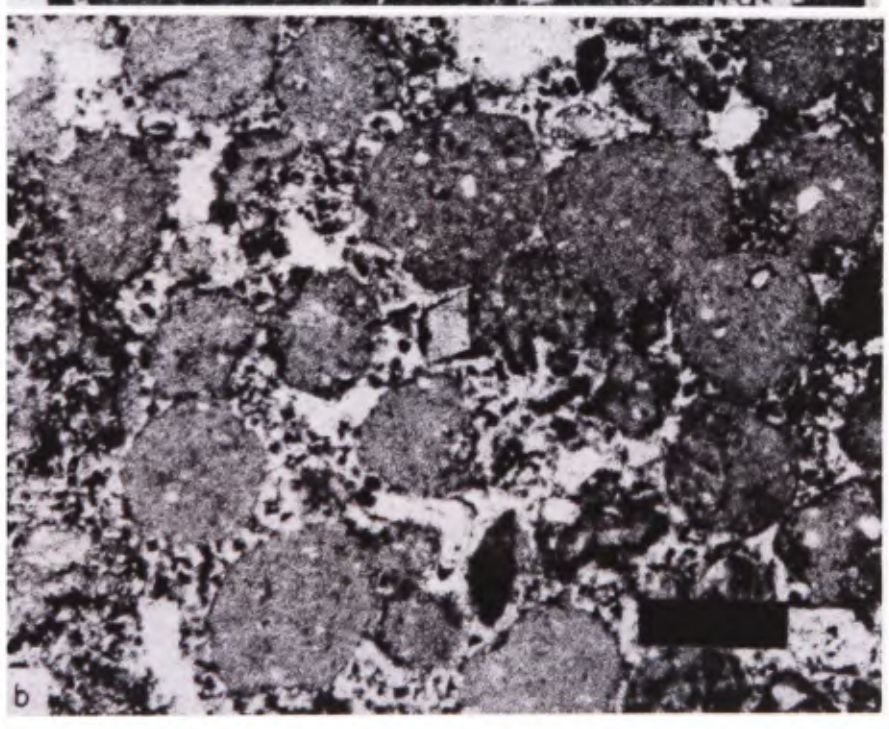
Pelletal micrite of accretionary origin in veins of the upper calcrete of the Ndolanya Beds Tanzania. Cement is largely **microspar**, and the fabric appears to be grain supported. This fabric is identical to the *structure grumeleuse* of Cayeaux (1935). Photo is of an acetate peel. (Hay & Reeder, `78)



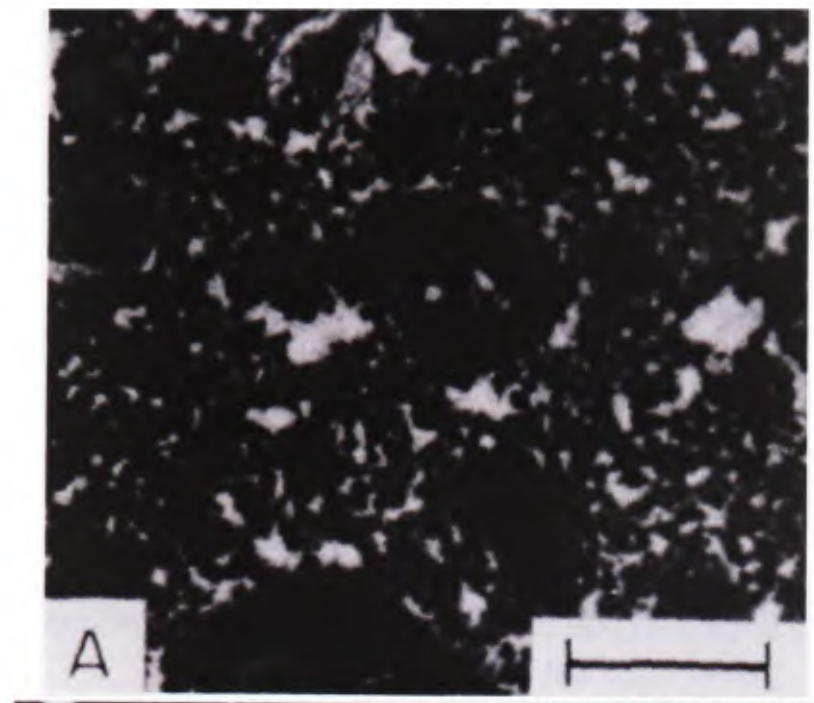
Pelletal micrite of accretionary origin in veins of the upper calcrete of the Ndolanya Beds Tanzania. Cement is largely **microspar**, and the fabric appears to be grain supported. This fabric is identical to the *structure grumeleuse* of Cayeaux (1935). Photo is of an acetate peel. (Hay & Reeder, `78)



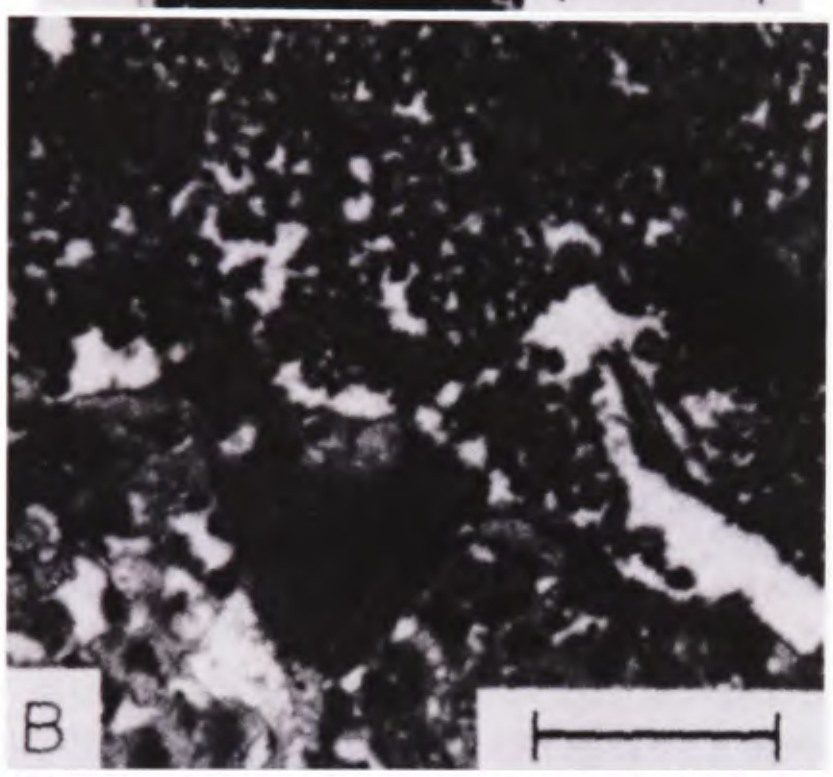
Pelletal micrite as seen in thin section, using plane light. The photo is of pelletal limestone from a filled fracture in the calcrete of Kyle Canyon, USA. Pellets were formed by cementation of pellet-shaped bodies of porous **micrite**. This photo shows an early stage in the separation of pellets from less-cemented matrix. Solid lines are drawn over clearly deflned pellet margins and dashed lines indicate poorly defined or incompletely developed pellet margins. (Hay & Wiggins, `80)



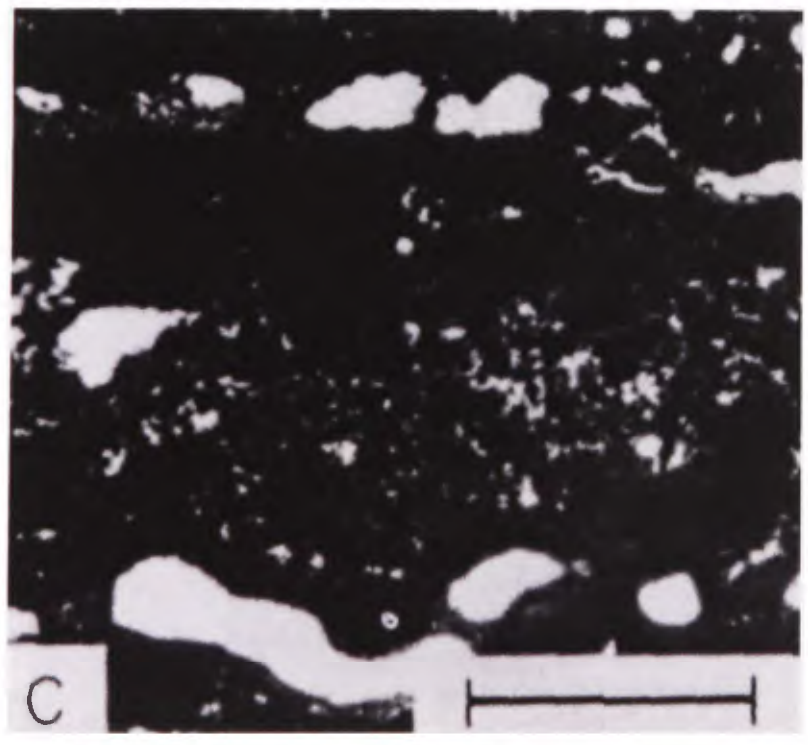
Pelletal sediment from the interstices of uncemented gravel overlying a thin laminar layer of calcrete of surface 2 in Kyle Canyon, USA. Pellets lie in a matrix of silt, sand and micrite crumb aggregates. (Hay & Wiggins, `80)



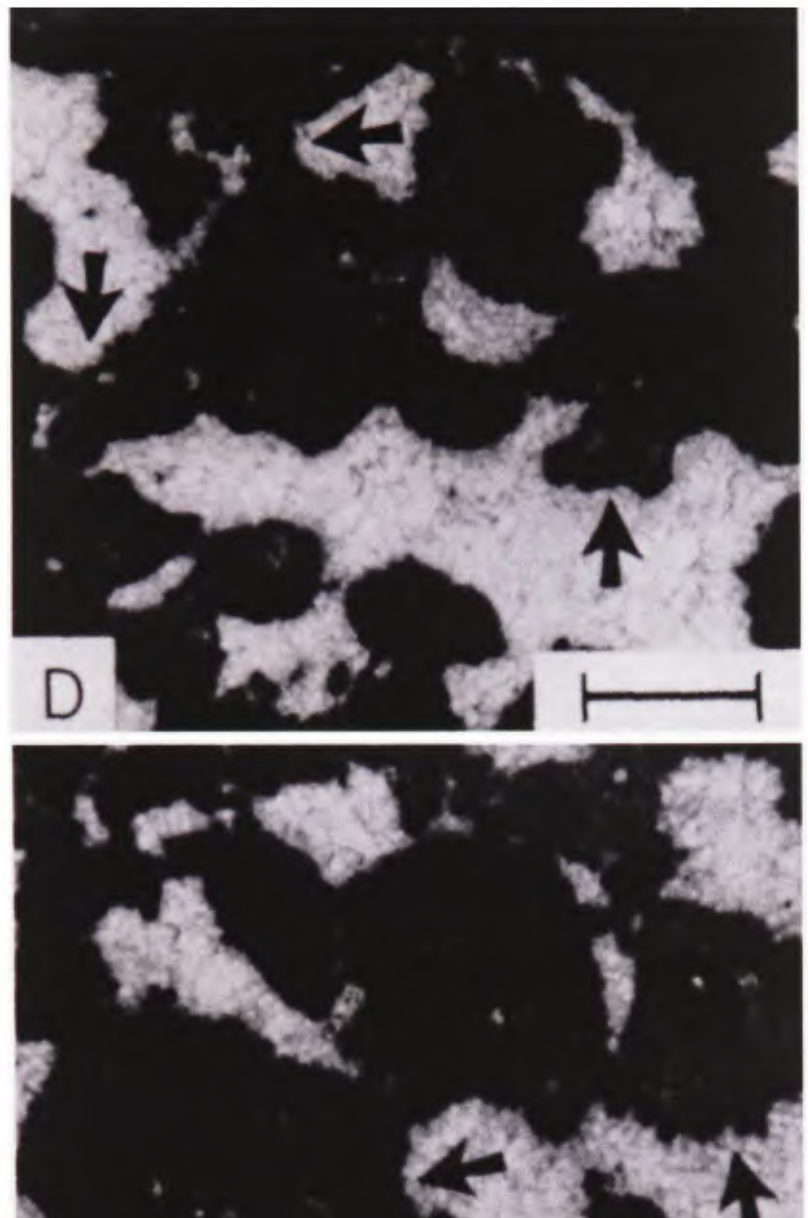
Small pellets occurring between the larger **peloids**. Scale bar is 1 mm long. (Wright, `83)



Concentration of **pellets** in the upper half of the photo overlying an area of poorly sorted **peloids** with **irregular calcite coatings**. Many of the pellets are compacted (welded) together. Scale bar is 1 mm long. (Wright, `83)

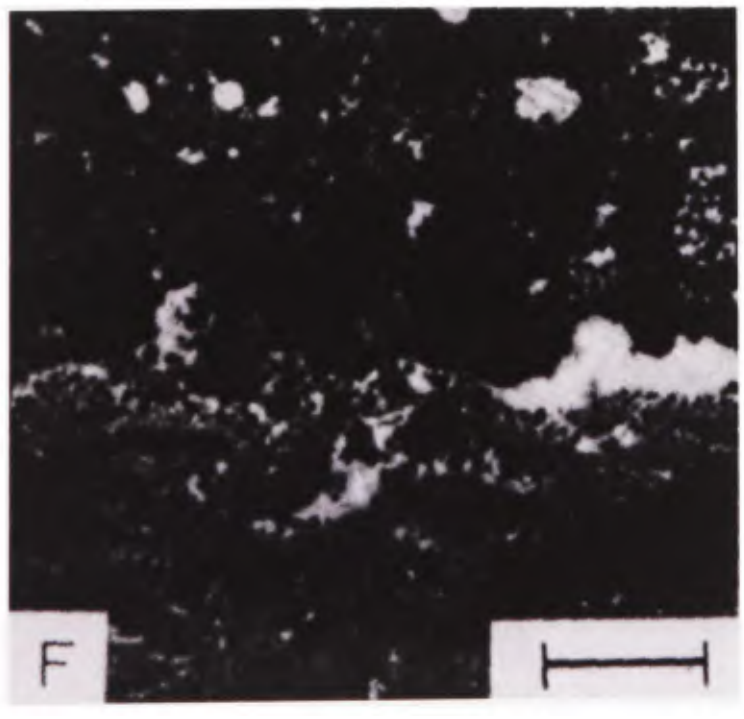


Area of compacted **pellets** traversed by **tubular fenestrae**; note the **pellets** in the **fenestrae** at the top left, and then **septa-like structures** in some of the **fenestrae**. Scale bar is 2 mm long. (Wright, `83)

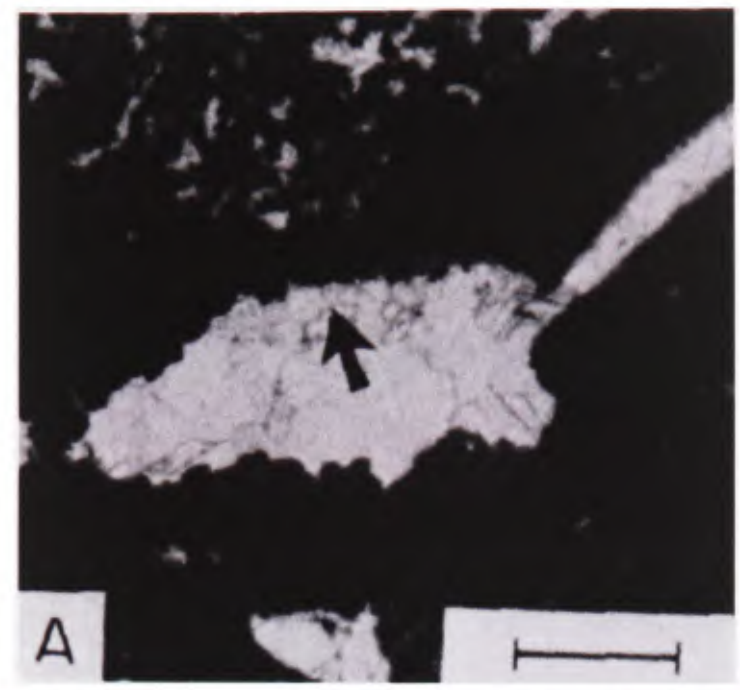


Pellet coatings and **bridges** (arrowed) on larger **sediment-grain peloids**. Scale bar is 0.5 mm long. (Wright, `83)

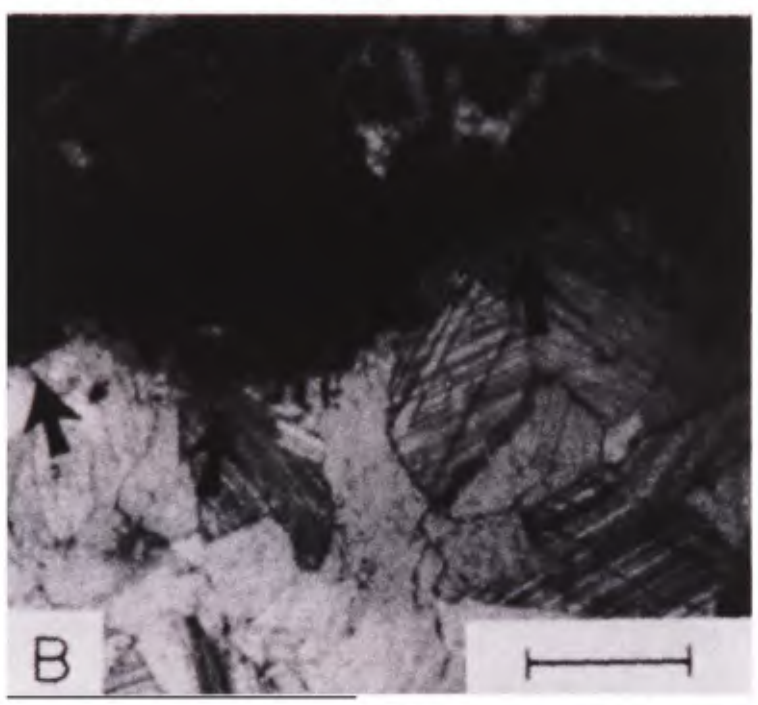
Pellet coatings (arrowed) on **peloids**. Scale bar is 0.5 mm long. (Wright, `83)



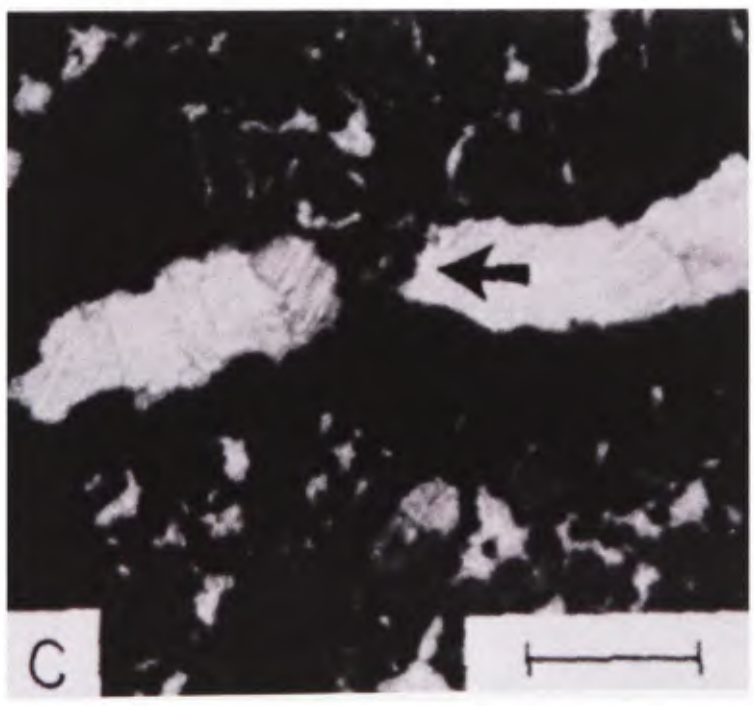
Tubular fenestra (burrow ?) partially filled with **pellets**. Note the irregular domed roof and chamber-like termination. The **matrix** consists of compacted **pellets**. Scale bar is 1 mm long. (Wright, `83)



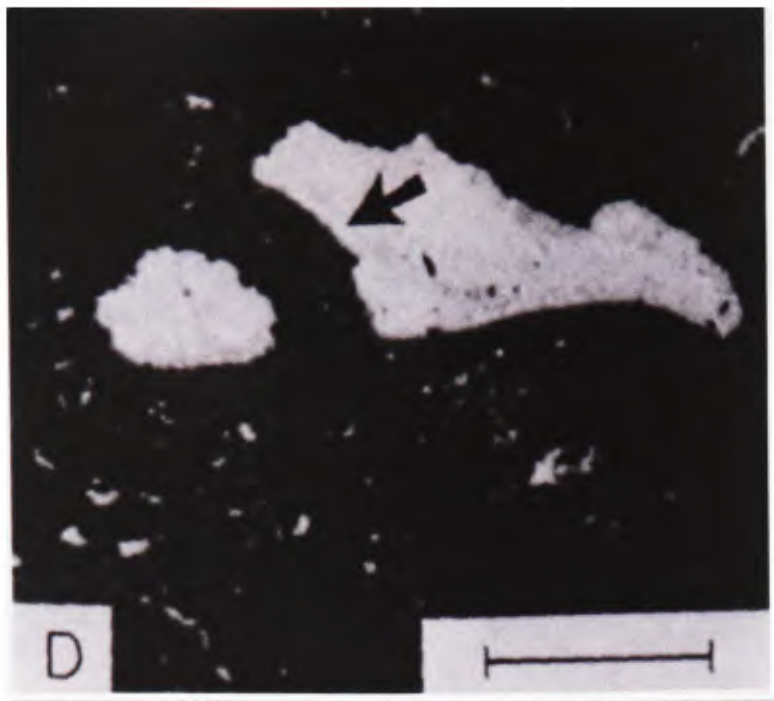
Chamber-like structure within a complex **tubular fenestrae** showing **pellets** in the roof (arrowed). The **pellets** are coated by a fine crust of **fibrous calcite**. Scale bar is 0.5 mm long. (Wright, `83)



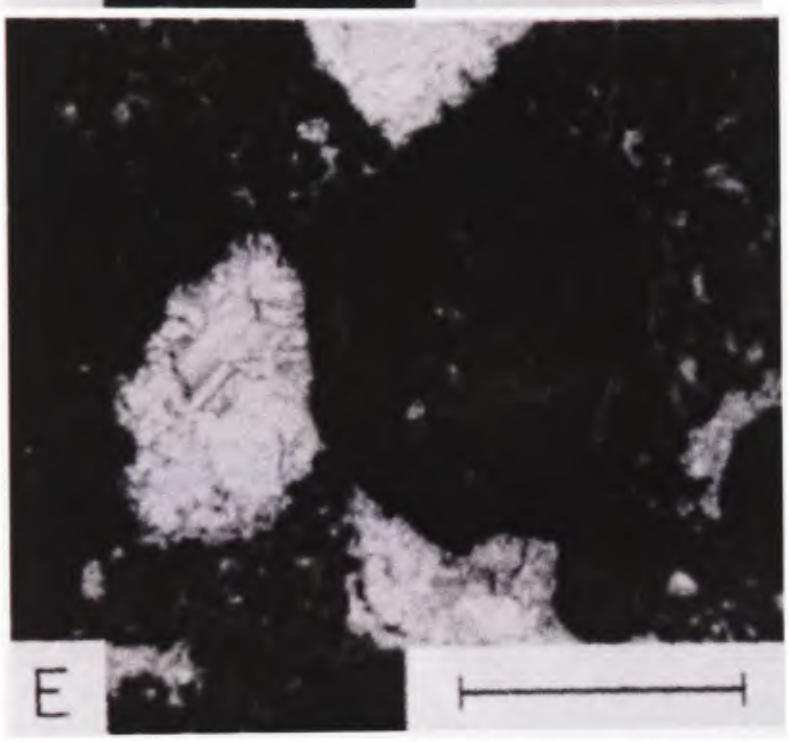
Pellets in the roof (arrowed) of a large chamber-like structure in a complex tubular **fenestrae**. The **pellets** also have a fine **fibrous crust**. Note the **sparry haloes** around the **peloids** above the roof. Scale bar is 0.5 mm long. (Wright, `83)



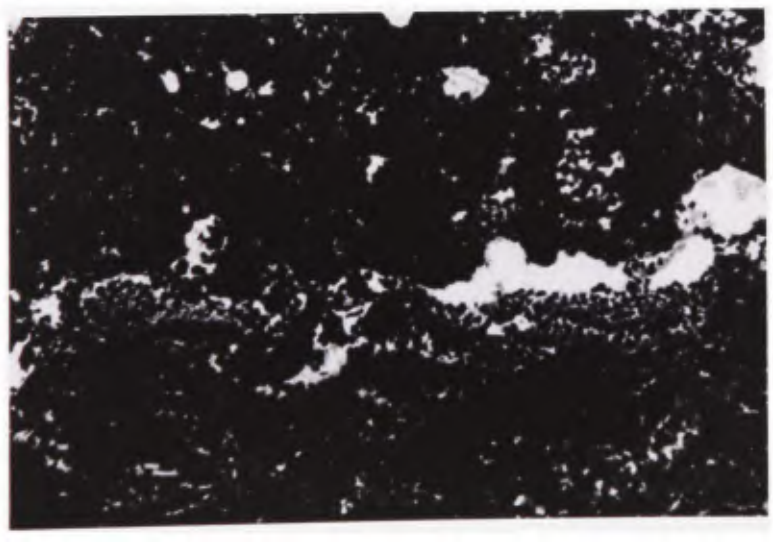
Pellet septa (arrowed) in a tubular fenestrae. Note the sparry haloes around the overlying peloids. The small pellets are packed in between the large peloids. Scale bar is 0.5 mm long. (Wright, `83)



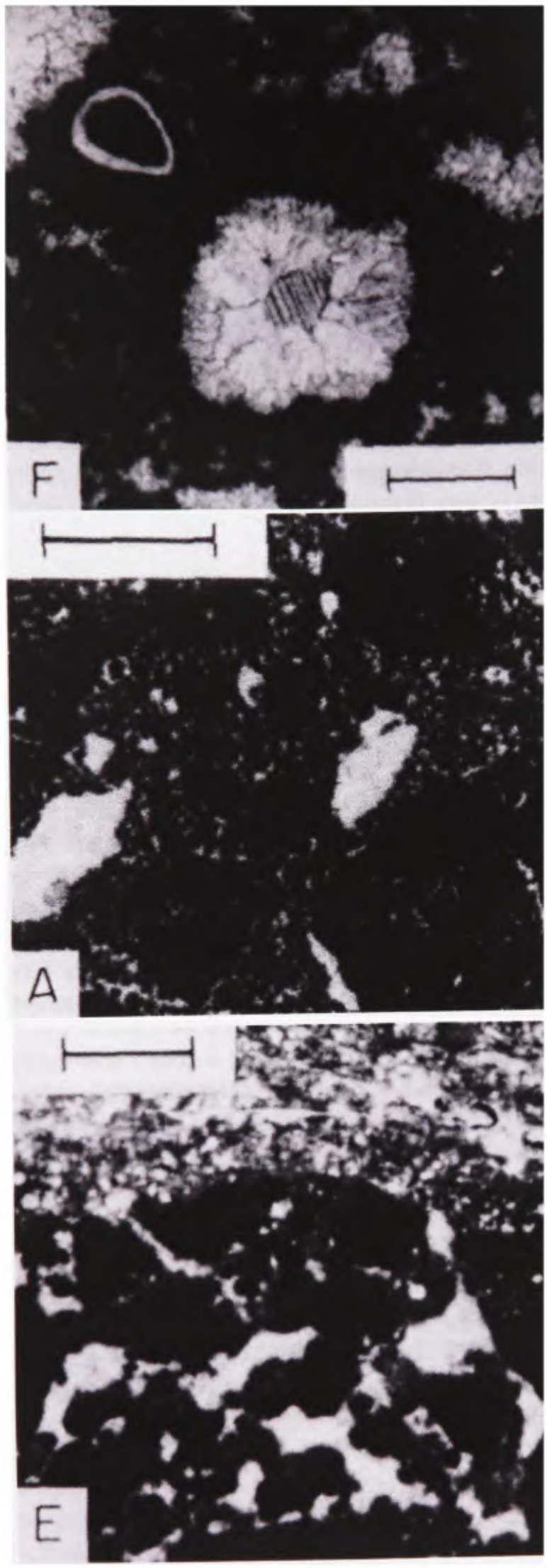
Irregular fenestrae containing a **pellet** arch (arrowed). Note **geopetal crystal silt** overlying a **pellet** layer. The **matrix** consists of compacted **pellets.** Scale bar is 1 mm long. (Wright, `83)



Pellet bridge structure. Is this a simple **pellet bridge** or a **pellet tube-lining** formed by some organism? Scale bar is 1 mm long. (Wright, `83)



Pellets in a burrow. Field of view is 6 mm wide. Lower Carboniferous Darren Felen geosol. (Wright)



A **pellet tube structure.** This is not simply a series of **pellet bridges** connecting **peloids** but a distinct **pellet tube.** But was it formed by a root simply pushing pellets aside or by some animal constructing a protective tube? Note the regular **sparry halo** around the **peloid** in the upper left quadrant. Scale bar is 0.5 mm long. (Wright, `83)

Large **compound pellets** set in a **matrix** of smaller **pellets.** Many of these compound pellets resemble earthworm fecal material. Scale bar is 2 mm long. (Wright, `83)

The upper third of the photo shows a **silt-rich clay laminae** thought to represent an argillan. This overlies **peloids.** Scale bar is 1 mm long. (Wright, `83)

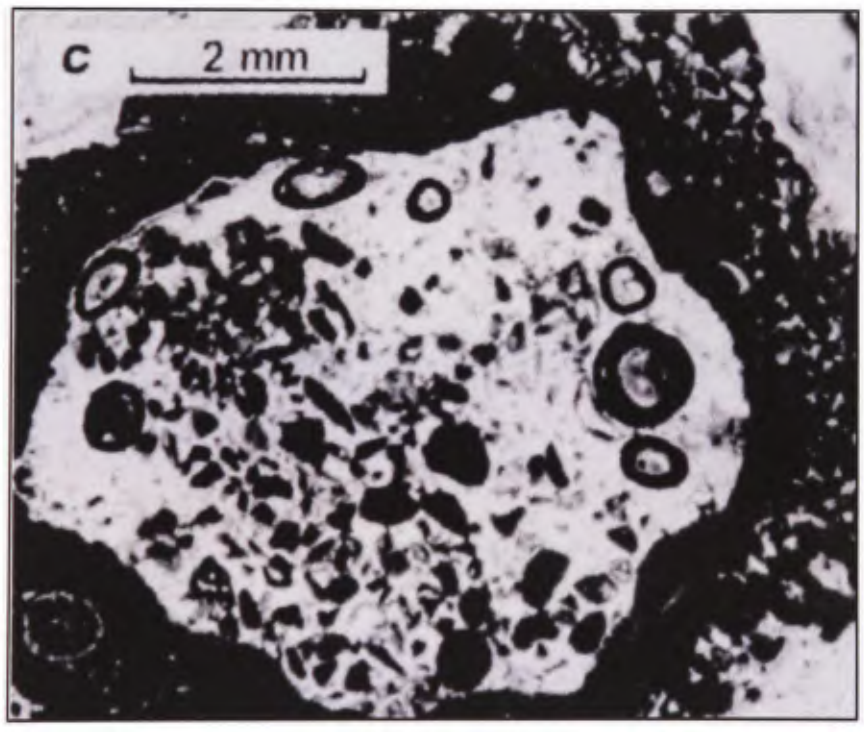
Pellets

Pellets are the excreta (coprolites) of various organisms. These grains typically collect in lakes and shallow ponds, but also occur in pedogenic environments. Pellets commonly are not preserved but disaggregate into micrite during desiccation and compaction associated with shallow burial.

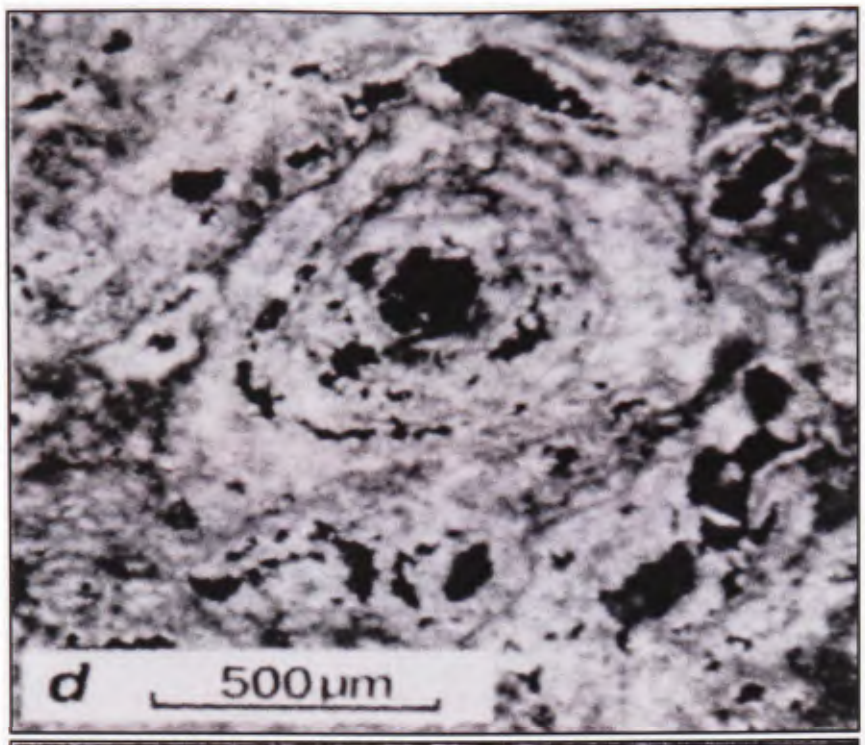
Peloids

A peloid is a rounded grain of homogeneous micrite. The term does not imply any particular mode of formation. Most peloids are probably faecal pellets, strongly micritised grains or are simply rounded fragments of reworked carbonate mud sediment (Adams and Mackenzie, 1998). It is also believed that some peloids are produced directly by calcified algae and cyanobacteria or are the cements formed with microbial involvement (Tucker and Wright, 1990). Due to the difficulty in identifying the origin of these micritic particles, the non-genetic descriptive term 'peloid' is commonly used. Clotted micrite is a fabric made up of discrete aggregated bodies (peloids) composed of micrite (Bathurst, 1975).

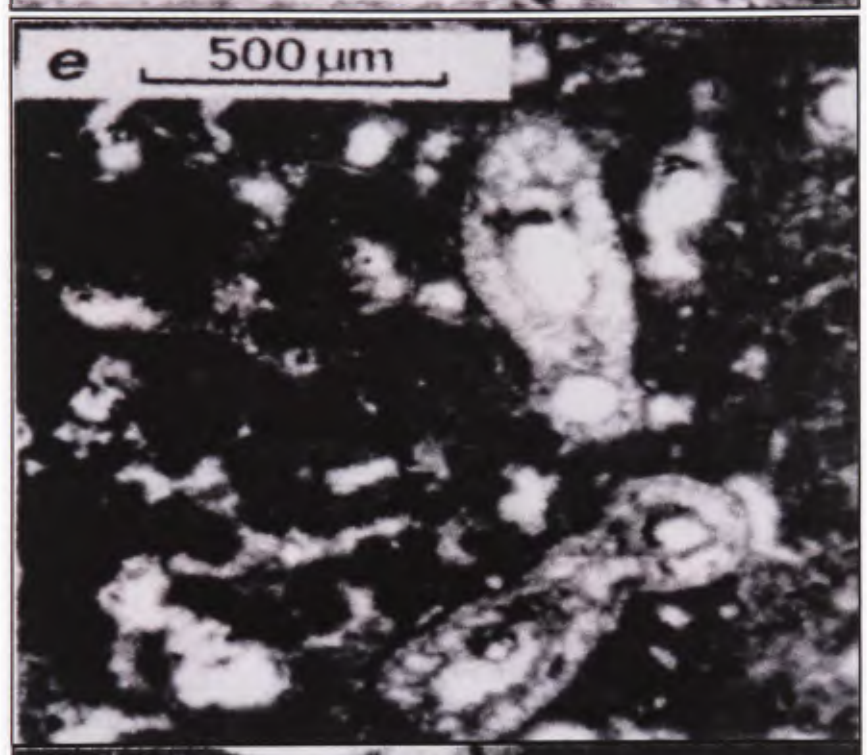
Rhizoliths



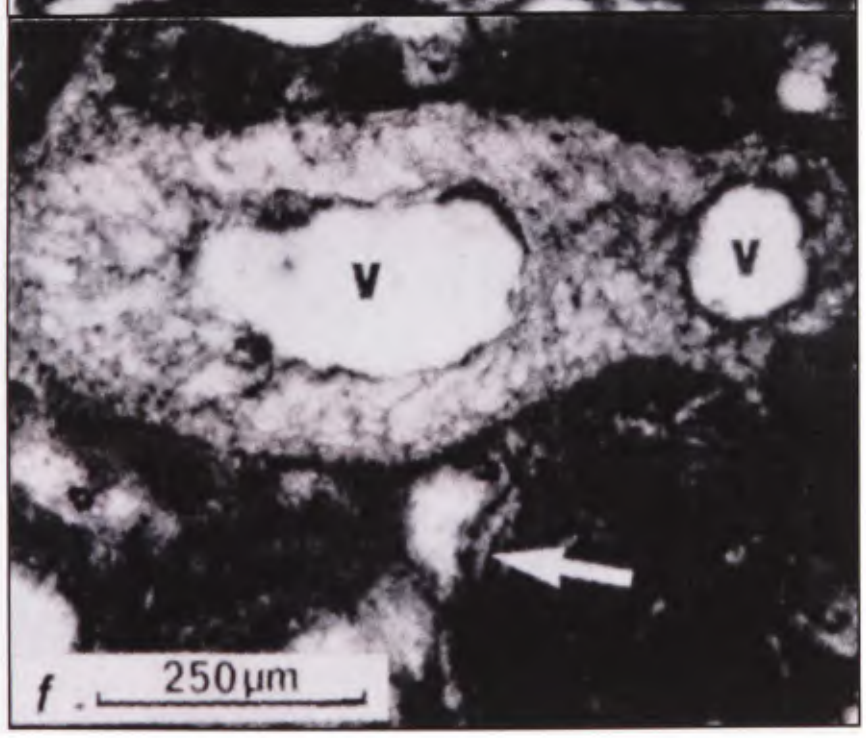
Transverse section through **rhizocretion**. Cemented cylinder is composed of calcareous wind-deposited sand grains; cement is **cryptocrystalline calcite**. Roots (outlined in ink) and weakly cemented sand grains within cylinder. Note: **rhizocretion** will become a **root tubule** if roots decay completely. Thin section, PPL. (Klappa,`80)



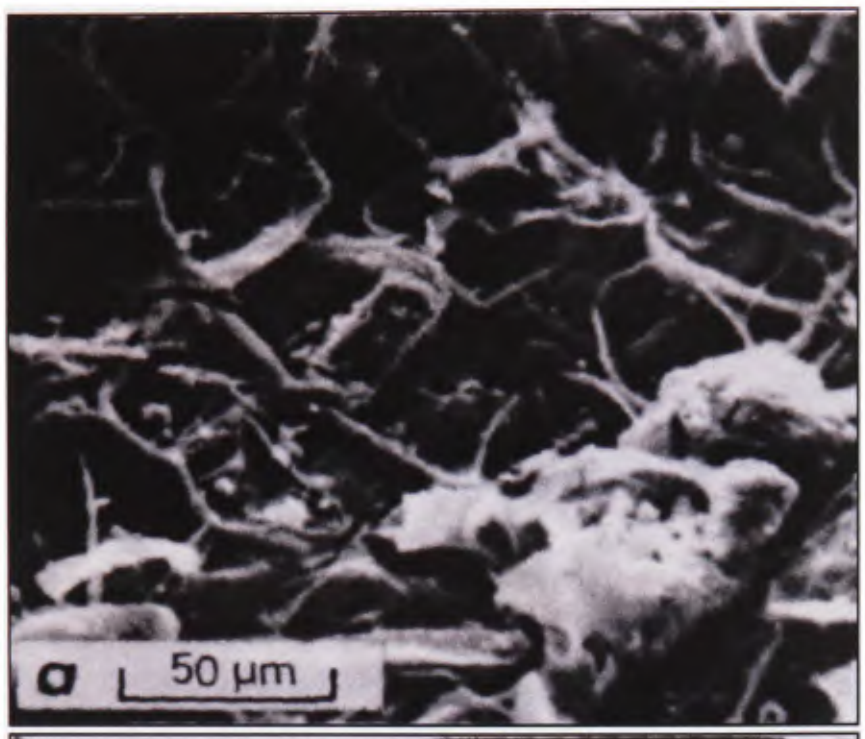
Rhizolith lacking fine cellular details. Note vague **concentric** arrangement of **micritic** layers. Black areas are **voids**. Thin section, crossed polarized light. Location: Cala Bassa, Ibiza. (Klappa, `80)



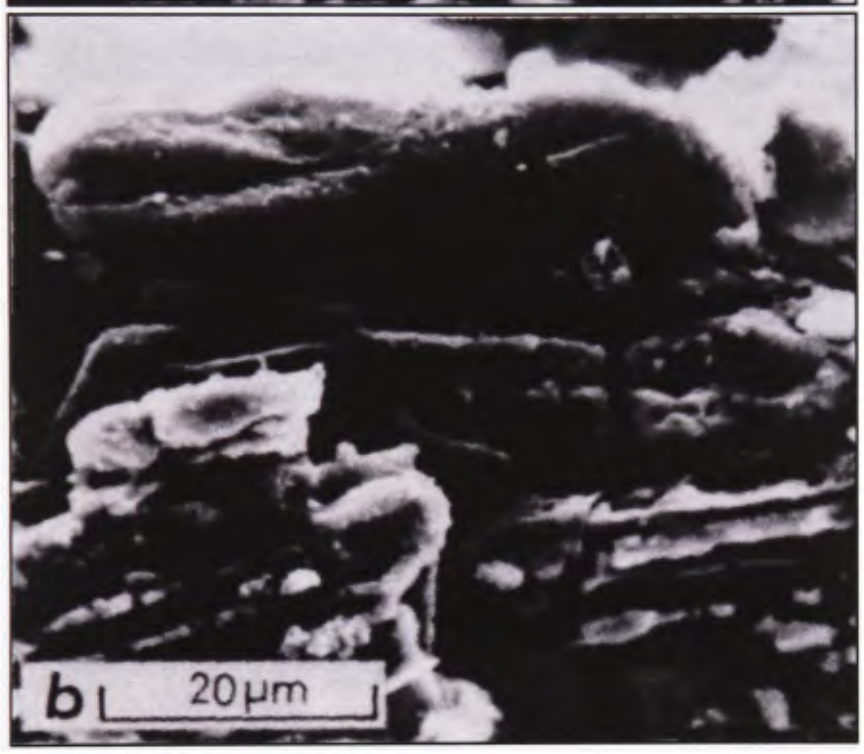
Oblique sections through **bifurcating calcified roots.** Epidermis and cortical cells have been calcified. **Clotted micrite** matrix is composed of **calcified faecal pellets.** Thin section, PPL. Calcrete hardpan of Pleistocene age. Location: Cala Bassa, Ibiza. (Klappa, `80)



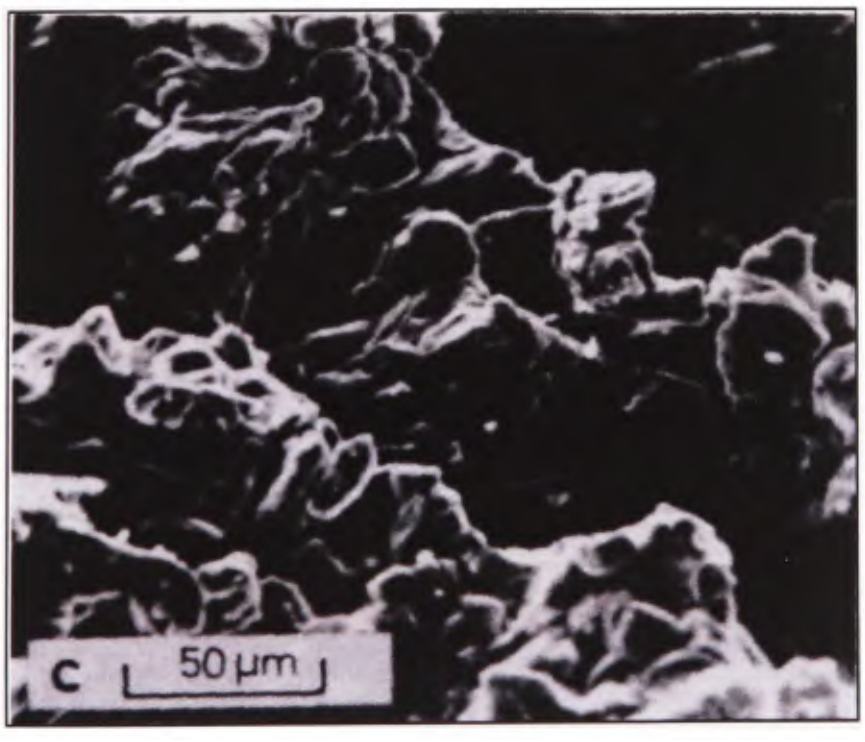
Detail of upper **rhizolith** shown in (e) above. **Voids** (v) mark positions of former vascular systems. **Micritic** matrix, which has a **vermicular texture,** contains calcified root hairs (arrow). Thin section, PPL. (Klappa, `80)



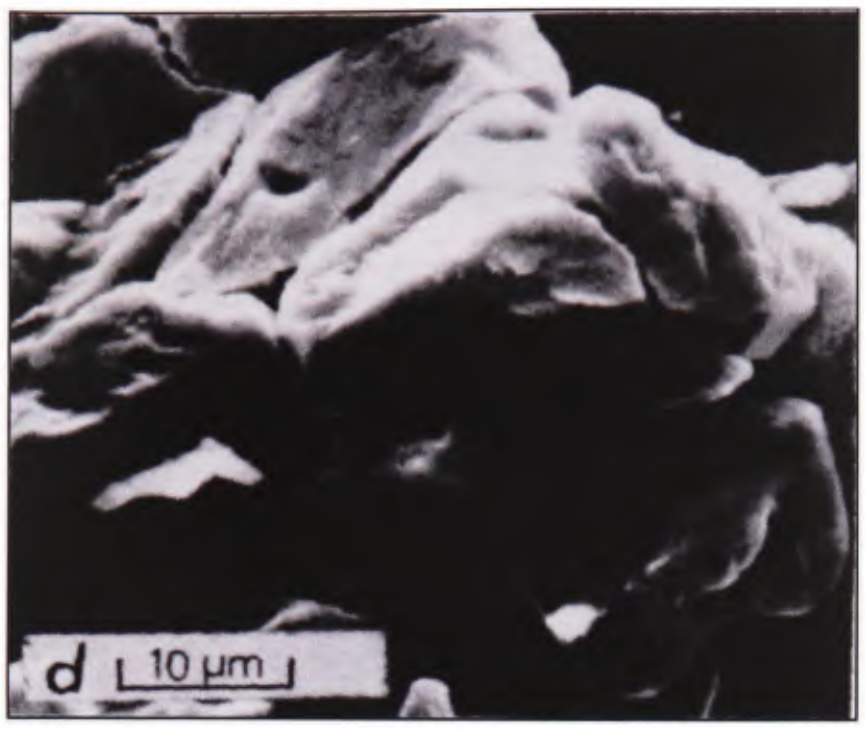
Partially decomposed Recent root showing **collapsed, parenchymatous cells** of cortex. Cell contents have been lost. Fine filaments on surface are **fungal hyphae**; spheres are **comidia**. SEM. Location: Vandellos, NE Spain; chalky horizon of Pleistocene calcrete. (Klappa, `80)



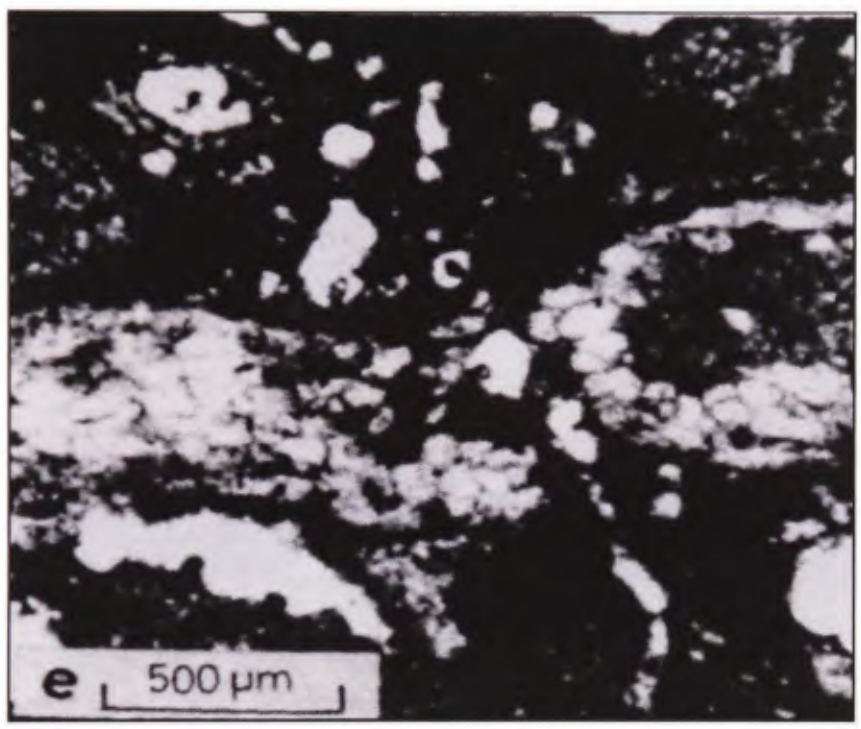
Epidermis (lower part) and partly decayed **cortical cells** of Recent root. Note that **cell walls** have decomposed. SEM. Location: Vandellos, NE Spain. (Klappa, `80)



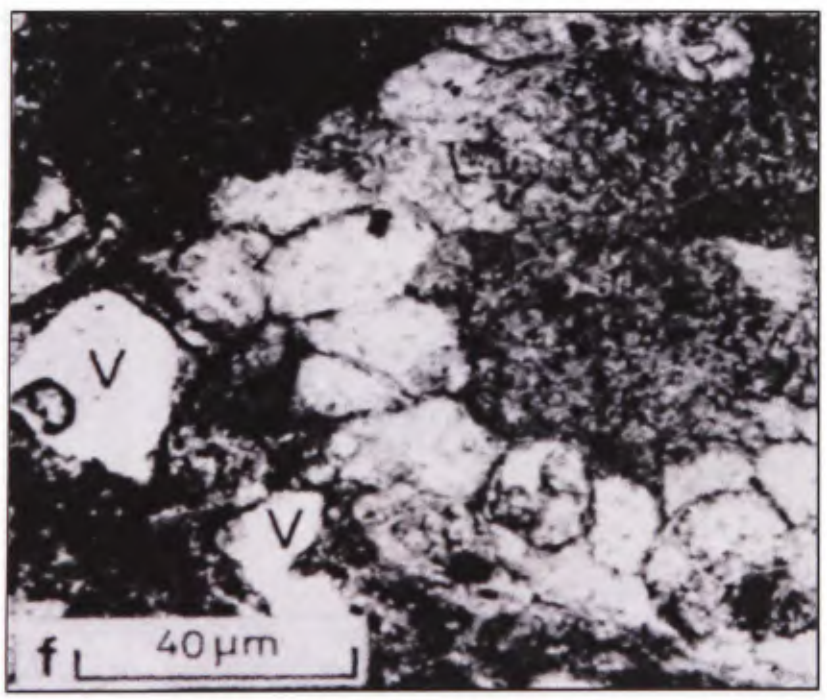
Calcified **cortex of root**. **Isodiametric calcite grains pseudomorph parenchymatous cells.** SEM. Location: Falset, NE Spain; sheet calcrete horizon of Pleistocene calcrete. (Klappa, `80)



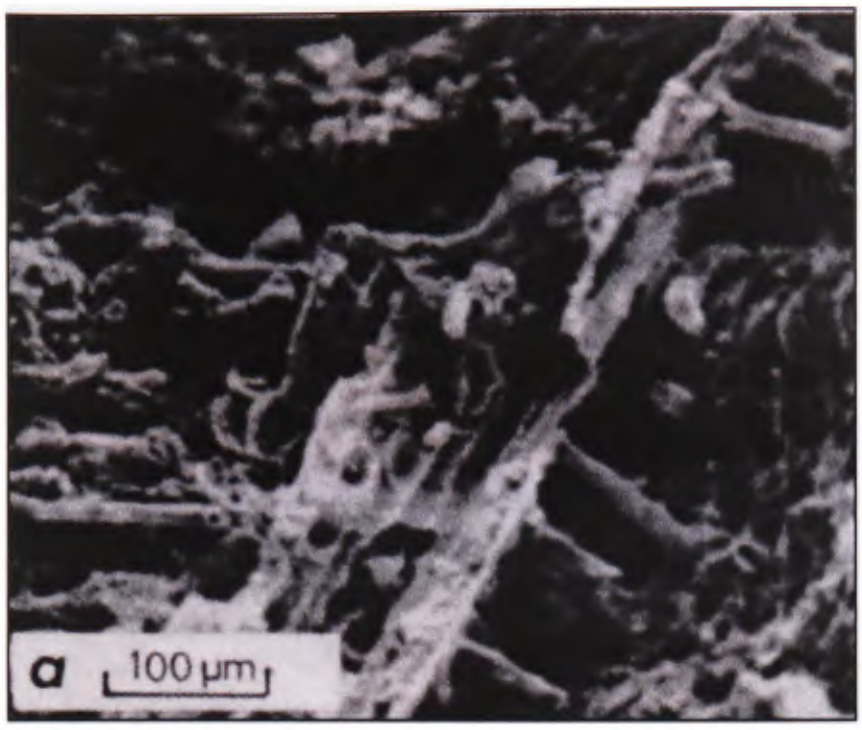
Detail of (c) above. **Isodiametric calcite grains.** Note **curved boundaries and intergranular voids. Intergranular voids** mark positions of **cell walls**. SEM. (Klappa, `80)



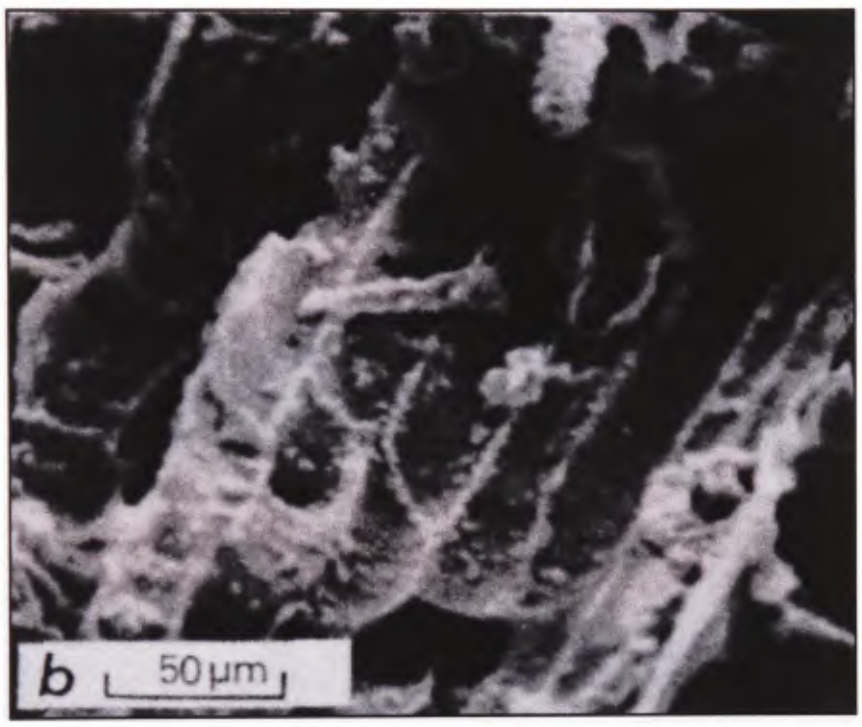
Oblique sections through **calcified root. Parenchymatous cells** of **root cortex** have been replaced by **calcite.** Anatomy of central vascular system has not been preserved. Thin section, PPL. Location: Es Cana, Ibiza; Hardpan horizon of Pleistocene (or older) calcrete. (Klappa, `80)



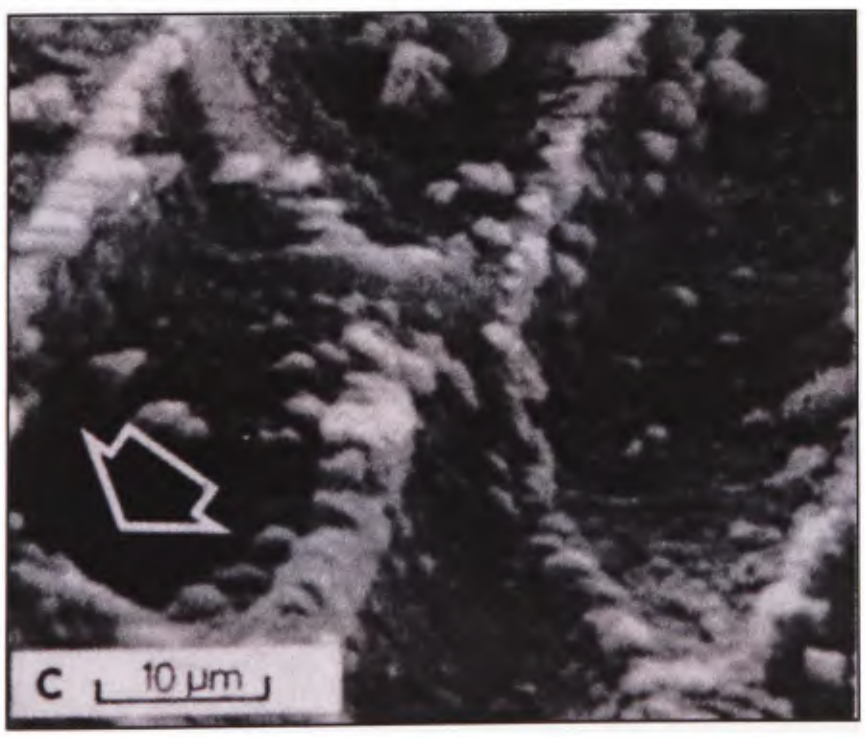
Detail of (e) above. Individual **calcite grains** of **calcified root cortex** extinguish as single crystals. **Voids** (v) of channel shown in (e). Thin section PPL. (Klappa, `80)



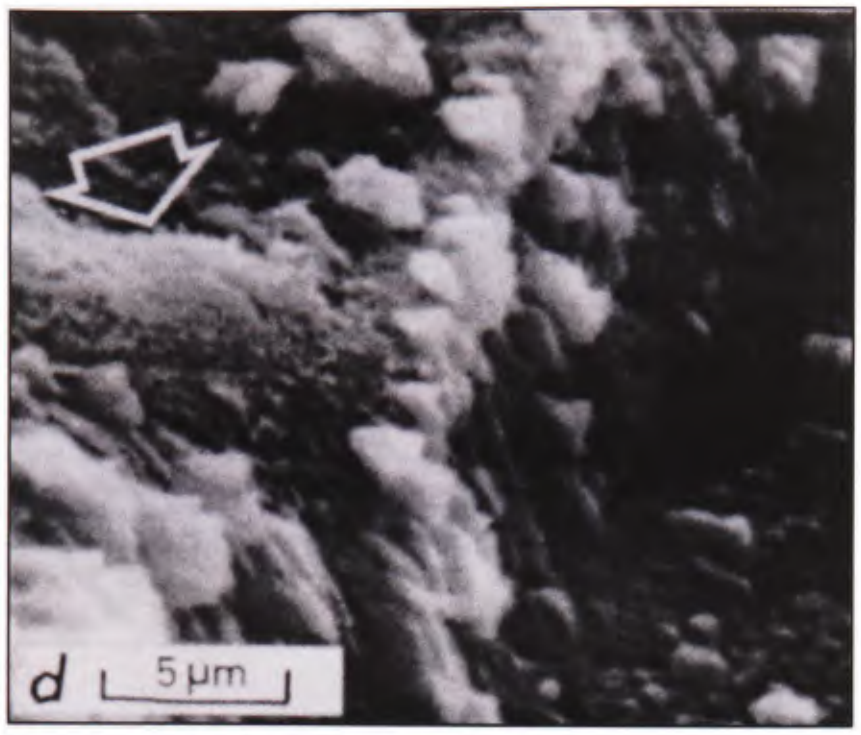
Calcified **epidermis** of root. Tubular extensions are **root hairs**. Calcified **fungal hyphae** and sloughed off calcified **root hairs** are present in the surrounding **micritic** matrix. SEM. Location: Albacete, SE Spain. (Klappa, `80)



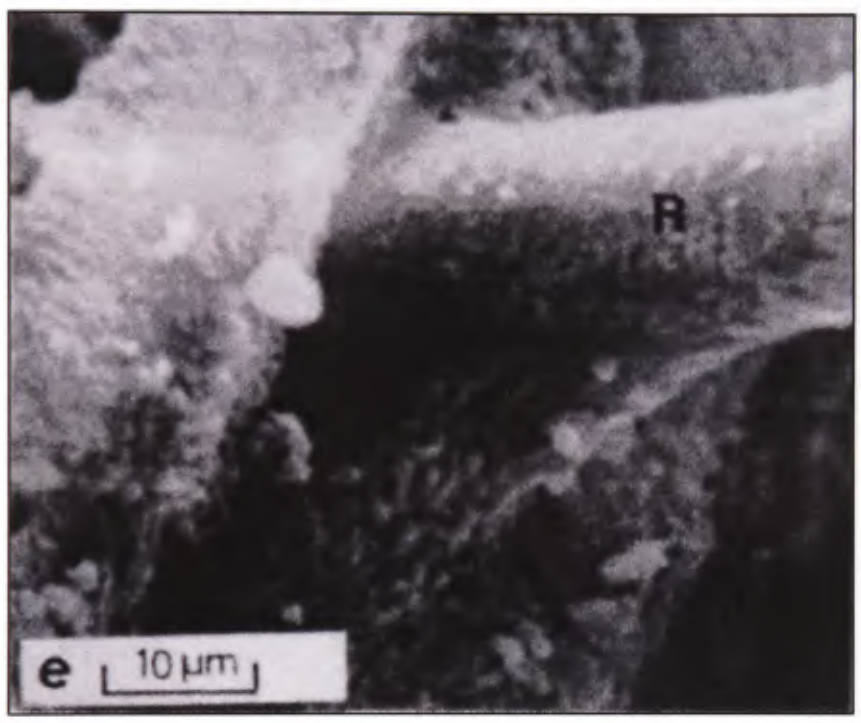
Detail of (a) above. Note ridges between **cells**. SEM. (Klappa, `80)



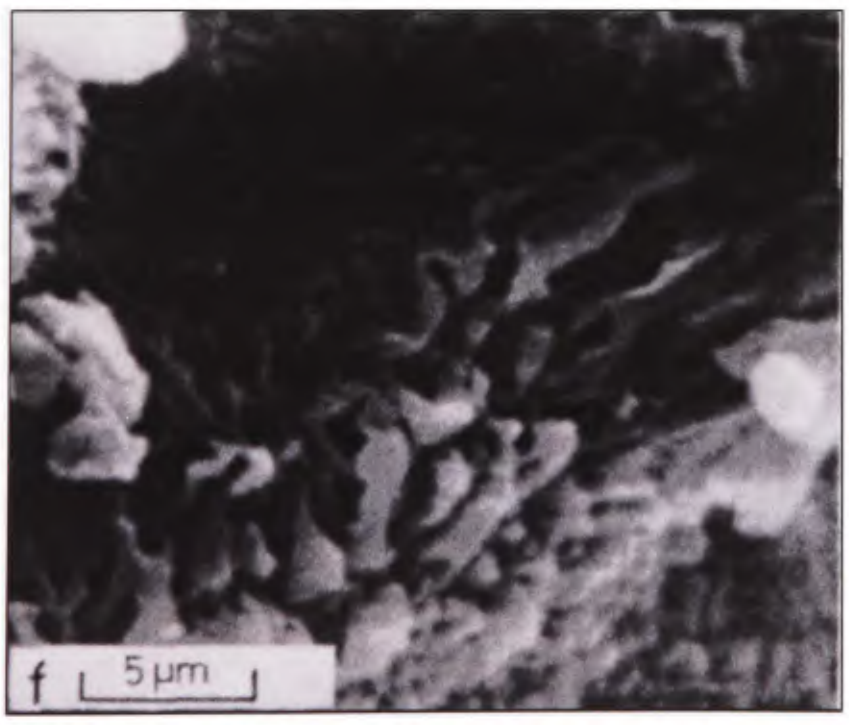
Detail of (b) above. Ridges consist of **micron-sized calcite grains**. Arrow points to interior of **root hair** tube. SEM. (Klappa, `80)



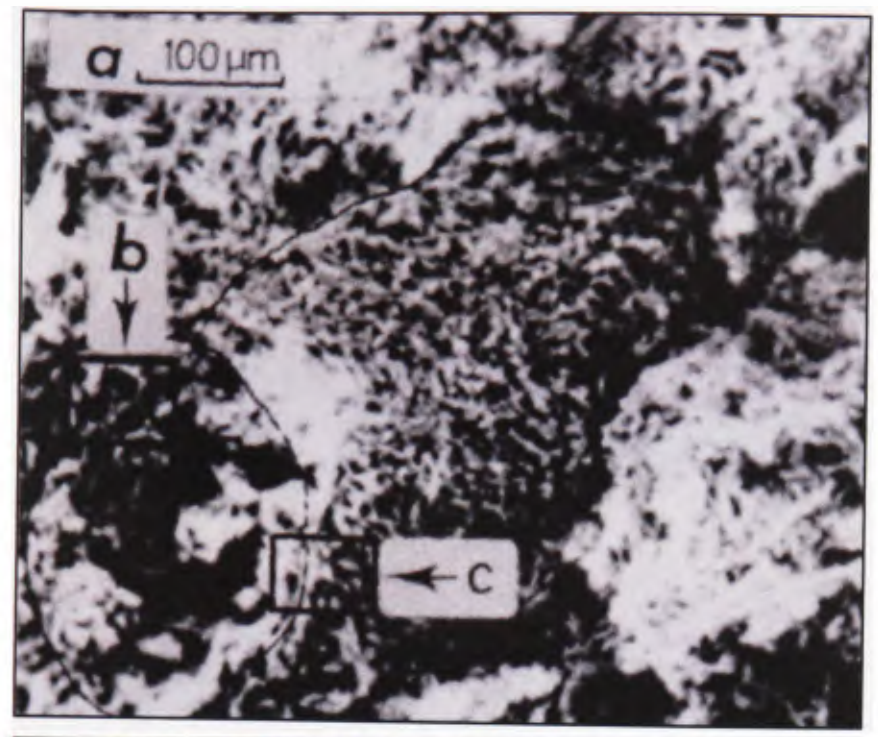
Detail of central part of (c) above. Fibrillar material (arrow) is **cell wall** material; composition not determined, possibly cellulose. **Micron-sized calcite plates** are located between **cells** in position of **middle lamella**. SEM. (Klappa, `80)



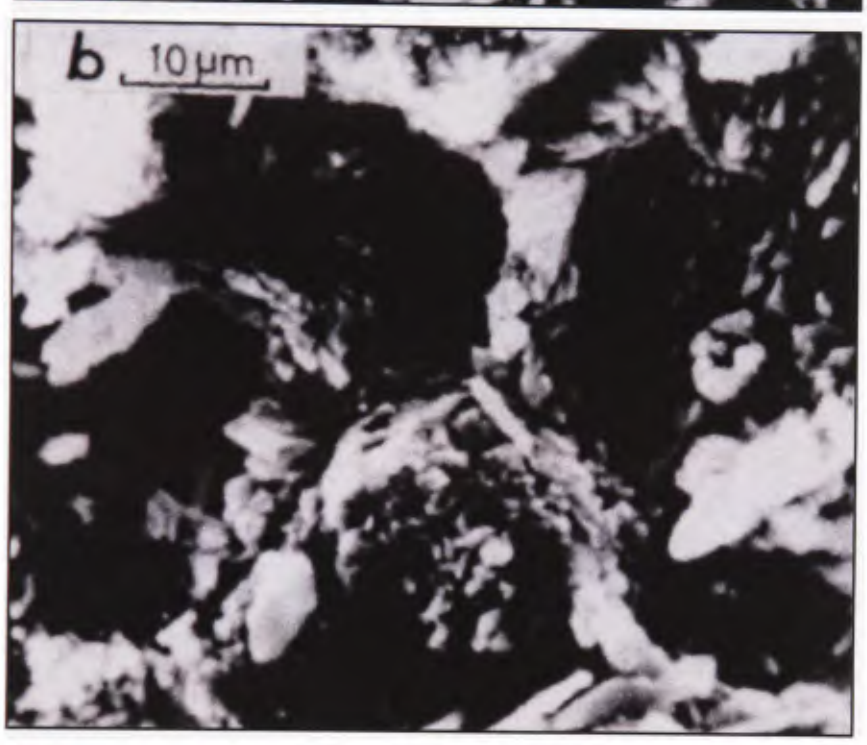
Outer surface of **epidermis**, including **root hair** (R). Composition not determined. SEM. Location: top right of (a) above. (Klappa, `80)



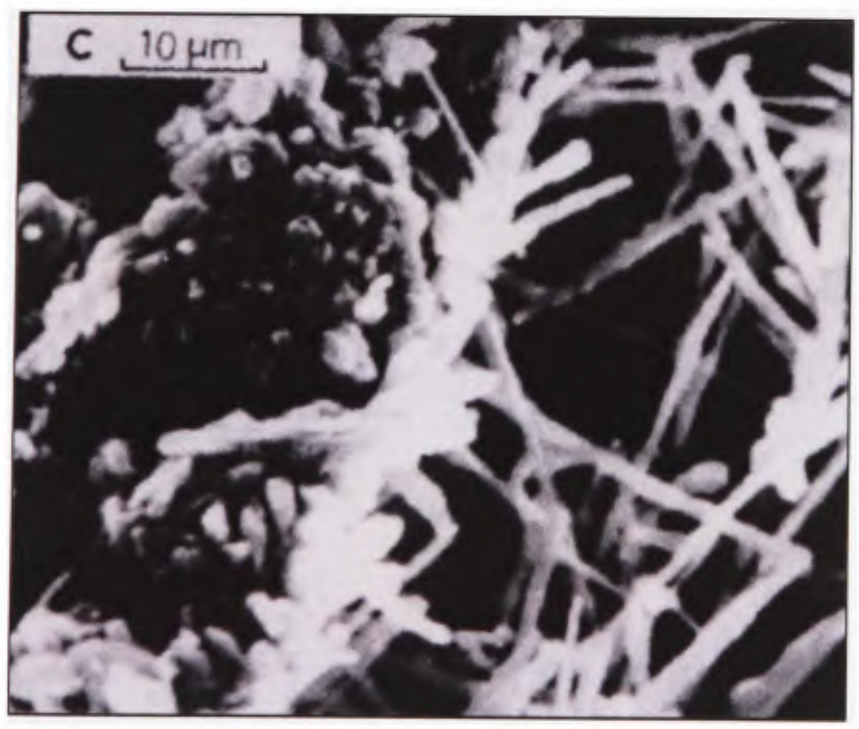
Detail of (e) above. Note **microporosity** resulting from selective loss of **cell wall material**. SEM. (Klappa, `80)



Calcified root with long axis lying NE-SW in photomicrograph. SEM. Location (and for fig. b-f): Salou, NE Spain; hardpan of Pleistocene calcrete. (Klappa, `80)



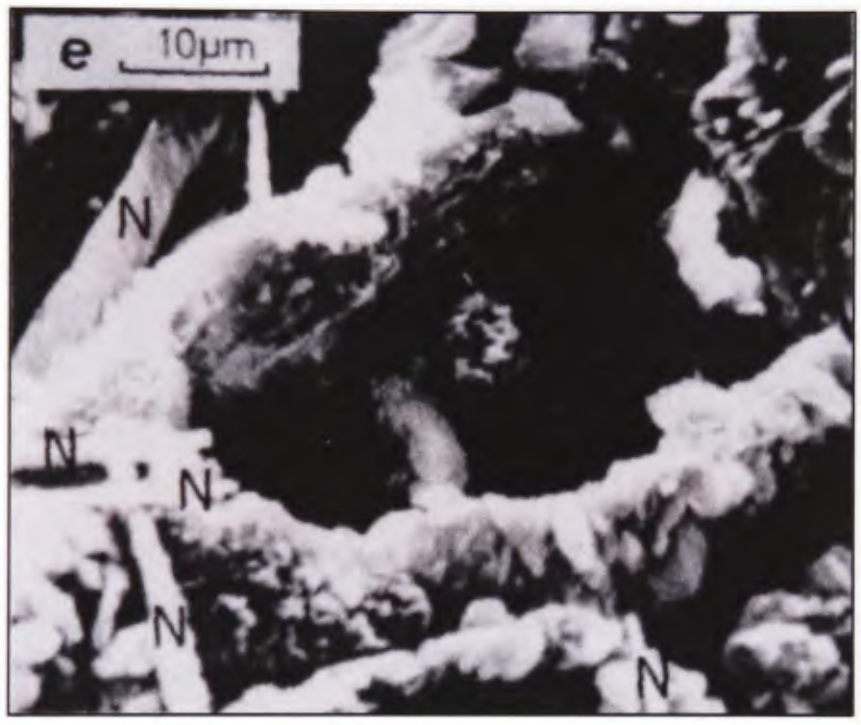
Calcified walls of (?) xylem vessels composed of **rhombic micrite (micron-sized calcite grains)**. SEM. (Klappa, `80)



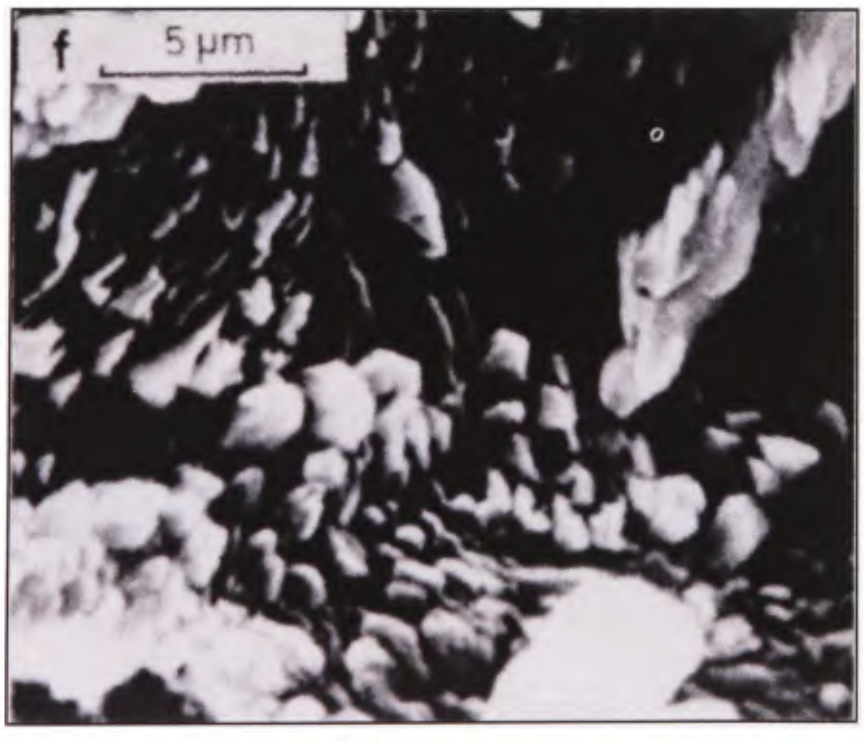
Outer wall of **rhizolith** shown in (a) above. Wall is composed of **micron-sized calcite grains**. Hyphantic **needle-fibre calcite** occurs in **voids** within and around rhizolith. SEM. (Klappa, `80)



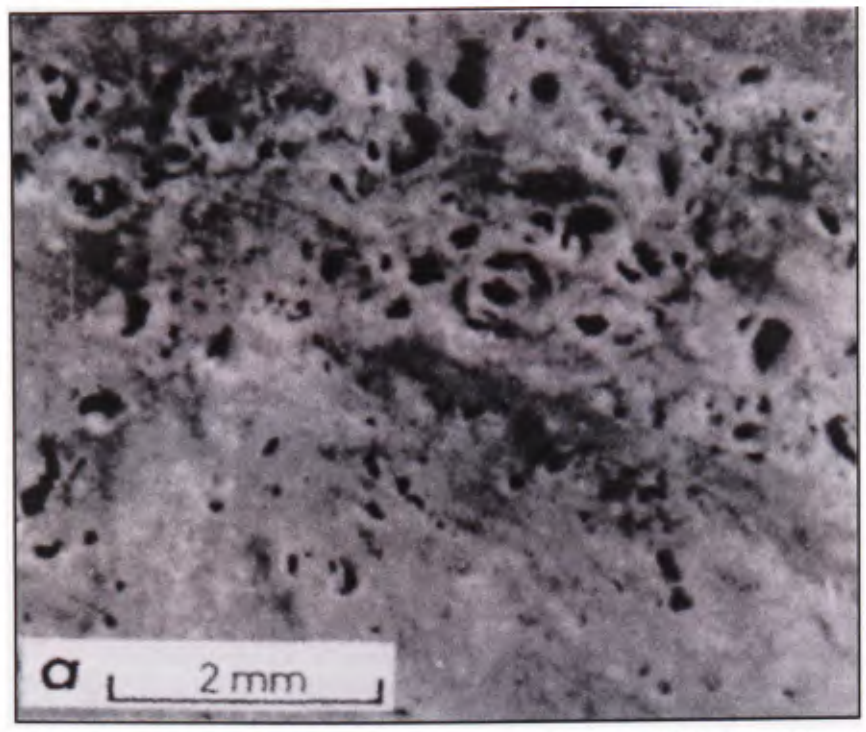
Calcified parenchymatous cells of root. Note cell contents have not been calcifled; cells are empty. SEM. (Klappa, `80)



Detail of top right cell in (d) above showing empty cell. **Calcite needles** (N) show a random distribution. SEM. (Klappa, `80)



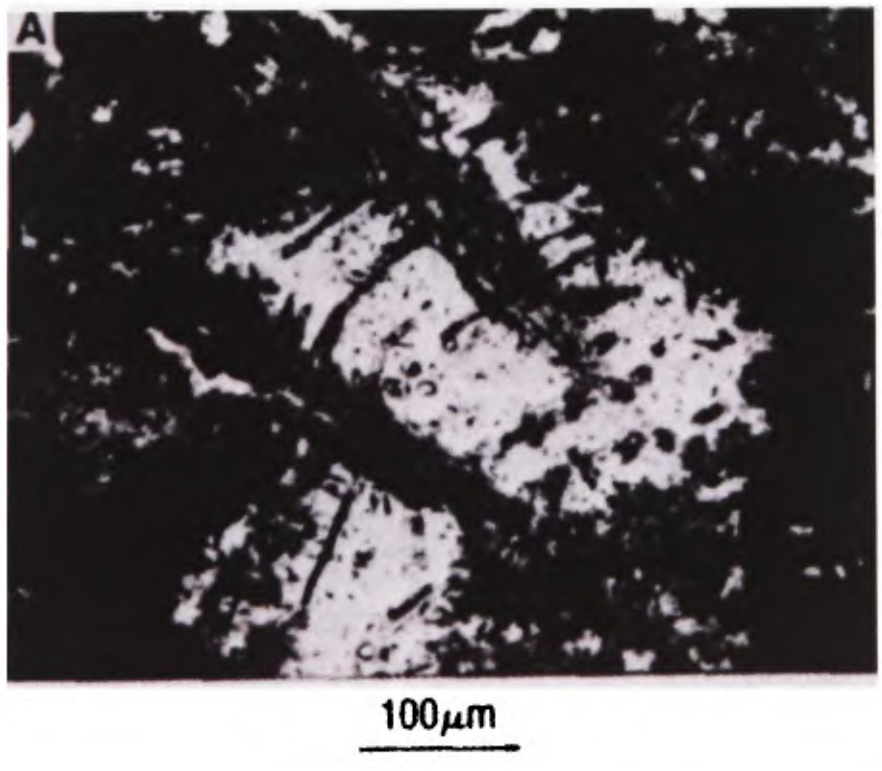
Detail of inner surface of calcified cell wall shown in (e) above. **Calcite** consists of **micron-sized plates** oriented perpendicular to the wall surface. Plates have been overlain partly by a **second generation equant micron-sized epitaxial calcite**. SEM. (Klappa, `80)



Vertical section through calcrete hardpan. **Tubular voids** are **root moulds.** Some moulds contain cylinders composed of **microcrystalline calcite** to give an **alveolar texture.** Polished slab. Cala Bassa, Ibiza; calcrete hardpan of Pleistocene age. (Klappa, `80)



Photo showing irregular **spar-filled voids** surrounded by coatings of vaguely **laminated micrite.** Interpreted as **rhizocretions.** Scale bar represents 0.5 mm. (Adams, `80)

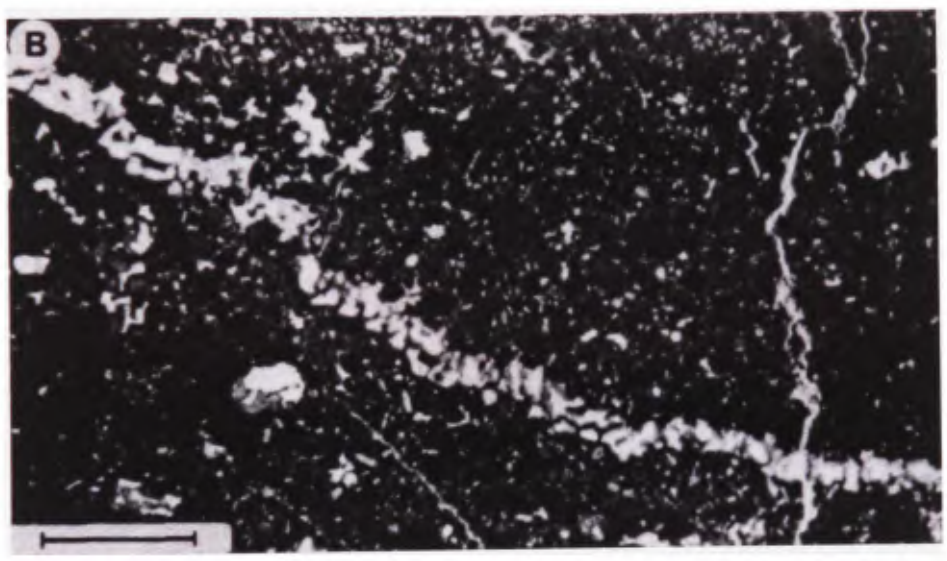


Thin section photo of the interior of a caliche **pisolite, showing roolets** of dune plants. (Beier, `87)

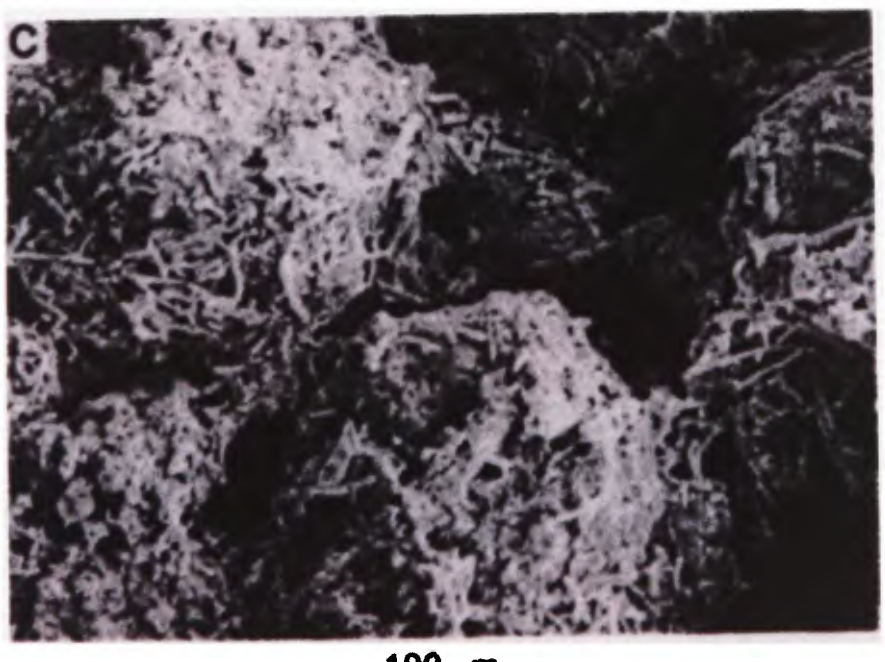


SEM photo. **Plant fibres** in a calcareous crust. Insert shows the same type of structure as seen in thin section with a petrographic microscope. Maximum width of the structure shown in the insert is 20 µm. (Kahle, '77)

Tubular Structures



A **lithoclast** from Heatherslade Geosol at Miskin. A **bifurcating tubular structure** runs from the upper left corner of the sample. The lithoclast is an **oolitic** grainstone. The tube is cross-cut by **irregular, arcuate, bifurcating micrite septae** forming an **alveolar-spetal structure**. Scale bar represents 3 mm. (Wright, '86)



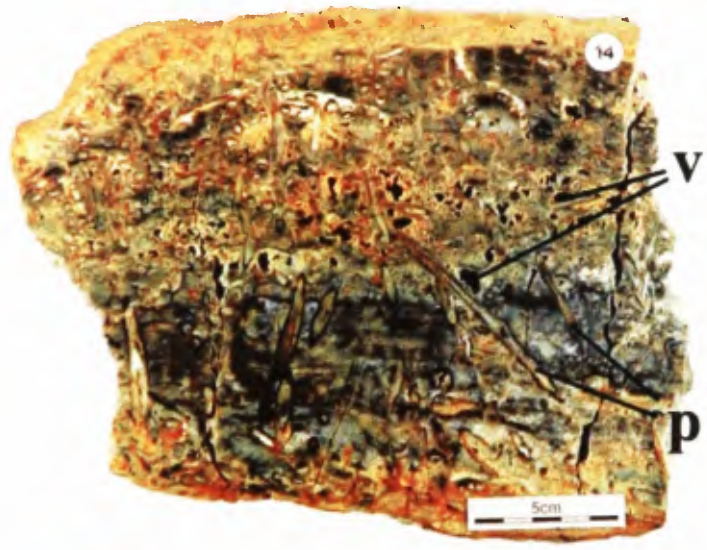
SEM photo of **calcified tubules**, probably of algal origin, which coat and bind together grains inside the **pisolite**, and appear as **micrite cement** in thin section. (Beier, '87)



SEM photo. Structures interpreted as **worms** in a calcareous crust. (Kahle, '77)

Vugs

Cherts and carbonates may contain well-preserved plants, the latter often **autochthonous** with upright stems, prostrate or flattened stems; or **allochthonous**, inverted stems. Sediment and silica and calcite cement forming geopetal in-fills are often seen within plant straws and vugs or cavities within the chert or carbonate. Vugs that have not been totally occluded by silica or calcite cements are typically lined by euhedral (well formed) quartz or calcite crystals.

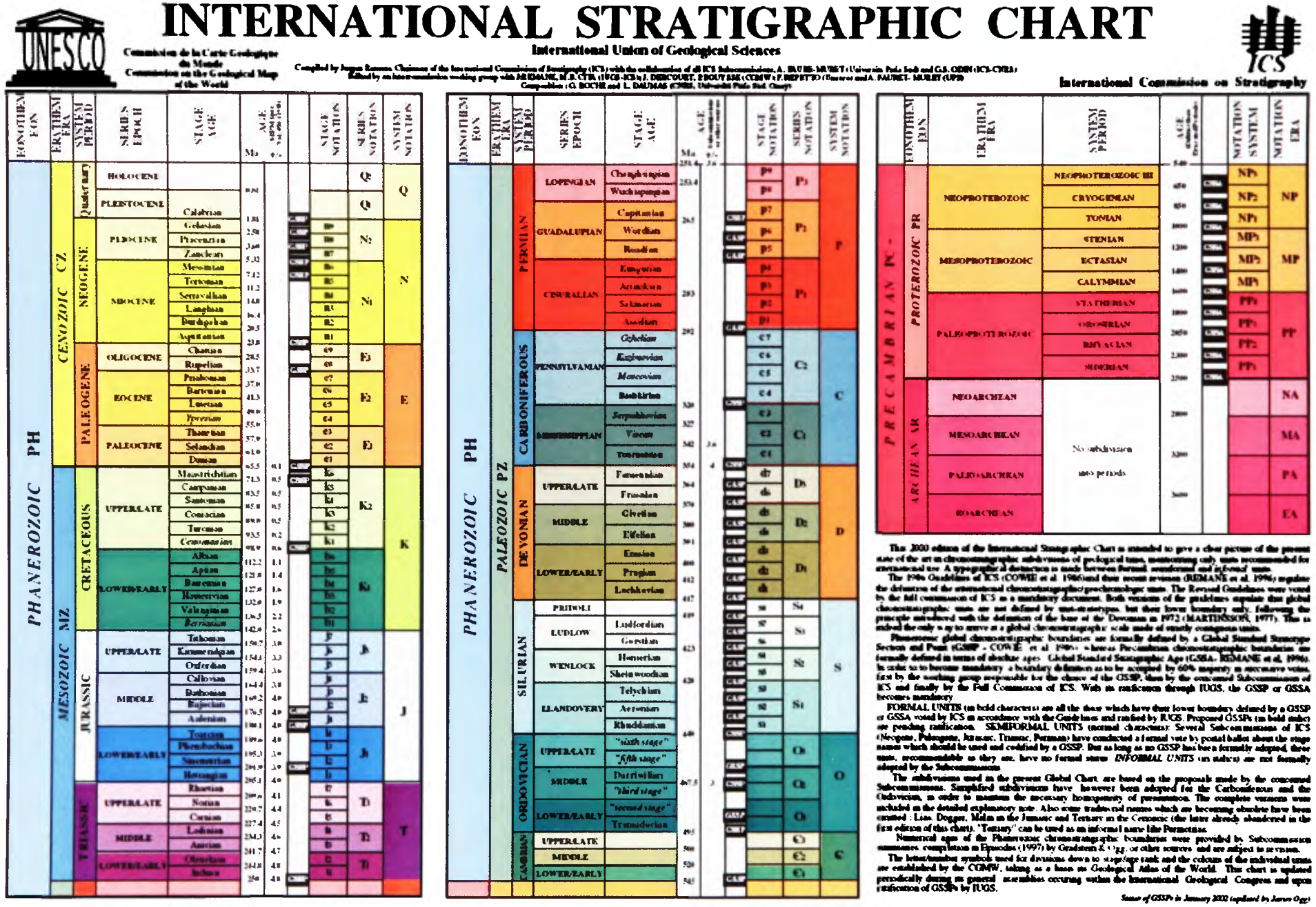


Bed of predominantly massive and vuggy chert showing vugs (**v**) and well preserved, inverted plant stems of *Ventarura lyonii* (**p**). In this case these plants have been transported and were then preserved in the chert upside down.



Polished slab of predominantly massive and vuggy chert with exceptionally well preserved stems of the plant *Rhynia gwynne-vaughanii* in growth position. The crude lamination in the centre of the bed most likely represents a silicified microbial mat that in life probably bound the plant stems.

APPENDIX 2


INTERNATIONAL STRATIGRAPHIC CHART
International Union of Geological Sciences
International Commission on Stratigraphy
UNESCO
Commission de la Carte Géologique du Monde
Commission for the Geological Map of the World
ICS
PHANEROZOIC PH
CENOZOIC CZ
MESOZOIC MZ
PALEOZOIC PZ
PRECAMBRIAN PC - PROTEROZOIC PR - ARCHEAN AR
Quaternary
NEOGENE
PALEOGENE
CRETACEOUS
JURASSIC
TRIASSIC
PERMIAN
CARBONIFEROUS
DEVONIAN
SILURIAN
ORDOVICIAN
CAMBRIAN
NEOPROTEROZOIC
MESOPROTEROZOIC
PALEOPROTEROZOIC
NEOARCHEAN
MESOARCHEAN
PALEOARCHEAN
MESOARCHEAN
NEOPROTEROZOIC III
CRYOGENIAN
TONIAN
STENIAN
ECTASIAN
CALYMMIAN
STATHERIAN
OROSIRIAN
RHYACIAN
SIDERIAN
No subdivision into periods
Compiled by Jacques Remane, Chairman of the International Commission of Stratigraphy (ICS) with the collaboration of all ICS Subcommissions, A. BAUDIS-MURET (Université Paris Sud) and G.S. ODIN (ICS-CNRS)
Edited by an intercommission working group with M.REMANE, M.B.CITA (ICGI-ICS) & J. DERCOURT, P.BOUYSSE (CCMW) F.BIJPETTO (Florence) and A. FAURET- MURET (UPS)
Composition : G. BOCHE and L. DAUMAS (CNRS, Université Paris Sud, Orsay)
The 2000 edition of the International Stratigraphic Chart is intended to give a clear picture of the present state of the art in chronostratigraphic subdivisions of geological times, monitoring only units recommended for international use. A typographical distinction is made between Formal, unconfirmed and informal units.
The 1996 Guidelines of ICS (COWIE et al. 1986)and their recent revisions (REMANE et al. 1996) regulate the definition of the international chronostratigraphic/geochronologic units. The Revised Guidelines were voted by the full commission of ICS as a mandatory document. Both versions of the guidelines stipulate that global chronostratigraphic units are not defined by unit-stratotypes, but there lower boundary only, following the principle introduced with the definition of the base of the Devonian in 1972 (MARTINSSON, 1977). This is indeed the only way to arrive at a global chronostratigraphic scale made of exactly contiguous units.
Phanerozoic global chronostratigraphic boundaries are formally defined by a Global Standard Stratotype Section and Point (GSSP - COWIE et al. 1986) whereas Precambrian chronostratigraphic boundaries are formally defined in terms of absolute ages: Global Standard Stratigraphic Age (GSSA- REMANE et al, 1996). In order to so become mandatory a boundary definition as to be accepted by 60% majority in successive votes, first by the working group responsible for the choice of the GSSP, then by the concerned Subcommissions of ICS and finally by the Full Commission of ICS. With its ratification through IUGS, the GSSP or GSSA becomes mandatory.
FORMAL UNITS (in bold characters) are all the those which have their lower boundary defined by a GSSP or GSSA voted by ICS in accordance with the Guidelines and ratified by IUGS. Proposed GSSPs (in bold italic) are pending ratification. SEMIFORMAL UNITS (normal characters): Several Subcommissions of ICS (Neogene, Paleogene, Jurassic, Triassic, Permian) have conducted a formal vote by postal ballot about the stage names which should be used and codified by a GSSP. But as long as no GSSP has been formally adopted, these units, recommendable as they are, have no formal status. *INFORMAL UNITS* (in italics) are not formally adopted by the Subcommissions.
The subdivisions used in the present Global Chart, are based on the proposals made by the concerned Subcommissions. Simplified subdivisions have however been adopted for the Carboniferous and the Ordovician, in order to maximum the necessary homogeneity of presentation. The complete versions were included in the detailed explanatory note. Also some traditional names which are becoming obsolete have been retained : Lias, Dogger, Malm in the Jurassic and Tertiary in the Cenozoic (the latter already abandoned in the first edition of this chart). "Tertiary" can be used as an informal name like Permetrias.
Numerical ages of the Phanerozoic chronostratigraphic boundaries were provided by Subcommission summaries compilation in Episodes (1997) by Gradstein & Ogg, or other sources and are subject to revision.
The letter/number symbols used for divisions down to stage/age rank and the colours of the individual units are established by the CCMW, taking as a base the Geological Atlas of the World. This chart is updated periodically during its general assemblies occuring within the International Geological Congress and upon ratification of GSSPs by IUGS.
Status of GSSPs in January 2002 (updated by Jansen Ogg)

Appendix 3: Inventory of sediments analysed.

Appendix 3: Inventory of sediments analysed.

Site	Sample No.	Description	GPS	Depth	Environment
		BOTSWANA			
B-NG1		A large calcrete quarry on the eastern edge of Ngwaku Pan exposes a 3.0 m sequence.	20`38.23 S / 22`45.15 E		Ngwaku Pan
	NG1a	Calcrete cemented conglomerate containing very poorly sorted well rounded quartz clasts.		Surface	
	NG1b	Finely laminated calcrete.		0.5 m below the surface.	
	NG1 - 1.5 m	Massive calcrete.		1.5 m below the surface.	
	NG - 3.0 m	Ghanzi Group basement.		3.0 m below the surface.	
B01	B/2000/01/A	Sample collected from a shallow borrow in the base of the Molopo Valley. Sample is very soft and only poorly indurated. The calcrete is capped by Kalahari dunes on either side of the valley.	26`37.39 S / 22`03.50 E	10 m below surface	Molopo River valley
B02		A 4.0 m sequence exposed in the southern calcrete terrace of Molopo Valley.	26`34.39 S / 22`05.64 E		Molopo River valley
	B/2000/02/A	Upper surface of southern bank / terrace. Hardpan / massive calcrete.		surface	
	B/2000/02/B	Nodular calcrete.		2.5 m below the surface.	
	B/2000/02/C	Massive calcrete.		4.0 m below the surface.	
B03		Borrow pit in the upper northern bank of the Molopo River. Section is approx. 1.75 m deep exposed 1 m below the surface, upper 1 m is composed of Kalahari sand.	26`12.34 S / 22`19.61 E		Kalahari surface above the Molopo Valley

Appendix 3: Inventory of sediments analysed.

	B/2000/03/A	Hardpan calcrete with nodules and laminations on the upper surface. Located approx. 1 m below the surface. Upper 1 m is Kalahari sand. Zone is approx 0.3 m thick.		1 m below the surface.	
	B/2000/03/B	Powdery calcrete poorly consolidated, although it contains patches and horizons which are more consolidated. Zone is approx 1.3 m thick.		2 m below the surface	
	B/2000/03/C	Honeycomb nodular calcrete with associated powdery calcrete forming the matrix. Zone exposed is approx 0.3 m thick.		2.8 m below the surface.	
B04		3.0 m section of calcrete exposed in borrow pit on the Kalahari plain above the northern bank of the Molopo Valley. Calcrete buried by approx. 1.0 m of Kalahari sand. Veg comprises large Acacia trees and grassy understory.	25`57.77 S / 22`27.03 E		Kalahari surface above the Molopo Valley
	B/2000/04/A	Hardpan calcrete approx 1 m below Kalahari dune sand. Zone of hardpan is approx. 0.5 m thick.		1 m below the surface.	
	B/2000/04/B	Nodular / powdery calcrete. Zone is approx. 1.0 m thick.		2.5 m below the surface.	
	B/2000/04/C	Massive calcrete. Zone exposed is 0.5 m thick.		3.5 m below the surface.	
B05		Borrow pit located on the Kalahari plain above the northern bank of the Molopo Valley. Upper 2 m is composed of a poorly developed soil within the aeolian sand. Between the two sample positions is approx. 1.0 m of nodular poorly lithified calcrete with a powdery matrix. Veg comprises approx. 5 m tall Acacia trees with grassy understory.	25`41.82 S / 22`42.37 E		Kalahari surface above the Molopo Valley
	B/2000/05/A	Hardpan calcrete.		2 m below the surface	
	B/2000/05/B	Massive calc-silcrete		3.2 m below the surface	

Appendix 3: Inventory of sediments analysed.

B24		A 3.0 m deep borrow pit at Moremaoto exposed a 1.0 m thick upper brown organic rich soil which is underlain by a nodular/massive moderately consolidated calc-silcrete which grades into a powdery poorly consolidated silcrete. Vegetation is Accacia woodland.	20`22.29 S / 24`21.13 E		
	B/2000/24/A	Nodular/massive calc-silcrete.		1.5 m below the surface	
	B/2000/24/B	Massive poorly consolidated silcrete.		3.0 m below the surface.	
B25	B/2000/25/A	A sample of poorly consolidated sandy calc-silcrete containing small silica nodules was collected from the upper horizon on the western side of the 5 m high Boteti River terrace.	20`17.12 S / 24`16.07 E	0.5 m below the surface.	
B26		A large quarry on the north bank of the Boteti River near Lebane exposes a 4.0 m profile. The sequence consists of an upper 1.5 m thick brown sandy soil which grades into sandy sil-calcrete containing numerous silcrete nodules. At 2.0 m there is a distinct unconformity and the sil-calcrete is replaced by green coloured powdery silcrete which shows increased calcite levels down-profile. At 4.0 m there is another unconformity with the underlying massive green/grey coloured quartzitic silcrete.	20`12.47 S / 24`07.70 E		
	B/2000/26/A	Massive sandy sil-calcrete with silica nodules.		1.75 m below the surface	
	B/2000/26/B	Green coloured massive, powdery, sandy silcrete.		3.0 m below the surface.	
	B/2000/26/C	Massive powdery calc-silcrete lying above a very distinct contact with the silcrete horizon at 4.0 m below the surface.		3.7 m below the surface.	

Appendix 3: Inventory of sediments analysed.

B27		A borrow pit in the northern bank of the Boteti River exposes a 2.0 m section. The profile consists of 1.0 m of brown sandy soil underlain by massive calc-silcrete which becomes increasingly green with depth. Vegetation is bushveld with scattered trees.	20`11.23 S / 23`54.48 E		Boteti River
	B/2000/27/A	Massive powdery calc-silcrete.		1.5 m below the surface	
	B/2000/27/B	Massive powdery calc-silcrete with a strong green colouration.		2.0 m below the surface.	
B28		Borrow pit on the southern bank of the Thamalakane River exposes a 2.5 m section. The upper 0.5 m is composed of a grey alluvium.Vegetation is dominated by Mopane trees.	19`53.60 S / 23`33.06 E		
	B/2000/28/A	Powdery massive sil-calcrete.		0.5 m below the surface.	
	B/2000/28/B	Powdery massive calc-silcrete with a slight green colour.		1.5 m below the surface	
B29	B/2000/29/A	A 4.2 m profile is exposed in a borrow pit near Shorobe. The upper 0.2 m is a thin poorly developed soil which is underlain by 4 m of powdery massive calc-silcrete. The lower 2.5 m of the profile is characterised by extensive iron mottling.	19`45.37 S / 23`40.55 E	2.5 m below the surface	
B30		A borrow pit exposed a 1.8 m profile. The upper 1.0 m of the profile is characterised by brown sandy soil which overlies beige powdery dolomitic calcrete. Veg is dense Mopane forest.	19`36.82 S / 23`48.18 E		
	B/2000/30/Aa	Massive powdery dolomitic calcrete with small nodules collected at contact with the overlying poorly developed sandy brown soil.		1.0 m below the surface.	
	B/2000/30/Ab	Massive powdery dolomitic calcrete.		1.3 m below the surface.	

Appendix 3: Inventory of sediments analysed.

	B/2000/30/B	Powdery massive dolomitic calcrete, less well consolidated and friable, breaks into pellets along pseudo laminations.		1.8 m below surface.	
B31	B/2000/31/A	A 1.75 m trench exposes massive powdery sil-calcrete below a 1.2 m capping brown grey sandy soil. Surface vegetation consists of moderately thick Accacia and Combretum forest with a grassy understory.	20`23.21 S / 22`48.17 E	1.5 m below the surface	
B32	B/2000/32/A Nodules	A borrow pit exposes a 1.75 m profile showing very poorly consolidated massive sandy (creamy white colour) silcrete containing nodules developed below a 1.3 m thick poorly developed grey soil. Vegetation dominated by 15 m tall Accacia trees with smaller Accacia bushes and grassy understory.	20`17.95 S / 22`35.81 E	1.5 m below the surface	
	B/2000/32/A Matrix			1.5 m below the surface	
B33	B/2000/33/A Nodules	A borrow pit exposes a 3.2 m profile of 1.2 m thick poorly developed brown grey sandy soil capping a massive sandy calcrete profile containing nodules. The vegetation is dominated by 5 m tall Accacia trees, with 1.5 - 2 m tall Accacia bushes and grass as understory.	20`03.04 S / 22`19.03 E	2.5 m below the surface	
	B/2000/33/A Matrix			2.5 m below the surface	
B34	B/2000/34/A	A borrow pit next to the confluence of the Nhoma/Xaudun and Thaoge Rivers exposed a 4.5 m profile. An upper 0.5 m thick brown sandy soil caps a massive powdery calcrete with increasing nodule content with depth. Nodules collected at 3.5 m. Vegetation comprises thick Accacia thornveld.	19`18.75 S / 22`09.99 E	3.5 m below the surface.	Nhoma/Xaudum and Thaoge Rivers

Appendix 3: Inventory of sediments analysed.

B35	B/2000/35/A	A 0.5 m deep borrow pit close to Etsha Village revealed grey/brown alluvium overlying massive poorly consolidated calcretised sand. Surrounding vegetation is a Mopane forest with mature trees in excess of 8 m and juveniles of 3 m.	19`04.14 S / 22`16.32 E	0.5 m below the surface.	
B36		A large borrow west of Etsha 6 Village exposes a 4.0 m calc-silcrete profile. The upper 1.2 m of sediment consists of grey alluvium containing small pisoliths. Vegetation comprises Mopane forest with mature and juvenile trees.	18`57.43 S / 22`16.23 E		
	B/2000/36/A	Massive reasonably consolidated calc-silcrete with nodules.		2.0 m below the surface	
	B/2000/36/B	Large calc-silcrete nodules within the powdery matrix.		4.0 m below the surface.	
	B/2000/36/C	Nodules collected from the capping grey / light brown soil. Nodules are evident throughout the soil horizon.		0.75 m below the surface	
B37	B/2000/37/A	Hardpan/massive calc-silcrete with iron mottling exposed in a 1.5 m deep trench. Upper 1.2 m consists of grey alluvium. Vegetation comprises mixed savanna woodland.	18`48.70 S / 22`12.52 E	1.5 m below the surface	
B38		Borrow pit exposes a 2.8 m profile. Profile capped by a thin 0.3 m thick poorly developed soil. Calc-silcrete grades down-profile from nodular to massive. Surrounding vegetation is mixed savanna woodland.	18`44.59 S / 22`10.03 E		
	B/2000/38/A	Powdery calc-silcrete with small nodules.		0.5 m below the surface.	
	B/2000/38/B	Nodular calc-silcrete with powdery matrix.		1.2 m below the surface.	
	B/2000/38/C	Nodular calc-silcrete with powdery matrix. Nodules increase in size with depth.		2.8 m below the surface.	

Appendix 3: Inventory of sediments analysed.

B39		A 2.0 m profile is exposed in a borrow pit. Powdery massive calc-silcrete is developed below a 0.4 m capping of brown sandy soil.	18`27.26 S / 21`53.91 E		
	B/2000/39/A Nodules	Powdery massive calcrete with small nodules. Sample collected below the capping poorly developed sandy brown soil.		1.0 m below the surface.	
	B/2000/39/A Matrix			1.0 m below the surface.	
	B/2000/39/B Nodules	Powdery massive calcrete with small nodules.		2.0 m below the surface.	
	B/2000/39/B Matrix			2.0 m below the surface	
	B/2000/39/C	Nodules collected from the fioor of the pit where they have accumulated after weathering out of the exposed calcrete profile.		Floor of the pit, not *in situ*	
B40	B/2000/40/A	A 1.5 m deep trench near Nokaneng exposed an upper 1.0 m grey alluvium overlying massive calcrete with small poorly developed nodules and iron mottling. Vegetation comprises mixed savanna woodland.	19`41.28 S / 22`11.80 E	1.5 m below the surface.	
B41		A large borrow pit, exposes a 4.5 m section on the western bank of the Thaoge River. The upper 0.3 m consists of grey alluvium which has a sharp contact with the underlying massive, nodule free, poorly consolidated powdery silcrete.	20`10.71 S / 22`27.81 E		
	B/2000/41/A	Massive powdery silcrete.		2.0 m below the surface.	
	B/2000/41/B	Massive powdery silcrete.		4.5 m below the surface.	
B42		A 1.5 m deep trench exposes a sequence of Kalahari sand (0.5 m) overlying massive honeycomb calcrete which overlies massive silcrete. Vegetation is grassland with scattered trees.	20`33.03 S / 22`44.88 E		

Appendix 3: Inventory of sediments analysed.

	B/2000/42/A	Massive honeycomb calcrete.		0.75 m below the surface.	
	B/2000/42/B	Massive brecciated silcrete.		1.2 m below the surface.	
B43		An outcrop of hardpan calcrete underlain by silcrete on the southern maximum strandline.	20`32.94 S / 22`44.76 E		
	B/2000/43/A	Hardpan calcrete containing rounded silcrete nodules.		Surface	
	B/2000/43/B	Laminated silcrete exposed on the surface were the calcrete has eroded away.		Surface	
B44		A 2.0 m section in a borrow pit within a strandline exposed a of hardpan with silcrete nodules grading into a grey becoming beige carbonaceous siltstone. Surrounding vegetation is dominated by 3.5 m tall closely spaced Acacia trees with a thick grassy understory.	20`31.88 S / 22`45.23 E		Lake Ngami
	B/2000/44/A	A very hard, extremely well consolidated upper hardpan with green silcrete nodules.		Surface	
	B/2000/44/B	Grey carbonaceous siltstone.		1.0 m below the surface.	
	B/2000/44/C	Massive poorly consolidated beige carbonaceous sand.		1.5 m below the surface	
	B/2000/44/D	Massive moderately consolidated beige carbonaceous sand.		2.0 m below the surface.	
B45		A 2.0 m sequence exposed in a strandline quarry.	20`23.89 S / 22`56.17 E		Lake Ngami
	B/2000/45/A	Hardpan calc-silcrete.		Upper surface of strandline.	
	B/2000/45/B	Massive powdery sil-calcrete containing nodules.		1.5 m below the surface.	

Appendix 3: Inventory of sediments analysed.

	B/2000/45/C	Massive powdery sil-calcrete.		2.0 m below the surface.	
B46	B/2000/46/A	A 0.5 m profile exposed in a strandline south of the Nhabe River. Surface hardpan grades down-profile into massive calcrete with poorly consolidated nodules. Underlying the calcrete is a massive grey silty sand with silcrete nodules and fine grained basement at the base of the sequence. Vegetation is typical thornveld - Acacia trees (2.5 m tall) with thin grassy understory.	20`24.85 S / 22`56.64 E	0.3 m below surface level.	Lake Ngami
B47		A 2.0 m section exposed in a borrow pit. Upper 0.3 m of grey sand overlies massive nodular calcrete which grades into massive calcrete with floating nodules. At 1.7 m there is a poorly developed hardpan which grades down-profile into friable massive calcrete. Vegetation is Acacia dominated thornveld.	20`26.09 S / 22`55.69 E		
	B/2000/47/A	Massive nodular calcrete.		0.5 m below the surface.	
	B/2000/47/B	Massive calcrete containing small floating nodules.		1.3 m below the surface.	
	B/2000/47/C	Friable massive powdery calcrete.		2.0 m below the surface.	
B48		A borrow pit near Mogapelwa Village exposed a 2.5 m profile consisting of a thin sandy soil (0.2 m) underlain a laminated hardpan which grades into nodular calcrete. Vegetation is dominated by Acacia thornveld.	20`28.45 S / 22`54.79 E		
	B/2000/48/A	Laminated hardpan.		0.2 m below the surface.	
	B/2000/48/B	Nodular calcrete (clast supported with the nodules varying in size from 2 - 10 cm).		0.5 m below the surface.	
	B/2000/48/C	Nodular calcrete. Nodules are large (up to 20 cm) and irregularly shaped. The calcrete is clast supported.		1.5 m below the surface.	

Appendix 3: Inventory of sediments analysed.

	B/2000/48/D	Nodular calcrete. Nodules are of mixed size - some large nodules (20 cm) and some smaller of regular and irregular shape.		2.0 m below the surface.	
B49		A 4.0 m quarry section on the edge of Tswelenyane Pan showing a range of calcrete morphologies. Vegetation is mixed, very thick Acacia forest (10 m tall trees) with a thick bushy understory.	20`31.28 S / 22`51.47 E		Tswelenyane Pan
	B/2000/49/A	Hardpan calcrete collected from below a 1.2 m thick capping brown/grey sandy soil.		1.3 m below the surface.	
	B/2000/49/B	Granular/nodular calcrete with a powdery matrix. Poorly consolidated.		2.5 m below the surface	
	B/2000/49/C	Massive poorly consolidated powdery calcrete.		3.0 m below the surface.	
	B/2000/49/D	Massive calcrete, moderately consolidated with angular and rounded lithic fragments.		3.8 m below the surface.	
B50		A 2.0 m section exposed in a quarry on the edge of Tale Pan. Profile consists of 0.5 m of grey sandy soil overlying a 0.5 m thick hardpan which grades into green coloured sandstone. Vegetation is dominated by scattered Acacia trees (3 m tall) with a grassy understory.	20`33.92 S / 22`48.86 E		Tale Pan
	B/2000/50/A	Hardpan calcrete with lithic fragments included.		0.5 m below the surface.	
	B/2000/50/B	Green sandstone.		1.4 m below the surface.	
B51	B/2000/51/A	A shallow borrow pit (1.2 m) on the northern edge of Ngwaku Pan. The upper 1.0 m comprises brown sandy soil which is underlain by hardpan calcrete containing lithic fragments. Vegetation is thick bushveld.		1.0 m below the surface.	Ngwaku Pan

Appendix 3: Inventory of sediments analysed.

B52		A 2.0 m section exposed in a borrow pit on the edge of Txenga Pan. Sequence consists of a thin 0.2 m grey sandy soil underlain by hardpan which grades into powdery becoming massive calcrete. The base of the sequence exposes partially calcretised Ghanzi Group basement.	20`47.59 S / 22`40.73 E		Txenga Pan
	B/2000/52/A	Hardpan calcrete.		0.2 m below the surface.	
	B/2000/52/B	Moderately consolidated massive calcrete.		1.5 m below the surface.	
	B/2000/52/C	Calcretised bedrock.		2.0 m below the surface.	
B53		A large quarry adjacent a dry river bed exposes a 3.75 m profile. The sequence consists of an 1.0 m thick grey alluvium which overlies nodular calcrete which grades down-profile into boulder calcrete. At 2.5 m there is an unconformity and the boulder calcrete is replaced by massive friable calcrete which grades down-profile into the calcretised bedrock. Vegetation is Acacia thorn/bushveld.	20`55.64 S / 22`33.53 E		
	B/2000/53/A	Nodular calcrete with a powdery matrix. Nodules are of mixed size and range from 2-15 cm and are regular and irregular in shape.		1.0 m below the surface.	
	B/2000/53/B	Large nodular / boulder calcrete.		2.0 m below the surface.	
	B/2000/53/C	Massive calcrete which breaks along sub vertical planes of weakness.		2.5 m below the surface	
	B/2000/53/D	Massive calcrete, creamy colour, breaks along sub vertical planes of weakness.		3.0 m below the surface.	
	B/2000/53/E	Massive carbonate cemented sandstone with lithic fragments.		3.5 m below the surface.	

Appendix 3: Inventory of sediments analysed.

B64	B/2000/64/A	Massive calcrete grading down-profile into calc-silcrete collected from below 0.5 m of red/brown sandy soil (Kalahari dune sand) in borrow pit.	23`18.89 S / 22`26.75 E	1.0 m below the surface	Pedogenic
B65	B/2000/65/A	Massive cal-silcrete collected from below 0.75 m of Kalahari sand in a borrow pit.	23`37.60 S / 22`42.44 E	1.5 m below the surface	Pedogenic
B66	B/2000/66/A	Massive calcrete with nodules collected below 0.5 m capping of red/brown Kalahari sand in trench excavated for a pipeline. Vegetation is grassveld with scattered Accacia trees and small bushes.	23`46.67 S / 22`30.23 E	1.0 m below the surface	Pedogenic
B67	B/2000/67/A	Massive calcrete with nodular inclusions. Sample collected below 1.0 m of Kalahari sand in trench excavated for pipeline.	23`50.37 S / 22`15.73 E	1.3 m below the surface	Pedogenic
B68	B/2000/68/A	Massive cal-silcrete collected below 0.5 m of Kalahari sand. Sample collected from a trench excavated for a pipeline.	23`55.27 S / 22`01.21 E	1.0 m below the surface	Pedogenic
B69	B/2000/69/A	Hardpan/massive calcrete sample collected from the exposed surface north of Tshane. Shows distinct hardpan laminations and nodules within the matrix. Surface covered by thin horizon of red Kalahari sand. Vegetation is thick bushveld/thornveld (Accacia trees 2.5/3.0 m tall very close together) with heavily overgrazed grassy understory.	23`59.56 S / 21`51.50 E	Surface	Pedogenic
B70	B/2000/70/A	Massive/hardpan calcrete collected in 1 m above Kakwe Pan. Surrounded by very sandy (white fluvial sand) surface material probably deflated from the pan. Vegetation comprises scattered Acaccia trees with no grassy understory.	24`01.81 S / 21`52.32 E	1.0 m above the pan floor	Kakwe Pan
B71	B/2000/71/A	Hardpan/massive calcrete collected from outcropping ridge. Sample shows a range of structures: laminations on the outer surface, brecciation, veining, etc.	23`56.84 S / 21`49.88 E	Surface	Pedogenic

Appendix 3: Inventory of sediments analysed.

B72	B/2000/72/A	Hardpan/massive calcrete collected from outcropping terrace on the northern rim of Pepane Pan at the interface between the red Kalahari dune sand and the grey sandy silt of the pan surface.	23`52.99 S / 21`48.27 E	0.2 m above the pan floor in terrace	Pepane Pan
B73	B/2000/73/A	Massive calcrete collected from a shallow terrace on the eastern rim of Tshotswa Pan which is covered by a thin layer (20 cm) of grey/red/brown fine silt and sand. Vegetation on the pan perimeter is grass with a few low Accacia bushes. Pan is completely devoid of vegetation.	23`44.31 S / 21`43.73 E	0.2 m above the pan floor in terrace	Tshotswa Pan
B74	B/2000/74/A	Calc-dolocrete collected from an outcrop in the floor of the silty, grass covered Ohe Pan.	23`32.96 S / 21`38.04 E	Pan surface	Ohe Pan
B75	B/2000/75/A	Massive/hardpan calcrete collected from a shallow terrace on the eastern margin of the grass covered Hunhukwe Pan. Surrounding vegetation comprises Accacia Tortilus (scattered) with grassy understory - savanna woodland.	23`26.16 S / 21`29.45 E	0.2 m above the pan floor in terrace	Hunhukwe Pan
B76	B/2000/76/A	Massive sandy calcrete was collected from a surface outcrop in the inter-dunal depression between two linear Kalahari dunes on the edge of Mamasi Pan.	23`18.08 S / 21`07.43 E	Surface	Mamasi Pan
B-RC		A large linear dune has been disected by the Okavango River and exposes a 15 m section. The upper 11 m of the dune comprise red Kalahari aeolian sand. Below this there is a gradational boundary with a underlying calcrete sequence which is in excess of 4 m thick (only 4 m is exposed above the water level). The upper dune surface is characterised by thick forest cover and as one travels further north one noticies these large linear dunes spaced approx. every 2 km.	18`28.77 S / 22`04.81 E		Okavango River
	11 m	Sample collected from the upper calc-silcrete horizon.		11 m below surface	

Appendix 3: Inventory of sediments analysed.

	12 m	Well consolidated silcrete.		12 m below upper surface	
	13 m	Well consolidated calc-silcrete.		13 m below upper surface	
B-Sepupa		A sample of consolidated massive sil-calcrete collected from an outcrop next to Sepupa Village on the western terrace of the Okavango River.	18`46.27S / 22`14.56 E	Surface	Okavango River
B-3BRDG		A sample of very well consolidated massive calcrete was collected from a shallow borrow pit close to the 3rd Bridge in Moremi.	19`15.31 S / 23`20.70 E	0.5 m below the surface.	
OK12		Sample collected from 2.5 m high terrace of grey calc-silcrete on the western bank of the Okavango River.	18`21.58 S / 21`50.77 E	2.5 m below the surface.	Okavango River
OK13		A 4.5 m silcrete terrace on the western bank of the Okavango River. Vegetation characterised by very large trees.	18`16.67 S / 21`47.20 E		Okavango River
	2.0 m	Moderately consolidated silcrete cemented sand.		2.0 m below the surface.	
	4.0 m	Very poorly consolidated and highly porous silty material collected just above the water level.		4.0 m below the surface.	
Mosupatsela Island		Samples collected from Mosupatsela Island on the Jao River.	19`08.08 S / 22`37.01 E		
	Mosupatsela A 150 cm	Sample collected 5 m from the perimeter of the island. Veg dense ripariari woodland.		1.5 m below the surface.	
	Mosupatsela B 200 cm	Sample collected 50 m from the perimeter of the island. Veg mixed woodland, palms and grass.		2.0 m below the surface.	
	Mosupatsela C surface	Sample grey biocrust collected from surface of a 0.75 m inspection pit dug at centre of the island 200 m from the perimeter.		Surface	
	Mosupatsela C 20 cm	Grey alluvial sand.		0.2 m below the surface.	

Appendix 3: Inventory of sediments analysed.

	Mosupatsela C 50 cm	Grey alluvial sand with mottles.		0.5 m below the surface.	
Gaenga Island		Samples collected a 0.4 m inspection pit dug in the centre of Gaenga Island on the Nqoga River.	19`04.11 S / 22`49.24 E		
	Gaenga surface	White biocrust collected from the surface.		Surface	
	Gaenga 20 cm	Grey fluvial sand.		0.2 m below the surface.	
	Gaenga 40 cm	Dark grey fluvial sand.		0.4 m below the surface.	
Xhamoga Island		Samples were collected from 4 inspection pits dug in a transect across Xhamoga Island on the Santantadibe River.	19`09.84 S / 23`07.94 E		
	Xhamoga A surface	Surface sample collected from inspection pit dug 10 m from the active channel.		Surface	
	Xhamoga A 20 cm			0.2 m below the surface.	
	Xhamoga A 40 cm			0.4 m below the surface.	
	Xhamoga A 60 cm			0.6 m below the surface.	
	Xhamoga B surface	Surface sample collected from inspection pit dug 50 m from the active channel.		Surface	
	Xhamoga B 20 cm			0.2 m below the surface.	
	Xhamoga B 40 cm			0.4 m below the surface.	
	Xhamoga B 60 cm			0.6 m below the surface.	
	Xhamoga B 80 cm			0.8 m below the surface.	
	Xhamoga B 100 cm			1.0 m below the surface.	

Appendix 3: Inventory of sediments analysed.

	Xhamoga B 120cm			1.2 m below the surface.	
	Xhamoga B 140 cm			1.4 m below the surface.	
	Xhamoga B 160 cm			1.6 m below the surface.	
	Xhamoga B 180 cm			1.8 m below surface.	
	Xhamoga C surface	Surface sample collected from inspection pit dug 75 m from the active channel.		Surface	
	Xhamoga C 20 cm			0.2 m below the surface.	
	Xhamoga C 40 cm			0.4 m below the surface.	
	Xhamoga C 60 cm			0.6 m below the surface.	
	Xhamoga C 90 cm			0.9 m below the surface.	
	Xhamoga D surface	Surface sample collected from shallow inspection pit dug 85 m from the active channel on the edge of the central pan.		Surface	
	Xhamoga D 20 cm			0.2 m below the surface.	

NAMIBIA					
L1A	L/1999/1/A	Sample taken from the top of a sloping sequence which was approx. 3.5 m above the contemporary floodplain. Sample is a pedogenic calc-silcrete developed beneath a thin capping of Kalahari sand.	18`01.79 S / 23`19.08 E	Calcrete sampled 0.1 m below the surface.	Incised bank on the edge of the Kwando fioodplain.

Appendix 3: Inventory of sediments analysed.

L1B		Calcrete quarry, alternating horizons of powdery calcrete with nodules and massive calcrete.			Terrace on the edge of the Kwando River floodplain.
	L/1999/1B 2.0 m	Powdery calcrete with nodules. Colour 5Y 8/2		2.0 m below the surface.	
	L/1999/1B 2.5 m	Massive calcrete. Colour 10YR 8/1		2.5 m below the surface.	
	L/1999/1B 3.0 m	Powdery calcrete with nodules. Colour 5Y 8/2		3.0 m below the surface.	
	L/1999/1B 3.5 m	Massive calcrete. Colour 5Y 8/2		3.5 m below the surface.	
L3		Calcrete quarry in the terrace on the edge of the Kwando fioodplain. Grey aeolian reworked/fluvial sand overlying a horizon of powdery calcrete (0.5 m thick) underlain by massive calcrete with small nodules.	18`02.48 S / 23`19.24 E		Terrace on the edge of the Kwando River fioodplain.
	L/1999/3 - 1.5m	Partially calcretised fluvial sand.		1.5 m below the surface.	
	L/1999/3 - 2.0m	Powdery calcrete with minor nodules.		2.0 m below the surface.	
	L/1999/3 - 2.5m	Indurated massive calcrete with nodules.		2.5 m below the surface.	
	L/1999/3 - 3.0m	Indurated massive calcrete with nodules.		3.0 m below the surface.	
	L/1999/3 - 3.5m	Less well indurated calcrete with nodules.		3.5 m below the surface.	
L4A	L/1999/4/A	A large Borrow pit. Upper 0.75 m comprises brownish/grey fluvial/aeolian soil. Below 0.75 m the calcium carbonate content increases down profile and at 2.5 m massive calcrete replaces the powdery calcrete which has become more indurated with depth. Surface vegetation is stunted Mopane woodland.	18`12.11 S / 23`30.90 E		Pedogenic

Appendix 3: Inventory of sediments analysed.

L4B	L/1999/4B - 2.0 m	Well indurated massive calcrete.		2.0 m below the surface.	
	L/1999/4B - 3.0 m	Calcrete quarry, extremely hard massive calcrete		3.0m below the surface.	
L5		A very large calc-silcrete quarry close to Lake Liambezi. A poorly developed soil overlies sandy silcrete with carbonate nodules, underlain by massive silcrete.	17`49.42 S / 24`11.18 E		Littoral sediments of Lake Liambezi
	L/1999/5 - 1.0 m	Friable poorly developed soil.		1.0 m below the surface.	
	L/1999/5 - 1.5 m	Intermediate friable sand containing carboante nodules.		1.5 m below the surface.	
	L/1999/5 - 2.0 m	Sample from top of massive silcrete.		2.0 m below the surface.	
	L/1999/5 - 2.5 m	Sample from massive silcrete at the base of the quarry.		2.5 m below the surface.	
Ekuma River / E003		Calcrete nodules collected from western bank of the Ekuma River	18`34.14 S / 15`58.62 E		Ekuma River
EO 01		Shallow borrow pit sample within the strandlines of palaeo-lake Etosha.	18`23.95 S / 16`38.14 E		Lacustrine/palustrine/pedogenic
EO 02		Shallow borrow pit north of Andoni.	18`26.54 S / 16`45.79 E		Lacustrine/palustrine/pedogenic
EO 03		Upper terrace of the Omuramba Ovambo.	18`36.51 S / 17`09.67 E		Lacustrine/palustrine/pedogenic/fluvial
Etaka / Ekuma River / T1 16		Sample collected from quarry in the eastern bank of the Ekuma/Etaka River.	17`51.40 S / 15`13.24 E	3.5 m below the surface.	Ekuma/Etaka River
Halali		Surface sample collected at Halali		Dolomite inselberg	Etosha Pan
Kapupuhedi		Surface sample collected at Kapupuhedi		Surface	Etosha Pan
Namutoni 10 / EO 05		Surface sample, 10 km east of Namatoni.	18`38.51 S / 17`10.51 E	Surface	Etosha Pan
Namutoni 12		Surface sample collected 12 km west of Namutoni		Surface	Etosha Pan

Appendix 3: Inventory of sediments analysed.

Ohangwena / T3 01		Sample collected from large borrow pit south of Oshikango.	17`24.77 S / 15`53.31 E	4.5 m below the surface.	Pedogenic
Okaukuejo		Surface sample collected at Okaukuejo - west		Surface	Etosha Pan
Ondangwa north / T3 02		Borrow pit north of Ondangwa. Sample collected at 5.0 m below surface, overlain by red aeolian sand 2 -2.5 m thick.	17`37.14 S / 15`54.79 E	5.0 m below the surface.	Pedogenic
Oshigambo River / E002	E002 - 1.0 m	Massive calcrete collected from eastern bank of the Oshigambo River	18`30.10 S / 16`05.87 E	1.0 m below the surface.	Oshigambo River
	E002 - 3.5 m	Sample collected at the base of exposed bank.	18`30.10 S / 16`05.87 E	3.5 m below the surface.	Oshigambo River
Odila River / OWL C1	OWL C1 - 1.8 m	Rhizolith and nodule rich upper fluvial sand with a poorly developed 0.4 m thick surface soil. Nodular calcrete horizon 0.2 m thick at 1.8 m.	18`13.91 S / 16`25.84 E	1.8 m below the surface	Odila River
	OWL C2 - 2.7 m	Massive basal calcrete with distinct contact with the overlying fluvial sand.	18`13.91 S / 16`25.84 E	2.7 m below the surface.	Odila River
Sueda		Surface sample collected at Sueda		Surface	Etosha Pan
N1	N/2000/1/A	Massive calcrete was collected from beneath a thin covering of Kalahari sand in a shallow borrow pit between the Chapmans and Rietfontein Rivers. Veg is Accacia thornveld with a grassy understory.	22`20.38 S / 19`26.64 E	0.5 m below the surface	Palustrine/pedogenic - interfluve
N3	N/2000/3/A	Sample of Karibib formation dolomitic limestone collected 2.5 m below the surface in a road cutting.	20`07.01 S / 16`09.30 E	2.5 m below the surface.	Precambrian basement
N10	N/2000/10/A	Nodular/honeycomb/hardpan calcrete exposed in an erosion gully on the western side of the Skaap River. The calcrete is developed beneath a thin veneer of red gritty sand. Vegetation is grassland with scattered Accacia trees (approx. 3 m tall) and a lot of camphor bushes.	22`56.65 S / 17`40.04 E	In situ just below surface vineer.	Skaap River
N11	N/2000/11/A	Hardpan/massive calcrete collected from a shallow borrow pit in the floor of Olifants Valley. A thin grey alluvial soil caps the calcrete. Vegetation is grassveld, no trees or bushes.	23`00.89 S / 17`51.67 E	0.2 m below the surface.	Confluence of the Skaap and Olifants Rivers

Appendix 3: Inventory of sediments analysed.

N12	N/2000/12/A	Hardpan/massive calcrete collected from below a thin covering of grey/brown alluvial soil. Surface vegetation is grassveld with a few scattered trees.	23`09.27 S / 18`08.44 E	0.2 m below the surface.	Olifants River valley
N13	N/2000/13/A	Hardpan and a conglomeratic calcrete is exposed in a 2.0 m road cutting on the western side of the Nossob River Valley. Vegetation is grassland with scattered Accacia bushes.	23`35.83 S / 18`46.76 E	2.0 m below the surface.	Nossob River valley
N14	N/2000/14/A	Hardpan and conglomeratic calcrete collected from a 1.75 m road cutting on the western side of the Nossob Valley.	24`09.42 S / 19`06.20 E	1.75 m below the surface.	Nossob River valley
N15	N/2000/15/A	Hardpan and conglomeratic calcrete was collected from a small quarry on the western side of the Nossob Valley.	24`38.35 S / 19`42.16 E	1.0 m below the surface	Nossob River valley
N16		A 1.5 m road cutting on the western bank of the Olifants River. Vegetation is grassland with scattered Accacia trees and bushes.	24`46.22 S / 18`59.11 E		Olifants River valley
	N/2000/16/A	Hardpan calcrete collected from the upper surface of a road cutting. To the east and west are large Kalahari linear dunes.		Surface.	
	N/2000/16/B	Massive dolomitic calcrete.		1.5 m below the surface.	
N17		A road cutting on the western side of the Auob River Valley.	24`51.44 S / 18`48.56 E	Auob River	
	N/2000/17/A	Hardpan calcrete from the top surface of the road cutting. Sample capping a conglomeratic horizon.		Surface	
	N/2000/17/B	Massive dolomitic calcrete.		1.5 m below the surface.	
	N/2000/17/C	Fine grained dolomitic calcrete.		4.0 m below the surface.	
N18	N/2000/18/A	Hardpan calc-silcrete collected from beneath a thin veneer of brown sandy soil. Vegetation is dominated by Accacia bushes and grass.	25`15.35 S / 18`32.67 E	Surface	Pedogenic

Appendix 3: Inventory of sediments analysed.

N19	N/2000/19/A	Massive calc-silcrete collected from beneath 0.3 m of brown sandy soil. Vegetation is grassland with occasional Accacia bushes.	25`45.93 S / 18`36.77 E	Surface	Pedogenic
N20	N/2000/20/A	Massive dolomitic-calcrete collected beneath a thin veneer of sandy soil. Vegetation is grassland with occasional Accacia bushes.	25`52.60 S / 18`45.61 E	Surface	Pedogenic
N21	N/2000/21/A	Honeycomb calc-silcrete collected from the southern edge of a 500 m diameter pan. Vegetation is grassland.	25`55.37 S / 18`59.50 E	Surface	Pan/pedogenic
N22	N/2000/22/A	Massive calc-silcrete collected from beneath a thin veneer of sediment. Slight undulations visible on the fiat plain. Vegetation is grassland with scattered bushes.	25`59.04 S / 19`14.13 E	Surface	Pedogenic
N23	N/2000/23/A	A massive calc-silcrete sample was collected from the edge of a small pan close to the western marginal of the Kalahari dunesfield (typical red aeolian sand). Further to the west the landscape becomes a fiat grassy plain.	26`16.31 S / 19`34.36 E	Surface	Pan/pedogenic
N24	N/2000/24/A	Massive calc-silcrete collected from beneath a thin veneer of sandy soil close to a series of linear Kalahari dunes. Vegetation is grassland.	26`42.18 S / 19`38.71 E	Surface	Pedogenic
		NORTHERN CAPE			
NC12		A 2.5 m borrow pit in the bank of the Doringdam River. Veg comprises small acacia bushes and grass and very scattered trees approx. 3 m tall.	28`06.34 S / 20`40.65 E		Doringdam River
	NC/2000/12/A	Sil-calcrete (very hard).		surface	
	NC/2000/12/B	Contact between the overlying hardpan / nodular sil-calcrete and the underlying Dwyka. Hard.		1.0 m below surface.	
	NC/2000/12/C	Base of the profile. Calcium carbonate replacement of the Dwyka bedrock which appears to have wavy laminations, possible bedding structures. Not very hard.		2.5 m below surface.	Bedrock

Appendix 3: Inventory of sediments analysed.

NC13		Incised Molopo River floodplain. Sample site on the eastern side of valley. Valley incised 50 m into a Nama Group plateau which forms steep scarps on either side of the valley.	28`04.04 S / 20`34.42 E		Molopo River valley
	NC/2000/13/A	Sample collected slightly above the level of the floodplain (approx. 1.5 m).		surface	
	NC/2000/13/B	Sample collected at floodplain level. Nodular silcrete / calcrete.		surface	
NC14		A 1.5 m profile exposed in a borrow pit in an interdune depression at the southern end of Vroueris Pan.	27`54.99 S / 20`27.56 E		Interdune depression in Vrouens Pan.
	NC/2000/14/A	Nodular and massive calcrete.		surface	
	NC/2000/14/B	Massive calcrete with Nababis formation bedrock influence.		1.0 m below surface	
NC15		Interdune depression, dune spacing 150-200 m apart on the western edge of the Molopo Valley. Sample from a1.5 m section in a borrow pit. Veg comprises small bushes and very little grass, lots of open space between veg and exposed sand.	27`45.65 S / 20`22.79 E		Molopo Valley/interdune depression
	NC/2000/15/A	Hardpan massive / nodular calcrete.		surface	
	NC/2000/15/B	Interface between overlying massive calcrete and underlying Nama Group bedrock.		1.0 m below surface	
NC16		Albion Pan, old Molopo floodplain north of the zone of linear Kalahari dunes. 1.5 m profile exposed in a borrow pit. Veg dominated by grass, a few bushes but no trees.	27`43.14 S / 20`21.60 E		Albion Pan/floodplain
	NC/2000/16/A	Massive and nodular calcrete (very hard).		surface	
	NC/2000/16/B	Calcification of bedrock		1.5 m below surface	
NC17	NC/2000/17	Massive / nodular calcrete sample. 2.0 m section in Hol Pan revealed that calcrete is only present as nodules in the soil horizon. Nodules are very pentiful on the surface, they have probably weathered out of the soil horizon.	27`14.54 S / 20`02.21 E	surface	Hol Pan/floodplain

Appendix 3: Inventory of sediments analysed.

NC18	NC/2000/18	Calcrete nodules collected from the upper horizon (0.5 m thick). 4 m section exposed in the borrow pit. Below the upper horizon is Dwyka bedrock. Located in an interdune depression with flanking dunes approx. 250 m apart.	27`11.12 S / 20`05.09 E	upper 0.5 m of profile	Interdune depression/bedrock
NC19	NC/2000/19	Sample of hardpan collected on the surface of Uitsakpan, flanked by Kalahari sand dunes and Prince Albert formation ridges. Also evidence of small pans which have formed on the floodplain.	27`04.99 S / 20`05.17 E	surface	Uitsak Pan/floodplain
NC20	NC/2000/20	Hardpan calcrete collected from lunnettes on the northern boundary of Koppieskraal Pan. Pan is surrounded by Prince Albert formation to the south and Kalahari dunes.	26`55.61 S / 20`16.13 E	surface	Koppieskraal Pan
NC21	NC/2000/21	Large calcrete boulders in floor of Koppieskraal Pan.	26`56.74 S / 20`19.19 E	surface	Koppieskraal Pan
NC22		Roadcutting through a Prince Albert formation. Bedrock has been calcified.	26`58.00 S / 20`22.29 E		
	NC/2000/22/A	Hardpan calcrete boulder showing laminations on its upper surface.		surface	
	NC/2000/22/B	Hardpan calcrete or silcrete (very hard) collected from road cutting through sloping hill.		surface	
NC22b		A large 3.0 m deep borrow pit in an inter-dune depression close to Inkbosch Pan. Very silty, poorly consolidated diatomaceous carbonate.	27`00.52 S / 20`28.09 E	1.0 m	Interdune depression/pan
NC23		Molopo Valley, 20 m high steeply sloping calcrete valley wall (terrace) to the south and 15/20 m high Kalahari dunes to the north. Veg in the valley comprised large trees and on the upper surface bushes and grass.	27`01.72 S / 20`34.35 E		Molopo River valley
	NC/2000/23/A	Hardpan calcrete.		surface	
	NC/2000/23/B	Massive / nodular calcrete.		1.5 m below surface	

Appendix 3: Inventory of sediments analysed.

	NC/2000/23/C	Massive calcrete.		5.0 m below surface	
	NC/2000/23/D	Massive / nodular calcrete		10 m below surface	
	NC/2000/23/E	Massive calcrete		20 m below surface	
NC24		Nossob Valley, calcrete valley wall / terrace with Kalahari dunes present on the upper surface and a corresponding terrace to the NE which is mostly covered by ramping Kalahari dunes.	26`47.70 S / 20`38.21 E		Nossob River valley
	NC/2000/24/A	Hardpan calcrete		surface	
	NC/2000/24/B	Massive / nodular calcrete		2.5 m below surface	
	NC/2000/24/C	Massive calcrete. Distinctive unconformity between the overlying nodular (NC/2000/24/B) and underlying massive (NC/2000/24/C) calcretes at 4.0 m. Sample collected below unconformity.		4.0 m	
NC25		Nossob Valley with a 4.0 m terrace, close to Melkvlei	26`08.55 S / 20`51.29 E		Nossob River valley
	NC/2000/25/A	Sample taken from valley wall. Massive calcrete grading into conglomeratic calcrete.		2.0 m below surface	
	NC/2000/25/B	Rhizoliths and biotubes weathered out, due to differential weathering, of the massive calcrete.		2.5 m below surface	
NC26	NC/2000/26	Hardpan dolomitic calcrete with lithic clasts. Located on the western side of the Nossob Valley. The eastern flank calcrete terrace is overlain by Kalahari dunes. Veg is composed of scattered Acacia and Combretum trees approx. 5 m tall on the sides of the valley floor and grass and small bushes in the central section of the valley floor.	25`51.85 S / 20`48.12 E	Surface	Nossob River valley

Appendix 3: Inventory of sediments analysed.

NC27		Auob River. Valley consists of calcrete flanking terraces with Kalahari dunes capping. Samples taken from a 4.0 m exposure on the western side of the valley. Veg consists of grassland on the valley floor and sparse 10 m tall Acacia trees on the valley floor and on the banks.	26`00.79 S / 20`24.00 E		Auob River valley
	NC/2000/27/A	Hardpan calcrete collected on the western terrace / valley wall.		surface	
	NC/2000/27/B	Nodular / massive dolocrete		3.0 m below surface	
NC28		Auob River valley. The same cross section profile as at NC/2000/27. Valley sides approx. 25/30 m high. Section 3.5 m high exposed close to Gemsbokplein.	26`09.03 S / 20`31.58 E		Auob River valley
	NC/2000/28/A	Hardpan calcrete.		surface	
	NC/2000/28/B	Very nodular massive calcitic dolocrete - breaks into nodules very easily when hit with a hammar.		3.0 m below surface	
NC29	NC/2000/29	Auob River. Hardpan / massive nodular calcrete, showing minor laminations. Sample collected at upper surface of calcrete / contact between calcrete and overlying Kalahari dunes.	26`15.96 S / 20`34.56 E	calcrete surface	Auob River valley
NC30		Kuruman River. Quarry next to the road, exposing an 8 m section on the southern side of the valley. Valley is wide with a low terrace on either side (appox. 8 m). The northern terrace is covered by Kalahari dunes.	26`59.04 S / 20`51.65 E		Kuruman River valley
	NC/2000/30/A	Hardpan calcrete.		surface	
	NC/2000/30/B	Nodular calcrete.		0.5 m below surface.	
	NC/2000/30/C	Massive calcrete, no nodules. Contact between massive and overlying nodular calcrete very distinct at 1.5 m below the surface.		1.7 m below surface	
	NC/2000/30/D	Massive calcrete with 2 cm (average) diamter mottles. Also contains small round nodules approx. 5 cm in diameter.		5 m below surface	

Appendix 3: Inventory of sediments analysed.

	NC/2000/30/E	Massive calcrete with 2 cm (average) irregular mottles. Contains large nodules, irregular shaped between 5 and 10 cm in diameter.		8 m below surface	
NC31		Kuruman River. Samples taken from a 5.0 m borrow pit exposure of calcrete on the eastern flank of valley. Valley is flanked by Kalahari dunes. Veg dominated by bushveld type Acacias, small bushes approx. 1.0 m tall and scattered grass.	26`54.73 S / 21`57.42 E		Kuruman River valley
	NC/2000/31/A	Hardpan / massive calcrete		Calcrete surface below overlying dunes.	
	NC/2000/31/B	Very hard massive dolocrete		1.5 m below calcrete surface	
	NC/2000/31/C	Massive dolocrete, coarser grained.		3.0 m below calcrete surface	
	NC/2000/31/D	Massive dolocrete brown colour, coarser (sand textured).		5.0 m below calcrete surface	

Appendix 4: Summary of XRD results.

Appendix 4: Summary of XRD results.

| | Whole rock analyses | | | | | | | | | | | | | | | | | | | < 2µm fraction analyses | | | | | | | | | | | | | | | | | | |

Appendix 4 Summary of XRD results

LS 2.0m	91	-	8	-	-	-	-	-	-	-	-	-	-	-	-	-	-	-	1	
LS 2.5m	70	-	30	-	-	-	-	-	-	-	-	-	-	-	-	-	-	-	-	
LS Nodules	48	-	52	-	-	-	-	-	-	-	-	-	-	-	-	-	-	-	-	

Okavango

Mohembo Homogenised	96	-	1	-	-	-	-	-	-	-	-	-	-	-	-	-	-	-	4	
Shakawe	55	-	45	-	-	-	-	-	-	-	-	-	-	-	-	-	-	-	-	
Red Cliff 11m below surface	73	-	27	-	-	-	-	-	-	-	-	-	-	-	-	-	-	-	-	
Sepupa	21	-	77	-	-	-	-	-	-	-	-	-	-	-	-	-	-	-	2	
Sepupa	28	-	72	-	-	-	-	-	-	-	-	-	-	-	-	-	-	-	-	
B/2000/28A	25	-	71	-	-	-	-	-	-	-	-	-	2	-	-	2	-	-	-	
B/2000/29A	51	-	47	-	-	-	-	-	-	-	-	-	-	-	-	-	-	-	2	
B/2000/30A	56	-	37	4	-	-	-	-	-	-	-	-	-	3	-	-	-	-	-	
B/2000/31	46	-	48	-	-	-	2	-	-	-	-	-	-	-	-	-	-	-	4	
B/2000/32 Matrix	93	-	4	-	-	-	2	-	-	-	-	-	-	-	-	-	-	-	1	
B/2000/33 Matrix	94	-	6	-	-	-	-	-	-	-	-	-	-	-	-	-	-	-	-	
B/2000/34A	49	-	49	-	-	-	-	-	-	-	-	-	-	-	-	-	-	-	2	
B/2000/35A	54	-	46	-	-	-	-	-	-	-	-	-	-	-	-	-	-	-	-	
B/2000/36A	74	-	25	-	-	-	-	-	-	-	-	-	-	-	-	-	-	-	1	
B/2000/39B Matrix	83	-	15	-	-	-	-	-	-	-	-	-	-	-	-	-	-	-	2	
B/2000/41A	97	-	-	-	-	-	2	-	-	-	-	-	1	-	-	-	-	-	-	
B/2000/42A	7	-	83	-	-	-	8	-	-	-	-	-	-	-	2	-	-	-	-	
B/2000/42B	44	-	54	-	-	-	-	-	-	-	-	-	2	-	-	-	-	-	-	
B/2000/45C	39	-	58	-	-	2	-	-	-	-	-	-	-	-	-	-	-	-	1	
B/2000/47A	17	-	83	-	-	-	-	-	-	-	-	-	-	-	-	-	-	-	-	
B/2000/47B	13	-	87	-	-	-	-	-	-	-	-	-	-	-	-	-	-	-	-	
B/2000/47C	18	-	82	-	-	-	-	-	-	-	-	-	-	-	-	-	-	-	-	
B/2000/48A	21	-	79	-	-	-	-	-	-	-	-	-	-	-	-	-	-	-	-	
B/2000/49A	14	-	86	-	-	-	-	-	-	-	-	-	-	-	-	-	-	-	-	
B/2000/49B	29	-	71	-	-	-	-	-	-	-	-	-	-	-	-	-	-	-	-	
B/2000/49C	37	-	63	-	-	-	-	-	-	-	-	-	-	-	-	-	-	-	-	
B/2000/49D	30	-	70	-	-	-	-	-	-	-	-	-	-	-	-	-	-	-	-	
B/2000/53A	-	-	100	-	-	-	-	-	-	-	-	-	-	-	-	-	-	-	-	
B/2000/53B	-	-	100	-	-	-	-	-	-	-	-	-	-	-	-	-	-	-	-	
B/2000/53C	-	-	100	-	-	-	-	-	-	-	-	-	-	-	-	-	-	-	-	
B/2000/53D	-	-	100	-	-	-	-	-	-	-	-	-	-	-	-	-	-	-	-	
B/2000/53E	28	-	72	-	-	-	-	-	-	-	-	-	-	-	-	-	-	-	-	
NG 1	8	-	91	-	-	-	-	-	-	-	-	-	-	-	-	-	-	-	3	
3rd Bridge Moremi	23	-	77	-	-	-	-	-	-	-	-	-	-	-	-	-	-	-	-	
Gaenga Surface	98	-	2	-	-	-	-	-	-	-	-	-	-	-	-	-	-	-	-	
Gaenga 40cm	100	-	-	-	-	-	-	-	-	-	-	-	-	-	-	-	-	-	-	
OK 51A 60cm	92	-	8	-	-	-	-	-	-	-	-	-	-	-	-	-	-	-	-	
OK 51B 90cm	100	-	-	-	-	-	-	-	-	-	-	-	-	-	-	-	-	-	-	
OK 51C 20cm	100	-	-	-	-	-	-	-	-	-	-	-	-	-	-	-	-	-	-	
OK 51D 60cm	100	-	-	-	-	-	-	-	-	-	-	-	-	-	-	-	-	-	-	
OK 51D 120cm	98	-	2	-	-	-	-	-	-	-	-	-	-	-	-	-	-	-	-	
OK 51D 180cm	96	-	4	-	-	-	-	-	-	-	-	-	-	-	-	-	-	-	-	
Mosupatsela 5m	96	-	4	-	-	-	-	-	-	-	-	-	-	-	-	-	-	-	-	
Mosupatsela 50m	96	-	4	-	-	-	-	-	-	-	-	-	-	-	-	-	-	-	-	

Makgadikgadi & Boteti

B/2000/16B	17	-	83	-	-	-	-	-	-	-	-	-	-	-	-	-	-	-	-	
B/2000/17B	65	-	35	-	-	-	-	-	-	-	-	-	-	-	-	-	-	-	-	
B/2000/18A	8	-	92	-	-	-	-	-	-	-	-	-	-	-	-	-	-	-	-	
B/2000/18B	33	-	67	-	-	-	-	-	-	-	-	-	-	-	-	-	-	-	-	
B/2000/23/A	87	-	13	-	-	-	-	-	-	-	-	-	-	-	-	-	-	-	-	
B/2000/23/B	67	-	33	-	-	-	-	-	-	-	-	-	-	-	-	-	-	-	-	
B/2000/23/C	67	-	33	-	-	-	-	-	-	-	-	-	-	-	-	-	-	-	-	
B/2000/24B	83	-	17	-	-	-	-	-	-	-	-	-	-	-	-	-	-	-	-	
B/2000/25A	90	-	10	-	-	-	-	-	-	-	-	-	-	-	-	-	-	-	-	
B/2000/26A	30	-	70	-	-	-	-	-	-	-	-	-	-	-	-	-	-	-	-	
B/2000/26B	92	-	3	-	-	-	5	-	-	-	-	-	-	-	-	-	-	-	-	
B/2000/26C	32	-	68	-	-	-	-	-	-	-	-	-	-	-	-	-	-	-	-	
B/2000/27B	71	-	22	2	-	1	1	-	-	-	-	-	3	-	-	-	-	-	-	

Kgalagadi

B/2000/65	46	-	51	-	-	-	-	3	-	-	-	-	-	-	-	-	-	1	-	
B/2000/66	90	-	10	-	-	-	-	-	-	-	-	-	-	-	-	-	-	-	-	
B/2000/67	41	-	44	-	-	-	-	-	-	-	-	-	-	-	-	-	14	1	-	
B/2000/68	8	-	80	-	8	-	-	-	-	-	-	-	-	-	-	-	6	-	-	
B/2000/69	27	-	73	-	-	-	-	-	-	-	-	-	-	-	-	-	-	-	-	
B/2000/70A	54	-	46	-	-	-	-	-	-	-	-	-	-	-	-	-	-	-	-	
B/2000/71	15	-	84	-	-	-	-	-	1	-	-	-	-	-	-	-	-	-	-	
B/2000/72	24	-	76	-	-	-	-	-	-	-	-	-	-	-	-	-	-	-	-	
B/2000/73A	63	-	-	23	-	-	14	-	-	-	-	-	-	-	-	-	-	-	-	
B/2000/74A	39	-	24	40	-	-	-	-	-	-	-	-	-	-	-	-	-	-	-	
B/2000/75A	56	-	44	-	-	-	-	-	-	-	-	-	-	-	-	-	-	-	-	
B/2000/76A	21	-	79	-	-	-	-	-	-	-	-	-	-	-	-	-	-	-	-	

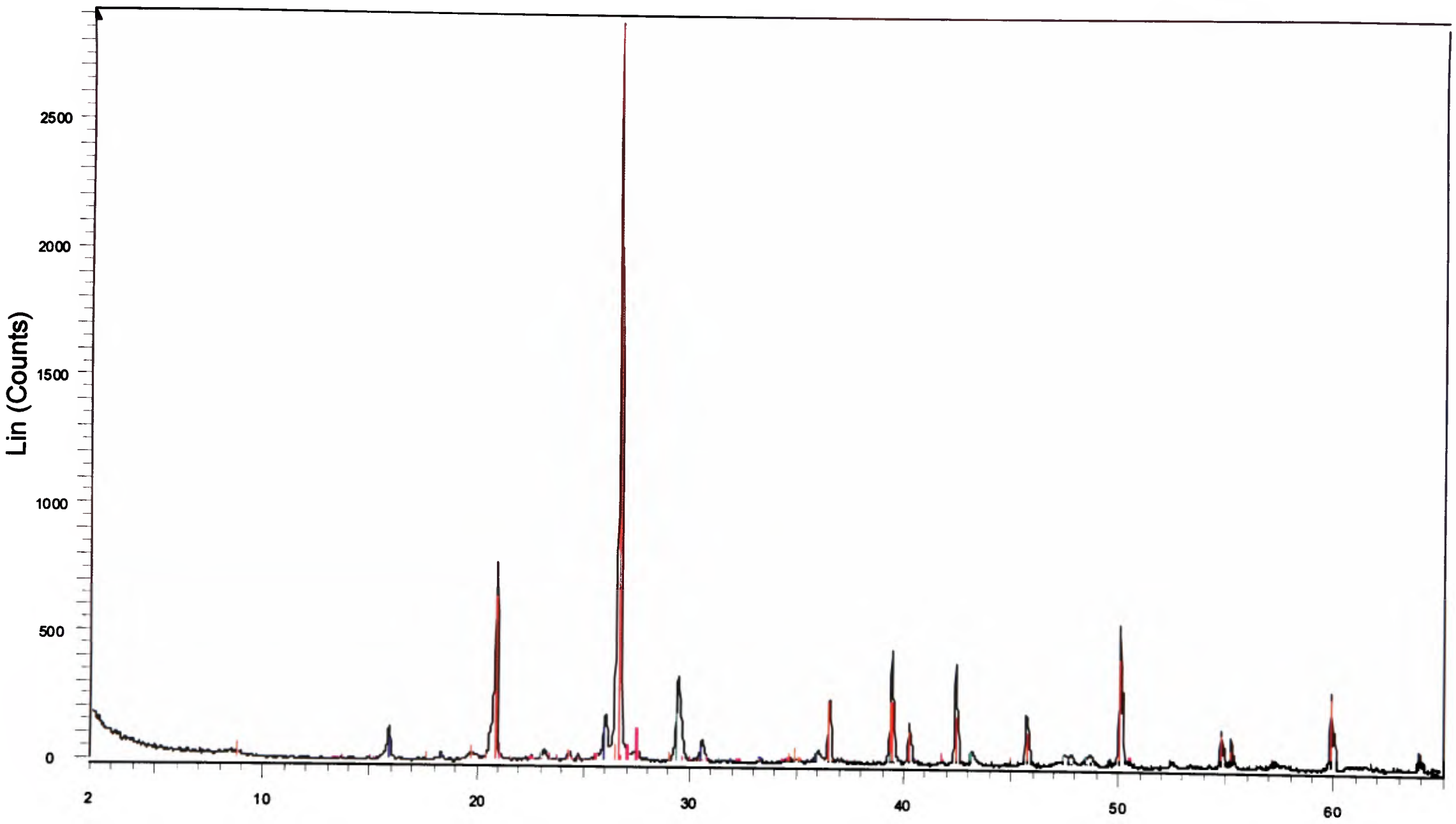
LS 2.0m	32	-	-	-	-	-	-	-	68	-	-	-	-	-	-	-				
LS 2.5m	-	-	-	-	-	-	-	-	-	-	-	-	11	-	-	-				
LS Nodules	9	86	-	-	-	-	-	-	-	-	-	-	5	-	-	-				
Mohembo Homogenised	37	-	-	-	-	-	-	15	-	47	-	-	-	-	-					
Shakawe	12	28	-	-	-	-	-	32	-	28	-	-	-	-	-					
Red Cliff 11m below surface	-	-	-	-	-	-	-	-	-	8	-	-	-	-	-					
Sepupa	31	3	-	-	-	-	-	-	-	14	-	52	-	-	-					
Sepupa	-	-	-	-	-	-	-	-	-	-	-	-	-	-	-					
B/2000/28A	17	-	-	-	27	-	-	19	-	37	-	-	-	-	-					
B/2000/29A	3	12	-	-	-	-	-	5	-	81	-	-	-	-	-					
B/2000/30A	8	-	-	-	-	-	-	40	-	52	-	-	-	-	-					
B/2000/31	-	40	-	-	-	-	-	14	-	-	-	49	-	-	-					
B/2000/32 Matrix	15	-	-	-	-	6	-	32	-	47	-	-	-	-	-					
B/2000/33 Matrix	18	-	-	-	6	-	-	39	-	39	-	-	-	-	-					
B/2000/34A	21	-	-	-	-	-	-	10	-	69	-	-	-	-	-					
B/2000/36A	24	10	-	-	-	-	-	-	-	15	51	-	-	-	-					
B/2000/38A	32	-	-	-	-	34	-	-	-	34	-	-	-	-	-					
B/2000/39B Matrix	10	-	-	-	-	10	-	14	-	69	-	-	-	-	-					
B/2000/41A	13	-	-	-	7	-	-	69	-	12	-	-	-	-	-					
B/2000/42A	no < 2µm fraction																			
B/2000/42B	64	17	-	-	-	-	-	-	-	19	-	-	-	-	-					
B/2000/46C	14	-	-	-	-	-	-	-	28	-	-	60	-	-	-					
B/2000/47A	-	-	-	-	-	-	-	-	-	-	-	-	-	-	-					
B/2000/47B	-	-	-	-	-	-	-	-	-	-	-	-	-	-	-					
B/2000/47C	-	-	-	-	-	-	-	-	-	-	-	-	-	-	-					
B/2000/48A	-	-	-	-	-	-	-	-	-	-	-	-	-	-	-					
B/2000/48A	-	-	-	-	-	-	-	-	-	-	-	-	-	-	-					
B/2000/49B	-	-	-	-	-	-	-	-	-	-	-	-	-	-	-					
B/2000/49C	-	-	-	-	-	-	-	-	-	-	-	-	-	-	-					
B/2000/49D	-	-	-	-	-	-	-	-	-	-	-	-	-	-	-					
B/2000/53A	-	-	-	-	-	-	-	-	-	-	-	-	-	-	-					
B/2000/53B	-	-	-	-	-	-	-	-	-	-	-	-	-	-	-					
B/2000/53C	-	-	-	-	-	-	-	-	-	-	-	-	-	-	-					
B/2000/53D	-	-	-	-	-	-	-	-	-	-	-	-	-	-	-					
B/2000/53E	-	-	-	-	-	-	-	-	-	-	-	-	-	-	-					
NG 1	20	35	-	-	-	-	-	-	-	-	-	45	-	-	-					
3rd Bridge Moremi	no < 2µm fraction																			
Gaenga Surface	82	15	-	-	-	-	-	8	-	15	-	-	-	-	-					
Gaenga 40cm	41	15	-	-	11	-	-	20	-	13	-	-	-	-	-					
OK 51A 60cm	30	56	-	-	-	-	-	8	-	-	8	-	-	-	-					
OK 51B 90cm	17	-	-	-	15	-	-	49	-	19	-	-	-	-	-					
OK 51C 20cm	33	-	-	-	12	-	-	44	-	-	-	11	-	-	-					
OK 51D 60cm	29	-	-	-	-	-	-	53	-	-	10	-	8	-	-					
OK 51D 120cm	27	-	-	-	9	-	-	57	-	-	7	-	-	-	-					
OK 51D 180cm	19	57	-	-	-	-	-	17	-	-	7	-	-	-	-					
Mosupatsela 5m	21	37	-	-	-	-	-	14	-	28	-	-	-	-	-					
Mosupatsela 50m	18	54	-	-	-	-	-	14	-	14	-	-	-	-	-					

B/2000/16B	-	-	-	-	-	-	-	-	-	-	-	-	-	-	-					
B/2000/17B	-	-	-	-	-	-	-	-	-	-	-	-	-	-	-					
B/2000/18A	-	-	-	-	-	-	-	-	-	-	-	-	-	-	-					
B/2000/18B	-	-	-	-	-	-	-	-	-	-	-	-	-	-	-					
B/2000/23/A	-	-	-	-	-	-	-	-	-	-	-	-	-	-	-					
B/2000/23/B	-	-	-	-	-	-	-	-	-	-	-	-	-	-	-					
B/2000/23/C	-	-	-	-	-	-	-	-	-	-	-	-	-	-	-					
B/2000/24B	-	-	-	-	-	-	-	-	-	-	-	-	-	-	-					
B/2000/25A	46	-	-	-	-	-	-	-	-	54	-	-	-	-	-					
B/2000/25A	-	-	-	-	-	-	-	-	-	-	-	-	-	-	-					
B/2000/26B	-	-	-	-	-	-	-	-	-	-	-	-	-	-	-					
B/2000/26C	-	-	-	-	-	-	-	-	-	-	-	-	-	-	-					
B/2000/27B	22	-	-	-	-	-	46	-	-	32	-	-	-	-	-					

B/2000/65	-	-	-	-	-	-	-	-	-	-	-	-	-	-	-					
B/2000/66	-	-	-	-	-	-	-	-	-	-	-	-	-	-	-					
B/2000/67	-	-	-	-	-	-	-	-	-	-	-	-	-	-	-					
B/2000/68	-	-	-	-	-	-	-	-	-	-	-	-	-	-	-					
B/2000/69	-	-	-	-	-	-	-	-	-	-	-	-	-	-	-					
B/2000/70A	-	-	-	-	-	-	-	-	-	-	-	-	-	-	-					
B/2000/71	-	-	-	-	-	-	-	-	-	-	-	-	-	-	-					
B/2000/72	-	-	-	-	-	-	-	-	-	-	-	-	-	-	-					
B/2000/73A	-	-	-	-	-	-	-	-	-	-	-	-	-	-	-					
B/2000/74A	-	-	-	-	-	-	-	-	-	-	-	-	-	-	-					
B/2000/75A	-	-	-	-	-	-	-	-	-	-	-	-	-	-	-					
B/2000/76A	-	-	-	-	-	-	-	-	-	-	-	-	-	-	-					

Appendix 5: A selection of 30 X-ray diffraction traces.

Sample 1



Y - 1.0 mm - Shaw A, sample 1 - File: 02136-1.raw - Type: 2Th/Th locked - Start: 2.012 ° - End: 65.010 ° - Step: 0.020 ° - Step time: 1. s

Operations: Displacement -0.021 | Smooth 0.060 | Import

33-1161 (*) - Quartz, syn - SiO2 - WL: 1.5406

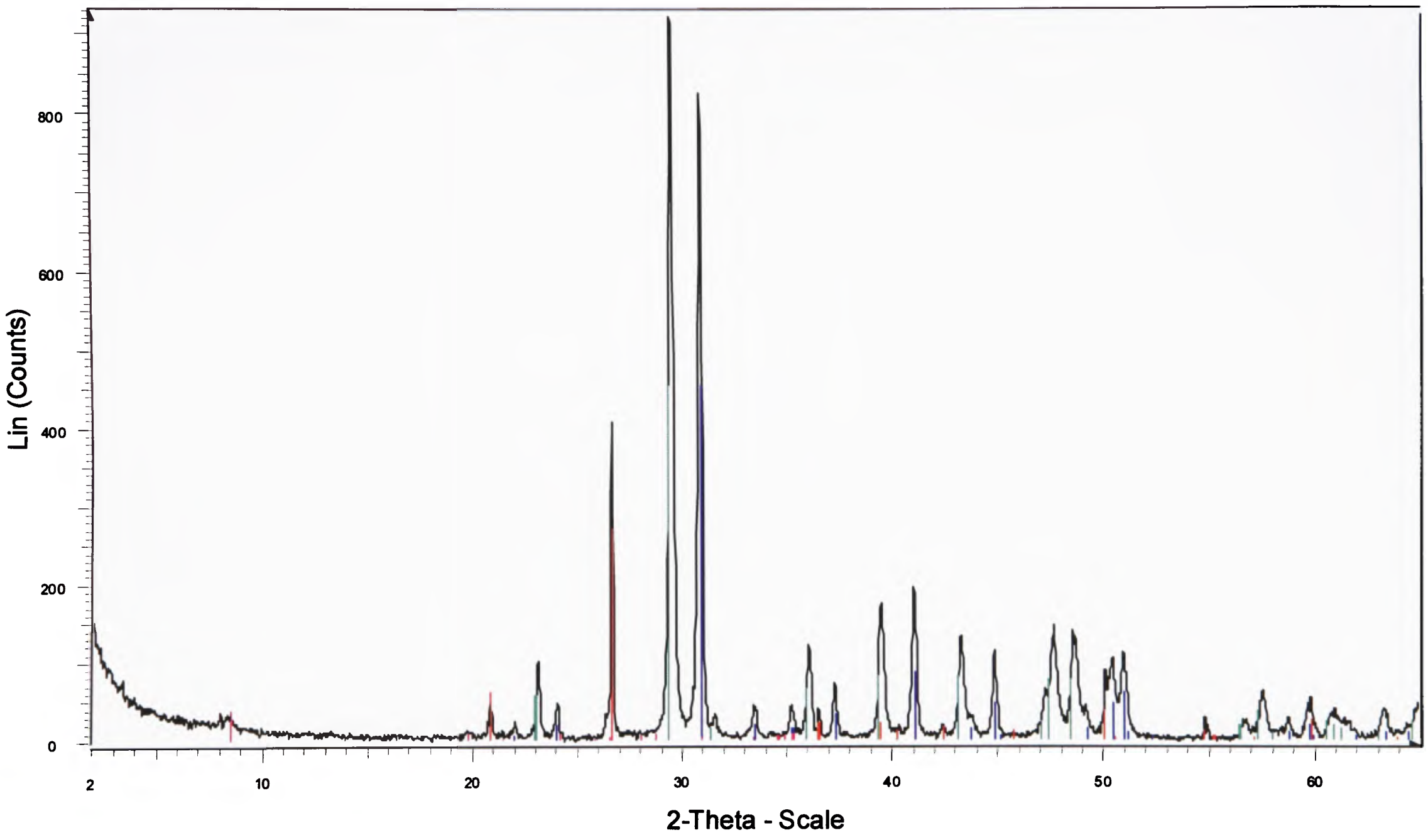
05-0586 (*) - Calcite, syn - CaCO3 - WL: 1.5406

41-1478 (*) - Analcime-C - Na(Si2Al)O6·H2O - WL: 1.5406

19-0932 (I) - Microcline, intermediate - KAlSi3O8 - WL: 1.5406

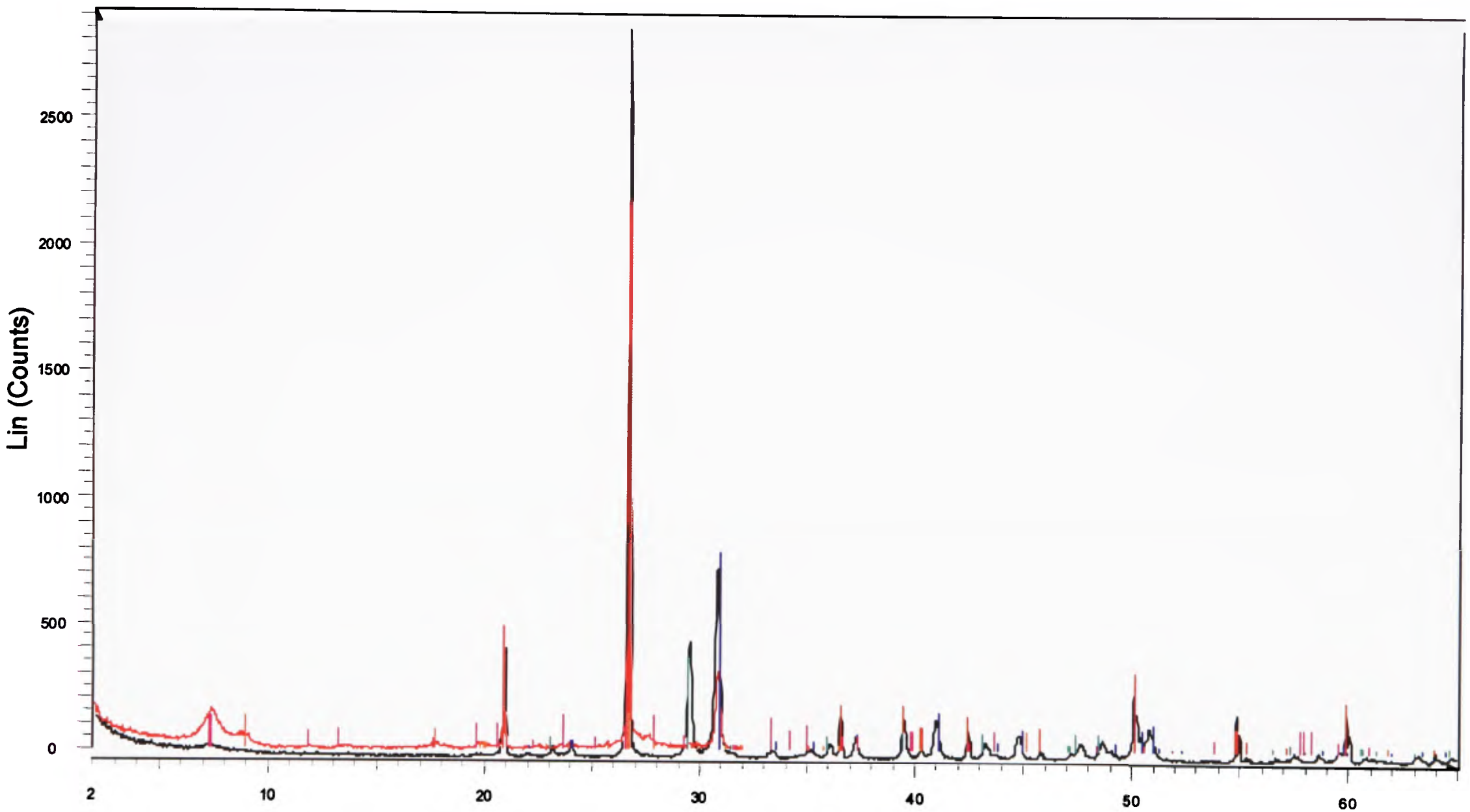
07-0025 (I) - Muscovite-1M, syn - KAl2Si3AlO10(OH)2 - WL: 1.5406

Sample 2



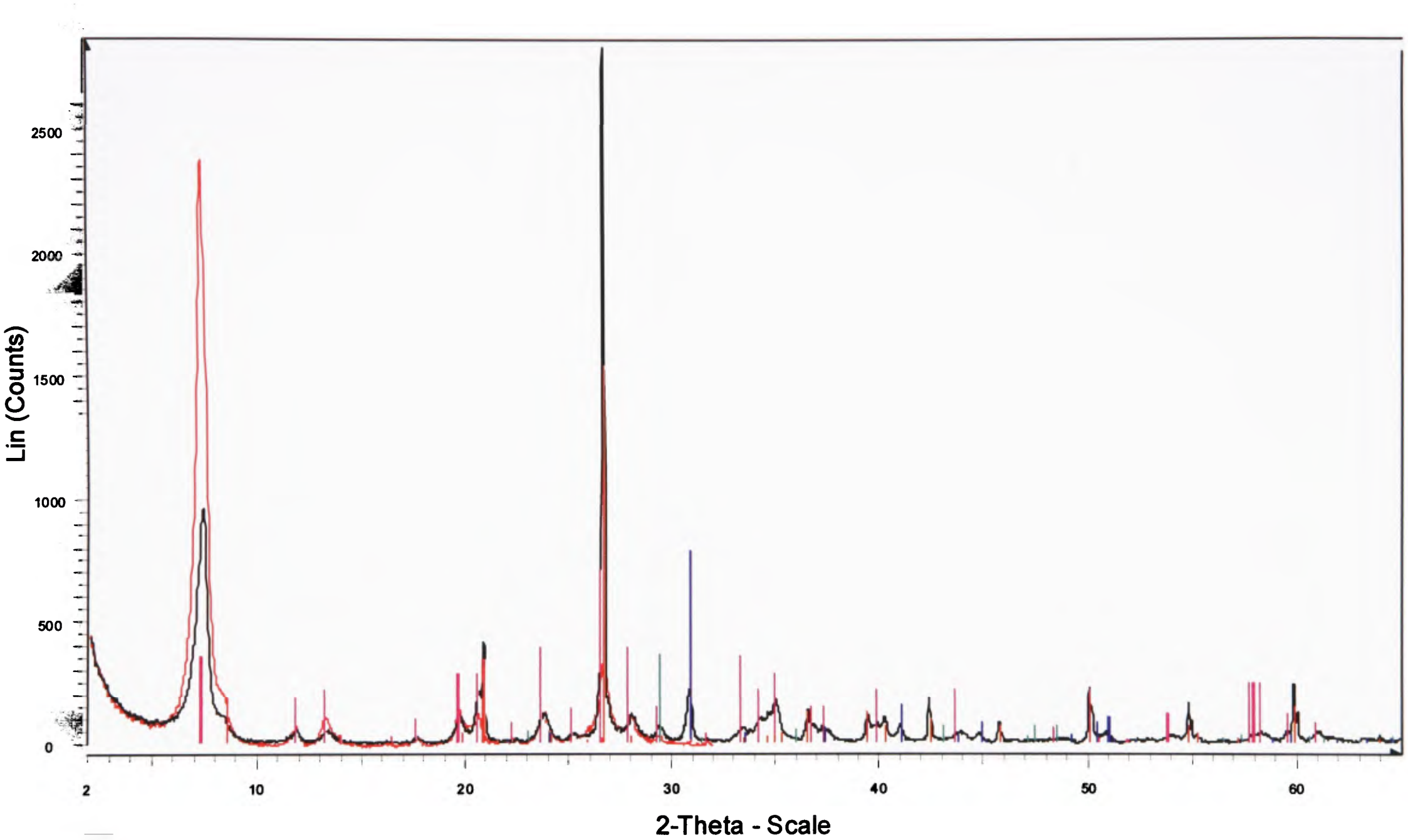
Y - 1.0 mm - Shaw A, sample 2 - File: 02136-2.raw - Type: 2Th/Th locked - Start: 1.982 ° - End: 64.985 ° - Step: 0.020 ° - Step time: 1. s
Operations: Displacement 0.031 | Smooth 0.060 | Import
33-1161 (*) - Quartz, syn - SiO2 - WL: 1.5406
36-0426 (*) - Dolomite - CaMg(CO3)2 - WL: 1.5406
05-0586 (*) - Calcite, syn - CaCO3 - WL: 1.5406
31-0783 (I) - Palygorskite - Mg5(Si,Al)8O20(OH)2·8H2O - WL: 1.5406

Sample 3



Y - 1.0 mm - Shaw A, sample 3: clay fraction - File: 02136-3clay.raw - Type: 2Th/Th loc
Operations: Displacement 0.073 | Smooth 0.060 | Import
Y - 2.0 mm - Shaw A, sample 3 - File: 02136-3.raw - Type: 2Th/Th locked - Start: 2.024
Operations: Displacement -0.042 | Smooth 0.060 | Import
33-1161 (*) - Quartz, syn - SiO2 - WL: 1.5406
36-0426 (*) - Dolomite - CaMg(CO3)2 - WL: 1.5406
05-0586 (*) - Calcite, syn - CaCO3 - WL: 1.5406
26-1226 (I) - Sepiolite - Mg4Si6O15(OH)2·6H2O - WL: 1.5406
26-0911 (I) - Illite-2M1 - (K,H3O)Al2Si3AlO10(OH)2 - WL: 1.5406

Sample 4



Y - 1.0 mm - Shaw A, sample 4 - File: 02136-4.raw - Type: 2Th/Th locked - Start: 1.982
Operations: Displacement 0.031 | Smooth 0.060 | Import

Y - 2.0 mm - Shaw A, sample 4: clay fraction - File: 02136-4clay.raw - Type: 2Th/Th loc
Operations: Smooth 0.060 | Displacement 0.083 | Import

33-1161 (*) - Quartz, syn - SiO2 - WL: 1.5406

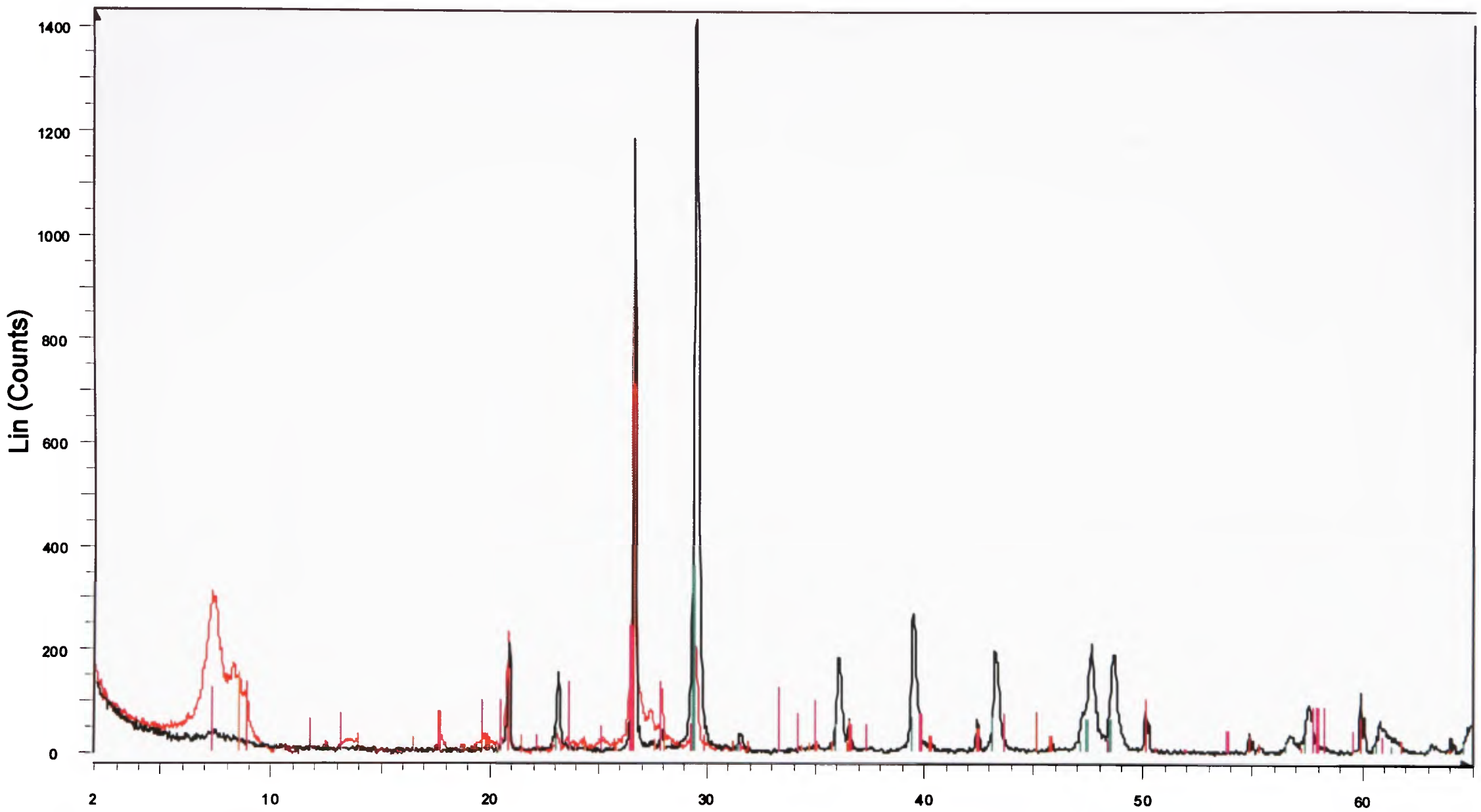
36-0426 (*) - Dolomite - CaMg(CO3)2 - WL: 1.5406

05-0586 (*) - Calcite, syn - CaCO3 - WL: 1.5406

26-1226 (I) - Sepiolite - Mg4Si6O15(OH)2·6H2O - WL: 1.5406

31-0783 (I) - Palygorskite - Mg5(Si,Al)8O20(OH)2·8H2O - WL: 1.5406

Sample 5



Y - 1.0 mm - Shaw A, sample 5 - File: 02136-5.raw - Type: 2Th/Th locked - Start: 1.988
Operations: Displacement 0.021 | Smooth 0.060 | Import

Y - 2.0 mm - Shaw A, sample 5: clay fraction - File: 02136-5clay.raw - Type: 2Th/Th loc
Operations: Displacement 0.021 | Smooth 0.060 | Import

33-1161 (*) - Quartz, syn - SiO2 - WL: 1.5406

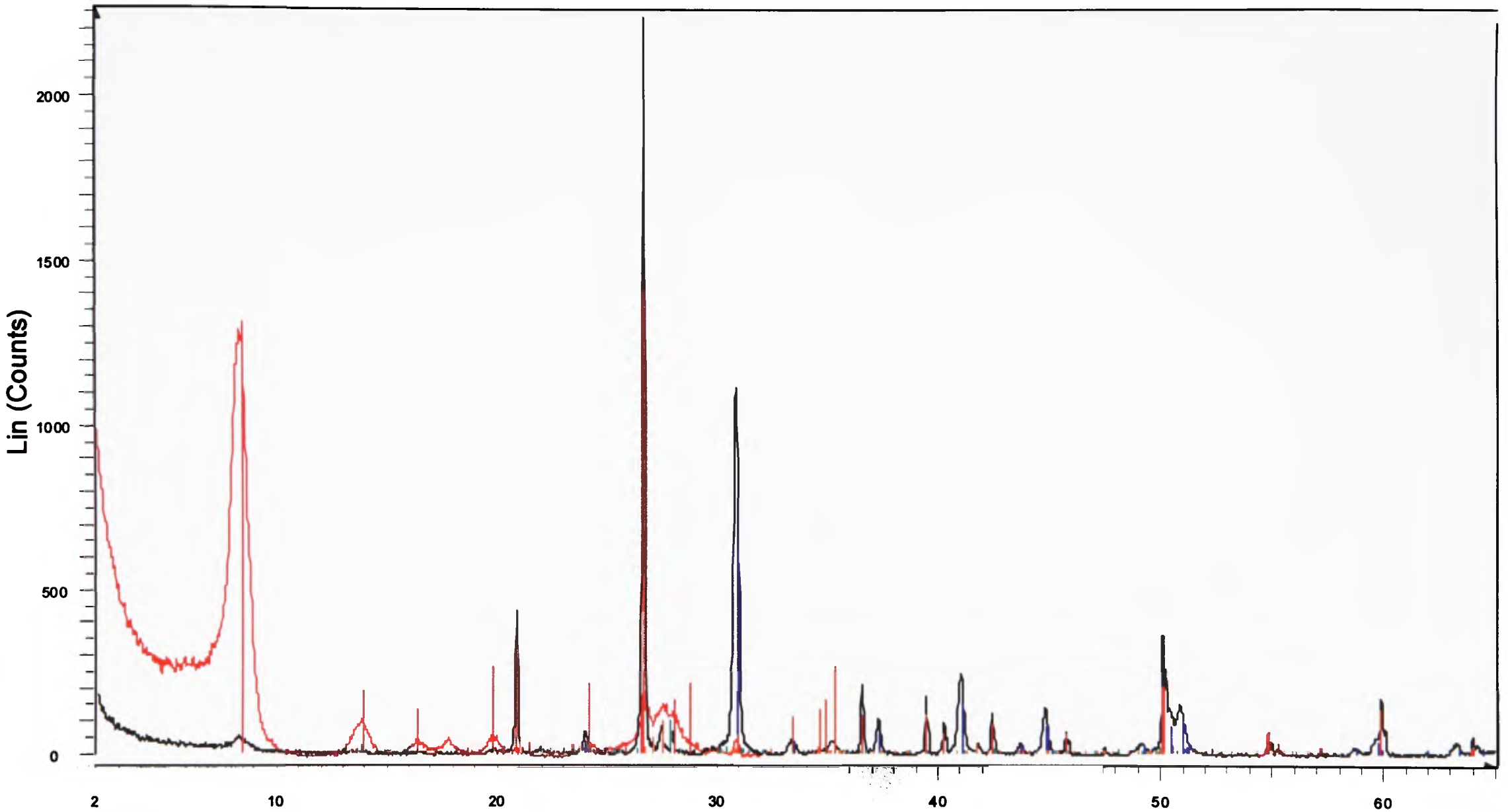
05-0586 (*) - Calcite, syn - CaCO3 - WL: 1.5406

26-1226 (I) - Sepiolite - Mg4Si8O15(OH)2·6H2O - WL: 1.5406

26-0911 (I) - Illite-2M1 - (K,H3O)Al2Si3AlO10(OH)2 - WL: 1.5406

21-0958 (I) - Palygorskite - (Mg,Al)5(Si,Al)8O20(OH)2·8H2O - WL: 1.5406

Sample 6



Y - 1.0 mm - Shaw A, sample 6 - File: 02136-6.raw - Type: 2Th/Th locked - Start: 2.024
Operations: Displacement -0.042 | Smooth 0.060 | Import

Y - 2.0 mm - Shaw A, sample 6: clay fraction - File: 02136-6clay.raw - Type: 2Th/Th loc
Operations: Displacement 0.052 | Smooth 0.060 | Import

33-1161 (*) - Quartz, syn - SiO2 - WL: 1.5406

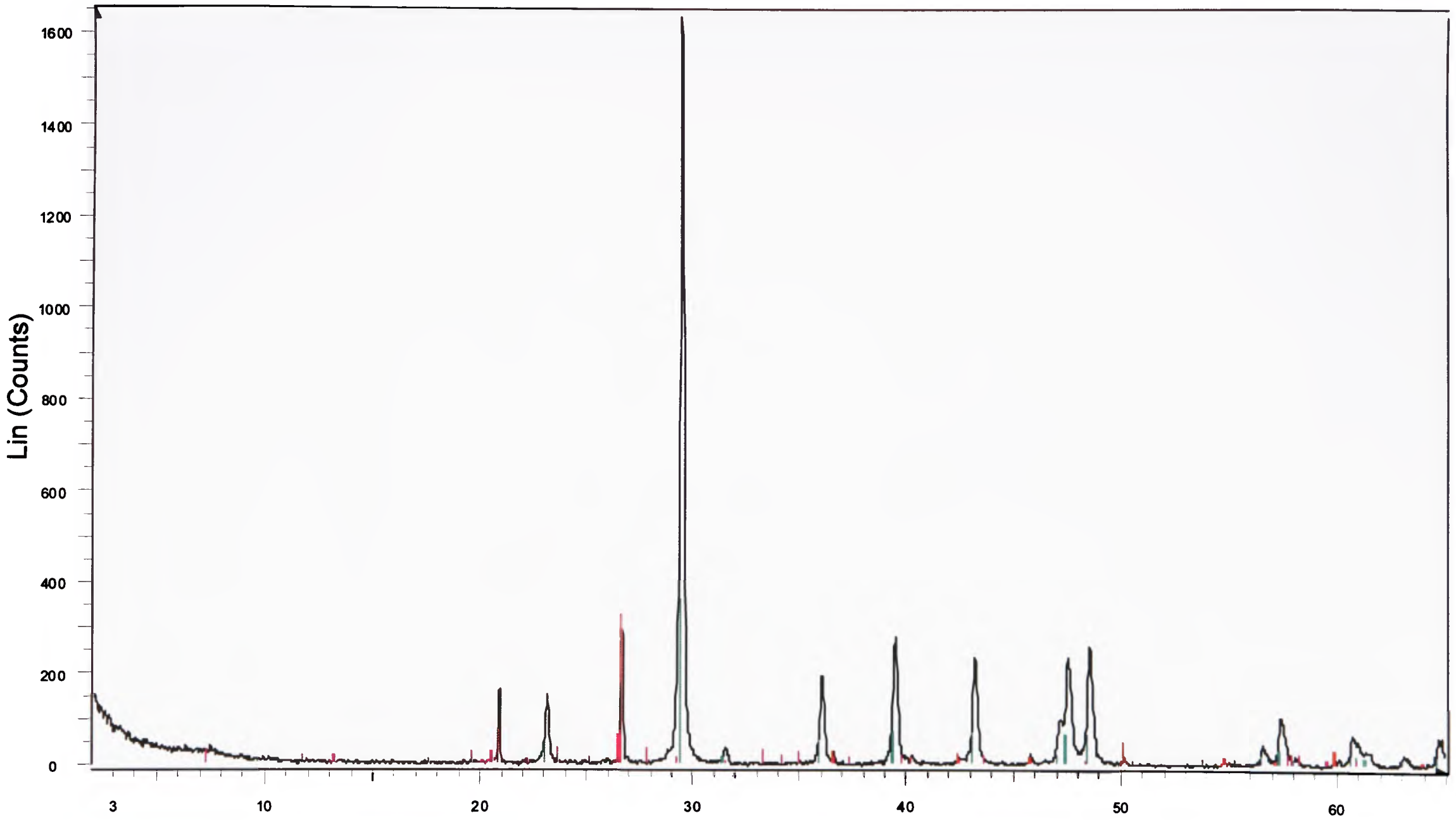
36-0426 (*) - Dolomite - CaMg(CO3)2 - WL: 1.5406

31-0783 (I) - Palygorskite - Mg5(Si,Al)8O20(OH)2·8H2O - WL: 1.5406

19-0932 (I) - Microcline, intermediate - KAlSi3O8 - WL: 1.5406

09-0466 (*) - Albite, ordered - NaAlSi3O8 - WL: 1.5406

Sample 7



Y - 1.0 mm - Shaw A, sample 7 - File: 02136-7.raw - Type: 2Th/Th locked - Start: 2.057 ° - End: 65.048 ° - Step: 0.020 ° - Step time: 1. s

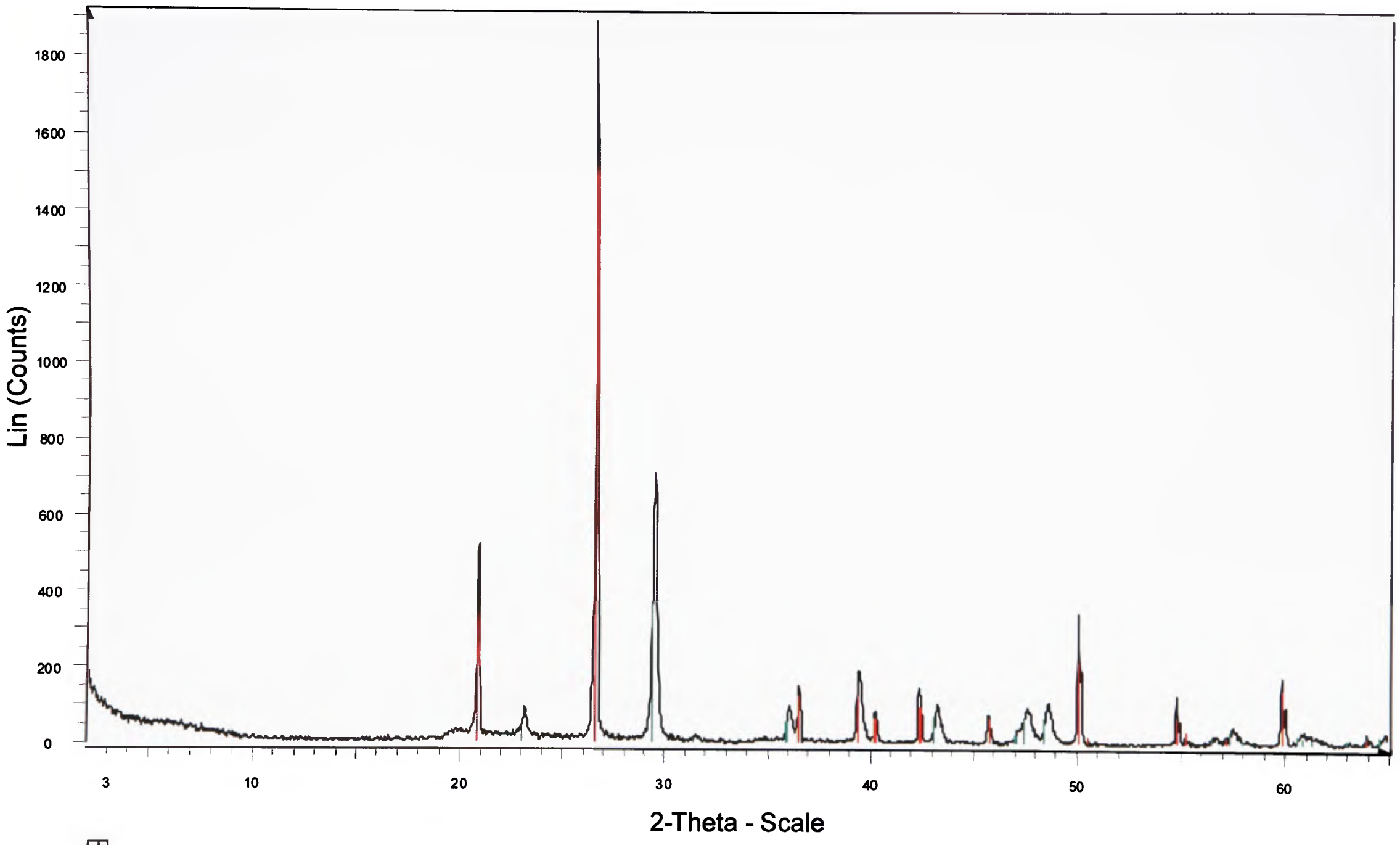
Operations: Displacement -0.100 | Smooth 0.060 | Import

33-1161 (*) - Quartz, syn - SiO2 - WL: 1.5406

05-0586 (*) - Calcite, syn - CaCO3 - WL: 1.5406

26-1226 (I) - Sepiolite - Mg4Si6O15(OH)2·6H2O - WL: 1.5406

Sample 8



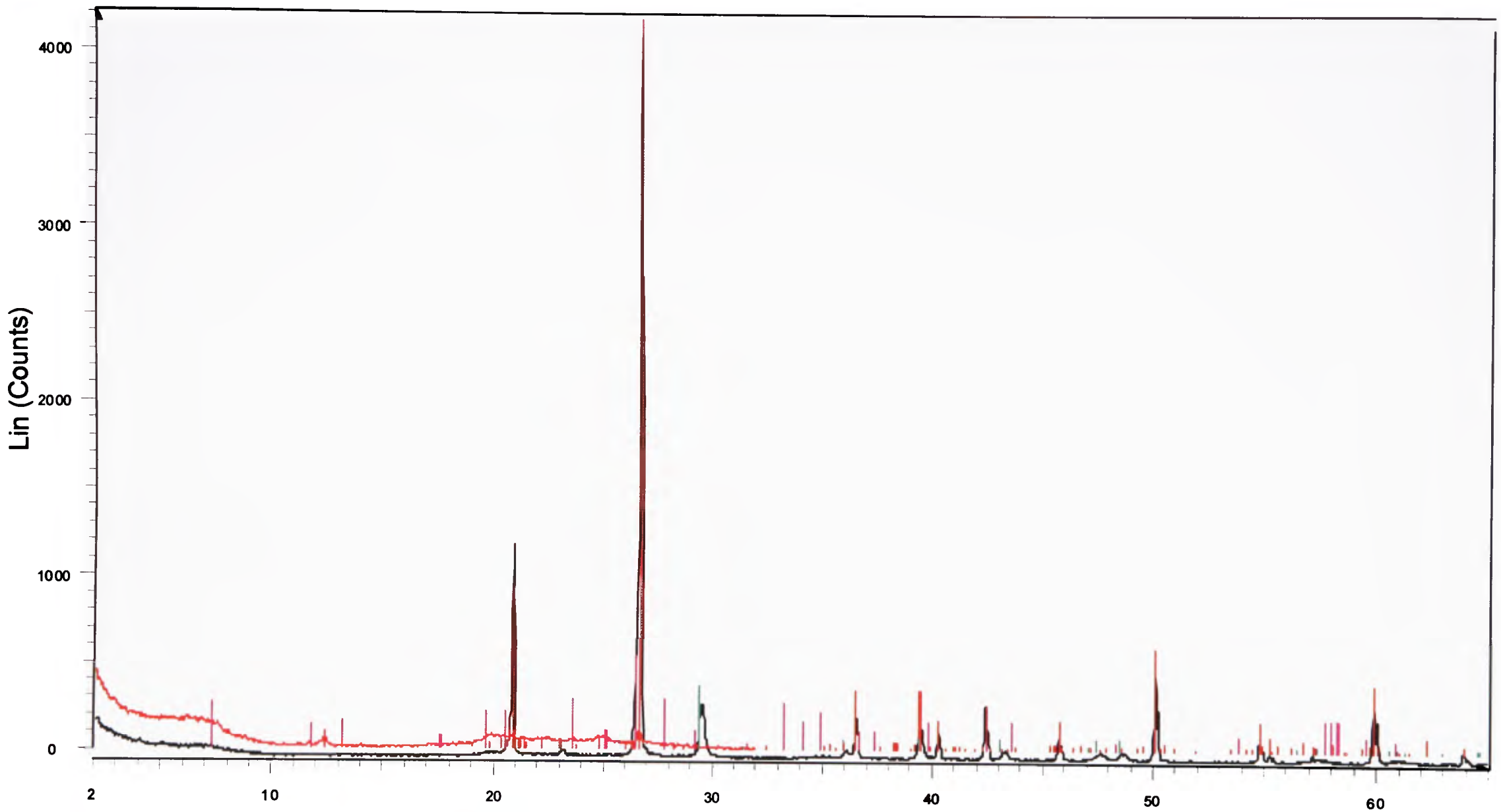
Y - 1.0 mm - Shaw A, sample 8 - File: 02136-8.raw - Type: 2Th/Th locked - Start: 2.042 ° - End: 65.035 ° - Step: 0.020 ° - Step time: 1. s

Operations: Displacement -0.073 | Smooth 0.060 | Import

33-1161 (*) - Quartz, syn - SiO_2 - WL: 1.5406

05-0586 (*) - Calcite, syn - $CaCO_3$ - WL: 1.5406

Sample 9



Y - 1.0 mm - Shaw A, sample 9 (clay fraction) - File: 02136-9clay.raw - Type: 2Th/Th locked - Start: 2.000 ° - End: 32.000 ° - Step: 0.020 ° - Step time: 1. s
Operations: Smooth 0.060 | Import

Y - 2.0 mm - Shaw A, sample 9 - File: 02136-9.raw - Type: 2Th/Th locked - Start: 2.036 ° - End: 65.030 ° - Step: 0.020 ° - Step time: 1. s
Operations: Displacement -0.063 | Smooth 0.060 | Import

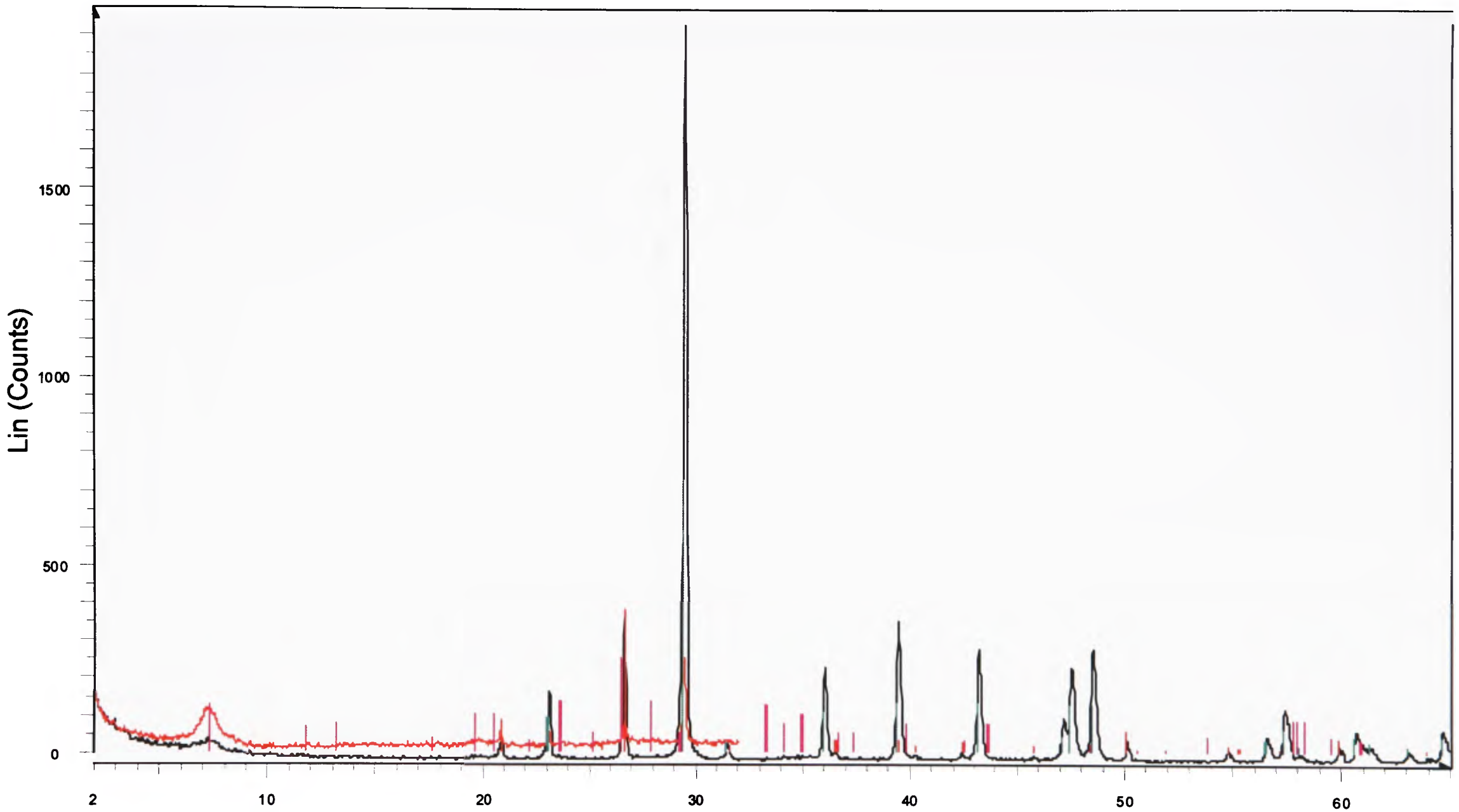
33-1161 (*) - Quartz, syn - SiO2 - WL: 1.5406

05-0586 (*) - Calcite, syn - CaCO3 - WL: 1.5406

26-1226 (I) - Sepiolite - Mg4Si6O15(OH)2·6H2O - WL: 1.5406

14-0164 (I) - Kaolinite-1A - Al2Si2O5(OH)4 - WL: 1.5406

Sample 10



Y - 1.0 mm - Shaw A, sample 10: clay fraction - File: 02136-10clay.raw - Type: 2Th/Th locked - Start: 2.000 ° - End: 32.000 ° - Step: 0.020 ° - Step time: 1. s
Operations: Smooth 0.060 | Import

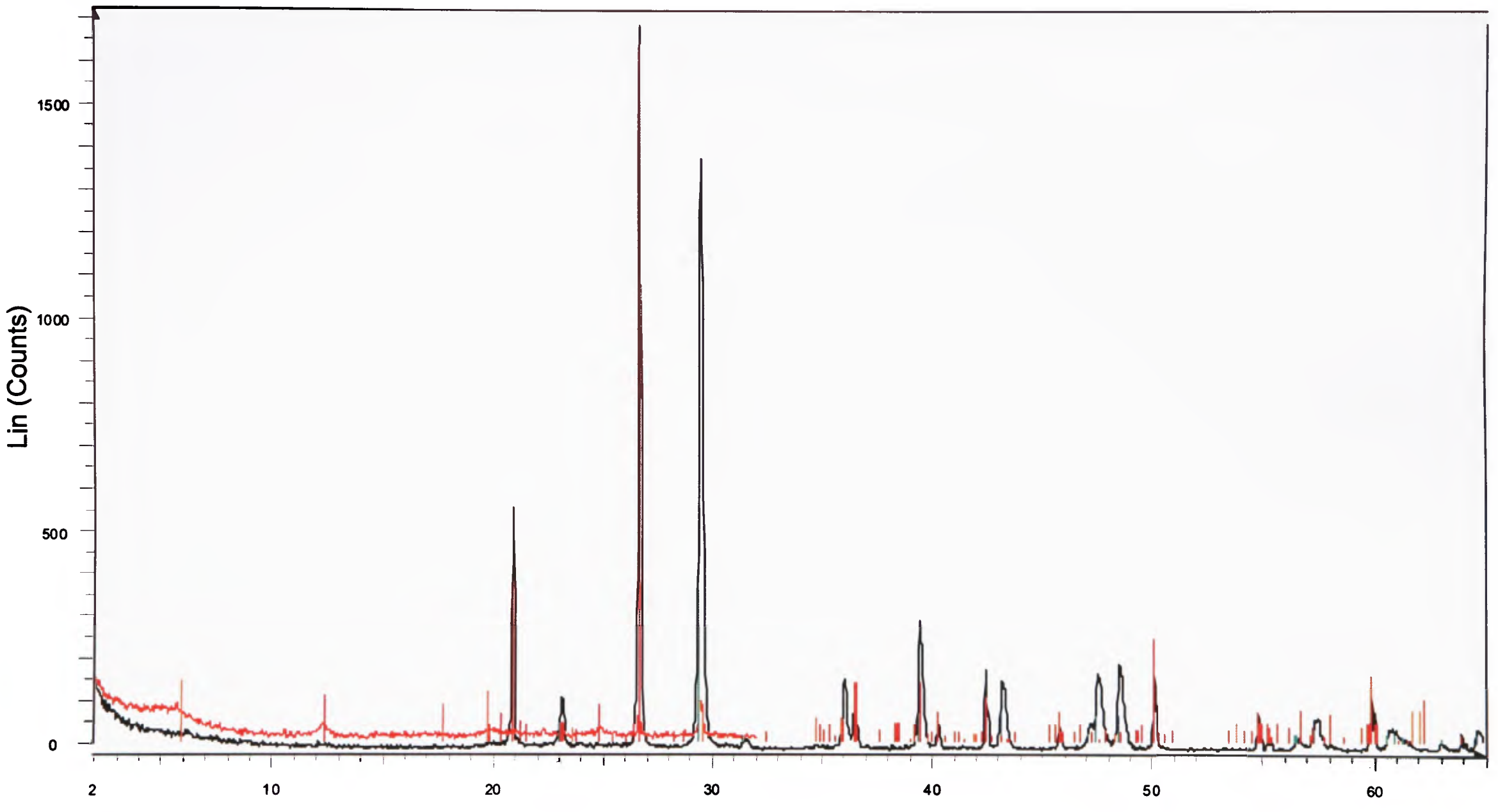
Y - 2.0 mm - Shaw A, sample 10 - File: 02136-10.raw - Type: 2Th/Th locked - Start: 2.030 ° - End: 65.025 ° - Step: 0.020 ° - Step time: 1. s
Operations: Displacement -0.052 | Smooth 0.060 | Smooth 0.060 | Import

33-1161 (*) - Quartz, syn - SiO2 - WL: 1.5406

05-0586 (*) - Calcite, syn - CaCO3 - WL: 1.5406

26-1226 (I) - Sepiolite - Mg4Si6O15(OH)2·6H2O - WL: 1.5406

Sample 11



Y - 1.0 mm - Shaw A, sample 11: clay fraction - File: 02136-11clay.raw - Type: 2Th/Th locked - Start: 2.000 ° - End: 32.000 ° - Step: 0.020 ° - Step time: 1. s
Operations: Smooth 0.060 | Import

Y - 2.0 mm - Shaw A, sample 11 - File: 02136-11.raw - Type: 2Th/Th locked - Start: 1.988 ° - End: 64.990 ° - Step: 0.020 ° - Step time: 1. s
Operations: Displacement 0.021 | Smooth 0.060 | Import

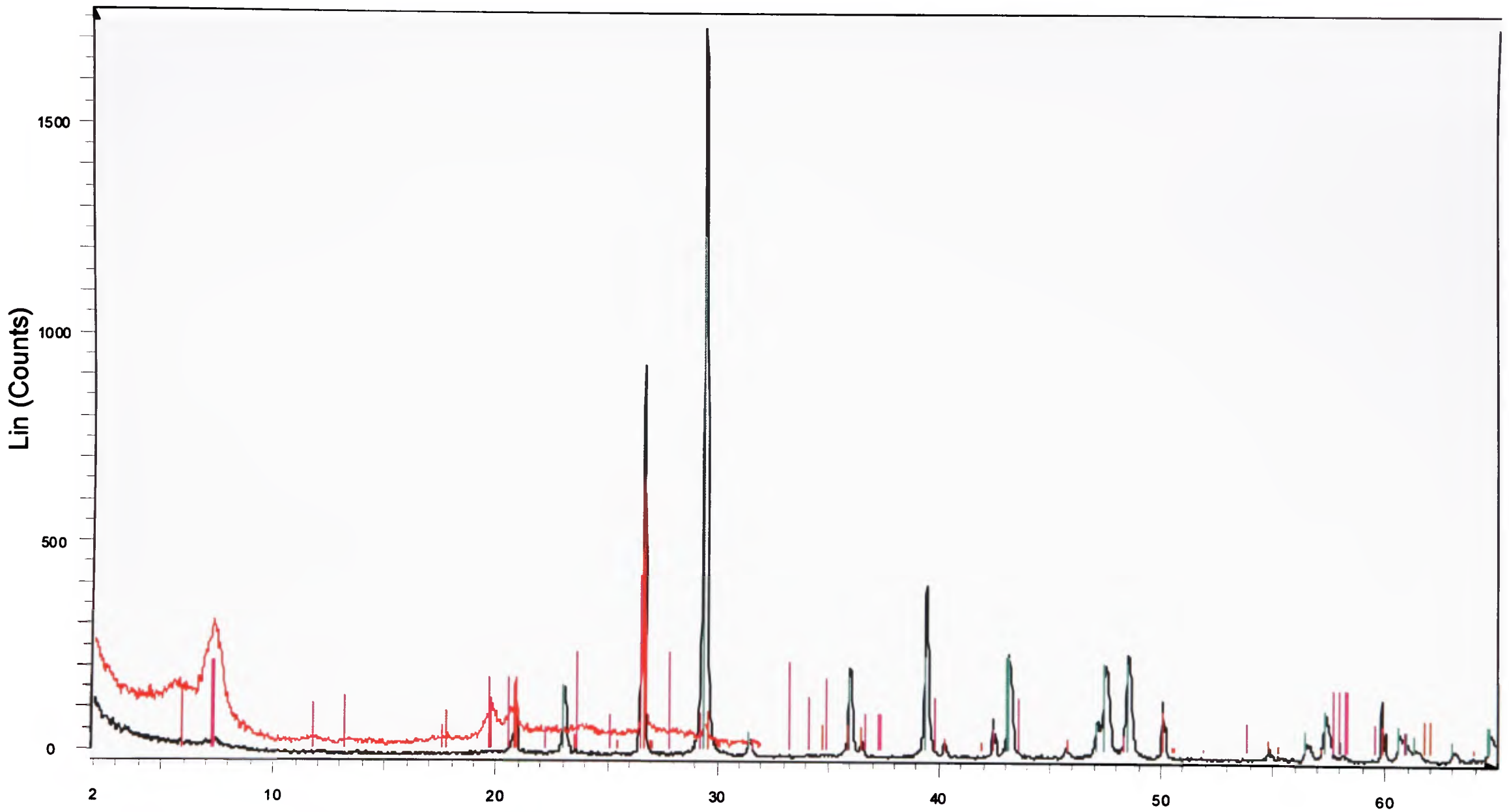
33-1161 (*) - Quartz, syn - SiO2 - WL: 1.5406

05-0586 (*) - Calcite, syn - CaCO3 - WL: 1.5406

14-0164 (I) - Kaolinite-1A - Al2Si2O5(OH)4 - WL: 1.5406

13-0135 (N) - Montmorillonite-15A - Ca0.2(Al,Mg)2Si4O10(OH)2·4H2O - WL: 1.5406

Sample 12



Y - 1.0 mm - Shaw A, sample 12 (clay fraction) - File: 02136-12clay.raw - Type: 2Th/Th locked - Start: 2.000 ° - End: 32.000 ° - Step: 0.020 ° - Step time: 1. s
Operations: Smooth 0.060 | Import

Y - 2.0 mm - Shaw A, sample 12 - File: 02136-12.raw - Type: 2Th/Th locked - Start: 1.929 ° - End: 64.940 ° - Step: 0.020 ° - Step time: 1. s
Operations: Displacement 0.125 | Smooth 0.060 | Import

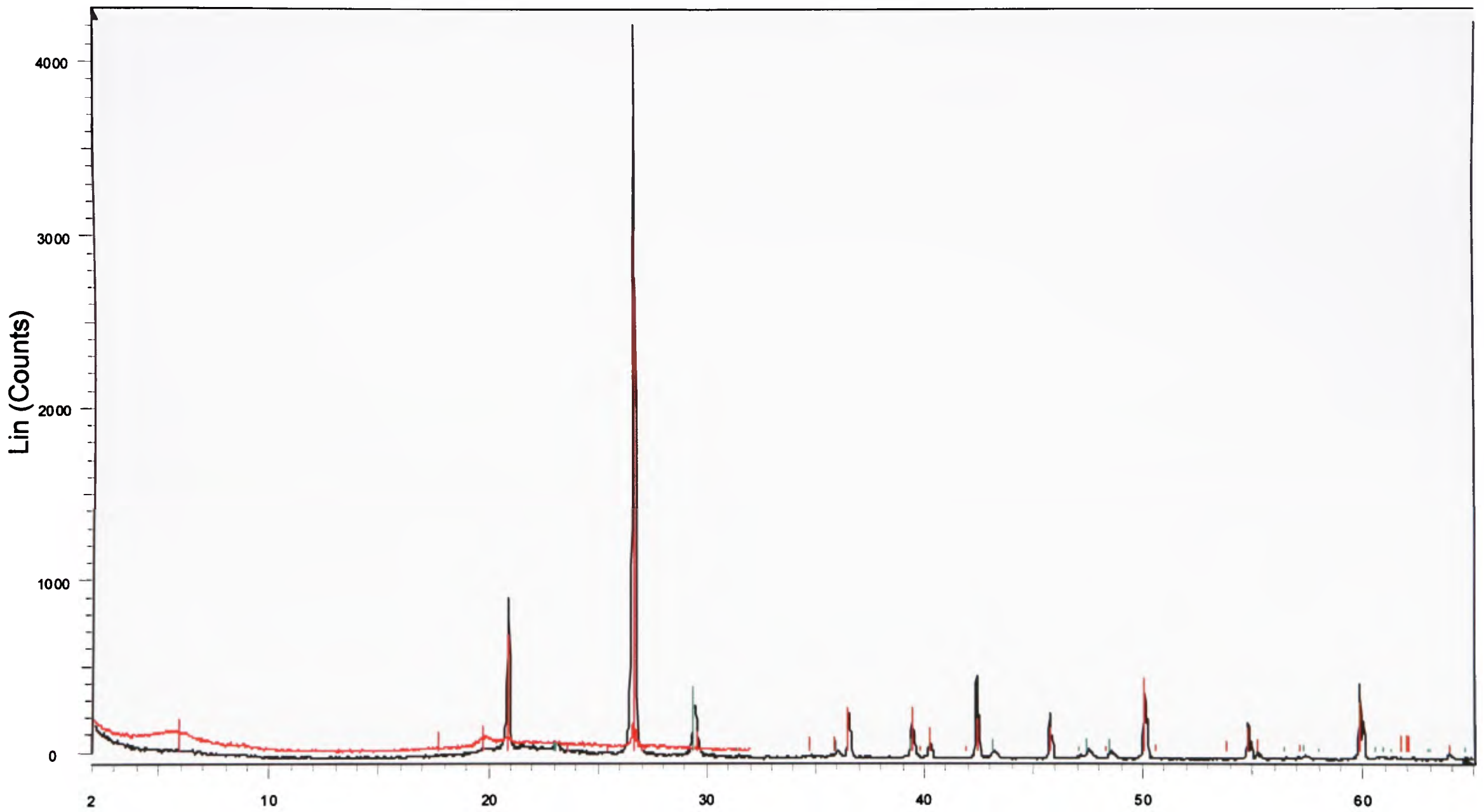
33-1161 (*) - Quartz, syn - SiO2 - WL: 1.5406

05-0586 (*) - Calcite, syn - CaCO3 - WL: 1.5406

26-1226 (I) - Sepiolite - Mg4Si6O15(OH)2·6H2O - WL: 1.5406

13-0135 (N) - Montmorillonite-15A - Ca0.2(Al,Mg)2Si4O10(OH)2·4H2O - WL: 1.5406

Sample 13



Y - 1.0 mm - Shaw A, sample 13 (clay fraction) - File: 02136-13clay.raw - Type: 2Th/Th locked - Start: 2.000 ° - End: 32.000 ° - Step: 0.020 ° - Step time: 1. s
Operations: Smooth 0.060 | Import

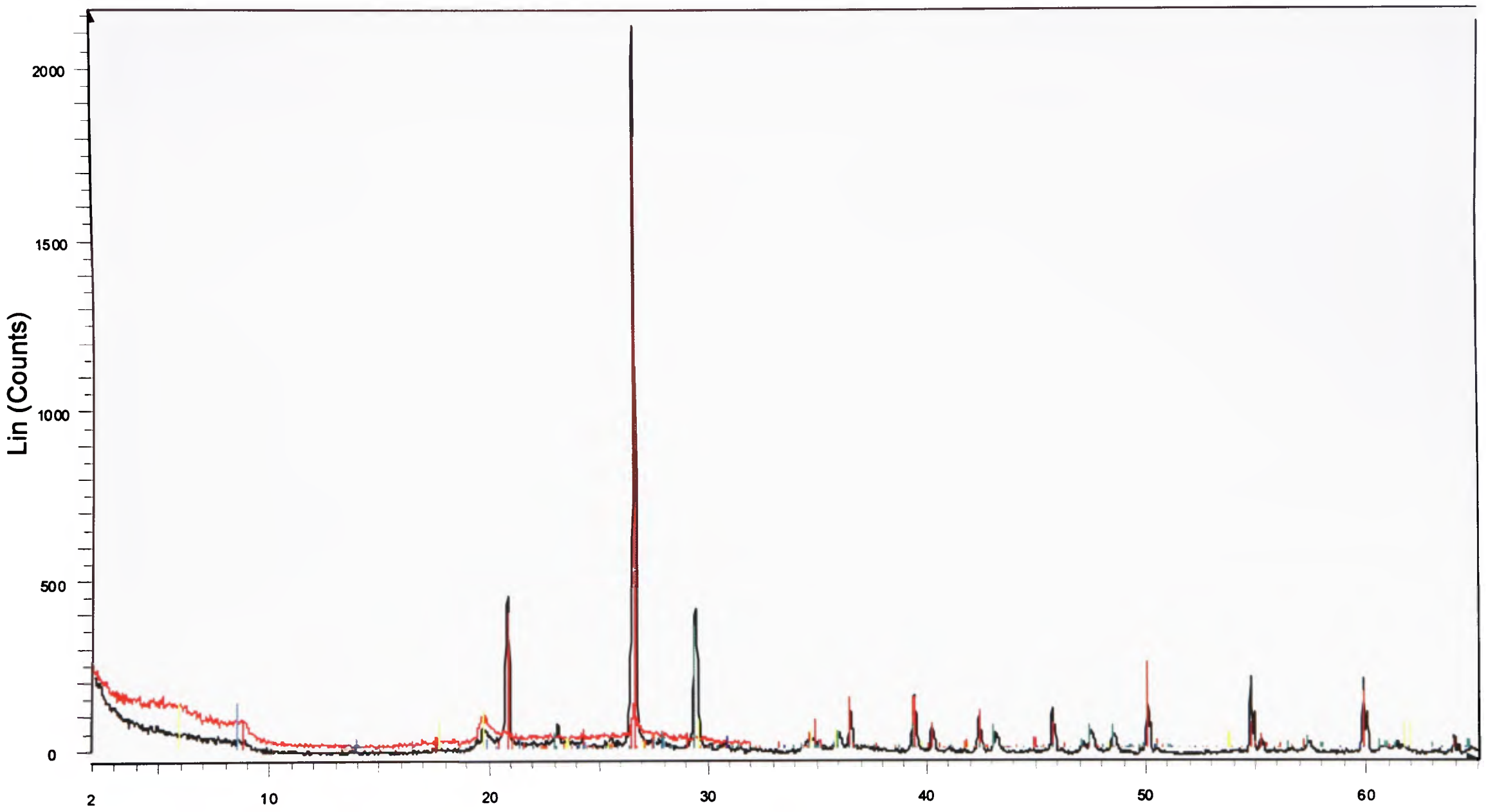
Y - 2.0 mm - Shaw A, sample 13 - File: 02136-13.raw - Type: 2Th/Th locked - Start: 2.018 ° - End: 65.015 ° - Step: 0.020 ° - Step time: 1. s
Operations: Displacement -0.031 | Smooth 0.060 | Import

33-1161 (*) - Quartz, syn - SiO2 - WL: 1.5406

05-0586 (*) - Calcite, syn - CaCO3 - WL: 1.5406

13-0135 (N) - Montmorillonite-15A - Ca0.2(Al,Mg)2Si4O10(OH)2·4H2O - WL: 1.5406

Sample 14



Y - 1.0 mm - Shaw A, sample 14 (clay fraction) - File: 02136-14clay.raw - Type: 2Th/Th l
Operations: Smooth 0.060 | Import

Y - 2.0 mm - Shaw A, sample 14 - File: 02136-14.raw - Type: 2Th/Th locked - Start: 2.0
Operations: Displacement -0.073 | Smooth 0.060 | Import

33-1161 (*) - Quartz, syn - SiO2 - WL: 1.5406

36-0426 (*) - Dolomite - CaMg(CO3)2 - WL: 1.5406

05-0586 (*) - Calcite, syn - CaCO3 - WL: 1.5406

07-0025 (I) - Muscovite-1M, syn - KAl2Si3AlO10(OH)2 - WL: 1.5406

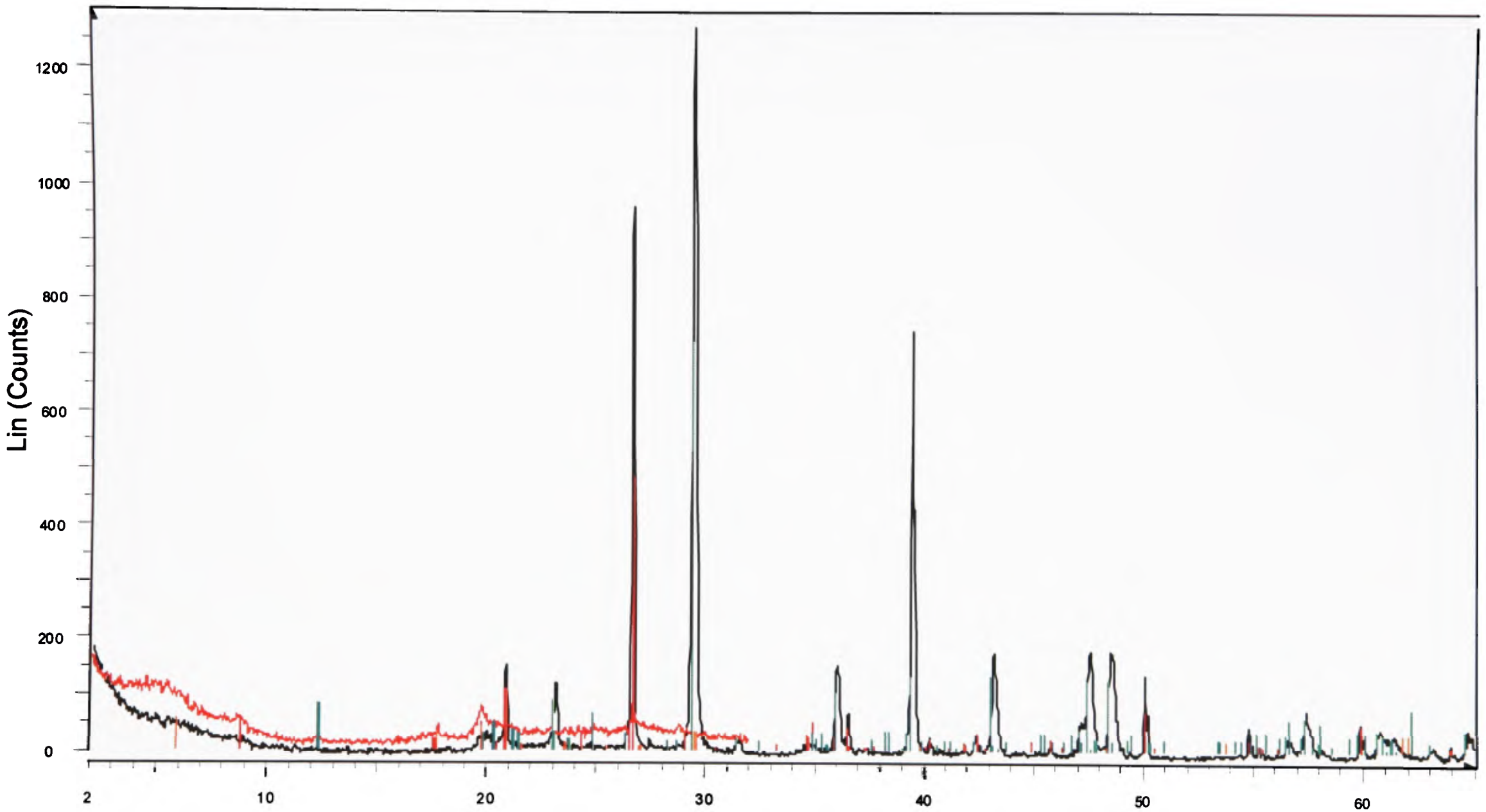
19-0932 (I) - Microcline, intermediate - KAlSi3O8 - WL: 1.5406

09-0466 (*) - Albite, ordered - NaAlSi3O8 - WL: 1.5406

21-0958 (I) - Palygorskite - (Mg,Al)5(Si,Al)8O20(OH)2·8H2O - WL: 1.5406

13-0135 (N) - Montmorillonite-15A - Ca0.2(Al,Mg)2Si4O10(OH)2·4H2O - WL: 1.5406

Sample 15



Y - 1.0 mm - Shaw A, sample 15 (clay fraction) - File: 02136-15clay.raw - Type: 2Th/Th l
Operations: Smooth 0.060 | Import

Y - 2.0 mm - Shaw A, sample 15 - File: 02136-15.raw - Type: 2Th/Th locked - Start: 2.0
Operations: Displacement -0.125 | Smooth 0.060 | Import

33-1161 (*) - Quartz, syn - SiO2 - WL: 1.5406

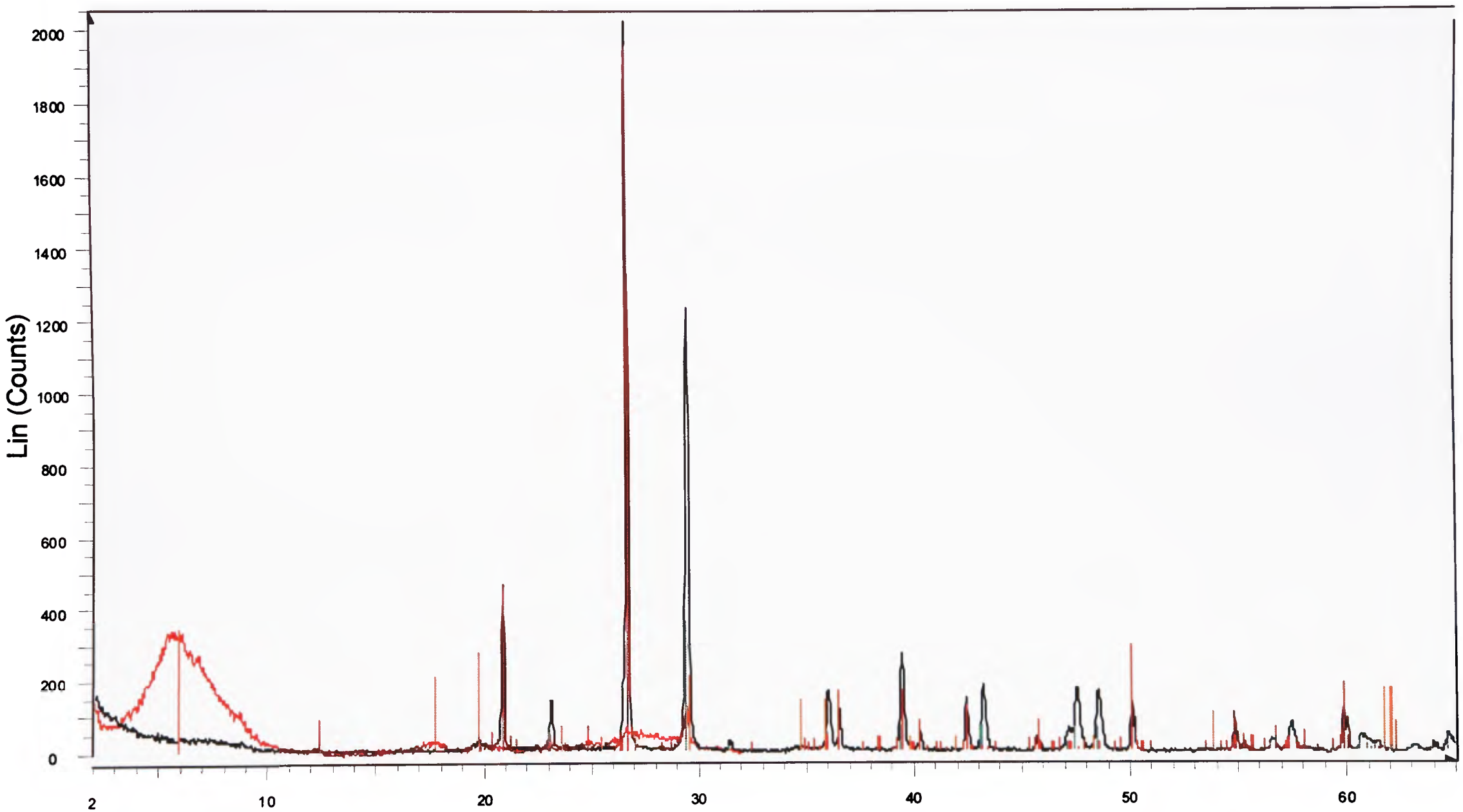
05-0586 (*) - Calcite, syn - CaCO3 - WL: 1.5406

07-0025 (I) - Muscovite-1M, syn - KAl2Si3AlO10(OH)2 - WL: 1.5406

13-0135 (N) - Montmorillonite-15A - Ca0.2(Al,Mg)2Si4O10(OH)2·4H2O - WL: 1.5406

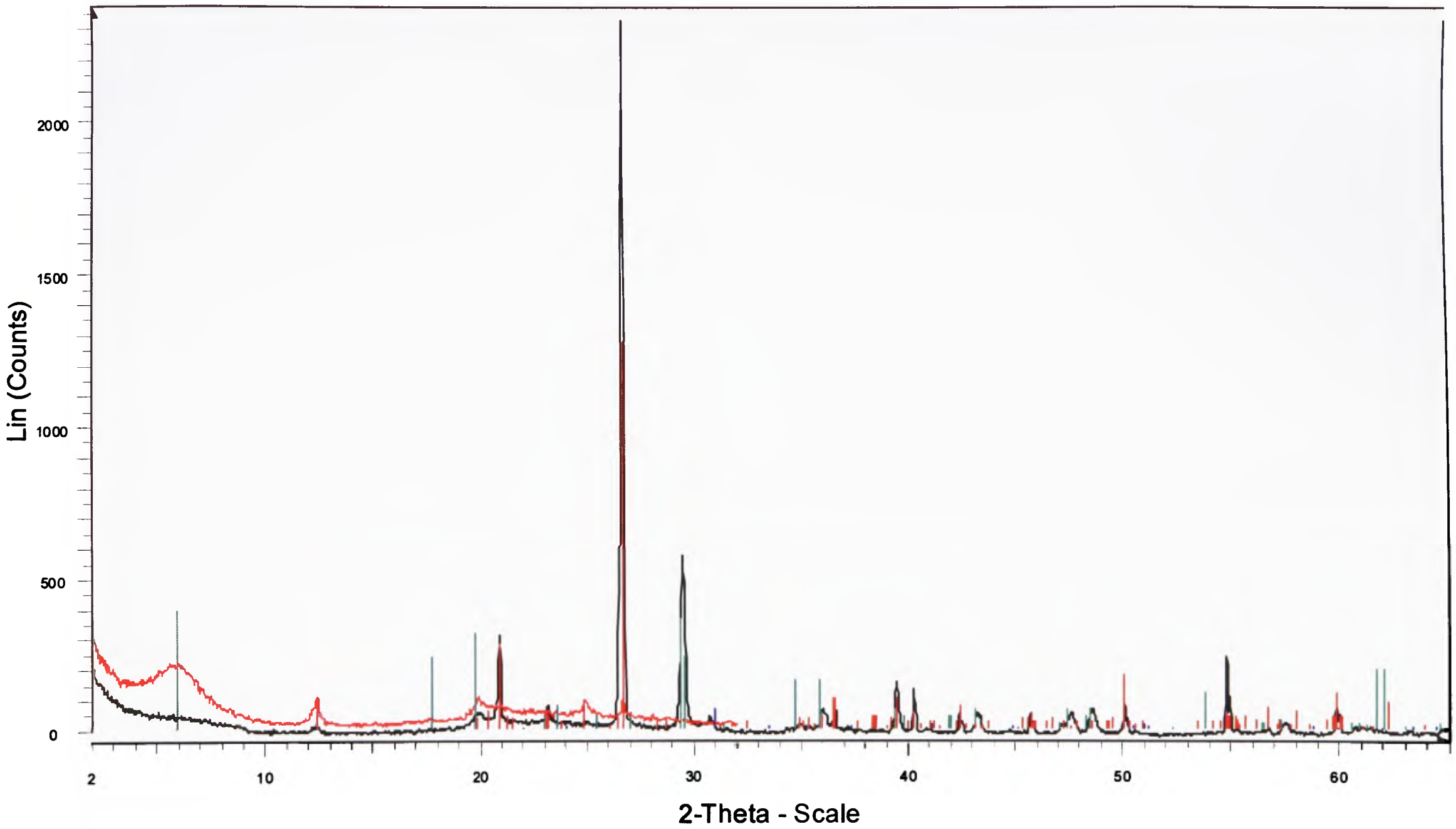
14-0164 (I) - Kaolinite-1A - Al2Si2O5(OH)4 - WL: 1.5406

Sample 16

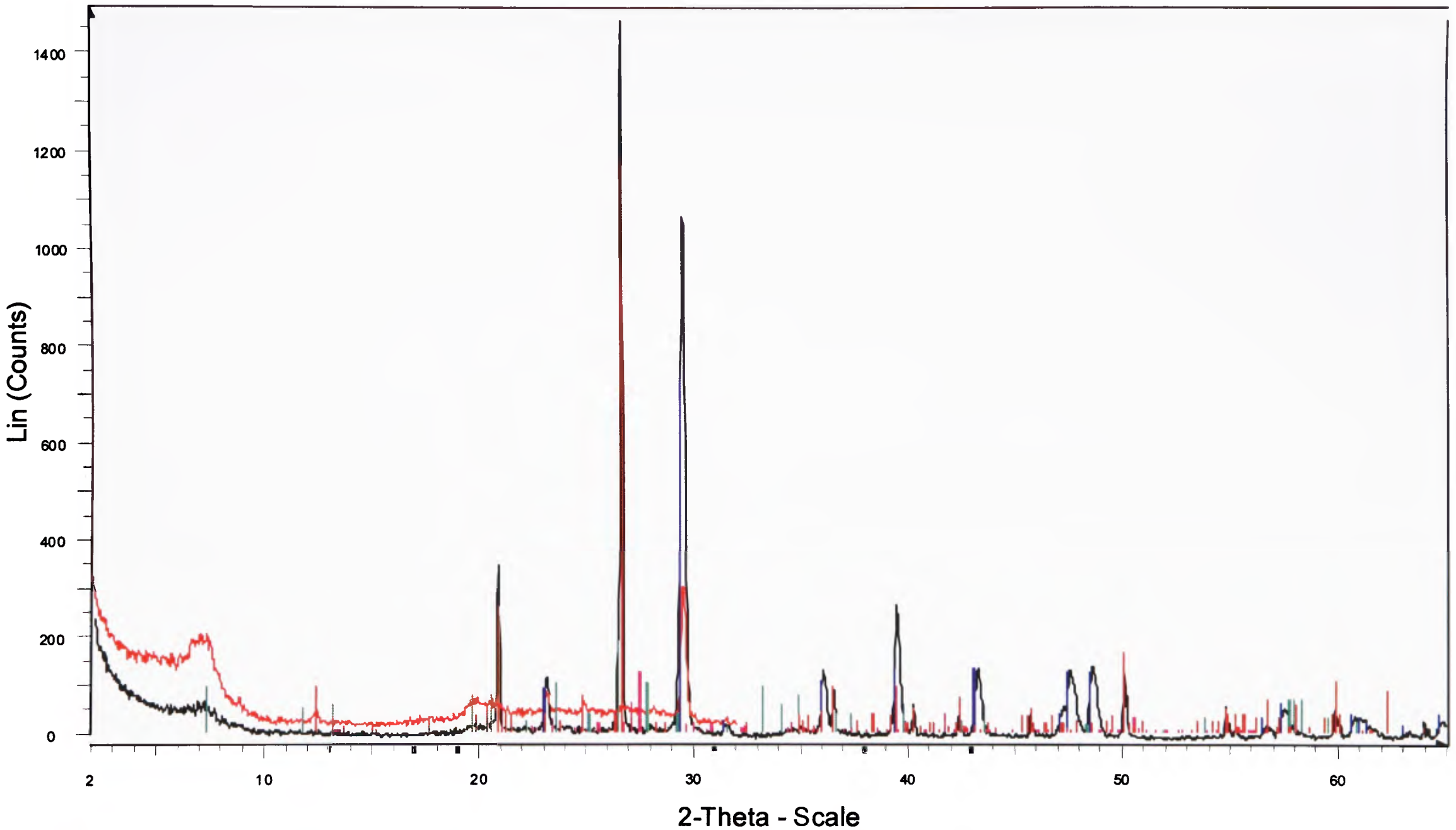


Y - 1.0 mm - Shaw A, sample 16 - File: 02136-16.raw - Type: 2Th/Th locked - Start: 2.036 ° - End: 65.030 ° - Step: 0.020 ° - Step time: 1. s
Operations: Displacement -0.063 | Smooth 0.060 | Import
Y - 2.0 mm - Shaw A, sample 16: clay fraction - File: 02136-16clay.raw - Type: 2Th/Th locked - Start: 2.000 ° - End: 32.000 ° - Step: 0.020 ° - Step time: 1. s
Operations: Smooth 0.060 | Import
33-1161 (*) - Quartz, syn - SiO2 - WL: 1.5406
05-0586 (*) - Calcite, syn - CaCO3 - WL: 1.5406
14-0164 (I) - Kaolinite-1A - Al2Si2O5(OH)4 - WL: 1.5406
13-0135 (N) - Montmorillonite-15A - Ca0.2(Al,Mg)2Si4O10(OH)2·4H2O - WL: 1.5406

Sample 17


Lin (Counts)
2000
1500
1000
500
0
2
10
20
30
40
50
60
2-Theta - Scale
Y - 1.0 mm - Shaw A, sample 17 (clay fraction) - File: 02136-17clay.raw - Type: 2Th/Th l
Operations: Smooth 0.060 | Import
Y - 2.0 mm - Shaw A, sample 17 - File: 02136-17.raw - Type: 2Th/Th locked - Start: 2.0
Operations: Smooth 0.060 | Import
33-1161 (*) - Quartz, syn - SiO2 - WL: 1.5406
36-0426 (*) - Dolomite - CaMg(CO3)2 - WL: 1.5406
05-0586 (*) - Calcite, syn - CaCO3 - WL: 1.5406
14-0164 (I) - Kaolinite-1A - Al2Si2O5(OH)4 - WL: 1.5406
13-0135 (N) - Montmorillonite-15A - Ca0.2(Al,Mg)2Si4O10(OH)2·4H2O - WL: 1.5406

Sample 18



Y - 1.0 mm - Shaw A, sample 18: clay fraction - File: 02136-18clay.raw - Type: 2Th/Th l
Operations: Smooth 0.060 | Import

Y - 2.0 mm - Shaw A, sample 18 - File: 02136-18.raw - Type: 2Th/Th locked - Start: 2.0
Operations: Displacement -0.104 | Smooth 0.060 | Import

33-1161 (*) - Quartz, syn - SiO2 - WL: 1.5406

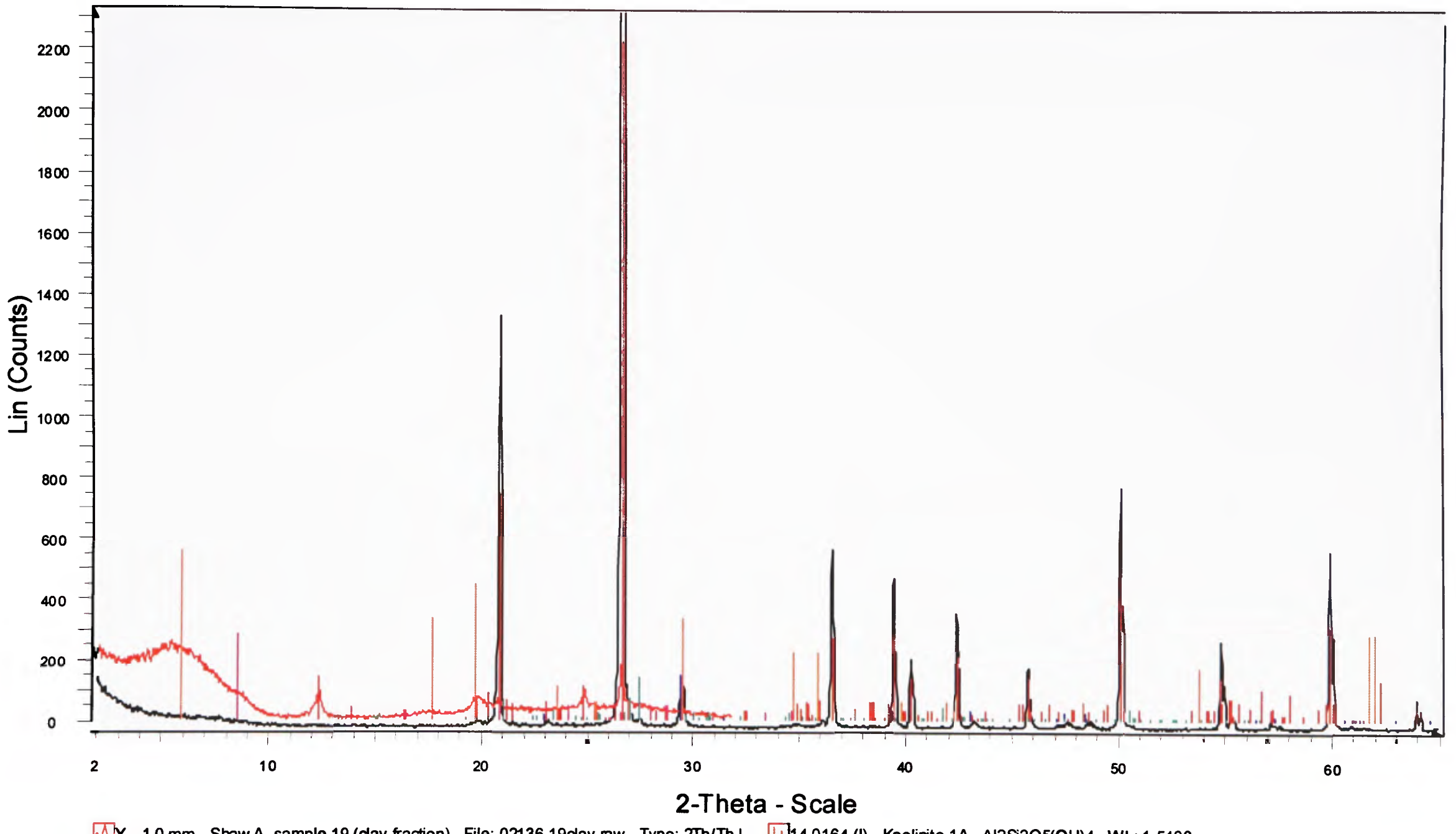
05-0586 (*) - Calcite, syn - CaCO3 - WL: 1.5406

26-1226 (l) - Sepiolite - Mg4Si6O15(OH)2·6H2O - WL: 1.5406

19-0932 (l) - Microcline, intermediate - KAlSi3O8 - WL: 1.5406

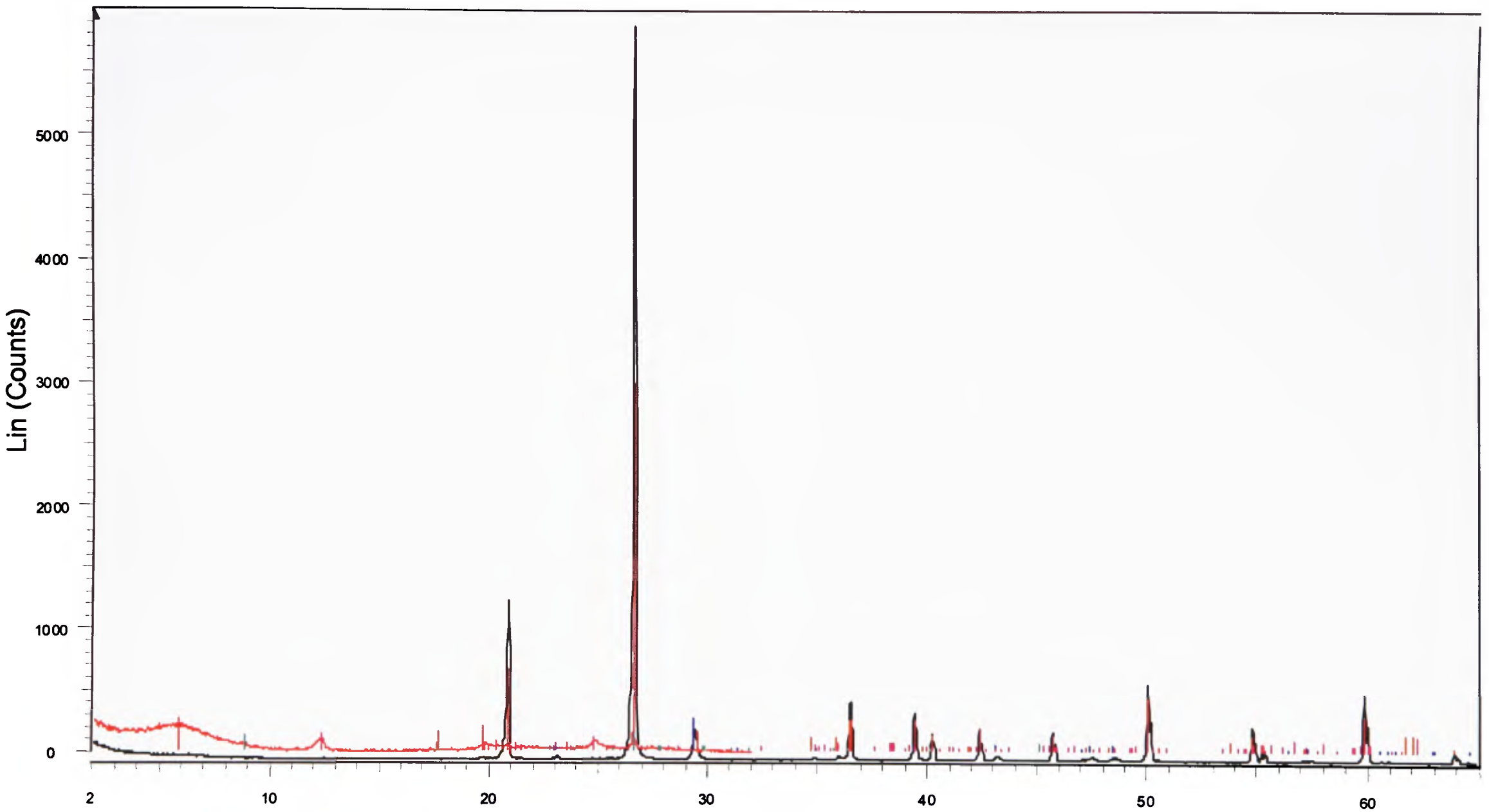
14-0164 (l) - Kaolinite-1A - Al2Si2O5(OH)4 - WL: 1.5406

Sample 19



Y - 1.0 mm - Shaw A, sample 19 (clay fraction) - File: 02136-19clay.raw - Type: 2Th/Th l
Operations: Displacement 0.373 | Displacement 0.250 | Smooth 0.060 | Import
Y - 2.0 mm - Shaw A, sample 19 - File: 02136-19.raw - Type: 2Th/Th locked - Start: 1.9
Operations: Displacement 0.062 | Smooth 0.060 | Import
33-1161 (*) - Quartz, syn - SiO2 - WL: 1.5406
05-0586 (*) - Calcite, syn - CaCO3 - WL: 1.5406
19-0932 (I) - Microcline, intermediate - KAlSi3O8 - WL: 1.5406
31-0783 (I) - Palygorskite - Mg5(Si,Al)8O20(OH)2·8H2O - WL: 1.5406
14-0164 (I) - Kaolinite-1A - Al2Si2O5(OH)4 - WL: 1.5406
13-0135 (N) - Montmorillonite-15A - Ca0.2(Al,Mg)2Si4O10(OH)2·4H2O - WL: 1.5406

Sample 20



Y - 1.0 mm - Shaw A, sample 20 (clay fraction) - File: 02136-20clay.raw - Type: 2Th/Th l
Operations: Displacement -0.088 | Smooth 0.060 | Import

Y - 2.0 mm - Shaw A, sample 20 - File: 02136-20.raw - Type: 2Th/Th locked - Start: 1.9
Operations: Displacement 0.034 | Smooth 0.060 | Import

33-1161 (*) - Quartz, syn - SiO2 - WL: 1.5406

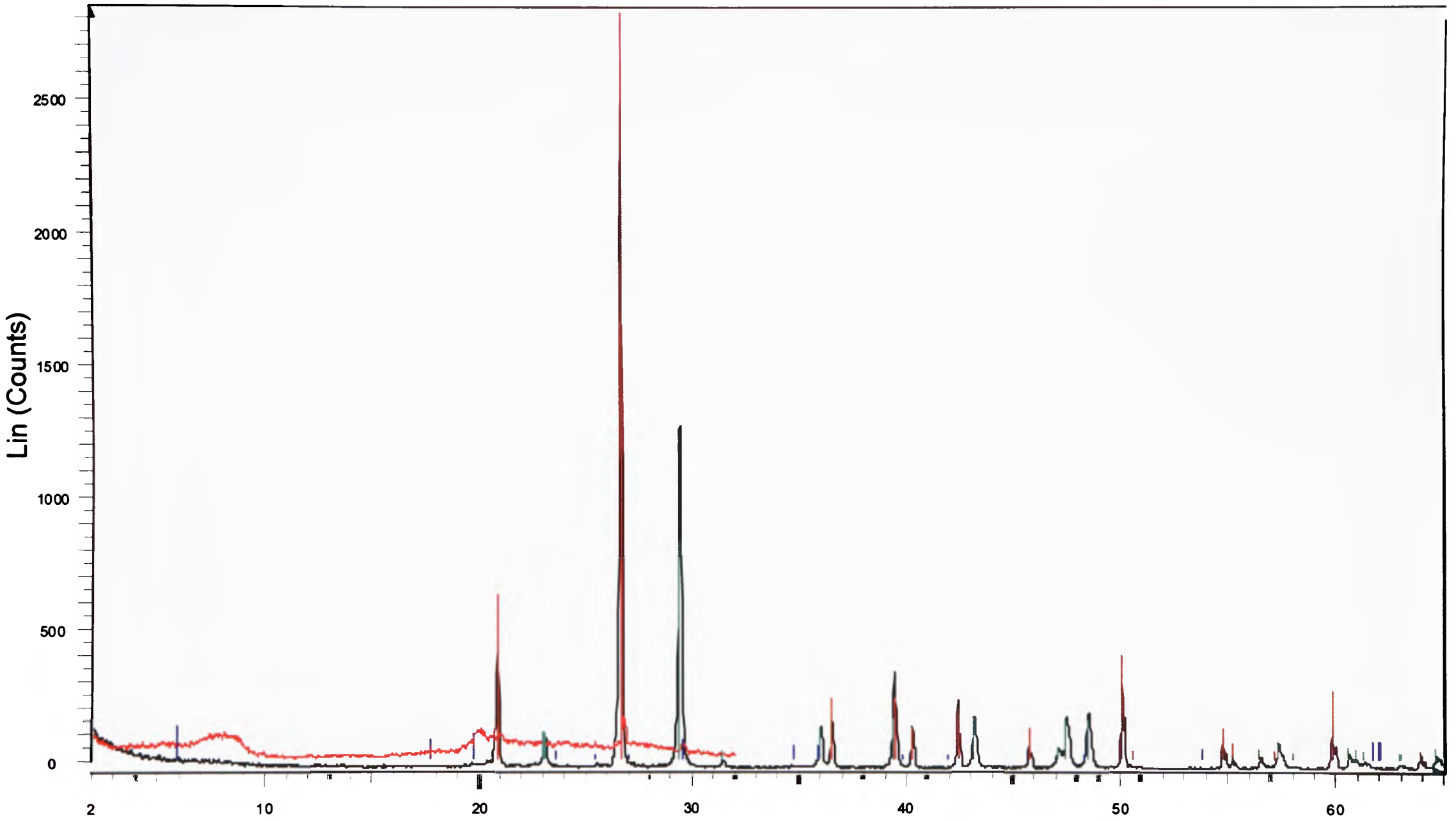
05-0586 (*) - Calcite, syn - CaCO3 - WL: 1.5406

26-0911 (I) - Illite-2M1 - (K,H3O)Al2Si3AlO10(OH)2 - WL: 1.5406

14-0164 (I) - Kaolinite-1A - Al2Si2O5(OH)4 - WL: 1.5406

13-0135 (N) - Montmorillonite-15A - Ca0.2(Al,Mg)2Si4O10(OH)2·4H2O - WL: 1.5406

Sample 21



Y - 1.0 mm - Shaw A, sample 21 (clay fraction) - File: 02136-21clay.raw - Type: 2Th/Th locked - Start: 2.000 ° - End: 32.000 ° - Step: 0.020 ° - Step time: 1. s
Operations: Smooth 0.060 | Import

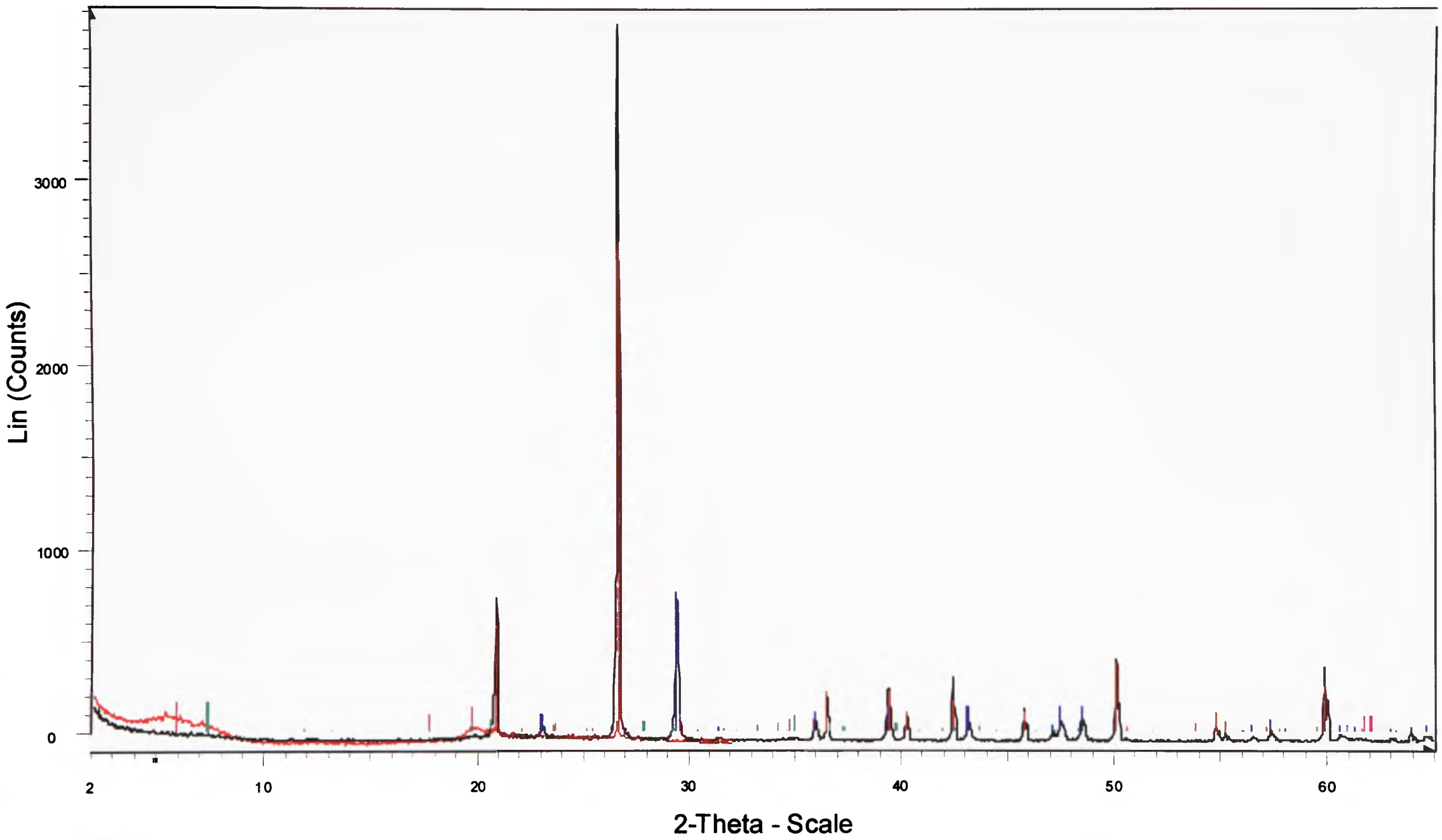
Y - 2.0 mm - Shaw, sample 21 - File: 02136-21.raw - Type: 2Th/Th locked - Start: 2.018 ° - End: 65.015 ° - Step: 0.020 ° - Step time: 1. s
Operations: Displacement -0.031 | Smooth 0.060 | Import

33-1161 (*) - Quartz, syn - SiO2 - WL: 1.5406

05-0586 (*) - Calcite, syn - CaCO3 - WL: 1.5406

13-0135 (N) - Montmorillonite-15A - Ca0.2(Al,Mg)2Si4O10(OH)2·4H2O - WL: 1.5406

Sample 22



Y - 2.0 mm - Shaw, sample 22 - File: 02136-22.raw - Type: 2Th/Th locked - Start: 2.024 ° - End: 65.020 ° - Step: 0.020 ° - Step time: 1. s
Operations: Displacement -0.042 | Smooth 0.060 | Import

Y - 3.0 mm - Shaw A, sample 22 (clay fraction) - File: 02136-22clay.raw - Type: 2Th/Th locked - Start: 2.000 ° - End: 32.000 ° - Step: 0.020 ° - Step time: 1. s
Operations: Smooth 0.060 | Import

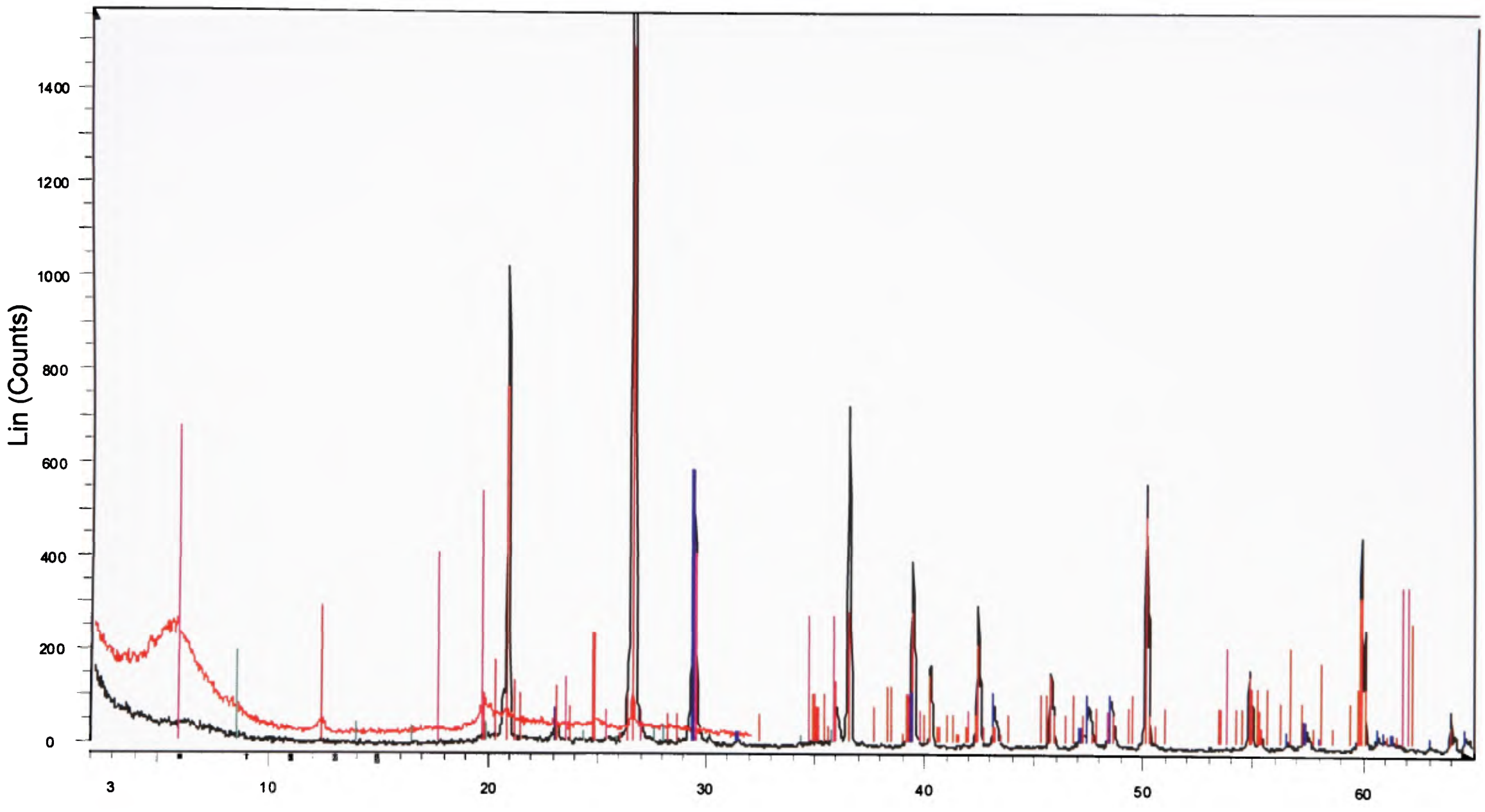
33-1161 (*) - Quartz, syn - SiO2 - WL: 1.5406

05-0586 (*) - Calcite, syn - CaCO3 - WL: 1.5406

13-0135 (N) - Montmorillonite-15A - Ca0.2(Al,Mg)2Si4O10(OH)2·4H2O - WL: 1.5406

13-0595 (I) - Sepiolite - Mg4Si6O15(OH)2·6H2O - WL: 1.5406

Sample 23



Y - 1.0 mm - Shaw A, sample 23 (clay fraction) - File: 02136-23clay.raw - Type: 2Th/Th l
Operations: Displacement -0.104 | Smooth 0.060 | Import

Y - 2.0 mm - Shaw, sample 23 - File: 02136-23.raw - Type: 2Th/Th locked - Start: 2.042
Operations: Displacement -0.073 | Smooth 0.060 | Import

33-1161 (*) - Quartz, syn - SiO2 - WL: 1.5406

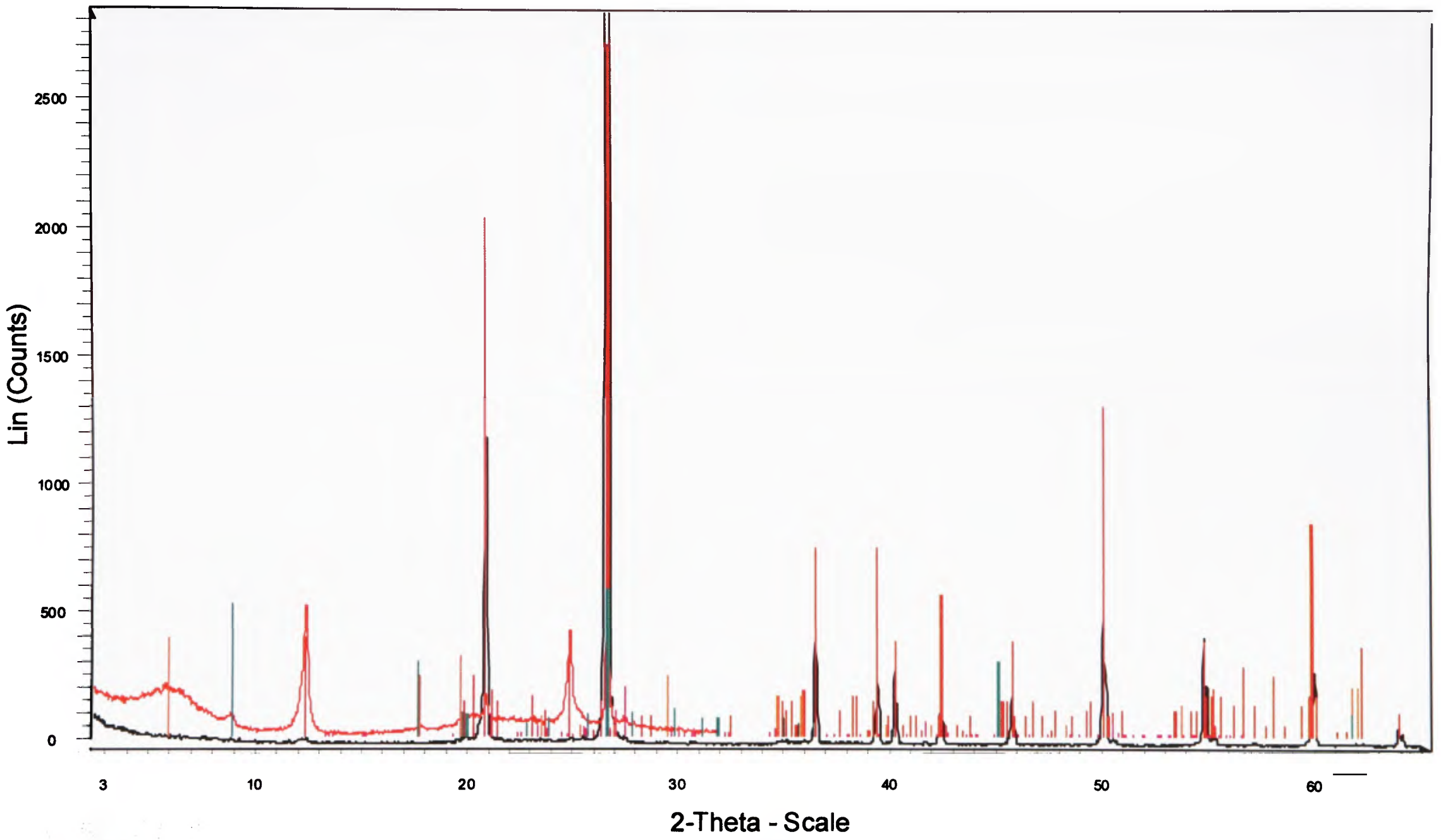
05-0586 (*) - Calcite, syn - CaCO3 - WL: 1.5406

21-0958 (I) - Palygorskite - (Mg,Al)5(Si,Al)8O20(OH)2·8H2O - WL: 1.5406

13-0135 (N) - Montmorillonite-15A - Ca0.2(Al,Mg)2Si4O10(OH)2·4H2O - WL: 1.5406

14-0164 (I) - Kaolinite-1A - Al2Si2O5(OH)4 - WL: 1.5406

Sample 24



Y - 1.0 mm - Shaw sample 24 (Clay prep) - File: 02136-24clay.raw - Type: 2Th/Th locke
Operations: Smooth 0.060 | Import

Y - 2.0 mm - Shaw, sample 24 - File: 02136-24.raw - Type: 2Th/Th locked - Start: 2.000
Operations: Smooth 0.060 | Import

33-1161 (*) - Quartz, syn - SiO2 - WL: 1.5406

14-0164 (I) - Kaolinite-1A - Al2Si2O5(OH)4 - WL: 1.5406

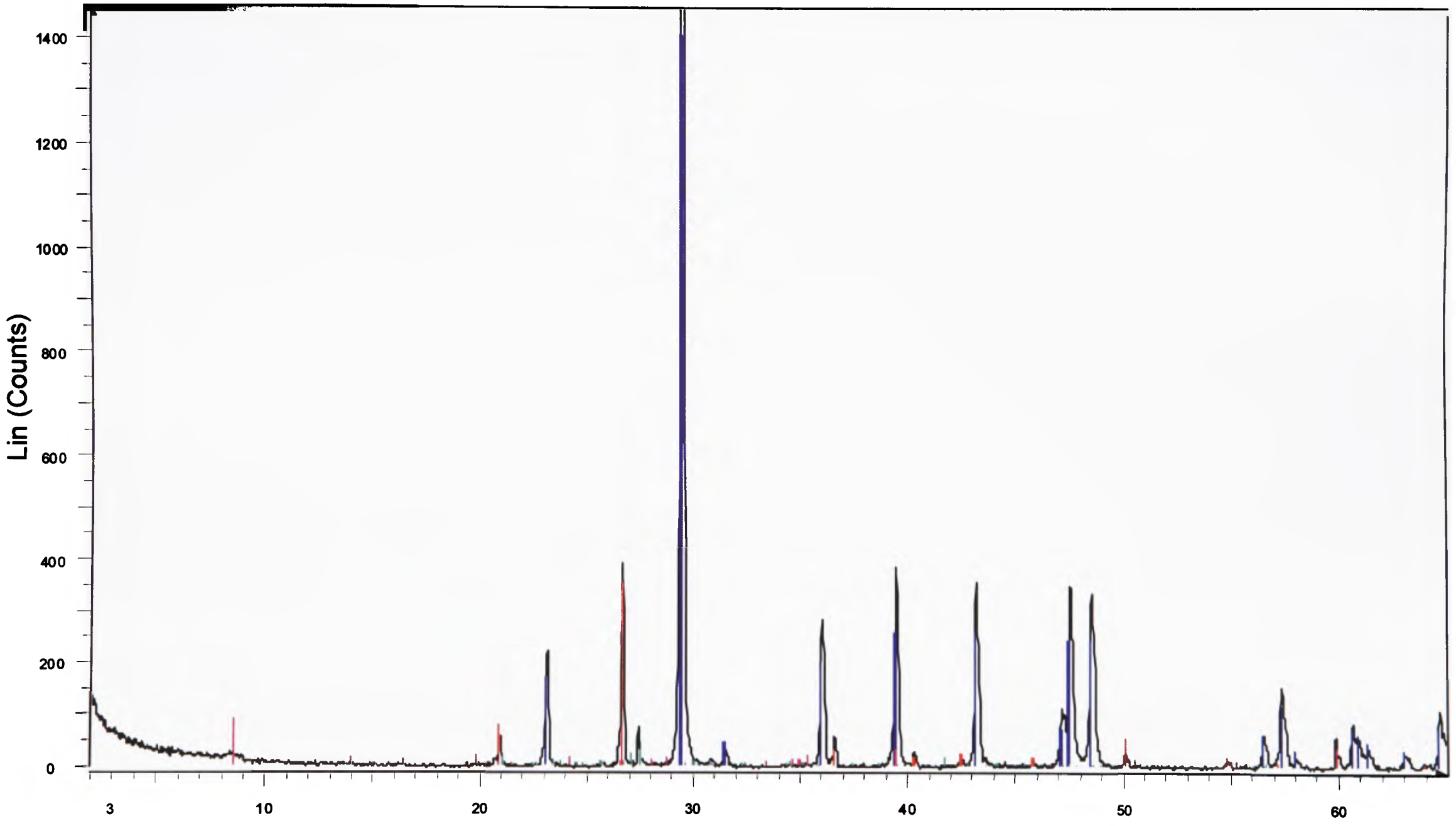
19-0932 (I) - Microcline, intermediate - KAlSi3O8 - WL: 1.5406

14-0164 (I) - Kaolinite-1A - Al2Si2O5(OH)4 - WL: 1.5406

13-0135 (N) - Montmorillonite-15A - Ca0.2(Al,Mg)2Si4O10(OH)2·4H2O - WL: 1.5406

26-0911 (I) - Illite-2M1 - (K,H3O)Al2Si3AlO10(OH)2 - WL: 1.5406

Sample 25



Y - 1.0 mm - Shaw, sample 25 - File: 02136-25.raw - Type: 2Th/Th locked - Start: 1.976 ° - End: 64.980 ° - Step: 0.020 ° - Step time: 1. s

Operations: Displacement 0.042 | Smooth 0.060 | Import

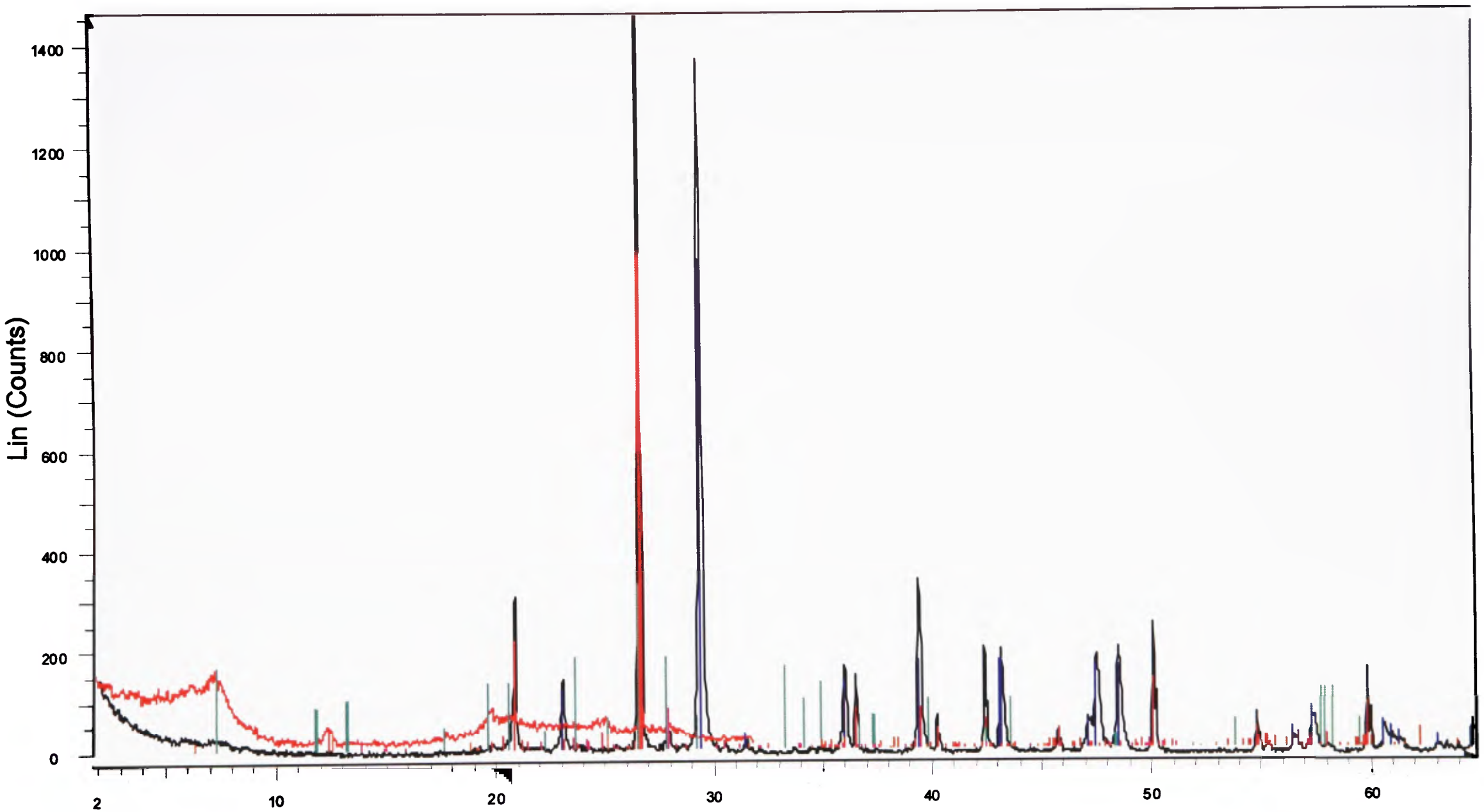
33-1161 (*) - Quartz, syn - SiO2 - WL: 1.5406

05-0586 (*) - Calcite, syn - CaCO3 - WL: 1.5406

19-0932 (I) - Microcline, intermediate - KAlSi3O8 - WL: 1.5406

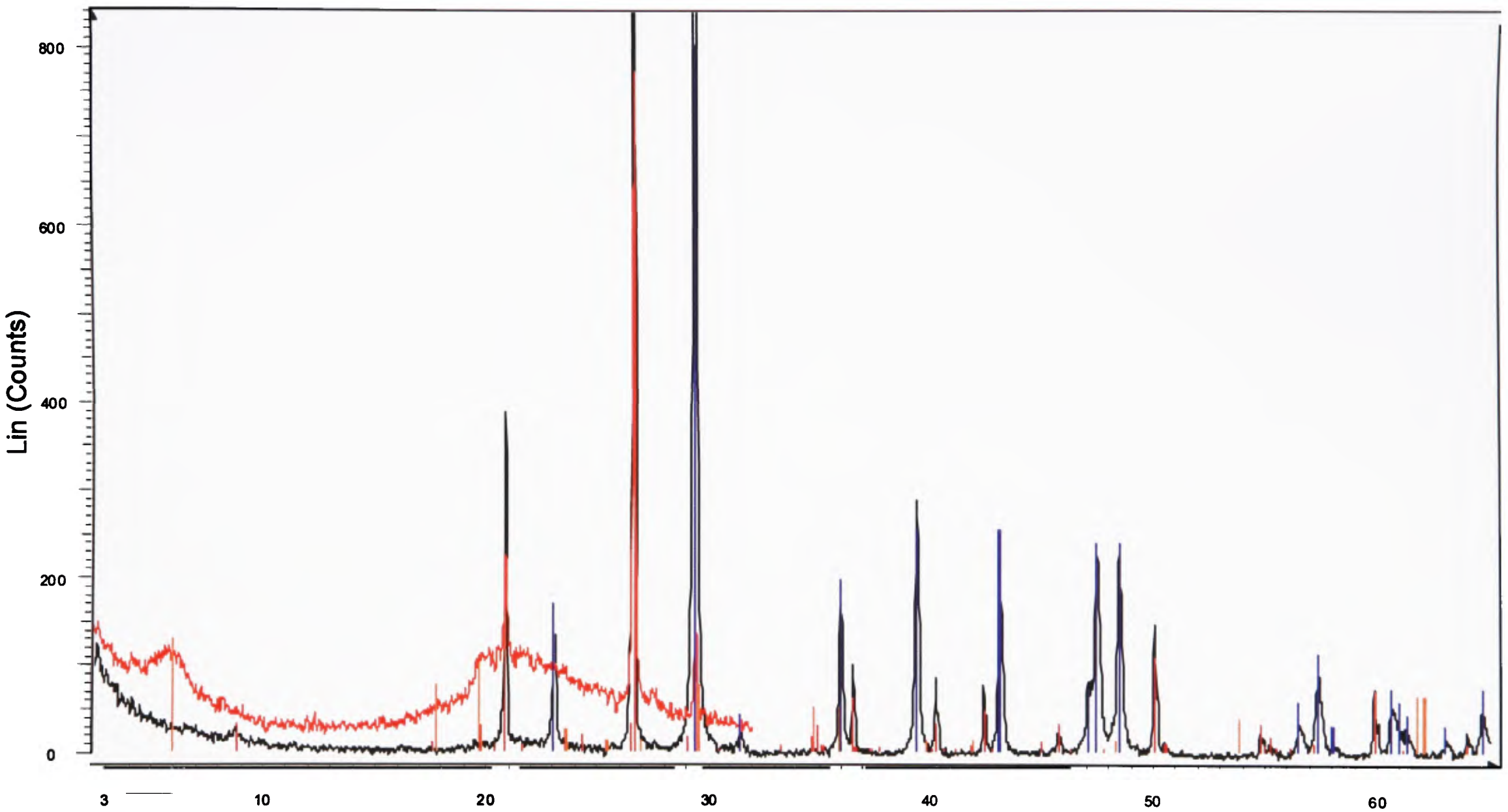
31-0783 (I) - Palygorskite - Mg5(Si,Al)8O20(OH)2·8H2O - WL: 1.5406

Sample 26



Y - 1.0 mm - Shaw sample 26 (Clay prep) - File: 02136-26clay.raw - Type: 2Th/Th locke
Operations: Displacement 0.370 | Displacement 0.250 | Smooth 0.060 | Import
Y - 2.0 mm - Shaw A, sample 26 - File: 02136-26.raw - Type: 2Th/Th locked - Start: 2.0
Operations: Smooth 0.060 | Import
33-1161 (*) - Quartz, syn - SiO2 - WL: 1.5406
26-1226 (I) - Sepiolite - Mg4Si6O15(OH)2·6H2O - WL: 1.5406
09-0466 (*) - Albite, ordered - NaAlSi3O8 - WL: 1.5406
05-0586 (*) - Calcite, syn - CaCO3 - WL: 1.5406
14-0164 (I) - Kaolinite-1A - Al2Si2O5(OH)4 - WL: 1.5406
29-0701 (I) - Clinochlore-1MIIb, ferroan - (Mg,Fe)6(Si,Al)4O10(OH)8 - WL: 1.5406

Sample 27



Y - 1.0 mm - Shaw sample 27 (Clay prep) - File: 02136-27clay.raw - Type: 2Th/Th locked - Start: 1.981 ° - End: 31.982 ° - Step: 0.020 ° - Step time: 1. s
Operations: Displacement 0.033 | Smooth 0.060 | Import

Y - 2.0 mm - Shaw, sample 27 - File: 02136-27.raw - Type: 2Th/Th locked - Start: 2.031 ° - End: 65.027 ° - Step: 0.020 ° - Step time: 1. s
Operations: Displacement -0.055 | Smooth 0.060 | Import

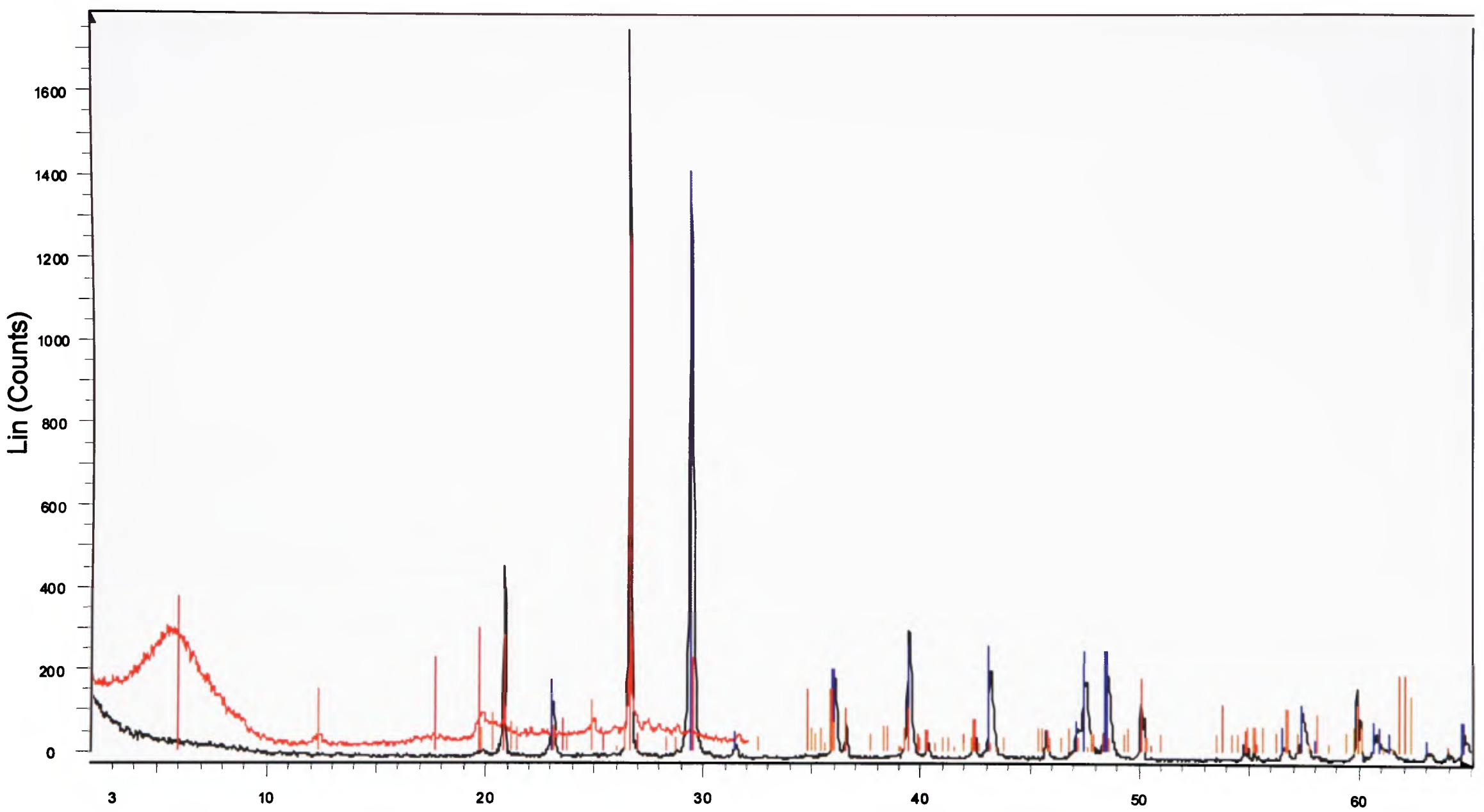
33-1161 (*) - Quartz, syn - SiO2 - WL: 1.5406

05-0586 (*) - Calcite, syn - CaCO3 - WL: 1.5406

07-0025 (I) - Muscovite-1M, syn - KAl2Si3AlO10(OH)2 - WL: 1.5406

13-0135 (N) - Montmorillonite-15A - Ca0.2(Al,Mg)2Si4O10(OH)2·4H2O - WL: 1.5406

Sample 28



Y - 1.0 mm - Shaw sample 28 (Clay prep) - File: 02136-28clay.raw - Type: 2Th/Th locked - Start: 2.042 ° - End: 32.040 ° - Step: 0.020 ° - Step time: 1. s
Operations: Displacement -0.073 | Smooth 0.060 | Import

Y - 2.0 mm - Shaw, sample 28 - File: 02136-28.raw - Type: 2Th/Th locked - Start: 2.062 ° - End: 65.052 ° - Step: 0.020 ° - Step time: 1. s
Operations: Displacement -0.108 | Smooth 0.060 | Import

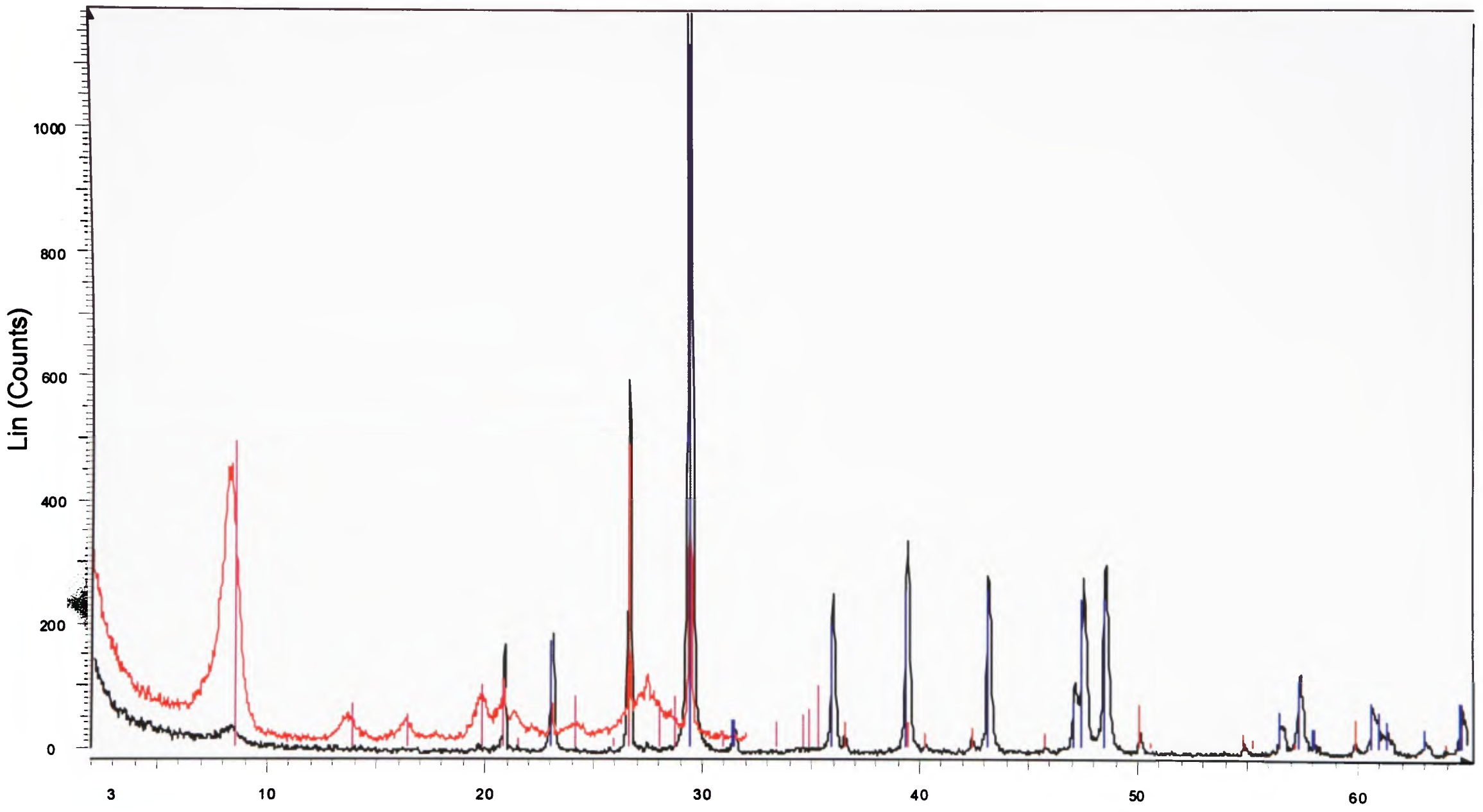
33-1161 (*) - Quartz, syn - SiO2 - WL: 1.5406

05-0586 (*) - Calcite, syn - CaCO3 - WL: 1.5406

13-0135 (N) - Montmorillonite-15A - Ca0.2(Al,Mg)2Si4O10(OH)2·4H2O - WL: 1.5406

14-0164 (I) - Kaolinite-1A - Al2Si2O5(OH)4 - WL: 1.5406

Sample 29



Y - 1.0 mm - Shaw sample 29 (Clay prep) - File: 02136-29clay.raw - Type: 2Th/Th locked - Start: 2.000 ° - End: 32.000 ° - Step: 0.020 ° - Step time: 1. s
Operations: Smooth 0.060 | Import

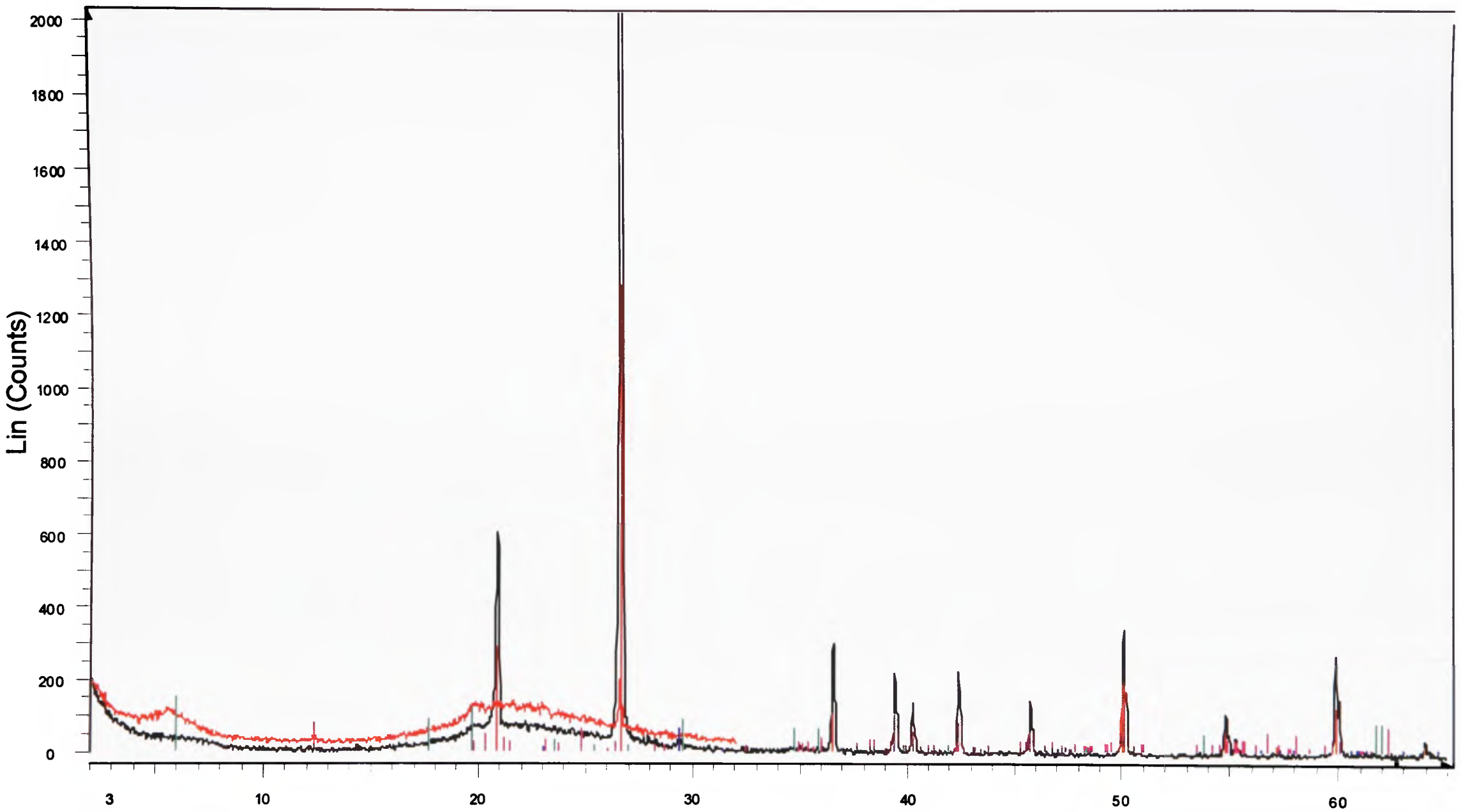
Y - 2.0 mm - Shaw, sample 29 - File: 02136-29.raw - Type: 2Th/Th locked - Start: 2.031 ° - End: 65.027 ° - Step: 0.020 ° - Step time: 1. s
Operations: Displacement -0.055 | Smooth 0.060 | Import

33-1161 (*) - Quartz, syn - SiO2 - WL: 1.5406

05-0586 (*) - Calcite, syn - CaCO3 - WL: 1.5406

31-0783 (I) - Palygorskite - Mg5(Si,Al)8O20(OH)2·8H2O - WL: 1.5406

Sample 30



Y - 1.0 mm - Shaw sample 30 (Clay prep) - File: 02136-30clay.raw - Type: 2Th/Th locked - Start: 2.000 ° - End: 32.000 ° - Step: 0.020 ° - Step time: 1. s
Operations: Smooth 0.060 | Import

Y - 2.0 mm - Shaw, sample 30 - File: 02136-30.raw - Type: 2Th/Th locked - Start: 2.031 ° - End: 65.027 ° - Step: 0.020 ° - Step time: 1. s
Operations: Displacement -0.055 | Smooth 0.060 | Import

33-1161 (*) - Quartz, syn - SiO2 - WL: 1.5406

05-0586 (*) - Calcite, syn - CaCO3 - WL: 1.5406

14-0164 (I) - Kaolinite-1A - Al2Si2O5(OH)4 - WL: 1.5406

13-0135 (N) - Montmorillonite-15A - Ca0.2(Al,Mg)2Si4O10(OH)2·4H2O - WL: 1.5406

Appendix 6: Summary of magnetic susceptibility.

Magnetic Susceptibility in CGS units	
Sample	**Average Value**
B/1999/NG1A	4.08
B/1999/NG1B	2.13
B/1999/NG1 1.5m	1.37
B/2000/25A	3.05
B/2000/26A	2.90
B/2000/26B	3.73
B/2000/26C Matrix	1.80
B/2000/26C Nodules	4.05
B/2000/27A	2.45
B/2000/27B	3.20
B/2000/28A	2.20
B/2000/29A	2.00
B/2000/30Aa Matrix	1.50
B/2000/30Aa Nodules	3.80
B/2000/30 Ab	1.15
B/2000/30B	2.10
B/2000/31A	1.05
B/2000/32A Matrix	0.42
B/2000/32A Nodules	0.38
B/2000/33A Matrix	0.33
B/2000/33A Nodules	0.62
B/2000/34A	3.95
B/2000/35A	1.20
B/2000/36A	0.37
B/2000/36B	1.17
B/2000/36C	1.12
B/2000/37A	1.43
B/2000/38A	1.87
B/2000/38B	1.43
B/2000/38C	1.15
B/2000/39A Matrix	1.90
B/2000/39A Nodules	1.38
B/2000/39B Matrix	1.53
B/2000/39B Nodules	5.80
B/2000/40 Matrix	3.52
B/2000/40 Nodules	1.98
B/2000/41A	0.57
B/2000/41B	2.03
B/2000/42A	0.77
B/2000/43A	12.93
B/2000/43B	30.87
B/2000/44A	1.98
B/2000/44B	1.12
B/2000/44C	0.78
B/2000/44D	0.58
B/2000/45A	5.52
B/2000/45B Matrix	1.52
B/2000/45B Nodules	3.68
B/2000/45C	1.03
B/2000/46A Matrix	2.32
B/2000/46A Nodules	4.47
B/2000/47B Matrix	1.27
B/2000/47B Nodules	12.10
B/2000/47C	5.25
B/2000/48A	1.53
B/2000/48B	0.32
B/2000/48C	0.42
B/2000/48D	0.15
B/2000/49D	0.28
B/2000/50A	2.87
B/2000/50B Rind	7.42
B/2000/50B Core	4.25
B/2000/51A	1.73
B/2000/52A	3.38
B/2000/52B	2.48
B/2000/52C	2.22
Mosupatsela A 150 cm	3.82
Mosupatsela B 200 cm	1.62
Mosupatsela C surface	0.83
Mosupatsela C 20 cm	0.97
Mosupatsela C 50 cm	0.58
Gaenga surface	0.50
Gaenga 20 cm	0.63
Gaenga 40 cm	0.13
Xhamoga A surface	3.85
Xhamoga A 20 cm	3.57
Xhamoga A 40 cm	3.48
Xhamoga A 60 cm	2.18
Xhamoga B surface	2.98
Xhamoga B 20 cm	4.95
Xhamoga B 40 cm	3.27
Xhamoga B 60 cm	4.07
Xhamoga B 80 cm	4.32
Xhamoga B 100 cm	3.98
Xhamoga B 120cm	3.97
Xhamoga B 140 cm	4.10
Xhamoga B 160 cm	3.80
Xhamoga B 180 cm	1.85
Xhamoga C surface	2.50
Xhamoga C 20 cm	1.83
Xhamoga C 40 cm	2.28
Xhamoga C 80 cm	2.97
Xhamoga C 90 cm	2.18
Xhamoga D surface	0.50
Xhamoga D 20 cm	0.28

Appendix 7: Summary table of loss on ignition (LOI) results.

Sample	% organic material	% carbonate	% other minerals
B/2000/25A	1.6	3.3	96.7
B/2000/26A	1.2	32.0	68.0
B/2000/26B	1.0	1.0	99.0
B/2000/26C Matrix	1.1	31.3	68.7
B/2000/26C Nodules	1.1	49.1	50.9
B/2000/27A	1.7	23.8	76.2
B/2000/27B	1.9	8.1	91.9
B/2000/28A	1.7	31.0	69.0
B/2000/29A	1.0	23.9	76.1
B/2000/30Aa Matrix	1.9	30.0	70.0
B/2000/30Aa Nodules	3.9	14.5	85.5
B/2000/30Ab	1.6	25.4	74.6
B/2000/30B	2.5	6.0	94.0
B/2000/31A	2.3	25.4	74.6
B/2000/32A Matrix	0.6	2.6	97.4
B/2000/32A Nodules	0.4	2.6	97.4
B/2000/33A Matrix	0.3	4.5	95.5
B/2000/33A Nodules	0.3	6.6	93.4
B/2000/34A	0.5	35.5	64.5
B/2000/36A	1.2	30.4	69.6
B/2000/36B	1.0	40.9	59.1
B/2000/36C	1.0	28.6	71.4
B/2000/37A	1.5	29.0	71.0
B/2000/38A	0.8	10.7	89.3
B/2000/38B	0.5	39.1	60.9
B/2000/38C	0.6	34.4	65.6
B/2000/39A Matrix	0.9	10.8	89.2
B/2000/39A Nodules	0.8	34.8	65.2
B/2000/39B Matrix	0.7	11.1	88.9
B/2000/39B Nodules	0.5	33.8	66.2
B/2000/40A Matrix	1.4	42.2	57.8
B/2000/40A Nodules	1.0	51.4	48.6
B/2000/41A	0.4	0.6	99.4
B/2000/41B	0.5	0.7	99.3
B/2000/42A	0.5	48.2	51.8
B/2000/43A	1.2	44.1	55.9
B/2000/43B	0.4	0.4	99.6
B/2000/44A	0.1	0.4	99.6
B/2000/44B	0.4	30.8	69.2
B/2000/44C	0.4	34.9	65.1
B/2000/44D	0.2	23.0	77.0
B/2000/45A	1.0	29.0	71.0
B/2000/45B Matrix	1.3	25.1	74.9
B/2000/45B Nodules	1.3	33.5	66.5
B/2000/45C	0.9	26.0	74.0
B/2000/46A Matrix	1.3	45.2	54.8
B/2000/46A Nodules	1.3	45.7	54.3
B/2000/47B Matrix	0.8	32.3	67.7
B/2000/47C	0.6	34.4	65.6
B/2000/48A	1.8	45.3	54.7
B/2000/48B	0.9	49.4	50.6
B/2000/48C	0.7	44.6	55.4
B/2000/48D	0.6	48.0	52.0
B/2000/49D	0.6	46.0	54.0
B/2000/50A	0.9	43.3	56.7
B/2000/50B Rind	1.4	25.2	74.8
B/2000/50B Core	0.3	3.3	96.7
B/2000/51A	0.7	44.5	55.5
B/2000/52A	1.4	31.2	68.8
B/2000/52B	0.5	41.0	59.0
B/2000/52C	0.7	35.8	64.2
EO 01	1.6	49.8	50.2
EO 02	1.0	36.8	63.2
EO 03	2.8	8.0	92.0
Kapupuhedi	3.3	48.2	51.8
L/1999/1b 2.5m	0.7	14.8	85.2
L/1999/1b 3m	0.6	14.5	85.5
L/1999/3 2.5m	0.9	22.0	78.0
L/1999/3 3m	0.5	9.4	90.6
L/1999/4b 2m	0.5	21.0	79.0
L/1999/5 2m	0.9	7.1	92.9
N/2000/1A	1.2	48.9	51.1
Nam 12	7.8	29.4	70.6
B/1999/NG1A	1.3	43.8	56.2
B/1999/NG1B	1.5	19.8	80.2
B/1999/NG1 1.5m	1.1	46.0	54.0
OK/2001/12	0.6	29.7	70.3
OK/2001/13 2m Matrix	0.9	2.1	97.9
OK/2001/13 2m Nodules	1.0	2.0	98.0
OK/2001/13 4m	0.6	1.3	98.7
OK/2001/Sepupa	0.8	37.6	62.4
OK/2001/3BRD	1.3	33.0	67.0
Okaukuejo	3.2	44.6	55.4
Oshigambo 1m	0.8	6.7	93.3
B/2001/RC 11m	0.6	11.3	88.7
B/2001/RC 12m	0.7	1.3	98.7
B/2001/RC 13m	0.5	6.5	93.5
Sueda	3.9	43.7	56.3
T1 16 3.5m	2.0	33.3	66.7
Mosupatsela A 150 cm	0.34	3.22	96.8
Mosupatsela B 200 cm	0.47	5.56	94.4
Mosupatsela C surface	0.10	0.10	99.9

Appendix 7: Summary table of loss on ignition (LOI) results.

Mosupatsela C 20 cm	0.07	0.09	99.9
Mosupatsela C 50 cm	0.07	0.10	99.9
Gaenga surface	0.93	1.71	98.3
Gaenga 20 cm	0.32	0.36	99.6
Gaenga 40 cm	0.24	0.35	99.7
Xhamoga A surface	9.15	3.73	96.3
Xhamoga A 20 cm	1.90	3.83	96.2
Xhamoga A 40 cm	1.18	4.64	95.4
Xhamoga A 60 cm	1.46	7.10	92.9
Xhamoga B surface	4.83	1.27	98.7
Xhamoga B 20 cm	2.29	0.86	99.1
Xhamoga B 40 cm	0.75	0.60	99.4
Xhamoga B 60 cm	0.82	0.75	99.3
Xhamoga B 80 cm	0.54	0.69	99.3
Xhamoga B 100 cm	0.46	0.97	99.0
Xhamoga B 120cm	0.36	0.98	99.0
Xhamoga B 140 cm	0.37	1.26	98.7
Xhamoga B 160 cm	0.52	2.16	97.8
Xhamoga B 180 cm	0.62	3.55	96.4
Xhamoga C surface	1.04	0.74	99.3
Xhamoga C 20 cm	0.47	0.59	99.4
Xhamoga C 40 cm	0.36	0.76	99.2
Xhamoga C 60 cm	0.49	1.12	98.9
Xhamoga C 90 cm	0.37	1.65	98.4
Xhamoga D surface	0.21	0.27	99.7
Xhamoga D 20 cm	0.10	0.24	99.8
E001 0.2m	7.32	3.37	96.6
E001 0.35m	5.28	2.83	97.2
E001 0.5m	1.33	0.95	99.0
E001 0.75m	7.31	4.64	95.4
E001 1.5m	8.19	4.70	95.3
E001 1.75m	8.70	4.83	95.2
E001 2.0m	1.98	2.01	98.0
E001 2.5m	2.39	1.90	98.1
E001 3.0m	3.75	2.42	97.6
E002 0.3m	3.14	6.59	93 4
E002 0.5m	2.63	6.54	93.5
E002 0.65m	1.71	3.42	96.6
E002 1.0m	3.36	6.85	93.1
E002 1.2m	2.55	10.49	89.5
E002 1.5m	3 24	5.54	94.5
E002 1.75m	2 97	7.22	92.8
EKA1 0.25m	0 65	0.12	99.9
EKA1 0.5m	0.53	0.23	99.8
EKA1 1.0m	0.93	0.52	99.5
EKA1 1.5m	1.04	1.24	98.8
EKA1 2.0m	0.94	2.23	97.8
EKA2 0.0m	1.21	49.83	50.2
EKA2 0.3m	6.06	24.13	75.9
EKA2 0.5m	0.36	7.58	92.4
EKA3 0.25m	0.46	0.15	99.9
EKA3 0.5m	0 51	0.26	99.7
EKA3 1.0m	0 11	0.17	99.8
EKA3 1.5m	0 12	0.14	99.9
EKA3 2.0m	0 07	1.24	98.8
EKA4 0.25m	0.43	1.86	98.1
EKA4 0.5m	0 53	1.97	98.0
E004A 0.15m		4.53	95.5
E004A 0.35m		3.75	96.3
E004A 0.8m		1.71	98.3
E004A 1.0m		1.56	98.4
E004A 1.2m		1.11	98.9
E004A 1.65m		1.89	98.1
E004A 1.8m		1.99	98.0
E004A 2.0m		9.89	90.1
E004A 2.3m		12.70	87.3
E004A 2.5m		5.70	94.3
E004B 0.3m		16.02	84.0
E004B 0.6m		15.25	84.7
E004B 1.5m		7.12	92.9
E004C 0.2m		0.56	99.4
E004C 0.5m		1.00	99.0
E004C 0.7m		1.88	98.1
E004D 0.1m		0.06	99.9
E004D 0.4m		0.09	99.9
E004D 0.65m		1.04	99.0
E004D 1.0m		1.07	98.9
E004D 1.5m		0.90	99.1
E004D 2.0m		1.34	98.7
E004D 2.5m		0.98	99.0
E004E 0.25m		1.31	98.7
E004E 0.5m		0.88	99.1
E004E 1.0m		1.63	98.4
E004E 1.3m		3.66	96.3
E004F 0.15m		2.13	97.9
E004F 0.3m		1.72	98.3
E004F 0.5m		0.95	99.1
E004F 1.0m		1.70	98.3
E004F 1.5m		1.64	98.4
E004F 1.8m		1.18	98.8
E004F 2.5m		2.78	97.2

Appendix 8: Summary table of the sediments EC.

Sample	EC µS
B/2000/31A	458.9
B/2000/32A	3089.2
B/2000/33A	439.5
B/2000/34A	1929.0
B/2000/36A	427.4
B/2000/36B	714.9
B/2000/36C	648.0
B/2000/37A	568.6
B/2000/39A	441.9
B/2001/RC 11m	5001.9
B/2000/RC 12m	360.7
B/2000/RC 13m	781.1
Gaenga Surface	2770.8
Gaenga 20cm	587.9
Gaenga 40cm	474.2
Mosupatsela Surface	445.7
Mosupatsela 20cm	378.7
Mosupatsela 40cm	790.5
Mosupatsela 5m	1541.4
Mosupatsela 50m	2654.3
OK 51A Surface	2318.2
OK 51A 20cm	3146.9
OK 51A 40cm	1482.1
OK 51A 60cm	797.6
OK 51B Surface	1900.1
OK 51B 20cm	3667.4
OK 51B 40cm	2962.9
OK 51B 60cm	2124.1
OK 51B 90cm	1514.5
OK 51C Surface	4027.4
OK 51C 20cm	816.4
OK 51D Surface	4829.9
OK 51D 20cm	6148.7
OK 51D 40cm	3198.8
OK 51D 60cm	2913.3
OK 51D 80cm	5095.8
OK 51D 100cm	3545.7
OK 51D 120cm	2662.4
OK 51D 140cm	2505.8
OK 51D 160cm	2040.5
OK 51D 180cm	2024.2

Appendix 9: Summary table of the water soluble cation content of the sediments.

	Li	Na	Mg	Al	K	Ca	V	Cr	Fe	Mn	Co	Ni	Cu	Zn	Rb	Sr	Ba	Th	U	Ca/Mg Ratio	Mg/Ca Ratio
	ppb	ppm	ppm	ppm	ppm	ppm	ppb	ppb	ppm	ppm	ppb	ppb	ppm	ppm	ppb	ppb	ppb	ppb	ppb		
B/1999/NG1A	11.51	3.52	6.96	6.37	21.85	39.77	13.56	0.90	0.00	3.41	2.86	7.61	13.23	0.05	6.85	829.94	506.50	0.03	4.34	5.71	0 17
B/1999/NG1B	17.56	72.10	2.18	20.90	9.97	19.69	134.91	0.78	0.00	1.33	1.31	5.50	16.15	0.07	5.93	509.99	206.86	0.05	2.91	9.12	0 11
B/1999/NG1 1.5 m	14.17	4.28	4.10	1.02	5.05	26.82	66.90	1.21	0.00	0.49	0.22	1.36	6.01	0.04	1.96	695.06	697.38	0.01	1 17	6.54	0 15
B/2000/25A	4.67	2.36	2.13	26.43	14.49	29.90	42.23	1.22	0.00	1.49	0 50	2.88	16.55	0.08	10.99	369.33	288.50	0.05	0.25	14 01	0.07
B/2000/26C Matrix	25.53	59.43	18.77	4.28	42.54	44.33	62.13	1.46	0.00	2.56	0.24	1.88	6.43	0.05	11.26	1712.26	566.79	0 00	1 10	2 64	0 38
B/2000/26A	9.53	8.18	4.40	10.73	3.88	22.85	73.20	1.13	0.00	0.51	0.12	1.13	4.75	0.06	1.61	394.64	476.54	0.01	0.10	5 19	0 19
B/2000/30 As Nodules	46.47	19.98	8.41	91.40	77.66	25.56	266.89	5.17	0.02	0.71	0.20	3.96	15.25	1.29	24 99	501.09	513.61	0.01	0.47	3 04	0.33
B/2000/32 Matrix	29.44	134.32	12.17	13.60	21.32	21.27	283.31	29.07	5.85	50.65	5.54	10.94	22.02	0.01	39.30	246.30	717 60	0.66	1.74	1 75	0.57
B/2000/32 Nodules	46.43	133.38	19.10	20.16	24.46	30.10	288.89	44.38	9.09	93.26	7.62	14.74	21.63	0.02	63 65	339.13	663.67	1 15	2.31	1 58	0.63
B/2000/33 Matrix	22.18	760.08	3.00	206.08	14.15	20.87	30.77	2.14	0.12	25.98	0.20	0.87	1.19	0.00	11.39	486.66	303.32	0.01	0.12	6.95	0.14
B/2000/35A	16.85	10.13	4.66	22.76	11.78	26.36	273.75	1.44	0.00	1.24	0.29	2.38	11.35	0.02	8.25	661.20	571.66	0.01	5.42	5.40	0.19
B/2000/36A	21.49	15.76	9.36	4.16	4.36	21.97	635.31	3.20	0.00	0.29	0.22	0.61	1.64	0.01	4.01	1546.91	568.29	0.00	4.80	2 35	0.43
B/2000/36B	9.46	1.67	9.01	5.95	4.49	27.44	196.67	5.61	0.00	0.56	0.26	1.13	5.32	0.00	5.81	822.43	1082.39	0.00	2.16	3 04	0.33
B/2000/36C	10.65	1.89	5.59	3.44	6.25	29.75	163.90	6.32	0.00	1.51	0.20	1.26	1.97	0.01	7.36	647.35	397.38	0.01	0.49	5.32	0.19
B/2000/37A	10.51	2.71	13.32	6.83	3.24	24.49	58.53	1.31	0.00	1.20	0.20	1.25	1.43	0.00	3.94	900.19	187.09	0.00	0.78	1 84	0 54
B/2000/38A	11.81	3.38	3.09	43.46	7.65	33.82	101.48	3.02	0.00	2.03	0.33	1.72	4.55	0.02	13.64	195.66	1127.12	0.01	0.51	10 86	0 09
B/2000/38B	7.16	1.58	3.57	5.70	5.77	27.65	76.84	7.61	0.00	0.87	0.11	0.66	4.75	0.00	10.32	229.73	1226.18	0.00	0.74	7 83	0 13
B/2000/38C	11.04	2.63	14.19	3.33	7.92	51.25	66.89	0.99	0.00	2.16	0.21	1.27	1.79	0.00	13.42	1116.59	3973 18	0.00	1.00	3 61	0 28
B/2000/39A Matrix	5.44	1.06	2.67	22.10	7.17	29.11	122.90	1.67	0.00	1.96	0.36	1.79	4.77	0.00	6.37	280 93	125.54	0.04	1.05	10 15	0 10
B/2000/39A Nodules	5.21	1.81	2.97	9.37	6.33	25.99	108.42	3.33	0.00	0.63	0.11	1.31	14.38	0.04	5.60	278.44	130 39	0 00	1 26	8 76	0 11
B/2000/39B Matrix	4.46	1.66	4.59	127.87	6.05	31.94	90.47	2.12	0.00	1.79	0.12	1.13	11 81	0.04	7.08	297 83	172.17	0 01	1 17	6 95	0 14
B/2000/39B Nodules	4.34	1.66	4.03	13.65	7.56	29.91	70.91	3.63	0.00	0.97	0.10	1.20	8.06	0.03	7.02	267 96	106.56	0.00	1 26	7 43	0 13
B/2000/40 Matrix	13.75	3.51	5.14	9.64	3.09	30.00	82.23	0.80	0.00	0.63	0.85	4.90	14.15	0.06	3.21	330 78	622 70	3.00	2 15	5 83	0 17
B/2000/40 Nodules	11.01	3.19	4.46	8.14	1.50	27.96	53.45	0.38	0.00	0.74	0.36	5.47	8.34	0.02	1.09	469.99	665 11	0.70	2 21	6 24	0 16
B/2000/41A	24.46	186.86	6.01	20.61	12.01	10.67	549.56	25.93	9.38	162.20	11.39	17.49	65.40	0.05	41.01	129.16	487.80	7 66	2.27	1 78	0.56
B/2000/41B	56.39	111.06	7.95	67.40	9.92	5.22	487.94	72.58	27.82	175.13	17.25	34.25	53.33	0.10	54.64	49.45	250.96	19 43	2 32	0 68	1 47
B/2000/42A	1.59	1.44	2.71	10.66	13.34	20.66	10.63	0.38	0.00	1.09	0.42	2.80	14.72	0.05	2.70	100.00	83.81	0.32	0 81	7 62	0 13
B/2000/43A	6.24	2.01	2.15	13.44	6.38	32.56	7.40	0.73	0.00	2.81	1.18	9.62	12.07	0.02	6.55	140.00	156.95	0 34	1 69	15 13	0 07
B/2000/43B	3 06	2.07	2.25	70.45	9.66	33.41	4.61	1.66	0.11	12.82	0.40	8.04	52.59	0.03	7.65	123.22	546.66	0 56	0 88	14 87	0 07
B/2000/44A	4.61	9.94	0.59	414.15	14 51	17.24	40.53	0.44	0.50	3.12	0.75	1.02	14 67	0.01	10.97	179.97	259.11	0 10	6 81	29 26	0 03
B/2000/44B	6.69	4.27	1.34	2 66	12 32	25.67	156.20	0.64	0.00	1.76	0.35	1 48	7.92	0.03	13.59	333.96	462.56	0 12	0 89	19 33	0 05
B/2000/44C	6 21	2.96	0.97	5.99	10 17	23.21	269.00	0.09	0.01	2.14	0.46	1.63	9.12	0.06	13.02	314.25	253.56	0 10	2.18	23 64	0 04
B/2000/44D	6.75	6.31	0.95	180.94	12 67	20.91	106.78	0.11	0.54	7.23	0.50	1.73	14.19	0.06	10.78	248.26	149.27	0 13	4.79	21 98	0 05
B/2000/45A	57.51	5.54	13.03	3.87	9.82	90.54	41.55	2.07	0.00	2.11	1.13	3.29	9.19	0.07	9.08	26648.08	100.77	0.15	9.06	6.95	0.14
B/2000/45B Matrix	45.02		2.15	2.23	59.90	20.12	54.12	0.49	0.00	0.33	0.36	1.51	13.01	0.05	13.80	1212.52	193 50	0 10	2.50	9.37	0.11
B/2000/45B Nodules	66.45		2.74	5.96	46.06	15.97	80.76	1.80	0.00	0.84	0.26	1.99	40.34	0.05	20.19	1063.82	245 12	0 09	2.86	5.83	0.17
B/2000/45C	22.33	20.90	3.06	1.63	30.89	20.21	21.00	1.23	0.00	1.03	0.20	1.23	3.52	0.02	13 48	858.30	360 00	0 04	0.50	6.57	0.15
B/2000/46A Matrix	12.71	7.83	3.12	4.40	3.81	25.04	42.43	0.68	0.00	0.62	0.35	2.73	3.67	0.02	3.80	252.86	472.50	0 05	0.86	8.03	0.12
B/2000/46A Nodules	31.85	11.15	4.97	7.77	9.51	28.78	89.51	2.12	0.00	1.33	0.41	4.56	16.33	0.03	10.07	343.07	321.25	0.04	0.61	5.79	0.17
B/2000/47B Matrix	16 16	20.47	2.16	2.19	2.05	24.42	60.62	1.42	0.00	0.49	0.68	2.47	5.69	0.02	1.62	224.65	433.54	0.06	0.46	11.29	0.09
B/2000/47B Nodules	89.01	15.61	8.14	11.47	9.35	26.75	76.95	1.35	0.00	1.43	0.39	4.21	16.44	0.06	10.69	287.15	502.40	0.05	1.94	3.29	0.30
B/2000/47C	14.27	26.02	1.62	4.69	1.16	14.19	73.19	0.84	0.00	0.72	0.24	1.37	10.12	0.07	0.59	216.03	197.76	0.02	0.47	7.80	0.13
B/2000/48A	19.33	16.08	6.89	4.28	14.86	70.10	34.49	1.92	0.00	5.62	6.52	6.93	17.00	0.03	7.48	633.46	299.74	0.07	0.70	8.07	0.12
B/2000/48B	8.74	3.29	2.57	11.51	5.12	26.85	28.80	0.55	0.00	0.84	0.81	2.66	4.63	0.34	3.72	329.46	322.00	0.02	0.53	10.43	0.10
B/2000/48C	12.63	12.71	3.96	2.19	3.55	23.49	55.54	1.09	0.00	1.00	0.40	1.51	6.89	0.02	2.03	431.56	637.50	0.02	0.36	5.93	0.17
B/2000/48D	12.82	36.46	2.72	6.63	2.35	14.96	174.50	1.06	0.00	0.78	0.99	1.34	9.59	0.05	1.46	292.40	106.35	0.02	0.58	5.50	0.18
B/2000/49D	12.46	23.85	4.12	3.35	5.02	14.14	597.42	1.94	0.00	0.53	0.59	1.37	7.76	0.05	1.59	868.64	201 76	0.01	4.16	3.43	0.29
B/2000/50A	10.06	4.02	2.94	10.62	4.43	30.80	26.34	0.93	0.00	1.04	0.67	4.60	11.59	0.09	2.66	411.04	417.29	0.03	1.78	10.41	0.10
B/2000/50B Rind	25.86	7.63	4.10	2.06	3.42	32.86	56.66	0.53	0.00	1.96	0.64	3.23	6.76	0.03	1.92	648.44	491.73	0.02	0.89	8.05	0.12
B/2000/50B Core	24.20	10.80	2.91	16.37	2.37	29.96	106.53	0.46	0.00	1.62	0.26	1.85	9.65	0.06	0.75	351.65	230.66	0.01	0.35	10.28	0.10
B/2000/51A	16.36	8.47	2.03	22.55	89.40	15.46	45.02	1.42	0.00	1.02	0.56	3.31	6.50	0.02	18.18	197.63	171.67	0.03	0.90	7.64	0.13
B/2000/52A	22.32	15.06	7.11	3.13	7.21	67.31	63.44	0.54	0.00	26.73	2.81	17.27	13.27	0.07	3.37	1185.33	730.66	0.07	3.33	9.47	0.11
B/2000/52B	11.73	3.41	3.35	10.09	5.49	24.66	30.63	0.21	0.00	0.92	0.34	2.26	6 22	0.05	2.64	433.24	186.66	0.02	0.96	7.36	0.14
B/2000/52C	12.50	14.39	4.49	3.29	4.00	25.39	63.04	0.44	0.00	1.09	0.56	3.79	9.93	0.03	1.66	602.16	371.92	0.02	1.25	5.66	0.16
Gaenga surface	37.12	43.37	17.31	5.65	112.06	6.86	1.33	1.65	0.01	3.73	0.45	1.09	4.85	0.01	96.17	360.19	400.06	0.03	0.07	0.51	1.95
Gaenga 20 cm	5.06	2.09	2.21	46.20	17.69	19.10	37.91	0.76	0.02	32.14	0.54	2.37	10.82	0.01	19.22	165.00	526.33	0.07	0.19	8.63	0.12
Mosupetsela A 150 cm	11.77	6.02	4.64	0.01	12.83	43.64	28.94	1.40	0.00	16.20	0.20	1.83	5.77	0.01	9.39	485.61	662.20	0.05	0.07	9.02	0.11
Mosupetsela B 200 cm	7.45	109.70	1.41	0.27	10.77	4.61	63.21	1.66	0.16	27.19	0.41	1.25	7.29	0.01	3.07	169.76	255.50	0.10	2.80	3.27	0.31
Mosupetsela C surface	5.80	7.73	1.78	3.41	6.16	2.48	4.92	3.33	2.43	371.57	1.72	2.04	5.01	0.02	12.35	55.80	59.75	0.13	0.06	1.39	0.72
Mosupetsela C 20 cm	17.55	12.72	0.86	1.94	9.54	4.41	2 67	2.58	1.53	516.17	4.57	4.16	5.05	0.05	7.20	73.97	82.55	0.05	0.03	5.02	0.20
Mosupetsela C 50 cm	19.97	15 98	2.62	16.16	7 01	0.93	26.92	14.20	10.93	363.62	7.20	7.98	9.46	0.04	37.36	36.76	97.36	0.00	0.00	0.35	2.83
Xhemoga A surface	45.74	116 24	7 99	96.70	83.31	24.29	150 10	2.55	0 04	123.06	5.30	8.40	32.21	0.07	59.75	297.44	508.51	1.41	2.29	3.04	0.33
Xhemoga A 20 cm	69.24	141.47	9.73	25.44	87 18	22 78	109.66	1.35	0.01	343.37	3.97	8.06	21.15	0 17	61.05	366.55	701.72	2.53	2.97	2.34	0.43
Xhemoga A 40 cm	37.16	72 22	7.16	2 96	36.46	7.32	145.72	1.15	0.00	4.30	0.26	1.67	9.78	0.00	31 67	186.42	261.42	0.35	0.71	1.02	0.98
Xhemoga A 60 cm	9.61	17 16	21.69	0.94	9.49	19 78	80.74	1.96	0.00	9.26	0.33	2.92	4.64	0.04	10.28	161.59	82.55	0.16	0.56	0.91	1.10
Xhemoga B surface	13 87	2.25	21 78	53.56	66.44	65.65	5.61	3.49	0.06	977.16	4.56	6.53	25.51	0.01	32.65	3179.52	7259.76	0.25	0.13	3.03	0.33
Xhemoga B 20 cm	26 90	2 63	26.22	45.55	60.96	80.71	8.57	4.22	0.06	1531.03	4.84	8.32	26.16	0.04	27.24	2904.05	4823.61	0.28	0.25	2.86	0.35
Xhemoga B 40 cm	24.39	2 90	10.64	27 53	49.07	26.12	32.77	1.79	0.03	1300.02	7.07	7.25	15.82	0.03	22.02	647.24	737.71	0.12	0.16	2.59	0.39
Xhemoga B 60 cm	17 05	4 66	9.40	23 57	65.08	24.32	47 37	2.17	0.01	376.76	3.99	5.55	9.90	0.02	22.33	427 56	176.76	0.26	0.13	2.59	0.39
Xhemoga B 80 cm	37 76	88.26	4.69	1297.01	77 46	12.75	87.62	3.58	0.66	360.65	10 70	14.36	16 46	0.02	22.02	229.53	121.64	2.27	1.05	2.61	0.38
Xhemoga B 100 cm	58 33	90 66	20.70	94.26	116.21	15.15	383.73	105.67	52.49	1063.10	23 56	41 26	37.06	0 09	178 00	204 17	289.50	0.00	2.26	0.73	1.37
Xhemoga B 120cm	51 36	78.27	21.02	84.61	94.06	10 60	420.49	75.71	37.46	1045.94	17 85	30 68	36 24	0.06	136 43	199 33	338.42	0.00	1.73	0.51	1.95
Xhemoga B 140 cm	47 59	77.42	15.67	50.78	83.79	7 56	1075.93	59.47	27.50	582.51	11.51	22 10	22.87	0 05	98 40	169 60	337.47	0.00	1.44	0.48	2 09
Xhemoga B 160 cm	14 75	51.00	1.67	51.67	69.47	8.02	951.17	1.91	0.04	22.41	0.66	2.30	14.71	0.02	20 97	171 79	213.86	1.21	0.60	4.82	0.21
Xhemoga B 180 cm	6.40	40.99	4.17	6.18	69.94	6.67	558.78	2.56	0.01	5.61	0.33	1.84	5 59	0.00	22 04	250 74	158.00	0 17	0.72	1.85	0 61
Xhemoga C surface	7 10	23.05	6.46	122.16	53.62	22.10	33.57	2.85	0.05	20.70	1.07	3.93	12 02	0 05	15 46	260.34	262.01	0.37	0.46	3.41	0.29
Xhemoga C 20 cm	35.96	89.06	22.64	75.93	89.15	16.89	259.56	86.40	42.19	1650.93	30.74	48 90	66 06	0 12	146.20	317 13	680.46	0.00	2.19	0.74	1 36
Xhemoga C 40 cm	37 34	90 02	24.40	75.46	104.91	12.37	312.25	85.89	43.03	1510.77	24.25	40 59	53 01	0 09	155 70	325.93	674.55	0 00	1.34	0.51	1 97
Xhemoga C 60 cm	44.02	112.67	36.90	61.15	135.61	18.23	629.35	92.11	44.84	2325.06	32.32	51 34	61 37	0 09	180 90	561.30	1469.30	0 00	1.40	0.49	2 02
Xhemoga C 90 cm	4 65	100.69	2.63	680.12	86.09	3.47	302.98	4.42	0.51	71.35	1 13	2 59	9 30	0 01	15 50	88.25	148.55	0.79	0.51	1.32	0 76
Xhemoga D surface	14.22	61.22	6.77	2.49	91.72	10.01	10 48	4.00	1.88	431.73	3.33	3 48	11 40	0 02	24 05	216 41	351.82	0.51	0.22	1.48	0.68
Xhemoga D 20 cm	14.15	10.09	10.79	29.13	29.11	3.96	71.05	31.16	16.92	782.17	13.96	14 27	12 78	0.04	52.26	137 10	298.42	0.00	0.00	0.37	2.73

Appendix 10: Summary table of the water soluble anion content of the sediments.

Sample	Chloride	Nitrite	Phosphate	Sulphate	Nitrate
Gaenga Surface	55.60	0.00	0.00	15.72	0.00
Gaenga 20cm	11.98	0.00	0.00	6.93	0.00
Gaenga 40cm	10.96	0.00	0.00	0.00	0.00
Mosupatsela Surface	37.58	0.00	0.00	23.23	11.00
Mosupatsela 20cm	16.70	0.00	0.00	8.16	0.00
Mosupatsela 40cm	0.00	0.00	0.00	0.00	0.00
Mosupatsela 5m	0.00	0.00	0.00	0.00	0.00
Mosupatsela 50m	0.00	0.00	0.00	0.00	0.00
OK 51A Surface	42.04	0.00	0.00	20.97	0.00
OK 51A 20cm	81.33	0.00	0.00	22.28	6.14
OK 51A 40cm	56.01	0.00	0.00	5.76	0.00
OK 51A 60cm	22.95	0.00	0.00	4.69	0.00
OK 51B Surface	30.82	0.00	0.00	27.72	0.00
OK 51B 20cm	201.66	111.86	0.00	40.20	0.00
OK 51B 40cm	200.09	29.52	0.00	23.16	0.00
OK 51B 60cm	187.33	0.00	0.00	0.00	0.00
OK 51B 90cm	67.81	0.00	0.00	10.04	0.00
OK 51C Surface	182.74	9.51	0.00	22.10	40.88
OK 51C 20cm	140.63	0.00	0.00	0.00	0.00
OK 51D Surface	303.03	412.44	0.00	37.14	388.90
OK 51D Surface_2	259.31	283.33	0.00	31.23	332.26
OK 51D 20cm	439.34	6.56	0.00	111.54	537.40
OK 51D 20cm_2	396.30	0.00	0.00	95.90	487.90
OK 51D 40cm	240.34	5.67	0.00	81.23	133.65
OK 51D 60cm	340.32	20.28	0.00	42.76	63.34
OK 51D 80cm	1107.23	0.00	0.00	85.41	6.33
OK 51D 80cm_2	818.50	0.00	0.00	79.40	0.00
OK 51D 100cm	493.99	63.22	0.00	18.60	24.20
OK 51D 100cm_2	436.64	60.60	0.00	20.00	23.48
OK 51D 120cm	172.81	0.00	0.00	14.15	11.85
OK 51D 140cm	389.48	0.00	0.00	10.89	20.06
OK 51D 160cm	220.06	0.00	0.00	15.91	15.47
OK 51D 180cm	366.54	0.00	0.00	11.20	6.72
OK 51D 180cm_2	315.67	0.00	0.00	10.14	0.00

Appendix 11: Summary of isotope analysis.

		Inorganic δ13C PDB	Organic δ13C PDB	δ18O PDB
1	B/1999/NG1a	-2.38		-4.84
2	B/1999/NG1 - 1.5 m	-3.97		-7.05
3	B/1999/NG1 - 2.0 m	-2.26		-7.52
4	EO 01/1999	-4.69		-7.23
5	EO 02/1999	0.15		-5.86
6	EO 03/1999	-2.59		-4.43
7	Kapupuhedi	-3.26		-5.50
8	L/1999/1B - 2.5m	-4.73		-7.63
9	L/1999/1B - 3.0m	-5.98		-8.17
10	L/1999/3 - 2.5m	-5.26		-6.62
11	L/1999/3 - 3.0m	-3.94		-4.83
12	L/1999/4 - 2.0m	-1.94		-3.42
13	L/1999/5 - 2.0m	-2.73		-1.50
14	Namutoni 12	-0.16		-4.18
15	Okaukuejo	-1.57		-4.60
16	Oshigambo River / E002	-2.59		-7.01
17	Sueda	-1.13		-4.00
18	T1 16/1999	-2.89		-6.30
19	B/2000/25A	-6.65		-6.18
20	B/2000/26A	-1.88		-5.96
21	B/2000/26B	-4.12		-4.27
22	B/2000/26C Matrix	-2.09		-5.29
23	B/2000/26C Nodules	-2.91		-5.55
24	B/2000/27A	-1.46		-6.13
25	B/2000/27B	-2.20		-5.95
26	B/2000/28A	-4.03		-6.00
27	B/2000/29A	-5.86		1.55
28	B/2000/30Aa Matrix	0.82		-2.23
29	B/2000/30Aa Nodules	0.42		-2.64
30	B/2000/30Ab	-0.81		-2.59
31	B/2000/30B	-3.72		-2.04
32	B/2000/31A	1.35		0.29
33	B/2000/32A Matrix	-1.65		-1.16
34	B/2000/32A Nodules	-0.92		-1.71
35	B/2000/33A Matrix	-5.49		-4.71
36	B/2000/33A Nodules	-5.90		-4.47
37	B/2000/34A	0.54		-7.01
38	B/2000/35A	-0.21		-6.60
39	B/2000/36A	-0.58		-7.17
40	B/2000/36B	-0.43		-7.98
41	B/2000/36C	0.63		-7.57
42	B/2000/37A	0.49		-5.21
43	B/2000/38A	-2.79		-8.15
44	B/2000/38B	0.65		-9.01
45	B/2000/38C	0.16		-8.18
46	B/2000/39A Matrix	-3.94		-8.15
47	B/2000/39A Nodules	0.88		-7.57
48	B/2000/39B Matrix	-3.78		-8.46
49	B/2000/39B Nodules	0.84		-7.99
50	B/2000/40A Matrix	-2.24		-5.68
51	B/2000/40A Nodules	-1.29		-6.37
52	B/2000/41A	-3.89		-5.43
53	B/2000/41B	-5.04		-6.84
54	B/2000/42A	-2.85		-6.66
55	B/2000/43A	-4.47		-5.83
56	B/2000/43B	-5.34		-6.99
57	B/2000/44A	-9.89		-9.56
58	B/2000/44B	-4.02		-4.63
59	B/2000/44C	-3.57		-5.75
60	B/2000/44D	-3.25		-4.90
61	B/2000/45A	-0.53		-1.18
62	B/2000/45B Matrix	-3.51		-2.53
63	B/2000/45B Nodules	-1.71		-2.29
64	B/2000/45C	-4.00		-2.18
65	B/2000/46A Matrix	0.36		-5.60
66	B/2000/46A Nodules	-0.67		-5.79

Appendix 11: Summary of isotope analysis.

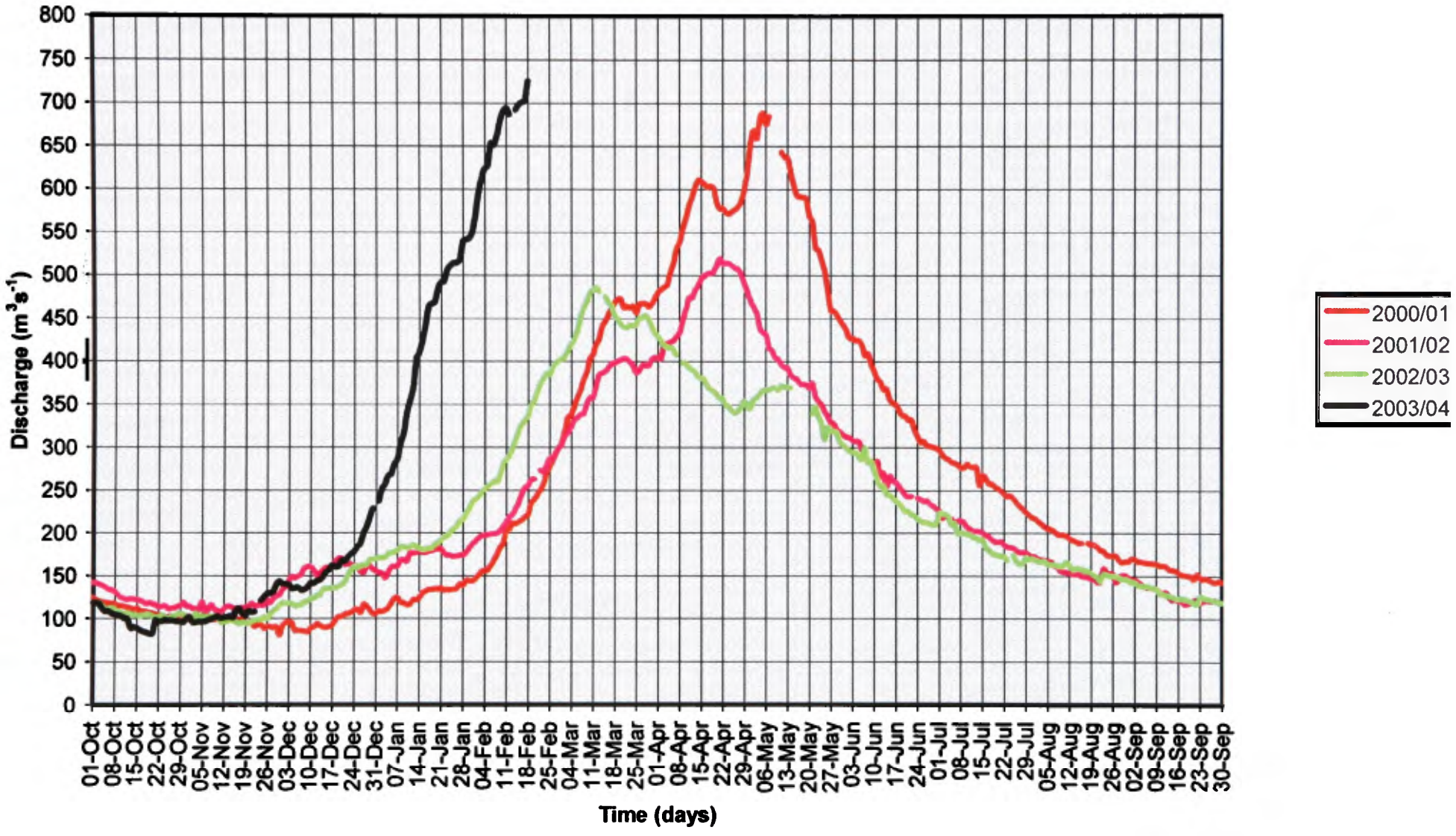
67	B/200047A	0.19		-6.67
68	B/2000/47B Matrix	-1.22		-5.79
69	B/2000/47B Nodules	-1.73		-6.28
70	B/2000/47C	-2.93		-6.25
71	B/2000/48A	-2.26		-4.32
72	B/2000/46B	-1.28		-6.40
73	B/2000/48C	-1.84		-6.90
74	B/2000/48D	-2.30		-6.49
75	B/2000/49D	-4.65		-7.07
76	B/2000/50A	-2.63		-6.35
77	B/2000/50B Core	-2.72		-7.96
78	B/2000/50B Rind	-2.98		-7.50
79	B/2000/51A	-2.00		-6.87
80	B/2000/52A	-4.63		-6.00
81	B/2000/52B	-4.77		-8.29
82	B/2000/52C	-4.58		-7.95
83	N/2000/1A	-0.8		-3.6
84	NC/2000/14B	-2.88		-3.91
85	NC/2000/27B	-3.44		-0.94
86	B/2001/RC - 11m	-1.23		-6.94
87	B/2001/RC - 13m	-5.96		-8.79
88	B/2001/Sepupa	-1.17		-7.08
89	B/2001/3BRDG	-4.68		-5.18
90	OK/2001/12	-1.93		-8.84
91	OK/2001/13 - 2.0 m Matrix	-9.15		-8.03
92	OK/2001/13 2.0 m Nodule	-8.80		-9.51
93	Gaenga Island Surface 1A (<80) - fine	5.08	-19.8	5.17
94	Gaenga Island Surface 1A (>80) - coarse	7.05		3.50
95	Gaenga Island Surface 1B (<80) - fine	-0.40	-19.9	1.60
96	Gaenga Island Surface 1B (>80) - coarse	-0.41		-0.26
97	Gaenga Island Precipitant below surface (<80)	1.47	-19.2	0.80
98	Gaenga Island Precipitant below surface (>80)	1.61		2.28
99	Gaenga Island 20 cm (<80) - fine	-6.33	-18.1	-0.78
100	Gaenga Island 20 cm (>80) - coarse			
101	Gaenga Island 40 cm (<80) - fine	-6.80	-18.4	-2.32
102	Gaenga Island 40 cm (>80) - coarse	-7.08		-5.61
103	Mosupatsela Island Surface	-17.34		
104	Mosupatsela Island Surface 0.5m	-5.77		
105	Mosupatsela Island 5 m (< 80) - coarse	-6.17		-5.45
106	Mosupatsela Island 50 m (>80) - fine	-6.27		-4.43
107	Mosupatsela Island 50 m (< 80) - coarse	-3.24		-6.02
108	Xhamoga Island P-A Surface (<80) - fine	-11.33	-27.1	-4.87
109	Xhamoga Island P-A Surface (>80) - coarse			
110	Xhamoga Island P-A 20 cm (<80)	-10.95	-25.0	-4.12
111	Xhamoga Island P-A 20 cm (>80)	-10.33		-2.62
112	Xhamoga Island P-A 40 cm (<80)	-9.60	-23.4	-4.00
113	Xhamoga Island P-A 40 cm (>80)			
114	Xhamoga Island P-A 60 cm (<80)	-8.60	-23.7	-3.30
115	Xhamoga Island P-A 60 cm (>80)	-7.66		-2.35
116	Xhamoga Island P-B Surface (<80) - fine	-21.07	-26.3	-14.10
117	Xhamoga Island P-B 20 cm (<80) - fine	-25.06	-25.3	-21.20
118	Xhamoga Island P-B 40 cm (<80) - fine	-24.00	-22.7	-16.85
119	Xhamoga Island P-B 60 cm (<80) - fine	-8.75	-22.8	-4.82
120	Xhamoga Island P-B 80 cm (<80) - fine	-8.25	-23.1	-0.65
121	Xhamoga Island P-B 80 cm (>80) - coarse	-10.24		-8.05
122	Xhamoga Island P-B 100 cm (<80) - fine	-8.60	-22.2	-2.58
123	Xhamoga Island P-B 100 cm (>80) - coarse	-8.73		-5.77
124	Xhamoga Island P-B 120 cm (<80) - fine	-7.16	-20.7	-2.65
125	Xhamoga Island P-B 120 cm (>80) - coarse	-7.68		-5.06
126	Xhamoga Island P-B 140 cm (<80) - fine	-7.19	-21.6	-4.22
127	Xhamoga Island P-B 140 cm (>80) - coarse	-7.11		-3.95
128	Xhamoga Island P-B 160 cm (<80) - fine	-7.21	-24.5	-4.78
129	Xhamoga Island P-B 160 cm (>80) - coarse	-6.65		-6.49
130	Xhamoga Island P-B 180 cm (<80) - fine	-6.59	-23.6	-1.92
131	Xhamoga Island P-B 180 cm (>80) - coarse	0.08		-6.76
132	Xhamoga Island P-C Surface (<80)	-6.27	-23.4	
133	Xhamoga Island P-C 20 cm (<80)	-7.66	-19.7	0.59
134	Xhamoga Island P-C 40 cm		-19.7	
135	Xhamoga Island P-C 60 cm		-21.2	
136	Xhamoga Island P-C 90 cm (<80)			-2.18
137	Xhamoga Island P-D Surface (<80)		-18.4	2.89

Appendix 12: Summary table of nitrogen and organic carbon content of the island sediments.

Sample	% N	% C	C/N
Mosupatsela Surface	0.01	0.09	8.18
Mosupatsela 20cm	0.00	0.03	6.50
Mosupatsela 50cm	0.00	0.02	8.00
M17 5m	0.02	0.13	7.82
M17 50m	0.01	0.06	8.43
Gaenga Island surface 1A	0.15	1.81	12.51
Gaenga Island surface 1B	0.10	0.80	8.11
Gaenga Precip Below Surface	0.28	2.57	9.27
Gaenga Island 20cm	0.02	0.22	12.28
Gaenga Island 40cm	0.11	1.28	11.20
OK 51 A surface	0.43	11.34	26.32
OK 51 A 20cm	0.06	0.96	14.98
OK 51 A 40cm	0.04	0.38	10.16
OK 51 A 60cm	0.04	0.55	14.10
OK 51 B surface	0.36	0.52	6.57
OK 51 B 20cm	0.11	2.14	19.45
OK 51 B 40cm	0.05	0.85	16.61
OK 51 B 60cm	0.04	0.68	17.38
OK 51 B 80cm	0.04	0.51	13.29
OK 51 B 100cm	0.02	0.23	10.76
OK 51 B 120cm	0.01	0.09	6.71
OK 51 B 140cm	0.01	0.10	7.69
OK 51 B 160cm	0.02	0.16	10.40
OK 51 B 180cm	0.02	0.14	9.00
OK 51 C surface	0.07	0.81	11.87
OK 51 C 20cm	0.02	0.21	10.70
OK 51 C 40cm	0.01	0.12	8.64
OK 51 C 60cm	0.02	0.16	8.37
OK 51 C 90cm	0.01	0.07	6.45
OK 51 D surface	0.01	0.12	8.29
OK 51 D 20cm	0.01	0.03	6.60

APPENDIX 13

OKAVANGO RIVER AT MOHEMBO HYDROGRAPHS 2000/1 TO 2003/4



Appendix 14: Surface and ground water samples collected from the Okavango Delta March 2001-July 2002.

			11/17/2001	12/5/2001	1/22/2002						OK38	Boro	Xaxaba Lodge	19°32.69	23°02.85
			11/17/2001	12/5/2001	1/22/2002						OK39	Boro	Baboon Camp	19°30.52	23°01.65
			11/17/2001	12/5/2001	1/22/2002						OK40	Boro	Xakue	19°30.14	23°00.22
			11/17/2001	12/5/2001							OK41	Boro	Mpho's Camp	19°26.30	22°56.39
				12/6/2001	1/20/2002	2/15/2002	3/29/2002	4/16/2002	5/28/2002		OK42	Santantadibe	Ditshiping	19°39.90	23°27.70
				12/7/2001	1/30/2002					7/6/2002	OK43	Khwai	Kwai River Bridge	19°10.28	23°45.06
				12/7/2001							OK43 Borehole	Khwai	Kwai River Borehole	19°10.28	23°45.06
				12/7/2001	1/20/2002						OK44	Khwai	Tsaro Camp	19°09.99	23°44.05
01/03/01 (M1)	8/28/2001			12/8/2001	1/11/2002					7/6/2002	OK45	Maunachira	Xakanaxa	19°10.87	23°24.53
				12/8/2001							Rain		Xakanaxa	19°10.87	23°24.53
	8/28/2001			12/8/2001	1/16/2002						OK46	Maunachira	Gadikwe	19°09.33	23°15.07
	8/28/2001			12/8/2001	1/16/2002						OK47	Maunachira	Xobega	19°11.69	23°12.66
	8/28/2001			12/9/2001	1/17/2002						OK48	Maunachira	Xugana	19°04.06	23°06 05
				12/9/2001	1/16/2002						OK49	Mboroga	Lopis Island	19°09.84	23°07 94
				12/9/2001							OK50	Santantadibe	Xhamoga Channel		
				12/9/2001							OK51A	Santantadibe	Xhamoga Island		
				12/10/2001							OK51B	Santantadibe	Xhamoga Island		
				12/10/2001							OK51C	Santantadibe	Xhamoga Island		
				12/10/2001							OK51D	Santantadibe	Xhamoga Island		
				12/9/2001							OK51 Vlei	Santantadibe	Xhamoga Island		
				12/12/2001				4/28/2002	5/28/2002	7/7/2002	Shashe 1 # 7935	Shashe	Shashe Valley	20°00.79	23°23.19
				12/12/2001	1/30/2002			4/1/2002	5/28/2002	7/7/2002	Shashe 4 # 7937	Shashe	Shashe Valley	20°00 85	23°22.68
				12/12/2001	1/30/2002			4/28/2002	5/28/2002	7/7/2002	Shashe 6 # 7938	Shashe	Shashe Valley	19°59.24	23°21.58
				12/12/2001	1/30/2002		3/27/2002	4/28/2002	5/28/2002	7/7/2002	Shashe 10 # 7962	Shashe	Shashe Valley	19°56.95	23°19.83
	8/28/2001										OK52		Txichira	19°20'06.9	22°42'40 5
01/03/01 (M13)	8/23/2001										OK53	same as M13	Gogontie	19°16'25.9	22°41'52.4
01/03/01 (M15)	8/23/2001				1/30/2002						OK54	same as M15	Mmadinare	19°11'25.9	22°40'22
											OK55		Mogogelo = OK47	19°12'10.7	23°12'49.2
											OK56	same as OK29	Old Matiapana Bridge		
01/03/01 (Maun 1)		9/29/2001			1/11/2002		3/29/2002	4/19/2002			OK57	same as Maun1	Pontoon Site		
			11/5/2001		1/13/2002	2/12/2002					OK58	Kunyere	Matsebe		
					1/17/2002						OK 59		Txaba		
											OK 60	same as OK 42	Ditshiping		
					1/20/2002						OK 60 Borehole	same as OK 42 Borehole	Ditshiping (groundwater)		
					1/13/2002	2/12/2002	3/28/2002				OK 61		Dikgathong		
										7/3/2002	OK 62		Tubu Channel		
										7/3/2002	OK 63		Tubu Borehole		
										7/3/2002	OK 64	same as M32	Shakawe Lodge		
										7/6/2002	OK 65		3rd Bridge		
					1/28/2002						OK 67		Xurube		

Appendix 15: Summary table of TDS (mg/l) in the surface Okavango water.

Mar-01	Aug-01	Sep-01	Nov-01	Dec-01	Jan-02	Feb-02	Mar-02	Apr-02	May-02	Jul-02	
M02	68.5 OK01	60.6 OK27	116.5 OK01	101.5 OK14	61.6 OK01	98.7 OK28	109.6 OK27	156.6 OK28	129.9 OK42	65.7 OK12	28.6
M03	62.7 OK02	88.7 OK28	137.3 OK02	149.7 OK15	41.1 OK03	83.1 OK29	103.4 OK28	117.9 OK29	127.3	OK24	25.6
M04	72.5 OK03	68.4 OK29	118.5 OK03	112.0 OK16	72.6 OK04	120.4 OK35	120.9 OK29	124.3 OK42	73.1	OK27	217.1
M05	67.9 OK04	79.5 OK57	125.2 OK04	122.8 OK17	45.6 OK11	38.3 OK42	110.9 OK42	100.5 OK57	145.2	OK28	220.1
M06	78.8 OK12	36.3	OK05	102.5 OK18	41.4 OK12	35.0 OK58	144.3 OK57	131.4		OK29	191.8
M08	81.6 OK13	42.2	OK06	119.5 OK19	52.7 OK13	45.1 OK61	123.3 OK61	130.2		OK43	100.4
M09	93.5 OK14	53.6	OK07	128.7 OK21	49.0 OK15	49.2				OK45	41.5
M11	108.9 OK16	35.5	OK08	88.9 OK22	34.8 OK16	55.6				OK62	94.5
M12	91.7 OK17	37.4	OK09	49.8 OK23	35.6 OK17	43.3				OK64	33.3
M14	91.2 OK18	36.5	OK10	59.3 OK24	35.6 OK18	34.1				OK65	55.3
M16	93.0 OK21	39.0	OK11	54.9 OK25	228.8 OK21	45.0					
M19	100.7 OK22	40.1	OK12	31.0 OK26	136.7 OK22	42.0					
M20	99.0 OK23	31.9	OK13	45.3 OK27	113.1 OK23	43.2					
M21	95.4 OK24	38.1	OK26	131.2 OK28	113.6 OK26	153.1					
M22	92.0 OK45	61.5	OK31	113.7 OK29	116.2 OK27	68.6					
M23	67.2 OK46	49.5	OK32	103.0 OK30	103.0 OK28	96.9					
M24	70.3 OK47	49.0	OK33	102.6 OK31	99.7 OK29	103.4					
M26	70.6 OK48	43.7	OK34	102.5 OK32	92.2 OK31	95.5					
M27	67.5 OK52	38.3	OK35	85.9 OK33	91.4 OK32	84.4					
M28	57.3 OK53	37.6	OK36	88.9 OK34	105.1 OK33	142.9					
M29	56.3 OK54	32.6	OK37	89.4 OK35	94.0 OK34	87.4					
M30	55.3		OK38	92.0 OK36	93.6 OK35	85.7					
M31	55.2		OK39	104.1 OK37	89.3 OK36	98.3					
OK12	47.7		OK40	89.2 OK38	85.4 OK37	92.5					
OK13	52.4		OK41	86.0 OK39	90.0 OK38	91.3					
OK17	87.3		OK58	136.3 OK40	91.9 OK39	99.3					
OK19	124.5			OK41	87.8 OK40	86.1					
OK21	86.1			OK42	138.3 OK42	109.7					
OK22	72.4			OK43	161.7 OK43	154.0					
OK24	63.6			OK44	165.0 OK44	157.1					
OK26	335.3			OK45	69.1 OK45	59.7					
OK28	83.0			OK46	74.5 OK46	65.5					
OK29	119.1			OK47	76.5 OK47	73.5					
OK45	63.1			OK48	73.0 OK48	38.9					
OK53	87.9			OK49	81.1 OK49	67.5					
OK54	95.3			OK50	106.2 OK54	21.6					
OK64	51.4				OK57	99.4					
					OK58	123.8					
					OK59	92.2					
					OK61	138.2					
					OK67	50.4					

Appendix 16: Summary table of groundwater TDS (mg/l) levels in the Okavango region.

Sample	Date	TDS (mg/l)
NG01	2/24/2001	5759.46
NG02	3/8/2001	6516.27
OK02	11/27/2001	149.72
OK43	12/7/2001	424.49
Gaenga (OK23)	12/2/2001	631.48
Gaenga Vlei (OK23)	12/2/2001	694.53
Mosupatsela (50m) (OK21)	3/13/2001	482.60
Mosupatsela (5m) (OK21)	3/13/2001	7090.32
Xhamoga Island (OK51) A	12/9/2001	1822.17
Xhamoga Island (OK51) B	12/10/2001	2199.38
Xhamoga Island (OK51) C	12/10/2001	5602.02
Xhamoga Island (OK51) D	12/10/2001	748.17
Xhamoga Island (OK51) Vlei	12/9/2001	284.60
Shashe Borehole 7935	12/11/2001	1367.65
Shashe Borehole 7935	4/28/2002	1287.35
Shashe Borehole 7935	5/28/2002	1119.33
Shashe Borehole 7935	7/7/2002	1495.16
Shashe Borehole 7937	12/11/2001	1065.11
Shashe Borehole 7937	1/30/2002	1146.53
Shashe Borehole 7937	4/1/2002	1233.88
Shashe Borehole 7937	5/28/2002	1213.24
Shashe Borehole 7937	7/7/2002	1227.91
Shashe Borehole 7938	12/11/2001	1016.60
Shashe Borehole 7938	1/30/2002	1112.75
Shashe Borehole 7938	4/28/2002	1065.11
Shashe Borehole 7938	5/28/2002	1099.23
Shashe Borehole 7938	7/7/2002	3254.11
Shashe Borehole 7962	12/11/2001	1126.41
Shashe Borehole 7962	1/30/2002	1029.92
Shashe Borehole 7962	3/27/2002	1048.06
Shashe Borehole 7962	4/28/2002	1055.94
Shashe Borehole 7962	5/28/2002	1046.12
Shashe Borehole 7962	7/7/2002	1003.70
Tubu Borehole	7/3/2002	276.09

Appendix 17: Summary table of groundwater cations in the Okavango region.

Sample Name	Li (ppb)	Na (ppm)	Mg (ppm)	Al (ppb)	K (ppm)	Ca (ppm)	V (ppb)	Cr (ppb)	Fe (ppb)	Mn (ppm)	Co (ppb)	Ni (ppb)	Cu (ppb)	Zn (ppb)	Rb (ppb)	Sr (ppb)	Ba (ppb)	U (ppb)	Ca/Mg Ratio
Gaenga Groundwater	18.324	9.263	22.331	0	56.942	97.786	2.548	0.528	0	1.262	0.870	5.289	2.028	9.017	50.089	623.692	2819.972	0.831	4.38
Gaenga Vlei	31.631	55.066	29.140	trace	110.324	23.076	0.237	0.227	0	26.464	0.140	0.771	1.877	5.354	57.848	594.098	1309.644	0.087	0.79
OK 43 Groundwater	7.148	7.901	5.802	0	4.219	80.859	trace	trace	120.440	0.306	0.359	2.899	1.255	168.344	4.527	444.942	584.141	1.110	13.94
Xhamoga Island (OK 51) A	158.753	103.628	377.591	6.178	20.576	78.004	12.295	0.206	0	0.436	0.931	4.633	1.952	8.066	21.490	888.025	341.274	2.792	0.21
Xhamoga Island (OK 51) B	94.634	347.012	94.168	48.600	289.242	49.049	98.870	0.485	20.545	57.720	1.678	6.415	6.706	8.443	118.397	3012.103	3680.505	4.166	0.52
Xhamoga Island (OK 51) C	39.321	787.290	79.065	6.071	373.857	16.076	269.826	0.507	0	73.007	1.523	7.063	19.377	5.162	185.490	1373.212	1990.618	4.148	0.20
Xhamoga island (OK 51) Vlei	2.426	52.825	0.890	13.517	20.628	4.095	1.934	0	22.352	18.987	trace	trace	2.012	5.832	11.115	29.164	33.971	0.192	4.60
Shashe Borehole 7935	9.539	445.047	2.064	0	13.119	7.241	3.008	0	17.056	6.730	trace	trace	7.995	8.582	4.179	135.133	77.031	3.544	3.51
Shashe Borehole 7937	7.586	360.955	1.043	0	11.033	2.992	7.093	0	0	0.767	0.000	trace	7.927	2.951	3.087	93.329	52.009	9.207	2.87
Shashe Borehole 7938	9.900	293.492	2.806	trace	10.554	3.404	18.457	0	0	1.572	0.000	trace	10.349	4.297	3.542	145.464	41.117	17.296	1.21
Shashe Borehole 7962	9.571	270.346	9.879	0	11.380	38.414	8.140	0	0	116.724	trace	1.049	5.086	4.961	6.267	434.474	212.057	13.872	3.89
NG 1 March 2001	178.036	31.116	65.323	0.583		95.341	101.525	3.998	3.9953	91.352	0.818	4.772	36.004	0.115	39.149	3265.633	80.243	90.121	1.46
NG 2 March 2001	222.199	33.231	81.547	12.360	107.908	204.896	38.030	19.733	9.4417	92.089	3.682	11.706	29.867	0.068	24.342	19364.269	258.578	25.410	2.51